U.PORTO

DOUTORAMENTO

CIÊNCIAS BIOMÉDICAS

# DISCLOSING THE HEMATOPOIETIC NICHE AT THE DEVELOPING FETAL LIVER INTERSECTION

Márcia Mesquita Peixoto

**D**

**2023**

U.PORTO

**Márcia Mesquita Peixoto**. Disclosing the hematopoietic niche at the developing fetal liver intersection

**Disclosing the hematopoietic niche at the developing fetal liver intersection**

Márcia Mesquita Peixoto

INSTITUTO DE CIÊNCIAS BIOMÉDICAS ABEL ZALAZAR

**D** .ICBAS **2023**

MÁRCIA ISABEL MESQUITA PEIXOTO

# DISCLOSING THE HEMATOPOIETIC NICHE AT THE DEVELOPING FETAL LIVER INTERSECTION

Tese de Candidatura ao grau de Doutor em Ciências Biomédicas;
Programa Doutoral da Universidade do Porto (Instituto de Ciências Biomédicas Abel Salazar)

**Orientadora** – Doutora Perpétua Pinto-do-Ó
**Categoria** – Investigadora Principal
**Afiliação** – Instituto de Investigação e Inovação em Saúde, Instituto de Engenharia Biomédica; Instituto de Ciências Biomédicas Abel Salazar da Universidade do Porto

**Coorientadora** – Doutora Ana Cumano
**Categoria** – Investigadora Principal
**Afiliação** – Institut Pasteur, Paris

**Institutions involved in the development of this thesis work:**
















**Funding:**

This work was financed by national funds through FCT – Fundação para a Ciência e Tecnologia, I.P. in the scope of the project “2022.09110.PTDC” and FEDER - Fundo Europeu de Desenvolvimento Regional funds through the COMPETE 2020 - Programa Operacional Competitividade e Internacionalização (POCI), Portugal 2020, and by Portuguese funds through FCT/MCTES in the framework of the project "POCI-01-0145-FEDER-032656" granted to Perpétua Pinto-do-Ó, and by the Institut Pasteur, INSERM, ANR (grant Twothyme and grant Epi-Dev), REVIVE Future Investment Program and Pasteur-Weizmann Foundation through grants to Ana Cumano. Marcia Peixoto was a recipient of the grant FRH/BD/143605/2019.



















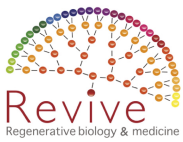

*“Sometimes, immersed in his books, there would come to him the awareness of all that he did not know, of all that he had not read; and the serenity for which he labored was shattered as he realized the little time he had in life to read so much, to learn what he had to know.”*
***— John Williams, Stoner***

# ACKNOWLEDGMENTS

*Et voilà*! The day has finally come!

Allow me to start by apologizing for the extensive list of names that follows, but I couldn't miss the opportunity to leave written the names of everyone who played a significant role in my life over the past years and in the progress of this scientific work. My apologies for the language blend, but I'll write as my thoughts flow. It's late, I'm tired, and coherence may falter, yet you can alternatively regard it as a stylistic choice.

First of all, I need to thank my supervisors Perpétua and Ana,

Perpétua, from you I inherited a deep passion for hematopoiesis and developmental biology, many years ago, while still a student. The passion you infused into your Stem Cell Biology course drew me to you, and here I am, eight years later, still inspired by you and your desire to truly understand how hematopoietic stem cells determine their fate. I am truly happy that you were part of mine.

Ana, your boundless energy and contagious enthusiasm are truly outstanding. I vividly remember the first time you taught me how to operate the sorting machine. Your passion was so captivating that it spurred my curiosity to the extent that I found myself absorbed in reading the entire machine's manual. Thanks for reminding me constantly how perfectionism is a curse; and how it is only worth it if we have fun. This Ph.D. was far from being easy, but even at the hardest moments, there was always something to make it fun.

For the team members,

António, it is hard to express how much I cherish our friendship and our deep long conversations. Thanks a lot for always being so encouraging. It is a great honor to be the "Sibila".

"Latas", the Power Rangers, the Band of Brothers. Elsinha, "chefe oficial das latas"; Ritinha "sub-chefe; responsável oficial pela Elsa"; Joana, "médica sem fronteiras, no hospital, em casa e em toda a parte"; Daniel, "que os panados para sempre te acompanhem". There are those friends from work, and then there are Latas, united by Sebastianism!

Lata Joana, with you I have life-long memories of pure excitement of performing 3D imaging for the first time; knocking on every i3S door looking for Agar; the rescue mission of a cat from under a car at 3 a.m.; night shifts in the lab, …! The dedication you pour into your work, and your patients, is not just inspirational, it's genuinely heartwarming.

Prerna, my sidecar, my bench partner, and my memes associate; thanks for allowing me to be your mentor and contribute a little bit to your way in science.

Rita Faria, you are another of my inspirations. I truly appreciated our teamwork, how disciplined you are, and how respectful you are of working in science! A tough, vibrant woman of science!

Inês Faria, a heritage from Rita, another of my duos, another great team! I had the best time in the lab with you in Paris, and I genuinely appreciate your refreshing feedback!

Mariana, Gonçalo, Francisca, Inês, Catarina e Tânia, the Portuguese crew in a foreign land. A special thanks to Mariana, for being so kind and always having wise words to give me.

Francisca, thanks for all the teachings, and for the teamwork, especially during COVID times! I have great memories of the two weeks pre-lockdown, when we wrote an entire review paper together, and the following summer, when we optimized many immunofluorescence stainings and started to see the fetal liver as no one had seen it before!

To ALL other current and former team members of both groups. To name a few, Diana Nascimento, Catarina Alves, Tânia Cruz, Luís Monteiro (a former team member from times not mine; a current friend), Marie-Pierre, Marie-Christine, Nathan Mackowski, Yanping Zhou, Françoise Guinet and,

Palomita, *mon cœur*, I promise I will learn how to cook “rissóis” and teach you!

Our dearest neighbors from Charles Baroud Lab, especially Charles himself, Gustave Ronteix, Valentin Bonnet, Andrey Aristov, Erik Maikranz and Sébastien Sart. Valentin, my latest duo, it was a great pleasure to work with you! I learned a LOT from you. It always brought me the most joy to learn a new coding shortcut with you.

I would like to extend my gratitude to the scientific platforms both at i3S and Institut Pasteur, and all the people involved, whose unwavering support and expertise were fundamental for this work. Because it is also worth mentioning by their names, a special thanks to Rossana Correia, Rui Fernandes, Nuno Mendes (HEMS), Catarina Meireles, Emília Cardoso (TraCy), Paula Sampaio, Maria Azevedo (ALM), Sofia Lamas (Animal Facility), Paula Magalhães, Tânia Meireles (CCGEN), Hugo Osório (Proteomics), María Lázaro, Eduardo Conde-Sousa (Bioimage) from i3S; and Sophie Novault, Sandrine Schmutz (CB UTechS); Julien Fernandes (PBI), and Tru Huynh (Gpulab) from Institut Pasteur. I am also deeply thankful to our collaborator Cédric Aït-Mansour (SONY), that was fundamental for the spectral cytometry analysis, and always available to answer my questions; and to João Pedro Pereira, with whom I had highly insightful and enriching discussions.

The friends,

Ana Filipa, my grammar and writing advisor, my partner of adventures, in Porto, in Paris, together or apart, the cities are for us to “desbravar”.

Joana Oliveira, my little sister, to whom I will always look after! I'm so proud of you!!

Domingos, Andreia, I have great memories with you, the summer 22' was a change of paradigm! Hope to see you in the next EuroTrips! Domingos, anytime you need, we'll drive you home!

Carlinhaaaaaa, it's done! I finished the thesis, but how does that compare to you, just giving birth a few hours before me writing this? I can't decide which makes me happier.

The family,

My family, that I will also enumerate because it's small and I love them all: pai, mãe, Vera (e respetivos), avó Fernanda, avô Joaquim‡ (já lá vão uns anos, mas como "antes assim que mais mal" se aqui aplica...), avó Patrocínia, avô Francisco, padrinho (que esta tese tenha a sua bênção), Ilda, Paulo, Natália, primooooss, ilustre Luís, Francisco, Andreia, e Maria; os avós emprestados (Sra. Zelinha e Sr. Carvalhais‡); a T e o Chitoooo.

Pai, mãe, Vera, a vós tenho a acrescentar "hum, hum, beijinhos e até amanhã"!

The one,

João, nem sei o que te diga, tenho tantas palavras para ti, "palavras impossíveis de escrever", que não cabem aqui. Não consigo imaginar este processo sem ti. Provavelmente teria demorado menos tempo a escrever a tese, mas não teria valido tanto a pena. Este Alto de l'Angliru já acabou, agora resta-nos subir o verdadeiro, juntos.

# RESUMO

No decorrer da embriogénese, o fígado fetal (FF) serve transitoriamente de nicho às células hematopoiéticas recém-formadas, proporcionando as condições necessárias à maturação, expansão e diferenciação de progenitores hematopoiéticos, nomeadamente células estaminais hematopoiéticas (CEHs). Apesar do papel preponderante do nicho hematopoiético do FF, este permanece pouco explorado.

Nesse âmbito, o presente projeto seguiu uma abordagem abrangente e minuciosa de caracterização do compartimento não-hematopoiético do FF durante o desenvolvimento embrionário. Esta incluiu a utilização de citometria de fluxo espectral aliada à análise de perfis de assinatura transcricional e mapeamento da localização de populações celulares *in situ*. O elevado número e qualidade de imagens de imunofluorescência geradas impulsionou a implementação de uma *pipeline* de *deep learning* personalizada (*Pyxidis*), a qual permitiu identificar padrões de distribuição celular e composição de redes celulares vizinhas com resolução ao nível da célula individual.

Os resultados obtidos sugerem uma contribuição multicelular das populações estromais para a produção de fatores hematopoiéticos, uma distribuição não aleatória de progenitores hematopoiéticos na periferia do fígado, e uma forte dependência de contacto direto entre populações de progenitores hematopoiéticos com hepatoblastos, os principais produtores de citocinas no FF. Identificamos ainda um papel até então não descrito das células mesoteliais na produção de citocinas hematopoiéticas.

Em suma, o trabalho realizado nesta tese contribuiu para uma melhor compreensão da composição celular do nicho hematopoiético do FF, bem como da sua topografia e interações celulares. Aprofundar este conhecimento poderá impulsionar a formulação de condições de cultura para a diferenciação de células estaminais pluripotentes (CEPs) em CEHs e para a manutenção e/ou expansão das mesmas *ex vivo*, o que, por sua vez, se traduzirá em avanços significativos nas aplicações clínicas destas células.

**Palavras-chave:** Hematopoiese, Fígado Fetal**,** Células Estaminais Hematopoiéticas, Nicho, Desenvolvimento, Citometria de Fluxo Espectral, Imagem 3D, Análise de Imagem, *Deep Learning*

# ABSTRACT

During embryogenesis, the fetal liver (FL) transiently serves as a niche for the newly generated hematopoietic cells, providing conducive conditions for the maturation, expansion and differentiation of hematopoietic progenitors, namely hematopoietic stem cells (HSCs). Despite the prominent role of the hematopoietic niche in the FL, it remains largely unexplored.

Within this context, this project adopted a comprehensive approach to thoroughly characterize the FL non-hematopoietic compartment during embryonic development. This involved the use of spectral flow cytometry, combined with transcriptional signature analysis and the mapping of the location of these populations *in situ*. The high quantity and quality of immunofluorescence images generated led to the implementation of a customized deep learning pipeline (*Pyxidis*), which allowed for the identification of cellular distribution patterns and the composition of neighboring cellular networks at the single-cell level.

The results obtained suggest a multicellular contribution of stromal populations to hematopoietic factors production, a non-random distribution of hematopoietic progenitors at the liver's periphery, and a strong dependence on direct contact between hematopoietic progenitor populations and hepatoblasts, the primary cytokine producers in the FL. Additionally, we identified a previously undescribed role of mesothelial cells in hematopoietic cytokine production.

In summary, the work conducted in this thesis has contributed to a better understanding of the cellular composition of the hematopoietic niche in the FL, as well as its topography and cellular interactions. Deepening this knowledge may drive the formulation of culture conditions for the differentiation of pluripotent stem cells (PSCs) into HSCs and for their maintenance and/or expansion *ex vivo*, ultimately leading to significant advancements in the clinical applications of these cells.

**Keywords:** Hematopoiesis, Fetal Liver, Hematopoietic Stem Cells, Niche, Development, Spectral Flow Cytometry, 3D Imaging, Image Analysis, Deep Learning

# TABLE OF CONTENTS

**ACKNOWLEDGMENTS** **v**

**RESUMO** **ix**

**ABSTRACT** **xi**

**LIST OF FIGURES** **xvi**

**LIST OF SUPPLEMENTARY FIGURES** **xvii**

**LIST OF TABLES** **xviii**

**LIST OF SUPPLEMENTARY TABLES** **xviii**

**LIST OF SUPPLEMENTARY VIDEOS** **xix**

**LIST OF ABBREVIATIONS** **xx**

**PREFACE** **1**

*LIST OF PUBLICATIONS* *3*

**CHAPTER I. INTRODUCTION** **5**

THE HEMATOPOIETIC SYSTEM 6

*An integrative view on hematopoiesis – old and new approaches* *6*

ONTOGENY OF THE HEMATOPOIETIC SYSTEM 11

*The different starting points* *11*

Yolk Sac 11

AGM 13

Placenta? 15

*Convergence point – the FL* *16*

*Settling down* *17*

*A layered organization* *17*

HSC EXPANSION – A DOGMA REVISITED 21

*The establishment of the HSC compartment* *21*

*A dogma on the edge?* *24*

FL – THE EMBRYONIC HEMATOPOIETIC HUB 26

*Liver development* *26*

*FL composition* *28*

Hepatic cells 28

Endothelial cells 30

Mesothelial cells 32
Mesenchymal cells 33
*An hematopoietic niche?* *35*
*Why the FL?* *38*
*Why no longer the FL?* *39*
AN OVERALL LOOK INTO HEMATOPOIETIC MICROENVIRONMENTS 41
TRACKING HSC LOCALIZATION IN THE NICHES 46
WRAP-UP, DISCUSSION AND *OPEN QUESTIONS* 51
PROJECT DESCRIPTION 53
**CHAPTER II. WHO, WHERE AND HOW: CHARACTERIZATION OF THE KEY PLAYERS IN THE FL HEMATOPOIETIC NICHE 55**
PREAMBLE 56
WHO: DISSECTING THE FL NON-HEMATOPOIETIC COMPARTMENT 58
*Autofluorescence as a parameter* *61*
WHERE: MAPPING THE FL 65
HOW: SCREENING FOR CYTOKINE PRODUCTION 70
DISCUSSION 74
MATERIALS AND METHODS 77
SUPPLEMENTARY INFORMATION 80
**CHAPTER III. DECODING THE VISUAL NARRATIVE: THE FL IN A DATAFRAME 89**
PREAMBLE 90
IMAGE ANALYSIS PIPELINE 91
*Nuclei segmentation* *92*
*Cell classification* *92*
*Spatial/network analysis* *94*
AF cells 94
Removal and selection of specific regions 95
Network construction 95
*Pipeline limitations* *97*
*Code availability* *97*
DISCUSSION 98
SUPPLEMENTARY INFORMATION 99
**CHAPTER IV. INTERACTIONS AT THE BORDER: A NOVEL NICHE FOR HEMATOPOIETIC PROGENITORS IN THE FL 101**

PREAMBLE 102

THE HEMATOPOIETIC COMPARTMENT 103

*Wild-HSC chase – an inglorious pursuit* *104*

*A bird's-eye view instead* *105*

FL NETWORK ANALYSIS 107

*Tissue composition* *107*

*E12.5* *108*

*E14.5* *110*

*E18.5* *112*

DISCUSSION 114

MATERIALS AND METHODS 116

SUPPLEMENTARY INFORMATION 119

**EPILOG** **127**

**REFERENCES** **131**

**ANNEX I** **160**

**ANNEX II** **162**

**ANNEX III** **182**

**ANNEX IV** **201**

**ANNEX V** **211**

**ANNEX VI** **228**

# LIST OF FIGURES

Figure 1. The hematopoietic tree model. 6
Figure 2. Model of lineage fate landscape in physiological hematopoiesis. 10
Figure 3. YS hematopoietic waves: blood islands and hemogenic vascular plexus. 13
Figure 4. Hematopoietic cell emergence at the major arteries in zebrafish and mouse. 15
Figure 5. Model of hematopoietic progenitor emergence in the embryo: sequential but overlapping waves. 20
Figure 6. Gut tube organogenesis and FL development. 27
Figure 7. Hepatocytes and cholangiocytes lineage segregation. 29
Figure 8. Early developmental stages of FL venous drainage. 31
Figure 9. Full spectrum of FL stromal cells obtained by spectral FC. 57
Figure 10. Global discrimination of the FL non-hematopoietic compartment. 59
Figure 11. Identification of two AF profiles in FL stromal cells. 61
Figure 12. The distinct AF signals define specific FL stromal populations. 62
Figure 13. AF-2 defines hepatoblast-like cells after birth. 64
Figure 14. FL landscape is dominated by hematopoietic cells. 65
Figure 15. LHX2, CD146 and HNF4$\alpha$ allow the discrimination of major FL stromal populations. 66
Figure 16. Vascular and perivascular compartments along FL development. 67
Figure 17. Mesothelium and sub-mesothelium. 68
Figure 18. Hepatic compartment along FL development. 69
Figure 19. Supportive hematopoietic cytokines are produced by multiple stromal populations. 70
Figure 20. The FL is a putative low cytokine environment. 72
Figure 21. Image analysis workflow. 91
Figure 22. Validation and quality control of image analysis. 94
Figure 23. Autofluorescent cells are removed from the analysis. 95
Figure 24. Analyzing cell distribution patterns: distance to a reference point and comparison with random. 96
Figure 25. Pipeline limitations. 97
Figure 26. Discrimination of the FL hematopoietic compartment at E12.5. 103
Figure 27. Composition of the $CD45^+$, DP and $KIT^+$ FL compartments. 106
Figure 28. Quantification of FL populations. 107
Figure 29. $KIT^+$ and DP progenitors accumulate at the periphery at E12.5 and are preferentially in contact with hepatoblasts, but not stellate or endothelial cells. 109

Figure 30. At later stages, opposite to KIT$^{+}$, DP progenitors display a homogeneous distribution throughout the parenchyma in response to CXCL12 levels. 111
Figure 31. Myeloid and lymphoid cells accumulate in the vessels and mesothelium at late gestation. 112
Figure 32. Quantification of mature hematopoietic lineages around vessels and near the mesothelium at late gestation. 113

# LIST OF SUPPLEMENTARY FIGURES

Supplementary Figure 1. FC profile of the FL non-hematopoietic compartment during development. 80
Supplementary Figure 2. Single-cell gene expression of FL non-hematopoietic populations. 81
Supplementary Figure 3. Single-cell gene expression of lineage-associated transcripts in FL non-hematopoietic populations. 82
Supplementary Figure 4. Single-cell gene expression of hematopoietic cytokines of FL major non-hematopoietic populations. 83
Supplementary Figure 5. Searching for an efficient staining strategy to enrich phenotypic HSCs. 119
Supplementary Figure 6. Technical difficulties encountered in the staining strategy combining KIT, CD48 and Sca-1. 120
Supplementary Figure 7. Quantification of mature hematopoietic lineages around vessels and near the mesothelium at late gestation. 121

# LIST OF TABLES

Table 1. Molecular signatures enriched with hematopoietic stem and/or progenitor cells in the adult mice. 8
Table 2. Reports quantifying HSCs at different developmental stages. 24
Table 3. A critical overview of the methodologies used to quantify HSC potential. 25
Table 4. Molecular signatures of mesothelial and major mesenchymal cells in the mouse FL. 35
Table 5. Fundamental signaling axis regulating hematopoiesis throughout development. 44
Table 6. Studies that assessed and quantified HSC localization in the BM microenvironment. 47
Table 7. Identification of hematopoietic progenitors during mouse ontogeny. 50
Table 8. FC panel assembled to discriminate the FL non-hematopoietic compartment. 58
Table 9. Network training. 117

# LIST OF SUPPLEMENTARY TABLES

Supplementary Table 1. Percentages of FL non-hematopoietic populations throughout development. 85
Supplementary Table 2. List of antibodies used for the analysis of FL stromal populations by spectral FC. 86
Supplementary Table 3. List of antibodies used for cell sorting of FL stromal populations. 86
Supplementary Table 4. List of antibodies used for cell sorting of BM stromal populations. 87
Supplementary Table 5. List of primers used for qRT-PCR. 87
Supplementary Table 6. List of primary antibodies used for IF. 88
Supplementary Table 7. List of secondary antibodies used for IF. 88
Supplementary Table 8. List of antibodies tested to optimize an HSC-enriched staining. 122
Supplementary Table 9. Percentages of enrichment for LT-HSCs and LSK $CD48^-$ considering different combinations of markers at E14.5 and E18.5. 123
Supplementary Table 10. Staining strategy combining KIT, Sca-1 and CD48. 123

Supplementary Table 11. List of antibodies used for the analysis of FL hematopoietic populations in Figure 26 and 27. 124
Supplementary Table 12. List of antibodies used for the analysis of FL hematopoietic populations in Supplementary Figure 5. 125
Supplementary Table 13. List of primary antibodies used for IF. 126
Supplementary Table 14. List of secondary antibodies used for IF. 126

# LIST OF SUPPLEMENTARY VIDEOS

Supplementary Video 1. The intricate vascular and perivascular network of the E18.5 FL. 84
Supplementary Video 2. ALCAM displays a widely distributed expression pattern across FL populations. 84
Supplementary Video 3. Pattern of expression of *Cxcl12* in *Cxcl12*-dsRed reporter mice at E12.5. 84
Supplementary Video 4. Pattern of expression of *Kitl* in *Kitl*-tdTomato reporter mice at E12.5. 84
Supplementary Video 5. Visual confirmation of the segmentation and classification using *Napari*. 99

# LIST OF ABBREVIATIONS[1]

**AF** – autofluorescence
**AFP** – alpha-fetoprotein
**AGM** – aorta-gonads-mesonephros
**ALB** – albumin
**ALCAM** – activated leukocyte cell adhesion molecule (or CD166)
**ANGPTL** – angiopoietin ligand
**BM** – bone marrow
**BMP** – bone morphogenetic protein
**CAR** – CXCL12 abundant reticular (cells)
**CFC** – colony forming cell
**CHT** – caudal hematopoietic tissue
**CK** – cytokeratin
**CLPs** – common lymphoid progenitors
**CSF** – colony stimulating factor
**CXCL12** – C-X-C motif chemokine ligand 12 (or stromal cell-derived factor 1, SDF1)
**DA** – dorsal aorta
**DLK1** – delta-like non-canonical notch ligand 1
**drMPP(s)** – developmental restricted multipotent progenitor(s)
**DV** – *ductus venosus*
**E-Cadh** – E-Cadherin (or cadherin 1, CDH1 or CD324)
**ECM** – extracellular matrix
**EGF** – epidermal growth factor
**EHT** – endothelial-to-hematopoietic transition
**EMP(s)** – erythro-myeloid progenitor(s)
**EMT** – epithelial-to-mesenchymal transition
**EpCAM** – epithelial cell adhesion molecule (or CD326)
**EPCR** – endothelial protein C receptor (or CD201)
**EPO** – erythropoietin
**EryP(s)** – primitive erythroid progenitor(s)
**EVI1** – ecotropic viral integration site
**FACS** – fluorescence-activated cell sorting
**FC** – flow cytometry
**FGF** – fibroblast growth factor
**FL** – fetal liver
**FLT3L** – Fms related receptor tyrosine kinase 3 ligand
**GFAP** – glial fibrillary acidic protein
**GMP(s)** – granulocyte-monocyte progenitor(s)
**GP38** – glycoprotein 38 (or podoplanin, PDPN)
**GPM6A** – glycoprotein M6A
**HE** – hemogenic endothelium
**HGF** – hepatic growth factor
**HLF** – hepatic leukemia factor
**HLX** – H2.0 like homeobox
**HNF4** – hepatic nuclear factor 4
**HS** – hematopoietic system
**HSC(s)** – hematopoietic stem cell(s)
**HSPC(s)** – hematopoietic stem and progenitor cell(s)

[1] Figure legends have independent abbreviations lists. Due to the high frequency of the terms HSC, FL, BM, YS, AF, FC and IF, these terms are not repeated in figure legends.

**IAHCs** – intra-aortic hematopoietic clusters
**IE** – intra-embryonic
**IF** – immunofluorescence
**IGF** – insulin growth factor
**IL** – interleukin
**KITL** – KIT ligand (or stem cell factor, SCF)
**LepR** – leptin receptor
**LGR5** – leucine-rich repeat-containing G-protein coupled receptor 5
**LHX2** – LIM homeobox 2
**LSECs** – liver sinusoidal endothelial cells
**LSK** – $Lin^{-}Sca\text{-}1^{+}KIT^{+}$ (cells)
**LT-HSC(s)** – long-term hematopoietic stem cells(s)
**LTi** – lymphoid tissue inducer (cells)
**LTR** – long term reconstitution
**MCs** – mesothelial cells
**MDK** – midkine
**Mks** – megakaryocytes
**MPPs** – multipotent progenitors
**MSLN** – mesothelin
**MtMV** – mouse-to-mouse variance
**OSM** – oncostatin M
**p75NTR** – p75 neurotrophin receptor (pr nerve growth factor receptor, NGFR)
**PCLP1** – podocalyxin-like protein 1 (or PODXL)
**PFs** – portal fibroblasts
**PTN** – pleiotrophin
**qPCR** – quantitative polymerase chain reaction
**qRT-PCR** – quantitative real time polymerase chain reaction
**PS** – portal sinus
**P-Sp** – para-aortic splanchnopleure
**RDs** – random dots
**scRNA-Seq** – single-cell RNA sequencing
**SCs** – stellate cells
**SLCs** – second layer cells
**SMA** – smooth muscle actin
**ST-HSC(s)** – short-term hematopoietic stem cell(s)
**STM** – septum transversum mesenchyme
**TPO** – thrombopoietin
**UA** – umbilical artery
**UVs** – umbilical veins
**VA** – vitelline artery
**VIM** – vimentin
**VVs** – vitelline veins
**WLSM** – Weighted Least Squares Method
**WT** – Wilms tumor (protein)
**YS** – yolk sac

# PREFACE

Hematopoietic stem cells (HSCs) are multipotent cells capable of generating a diverse repertoire of blood and immune cells. These cells were the first tissue-specific stem cells identified, in the early 60s. Remarkably, shortly after, in 1968, 3 patients with severe combined immunodeficiency syndromes were successfully treated after hematopoietic cell transplantation. 40 years later, more than 800.000 patients worldwide had been treated using this procedure[2].

Many scientists have been intensely dedicated to the study of the hematopoietic system (HS) for the past 6 decades. This intricate and complex system is established through multiple waves of hematopoietic emergence during embryonic development and a residence stage in the fetal liver (FL), before ultimately migrating to the bone marrow (BM), that will function as a main hematopoietic hub throughout life. Adult hematopoiesis and the BM microenvironment have been a major focus to study HSC biology. Countless studies have identified and characterized BM cell types, reporting some as key hematopoietic regulators.

The adult HSC compartment must be tightly regulated to ensure continuous production of mature blood cells while safeguarding its maintenance. However, despite major efforts, isolated and cultured HSCs rapidly lose their stemness properties, which limits their *ex vivo* manipulation. Being able to maintain and manipulate HSCs outside their native environment holds the potential to address and surpass certain limitations in the clinical application of these cells. However, the mechanisms that drive the stem cell fate choices towards self-renewal, differentiation and expansion remain largely unknown.

Our understanding of the HS is in constant remodeling. Established dogmas are regularly challenged, and subject to revision and reformulation. While the adult BM is widely accepted as a “maintenance” niche, during embryonic development the HSC compartment is thought to go through an expansion phase, most pronounced during the FL stage. Although the dogma concerning FL as an expansion niche can be questioned, as it will be discussed later in the introduction, the need to dissect the FL microenvironment, the major hematopoietic site during embryonic development, is of an unaltered urgency. Yet, only a few studies have addressed the FL to screen for putative hematopoietic niches.

[2]Milestones in Hematopoietic Cell Transplantation, 50 Years in Hematology: Research That Revolutionized Patient Care, American Society of Hematology (2008)

Understanding the role of the FL microenvironment in hematopoietic development is a long-lasting joint ambition of Perpétua Pinto-do-Ó and Ana Cumano labs. In previous work, Francisca Soares-da-Silva optimized the isolation of FL cell types and identified major hematopoietic cytokine producers in the FL at midgestation. My Ph.D. stands as a follow-up of this work, in collaboration with Soares-da-Silva. We improved the flow cytometric characterization of FL cell types, ascertaining the transcriptional signature of major non-hematopoietic populations and their *in-situ* localization at various stages of liver development. For the latter, we created a high-definition imaging dataset of hematopoietic and non-hematopoietic cell types.

Another key collaboration was established later in my Ph.D. with Charles Baroud's lab, initially through Gustave Ronteix and continued with Valentin Bonnet, to develop a pipeline to extract biological relevant data from our microscopy images. Together, we explored the FL, by quantifying the organs' composition, and by identifying patterns of cell distributions and the neighbor composition at the single-cell resolution. *"Has a cell type a higher propensity to be closer to another given cell type?"* is the type of question that we can address by our image analysis approach, while easily escaping the eye.

This thesis compiles this cooperative work as follows. This manuscript is organized in four chapters. **Chapter I** introduces relevant topics to contextualize this thesis work. It starts by exploring historical and up to date knowledge on the HS, and the evolving paradigm of hematopoiesis in a hierarchical tree structure. To understand how the adult HS is established, its embryonic development is described following the chronology of discoveries and controversies on the multiple and overlapping waves of hematopoietic cell generation. An effort to compile studies that aimed to quantify the HSC compartment during development was done to revisit the magnitude of expansion that putatively occurs in the FL. The FL development, composition and contribution to the embryonic HS were extensively addressed. Other hematopoietic niches were briefly revisited and efforts to localize HSCs *in situ* were identified and examined. When relevant, cited papers were extensively dissected and discussed. Unless explicitly specified, the referenced papers primarily center around the mouse model. The introduction ends with a brief description of the project outline, the initial aims and the experimental setup defined to address the underlying questions.

For a better follow-up and more detailed exploration of the experiments performed to dissect the FL hematopoietic microenvironment, the work enclosed in the publications [**3**] and [**5**] (see list below) was deconstructed and re-organized here in 3 sections of results (**Chapter II-IV**). **Chapter II** includes and integrates results from both publications, focusing on characterizing the FL non-hematopoietic compartment. **Chapter III** presents and describes step-by-step the image analysis pipeline adapted to FL sections [**5**].

As our attempts to develop a staining method specifically targeting HSCs did not yield successful results, we shifted our attention towards a simplified staining approach. This approach enabled the differentiation of two distinct progenitor populations, along with more mature hematopoietic cells. In **Chapter IV** we then applied the image analysis pipeline to characterize the distribution of these cell types during FL development and their relationship with the stromal[3] populations [**5**]. The efforts and difficulties faced to identify HSCs *in situ* are also discussed here.

**Epilog** is a general discussion of this thesis work, integrating all chapters, and pointing major conclusions, unresolved points, and future perspectives.

References from all sections are compiled at the end of the manuscript, followed by annexes. **Annex I** offers a concise overview of mouse development, as I deemed it necessary to have in mind some aspects related to mouse embryogenesis and anatomy to understand the emergence of the HS at different locations within the embryo. The remaining annexes comprise the publications in which I contributed during the course of this thesis, as detailed below.

### *LIST OF PUBLICATIONS*

*These authors contributed equally, #senior authorship, $corresponding authors

[**1**] Soares-da-Silva, F.*, **Peixoto, M.***, Cumano, A., Pinto-do-Ó, P. (2020) “Crosstalk between the hepatic and hematopoietic systems during embryonic development”. *Front. Cell Dev. Biol*. doi: 10.3389/fcell.2020.00612. (**Annex II**)

**This review focused on the interplay between the developing hepatic and hematopoietic tissues, detailing the ontogenic development of both systems, and discussing the role of the FL non-hematopoietic subsets and its molecular milieu in fetal hematopoiesis.**

[**2**] Elsaid, R.*; Soares-da-Silva, F.*; **Peixoto, M.**; Amiri, D.; Mackowski, N.; Pereira, P.; Bandeira, A.; Cumano, A. (2020) “Hematopoiesis: a layered organization across chordate species”. *Front. Cell Dev. Biol*. doi: 10.3389/fcell.2020.606642. (**Annex III**)

**This review revisited the hematopoietic/lymphoid development in key animal models, namely mouse, human, zebrafish, axolotl, *Xenopus*, and chicken, presenting evidence for an evolutionary conserved layered hematopoietic system spanning chordate species.**

[3] Throughout this manuscript, the terms "niche" and "stroma" will be recurrently employed. While these terms are often used interchangeably in the existing literature, in the context of this manuscript, I will designate "stroma/l" to encompass the non-hematopoietic compartment or any non-hematopoietic population of the respective organ, and "niche cells/niche” to refer to any cell with hematopoietic regulatory functions (e.g., cytokine secretion).

[**3**] **Peixoto, M.***; Soares-da-Silva, F.*; Schmutz, S.; Maïlhe, M.P.; Novault, S.; Cumano, A.; Aït-Mansour, C. (2021) "Identification of fetal liver stromal subsets in spectral cytometry using the parameter autofluorescence". *Cytometry: Part A*. doi: org/10.1002/cyto.a.24567. (**Annex IV**)

**Using the SONY ID7000 spectral analyzer we identified two distinct autofluorescence emission spectra within the FL non-hematopoietic compartment that were uniquely associated with specific cell types. This work reinforced the advantage of considering intrinsic autofluorescence properties of cells as additional parameters that herein allowed to refine the analysis of the FL stromal compartment and improve a sorting strategy by conventional cytometry.**

[**4**] Soares-da-Silva, F.*; Elsaid R.*, **Peixoto, M.***; Nogueira G.*, Bandeira A., Pereira P., Cumano A. (2021) "Assembling the layers of the hematopoietic system: a window of opportunity for thymopoiesis in the embryo". *Immunological Reviews.* doi: 10.1111/imr.13187. (**Annex V**)

**This review centered on the emergence of the HS during embryonic development in the mouse model, detailing the several independent waves of generation of hematopoietic cells, with an emphasis on lymphoid subsets and its impact on thymic development. Additionally, the establishment of the HSC compartment was revisited by compiling studies that aimed to quantify HSCs along development, and the dogma of HSC embryonic expansion re-analyzed and discussed.**

[**5**] **Peixoto, M.***; Soares-da-Silva, F.*; Bonnet, V.*; Ronteix, G.*; Faria, M.R.; Maïlhe, M.P.; Feng, X.; Pereira, J.P.; Azzoni, E.; Giorgi, A.; de Bruijn, M.; Baroud, C.[#]; Pinto-do-Ó, P.[#$]; Cumano, A.[#$] (2023) "Spatiotemporal dynamics of cytokines expression dictate fetal liver hematopoiesis". *BioRxiv.* doi: https://doi.org/10.1101/2023.08.24.554612 (*Manuscript under review*) (**Annex VI**)

**This work compiled an extensive characterization of the FL non-hematopoietic populations, achieved through a multi-faceted approach that involved imaging, flow cytometry and transcriptional signature profiling of the murine FL. A costume-designed image analysis pipeline, *Pyxidis*, was described and implemented for the analysis of a high-definition imaging dataset to quantify and characterize the distribution of hematopoietic and stromal cell types, with single-cell resolution.**

# CHAPTER I.

## INTRODUCTION

Part of the section “HSC expansion – a dogma revisited” was published as part of the following paper:

- Soares-da-Silva, F*; Elsaid R*, Peixoto, M*; Nogueira G*, Bandeira A, Pereira P, Cumano A., (2022) **“Assembling the layers of the hematopoietic system: a window of opportunity for thymopoiesis in the embryo”.** *Immunological Reviews. doi:* 10.1111/imr.13187. *These authors contributed equally (**Annex V**)

# THE HEMATOPOIETIC SYSTEM

***An integrative view on hematopoiesis – old and new approaches***

The organization of the hematopoietic system (HS) is classically viewed as a hierarchical tree, with hematopoietic stem cells (HSCs) sitting at the top and continuously generating all mature blood lineages – myeloid and lymphoid cells, erythrocytes, and megakaryocytes (Mks) – throughout life (**Figure 1**). In humans, hematopoietic cells comprise ~85% of the daily cell production, with an estimated turnover of $2.8x10^{11}$ hematopoietic cells per day (**Sender & Milo**, **2021**). Considering the proportions of the different mature hematopoietic compartments, all with different turnover rates, the flux into each compartment must be tightly regulated, specially at the apex of the tree, to ensure continuous and balanced blood production, according to the organism's needs.

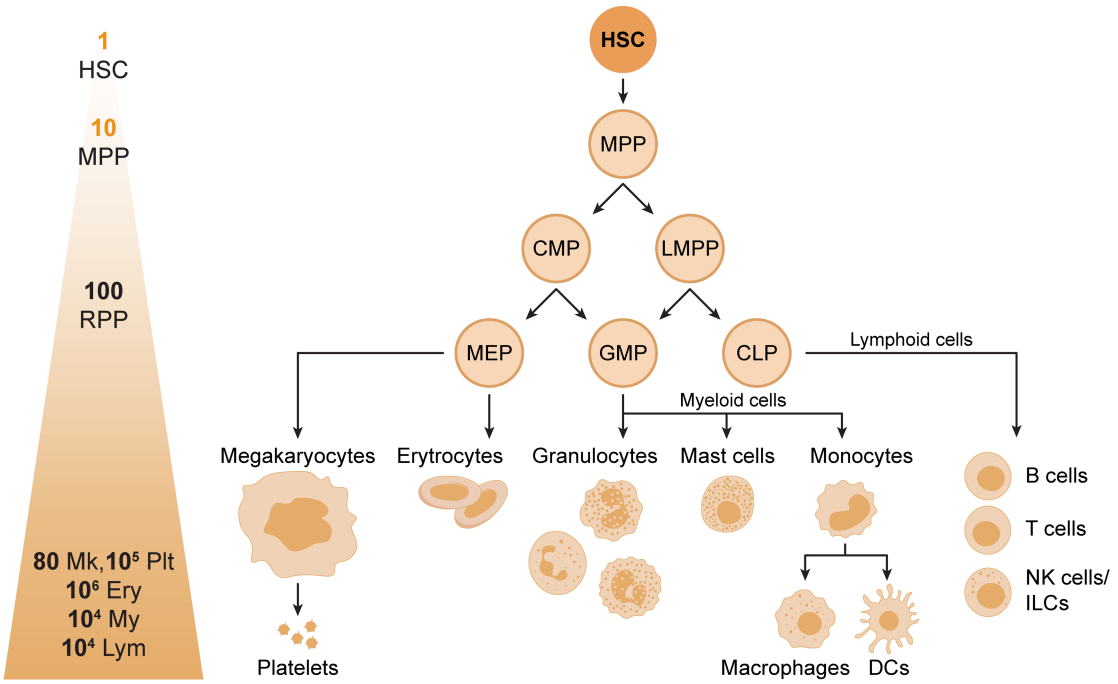


**Figure 1. The hematopoietic tree model.**
In a classical view of hematopoiesis, the HSC generates the mature blood lineages through a stepwise differentiation program of cells with increasingly limited lineage potential, from multi- to -bi, and ultimately unipotent progenitors. Cell numbers relative to 1 HSC were estimated based on (**Cosgrove et al.**, **2021**), considering main hematopoietic organs in 12-week-old, 22g female C57BL/6J mice.
CLP – common lymphoid progenitor; CMP – common myeloid progenitor; DCs – dendritic cells; Ery – erythrocytes; GMP – granulocyte-monocyte progenitor; ILCs – innate lymphoid cells; LMPP – lympho-myeloid progenitor; Lym – lymphoid cells; MEP – megakaryocyte/erythroid progenitor; Mk – megakaryocytes; MPP – multipotent progenitor cell; My – myeloid cells; NK – natural-killer cells; Plt – platelets; RPP – restricted potential progenitors (includes CMPs, CLPs, GMPs, MEPs and Mk progenitors).

HSCs were first identified in a series of seminal studies by Till and McCulloch in the '60s which were the foundation of the HSC concept: a cell with multilineage potential,

capable of continuously generating all blood cell types while maintaining its self-renewal ability. These studies showed that: 1. Transplanted bone marrow (BM) hematopoietic cells into sub-lethally irradiated mice had multilineage differentiation potential (generating granulocytes, macrophages, erythrocytes, and Mks) in spleen nodules, designated as colony-forming units-spleen (CFU-S) (**Becker et al.**, **1963**; **Till & McCulloch**, **1961**); 2. The number of transplanted cells correlated with the number of CFU-S (**Till & McCulloch**, **1961**); 3. Radiation-induced clonal markers allowed the tracing of transplanted cells, proving the clonality of each CFU-S (**Becker et al.**, **1963**) and its multipotent potential (**A. M. Wu et al.**, **1967**); 4. Cells isolated from CFU-S and re-injected could also form CFU-S, suggesting that some of the cells possess the capacity to self-renew (**Siminovitch et al.**, **1963**); 5. Common chromosomal abnormalities in lymphoid cells and cells from CFU-S were found, revealing that lymphoid cells can also be generated from CFU-S or that they share a common progenitor (**A. M. Wu et al.**, **1968**). BM transplantation into irradiated recipients and the CFU-S assay were then the first functional assays to evaluate stemness for the HS, pioneering the stem cell biology field. However, only the transplantation itself can fully ascertain a cell as a *bona fide* stem cell, as the long-term reconstitution (LTR) capacity can be demonstrated by assessing the reconstitution potential of the donor cells after a minimum of 16 weeks post-transplantation or after secondary transplantation (**Purton & Scadden**, **2007**). These and additional *in vitro* and *in vivo* functional assays to screen putative HSCs are detailed in (**Eaves**, **2015**; **Purton & Scadden**, **2007**; **Rodriguez y Baena et al.**, **2021**; **van Os et al.**, **2004**).

Advances in flow cytometry (FC) and monoclonal antibodies availability, started by Weissman's lab, opened doors to prospectively isolate and purify HSCs (**Spangrude et al.**, **1988**; **Weissman & Shizuru**, **2008**). Combining fluorescence-activated cell sorting (FACS) with *in vitro* clonal assays and *in vivo* reconstitution analysis, phenotypic characterization of cell surface markers for the HS was subsequently refined and compartmentalized, which ultimately led to the tree model (**Figure 1**). It is well established that HSCs lack lineage markers (that identify erythrocytes, granulocytes, macrophages, B and T cells), but express Sca-1 and c-Kit (KIT) (**Okada et al.**, **1992**). However, multipotent progenitors (MPPs) downstream of HSCs with different reconstitution capacities and tendencies to generate differentiated output (balanced or lineage-biased) are also included in the $Lin^{-}Sca\text{-}1^{+}KIT^{+}$ (LSK) compartment. Considering CD34 expression, HSCs were classified as long-term (LT, LSK $CD34^{-}$) or short-term (ST, LSK $CD34^{+}$), depending on the longevity of their reconstitution capacity (**Yang et al.**, **2005**). Currently, the most common strategy to isolate a population enriched in LT-HSCs is to select cells with an LSK $CD150^{+}$ $CD48^{-}$ phenotype. Approximately 1 out of 2 cells of this population was shown to successfully engraft and

reconstitute the HS in single-cell transplantation assays (at least up to 6 months) (**Kiel et al.**, **2005**), being the biggest enrichment reported so far.

The high complexity of the differentiation roadmap of HSCs makes the hematopoietic tree a paradigm still under construction. From its original version, in the early 2000s, the branching point between lymphoid and myeloid fates has been reformulated (**Adolfsson et al.**, **2005**), early Mk branching has been proposed (**Sanjuan-Pla et al.**, **2013**; **Yamamoto et al.**, **2013**), and the stem cell and downstream MPP compartments extensively sub-categorized (**Cabezas-Wallscheid et al.**, **2014**; **Dykstra et al.**, **2007**; **Pietras et al.**, **2015**). In consequence, different groups have been using different nomenclatures and gating strategies to isolate these cells (extensively reviewed by (**Cheng et al.**, **2020**; **Laurenti & Göttgens**, **2018**) and summarized in **Table 1**).

**Table 1. Molecular signatures enriched with hematopoietic stem and/or progenitor cells in the adult mice.**
CLP – common lymphoid progenitor; CMP – common myeloid progenitor; GMP – granulocyte/monocyte progenitor; Lin$^-$Sca-1$^+$KIT$^+$; LT – long-term; MPP – multipotent progenitor cell; MEP – megakaryocyte/erythroid progenitor; ST – short term.

| *POPULATION* | *LINEAGE POTENTIAL* | *PHENOTYPE* | *REFERENCE* |
|---|---|---|---|
| **HSC/LT-HSC** | All lineages | LSK CD135$^-$ CD34$^-$ CD150$^+$ CD48$^-$ (CD244$^-$ CD41$^-$) | (**Kiel et al.**, **2005**; **Yang et al.**, **2005**) |
| **MPP1/ST-HSC** | All lineages | LSK CD135$^-$ CD34$^+$ CD150$^-$ CD48$^-$ | (**Kiel et al.**, **2005**; **Yang et al.**, **2005**) |
| **MPP2** | All lineages, MEP-biased | LSK CD135$^-$ CD34$^+$ CD150$^+$ CD48$^+$ | (**Cabezas-Wallscheid et al.**, **2014**; **Pietras et al.**, **2015**) |
| **MPP3** | All lineages, Myeloid-biased | LSK CD135$^-$ CD34$^+$ CD150$^-$ CD48$^+$ | (**Cabezas-Wallscheid et al.**, **2014**; **Pietras et al.**, **2015**) |
| **MPP4/LMPP** | All lineages, Lymphoid-biased | LSK CD135$^+$ CD34$^+$ CD150$^-$ CD48$^+$ | (**Cabezas-Wallscheid et al.**, **2014**; **Pietras et al.**, **2015**) |
| **CLP** | Lymphoid | Lin$^-$ IL7rα$^+$ KIT$^{lo}$ Sca-1$^{lo}$ | (**Kondo et al.**, **1997**) |
| **CMP** | Myeloid | Lin$^-$ IL7rα$^-$ KIT$^+$ Sca-1$^-$ CD34$^+$ CD16/32$^-$ | (**Akashi et al.**, **2000**) |
| **GMP** | Granulocytes Monocytes | Lin$^-$ IL7rα$^-$ KIT$^+$ Sca-1$^-$ CD34$^+$ CD16/32$^+$ | (**Akashi et al.**, **2000**) |
| **MEP** | Megakaryocytes Erythrocytes | Lin$^-$ IL7rα$^-$ KIT$^+$ Sca-1$^-$ CD34$^-$ CD16/32$^-$ | (**Akashi et al.**, **2000**) |

It is worth noting that the HSC concept only has an "*ex vivo*" validity, as it requires a retrospective assessment of the two hallmarks of stemness – self-renewal and multipotency – upon isolation and transplantation into myeloablated recipients, which might not reflect the native fate of the cells *in vivo*. In recent years, different lineage-tracing mouse models, genetic barcoding technologies, and RNA sequencing have been increasingly

implemented to analyze the HS in unperturbed settings (reviewed in (**Pucella et al.**, **2020**; **Rodriguez-Fraticelli & Camargo**, **2021**)). These studies have shed light on the physiological hematopoietic flow throughout its hierarchical structure, questioning the validity of a discrete differentiation model in physiological conditions (**Pei et al.**, **2017**; **Rodriguez-Fraticelli et al.**, **2018**; **Sun et al.**, **2014**) **(Figure 2)**.

Camargo's lab used a doxycycline-induced Sleeping Beauty transposon tagging system to follow the output of hematopoietic progenitors in native conditions. They showed that over one year, only rare clones were found simultaneously in phenotypic HSCs and mature lineages, suggesting a minimal contribution of HSCs to blood production, which would instead be ensured by MPPs (**Sun et al.**, **2014**). They additionally found that the Mks arise largely independent from other lineages, and it is the predominant fate of HSCs *in situ* (**Rodriguez-Fraticelli et al.**, **2018**). Using two different approaches, *Tie2*-driven lineage tracing and *Polylox* barcoding, Rodewald's lab showed that adult hematopoiesis is also largely HSC-independent, while HSCs are actively contributing to the establishment of the immune and blood system in fetal and early postnatal life (**Busch et al.**, **2015**; **Pei et al.**, **2017**). In contrast to these works, Sawai et al. claimed a substantial HSC output in the adult by following the progeny of *Pdzk1ip1*-CreER (**Sawai et al.**, **2016**). However, the same fate mapping approach, combined with DNA barcoding revealed a low frequency of shared barcodes between HSCs and mature cells over a 6 month period (**Feng et al.**, **2022**). The disparities between the different studies are likely to arise from the inherent caveats of the respective methodologies employed (e.g., single-color fate mapping unspecific Cre drivers; leaky transposase expression after induction; low labeling efficiencies). A low influx from HSCs into downstream compartments is consistent with the prevailing notion that the adult stem cell compartment remains predominantly quiescent at steady state (**Cheshier et al.**, **1999**; **Pietras et al.**, **2011**). However, substantial evidence is still needed to disclose the extent of HSCs' contribution to active blood production.

Although downstream MPPs might have robust *in vivo* self-renewability, sustaining adult hematopoiesis (**Sun et al.**, **2014**), when transplanted, their repopulating ability is limited, and exhausted after a few weeks (**Harrison & Zhong**, **1992**). Therefore, they are not sufficient for LTR therapies. The mechanisms regulating the cell fate decision between self-renewal or differentiation are still largely unknown and their understanding is expected to open doors to the development of efficient HSC manipulation and expansion protocols *ex vivo*. To unravel the mysteries of HSC biology, it is fundamental to understand how the adult HS is established. As such, its cross-tissue embryonic development will be revisited next.

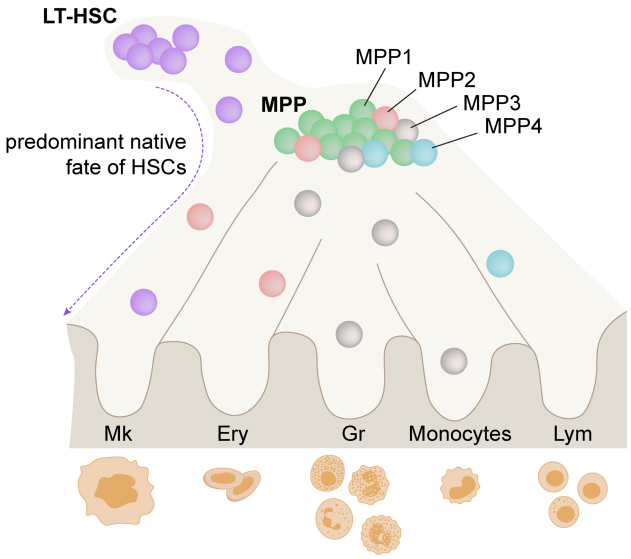


**Figure 2. Model of lineage fate landscape in physiological hematopoiesis.**
Recent studies indicate that LT-HSCs have low input in daily blood production and preferentially contribute to the Mk lineage. By contrast, the heterogenous pool of MPPs ensures the production of all mature lineages. Recent single-cell studies suggest that progenitors do not go through stable, discrete intermediate stages, but gradually acquire lineage-committed states in a continuous manner. Different MPP sorting gates enrich for different lineage-primed cell states, which results in differentiation bias.
Ery – erythrocytes; Gr – granulocytes; LT – long term; Lym – lymphoid cells; Mk – megakaryocytes; MPP – multipotent progenitor cell.

# ONTOGENY OF THE HEMATOPOIETIC SYSTEM

Although an HSC can generate a plethora of hematopoietic cell types, the first hematopoietic cells to appear during development are not HSCs, but rather committed erythroid progenitors, which originated extra-embryonically. These quickly differentiate to ensure rapid oxygenation of the developing embryo. It is only three days later that fated HSCs start to arise in large arterial vessels of the embryo. By this time, the embryo is already full of multiple hematopoietic lineages that can ensure the survival of the embryo until the end of gestation, even in the absence of HSCs (**Palis**, **2016**). This section focuses on the embryonic hematopoietic locations, the lineage potential of each hematopoietic wave ("layers"), and how they contribute to the adult HS.

## *The different starting points*[4]

### *Yolk Sac*

During embryonic development, the onset of hematopoiesis is marked by the emergence of clusters of primitive erythroid progenitor cells (EryPs) enveloped by endothelial precursors within structures known as blood islands, in the inner (mesodermal) layer of the proximal yolk sac (YS) (**Moore & Metcalf**, **1970**) (**Figure 3A**). Cells with primitive erythroid potential in clonal assays (EryP-CFCs, CFCs – colony forming cells) were detected as early as E7.0, peaked at E8.25 and were barely detectable by E9 (**Palis et al.**, **1999**). Two other lineages were recognized in blood islands by clonal assays, although to a much lesser extent: bipotent erythroid/Mk (**Tober et al.**, **2007**; **M. Xu et al.**, **2001**) and macrophage progenitors (**Palis et al.**, **1999**).

This first hematopoietic wave is commonly designated as primitive since it comprises a transient cohort of cells with distinct characteristics from their adult counterparts: 1. EryPs are larger, have increased capacity to transport oxygen, express both embryonic ($\beta$H1 and $\varepsilon\gamma$) and adult hemoglobin chains, mature semi-synchronously in circulation, and remain nucleated for several days (**Baron et al.**, **2012**); 2. Primitive Mks are smaller, can generate platelets faster in culture, and have lower ploidy class (**Tober et al.**, **2007**; **M. Xu et al.**, **2001**); 3. Primitive macrophages are recognized as large cells (larger than EryPs) with a macrophage morphology, lack detectable phagocytic activity and do not differentiate through a monocyte stage (**Takahashi et al.**, **1989**). The prime role of primitive hematopoiesis is to promptly fulfill the developing embryo's demands. EryPs are essential

[4] This section is solely focused on the hematopoietic emergence at different embryonic locations. For a deeper understanding of mouse development and the organization of each hematopoietic site, a concise overview is provided in **Annex I**.

for rapid oxygenation, macrophages facilitate early tissue remodeling and defense, and Mks contribute to maintaining vascular integrity.

Given that the first hematopoietic cells appear concomitantly with endothelial cells in the blood islands, and both are mesoderm-derived, a common origin for the two lineages would not be surprising and was first proposed nearly one century ago, introducing the term "hemangioblast" (**Murray & Wilson**, **1997**). However, clonal analysis of the blood islands failed to find a common progenitor (**Ueno & Weissman**, **2006**). This distinguishes the first hematopoietic wave from subsequent ones, which are now consensually accepted to arise from endothelial cells through an endothelial-to-hematopoietic (EHT) transition.

A second hematopoietic wave also arises in the YS, one day later (E8.25-E8.5), now generating less committed erythro-myeloid progenitors (EMPs) from the recently remodeled vascular plexus of the YS (larger and small vessels), with hemogenic endothelium (HE) potential (**Figure 3A, B**), in a time-window that lasts around 3 days (**Frame et al.**, **2016**; **Kasaai et al.**, **2017**; **McGrath et al.**, **2015**). EMPs can generate definitive erythroid progenitors (burst forming unit-erythroid – BFU-E and colony forming unit-erythroid – CFU-E colonies), bi-potent macrophage-granulocyte progenitors, mast cells and Mks (**Palis et al.**, **1999**, **2001**; **Perdiguero et al.**, **2015**). Even though it represents a transient population, the characteristics of the erythroid output led to the classification of these cells/wave as "definitive". Namely, the erythroid progenitors are smaller in size (comparable with adult ones), mature extravascularly in the FL, enucleate shortly after formation, and before re-entering circulation, and express adult-type globins exclusively ($\beta$1 and $\beta$2) (**Palis**, **2014**).

Both waves can generate macrophages and Mks in clonal assays. However, by the time the first Mks/macrophages are found in the blood islands, at E8.5 and E9.0, respectively (**Takahashi et al.**, **1989**; **M. Xu et al.**, **2001**), the second wave has already started, hindering a clear identification of its source.

With the onset of cardiac function as early as E8.25, the first EryPs enter the embryo proper (**McGrath et al.**, **2003**). EMPs expand considerably *in situ,* before being massively released into circulation (**Palis et al.**, **1999**, **2001**). Remarkably, YS-derived macrophages enter circulation and colonize all tissues from E8.5 to E12.5, contributing to a pool of tissue-resident macrophages that will acquire specific signatures and functions and can self-renew and persist throughout life (**Ajami et al.**, **2007**; **Jenkins et al.**, **2011**; **Merad et al.**, **2002**; **Perdiguero et al.**, **2015**; **Stremmel et al.**, **2018**).

At E12.5, EryPs start to enucleate and overall decline in the bloodstream. This coincides with the first appearance of enucleated definitive erythrocytes, which already represent more than half of all circulating cells by E13.5. By E16.5, circulating erythrocytes are virtually all enucleated, with a minor proportion of EryPs. EryPs continue to decrease to

residual levels, persisting for some days after birth (**Fraser et al.**, **2007**; **Kingsley et al.**, **2004**).

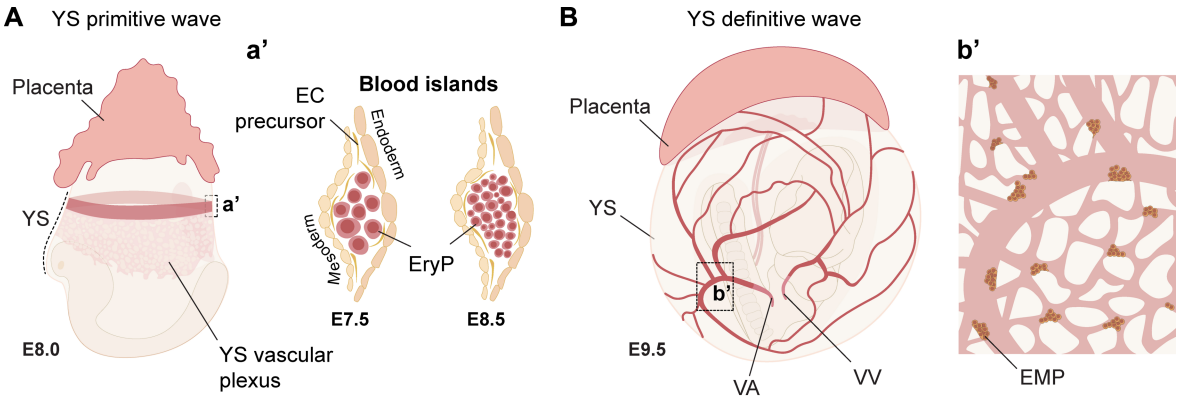


**Figure 3. YS hematopoietic waves: blood islands and hemogenic vascular plexus.**
(**A**) At E8.0, the YS is a simple bilayer of inner mesoderm and outer visceral endoderm above the embryo. Hematopoietic cells are first observed during development within blood islands (**a'**) – clusters mainly composed of EryPs, with sparse endothelial cells that form a complete band in the proximal YS. Concurrently, vasculogenesis starts to occur without visible hematopoiesis within the distal YS. Blood islands start to develop as early as E7.0 and become dispersed into circulation after E8.5. (**B**) At E9.5, the embryo is involved in the amniotic and YS membranes. Arterial specification has occurred, and YS circulation is connected to the embryo. Numerous clusters containing EMPs are emerging and expanding from arterial and venous HE of the YS. For simplification purposes, the remodeled vascular plexus of the YS is only shown in the zoom-in (**b'**) and cells in circulation are omitted.
EC – endothelial cell; EMPs – erythron-myeloid progenitors; EryPs – primitive erythroid progenitors; HE – hemogenic endothelium; VA - vitelline artery; VV – vitelline vein.

The YS was initially thought to be the source of HSCs, as CFU-S activity was first identified in the YS at E8 (**Moore & Metcalf**, **1970**). The first evidence for intra-embryonic (IE) generation of cells with lymphoid potential came from chick-quail and chick-chick chimeras (**Dieterlen-Lievre**, **1975**; **Lassila et al.**, **1978**). In these studies, the central area (that gives rise to the embryo proper, amnion and allantois) of a quail blastoderm was grafted in a chick area opaca (giving rise to the YS). The result was that only cells of quail origin (identifiable by the nuclear marker) were represented in the lymphoid organs of the chimeras, while the majority of erythrocytes in circulation were of chick origin. The YS was then considered to be an unlikely source of multipotent cells with lymphoid potential (**Dieterlen-Lievre**, **1975**). Experiments in mice then focused on evaluating if the embryo proper could also generate hematopoietic progenitors.

### *AGM*

Throughout the two decades at the turning of the century, there was a fervent effort to pinpoint the precise emergence site of HSCs. Because hematopoietic cells are formed at different locations, in overlapping time windows, and rapidly change location through

circulation, the task was a challenging pursuit. Cumulative evidence supported an IE origin of HSCs, from the aorta-gonads-mesonephros (AGM) region of the embryo: 1. The AGM contains significant numbers of CFU-S beginning at E9.5, in higher numbers than the YS (**A. L. Medvinsky et al.**, **1993**), and LTR-HSCs have only been found in the AGM at E10, slightly earlier than the YS and FL (**Müller et al.**, **1994**); 2. Before the establishment of circulation, the YS lacks lymphoid potential. However, the para-aortic splanchnopleure (P-Sp) that will originate the AGM can develop multilineage progenitors *in vitro* and *in vivo* when isolated as early as E7.5 (**Cumano et al.**, **1996**, **2001**); 3. Only the P-Sp/AGM can autonomously generate HSCs in *in vitro* culture systems (**Godin et al.**, **1999**; **A. Medvinsky & Dzierzak**, **1996**).

The first observation of hematopoietic clusters adhering to the endothelial layer of the aorta was made over a century ago in the avian model (**Jordan**, **1917**) and confirmed in multiple later studies, including in the mouse and human (**Garcia-Porrero et al.**, **1995**; **Jaffredo et al.**, **2000**; **Tavian et al.**, **1996**). However, robust direct visual evidence for hematopoietic generation from the aorta arose much later in zebrafish from three independent studies, revealing the EHT (**Bertrand et al.**, **2010**; **Kissa & Herbomel**, **2010**; **Lam et al.**, **2010**). These studies reported the budding of endothelial cells from the dorsal aorta (DA) floor into the sub-aortic space and subsequent migration toward the caudal vein (**Figure 4A**). In mice embryos, the emergence of intra-aortic hematopoietic clusters (IAHCs) from the endothelium could also be visualized using non-fixed E10 embryo slices (**Boisset et al.**, **2010**). Contrarily to the zebrafish, the nascent hematopoietic cells budded directly into aortic circulation (**Yokomizo et al.**, **2011**, **2012**) (**Figure 4B**). IAHCs were first detected in the DA at E9.5, peaked at E10.5 and decreased thereafter. Additionally, the umbilical (UA) and vitelline arteries (VA), that branch from the posterior DA, were also identified as potent sources of HSCs starting at E10.5 (**de Bruijn**, **2000**).

The EHT process varies among different animal models. IACHs in zebrafish, chicken and humans were only found on the ventral floor of the DA (**Bertrand et al.**, **2010**; **Ivanovs et al.**, **2017**; **Kissa & Herbomel**, **2010**; **Mascarenhas et al.**, **2009**; **Tavian et al.**, **1996**; **Yvernogeau & Robin**, **2017**). In contrast, in the mouse, IACHs were also found in the lateral and dorsal luminal surfaces of the DA. However, LTR activity was exclusively found in the explant cultures of the ventral domain, whereas CFC activity was observed in both (**Taoudi & Medvinsky**, **2007**). In the avian model, the DA was shown to have a dual origin – the floor from the splanchnic mesoderm and the roof from the somites (**Sato**, **2013**) (**Annex I**) – which might explain the ventral polarity of the this vessel regarding its HE potential.

Therefore, a third hematopoietic wave occurs at the major arteries of the mouse embryo, generating multipotent cells (**Godin et al.**, **1999**), some of which will acquire LTR

and contribute to the pool of adult HSCs. It is only in the FL, presumably due to a maturation requirement and upregulation of MHC class I molecules, that these cells transition into an adult HSC phenotype (LSK $CD150^{+}CD48^{-}$) and gain LTR activity in $Rag2^{-/-}$ or conventional mice (**Kieusseian et al.**, **2012**).

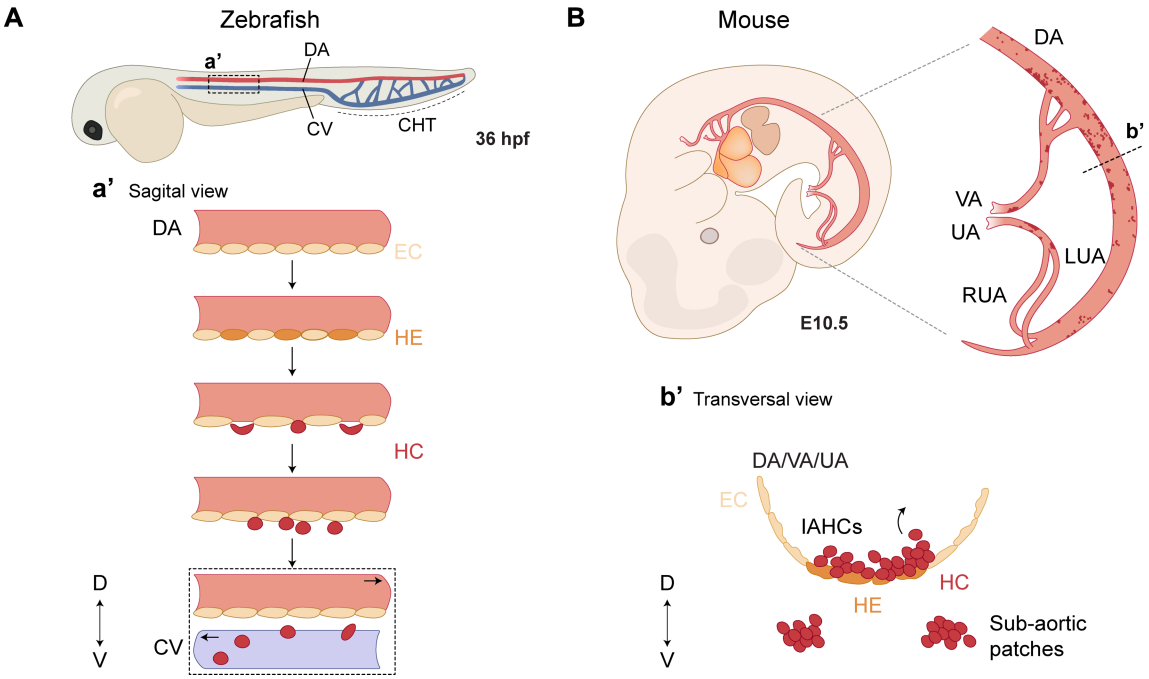


**Figure 4. Hematopoietic cell emergence at the major arteries in zebrafish and mouse.**
The first definitive multipotent blood cells arise from endothelial cells through an EHT. (**A**) In zebrafish, HE cells start to bud from the ventral wall of the DA into the sub-aortic space, joining the adjacent endothelial cells to close the gap. They acquire a round shape and hematopoietic markers (e.g., *cd41*) and migrate into the caudal vena, entering circulation. (**B**) In mice, endothelial cells also bud from the wall of the aorta (dorsal and ventral) and other major arterial vessels (VA and UA), and cluster adherently to the endothelium, before entering into circulation. Restricted to the ventral aspect of the aorta, sub-aortic patches of hematopoietic cells can be found from E10.5-E12.5.
CV – caudal vena; CHT – caudal hematopoietic tissue; D – dorsal; DA – dorsal aorta; EC – endothelial cell; IAHCs – intra-aortic hematopoietic clusters. HC – hematopoietic cell; HE – hemogenic endothelium; hpf – hours post fertilization; LUA – left UA; RUA – right UA; V – ventral; VA – vitelline artery; UA – umbilical artery.

Although adult HSCs produce all major blood cell types, some specific lymphoid lineages are only produced during embryonic development, namely dendritic epidermal T cells $V\gamma5^{+}$ (**Ikuta et al.**, **1990**), lymphoid tissue inducer (LTi) cells (**Eberl et al.**, **2004**), and a subset of IL-17-producing γδ T cells ($V\gamma6^{+}$) (**Haas et al.**, **2012**). Multipotent cells with a lymphoid bias can be hypothesized to also be generated within this wave, uncoupled from HSCs, and will be further discussed later on.

### *Placenta?*

Early multipotent clonogenic progenitors were found in the placenta at E10.5, one day earlier than in the FL (**Alvarez-Silva et al.**, **2003**). Two groups have further shown that

the placenta harbors a considerable pool of LTR hematopoietic progenitors ($KIT^{hi}$ $CD34^{+}$) during midgestation (**Gekas et al.**, **2005**; **Ottersbach & Dzierzak**, **2005**), with a sharp increase in the detected numbers between E11.5 and E12.5 (**Gekas et al.**, **2005**). *Sca1-GFP*$^{+}$ placental cells were found to contain all HSC activity and to cluster in placental vascular beds (**Ottersbach & Dzierzak**, **2005**). Rare multipotent cells were still found in the placenta of *Ncx1*$^{-/-}$ mouse embryos, with impaired heartbeat and consequently defects in blood circulation, suggesting *de novo* generation *in situ* (**Rhodes et al.**, **2008**). However, *Ncx1*$^{-/-}$ placenta explant cultures failed to autonomously generate HSCs (**Robin et al.**, **2006**). Whether the placenta is a reservoir of transient circulating HSCs or sustains *de novo* generation is yet to be clarified.

***Convergence point – the FL***

The outcomes of the multiple hematopoietic waves eventually migrate to the FL. In grafting experiments, the hepatic primordium, prior to the emergence of hematopoietic cells, proves insufficient to support hematopoietic development unless supplemented with exogenous hematopoietic cells (**Houssaint**, **1981**; **Johnson & Moore**, **1975**). This underscores its role as a recipient rather than an inducer of hematopoietic cells.

After E10.5, EMPs are reduced in circulation, as they ingress into the FL. By E11.5, myelopoiesis is already evident in the FL, with Mks and macrophages compromising the majority of non-erythroid hematopoietic cells. Macrophage progenitors expand considerably in the FL between E10.5 and E11.5 (**Palis et al.**, **1999**). However, it is not clear whether these cells result from the differentiation of EMPs or if they derive from the primitive wave. After E12.5 and at least until E16.5, EMPs produce monocytes in the FL and release them into circulation, which leads to the colonization of all tissues but the brain (**Hoeffel et al.**, **2012**, **2015**; **Perdiguero et al.**, **2015**). Interestingly, while EMPs exhibit broad granulocytic potential in clonal assays, only neutrophils are found in early stages, appearing by E11.5 in the FL and bloodstream, and rapidly expanding in both places (**McGrath et al.**, **2015**). Contrary to EryPs, EMP-derived erythrocyte progenitors do not mature in the bloodstream, and cells at the different stages of maturation are found in the FL, surrounding a central macrophage, in structures known as erythroblastic islands (**Palis et al.**, **1999**). Their maturation occurs through a similar process as their BM counterparts, culminating with the nuclei being expelled and engulfed by the macrophage (**Mohandas & Prenant**, **1978**). EryPs were initially thought to only mature in circulation without losing their nuclei. However, using a reporter mice model for embryonic globins (only expressed by EryPs), these cells were also found to mature in FL erythroblastic islands and to enucleate (**Isern et al.**, **2008**;

**Kingsley et al.**, **2004**). Nucleated EryPs accumulate in the FL until E14.5, but by E15.5 nearly all have undergone enucleation and reentered the circulation (**Isern et al.**, **2008**).

No CFU-S or LTR activity is detected in the FL until E11 (**Dzierzak et al.**, **1997**; **Müller et al.**, **1994**), increasing substantially thereafter (**H. Ema & Nakauchi**, **2000**). The FL is a place for maturation (**Kieusseian et al.**, **2012**) and eventual expansion of HSCs. The extent to which HSCs differentiate in the FL is still unclear and will be explored in more detail below.

***Settling down***

The BM is the ultimate destination of the HS journey in the embryo, being the production hub for blood cells throughout life. LSK cell homing and colonization of mouse BM was reported at E15.5–E16.5, coinciding with the fetal BM vascularization (**Cao et al.**, **2019**; **Coşkun et al.**, **2014**; **Gekas et al.**, **2005**; **Hall et al.**, **2022**). Yet, LT-HSC activity cannot be detected before E17.5 (**Christensen et al.**, **2004**). HSCs migrating out of the FL also seed the spleen, starting at E15.5. Although HSC activity remains detectable for a few weeks after birth (**Bertrand et al.**, **2006**; **Christensen et al.**, **2004**; **Wolber et al.**, **2002**), there is limited evidence of substantial expansion, and these cells primarily differentiate into the macrophage lineage (**Bertrand et al.**, **2006**).

***A layered organization***

As described, the formation of the HS unfolds through multiple steps, each generating a cohort of hematopoietic cells with distinct characteristics. A development based on layers of increasingly sophisticated cell populations that tailor themselves to the demands of advancing immune functions was first proposed by the Herzenbergs (**Herzenberg & Herzenberg**, **1989**). Remarkably, multiple fetal immune cells, including macrophages, mast cells, some $\gamma\delta$ T cells, B-1 B cells, and innate lymphoid cells, play not only a pivotal role in orchestrating the proper development of the organs they populate but also ensure life-long tissue homeostasis and immune protection. To this day, substantial evidence supports a layer organization, and this strategy appears to stand out as evolutionarily effective, being highly conserved across chordate species (extensively explored in (**Elsaid et al.**, **2020**)**, Annex III**). Tissue-resident macrophages, a diverse family of innate immune cells found in all organs and body cavities (e.g., liver Kupffer cells, brain microglia, splenic red pulp macrophages and epidermal Langerhans cells) are a remarkable example. The current paradigm states a sequential tissue colonization through three layers of macrophages: 1. YS-derived *Myb*-independent macrophages (**Hoeffel et al.**, **2015**; **Perdiguero et al.**, **2015**); 2. FL EMP-derived monocytes (**Hoeffel et al.**, **2012**, **2015**); 3.

HSC-derived monocytes that seed tissues postnatally and throughout life, in steady-state or after tissue inflammation (**Boyer et al.**, **2011**). However, it remains to be addressed whether the YS-derived macrophages are of primitive, EMP, or mixed origin, and at which point monocytes derived from HSC arise and colonize the tissues. Surprisingly, YS tissue-resident macrophages can self-renew locally throughout life (**Ajami et al.**, **2007**; **Jenkins et al.**, **2011**; **Merad et al.**, **2002**). YS-derived hematopoiesis has proven to also have a higher relevance than initially thought regarding other blood populations. Such is the case for mast cells, which are predominantly YS-derived in the embryo and at perinatal stages in most connective tissues (**Gentek et al.**, **2018**). Furthermore, recent evidence showed that, until birth, red blood cell production is maintained by YS EMPs with minimal contribution from HSCs (**Soares-da-Silva et al.**, **2021**).

So far, three waves of hematopoietic generation were described: YS primitive, YS-definitive, and IE-definitive. The first two possess erythroid and myeloid potential. The first emergence of cells with lymphoid potential is still under intense debate, as some studies suggest a late YS progenitor (EMP-independent) and others an early IE progenitor (HSC-independent) (reviewed in (**Soares-da-Silva et al.**, **2023**), **Annex V**). Genetic fate mapping has been the standard technique to track each wave. However, it is strongly limited by the waves' temporal/spatial overlap and lack of specificity and labeling efficiency of the Cre-driven targets, precluding robust conclusions.

While it is not possible to completely rule out a YS origin for a first wave of lymphoid progenitors, there is growing support for heterogeneity within the IE definitive wave, giving rise to additional developmentally restricted MPPs (drMPPs) independent of HSCs, with a bias toward lymphoid differentiation. Notably, Beaudin and colleagues used the FlkSwitch model and described a drMPP with higher lymphoid production (namely tissue-resident innate-like lymphocytes) and greater capacity to generate innate-like B and T cells in LTR assays, but that did not persist throughout life *in vivo* (**Beaudin et al.**, **2014**). Innate-lymphoid cells ($V\gamma5^+$ T cells and LTi) were labeled to the same extent as HSCs in the *Csf1r*$^{MERCreMER}$ mouse model, but not in the *Cdh5*$^{CreERT2}$ model, when induced at E10.5, suggesting that its specification from HE occurs before HSCs (**Elsaid et al.**, **2021**). More recently, Patel et al. combined cellular barcoding with a *Flk2*-Cre fate mapping model, and they also identified a drMPP population, specified within IAHCs, slightly earlier than HSCs. One year after transposon induction, drMPP clones showed a reduced myeloid output, but an extremely high contribution to the B cell compartment, revealing that they are contributing towards adult hematopoiesis for at least one year. Similar to barcoding studies in the adult, fetal HSCs had few common barcodes with mature lineages, suggesting that HSCs are not differentiating robustly within the FL (**Patel et al.**, **2022**). Yokomizo et al. showed that the hepatic leukemic factor (*Hlf)* is specifically expressed in $KIT^+$ cells within

IACHs in the DA, but not endothelial cells, nor EMPs. Using a *Hlf*$^{creERT2}$ mouse model induced at E9.0-E10.25, they also found a higher labeling frequency in the MPP compartments than in HSCs. They additionally showed that the input of HSCs into ST-HSCs is considerably low, suggesting a minimal contribution to the generation of downstream progenitors and a negligible role to fetal blood production (**Yokomizo et al.**, **2022**). HSC-independent progenitors and differentiation latency of HSCs have also been reported in the zebrafish (**Ulloa et al.**, **2021**).

These studies have challenged the dogma by which HSCs assume blood production from the moment they are generated and are the source of all hematopoietic lineages in the adult, thus providing evidence for the existence of a developmentally regulated "layered" HS (**Figure 5**). It is tempting to propose that the intricacy observed in the adult HS, characterized by significant heterogeneity within the progenitor compartment both in terms of phenotype and function (lineage-biases), may stem from distinct developmental origins, resulting also in a mosaic of layers at the progenitors' level.

Interestingly, Soares-da-Silva et al. showed that erythroid progenitors of YS origin (EMP-derived) require a 10-fold lower concentration of erythropoietin (EPO) compared to HSC-derived counterparts to efficiently support erythroid production (**Soares-da-Silva et al.**, **2021**). Progenitors that respond to lower concentrations of chemokines and cytokines, such as YS progenitors will have a selective advantage over HSC and their progeny (**Berthault et al.**, **2017**; **Soares-da-Silva et al.**, **2021**; **Wong et al.**, **2019**). One can speculate that, by taking over the production of mature cells throughout embryonic development, the YS-derived and other transient progenitors, are liberating the HSCs from fulfilling the needs of the embryo, allowing them to set up the stem cell pool.

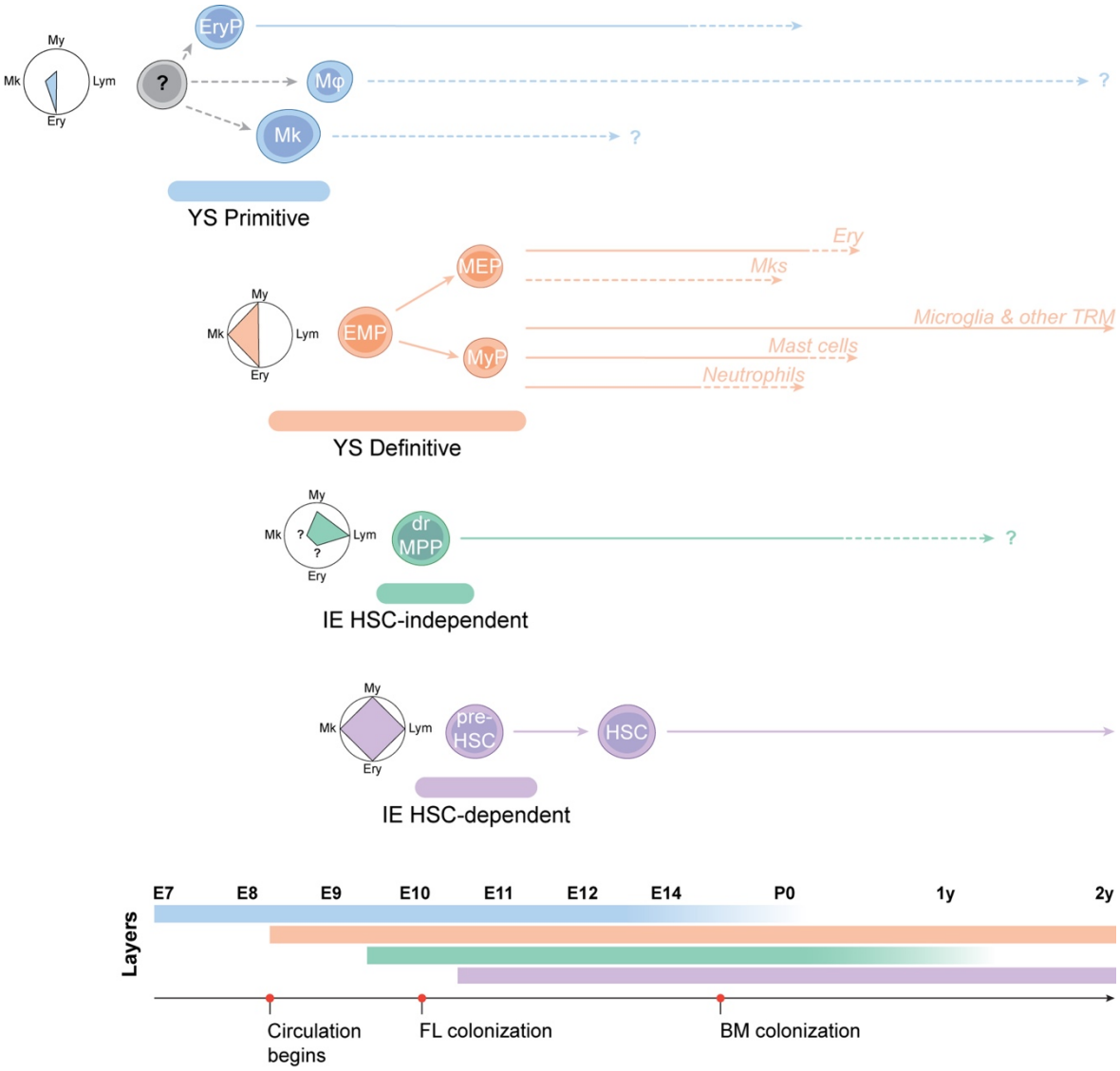


**Figure 5. Model of hematopoietic progenitor emergence in the embryo: sequential but overlapping waves.**

The first blood progenitors are found in the YS blood islands at E7.5 and generate mostly primitive erythrocytes and low numbers of Mks and macrophages. Whether these primitive cells arise from a common progenitor is currently unknown. Primitive erythrocytes can still be found at a low frequency around birth (blue). At E8.5, in the YS vascular plexus, EMPs emerge through EHT and generate erythrocytes, myeloid cells and Mks, but not lymphocytes. EMP-derived hematopoietic cells can persist until adulthood (microglia and other tissue-resident macrophages) or until perinatal stages (erythrocytes and mast cells) (orange). EMP-derived myelopoiesis seems to be restricted to neutrophils. Starting at E9.5, within the AGM, VA and UA of the embryo, a heterogeneous population of multipotent cells arises through EHT, some of them fated to become HSCs (pre-HSCs). drMPP (green) with a lymphoid bias can also be detected and seem to appear slightly earlier than pre-HSCs. Their contribution to hematopoiesis is not yet fully established. Pre-HSCs with multipotent potential but lacking LTR migrate to the FL where they mature into functional HSCs and contribute to the adult HSC pool (purple).

AGM – aorta-gonads-mesonephros; drMPPs – developmental restricted multipotent progenitors; EMPs – erythro-myeloid progenitors; EHT – endothelial-to-hematopoietic transition; Ery – erythroid; EryP – primitive erythroid progenitor; IE – intra-embryonic; LTR – long term reconstitution; Lym – lymphocytes; Mφ – primitive macrophages; MEP - megakaryocytic-erythroid progenitors; Mks – megakaryocytes; My – myeloid; MyP – myeloid progenitor; TRM – tissue-resident macrophages; UA – umbilical artery; VA – vitelline artery.

## HSC EXPANSION – A DOGMA REVISITED

In contrast to the adult system, it has been widely accepted that HSCs are highly proliferative during embryonic development, expanding massively in the FL (**H. Ema & Nakauchi**, **2000**), thus rendering this organ an ideal site to study the mechanisms driving HSC proliferation. However, this dogma was recently challenged (**Ganuza, Hall, et al.**, **2017**; **Ganuza et al.**, **2022**). To dissect how the adult HSC pool is established, from its generation at the AGM and major vessels region, until its settlement in the BM, reports that aimed to quantify HSCs throughout development are revisited here.

***The establishment of the HSC compartment***

Only 1-2 HSCs (cells with LTR potential) were detected in the AGM at E10.5-E11.5 (**A. Medvinsky & Dzierzak**, **1996**; **Müller et al.**, **1994**). Given the extremely low reconstitution activity of the emerging hematopoietic cells in this region, the term pre-HSC was introduced to identify immature precursors that acquired LTR potential after *ex vivo* cultures (**Rybtsov et al.**, **2016**). Using this system, Rybtsov and colleagues identified around 20 pre-HSCs in E10.5 AGM, peaking at E11.5 (40-60 cells). They further showed that the number of pre-HSCs in E11.5 AGM matched the number of mature HSCs in E12.5 FL (~60 cells), suggesting that maturation, rather than proliferation, takes place during the migration of cells from the AGM to the FL. This latter value compares well with the ~50 repopulating units (RU) described by Ema and Nakauchi in E12.5 FL (**H. Ema & Nakauchi**, **2000**).

The notion that the FL is a site of significant HSC expansion comes mainly from the work of Ema and Nakauchi who quantified LTR potential from FL cells at different developmental stages. They showed a 33-fold expansion from E12.5 (50 RUs) to E16.5 (1626 RUs), corresponding to about 5 rounds of symmetric division. Despite variable estimates in the number of RUs in E14 FL between different studies, ranging from 440 to 2000 (**Table 2**), most studies converge to the conclusion that the FL contributes to the generation of 1000-2000 HSCs. These numbers represent about 10% of the estimated number of HSCs in the adult (**Table 2**). Accordingly, 3 additional rounds of symmetric division should take place after HSCs leave the FL.

Recent reports not only questioned the concept that the FL is a privileged niche for active HSC expansion without differentiation but also concluded that the estimated cohort of HSCs generated in the AGM only doubles in size during fetal life. Using a multi-color ROSA26−*Confetti* reporter system and based on mouse-to-mouse variance (MtMV) in the composition of adult blood, Ganuza et al. traced back the hemopoietic hierarchical tree to

~ 600 E7-E10.5 AGM precursors, a number 10-fold higher than the above-cited number of pre-HSCs in E11.5 AGM. In *Conf-Ubiq*$^{ERT2\text{-}Cre}$ mice treated with tamoxifen at different stages, they further refined their estimations by showing that the HSC compartment in the BM of 6-month-old mice derived from about 850 E8-E10 endothelial progenitors and 1.700 E12–14 hematopoietic progenitors, with this number remaining constant up at least 9 days postnatally. Altogether, these results indicate that the size of the embryonic pool of HSCs is primarily determined by the very high number of pre-HSCs generated in the AGM, with no more than 1 round of division occurring at a later stage during embryonic development, eventually in the FL (**Ganuza et al.**, **2022**), not corroborating a FL massive HSC expansion.

Numerous studies showed that essentially all FL cells are in active division. Between E12.5 and E14.5, all Sca-1$^{+}$KIT$^{+}$ cells are in cycle, as demonstrated by BrdU uptake analysis (**Nygren et al.**, **2006**). Notably, Ganuza et al. also estimated 4 rounds of division of CD45$^{+}$KIT$^{+}$Lin$^{-}$ progenitors from E12.5 to E14.5 (**Ganuza et al.**, **2022**) in line with (**H. Ema & Nakauchi**, **2000**). Notwithstanding, an active cycling HSC population is not necessarily in contradiction with a low net expansion, as asymmetric division or differentiation might occur, preventing the duplicating of the stem cell pool at each division. Ganuza et al. suggest that FL HSCs are actively dividing but most daughter cells are biased for differentiation, implying that the FL is not a privileged niche for active HSC expansion without differentiation. Contradictingly to this, others suggest that similarly to the adult, embryonic HSCs are not actively contributing to blood production, while MPPs (originated from HSC-independent waves) undergo the task (**Freyer et al.**, **2020**; **Patel et al.**, **2022**; **Soares-da-Silva et al.**, **2021**).

Although HSCs migrate to the BM as early as E15.5, only minimal HSC activity can be detected during fetal stages (**Bowie et al.**, **2006**; **Hall et al.**, **2022**; **Qian, Georges-Labouesse, et al.**, **2007**). This might indicate that the migration from the FL to the BM occurs progressively, or massively only after birth, or that the establishment in the new niche might temporarily compromise their LTR potential. Although quantification of transplantable HSCs throughout the first days after birth has not been performed, the entire HSC population was reported to be in cycle during the first weeks after birth, switching to a quiescence state that is fully acquired by the end of the fourth week (**Bowie et al.**, **2006**). An increasing contribution of precursor cells to the adult BM pool could be estimated using the *Conf-Ubiq*$^{ERT2\text{-}Cre}$ model, from ~2.000 around birth to ~5.700 at 3 weeks (**Ganuza et al.**, **2022**). Overall, these results are also in line with the classical notion that, after birth, the HSC compartment must expand about 10-fold (~3 rounds of symmetric division) to reach the 10.000-20.000 HSCs in adult BM (**Table 2**).

| | AGM | | | | | FL | | | | | BM | | | | | |
|---|---|---|---|---|---|---|---|---|---|---|---|---|---|---|---|---|
| **Method** | **E8** | **E9** | **E10** | **E11** | **E12** | **E11** | **E12** | **E14** | **E16** | **E18** | **E18** | **2wk** | **3wk** | **4wk** | **Adult** | **Reference** |
| LTRA; LDA | - | - | - | - | - | - | - | - | - | - | - | - | - | - | 1 CRU/ 10.000 **(20.000) *** | (**Szilvassy et al., 1990**) |
| LTRA; LDA | - | - | - | - | - | - | - | - | - | - | - | - | - | - | 1 CRU/ 11.200 **(18.000) *** | (**Trevisan et al., 1996**) |
| LTRA | - | - | - | - | - | - | - | 1/15.700 **(1300) ** ** | - | - | - | - | - | - | - | (**Morrison et al., 1995**) |
| LTRA | - | - | - | - | - | - | - | 1/17.300 (1200) ** | - | - | - | - | - | - | - | (**Rebel et al., 1996**) |
| LTRA; LDA | - | - | - | - | - | - | - | 1.100 CRU | - | - | - | - | - | - | - | (**Miller et al., 1997**) |
| LTRA; LDA | - | - | - | - | - | n.d. | 1/39.840 (50) 40 CRU | 1/40.980 (488) | 1/36.900 (1.626) 1.538 CRU | 1/43.487 (1.035) | - | - | - | - | - | (**H. Ema & Nakauchi, 2000**) |
| LTRA | - | - | - | - | - | - | - | 1/23.000 **(900) ** ** | - | - | - | - | - | - | 1/20.000 **(10.000) *** *** | (**Szilvassy et al., 2003**) |
| LTRA | - | - | - | n.d. | < 5 | n.d. | 30 | ~500 | 1000 | - | < 10 | - | - | - | - | (**Gekas et al., 2005**) |
| LTRA; LDA | - | - | - | - | - | - | - | 2.000 CRU 1/35.000 ($Ter119^-$) | - | 1/73.000 | 1/95.000 or 1/6.600 | - | 1/6.500 ($Lin^-$) | 1/6.300 ($Lin^-$) | 1/5.500 ($Lin^-$) | (**Bowie et al., 2006**) |
| LTRA | - | - | - | - | - | - | - | 443 ESLAM *** | - | 1044 ESLAM | 7 ESLAM | - | 1016 ESLAM | 983 ESLAM | 1700 ESLAM | (**Benz et al., 2012**) |
| LTRA; LDA | - | - | - | - | - | <1 | 35 30 CRU | 600 SLAM*** | 600 (E15.5) | - | - | - | - | - | - | (**Zhao et al., 2015**) |
| LTRA (cultured explants) | - | - | - | 55 | 10 | n.d. | 60 | - | - | - | - | - | - | - | - | (**Rybtsov et al., 2016**) |
| *MtMV of Confetti-reporter labeling* | 600 Pre. (E7.5) | 850 Pre. | | - | - | - | 1700 Pre. | | - | - | - | 3.000 Pre. | 5.700 Pre. | - | 1/18.320 (11.000) * | (**Ganuza et al., 2017, 2022**) |

**Table 2. Reports quantifying HSCs at different developmental stages.**
Unless otherwise stated, cell numbers or frequencies are indicated as RUs relative to the respective organ's total cell number and some values were rounded for simplification. *Total cell number estimated considering $2\times10^8$ total BM cells; **Total cell number estimated using the total cell number per FL from (Ema & Nakauchi, 2000); ***ESLAM ($CD45^+EPCR^+CD48^-CD150^+$) or SLAM (LSK $CD48^-CD150^+$) cells with LTR potential.
CRU – competitive repopulating unit; LDA – limiting dilution assay; LTRA – long-term reconstitution assay (transplantation assays) – reconstitution potential was considered for at least 16 weeks after transplantation. n.d. - not detected. Pre. – precursors.

(Table previous page)

Discrepancies of estimated contributor cells to adult peripheral blood hematopoietic cells using the *Confetti*-reporter model when analyzed at 2 or 6 months (higher numbers at 2 months) suggest transient contributors in early adult life. Although we cannot disregard the fact that these values fall outside the window of precision (**Ganuza et al.**, **2022**), they might represent drMPPs that are active only for a few months after birth (**Patel et al.**, **2022**).

### *A dogma on the edge?*

Although there is some variability in the estimations of fetal HSCs numbers (**Table 2**), the most conflicting value that impacts the extent of embryonic HSC expansion is the starting number of AGM progenitors: ~60 immature HSC precursors (**Rybtsov et al.**, **2016**) vs. ~600 precursors fated to become HSCs (**Ganuza, Hall, et al.**, **2017**). **Table 3** enumerates the major limitations of the main methods used to quantitatively assess HSCs. Numbers based on transplantation systems are likely to be underestimations, as LTR ability might be acquired only a few days after emergence. Also, it should be noted that the work of Ema and Nakauchi is not informative as to whether the increase in RU they observed was due to expansion of HSCs or to maturation of multipotent cells into cells with LTR activity. While the strategy of Ganuza et al. is of considerable interest, it is also prone to overestimations. Newly generated progenitors are actively cycling, and the progeny of single cells can be marked more than once during the period of tamoxifen activity. Furthermore, their view does not easily accommodate increasing evidence suggesting that, similarly to adult HSCs, the bulk of embryonic HSCs are not actively contributing to blood production (**Patel et al.**, **2022**; **Soares-da-Silva**, **2020**; **Yokomizo et al.**, **2022**).

A precise quantification of the stem/progenitor cell compartments throughout ontogeny, contemplating the layered organization, is still missing. Figuring out the kinetics of the different waves and progenitors in the FL and fetal and neonatal BM will be fundamental to understanding the establishment of the adult HS and the impact of different niches in hematopoietic development.

**Table 3. A critical overview of the methodologies used to quantify HSC potential.**
EHT – endothelial-to-hematopoietic transition; LTR – long term reconstitution; LTRA – LTR assay (transplantation assays); MtMV – mouse-to-mouse variance.

| *METHODOLOGY* | *ADVANTAGES* | *DISADVANTAGES* |
|---|---|---|
| LTRA (freshly isolated cells) | Well-established<br>Simple and intuitive calculations<br>Only functional readout to prove stemness | Does not account for emerging HSC precursors that have not yet acquired LTR potential<br>Does not reflect the native cell fate<br>Overestimation when using neonatal recipients, suggesting a miscalculation of embryonic HSCs due to the complexity of the assay (cells must successfully engraft the adult marrow to be accounted for) |
| LTRA (cultured explants) | Allows quantification of immature HSC precursors before the FL stage | Might represent or account for *de novo* EHT and/or *ex vivo* expansion rather than maturation |
| MtMV of *Confetti*-reporter labeling | Reveals native development | Individual clones cannot be tracked<br>Accurate estimations limited to a range of 50-2500 cells<br>High intervals of confidence<br>Due to low labeling efficiency, cell number has to be extrapolated proportionally, increasing error propagation<br>Can lead to overestimation, if during the window where tamoxifen is still active, Confetti$^{-}$ cells divide and both daughter cells are labeled<br>Formulated in a system where cells are expected to divide at similar rates, which cannot be assumed for the *in vivo* system<br>Does not necessarily reflect the size of the compartment at the time point of labeling, but rather the size of the compartment that originated the analyzed output |

## FL – THE EMBRYONIC HEMATOPOIETIC HUB

The adult liver is a metabolic regulator organ, with major functions in blood detoxification, protein synthesis and immune responses (**Zorn**, **2008**). However, soon after the emergence of the liver primordium, the developing liver is hijacked by the HS to host the establishment and maturation of embryonic hematopoiesis, resulting from the convergence of cells from multiple origins. To understand how the FL microenvironment impacts hematopoietic development it is important to know the organ itself, its architecture and cellular composition, and the molecular milieu that might impact and regulate hematopoietic cell behavior (e.g., proliferation, fate choices, migration).

### *Liver development*

A primitive gut tube is formed soon after gastrulation from the endoderm germ layer and patterned into different regions: foregut, midgut, and hindgut (**Figure 6A**). The foregut, positioned in the anterior endoderm, generates the esophagus, trachea, thyroid, stomach, lungs, liver, biliary system, and pancreas. Gene expression patterns determine domains along the gut tube in which some specific organs will form (**Figure 6B**), several of them starting from an outgrowth of the endoderm epithelium into the surrounding mesenchyme, followed by extensive proliferation (**Zorn & Wells**, **2009**) (**Figure 6C**).

The liver development is initiated at around E8.5 with the specification of cells in the midline of the ventral foregut endoderm towards a hepatic fate by the expression of hematopoietically-expressed homeobox protein (*Hhex)* (**Bogue et al.**, **2000**) and prospero homeobox protein 1 (*Prox1*) (**Burke & Oliver**, **2002**), and the liver genes $\alpha$-fetoprotein (*Afp*), albumin (*Alb*) (**Gualdi et al.**, **1996**), and hepatic nuclear factor 4$\alpha$ (*Hnf4a*) (**Watt**, **2003**). By E9, these cells protrude from the foregut, forming a liver diverticulum – a single layer of cuboidal cells (**Figure 6D**) – that soon proliferates and switches into a pseudo-stratified epithelial morphology (**Bort et al.**, **2006**). Juxtaposed hepatic progenitor cells (hepatoblasts) downregulate E-Cadherin (E-Cadh), proliferate and delaminate into the surrounding mesenchyme, disrupting a basal lamina in between (enriched in laminin, collagen IV, and fibronectin), forming a growing liver bud (**Figure 6E**) (**Zorn**, **2008**).

The evagination of the foregut takes place towards the adjacent septum transversum mesenchyme (STM) and extends posteriorly to the cardiac mesoderm (**Figure 6Aa'**). Coordinated signaling from liver surroundings is critical for its development. Hepatic induction is dependent on fibroblast growth factor (FGF) signaling from the pre-cardiac mesoderm (**Jung et al.**, **1999**) while bone morphogenetic protein (BMP) signaling through the STM is required to induce endodermal hepatic specification and to exclude a pancreatic

fate (**Rossi et al.**, **2001**). Endothelial cells were found delimiting the STM, around the liver diverticulum, at E8.5 (**Figure 6D**), resembling a "loose necklace" of cells. In *Flk1*-null embryos (lacking endothelial cells), liver specification occurs, but subsequent organogenesis is impaired, with no liver bud formation (**Matsumoto et al.**, **2001**).

It has been hypothesized that during early hepatoblast proliferation and delamination from the foregut, STM's mesenchymal and endothelial cells become entrapped, integrating the liver bud, and contributing to the perivascular and vascular systems of the FL's parenchyma (**Enzan et al.**, **1997**; **Zorn**, **2008**). At E10.5, the margins of the liver are still poorly defined, but significant developments are observed in the liver rudiment, as large sinusoids filled with hematopoietic cells are already present (**Figure 6F**). Subsequently, within one day, a massive colonization of hematopoietic cells occurs, substantially increasing the liver's volume, the hepatic lobes become distinct, with deep fissures between them, and are demarcated by an epithelial layer (**Kaufmann & Bard**, **1999**; **Swartley et al.**, **2016**). The development throughout gestation of each liver's compartment is further explored below.

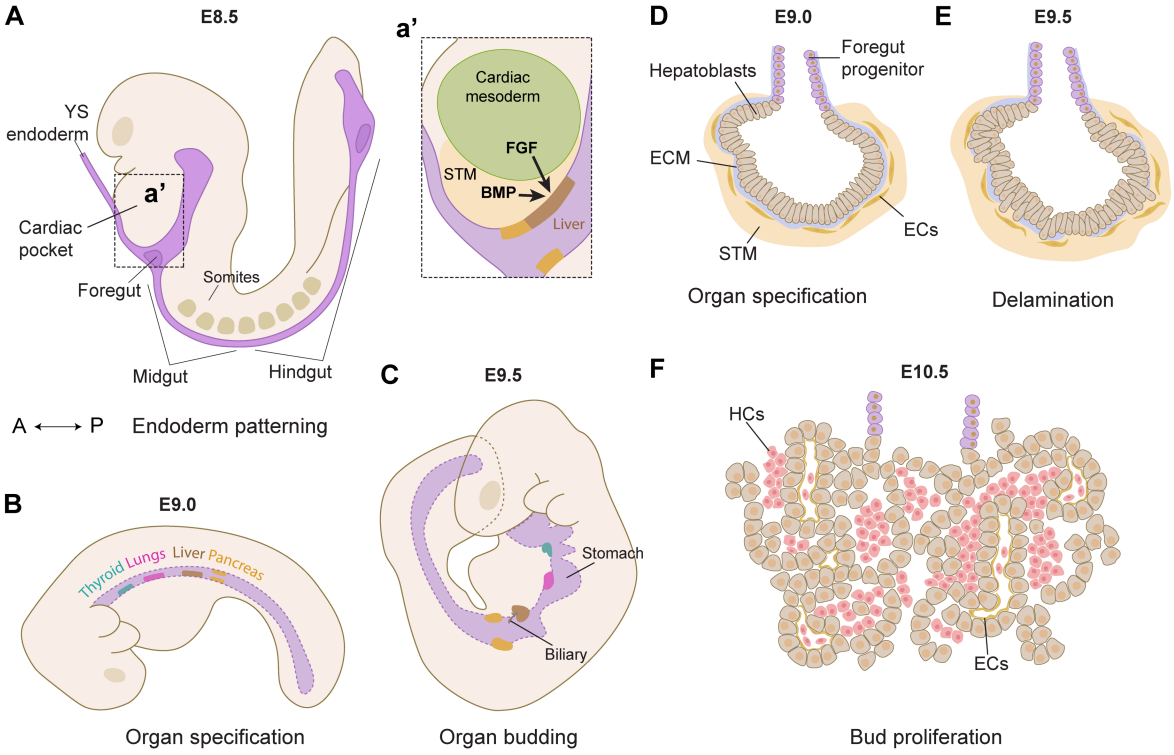


**Figure 6. Gut tube organogenesis and FL development.**
Schemes (**A**-**C**) represent mouse embryos at different stages with the endoderm tissue in purple, and schemes (**D**-**F**) show transverse sections of the gut tube at the level of the liver diverticulum at different stages in liver bud formation. Major events in liver development are: (**A**) Soon after gastrulation, the recently formed endoderm germ layer is patterned along the anterior-posterior (A-P) axis into foregut, midgut, and hindgut domains, and undergoes morphogenesis, forming foregut and hindgut pockets at its extremities. By E8.5, the hepatic fate is specified into a portion of the ventral foregut adjacent to the heart and STM, receiving instructive FGF and BMP signals (**a'**); (**B**) Along with the embryo turning, the endoderm undergoes ventral folding, being transformed into a gut

tube. The foregut is already patterned along its A-P axis into organ specific-territories; (**C**) As an internalized tube, outpocketings start to emerge from the gut tube, initiating tissue-specific organogenesis programs; (**D**) Shortly after hepatic specification (E8.5-E9.0), marked by the activation of liver-specific genes, the foregut epithelium thickens (as represented), and then transitions to a pseudostratified columnar epithelium – the liver diverticulum; (**E**) Between E9.0-E9.5 the basal lamina (rich in ECM protein, namely laminin) that surrounds the liver diverticulum from the adjacent mesenchyme breaks down and hepatoblasts delaminate, migrating into the STM, forming the liver bud; (**F**) As the liver bud outgrows into the STM, mesenchymal and endothelial cells are entrapped within the hepatic chords, and contribute to the formation of a vascular plexus, that is soon colonized by hematopoietic cells, that will integrate into the liver's parenchyma, and establish a fetal hematopoietic center until the end of gestation.
BMP – bone morphogenetic protein; ECs – endothelial cells; ECM – extracellular matrix; FGF – fibroblast growth factor; HCs – hematopoietic cells; STM – septum transversum mesenchyme.

### *FL composition*

#### *Hepatic cells*[5]

The liver parenchyma consists of two primary epithelial cell types: 1. Hepatocytes, the main functional units of the liver, represent around 70% of the adult organ. These are big polygonal cells that secrete serum albumin, bile, and blood clotting factors.; 2. Cholangiocytes are specialized epithelial cells that line bile ducts, regulating bile composition and transport. These originated from a common bi-potent progenitor, the endoderm-derived hepatoblasts, as discussed above (**Zorn**, **2008**).

Bipotent hepatoblasts express AFP and markers of hepatocytes (ALB, HNF4$\alpha$, keratin 18 (CK18)), and cholangiocytes (CK19). Delta-like non-canonical Notch ligand 1 (DLK1) was abundantly expressed in the E10.5 liver bud, and until E16.5, but downregulated thereafter. DLK1$^+$ sorted cells expressed *Alb* and *Ck19* and could differentiate into hepatocytes and cholangiocytes in culture (**Tanimizu et al.**, **2003**). DLK1 has then been frequently used to identify and isolate hepatoblasts during liver development. E-Cadh (**Nitou et al.**, **2002**) and Liv2 (**Prior et al.**, **2019**; **Watanabe et al.**, **2002**) were found to specifically label hepatoblasts and epithelial cell adhesion molecule (EpCAM) expression was reported in early hepatoblasts and differentiated cholangiocytes (**Tanaka et al.**, **2009**). Combining lineage tracing, organoid cultures and single-cell RNA-sequencing (scRNA-seq) analysis, Prior et al. revealed an heterogeneous population of hepatoblasts and identified Lgr5$^+$ hepatoblasts at the apex of the hepatoblasts hierarchy (**Prior et al.**, **2019**).

During development, hepatoblasts that receive instructive signals from the portal mesenchyme differentiate into cholangiocytes, following a well-orchestrated bile duct morphogenesis, while the majority of parenchymal hepatoblasts differentiate into hepatocytes, the default pathway (**Figure 7**) (**Yang et al.**, **2017**). Cholangiocyte

[5] While any cell within the liver cell might be considered hepatic, here we restrict the term hepatic cells for hepatoblasts and their progeny.

specification occurs as early as E11.5 and is completed by E14.5 (**Yang et al.**, **2017**). The formation of a ductal plate, a monolayer of cholangiocyte precursors CK19$^{high}$, around portal veins is the first sign of bile duct development (**Figure 7A**). At around E16.5, the ductal plate duplicates (**Figure 7B**), and luminal pockets start to arise in between the two layers (**Figure 7C**). Some of these mature into functional cholangiocytes forming bile ducts, while the remaining ductal plate regresses (**Figure 7D**). Hepatoblasts away from the portal vessels mature into hepatocytes and downregulate CK19. Although hepatoblast differentiation has been reported to start at E13.5 (**Su et al.**, **2017**; **Yang et al.**, **2017**), it is not before late gestation that the FL starts to resemble its adult counterpart, with hepatocyte chords juxtaposed in the parenchyma, and evident tubular structures around portal veins. Bile duct development occurs first near the liver's hilum and progresses towards the periphery of the lobes (**Yang et al.**, **2017**), with a continuous luminal network of intrahepatic bile ducts being established only 1 week after birth (**Ober & Lemaigre**, **2018**; **Tanimizu et al.**, **2016**). Three-dimensional reconstructions of serial cross-sections/whole-mount immunostained FL and carbon ink injection have been used to disclose the morphogenesis of intrahepatic bile ducts (**Takashima et al.**, **2015**; **Tanimizu et al.**, **2016**; **Vestentoft et al.**, **2011**).

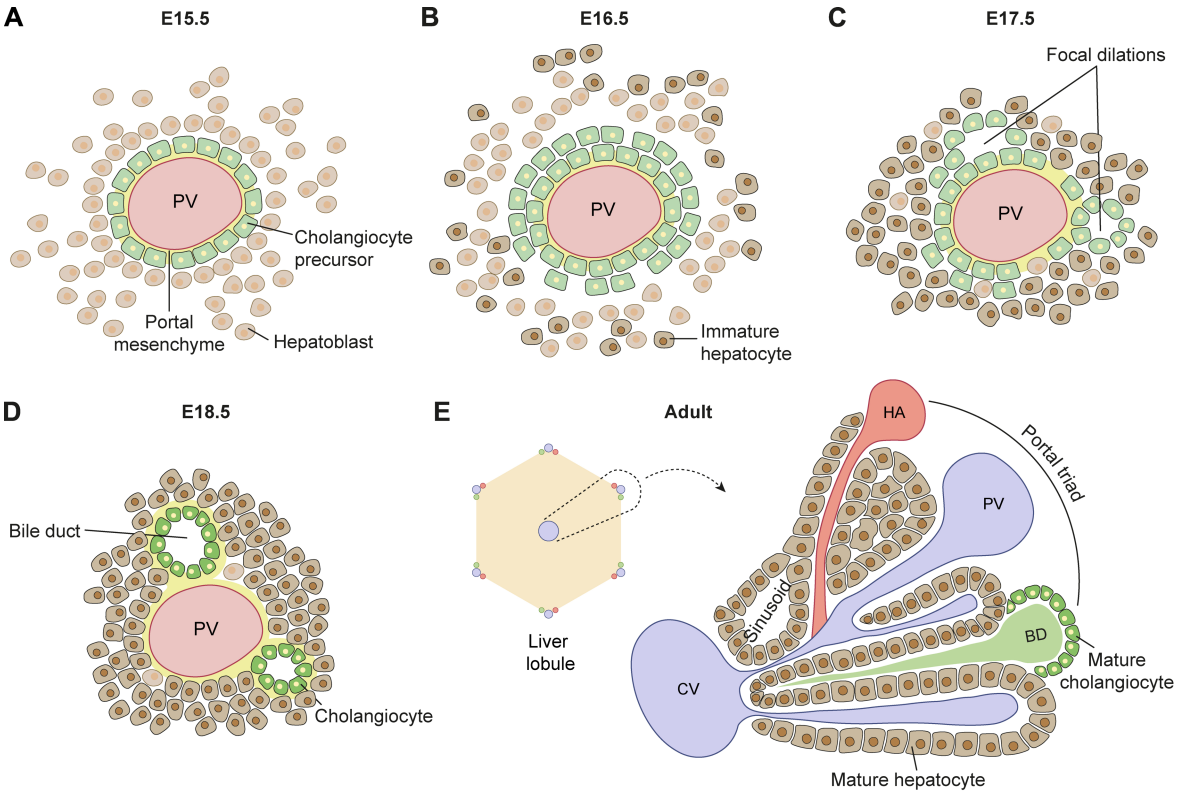


**Figure 7. Hepatocytes and cholangiocytes lineage segregation.**
(**A**) Hepatoblast-to-cholangiocyte specification occurs around the portal vessels by the acquisition of a cuboidal shape, forming a monolayered ductal plate. (**B**) At around E16.5, the ductal plate becomes bilayered. (**C**) Luminal dilations arise between the bilayered ductal plates. (**D**) Luminal dilations evolve into bile duct structures in late gestation, that become surrounded by the portal mesenchyme,

while the remaining bilayer cells regress. Hepatocytes in the parenchyma differentiate into hepatocytes. (**E**) Liber lobule architecture. A lobule has an hexagonal structure, with portal triads at the vertices, comprising a hepatic artery, a portal vein and a bile duct and a central vein in the center, around which plates of hepatocytes, lined by sinusoids, converge.
BD – bile duct; CV – central vein; HA – hepatic artery; PV – portal vein.

### *Endothelial cells*

The adult liver has two afferent vascular systems, the portal veins, and hepatic arteries and one efferent system, the central veins. The portal vein drains nutrient-rich blood from various abdominal organs while the hepatic artery delivers oxygenated blood from the heart. The central veins then carry the deoxygenated blood and waste products directly into the inferior vena cava, back to the heart. However, this vascular structure is only established after birth with the ligation of the umbilical inlet. During embryonic development, the vitelline veins (VVs) drain the YS at early stages of gestation, and the developing gut at later stages. The umbilical veins (UVs) return oxygenated blood from the placenta, and the posterior cardinal veins drain the lower limbs and the body wall below the heart.

At the onset of liver formation, left and right vitelline plexus develop in the STM and connect to the VVs (**Figure 8A**). When the hepatoblasts invade the STM, the vitelline venous plexus is disrupted and becomes intermingled with the liver bud. VVs continue to branch within the liver bud, forming venous channels, clearly evident at E10, that will mature into hepatic sinusoids (**Swartley et al.**, **2016**) (**Figure 8B**). *In vitro* cultures of FL cells depleted of hepatoblasts had impaired endothelial growth and capillary formation, suggesting a role of hepatoblasts in the stimulation of sinusoid morphogenesis (**Takabe et al.**, **2012**). Liver sinusoidal endothelial cells (LSECs) start to express stabilin 2 (STAB-2) and lymphatic vessel endothelial hyaluronic receptor 1 (LYVE-1) – hyaluronan receptors – at E9.5 and E10.5, respectively, and continue to express them thereafter. CD31/PECAM1 and FLK1 (also known as VEGFR2/KDR) expression is strong in early stages of development but is downregulated with time (**Y. Sugiyama et al.**, **2010**; **Takabe et al.**, **2012**).

Between E11.5 and E12.5, the *ductus venosus* (DV) is formed from the left UV, serving as an intrahepatic shunt to drain blood from the left UV directly to the caudal vena cava, and subsequently to the heart, bypassing the liver (**Swartley et al.**, **2016**) (**Figure 8C, D**). After E14.5, the major vessels continue to grow in size, adapting by elongation and increasing in diameter, but their fundamental structure and arrangement are already established and remain largely unchanged until the end of gestation. After birth, the umbilical vessels are closed, shutting down the flow to the DV, which soon constricts into fibrous cords – the *ligamentum teres hepatis* and the *ligamentum venosum* (**Kaufmann & Bard**, **1999**).

During embryonic liver development, portal vessels express the arterial markers Ephrin-B2 and Neuropilin-1, but not the venular marker EphB4. This expression profile is inverted at the end of gestation, with the transition into a venular phenotype (**Khan et al.**, **2016**; **Wang et al.**, **1998**). Both portal and hepatic (central) veins strongly express CD31, but only weakly FLK1 (**Y. Sugiyama et al.**, **2010**; **Takabe et al.**, **2012**). Although liver endothelial cells are heterogeneous, and different markers can be used for their identification, they are more easily identified by their spatial location and perivascular constituents, as discussed below.

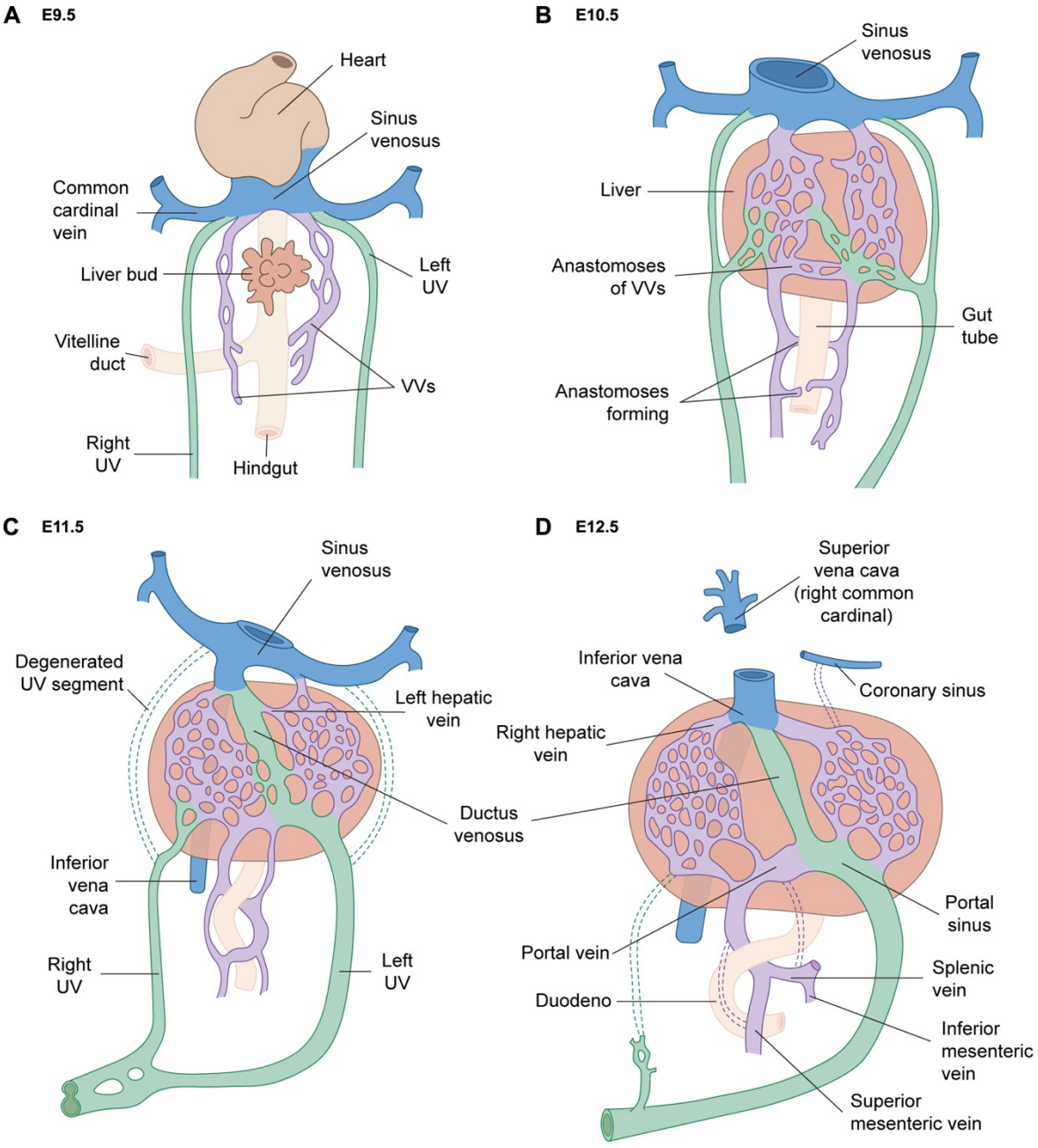


**Figure 8. Early developmental stages of FL venous drainage.**
(**A**) By E9.5, the embryonic heart receives a continuous influx of blood through the convergence of three symmetrical pairs of veins into the sinus venosus: the VVs, which drain the YS and gut (semi-

oxygenated blood); the UVs, which drain the placenta (oxygenated blood); and the cardinal veins, which drain the upper and lower body parts (venous blood). As the liver bud grows, the VVs ramify within the STM, forming a venous plexus that later intermingles with the growing hepatic cords. (**B**) The vitelline venous plexus continues to branch within the liver parenchyma, giving rise to primitive liver sinusoids – large venous channels, blood-filled, capillary-like vessels throughout the liver. Meanwhile, the two UVs give rise to both intra- and extra-hepatic branches. (**C**) Due to a marked increase in placental circulation, the intra-hepatic left UV starts to form a large diameter channel, the DV, bypassing the sinusoidal network of the liver, and delivering oxygenated blood from the placenta directly into the right atrium. The proximal portions of both UVs regress. (**D**) Caudal to the liver, the VV anastomotic network around the duodenum fuses to form a single trunk – the portal vein. The right VV ultimately originates the superior mesenteric vein, which drains the primitive intestinal loop, the left to right vitelline anastomoses originate the splenic vein and the inferior mesenteric vein, while the left VV regresses. The remainder of the right UV (hepatic branch) also disappears, leaving the UV as the sole conduit responsible for delivering reoxygenated blood to the embryo. At this stage, a large intrahepatic structure, the portal sinus, transports blood from the left UV to the DV (now a narrow, branchless, tubular structure, that ascends cranially toward the caudal vena cava) and into the sinusoids through the portal system. Cranial to the liver, the left VV regresses with the left sinus horn, and the right VV enlarges and becomes the hepatic portion of the inferior vena cava.
DV – *ductus venosus*; STM – septum transversum mesenchyme; UVs – umbilical veins; VVs – vitelline veins.

The morphology and topology of all functional important veins at midgestation in 3D reconstructions can be visualized in (**Geyer et al.**, **2022**; **Hikspoors et al.**, **2017**). Of note, the lymphatic vessels and hepatic artery only start to form after birth, in the vicinity of the portal veins (**Swartley et al.**, **2016**).

### *Mesothelial cells*

Mesothelial cells (MCs) form a single epithelial layer around the liver lobes – the mesothelium – a serous membrane, easily recognized in microscopy by its squamous morphology. While acting as a barrier surface, with lubricating properties, some studies suggest a major role in liver development and injury (**Lua & Asahina**, **2016**).

During development, the STM forms from the aggregation of mesenchymal tissue (originated from the splanchnic mesoderm) (see **Annex I**) that develops within the caudal part of the ventral mesentery of the foregut at around E8.5 (**Figure 6a'**) (**Kaufmann & Bard**, **1999**). This mesenchyme is soon invaded by the liver bud and umbilical and vitelline venous systems, contributing to the vascular and perivascular network of the FL (**Kaufmann & Bard**, **1999**). The STM expresses forkhead box F1 (FOXF1), GATA4, LIM homeobox protein 2 (LHX2), heart and neural crest derivatives expressed transcript 1 (HAND1), H2.0-like homeobox (HLX), mab-21-like 2 (MAB21L2), T-box transcription factor 18 (TBX18), zinc finger protein multitype 2 (ZFPM2/FOG2), activated leukocyte cell adhesion molecule (ALCAM/CD166), and Wilms' tumor gene 1 (WT1) (**Lua & Asahina**, **2016**). Some of these markers are also found in MCs and/or fibroblasts. Cell tracing of MesP1-Cre identified early mesodermal cells as the source of STM cells, which in turn contribute to the liver's MCs and fibroblasts. This finding was also corroborated using *Wt1*-Cre$^{ERT2}$ and STM-specific *Gata4*-

Cre mice models (**Asahina et al.**, **2011**; **Delgado et al.**, **2014**; **Rojas et al.**, **2005**). The STM also contributes towards heart development and diaphragm formation (**Kaufmann & Bard**, **1999**).

As the liver bud invades the STM, the surrounding mesenchyme becomes thinner. A flat layer of MCs is only evident on the liver surface by E11.5. MCs express Mesothelin (MSLN), CD200, Vimentin (VIM), ALCAM, and Podocalyxin-like protein 1 (PCLP1/PODXL), glycoprotein M6A (GPM6A) and Podoplanin (Gp38/PDPN) in both embryonic and adult stages (**Asahina et al.**, **2009**, **2011**) (**Table 4**). PCLP1 was shown to be highly expressed on the liver's surface at embryonic stages, but downregulated with time, while MSLN is upregulated (**Onitsuka et al.**, **2010**). A basal lamina (enriched in type IV collagen) lays adjacent to the mesothelium, separating it from underlying cells with a mesenchymal phenotype, called sub-mesothelial cells (sub-MCs) or capsular fibroblasts. Sub-MCs also express ALCAM and WT1, but have a typical mesenchymal transcriptional profile, expressing platelet-derived growth factor receptor α (PDGFRα), Desmin, LHX2, and also nerve growth factor receptor (NGFR/p75NTR) (**Asahina**, **2012**). This suggests that this population represents an intermediate cell type between MCs and hepatic fibroblasts. This hypothesis is reinforced by lineage tracing studies, showing that $WT1^+$ MCs/sub-MCs or $MSLN^+$ MCs migrate inward from the liver surface and give rise to mesenchymal cell types through an epithelial-to-mesenchymal transition (EMT) (**Asahina et al.**, **2011**; **Rinkevich et al.**, **2012**).

Different mouse models of depletion of MC-target genes, namely *Wt1*, *Gata4*, and *Hlx,* present impaired hematopoiesis and liver growth, revealing a major role of this peripheral membrane in the organ's development (**Delgado et al.**, **2014**; **Hentsch et al.**, **1996**; **Ijpenberg et al.**, **2007**; **Onitsuka et al.**, **2010**). MCs secrete hepatic growth factors, such as pleiotrophin (PTN), hepatic growth factor (HGF), epidermal growth factor (EGF) and Midkine (MDK). These factors are downregulated with time but can be activated after injury, suggesting their role in liver organogenesis and regeneration by stimulating hepatoblasts proliferation (**Inagaki et al.**, **2015**; **Onitsuka et al.**, **2010**).

MCs/sub-MCs are also documented to be a life-long source of mesenchymal cells in other organs, namely the heart, lungs, and gut (**Cano et al.**, **2013**; **Dixit et al.**, **2013**; **Que et al.**, **2008**; **Rinkevich et al.**, **2012**; **Wilm et al.**, **2005**), particularly active during organogenesis and injury.

### *Mesenchymal cells*

Four types of liver mesenchymal cells, here referred to as fibroblasts, can be considered regarding their location: portal fibroblasts (PFs, around portal veins), fibroblasts surrounding the central veins (second-layer cells, SLCs), capsular fibroblasts (sub-MCs),

and perisinusoidal fibroblasts, commonly known as hepatic stellate cells (SCs). Although some studies suggest different contributions to liver fibrosis (**Bhunchet & Wake**, **1992**), little is known about the functional differences between these cell types, and if they have specific signatures.

SCs, the most abundant and well-studied, were first observed by Kupffer in the 19$^{th}$ century, using a coloration method for vitamin A-containing droplets. The same cells were later identified using multiple coloration methods, resulting in different nomenclatures: hepatic pericytes, Ito cells or fat-storing cells, interstitial cells, lipocytes, and perisinusoidal cells (**Friedman**, **2008**; **Wake**, **1971**). In the adult liver, these cells are located in the space of Disse, between the basolateral surface of hepatocytes and the anti-luminal side of LSECs, constituting the major mesenchymal compartment of the liver. When quiescent, they act as a reservoir for vitamin A, stored in cytoplasmic lipid droplets. When activated (e.g., during liver injury or infection) they transition into a myofibroblast-like phenotype, proliferative and contractible, with up-regulation of alpha-smooth muscle actin ($\alpha$SMA). These cells become major regulators of liver fibrosis, by producing excessive amounts of extracellular matrix (ECM) proteins, namely collagen, leading to the formation of fibrotic scar tissue (**Friedman**, **2008**).

Different markers have been described for hepatic fibroblasts, namely Desmin, Fosf1, LHX2, and HLX (further detailed in **Table 4**). Notably, the markers listed should not be interpreted as specific, as most studies were focusing on a specific population. Because SCs also express Nestin, glial fibrillary acidic protein (GFAP), p75NTR, markers typically associated with neural cells, a possibility was raised that SCs could have a neural crest origin. However, a *Wnt1-Cre* lineage tracing model did not provide evidence for that hypothesis (**Cassiman et al.**, **2006**). As mentioned before, the origin of SCs and other mesenchymal cell types can be traced back to MCs originating from the STM (**Asahina et al.**, **2011**; **Rinkevich et al.**, **2012**).

Lua and colleagues compared the contribution of SCs, PFs, and MCs to myofibroblasts by inducing liver fibrosis in *Col1a1*$^{GFP}$ mice, showing that PFs partly participate in biliary fibrosis, but SCs are the dominant source of myofibroblasts in the liver (**Lua et al.**, **2016**).

During development, and similarly to MCs, SCs also support the proliferation of hepatoblasts by secretion of growth factors, such as HGF (**Maher**, **1993**), PTN (**Asahina et al.**, **2002**), Wnt family member 9a (Wnt9a) (**Matsumoto et al.**, **2008**), EGF and FGF10 (**Berg et al.**, **2007**).

**Table 4. Molecular signatures of mesothelial and major mesenchymal cells in the mouse FL.**
When the study only reports the transcript, the marker is written in *italics*.
MCs – mesothelial cells, SCs – stellate cells, PFs – portal fibroblasts; Pop. - population.

| *POP.* | *STAGE* | *ISOLATION* | *Also expressed (Gene,* PROTEIN*):* | *REFERENCE* |
|---|---|---|---|---|
| *MCs* | Fetal | - | GATA4, WT1 | (**Ijpenberg et al.**, **2007**) |
| | E12.5 | FLK1$^-$ PCLP1$^+$ | *Ptn, Mdk, Hgf, Wt1* | |
| | E18.5 | PCLP1$^+$ MSLN$^+$ | *Wt1* | (**Onitsuka et al.**, **2010**) |
| | Adult | MSLN$^+$ | *Wt1* | |
| | Fetal | - | Gp38, WT1, ALCAM | (**Asahina et al.**, **2009**, **2011**) |
| | Adult (*Col1a1$^{GFP}$* mouse) | Vit-A$^-$ *Col1a1$^{GFP+}$* GPM6A$^+$ | *Upk1b, Enl,* MSLN, Gp38, KRT19, GPM6A | (**Lua et al.**, **2016**) |
| | Adult | GPM6A$^+$ | - | (**Li, Lua, et al.**, **2013**) |
| | Fetal | ALCAM$^+$ Gp38$^+$ | *Mdk, Ptn,* NG2 (low), ITGA8, GPM6A, WT1, | (**Ogawa et al.**, **2018**) |
| *Sub-MCs* | Fetal | - | GATA4, Desmin | (**Ijpenberg et al.**, **2007**) |
| | Fetal | - | WT1, Desmin, ALCAM, p75NTR, PDGFRα | (**Asahina et al.**, **2009**, **2011**) |
| | Fetal | ALCAM$^+$ Gp38$^-$ | Desmin, NGFR, ITGA8 | (**Ogawa et al.**, **2018**) |
| *SCs* | Fetal | - | GATA4, Desmin | (**Ijpenberg et al.**, **2007**) |
| | Fetal | - | p75NTR, GFAP | (**Suzuki et al.**, **2008**) |
| | Fetal | - | Desmin, p75NTR, αSMA | (**Asahina et al.**, **2009**, **2011**) |
| | Adult | Vit-A$^+$ | *Gfap, Lrat, Reln,* RELN, Desmin, | (**Lua et al.**, **2016**) |
| | Fetal | ALCAM$^+$ Gp38$^-$ | Desmin, NGFR, ITGA8 | (**Ogawa et al.**, **2018**) |
| *PFs* | Fetal | - | p75NTR | (**Suzuki et al.**, **2008**) |
| | Adult | Vit-A$^-$ *Col1a1$^{GFP+}$* GPM6A$^-$ | DES, ELN, THY1, ENTPD2, αSMA, | (**Lua et al.**, **2016**) |
| | E14.5 | Nestin$^+$ | NG2, αSMA, CD105, CD106, CD51, CD146, PDGFRα, PDGFRβ, DLK1 | (**Khan et al.**, **2016**) |
| | Fetal | - | NG2 | (**Ogawa et al.**, **2018**) |

Between E9.5 to E15, the liver undergoes substantial growth and becomes the major site of fetal hematopoiesis. Gene mutations affecting liver development often result in impaired hematopoiesis, underscoring the pivotal role of the FL in supporting fetal blood production. Next, the molecular and cellular constituents of the FL microenvironment that might regulate the hematopoietic development will be discussed.

### *An hematopoietic niche?*

Moore et al. generated over 200 immortalized stromal cell lines from the FL to screen for their ability to support hematopoiesis *in vitro*. However, only a few clones were able to maintain LTR activity over a 3-week period. These clones had in common the

expression of DLK1, and overexpression of this factor was sufficient to enable hematopoietic support (**Moore et al.**, **1997**). Moreover, DLK1 knockdown in human hepatoblasts resulted in decreased hematopoietic support *in vitro* (**Gerlach et al.**, **2019**). While DLK1 has been used to identify hepatoblasts *in vivo*, it is also expressed by the majority of Nestin$^+$ PFs (**Khan et al.**, **2016**). Although FL cell lines can temporarily sustain HSCs *in vitro*, they cannot significantly expand the HSC population.

The first indication that the FL microenvironment could sustain HSC expansion came from primary cultures with isolated DLK1$^+$ cells, presumably hepatoblasts (**Chou et al.**, **2013**; **Chou & Lodish**, **2010**; **Zhang & Lodish**, **2004**). These cells expressed hematopoietic supportive factors, namely angiopoietin ligand 3 (Angptl3), KITL ligand (KITL or Stem Cell Factor, SCF), C-X-C motif chemokine 12 (CXCL12 or Stromal cell-derived factor 1, SDF-1), insulin growth factor (IGF)-2 and thrombopoietin (TPO) (**Chou & Lodish**, **2010**; **Zhang & Lodish**, **2004**). DLK1$^+$ cells were able to expand LT-HSCs around 20-fold after a 3-week co-culture period, supplemented with hematopoietic cytokines (**Chou et al.**, **2013**). This expansion was reliant on direct contact, as the conditioned medium alone was unable to maintain LT-HSCs, and co-cultures in a Transwell system displayed only limited expansion.

Hepatoblasts were also shown to support lineage differentiation and maturation. They produce EPO, required for terminal proliferation and differentiation of erythroid progenitors (**Sugiyama et al.**, **2011**). *In situ* maps further confirmed that *Kitl*-expressing hepatoblasts were usually near a *Kit*-positive erythroid progenitor (**Gao et al.**, **2022**). Hepatoblasts also support B-lineage development and Mk production by secretion of interleukin (IL)7 and TPO, respectively (**Brouard et al.**, **2017**; **Tsuneto et al.**, **2013**).

Nestin$^+$ NG2$^+$ PFs were also proposed as a key niche population, tightly related to the HSC compartment in the FL (**Khan et al.**, **2016**). Selective ablation of PFs (using NG2-*cre*/iDTA mice) showed no developmental defects at E12.5, but a reduction (~30%) in HSCs at E14.5, and a reduction in BrdU intake in the remaining HSC compartment, which can reflect a defect on HSC expansion. However, as Nestin$^+$ cells are relevant producers of *Cxcl12* at E14.5, the reduction of FL HSCs could also be interpreted as a displacement of cells into circulation. They additionally show that the HSC compartment grows (considering estimations from (**H. Ema & Nakauchi**, **2000**)) at the same rate as the Nestin$^+$ cells, suggesting a dependency. However, for this observation to be conclusive, it would require following the growth rate of the entire liver, to rule out the possibility of linear growth.

Hematopoietic stem and progenitor cells (HSPCs) expressing the Endothelial Protein C Receptor (EPCR) were found to interact with LSECs, in both luminal and parenchymal aspects (**Iwasaki et al.**, **2010**). LSECs were shown to express *Il7, Flt3l and Scf* and to promote B-cell lymphopoiesis in co-cultures with BM Lin$^-$ cells (**Wittig et al.**,

**2010**). A study in the zebrafish revealed a peculiar interaction between endothelial cells and HSPCs: endothelial cells surrounding a single HSPC attached to a single mesenchymal cell, resembling a pocket. Live imaging showed that the mesenchymal cell can anchor and orient the division plane of the HSPC. A similar process was observed in mice live imaging FL explants (**Tamplin et al.**, **2015**).

In addition to stromal populations, FL macrophages have also been indicated as niche regulators (**Gao et al.**, **2022**; **Kayvanjoo et al.**, **2023**). Their role in erythropoiesis has long been acknowledged (**Palis et al.**, **1999**), and more recently, a role in the HSC niche has been proposed. Macrophages were shown to establish frequent interactions with $KIT^+$ and $CD150^+$ progenitors. Moreover, the depletion of macrophages resulted in impaired erythrocyte maturation and induced transcriptional changes in HSCs, leading to a biased differentiation towards the granulocytic lineage, without affecting HSCPs numbers (**Kayvanjoo et al.**, **2023**). In a spatial transcriptomics study, macrophages were also suggested to localize close to HSPCs, in regions where growth factors were highly enriched, including MDK and PTN (**Gao et al.**, **2022**).

Recently, the role of KITL in fetal hematopoiesis was investigated through conditional depletion from various FL cell types, including hepatic, endothelial, perivascular, and hematopoietic cells (**Lee et al.**, **2021**). By employing reporter mice for *Cxcl12* and *Kitl*, the authors identified endothelial cells and SCs as the primary sources of *Kitl*, with SCs also being major producers of *Cxcl12*. Intriguingly, depleting *Kitl* from any of these cell types before birth did not lead to any discernible hematopoietic defects. However, a severe phenotype became evident postnatally when *Kitl* was depleted from SCs, and the impact was even more pronounced when endothelial cells were also depleted of *Kitl* (**Lee et al.**, **2021**). SCs had been previously proposed as likely niche cells, as $p75NTR^+$ isolated cells expressed a range of hematopoietic cytokines, namely colony stimulating factor 1 (C*sf1), Tpo, Kitl, Epo, Igf1, Il11,* FLT3 ligand *(Flt3l)* and oncostatin M (*Osm,* involved in hepatic maturation) and considerable high levels of *Igf2* (**Tan et al.**, **2017**).

While the role of FL cells in fetal hematopoiesis requires further clarification, it is also crucial to address other niche factors. For example, metabolism, endoplasmic reticulum stress and oxidative stress can also be extrinsically regulated, impacting HSC behavior. Liver's bile acids, freely dispersed until the formation of the bile canaliculus, were shown to regulate the numbers of HSPCs, functioning as chemical chaperones, critical to sustaining the high protein synthesis rates, without triggering endoplasmic reticulum stress (**Sigurdsson et al.**, **2016**). TPO, primarily produced by hepatocytes, while dispensable for HSCs at E14.5, it is required from E16.5 onwards and was reported to regulate mTOR and metabolism in HSCs (**Lee et al.**, **2022**).

The temporary residence of the HS in the FL is intriguing, giving rise to numerous questions about the FL microenvironment's role and the mechanisms governing its colonization and decolonization. To conclude this section, a closer look will be given at the mouse embryonic development in an effort to understand the "choice" of the FL as the embryonic hematopoietic host and why it eventually relinquishes its hematopoietic functions.

***Why the FL?***

The cardiovascular system is the first to develop and function during embryogenesis. The vascular network serves as a vital pathway for the transportation of essential nutrients and oxygen to all parts of the body while removing metabolic waste products. By the time the first blood islands become discernible in the YS mesoderm, the heart has already started to take shape, circa E7.5 (**Kaufmann & Bard**, **1999**). However, it is only nearly one day later that a connection between the two is established and with the onset of heartbeat, blood cells start to circulate through the body (**McGrath et al.**, **2003**). From E8.25-E8.5, circulation is characterized by the movement of a few EryPs into the DA, and an increase in blood flow thereafter (**McGrath et al.**, **2003**). Although EMPs arise from HE of YS vasculature at E8.25 onwards, they do not promptly integrate into the bloodstream. Instead, they undergo a phase of expansion in vascular beds, before massively entering circulation around E10, reaching the embryo through the VVs (**Kasaai et al.**, **2017**; **McGrath et al.**, **2003**, **2015**; **Palis et al.**, **2001**). By this time, HSPCs start to emerge in the major arteries of the embryo proper (DA, VA, UA), budding from arterial HE into circulation (**Boisset et al.**, **2010**; **de Bruijn**, **2000**), following two possible routes: the VA to the YS vasculature, and back to the embryo through the VVs; or the UA to the placenta, and back to the embryo through the UVs. In both cases, the first organ they encounter is the FL. At this point, the liver vasculature consists of only a primitive vascular plexus (filled with hematopoietic cells) formed from the VVs and connected to the UVs (**Figure 8B**). The DV, which allows direct passage of oxygenated blood to the heart only arises slightly later (**Figure 8C, D**). At this stage, cells from all hematopoietic waves can be found in circulation. Within one day, a substantial influx of hematopoietic cells occurs into the liver's parenchyma, and they become the predominant population, expanding considerably and transforming the FL into a potent hematopoietic center until the end of gestation.

Multiple factors might contribute to the colonization of the FL by hematopoietic cells, namely: 1. The topology of fetal circulation. Semi-oxygenated blood from the YS, oxygenated blood from the placenta, and venous blood from the gut meet in the intricate FL

vascular plexus, before converging into the sinus venosus and directed to the heart. 2. The distinctive characteristics of the FL sinusoidal network (reviewed in (**Wake & Sato**, **2015**)). In contrast with capillaries, liver sinusoids are large, particularly at early embryonic stages; have lower and discontinuous connective tissue (perisinusoidal SCs) with minimal basement membrane; are irregular, following the shape of the parenchymal tissue; and are highly fenestrated, being highly permeable to small molecules. 3. Low blood pressure within the FL sinusoids might facilitate the extravasation of circulating cells into the liver's parenchyma. Deletion of a floxed *Gata4* allele in *Stab2-Cre* and *Lyve1-Cre* (targeting LSECs) resulted in mutant embryos with hypoplastic livers, anemia, and prenatal lethality. LSECs in the mutant embryos were not fenestrated, exhibited upregulation of CD31 and VE-Cadh and a robust basement membrane. As a result, EMPs and HSPCs were markedly reduced in the liver and increased in the blood. Curiously, HSPCs did not exhibit any intrinsic defects, with similar LTR readouts as wild-type (**Géraud et al.**, **2017**). This study suggests that discontinuous sinusoids allow and are necessary for the transmigration of hematopoietic cells into the liver.

Liver colonization is also mediated by cell adhesion and chemoattraction (e.g., cytokines, chemokines, and growth factors) processes. Several cell adhesion molecules have been identified in embryonic HSPCs, including integrins, selectins, cadherins, and others, and some of their ligands can be found in liver cells and ECM components (reviewed in (**Hayashi et al.**, **2019**; **Soares-da-Silva et al.**, **2020**, **Annex II**). Variations in the expression of adhesion molecules during development might correlate with the mobilization of hematopoietic cells across various organs. For instance, HSPCs lacking β1 integrin had a severely impaired colonization of the FL, but were still present in circulation and with no differentiation defects, suggesting a role for integrin-mediated cell adhesion in FL colonization (**Hirsch et al.**, **1996**).

***Why no longer the FL?***

In mid-gestation, the embryonic liver works as a "bag" accommodating the expanding HS before BM development. From E12.5 to E16.5, the organ is essentially an hematopoietic tissue, with a ratio of non-hematopoietic cells/total liver cells very low. During this temporal window, the organ's architecture is far less complex than that of its adult counterpart. In the adult, hepatocytes are the main parenchymal cell type, organized in cords interspaced by an intricate vascular and biliary system (**Figure 7E**). Concomitantly with the start of the exodus of the HS from the FL and ingression in the developing BM (~E16.5) (**Christensen et al.**, **2004**), there is an observable maturation of the hepatic epithelium at a morphological level. This raises the possibility of a causal relationship

between these events. Transcriptomic and proteomic analysis throughout FL development identified E15.5 as the time of onset of metabolic, detoxification and immune programs (**Guo et al.**, **2009**), revealing a shift into hepatic functions.

Kinoshita et al. showed that hematopoietic cells expanded when cultured in a monolayer of primary fetal hepatic cells (in the presence of hematopoietic cytokines) and that the addition of OSM suppressed *in vitro* hematopoiesis, by inducing the maturation of the hepatic cells (**Kinoshita et al.**, **1999**). Since FL hematopoietic cells produce OSM, its expansion increases the local OSM concentration, consequently promoting hepatic development (**Kamiya et al.**, **1999**). In consequence, a metabolically active liver might no longer support hematopoiesis (**Miyajima et al.**, **2000**). However, it is still not clear whether the displacement of the hematopoietic cells out of the FL facilitates liver maturation or if the changes in the microenvironment no longer support hematopoiesis and/or trigger its migration.

The vasculature remodeling at the end of gestation was also correlated with the rapid loss of HSCs in the postnatal liver. After birth, the portal vein no longer receives blood from the VVs. It collects the blood from the gut, draining it to the central vein and the hepatic artery starts to form. With the ligation of the umbilical inlet, the portal vessels acquire a vein phenotype and lose the periportal pericytes (**Khan et al.**, **2016**).

The presence of fenestrated sinusoids exclusively in the liver, spleen, and BM, all of which are hematopoietic organs, is unlikely to be coincidental (**Griffin & Gao**, **2017**). As soon as the BM vascularization is initiated, hematopoietic cells initiate their colonization (**Coşkun et al.**, **2014**). CXCL12-deficient mice revealed that CXCL12 is not fundamental for early FL colonization, but it is required for the retention of hematopoietic cells in the FL until the end of gestation and subsequent migration to the BM (**Ara et al.**, **2003**). Other chemoattractive, adhesion molecules and ECM components that orchestrate the migration of hematopoietic cells from the FL to the BM were reviewed by (**Ciriza et al.**, **2013**).

## AN OVERALL LOOK INTO HEMATOPOIETIC MICROENVIRONMENTS

The challenge of fetal hematopoiesis is to quickly generate differentiated blood cells required for embryo growth and development, while simultaneously establishing a reservoir of conservatively self-renewing HSCs, before the development of its adult specialized niches. An independent origin of mature blood lineages and HSCs, with a low input for fetal blood production, might have arisen as an evolutionary advantage mechanism, as the extensive blood production required for embryogenesis could be too demanding for HSCs, leading to their exhaustion. The compartmentalization of fetal hematopoiesis into multiple sites is conserved across species (**Elsaid et al.**, **2020**, **Annex II**). Two initial distinct locations are associated with hematopoietic cell emergence (YS, or equivalent, and major arteries), followed by a temporary residence in a different location where all hematopoietic waves converge and blood cell production co-exists with HSC maintenance and (putative) expansion (the FL or caudal hematopoietic tissue, CHT, in the case of zebrafish), followed by the colonization of the adult niche later in gestation (BM, or kidneys in zebrafish). Here, aiming to identify common aspects shared among the diverse hematopoietic microenvironments, they will be briefly revisited, except the FL, previously discussed. **Table 5** summarizes the key hematopoietic factors and their respective sources throughout development.

Our understanding of the niche properties within the YS and the specific local signals that dictate hematopoietic specification and emergence remains limited. E9.5 YS-endoderm and mesoderm-derived cell lines were shown to express features of normal YS cells and to support the *in vitro* growth and differentiation of BM 5-Fluorouracil (5-FU) resistant hematopoietic cells. These cell lines seemed to recapitulate the original microenvironment, as they supported less neutrophil and greater macrophage differentiation than kidney and BM stromal cell lines (**Yoder et al.**, **1994**).

Recently, a human YS cell atlas was generated using scRNA-seq, light-sheet microscopy and RNAScope-based *in situ* hybridization (**Goh et al.**, **2023**). Beyond its role as an hematopoietic site, the authors identified the YS as a major regulator of metabolism, coagulation, and vascular development. They identified fibroblasts, smooth muscle cells, mesothelial, endothelial, and endodermal cells as the major non-hematopoietic subsets of the human YS. *ACTA2*$^{+}$ smooth muscle cells were visualized *in situ* forming a sub-layer between the mesoderm and endoderm. Interestingly, they found EPO and TPO expression in human and rabbit YS endodermal cells, but no expression in the murine YS (**Goh et al.**, **2023**). This species-specific difference aligns with the relatively low requirement of EPO for

pre-liver erythropoiesis in mice, as evidenced by the fact that *Epo/Epor*-deficient mice are only lethal around E13.5 (**Lin et al.**, **1996**; **H. Wu et al.**, **1995**).

KITL is a critical niche factor, regulating hematopoiesis across its multiple locations (**Table 5**). Using *Kitl*-tdTomato reporter mice, the sources of this cytokine were assessed *in situ* during embryonic development. At E8.5, *Kitl* was strongly expressed in the P-Sp and allantois (precursor structures of the AGM and umbilical vessels), and weakly expressed in the YS blood islands (in endothelial cells surrounding EryPs and some perivascular cells). *Kitl*-expressing endothelial cells near clusters of $KIT^+$ EMPs were still found at E10.5 in the YS vasculature, a time were Kitl expression was already apparent in the FL and the mesenchyme ventral to the DA (**Azzoni et al.**, **2018**). Endothelial-specific deletion of *Kitl* using $Tie2^{Cre}Kitl^{flox}$ mice resulted in a reduction of EMPs/HSPCs in the YS and AGM, respectively, but had a low impact on FL progenitor's numbers. The impact of lack of endothelium-derived *Kitl* phenocopied the *Kitl*-mutant mice in the YS and AGM, but not in the FL, suggesting that the requirements of endothelial *Kitl* vary between niches, likely due to compensatory effects in the FL (**Azzoni et al.**, **2018**). *Kitl*-producing endothelial cells were also found in the placenta (**Sasaki et al.**, **2010**).

The labyrinth vessels, a complex vascular network within the placenta, have been suggested as a unique hematopoietic niche conducive to HSPC proliferation (**Rhodes et al.**, **2008**). Nevertheless, direct evidence supporting this hypothesis is currently lacking. Furthermore, platelet-derived growth factor β (PDGFβ) was identified as an EPO regulator in the placenta, as its depletion induces trophoblast cells to upregulate *Epo* expression, causing ectopic erythropoiesis (**Chhabra et al.**, **2012**).

More than 100 stromal cell lines were established from sub-compartments of the AGM. HSC-supportive stromal clones were found in both the aorta-mesenchyme and urogenital ridges, the latter being the source of the most supportive isolated clone (**Oostendorp et al.**, **2002**). Tissues ventral to the AGM have been suggested as a supportive niche for hematopoietic generation (**Peeters et al.**, **2009**; **Taoudi & Medvinsky**, **2007**). Nerves of the central nervous system have been implicated as key components of the AGM niche, as HSC generation seems to be dependent on catecholamines (**Fitch et al.**, **2012**). Recently, YS-derived macrophages with a pro-inflammatory profile were shown to be abundant in the AGM. Remarkably, AGM explants depleted of macrophages revealed impaired HSC production, as cultured cells had little to no repopulation activity, revealing a positive regulation of macrophages in HSC emergence (**Mariani et al.**, **2019**). Blood flow was shown to be fundamental for a proper HSC emergence from the main arteries of the embryo. Although HSC precursors still emerged in from HE in $Ncx1^{-/-}$ embryos, they did not develop into functional HSCs. In the mutant embryos, $\alpha SMA^+$ cells were lost, subaortic

mesenchyme was thinner, macrophages were reduced and *Kitl* expression reduced in endothelial cells, indicating a strong impact in the hematopoietic niche **(Azzoni et al., 2021).**

Hematopoietic cells arrive in the BM as soon as circulation starts to be established. The BM is the most well-characterized hematopoietic niche. Extensive efforts to identify niche cell types within the adult BM have involved the optimization of stromal isolation protocols, gene expression analysis, conditional deletion studies targeting hematopoietic factors, cell ablation techniques, and *in situ* cell mapping. As a result, innumerous cell types were identified as positive/negative regulators of hematopoiesis, as reviewed by (**Comazzetto et al.**, **2021**; **Crane et al.**, **2017**; **Morrison & Scadden**, **2014**; **Pinho & Frenette**, **2019**).

In the adult BM, HSC niches are perisinusoidal (**Table 6**), with $LepR^+$ mesenchymal cells and endothelial cells producing the main factors required for HSC maintenance (**Table 5**) (**Ding et al.**, **2012**; **Ding & Morrison**, **2013**; **Greenbaum et al.**, **2013**; **Oguro et al.**, **2013**). However, fetal and neonatal BM differ substantially from the adult, with regards to cellular composition, gene expression and cell interactions (**Hall et al.**, **2022**; **Helbling et al.**, **2019**; **Liu et al.**, **2022**). Some reports suggest that HSCs are still proliferative when they arrive at the BM, and a shift to a quiescent state only occurs 3 weeks after birth (**Bowie et al.**, **2006**; **Coşkun et al.**, **2014**). This coincides with the time frame of intense bone remodeling, suggesting that HSC cycling is dependent on the cellular composition of the microenvironment. LSK cells isolated from $Osx^{-/-}$ fetal BM (lacking osteolineage cells and some mesenchymal populations (**Mizoguchi et al.**, **2014**; **Nakashima et al.**, **2002**)) form multi-lineage colonies *in vitro*, but fail to repopulate transplanted recipients. LSK cells exhibited dysregulated cell cycle progression and defective homing ability, suggesting that osteolineage and/or mesenchymal cells are necessary to establish and sustain BM LT-HSCs (**Coşkun et al.**, **2014**). Additionally, E15.5 $CD105^+Thy1^-$ mesenchymal progenitors transplanted under the kidney capsule give rise to donor-derived chondrocytes and can create an ectopic niche with the recruitment of host-derived marrow and HSCs, evidencing the importance of endochondral ossification for HSC niche formation (**Chan et al.**, **2009**).

Combining scRNA-Seq, FC, imaging and tissue-specific genetic mouse models, a recent study showed that the fetal BM is largely devoid of Leptin receptor (LepR)-expressing cells, a major cytokine producer population in the adult, and a role of arterial endothelial cells in HSPC expansion through Wnt signaling (**Liu et al.**, **2022**). A subset of osteochondro progenitors also appears to contribute to the fetal/neonatal BM niche, providing growth factors (e.g. IGF1/2) that regulate HSPC function (**Hall et al.**, **2022**).

**Table 5. Fundamental signaling axis regulating hematopoiesis throughout development.**
AECs – arterial endothelial cells; BIs – blood islands; CAR – CXCL12-adundant reticular (cells); ECs – endothelial cells; EryPs – primitive erythroid progenitors; HCs – hematopoietic cells; HE – hemogenic endothelium; HSPC – hematopoietic stem or progenitor cell; IACHs – intra-aortic hematopoietic clusters; LSECs – liver sinusoidal endothelial cells ; SCs – stellate cells; PFs – portal fibroblasts.

| *SIGNALING AXIS (FUNCTION)* | *SIGNAL's SOURCE:* |
|---|---|
| **KITL – KIT (CD117)**<br><br>HSC survival and self-renewal (**Miller et al.**, **1997**)<br>Regulates erythropoiesis, megakaryocytopoiesis, and mast cell generation (**Barker**, **1994**) | **YS**:<br>ECs surrounding BIs (**Azzoni et al.**, **2018**; **Isern et al.**, **2011**)<br>Perivascular cells (**Azzoni et al.**, **2018**)<br>Visceral endodermal cells (**Isern et al.**, **2011**)<br>**AGM**:<br>Para-aortic ECs,<br>Perivascular smooth muscle cells (**Azzoni et al.**, **2018**)<br>**Placenta** :<br>ECs (**Sasaki et al.**, **2010**)<br>**FL**:<br>ECs (**Lee et al.**, **2021**; **D. Sugiyama et al.**, **2011**)<br>LSECs (**Wittig et al.**, **2010**)<br>AECs (**Lu et al.**, **2021**)<br>Hepatoblasts (**Chou & Lodish**, **2010**; **Lu et al.**, **2021**; **D. Sugiyama et al.**, **2011**)<br>PFs (**Khan et al.**, **2016**)<br>SCs (**Lee et al.**, **2021**; **Tan et al.**, **2017**)<br>**BM**:<br>ECs (**Ding et al.**, **2012**); Arterial ECs (**Xu et al.**, **2018**)<br>CAR/LepR$^{+}$ perisinusoidal (**Comazzetto et al.**, **2019**; **Ding et al.**, **2012**)<br>NG2$^{+}$ peri-arteriolar (**Asada et al.**, **2017**)<br>Nestin (**Méndez-Ferrer et al.**, **2010**) |
| **CXCL12 – CXCR4**<br><br>Engraftment, trafficking, retention (**Ara et al.**, **2003**)<br>HSC maintenance (**T. Sugiyama et al.**, **2006**)<br>Regulates myelopoiesis and B cell development (**Nagasawa et al.**, **1996**) | **YS**:<br>**AGM**:<br>ECs, HE (**Mariani et al.**, **2019**)<br>**FL**:<br>Hepatoblasts (**Chou & Lodish**, **2010**; **Lu et al.**, **2021**)<br>PFs (**Khan et al.**, **2016**)<br>SCs (**Lee et al.**, **2021**)<br>AECs/perivascular (**Lu et al.**, **2021**)<br>**BM**:<br>ECs (**Ding & Morrison**, **2013**), Arterial ECs (**Xu et al.**, **2018**)<br>CAR/LepR$^{+}$ perisinusoidal (**Ding et al.**, **2012**; **Ding & Morrison**, **2013**; **T. Sugiyama et al.**, **2006**)<br>NG2$^{+}$ peri-arteriolar (**Asada et al.**, **2017**)<br>Nestin perivascular (**Greenbaum et al.**, **2013**; **Méndez-Ferrer et al.**, **2010**)<br>Osteoblasts (**Ding & Morrison**, **2013**) |

| | |
|---|---|
| **TPO – MPL (CD110)**<br><br>HSC survival and maintenance (**Kimura et al.**, **1998**; **Qian et al.**, **2007**)<br>Required for Mk and platelet production (**de Sauvage et al.**, **1994**; **Kaushansky et al.**, **1994**, **1995**) | **FL**:<br>Hepatoblasts (**Brouard et al.**, **2017**; **Chou & Lodish**, **2010**; **Sugiyama et al.**, **2011**)<br>Hepatocytes (**Lee et al.**, **2022**)<br>SCs (**Tan et al.**, **2017**)<br>Mesenchymal cells (**Brouard et al.**, **2017**)<br>***Adult**: liver hepatocytes (**Decker et al.**, **2018**; **Sungaran et al.**, **1997**) |
| **EPO – EPOR**<br><br>Regulates erythroid differentiation, maturation, proliferation, and survival in a hypoxia-inducible manner (**Lin et al.**, **1996**; **Watts et al.**, **2020**) | **Neural crest:**<br>Neural Epo-producing cells (**Suzuki et al.**, **2013**)<br>**Placenta**:<br>Sinusoidal trophoblast giant cells (**Chhabra et al.**, **2012**)<br>**FL**:<br>Hepatoblasts (**D. Sugiyama et al.**, **2011**)<br>**Adult kidney**:<br>Renal EPO-producing cells (**Souma et al.**, **2015**; **Suzuki et al.**, **2011**) |
| **CSF1 – CSF1R**<br><br>Commitment to myeloid lineage (**Mossadegh-Keller et al.**, **2013**) | **FL**:<br>SCs (**Tan et al.**, **2017**)<br>**BM**:<br>ECs,<br>Adipoq-lineage progenitors (**Inoue et al.**, **2023**) |
| **IL7 – IL7Rα**<br><br>Lymphocyte expansion,<br>B and T cell development<br>(**Peschon et al.**, **1994**) | **FL**:<br>LSECs (**Wittig et al.**, **2010**)<br>Hepatoblasts (**Tsuneto et al.**, **2013**)<br>**BM**:<br>CAR/LepR$^{+}$ perisinusoidal (**Cordeiro Gomes et al.**, **2016**)<br>Nestin (**Méndez-Ferrer et al.**, **2010**) |
| **FLT3L - FLT3/FLK2 (CD135)**<br><br>HSPC proliferation (**Lyman et al.**, **1993**) | **FL**:<br>SCs (**Tan et al.**, **2017**)<br>LSECs (**Wittig et al.**, **2010**)<br>**BM**:<br>HCs (**Tornack et al.**, **2017**) |
| **IGF2 – INSR/ IGF1R/ IGF2R**<br><br>HSC proliferation<br>(**Zhang & Lodish**, **2004**) | **YS**:<br>EryPs (**Isern et al.**, **2011**)<br>**AGM**:<br>ECs,<br>Smooth muscle cells,<br>IAHCs (**Mascarenhas et al.**, **2009**)<br>**Placenta**:<br>Endocrine cells (**Lopez-Tello et al.**, **2023**)<br>ECs,<br>Trophoblasts (**Sandovici et al.**, **2022**)<br>**FL**:<br>Hepatoblasts (**Chou & Lodish**, **2010**; **Zhang & Lodish**, **2004**)<br>PFs (**Khan et al.**, **2016**)<br>SCs (**Tan et al.**, **2017**) |

## TRACKING HSC LOCALIZATION IN THE NICHES

The understanding of where HSPCs are situated within their microenvironment and how they interact with their surroundings has made huge advances in the last decade due to improvements in imaging techniques. Histological techniques have been the standard procedure to investigate tissues. However, a clear understanding of biological mechanisms and tissue architecture requires an unbiased exploration of large specimens. For this, increasingly sophisticated tissue clearing methodologies, coupled with the capabilities of cutting-edge microscopes (such as confocal, multi-photon, and light-sheet) are currently on the rise. Tissue clearing techniques aim to render biological specimens transparent to mitigate light scattering and absorption, thereby facilitating in-depth acquisitions of large volume samples (extensively reviewed in (**Ariel**, **2017**; **Ueda et al.**, **2020**)).

Despite great advances, an accurate *in situ* identification of HSPCs in their microenvironments is still limited by the requirement for intricate combinations of cell-surface markers or the specificity of reporter mice and the lack of suitable tools for automated and quantitative computation analysis of (often terabyte-scale) imaging data. **Table 6** presents a literature overview summarizing quantitative results concerning the localization of HSCs in relation to BM niche populations. Some of these studies considered only a limited number of quantified target cells, and different bone types were analyzed, with contradictory results. Additionally, the quantification often relied on manual cell classification and calculation of near distances, which introduces subjectivity. Nevertheless, a recent study has shed light on the inconsistencies within the BM niche. Kokkaliaris and colleagues imaged 152 full-bone (femur and sternum) sections in a multiparameter strategy combining a total of 9 BM stromal cell types (4 simultaneous) and 3 HSC reporter lines (**Kokkaliaris et al.**, **2020**). They localized HSCs (in both bone types) close to sinusoids, CXCL12-expressing cells, Mks, and different combinations of these, but not to bone, adipocyte, periarterial or Schwann cells. However, their distribution pattern resembled that of random dots (RDs), reflecting the relative abundance of BM cell types rather than specific enrichment near these cell types.

The localization of HSCs during development is far less explored, in part due to the lack of understanding of the identity of the recently formed HSCs (or fated to be HSCs). Although adult HSCs can be highly purified using SLAM markers, with 1 in every 2.2 $CD150^{+}CD48^{-}CD41^{-}$ cells having LTR potential (**Kiel et al.**, **2005**), the phenotype of fetal HSCs is less clear. The SLAM phenotype is not acquired immediately as LTR can be found in $CD150^{-}CD48^{+/-}$ cells, which is also the case of other HSC typical markers, like Sca-1 and CD45 (**Table 7**).

**Table 6. Studies that assessed and quantified HSC localization in the BM microenvironment.**

n.d. – not determined. n.s. – not shown. RD – random dots. * As determined by (**Kiel et al., 2005**)

| *REFERENCE (Bone imaged)* | *STAINING STRATEGY* | *HSC PURITY* | *STAINING* | *QUANTIFICATION* | *# HSPCs* | *CONCLUSIONS* | *≠ from RDs* | *SECTION PREP.* |
|---|---|---|---|---|---|---|---|---|
| (**Kiel et al., 2005**) | $CD150^+$ $CD48^-$ $CD41^-$ $Lin^-$ | 1 in 2.2 | MECA-32 | Manual | 35 | ~60% perisinusoidal; 14% near the endosteum; | n.d. | Cryosections (7 μm) |
| (**Méndez-Ferrer et al., 2010**) | $CD150^+$ $CD41^-$ | n.d. | Nestin-GFP | Manual | 42 | 88% near $Nestin^+$ cells; 33% near bone; | n.d. | Sections |
| (**Yamazaki et al., 2011**) | $CD150^+$ $CD48^-$ $CD41^-$ $Lin^-$ | 1 in 2.2* | GFAP-GFP VE-Cadh Osteocalcin | ArrayScan | n.s. | ~13% near bone; 30% near vasculature; 23% near Schwann cells | n.d. | Cryosections |
| (**Nombela-Arrieta et al., 2013**) (Femur) | (1) $Lin^-$ $CD48^-$ $CD41^{-/low}$ $KIT^+$; (2) $KIT^+$ $Sca\text{-}1^+$ | n.d. | Laminin Sca-1 | iCys Cytometric Analysis Software (Compucyte); | 312(1) 1.589(2) | ~(1) 85%, (2) 70% perisinusoidal; ~(1) 23%, (2) 12% near the bone; | n.d. | Cryosections (5 μm) |
| (**Kunisaki et al., 2013**) (Sternum) | $Lin^-$ $CD150^+$ $CD48^-$ $CD41^-$ | 1 in 2.2* | VE-Cadh/CD31 Sca-1 *Nestin*-GFP *Col2.3*-GFP | Manual RDs (simulated in Matlab) | 217 | Contact: ~20% with $Nestin^{bright}$ cells, 15% with arterioles and 33% with sinusoids; <20μm: ~30% from arterioles and $Nestin^{bright}$ cells, 65% from sinusoids, 20% from bone | $Nestin^{bright}$: n.d. Arterioles: Yes (near) Sinusoids: No Bone: n.d. | Whole mount |
| (**Bruns et al., 2014**) (Sternum) | $Lin^-$ $CD150^+$ $CD48^-$ $CD41^-$ | 1 in 2.2* | CD150, CD41 (Mks) VE-Cadh/CD31 Sca-1 | Manual RDs (simulated in Matlab) | 252 | Contact: 20% with Mks; <15μm: ~45% from Mks; | Yes (near) | Whole mount |

**Table 6 (cont.).**

| *REFERENCE (Bone imaged)* | *STAINING STRATEGY* | *HSC PURITY* | *ADDITIONAL STAINING* | *QUANTIFICATION* | *# HSPCs* | *CONCLUSIONS* | *≠ from RDs* | *SECTION PREP.* |
|---|---|---|---|---|---|---|---|---|
| (**Zhao et al.**, **2014**) | $Lin^-$ $CD150^+$ $CD48^-$ $CD41^-$ | 1 in 2.2* | CD41 | Axiovision (Zeiss) | 72 | Contact: 20% with Mks | n.d. | Paraffin sections |
| (**Acar et al.**, **2015**) (Tibia) | $KIT^+$ α-catulin-$GFP^+$ | 1 in 3.1 | Laminin *Cxcl12*-dsRed *Lepr*-tdTomato GFAP | Imaris | 1588 | <10μm: 97% from $Cxcl12^+$ cells; 93% from $LepR^+$ cells; 15% from arterioles; 84% from sinusoids; 12% from transition vessels (TV); 6% from Schwann cells | Diaphysis: No Metaphysis: Yes (away) Arterioles: Yes (away) Sinusoids: No TV: Yes (away) Nerves: No | Whole mount, Murray' s or 3DISCO cleared |
| (**Chen et al.**, **2016**) (Tibia) | *Hoxb5*-$mCherry^+$ | 1 in 2.1 | VE-Cadh | Imaris | 287 | 94% perivascular | Yes (near) | Whole mount, CUBIC |
| (**Coutu et al.**, **2018**) | $Lin^-$ $Sca\text{-}1^+$ $KIT^+$ | n.d. | Col.1 GFAP Sca-1 CD105 OC-YFP | Imaris XiT (Imaging cytometry) | 1000 | Close to glial Schwann cells | Bone: No Nerves: Yes (near) | TDE cleared thick sections |
| (**Saçma et al.**, **2019**) | Label retaining $Lin^-$ $CD150^+$ $CD48^-$ $CD41^-$ | n.d. | Nestin-GFP FABP4 VE-Cadh/ CD31 | Volocity software (Perkin Elmer) | 137 | 83% perisinusoidal | Yes (near) | Whole mount |
| (**Christodoulou et al.**, **2020**) (Calvaria [(1)], femur [(2)]) | $Mds1^{GFP/+}$ $Mds1^{GFP/+}Flt3^{Cre}$ $Mds1^{GFP/+}Flt3^{Cre}KIT^+$ | 1 in 9 | CD105 Col.1 | Imaris XiT (Imaging cytometry) | 86 [(1)] 90 [(2)] | 94% perisinusoidal | Sinusoids: No Bone: No | Live imaging [(1)], TDE cleared thick sections [(2)] |
| (**Kokkaliaris**, **2020**) (Femur, sternum) | $KIT^+$ α-catulin-$GFP^+$ ($HSC^{α\text{-}cat}s$) $Mds1^{GFP/+}Flt3^{Cre}$ ($HSC^{MFG}s$) | 1 in 3.1 1 in 9 | Collagen.1, Opn GP1bb Laminin CD105 Sca-1 NG2 GFAP | Imaris XiT (Imaging cytometry) | 4067 $HSC^{α\text{-}cat}s$ 1336 $HSC^{MFG}s$ (115 full-bone sections) | Close to sinusoids, CXCL12-expressing cells, Mks, but not to bone, adipocyte, periarterial or Schwann cells | No (for all cell types) | TDE cleared thick sections |

**Table 7** provides a summary of the phenotype of hematopoietic progenitors originated during embryonic development. Recognizing the limitations of conventional staining strategies, that require the combination of multiple markers to HSCs, there has been a concerted effort to identify specific markers that could be traced using reporter mouse models, offering a promising strategy for *in situ* cell tracking. Numerous reporter lines are already accessible, facilitating HSC enrichment through a single-color staining approach, and often further enhanced by the inclusion of few additional markers, such as KIT (**Acar et al.**, **2015**). Key HSC reporter mouse models include α-catulin-GFP mice (**Acar et al.**, **2015**), *Evi1*-GFP (**Kataoka et al.**, **2011**), *Fgd5*-ZSGreen (**Gazit et al.**, **2014**), *HoxB4-YFP* (**Hills et al.**, **2011**), *Hoxb5*-tri-mCherry (**Chen et al.**, **2016**), *Pdzk1ip1*-GFP (**Sawai et al.**, **2016**), *Gprc5c*-eGFP (**Cabezas-Wallscheid et al.**, **2017**), and *Hlf*-tdTomato (**Yokomizo et al.**, **2019**). The specificity of some of these lines at embryonic stages still requires confirmation. *Evi1*- and *Hlf*-reporter mice are promising models to follow HSCs during embryonic development, as HSC specification was shown to be regulated by the EVI1/HLF axis. *Hlf* is exclusively expressed in $KIT^+$ cells within IAHCs, whereas *Evi1* is also expressed by endothelial cells. The level of expression of *Evi1* seems to regulate the fate of pre-HSCs, with $Evi1^{high}$ preferentially generating HSCs (**Yokomizo et al.**, **2019**, **2022**).

So far, only a few studies addressed the distribution of HSCs in the FL. Khan and colleagues reported that at E14.5, ~40% HSCs ($CD150^+CD48^-CD41^-Lin^-$) were at <20μm from $Nestin^+$ cells, and that there is a displacement of these cells away from portal vessels around birth (**Khan et al.**, **2016**). This resulted from the quantification of 12 whole-mount (not cleared) stained Nestin-GFP FLs, with a total of 105 cells classified as HSCs (at E14.5). This yields an average of only around 9 HSCs per whole liver. In the same study, ~500 HSCs/FL were estimated by FC, at the same time point, raising some concerns regarding the reliability of the staining method and consequent conclusions. Using the same staining strategy, Lee et al. contradictingly reported that candidate HSCs were in close association with $Laminin^+$ LSECs at E15.5 and P0 (**Lee et al.**, **2021**). Therefore, the precise localization of HSCs within the FL microenvironment remains to be determined.

**Table 7. Identification of hematopoietic progenitors during mouse ontogeny.**

AGM – aorta-gonads-mesonephros; DA – dorsal aorta; EMP – erythro-myeloid progenitors; EryP – primitive erythroid progenitor; HSPC – hematopoietic stem and progenitor cell; UA – umbilical artery; VA – vitelline artery.

| *CELL* | *EryP* | *EMP* | *Pre-HSC/HSPC* | *HSC/HSPC* | | |
|---|---|---|---|---|---|---|
| *STAGE* | Emergence E7.0 – E8.5 | Emergence E8.25-E10.5 | Emergence E9.5-E11.5 | Maturation E10.5 – E12.5 | Maturation E12.5-E16.5 | Steady state Adult |
| *LOCATION* | YS blood islands | YS vascular plexus | DA, VA, UA | AGM, Circulation, FL | FL | BM |
| *MARKERS* | | | | | | |
| KIT | low/+ (1) | + (3, 5, 6) | + (8, 9, 10) | + (9, 10) | + (4) | + (17) |
| CD41 | dim (1, 3) | + (3, 5) | + (8, 4) | +/- (4) | - (13) | - (17) |
| CD34 | + (2) | + (3) | + (9) | + (9) | + | - |
| CD31 | + (2) | + (7) | + (8) | + | + (10, 7) | + (7) |
| FLK1 | + (1, 2, 3) | | | | +/- (10) | - |
| TIE2 | + (1, 2) | | | | | |
| VE-Cadh | + (1, 2) | +/- (5) | + (11) | + (11) | +/- (10, 11) | - (11) |
| CD45 | | +/- (5, 6) | - (8, 4, 10) | +/- (4, 10) | + (11) | + |
| AA4.1 | | + (5, 6) | + (8) | + | + (14, 15, 25) | - |
| CD16/32 | | +/- (5) | | | | |
| Csf1r | | + (6) | | | | |
| Runx1 | + (24) | | + (10) | + (10) | + (10) | + |
| Sca-1 | | | - | -/+ (10, 12) | + (4, 13, 15, 16) | + (17) |
| Endomucin | - (4) | - (4) | + (4) | + (4) | + (4) | + (4) |
| Mac-1 | | | -/+ (9) | -/+ (9) | + (13, 16) | -/low (17) |
| CD150 | | | | | -/+ (13, 28) | + (17) |
| CD48 | | | | | - (13, 28) | - (17) |
| EVI1/MDS1 | | | + (18, 21) | + (18, 21) | + (18, 21) | + (19, 20) |
| HLF | | - (21) | + (21) | + (21) | + (21) | + (22,23) |
| EPCR | | | | | + (26, 28) | + (27,28) |
| ESAM | | | + (31) | + | + (29) | + (30) |

REFERENCES:

(1) (**Isern et al., 2011**), (2) (**Ema et al., 2006**), (3) (**Ferkowicz et al., 2003**), (4) (**Matsubara et al., 2005**), (5) (**McGrath et al., 2015**), (6) (**Perdiguero et al., 2015**), (7) (**Baumann et al., 2004**), (8) (**Bertrand et al., 2005**), (9) (**Sánchez et al., 1996**), (10) (**T. E. North et al., 2002**), (11) (**Taoudi et al., 2005**), (12) (**de Bruijn et al., 2002**), (13)P (**Kim et al., 2006**), (14) (**C. T. Jordan et al., 1990**), (15) (**C. T. Jordan et al., 1995**), (16) (**Morrison et al., 1995**), (17) (**Kiel et al., 2005**), (18) (**Yokomizo et al., 2022**), (19) (**Goyama et al., 2008**), (20) (**Kataoka et al., 2011**), (21) (**Yokomizo et al., 2019**), (22) (**Komorowska et al., 2017**), (23) (**Wahlestedt et al., 2017**) (24) (**T. North et al., 1999**), (25) (**Gao et al., 2022**), (26) (**Iwasaki et al., 2010**), (27) (**Balazs et al., 2006**), (28) (**Kent et al., 2009**), (29) (**Ueda et al., 2019**), (30) (**Lisa Ooi et al., 2009**), (31) (**Melig et al., 2023**)

## WRAP-UP, DISCUSSION AND *OPEN QUESTIONS*

The HS is the most rapidly regenerating system in homeostasis, ensuring immune surveillance and responses, tissue oxygenation, and blood clotting, with millions of cells being created and recycled every day to fulfill those functions. HSCs have been taking all the credit for ensuring the right equilibrium between their maintenance and differentiation into MPPs that can proliferate substantially and further differentiate into multiple lineages. Recent studies indicate a significantly lower contribution of HSCs to active blood production than previously believed (**Busch et al.**, **2015**; **Sun et al.**, **2014**). However, owing to the inherent caveats of cutting-edge technologies used to study hematopoiesis in its native conditions, namely barcoding and fate mapping, further research is warranted to elucidate *how much an HSC actually does*.

During development, the role of HSCs also seems to be secondary to fulfilling the developing embryo needs, as multiple mature lineages arise before the emergence of HSCs and build up a self-sustaining HS until the end of gestation, with some populations persisting throughout life (**Palis**, **2016**). *At which point in development do HSCs contribute to blood production?* An heterogeneous potential of HE cells of the major arteries and a subsequent heterogeneity in generated multipotent cells has been proposed. From these multipotent cells, only a fraction matures into LTR HSCs, contributing to the adult pool (**Yokomizo et al.**, **2022**) and an additional layer of long-lived drMPPs with a lymphoid bias has been proposed (**Beaudin et al.**, **2016**; **Patel et al.**, **2022**). *Is the adult HSPC compartment a mosaic of distinct developmental waves of multipotent cells?*

To understand the establishment of the adult HSC compartment it would be fundamental to precisely quantify *how many cells are generated from the HE fated to become HSCs*. As the estimations from explant cultures (**Rybtsov et al.**, **2016**) and the *Confetti* reporter system (**Ganuza et al.**, **2017**) differ in a big order of magnitude, it is not possible to draw robust conclusions. This knowledge will affect our perception of the FL as an hematopoietic niche. *How many rounds of division lead to the adult HSC pool? Does the FL microenvironment have a role in HSC proliferation?*

HSCs were reported to be in a proliferative state until 3 weeks after birth, shifting into quiescence thereafter (**Bowie et al.**, **2006**). *Does the neonatal BM also sustain HSC expansion? What contributes to the HSC shift into quiescence?* Given that HSC expansion only occurs during the initial stages of development, when the whole organism is growing, the possibility that a general mechanism, rather than a local one is the key to the conundrum, cannot be disregarded.

At mid-gestation, hepatic precursors protrude from the gut tube and expand in cords delaminating through the surrounding STM's cells, which became intermingled with the

hepatoblasts, forming a liver bud, just below a beating heart. Within the liver bud, a vascular plexus is established, connecting the heart to the major efferent vessel of the lower body. At this stage, the diverse hematopoietic layers that arise during development converge into the FL and extravasate into its parenchyma, where they meet conditions supportive/permissive for their proliferation and differentiation. Shortly after, a layer of epithelial cells from the STM surrounds the liver bud (~E11), forming its visceral serous membrane. The liver continues to grow at a fast pace, becoming the major organ of the embryo, easily identifiable by its large size and reddish color. Although the FL microenvironment has received much less attention in research compared to the BM, multiple FL cell types have been reported to play a regulatory role in fetal hematopoiesis at the progenitors' level (maintenance or expansion) and/or supporting the differentiation towards distinct lineages. However, most of these studies have concentrated on analyzing specific cell populations (**Chou & Lodish**, **2010**; **Khan et al.**, **2016**) or identifying the role of a particular cytokine (**Lee et al.**, **2021**), lacking a more comprehensive approach. As such, a clear picture of the interplay of HS-FL stroma is still lacking.

The pioneer stem cell niche hypothesis introduced by Schofield suggested that a stem cell's behavior is determined by its distinct spatial placement, effectively preventing its maturation, and ensuring its continuous maintenance (**Schofield**, **1978**). The posterior extensive research dissecting hematopoietic microenvironments, especially the BM, has gathered evidence that the reality is considerably more intricate. Gomes and colleagues showed that HSCs and MPPs can be in contact or in a short distance from the same mesenchymal progenitor (CAR cell). CAR cells are a potent source of multiple cytokines in the BM: CXCL12 and KITL that regulate the number of HSCs and MPPs, and IL7 that acts as a short-range signal for lymphoid differentiation, among others (**Cordeiro Gomes et al.**, **2016**). The work of Gomes et al. suggests that different signals from the same stromal cell can differentially impact fate decisions. Moreover, a recent study performed an extensive and robust quantitative analysis regarding the location of HSCs in the adult BM in relation to multiple stromal populations (**Kokkaliaris et al.**, **2020**). They found HSCs to be close/direct contact with some populations, but not with others. However, for all cell types assessed, the distribution of HSCs was comparable to the one of RDs. These studies suggest that HSCs do not reside in specific niches within the BM and might co-localize with other downstream progenitors. *What determines fate decisions? Is it a cell intrinsic mechanism?* Miao and colleagues showed that HSC expansion correlated with increased availability of membrane-bound KITL on stromal cell types after depletion of MPPs, suggesting that cellular competition for limiting hematopoietic factors might be fundamental to regulating cell fate (**Miao et al.**, **2022**). *Should we redefine the concept of hematopoietic niche?*

## PROJECT DESCRIPTION

Multiple parameters of a hematopoietic organ can influence the behavior of its cells. This includes not only cell communication but also physical properties, ECM composition and stiffness, the soluble molecular environment, oxygen levels, and more. Given that the FL cell composition has not been extensively studied, we aimed to dissect the FL hematopoietic niche “from the ground up”, by focusing primarily on its cellular content, and the molecular signaling that might be involved in the HS/stroma axis.

Our main aims and objectives were then:

**Aim 1**: Understand the spatial-temporal dynamics of the FL microenvironment during development

- Improve the discrimination of FL non-hematopoietic subsets by FC;
- Confirm their affiliation by single cell multiplex gene expression;
- Screen them for hematopoietic cytokines;
- Identify and quantify their location *in situ*;

**Aim 2**: Reveal HSPC localization in the FL during development

- Optimize a staining strategy robustly enriched for HSCs;
- Identify the location of HSPCs in FL sections throughout development;
- Identity and quantify patterns of cell distributions;

**Aim 3**: Understand the interaction HS/stromal compartment

- Identify and quantify neighbor distributions and distance to specific targets;

# CHAPTER II.

## WHO, WHERE AND HOW: CHARACTERIZATION OF THE KEY PLAYERS IN THE FL HEMATOPOIETIC NICHE

Part of the data in this chapter was published in the following papers:

- Peixoto, M.*; Soares-da-Silva, F.*; Schmutz, S.; Maïlhe, M.P.; Novault, S.; Cumano, A.; Aït-Mansour, C. (2021) "**Identification of fetal liver stromal subsets in spectral cytometry using the parameter autofluorescence**". *Cytometry: Part A.* doi: org/10.1002/cyto.a.24567 *these authors contributed equally (**Annex IV**)
- Peixoto, M.*; Soares-da-Silva, F.*; Bonnet, V.*; Ronteix, G.*; Faria, M.R.; Maïlhe, M.P.; Feng, X.; Pereira, J.P.; Azzoni, E.; Giorgi, A.; de Bruijn, M.; Baroud, C.#; Pinto-do-Ó, P.#; Cumano, A.# (2023) "**Spatiotemporal dynamics of cytokines expression dictate fetal liver hematopoiesis**". *BioRxiv*. doi: https://doi.org/10.1101/2023.08.24.554612 (Manuscript under review) *these authors contributed equally, #senior authorship (**Annex VI**)

## PREAMBLE

A seminal study reported a massive expansion of the HSC compartment in the FL, with a 33 fold increase in RUs from E12.5 to E16.5 (**H. Ema & Nakauchi**, **2000**). However, the extension of this expansion has been recently questioned, and it is still not clear how much maturation (acquisition of LTR potential) rather expansion is the cause of the massive RU increase during FL development. Understanding the contribution of the FL microenvironment to the expansion and/or establishment of the HS is fundamental, as it can enable the development of effective protocols for the HSC manipulation *ex vivo*, providing major clinical advances in the Hematology field.

Key FL non-hematopoietic populations have been identified and proposed to act as hematopoietic niche cells. Cells isolated as $DLK1^{+}SCF^{+}$, considered as hepatic progenitors (**Chou & Lodish**, **2010**), periportal $Nestin^{+}NG2^{+}$ (**Khan et al.**, **2016**), endothelial and SCs (**Lee et al.**, **2021**) were shown to produce hematopoietic supporting factors. Hepatic progenitor cells, endothelial and $Nestin^{+}$ cells were additionally studied in *in vitro* co-culture systems with hematopoietic cells (**Chou et al.**, **2013**; **Chou & Lodish**, **2010**; **Iwasaki et al.**, **2010**; **Khan et al.**, **2016**). However, the *in situ* assessment of the distribution of hematopoietic progenitor cells in the FL produced conflicting findings. One study proposed a close proximity with $Nestin^{+}$ cells (periportal location) (**Khan et al.**, **2016**) while another suggested an association with the sinusoidal vasculature (**Lee et al.**, **2021**). Because the studies conducted so far were focused on single populations or specific time points, a clear picture of how the different populations interact with the developing HS and their role is still lacking. To tackle this, we aimed to perform an extensive characterization of the organ during embryonic development, from early to late gestation, with robust isolation protocols (identifying all non-hematopoietic FL subsets), ascertain their location in the tissue, and screen them for cytokine production (multiple populations at multiple time points).

In previous work by our team, a protocol to isolate the FL stromal subsets was optimized, allowing their identification and characterization in terms of cytokine production (**Soares-da-Silva**, **2020**). Soares-da-Silva et al. identified a population of erythroid progenitors as $KIT^{+}Ter119^{-}CD45^{-}$, which constitutes a significant proportion of the $Ter119^{-}CD45^{-}$ compartment in FL (>70% at E14.5) (**Soares-da-Silva**, **2020**; **Soares-da-Silva et al.**, **2021**). The additional use of CD24/CD71 identified an extra erythroid-committed population, that hasn't yet acquired Ter119 expression. These findings allowed to better resolve the non-hematopoietic compartment in the FL, by excluding $Ter119^{+}$, $CD45^{+}$, $KIT^{+}$, $CD71^{+}$ cells.

Herein, we used spectral cytometry to refine the previous FC characterization of the FL by considering the cells' intrinsic autofluorescence (AF) properties. Spectral FC sets

itself apart from conventional FC through its utilization of prisms to capture a full spectrum of emitted light from laser-excited fluorophores across a range of detectors or channels, rather than detecting individual emitted photons collected by separate detectors. In a multiparametric staining, the resulting spectrum (as exemplified in **Figure 9**), corresponds to the sum of the fluorescence spectrum of each excited fluorochrome. The spectrum can then be deconvoluted, using a Weighted Least Squares Method (WLSM) (**Futamura et al.**, **2015**), to extract the intensities of each fluorochrome. This allows us to consider the intrinsic AF properties of cells, the baseline spectrum for unstained samples, and eliminate its signal from the analysis (**Schmutz et al.**, **2016**) or consider it as an additional independent fluorescent parameter (**Valente et al.**, **2019**; **Wanner et al.**, **2022**).

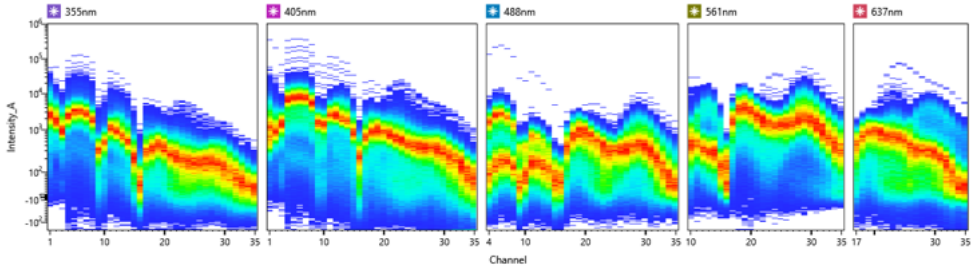


**Figure 9. Full spectrum of FL stromal cells obtained by spectral FC.**
The spectra of emission of E18.5 FL cells depleted of hematopoietic cells and gated on live single cells.

Proteins, NAD(P)H, flavins, and vitamin A are prominent endogenous fluorophores responsible for inducing AF in the adult liver (**Croce et al.**, **2004**, **2010**, **2018**). Cytoplasmatic storage of vitamin A is a unique characteristic of hepatic SCs. In the FL, vitamin A-specific autofluorescent cells were isolated when excited with ultraviolet light by FC (**Kubota et al.**, **2007**). However, this strategy limits the use of ultraviolet-excited fluorochromes. Here, we sought to analyze the AF properties of the FL non-hematopoietic compartment to better discriminate and affiliate these cells. We conducted an extensive spatial-temporal characterization of the FL stromal populations by FC, gene expression and *in situ* localization.

## WHO: DISSECTING THE FL NON-HEMATOPOIETIC COMPARTMENT

To better resolve the FL non-hematopoietic compartment (Ter119$^-$CD71$^-$CD45$^-$KIT$^-$ cells), hematopoietic cells, accounting for more than 90% of the total isolated FL cells were magnetically depleted. The remaining fraction was analyzed using the 14-marker panel described in **Table 8**, including endothelial, lymphatic, epithelial and mesenchymal markers, by spectral FC, at different developmental stages (E12.5, E14.5 and E18.5) (**Figure 10, Supplementary Figure 1, Supplementary Table 1**).

**Table 8. FC panel assembled to discriminate the FL non-hematopoietic compartment.**

| *MARKER* | *MOLECULE NAME* | *SPECTRUM* | *TARGET CELLS* |
|---|---|---|---|
| SAV | Streptavidin | PE-Cy5 | CD45, Ter119, CD71, KIT (hematopoietic cells) biotin |
| E-Cadh/CD324 | Epithelial-Cadherin | PE-Cy7 | Hepatic epithelial cells (hepatoblasts, hepatocytes and cholangiocytes) |
| CD31/PECAM1 | Platelet and endothelial cell adhesion molecule | PerCP-Cy5.5 | Endothelial cells |
| ALCAM/CD166 | Activated leukocyte cell adhesion molecule | FITC | Hepatic epithelial cells and stellate cells |
| PDGFR$\alpha$/CD140a | Platelet derived growth factor receptor | APC | Mesenchymal cells |
| Gp38/PDPN | Podoplanin | APC-Cy7 | Mesothelial cells and lymphatic endothelial cells |
| NG2/CSP4 | Neural glial 2/Chondroitin sulphate proteoglycan 4 | PE | A subset of perivascular cells |
| Sca-1/Ly6a | Stem cell antigen 1/Lymphatic antigen 6 family member A | BV711 | Endothelial cells |
| CD146/MCAM | Melanoma cell adhesion molecule | BV510 | Endothelial and mesenchymal cells |
| CD51/ITAV | Integrin $\alpha$V | BV421 | Mesenchymal and hepatic cells |
| EpCAM/CD326 | Epithelial adhesion molecule | BV605 | Cholangiocytes |
| CD54/ICAM1 | Intracellular adhesion molecule 1 | BUV395 | Hepatic and endothelial cells |
| CD90/Thy1.2 | Cluster of differentiation 90 | AF700 | Mesenchymal cells |
| PI | Dead marker | PI | Dead cells |

**Figure 10** shows a representative gating strategy used to discriminate the FL non-hematopoietic compartment at E18.5 (**Figure 10A**), the time point assessed where more cell types were represented, and how these populations evolve with time (**Figure 10B**, **C**). We categorized the different cell types here discriminated considering: 1. the markers expressed at the surface level (**Figure 10A, Supplementary Figure 1**); 2. cells' intrinsic AF

properties (**Figure 11, 12**); 3. gene expression (**Supplementary Figure 2, 3**); 4. cell localization *in situ* (section "**Where – Mapping the FL**").

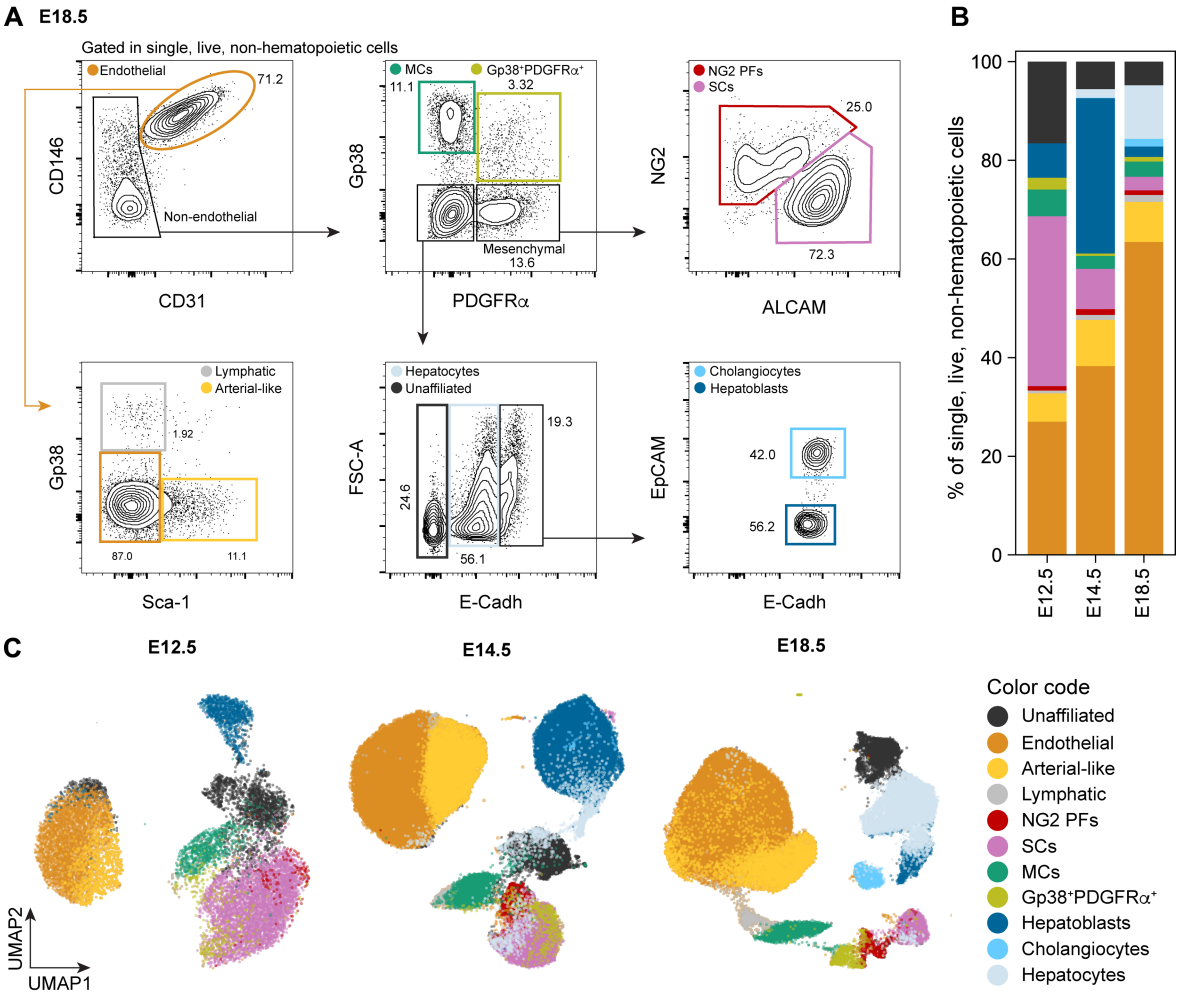


**Figure 10. Global discrimination of the FL non-hematopoietic compartment.**
(**A**) Representative gating strategy used to identify and/or isolate the FL non-hematopoietic cell types ($Ter119^-CD71^-KIT^-CD45^-$ cells) at E18.5, obtained by spectral cytometry, using a 14-marker panel (Table 8). The same strategy was applied to all time points (Supplementary Figure 1A, B). (**B**) Stacked bar plots showing representative proportions of the different non-hematopoietic cell types at E12.5, E14.5 and E18.5, as obtained by FC considering the gating strategy shown in (A). (**C**) Representative UMAP representations of the FL non-hematopoietic compartment throughout development (E12.5, E14.5, E18.5), obtained by spectral FC. Color code correlates to the gating strategy shown in (A).
MCs – mesothelial cells; PFs – portal fibroblasts; SCs – stellate cells.

Endothelial cells, the most represented population, were identified as $CD31^+CD146^+$ cells, expressed high levels of endothelial transcripts *Cdh5, Tek, Kdr, Endoglin,* and *Efnb2*, and were heterogeneous considering *Nestin* and *Lepr* expression (**Supplementary Figure 2A, 3**). Minor sub-populations can be proposed as arterial-like (~10%) and lymphatic (~1-2%), considering Sca-1 (**Kunisaki et al., 2013**) and Gp38 (**Breiteneder-Geleff et al., 1999**; **Saharinen et al., 2004**) expression, respectively. $Gp38^+$ endothelial cells set themselves

apart from the remaining endothelial cells, being $CD54^{-}CD51^{+}CD166^{+}NG2^{dim}$ (**Supplementary Figure 1C**), and clustering separately at the transcriptional level, with enrichment in the expression of *Dlk1, Wt1, Alcam, Krt18* and *Krt19*, and lower levels of *Endoglin, Cdh5* and *Tek* (Cluster II, **Supplementary Figure 2A**).

In non-endothelial cells, Gp38 and PDGFRα further defined two other main populations: $Gp38^{+}$ MCs, expressing the lineage-specific transgenes *Gpm6a, Msln, Wt1, Krt19*; and $PDGFR\alpha^{+}$ mesenchymal cells, expressing *Desmin, Nestin, Pdgfrb, Vcam1, Acta2, Lhx2, Ngfr* (**Supplementary Figure 2B, 3**). We also found a $CD31^{-}Gp38^{+}PDGFR\alpha^{+}$ population, of unclear affiliation. These cells, with some degree of heterogeneity, expressed transcripts of both mesothelial and mesenchymal (**Supplementary Figure 2B, 3**), potentially representing cells undergoing EMT.

Interestingly, not only mesenchymal, as previously described (**Khan et al.**, **2016**), but also lymphatic and MCs expressed high levels of the *Dlk1* transcript, a marker that has been used for the identification and isolation of hepatoblasts (**Chou et al.**, **2013**; **Chou & Lodish**, **2010**; **Tanaka et al.**, **2009**; **Tanimizu et al.**, **2003**).

The FL mesenchymal compartment includes multiple fibroblast cell types, that can be distinguished based on their spatial distribution within the tissue, sub-mesothelial or perivascular, the latter putatively heterogeneous. However, the divergence of these cells at the phenotypic and functional levels is not fully understood. To account for heterogenous perivascular populations, we used two additional markers described for perivascular populations in the FL, NG2 for PFs (**Khan et al.**, **2016**) and ALCAM for SCs (**Asahina et al.**, **2009**). However, identifying distinct populations within the mesenchymal compartment was not immediately evident. Nevertheless, as shown in detail below, considering the characteristic AF properties of SCs, we were able to establish a more solid gating strategy.

In the remaining fraction, E-Cadh and EpCAM identified hepatoblasts ($E\text{-}Cadh^{high}EpCAM^{-}$), hepatocytes ($E\text{-}Cadh^{dim}$) and cholangiocytes ($E\text{-}Cadh^{high}EpCAM^{+}$). At E12.5 and E14.5, hepatic cells consisted primarily of $E\text{-}Cadh^{+}EpCAM^{-}$ hepatoblasts, that expressed high levels of *Dlk1, Afp, Alb, Vcam1, Alcam* and *Hnf4a* (**Supplementary Figure 1, 2B**). A sub-population of these cells expressed the progenitor marker *Lgr5* and co-expressed the proliferative marker *ki67*, potentially representing cells at the apex of the hepatoblast pool, as suggested by Prior and colleagues (**Prior et al.**, **2019**).

With liver maturation, $E\text{-}Cadh^{+}$ hepatoblasts start to differentiate into hepatocytes and cholangiocytes. EpCAM is specifically expressed in cholangiocytes at late gestation (**Tanaka et al.**, **2009**) allowing its clear discrimination in the $E\text{-}Cadh^{+}$ population. While we observed a small fraction of cholangiocytes E14.5 onwards (**Supplementary Figure 1**), it was only after E17.5 that a significant population became distinctly apparent. Cholangiocytes lost expression of *Dlk1*, and *Lgr5,* but kept high levels of *Afp, Alb, Krt18,*

*Prox1, Onecut1,* and *Alcam* and upregulated the cholangiocyte transcripts *Sox4, Sox9, Krt19 and Spp1* (**Supplementary Figure 2C**, Cluster I). Conversely, the discrimination of hepatocytes within the E-Cadh$^{+}$ compartment was more challenging and, once again, was enhanced by incorporating an additional AF signal as a parameter.

### *Autofluorescence as a parameter*

Using the "Autofluorescence Finder" analytical tool of SONY ID7000 spectral cytometer, we found two major AF signals in FL stromal cells (**Figure 11**). One AF signal (AF-1) showed an emission spectrum with 3 emission peaks detected in the 355 and 405 lasers (around 510, 590 and 655 nm) and 2 small emission peaks in the 488 laser (around 510 e 590 nm). The other AF signal (AF-2) had similar emission peaks to AF-1, but additional peaks in the 488 (around 655nm) and 2 smaller peaks in the 561 laser (around 600 and 655 nm). While there was a significant overlap between the two spectra, they exhibited distinct shapes, allowing a proper unmixing, and were used as independent parameters to investigate whether they were specific of a given cell type.

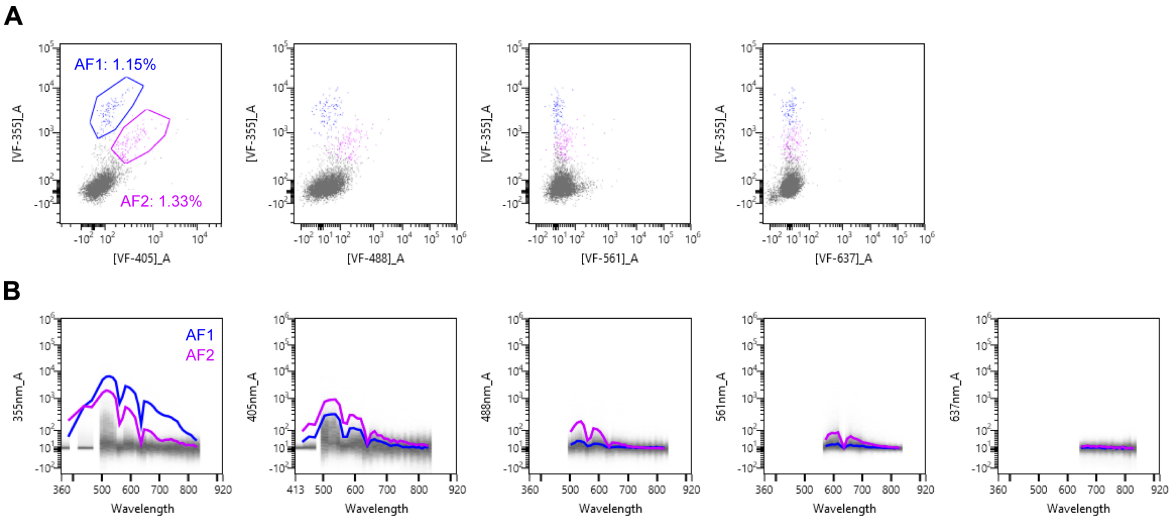


**Figure 11. Identification of two AF profiles in FL stromal cells.**
(**A**) AF is defined manually in the unstained sample, considering the lasers that allow better discrimination of different AF profiles. (**B**) The spectra of emission of the two AF signals in different lasers.

**Figure 12** shows the gating strategy employed in **Figure 10** to trace the affiliation of AF1$^{+}$ and AF2$^{+}$ cells at E18.5. AF1$^{+}$ cells were mainly CD31$^{-}$Gp38$^{-}$PDGFRα$^{+}$ALCAM$^{+}$ NG2$^{-/low}$, which define, with a high degree of enrichment, SCs. On the other hand, AF2$^{+}$ cells were mainly CD31$^{-}$Gp38$^{-}$PDGFRα$^{-}$E-Cadh$^{high}$EpCAM$^{+/-}$.

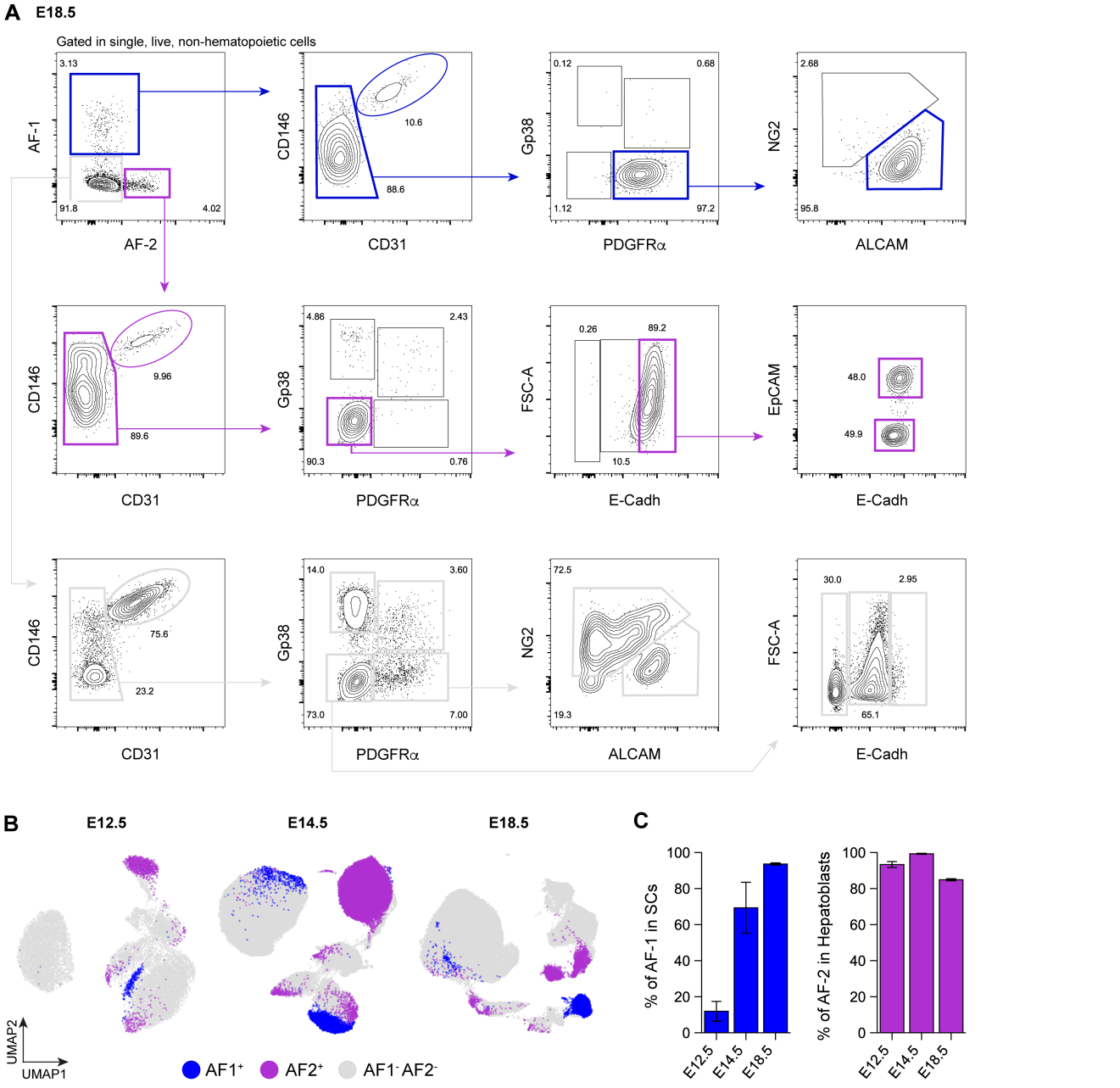


**Figure 12. The distinct AF signals define specific FL stromal populations.**
(**A**) Representative analysis of E18.5 FL live CD45$^-$Ter119$^-$CD71$^-$KIT$^-$ cells to identify AF-1$^+$ (top panel), AF-2$^+$ (middle panel) and AF-1$^-$AF-2$^-$ cells (lower panel) using the same gating strategy as displayed in Figure 10. (**B**) Representative UMAP representation of the FL non-hematopoietic compartment throughout development (E12.5, E14.5, E18.5), showing the overlap of cells that present a specific AF profile (AF1 or AF2), identified by spectral cytometry. (**C**) Percentage of AF1/2$^+$ cells in the cell type where they are mostly represented, PDGFRα$^+$ALCAM$^+$NG2$^{-/low}$ stellate and putative CD324$^{high}$EpCAM$^-$ hepatoblasts, respectively.

SCs AF is well-recognized to be due to the accumulation of vitamin A in cytoplasmatic granules, a hallmark for quiescent mature cells (**Friedman**, **2008**). The percentage of AF-1$^+$ cells in the CD31$^-$Gp38$^-$PDGFRα$^+$ALCAM$^+$NG2$^{-/low}$ increased drastically during liver development, starting at around 10% at E12.5, reaching 70% at E14.5 and surpassing 90% at E18.5 (**Figure 12B, C**), likely following the kinetics of

maturation of SCs. AF-1 was also represented in endothelial cells, but to a low extent. Considering AF-1, a phenotype for SCs was identified. A distinct population could then be discriminated inside the PDGFR$\alpha^+$ population, as NG2$^+$ALCAM$^{-/low}$ cells. These cells were barely detectable at E12.5 and increased in frequency as development progressed (**Figure 10**, **Supplementary Figure 1**). Comparing the two mesenchymal populations at the transcriptional level, we found a similar profile, considering the expression of *Endoglin, Nestin, Pdgfrb, Vcam1, Acta2, Desmin, Lhx2 and Ngfr* (**Supplementary Figure 2B, 3**).

The proportion of AF-2 within E-Cadh$^{high}$EpCAM$^-$ cell population consistently exceeded 80%, reaching nearly 100% at E14.5 (**Figure 12C**). Conversely, E-Cadh$^{dim}$ did not exhibit AF-2, while cholangiocytes were all AF-2$^+$ (**Figure 12A**). Based on this, we propose that AF-2 serves as a distinguishing feature of hepatoblasts, which is lost during hepatocyte differentiation while remaining present in newly differentiated cholangiocytes. Because we lack functional evidence for a hepatoblast affiliation of E-Cadh$^{hi}$EpCAM$^-$AF-2$^+$ (e.g., bipotentiality), we thereby call these cells hepatoblast-like.

To further characterize the AF of FL cells and determine whether this is a cell-intrinsic property, if it is induced by the enzymatic treatment or lost during manipulation we analyzed the AF profiles of mechanical/enzymatic dissociated FL cells and re-analyzed cells after sorting. The AF profiles were also detected after mechanical dissociation of the cells, however, the frequencies and numbers of AF-1$^+$, AF-2$^+$ and other stromal populations were remarkably reduced (data not shown), consistent with the previous observation that mechanical dissociation is not suited for FL viable stromal cell recovery (**Soares-da-Silva**, **2020**). Re-analyzing cells after sorting, considering the gating strategy employed in **Figure 10**, we confirmed that the majority of sorted SCs were AF-1$^+$, while E-Cadh$^{dim}$ were AF-1$^-$ AF-2$^-$ (**Annex IV**). As expected, because E-Cadh$^{dim}$ and E-Cadh$^{high}$ were not well separated, the sorting purity of E-Cadh$^{high}$ was compromised (only around 70%), but 40% of the cells retained AF-2 emission. These results indicated that AF in FL populations is a cell-intrinsic property.

We analyzed postnatal livers to see if hepatoblast-like cells were still present after birth. The previously detected AF signals remained present and specific to the same populations. However, by P3, we observed a significant reduction in the proportion of E-Cadh$^{high}$EpCAM$^-$ cells, which, notwithstanding, kept the same proportion of AF-2$^+$ cells as at E18.5 (**Figure 13**). Interestingly, the amount of AF-2$^+$ cells in the cholangiocytes population was considerably reduced from ~95% at E18.5, to ~20% at P3, suggesting that cholangiocytes lose the factors responsible for AF-2 during maturation. Considering the absence of specific markers for adult hepatic progenitor cells, these findings present a promising step toward enhancing their identification. However, further studies are warranted to validate AF-2 as a consistent hallmark of hepatoblast-like cells throughout ontogeny.

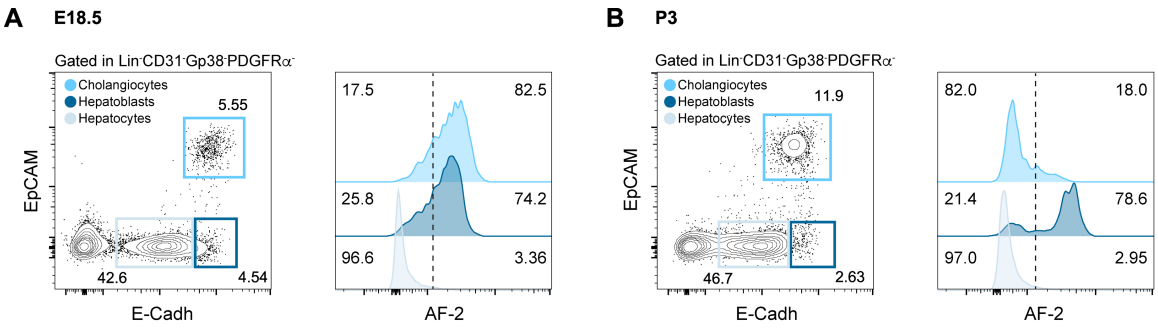


**Figure 13. AF-2 defines hepatoblast-like cells after birth.**

(**A-B**) Representative analysis of Lin (CD45, Ter119, KIT, CD71)$^{-}$CD31$^{-}$Gp38$^{-}$PDGFRα$^{-}$ E18.5 (A) and P3 (B) liver cells considering AF-2 emission.

## WHERE: MAPPING THE FL

The FL landscape is dominated by hematopoietic cells, mainly of erythroid affiliation (**Figure 14**). The hematopoietic composition of the FL will be detailed in **Chapter IV**.

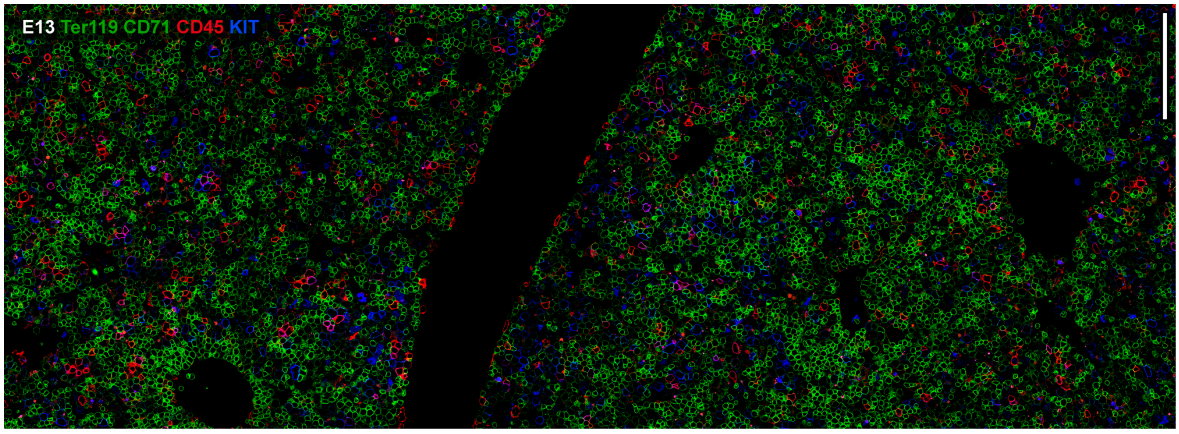


**Figure 14. FL landscape is dominated by hematopoietic cells.**
Single stack IF of E13.5 FL with Ter119 and CD71 (green), CD45 (red) and KIT (blue). Scale bar 200μm.

Previously, we identified the distribution of FL stromal populations *in situ,* by conventional IF in cryosections (7-10μm) (**Soares-da-Silva**, **2020**). However, the loose structure of the FL posed a significant challenge in obtaining high-quality sections. Additionally, we aimed to gain a deeper understanding of the intricate spatial organization of the organ and identify the cellular interactions between the hematopoietic/stromal compartments, to which we believed a good coverage of FL sections with 3D resolution was fundamental. We then optimized an IF protocol for vibratome sections (100-200μm) for multiple hematopoietic and stromal markers and we used a simple and robust commercially available clearing reagent (RapiClear®) to allow deep light penetration and good quality multi-stack image acquisitions.

From early stages, major stromal populations were easily identified with a simple 3-color staining strategy (**Figure 15**): hepatoblasts, evenly scattered throughout the parenchyma, were recognized by their expression of HNF4α; the intricate vascular and perivascular network of the FL, and additionally, the mesothelial layer at the periphery could be mapped using CD146; and LHX2 additionally helped to identify the perivascular and sub-mesothelial mesenchymal cells.

Except for the vascular network, which undergoes extensive remodeling during the early stages (**Crawford et al.**, **2010**), no major morphological changes occur during the organs' fast growth until E16.5, when the liver shifts into metabolic functions.

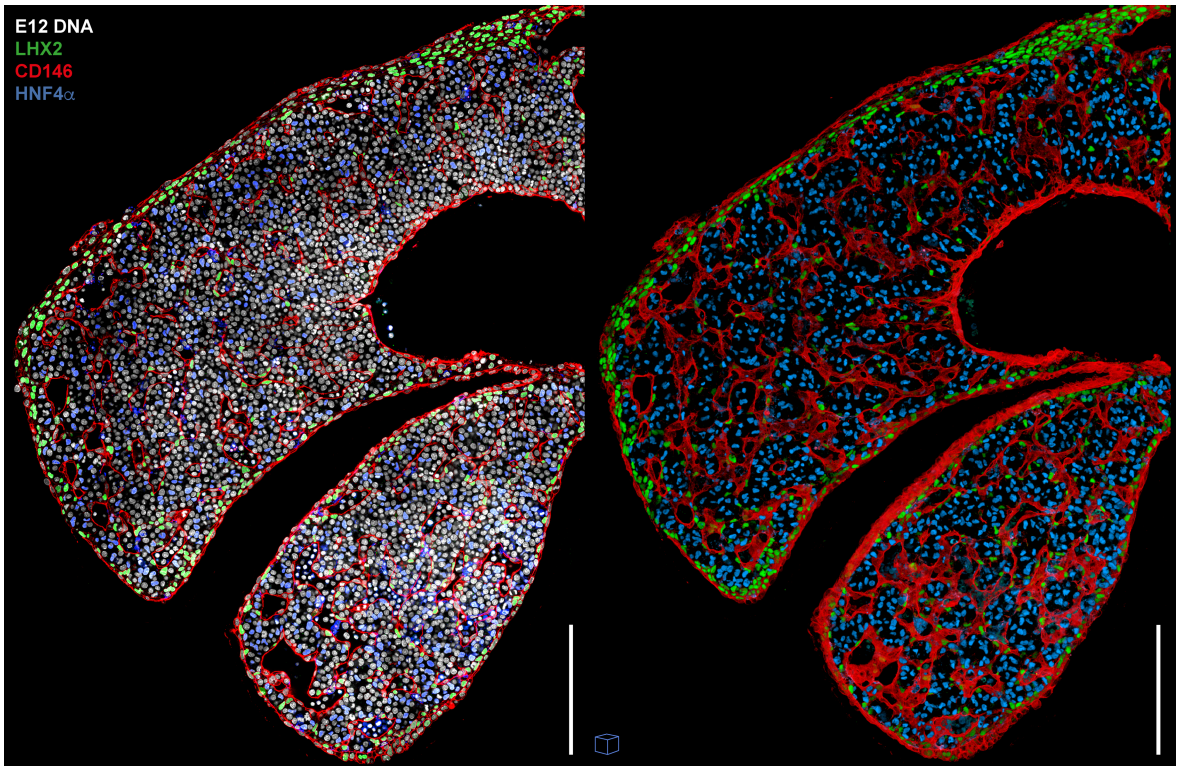


**Figure 15. LHX2, CD146 and HNF4α allow the discrimination of major FL stromal populations.** Single stack (left) or 3D view (15μm, right) IF of a E12 FL section with DAPI (white), LHX2 (green), CD146 (red), and HNF4α (blue). Scale bar 100μm.

At E11.5, the liver sinusoids appeared as large capillary-like channels (**Figure 16A**), which subsequently matured into a smaller and well-organized sinusoidal network (**Figure 16B**). Interestingly, we often observed sinusoids of larger caliber near the periphery (**Figure 16A,** *), suggesting that these regions might contain more immature sinusoids.

Sca-1 is commonly used in the BM to identify small-caliber arterioles (**Kunisaki et al., 2013**). We found a small fraction of endothelial cells expressing Sca-1 by FC, from early stages (**Figure 10, Supplementary Figure 1A, B**), that were also identified *in situ* (**Figure 16C**).

The mesenchymal compartment of the FL, which can be broadly evaluated using PDGFRα, exhibited two primary distribution patterns: perivascular and sub-capsular (**Figure 16B, D**). LHX2 and Desmin were also mesenchymal-specific, covering the majority of the compartment (**Figure 16A, B, D-F, Supplementary Video 1**). The expression of these 3 markers was found across any type of vascular structure: sinusoids, and main vessels. A distinguishing feature between the two was the expression of αSMA, only expressed by the main vessels: central and portal veins, with the latter being surrounded by a particular type of mesenchymal cells, the PFs, identified by the expression of NG2, and at late stages by the appearance of bile ducts ($EpCAM^+$) in their vicinity (**Figure 16G**). Consistent with the FC data, during early stages, NG2 perivascular cells were relatively

scarce, only found in the vicinity of the portal veins (portal sinus) in the center of the FL sections (**Figure 16H**). As development progressed, these cells became more abundant, and their spatial distribution expanded significantly, aligning with the growth of the portal network (**Figure 16G**). ALCAM allowed the discrimination between mesenchymal sub-compartments by FC, and we were able to assess its expression profile in the tissue (**Figure 16I**). However, ALCAM is not specific, having a broad expression across other stroma populations, namely hepatic (**Supplementary Figure 1C, Figure 16I, Supplementary Video 2**), hindering a clear visual discrimination between perivascular populations.

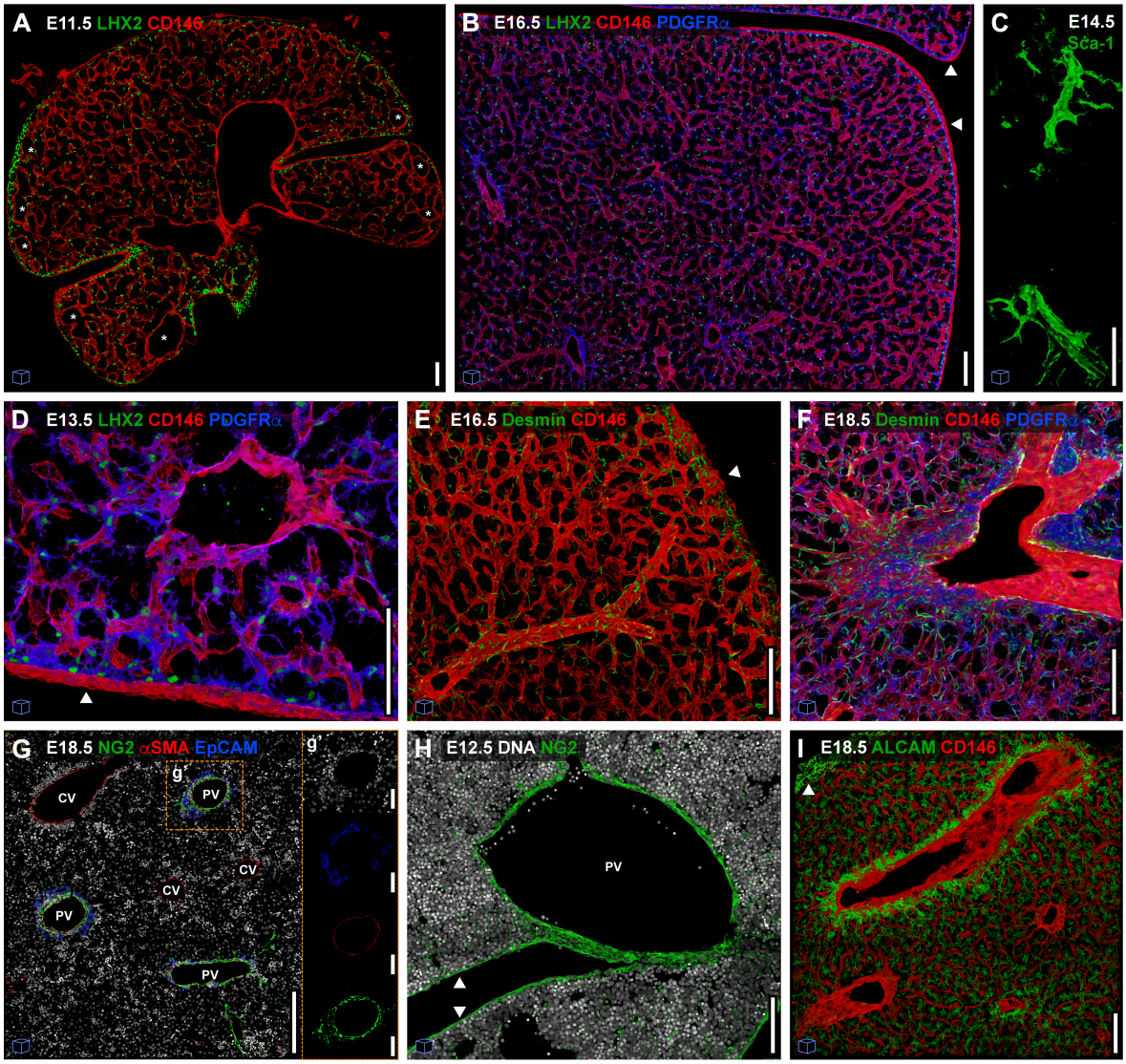


**Figure 16. Vascular and perivascular compartments along FL development.**
(**A**) 3D view (20 μm) IF of a E12 FL section with LHX2 (green) and CD146 (red). Asterisks represent large sinusoids at the liver's periphery. (**B**) 3D view (25 μm) IF of a E16.5 FL section with LHX2 (green) and CD146 (red) and PDGFRα (blue). (**C**) 3D view (50 μm) IF of a E14.5 FL section with Sca-1 (green). (**D**) 3D view (30 μm) IF of a E13.5 FL section with LHX2 (green), CD146 (red) and PDGFRα (blue). (**E**) 3D view (50 μm) IF of a E16.5 FL section with Desmin (green) and CD146 (red). (**F**) 3D view (50 μm) IF of a E18.5 FL section with Desmin (green), CD146 (red) and PDGFRα (blue). (**G**) 3D view (10 μm) IF of a E18.5 FL section with DNA (white), NG2 (green), αSMA (red) and EpCAM

(blue). The insert **g'** shows the channels separated for the selected region. (**H**) 3D view (20 μm) IF of a E12.5 FL section with DNA (white) and NG2 (green). (**I**) 3D view (50 μm) IF of a E18.5 FL section with ALCAM (green) and CD146 (red). Arrowheads indicate the mesothelium. Scale bars 100 μm.
CV – central vein; PV – portal vein.

At the periphery of the liver, MCs were easily recognized by their flattened morphology, forming a single epithelial layer, and expressing CD146, Gp38, and WT1 (**Figure 17A, B**). NG2 was commonly observed to be expressed in MCs (**Figure 16H**), as previously reported (**Ogawa et al.**, **2018**). However, its expression was not uniformly distributed throughout the entire area, with regions with low or no NG2 expression (data not shown). As reported (**Asahina et al.**, **2009**), WT1 stains either mesothelial and sub-MCs. We additionally found a few $WT1^+$ perivascular cells close to the periphery, but the intensity of staining decreased with the distance from the periphery, suggesting that WT1 is downregulated as sub-MCs migrate into the parenchyma (data not shown).

Interestingly, we often found at the tips of the liver lobes an accumulation of sub-MCs, expressing PDGFRα, LHX2, CD146 and Gp38 (**Figure 17C, D**). These cells are likely to represent the small population of $Gp38^+PDGFR\alpha^+$ cells we found by FC. Of note, at early stages we found a thick multi-layer of sub-MCs in some peripheral regions (**Figure 17E**), and the typical monolayer in others, once again, revealing some heterogeneity in the composition of cells of the liver's outermost layers. At later stages, we continued to find an accumulation of sub-MCs at the tips of the lobes, but no longer an organization in multi-layers elsewhere (**Figure 17F**).

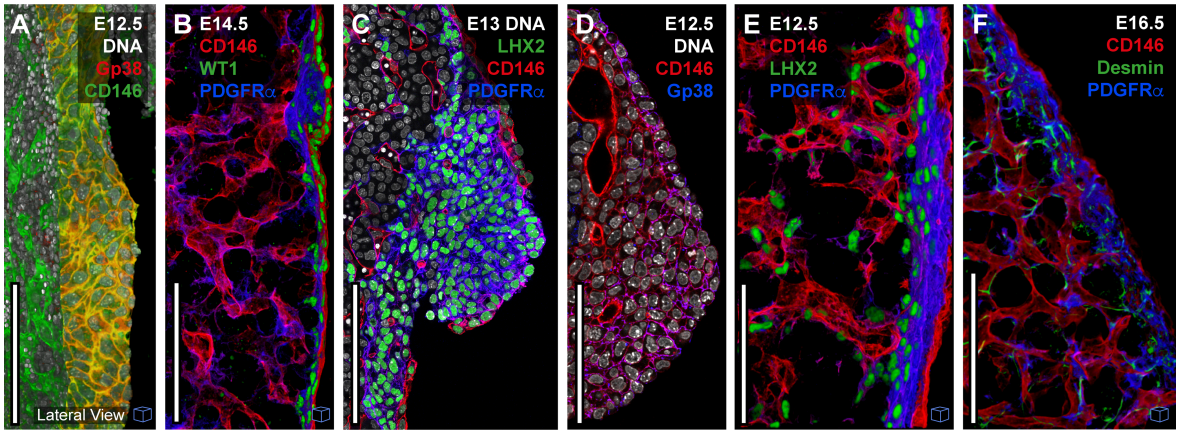


**Figure 17. Mesothelium and sub-mesothelium.**
(**A**) 3D view (50 μm) IF of a E12.5 FL section with DNA (white), Gp38 (red) and CD146 (green). (**B**) 3D view (30 μm) IF of a E14.5 FL section with CD146 (red), WT1 (green), and PDGFRα (blue). (**C**) Single stack IF of a E13 FL section with DNA (white), LHX2 (green), CD146 (red) and PDGFRα (blue). (**D**) Single stack IF of a E12.5 FL section with DNA (white), CD146 (red) and Gp38 (blue). (**E**) 3D view (50 μm) IF of a E12.5 FL section with CD146 (red), LHX2 (green) and PDGFRα (blue). (**F**) 3D view (50 μm) IF of a E16.5 FL section with CD146 (red), Desmin (green) and PDGFRα (blue). Scale bars 100 μm.

E16.5 marks a turning point in the liver's architecture: we observed a shift from a heavy densely packed organ, mainly constituted by hematopoietic cells, with an even distribution of hepatic cells (HNF4$\alpha^{+}$) (**Figure 18A**); to a less packed structure, with increased representation of hepatic cells, namely hepatocytes, that became juxtaposed, with a geometrical morphology (**Figure 18B, C**). Hepatocytes were identified as E-Cadh$^{dim}$, while E-Cadh$^{high}$ cells were only observed around the vessels, where EpCAM$^{+}$ cholangiocytes were starting to form.

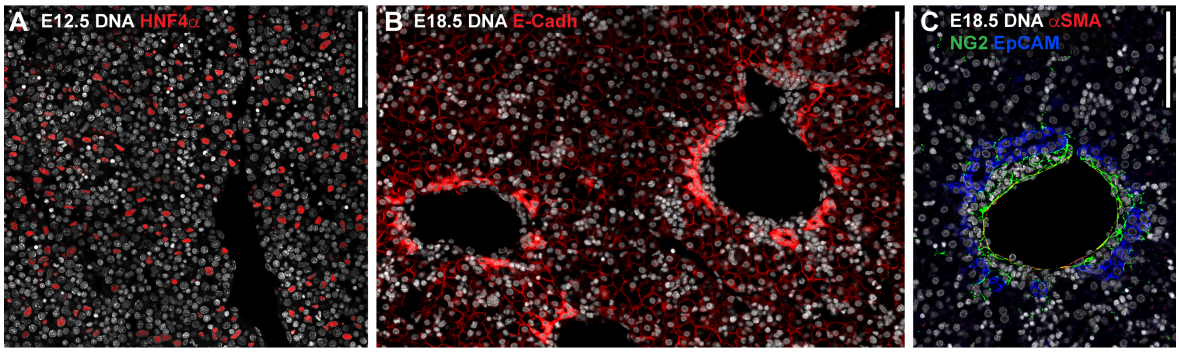


**Figure 18. Hepatic compartment along FL development.**
(**A**) Single stack IF of E12.5 FL with DNA (white), and HNF4$\alpha$ (red). (**B**) Single stack IF of E18.5 FL with DNA (white), and E-Cadh (red). (**C**) Single stack IF of E18.5 FL with DNA (white), $\alpha$SMA (red), NG2 (green) and EpCAM (blue). Scale bars 50 $\mu$m.

Although after E16.5 hepatocytes became the dominant liver population, the recovered yield we obtained after cell suspension preparation was very low and varied substantially between isolation (**Figure 11**, **Supplementary Table 1**).

## HOW: SCREENING FOR CYTOKINE PRODUCTION

Cytokines are instrumental in an hematopoietic microenvironment, as they regulate cell behavior, namely its maintenance, proliferation, differentiation, mobilization, and cellular interactions. We screened the expression of six relevant hematopoietic factors from the four major FL stromal populations ($CD31^{+}CD146^{+}$ endothelial, $CD31^{-}Gp38^{-}PDGFR\alpha^{-}E\text{-}Cadh^{high}$ hepatic, $CD31^{-}Gp38^{+}PDGFR\alpha^{-}$ mesothelial, and $CD31^{-}Gp38^{-}PDGFR\alpha^{+}$ mesenchymal) at multiple stages throughout liver development by bulk quantitative real-time polymerase chain reaction (qRT-PCR) to identify which stromal populations might have a role in hematopoietic development and the kinetics of cytokine expression (**Figure 19A**).

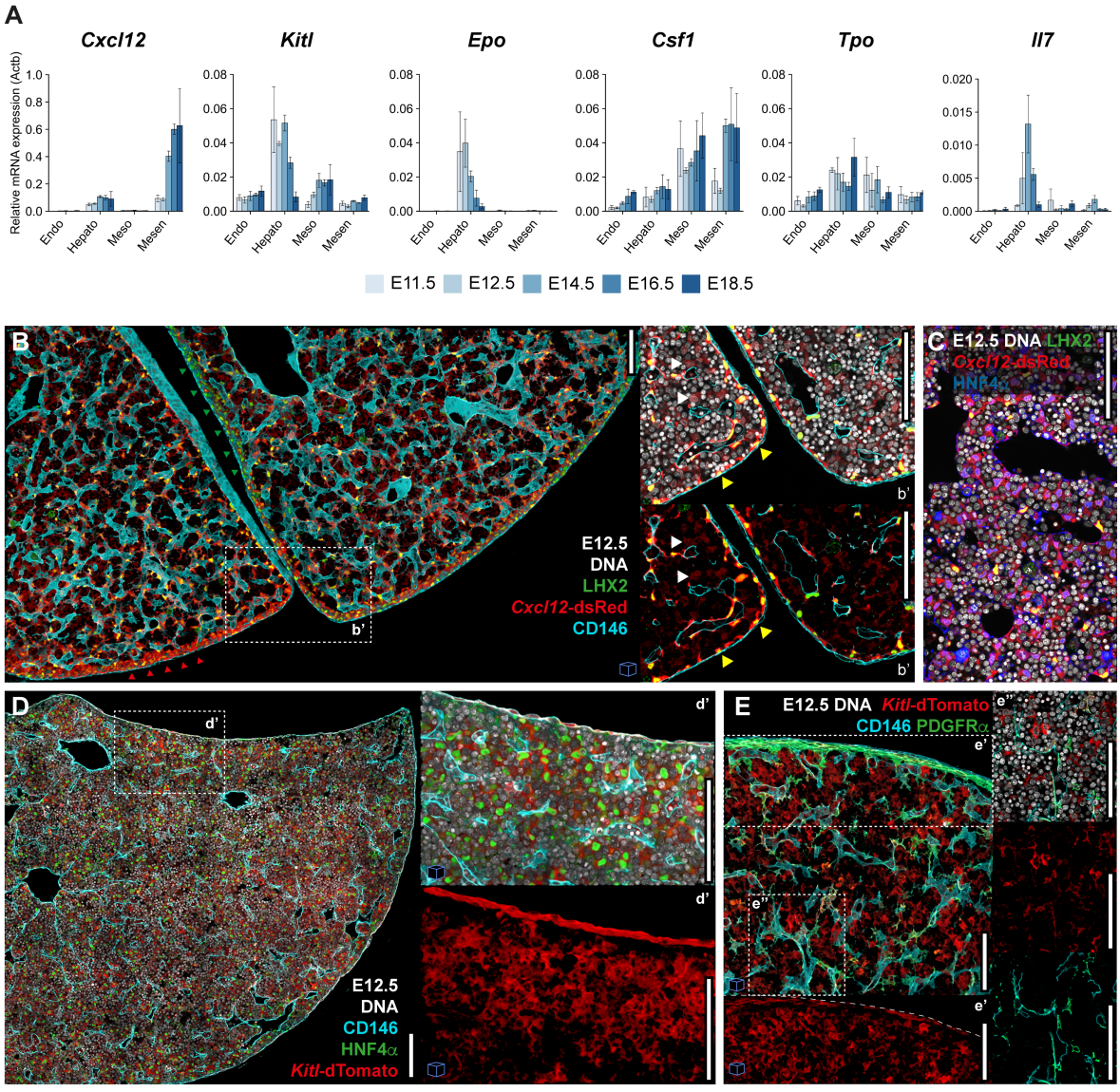


**Figure 19. Supportive hematopoietic cytokines are produced by multiple stromal populations.** (**A**) qRT-PCR analysis of the expression levels of the hematopoietic cytokines *Cxcl12, Kitl, Epo, Thpo, Il7, Csf1* in endothelial (Endo), hepatic (Hepa), mesothelial (Meso), and mesenchymal (Mesen) cells throughout development (E11.5, E12.5, E14.5, E16.5, E18.5) (n=3). (**B**) 3D view (25 μm) IF of

E12.5 FL (*Cxcl12*-dsRed mice) with LHX2 (green), *Cxcl12*-dsRed (red) and CD146 (cyan). Red arrowheads point to a periphery region with *Cxcl12*-dsRed$^{bright}$ cells, while green arrowheads indicate a region with *Cxcl12*-dsRed$^{dim}$ cells. Insert **b'** shows an enlarged single stack view of the selected region. DNA is represented in white. Yellow arrowheads indicate cells with high expression of *Cxcl12*, that co-stain LHX2. White arrowheads indicate cells with low expression of *Cxcl12*, LHX2$^{-}$. (**C**) Single stack IF of E12.5 FL (*Cxcl12*-dsRed mice) with DNA (white), LHX2 (green), *Cxcl12*-dsRed (red) and HNF4$\alpha$ (blue). (**D**) Single stack IF of E12.5 FL (*Kitl*-tdTomato mice) with DNA (white), HNF4$\alpha$ (green), *Kitl*-tdTomato (red) and CD146 (cyan). Inserts **d'** show an enlarged 3D view (20 $\mu$m) of the selected regions. (**E**) 3D view (15 $\mu$m) IF of E12.5 FL (*Kitl*-tdTomato mice) with PDGFR$\alpha$ (green), *Kitl*-tdTomato (red) and CD146 (cyan). Inserts **e'** and **e''** show an enlarged 3D view or single stack of the selected regions, respectively. The dashed line in e' represents the mesothelial layer. Scale bars 100 $\mu$m.

We found that hepatoblasts are major cytokine producers, expressing all cytokines assessed, at all stages, being the biggest producers of *Kitl* at early stages and the only producers of *Epo* and *Il7*. Endothelial cells, key cytokine producers in multiple hematopoietic microenvironments (**Azzoni et al.**, **2018**; **Ding et al.**, **2012**), expressed constant intermediate levels of *Kitl* and *Thpo*, and low, but increasing levels of *Csf1*. *Il7*, only expressed by hepatoblasts, was detected at very low levels, with a peak at E14.5. At early stages, *Cxcl12* was expressed by hepatoblasts and mesenchymal cells at similar levels, but while levels from hepatoblasts did not change considerably with time, mesenchymal cells strongly upregulated *Cxcl12* expression. *Kitl*, *Csf1*, and *Thpo* were expressed by the four stromal populations. Remarkably, MCs, that have not yet been implicated as hematopoietic regulators, expressed *Kitl* at comparable levels to endothelial cells at early stages, and higher from E14.5 onwards.

Interestingly, *Igf2*, encoding an important growth factor during development (**Sélénou et al.**, **2022**) was expressed at very high levels by nearly all FL stromal populations (**Supplementary Figure 2**).

To assess how the expression of *Cxcl12* and *Kitl*, major hematopoietic factors for progenitors, correlates with the cellular distribution of the expressing cells, we analyzed two reporter mice *in situ*, the *Cxcl12*-dsRed (**Ding & Morrison**, **2013**) (**Figure 19B, C, Supplementary Video 3**) and *Kitl*-tdTomato (**Buono et al.**, **2016**) (**Figure 19D, E, Supplementary Video 4**).

Two levels of intensity were discriminated for *Cxcl12*. *Cxcl12*-dsRed$^{brigh}$ cells co-expressed LHX2 in perivascular cells and sub-mesothelial regions (**Figure 19B**). However, the expression of *Cxcl12* in the sub-mesothelium was heterogeneous, with some regions highly expressing *Cxcl12* (**Figure 19B**, red arrowheads), while others appearing to express low-to-no levels (**Figure 19B**, green arrowheads). Cells with a dull expression of *Cxcl12* were evident in parenchymal cells (**Figure 19Bb'**, white arrowheads) co-expressing HNF4$\alpha$

(**Figure 19C**). In accordance with the single-cell gene expression analysis, all hepatoblasts and most mesenchymal cells expressed *Cxcl12* (**Supplementary Figure 4A**).

*Kitl* expression *in situ* could also be attributed to multiple cell types. Virtually all HNF4$\alpha^+$ cells, distributed throughout the parenchyma, were *Kitl*-tdTomato$^+$ (**Figure 19D**). As suggested by the single-cell data, a sub-population of MCs and a few mesenchymal cells also expressed *Kitl* (**Figure 19D, Ee'**; **Supplementary Figure 4A**). However, despite endothelial cells displaying a consistently high expression of Kitl, due to their flat morphology, the specific cellular source of *Kitl* in the vicinity of endothelial cells remains unclear *in situ*, as it often coincides with PDGFR$\alpha$ staining (**Figure 19Ee'', Supplementary Video 4**).

To understand how the FL cytokine levels compare to other hematopoietic microenvironments, we additionally assessed cytokine expression in the BM, from two major stromal populations: endothelial cells (CD31$^+$) and a population enriched in mesenchymal cells (CD51$^+$CD106$^+$), putatively CAR cells, the major cytokine producer in the BM (**Baryawno et al., 2019**) (**Figure 20A**). Because BM development is only initiated at the late stages of gestation and suffers major changes in the first weeks after birth, we analyze multiple time points, from postnatal days 7, 14 and 21 (**Figure 20B**). Except for *Epo*, which is expressed in the kidney from late gestation to adulthood (**Suzuki et al., 2011**), and not in the BM, all other cytokines were expressed at significantly higher levels by the CD106$^+$ BM cells. However, the levels of expression by FL cells were higher or similar to BM endothelial cells (**Figure 20B**). These observations indicate that the FL stromal populations are less proficient in cytokine production, which might result in a comparatively lower cytokine-rich environment in the FL, as compared to the BM.

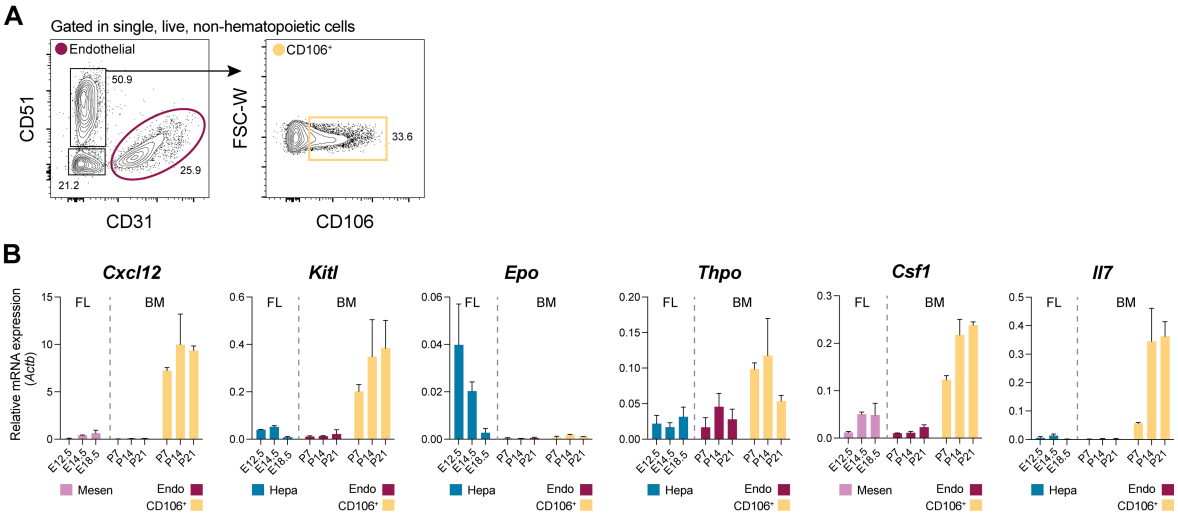


**Figure 20. The FL is a putative low cytokine environment.**
(**A**) Gating strategy used for the analysis of the stroma of P7, P14 and P21 BM using the surface markers CD51, CD31 and CD106. Representative profile of a P7 BM. The same strategy was applied to all time points. (**B**) qRT-PCR analysis of the expression levels of the hematopoietic cytokines

*Cxcl12, Kitl, Epo, Thpo, Csf1* and *Il7* in mesenchymal (pink) or hepatic (blue) cells of E12.5, E14.5 and E18.5 FL and endothelial (dark red) or $CD51^{+}CD106^{+}$ (yellow) cells of P7, P14 and P21 BM. For each cytokine, only the FL population with the highest expression level is represented: Mesen (pink) for *Cxcl12* and *Csf1* and Hepa (blue) for *Kitl, Epo, Thpo* and *Il7* (n=3).

## DISCUSSION

In this study, we conducted a comprehensive analysis of the FL stromal compartment over a significant embryonic time window, spanning from the early stages, shortly after the arrival of hematopoietic cells, to late gestation. By FC, we identified 10 cell types (some of which are specific to late stages) that could be classified into 4 major populations: endothelial ($CD31^+CD146^+$), hepatic ($CD31^-Gp38^-PDGFR\alpha^-E\text{-}Cadh^+$), mesenchymal ($CD31^-Gp38^-PDGFR\alpha^+$) and mesothelial $CD31^-Gp38^+PDGFR\alpha^-$).

The possibility of detecting specific AF profiles by using spectral FC enabled us to enhance our existing 14-markers panel by incorporating two additional parameters. As a result, we achieved a significant improvement in our ability to discern the FL stromal compartment. The two independent AF signals detected differed in shape and intensity along the spectrum and could be specifically assigned to different cell types.

Although lacking validation, as it was beyond this project's scope, our results suggest that AF-2 serves as a marker to identify hepatoblasts in adults. In accordance, we only found $E\text{-}Cadh^{high}$ cells in the portal zone, coherently with the current belief that a hepatic stem cell niche exists in the biliary tree at the level of the Canals of Hering (**Darwiche & Petersen**, **2010**).

We confirmed the affiliation of FC-resolved cell types by single-cell multiplexed gene expression and were able to identify their location *in situ* using multiple markers. Overall, 3 markers were sufficient to simultaneously identify the majority of FL stromal cell types at early stages by imaging: LHX2/Desmin/PDGFRα for the mesenchymal compartment; HNF4α for hepatic cells, and CD146 for the vascular and perivascular network, and additionally, the mesothelial layer.

The comparative analysis of all hematopoietic stromal subsets demonstrated that these cell types constitute a multicellular niche network, with promiscuous expression of hematopoietic factors. Hepatoblasts are major cytokine producers, being the most potent source of *Kitl*, a unique source of *Il7* and *Epo*, and also expressing *Cxcl12*, *Thpo* and *Csf1*. Notably, *Kitl* is also expressed by a subset of MCs, and to a lower extent, by endothelial and mesenchymal cells. At early stages, *Cxcl12* is expressed at comparable levels by both hepatoblasts and mesenchymal cells. While hepatoblasts maintain these levels nearly constant until the end of gestation, mesenchymal cells exhibit a significant upregulation of *Cxcl12* expression throughout liver development. Using the reporter mice model *Cxcl12*-dsRed (**Ding & Morrison**, **2013**), we confirmed that *Cxcl12* is restricted to hepatoblasts and mesenchymal populations (perivascular and sub-mesothelial). However, contrarily to what we could anticipate from the gene expression data, we saw two levels of expression of dsRed between cell types at E12.5: $dsRed^{dim}HNF4\alpha^+$ and $dsRed^{high}LHX2^+$ cells. This is also

not in agreement with the recent data from Hebling et al., which shows similar levels of expression between the two cell types using a similar knock-in mice model (*Cxcl12-GFP*) at E13.5 (**Helbling et al.**, **2023**, pre-print).

PFs Nestin$^{+}$NG2$^{+}$ were identified as major players in the FL hematopoietic niche, producing *Cxcl12, Kitl, Igf2 and Angptl3* (**Khan et al.**, **2016**). This work, however, did not compare this population with other stromal cell types, and the negative control used (Ter119$^{-}$CD45$^{-}$CD31$^{-}$Nestin$^{-}$) included a big population of erythroid committed progenitors, as shown elsewhere (**Soares-da-Silva et al.**, **2021**), diluting the contribution of other cytokine-expressing populations. In our data, *Cxcl12* is mainly expressed by mesenchymal cells, both PFs, SCs, and sub-MCs.

NG2 is also expressed in a subset of MCs, that we identify as a novel element of the FL hematopoietic niche, as *Kitl-, Csf1-* and *Thpo-* expressing cells. NG2$^{+}$ cell depletion might, therefore, result in unpredictable consequences for the integrity of the mesothelial compartment and for the organ architecture and could also contribute to the modest decrease in HSC observed by (**Khan et al.**, **2016**).

Cytokine/chemokine depletion in specific cell types is a widely employed approach to functionally assess stromal populations within hematopoietic microenvironments, particularly in the BM (reviewed by (**Crane et al.**, **2017**; **Gao et al.**, **2018**)). Following this strategy, Lee and colleagues constitutively depleted *Kitl* (*Scf*) from hepatic, hematopoietic, NG2$^{+}$ PFs, endothelial and SCs (**Lee et al.**, **2021**). At E15.5, depletion of *Kitl* from any of these FL populations demonstrated no discernible impact on the number or function of HSCs. However, deletion of *Kitl* from SCs led to a loss of HSCs at P0, and this decline in HSCs was strongly amplified when depleting *Kitl* from both endothelial and SCs. Our findings demonstrate that *Kitl* is produced by multiple cell types during liver development. Consequently, the depletion of *Kitl* from one source is likely to be compensated for by other cellular sources. Supporting this hypothesis is the observation that hepatoblasts function as the main producers of *Kitl* until E16.5, after which they exhibit a notable downregulation in *Kitl* expression. Thus, it is plausible that hepatoblasts alone may not be adequate to compensate for the depletion of *Kitl* at birth from SCs, let alone from both endothelial and SCs. This observation provides a valid explanation for the phenotypic outcomes reported by Lee et al. *Ezh2* inactivation in FL endothelial cells resulted in the overall depletion of the membrane-bound form of KITL, through overexpression of metalloproteinase (MMP)9. This, in turn, led to severe anemia and lethality at around E13.5 (**Neo et al.**, **2018**). These two studies suggest that the source of KITL in the FL does not seem to be determinant to FL hematopoiesis, as long as KITL availability is ensured.

Although the levels of *Il7* expression in hepatoblasts are very low, co-cultures with hepatoblasts (but not other stromal populations) and LSK supported B lineage cell

differentiation (Cumano's lab, *not published*). Moreover, the low concentrations of IL7 in the FL are pivotal for the generation of FL common lymphoid progenitors (FL CLPs), that will originate the first wave of thymic seeding progenitors (**Berthault et al.**, **2017**); and for B1 B cell selection for autoreactive specificities (**Wong et al.**, **2019**). YS-derived erythroid progenitors were shown to have a lower threshold response to EPO, being able to outcompete HSC-derived progenitors for access to low concentrations of EPO in the FL.

Using the reporter mice models, we showed here that *Cxcl12* and *Kitl* are broadly expressed throughout the FL. When comparing the levels of transcripts in sorted FL and BM stromal populations, we saw a big disparity between the two niches. Although we cannot directly infer the protein levels and availability of these factors, a relatively low cytokine environment and a higher threshold for cytokine response in HSC could explain their limited contribution to fetal hematopoiesis (**Yokomizo et al.**, **2022**). If this scenario holds true, a cytokine-protected environment could be fundamental to prevent differentiation of HSCs.

DLK1 expression has been considered a reliable marker for hepatoblasts (**Tanaka et al.**, **2009**; **Tanimizu et al.**, **2003**). However, the comparative analysis of all stromal subsets indicates that *Dlk1* is also expressed in lymphatic endothelial cells, mesothelial and mesenchymal cells. Consequently, relying solely on this marker for hepatoblast purification could inadvertently include additional stromal components within the isolated population, that also produce hematopoietic cytokines (**Chou et al.**, **2013**; **Chou & Lodish**, **2010**).

The phenotype of a considerable proportion of FL stromal cells could not be identified with the set of markers used (unaffiliated cells). Noteworthy, isolated CD31$^-$Gp38$^-$ PDGFR$\alpha^-$E-Cadh$^-$ cells express little or no levels of genes characteristic of the other non-hematopoietic or hematopoietic cell types and incorporate lower levels of Hoechst, compared to the other cell types, suggesting they are no longer viable cells (Cumano's lab, *not published*).

In parallel to this project, Helbling and colleagues also conducted an extensive characterization of the FL stroma (**Helbling et al.**, **2023**, pre-print). They employed *Cxcl12*$^{GFP}$ and *Kitl*$^{GFP}$ mouse models to screen for the expression of these cytokines in FL cells, reaching a similar conclusion regarding the broad expression of supportive HSC niche factors within FL stromal cells, and the downregulation of hematopoietic factors in hepatic cells with maturation, from E16.5 onwards.

## MATERIALS AND METHODS

### Mice

C57BL/6J mice were purchased from Envigo. Fixed *Cxcl12*$^{DsRed/+}$ (**Ding & Morrison**, **2013**) and *Kitl*-tdTomato (**Buono et al.**, **2016**) embryo samples were kindly provided by J. P. Pereira and M. FTR. de Bruijn, respectively. Timed pregnant females with vaginal plug after overnight mating were considered to be E0.5. Pregnant females were sacrificed by $CO_2$ inhalation, and cervical dislocation as a confirmation method. For embryos older than E15.5, decapitation was performed. All animal manipulations were performed according to the ethics charter approved by the French Agriculture Ministry and to the European Parliament Directive 2010/63/EU.

### Isolation of FL non-hematopoietic cells

E11.5 - E18.5 FLs were dissected under a binocular magnifying lens and recovered in Hanks' balanced-salt solution (HBSS) supplemented with 1% fetal calf serum (FCS) (Gibco), cut in 1 $mm^2$ pieces, and treated with 0.05 mg/mL Liberase TH (Roche) and 0.2 mg/mL DNase (Sigma) for 6-8 minutes at 37ºC. Enzymatic treatment was stopped by the addition of cold HBSS + 1%FCS followed by centrifugation. FLs were depleted of hematopoietic cells ($Ter119^+CD45^+KIT^+CD71^+$ cells) using MACS columns (Miltenyi Biotec) according to manufacturer instructions. Briefly, cells were incubated with biotinylated Ter119, CD45, Kit and CD71 antibodies for 20-30 min at 4ºC, washed twice, incubated with anti-biotin microbeads (Miltenyi Biotec) for 20 min at 4 ºC and passed through a LS column (Miltenyi Biotec). The flow-through was collected and used for cell surface staining, after filtered in a 100 μm cell strainer (BD). In an independent experiment, FL cells were analyzed after mechanical dissociation (in two biological replicates; *data not shown*).

### Isolation of BM non-hematopoietic cells

Femurs and tibias were isolated from P7, P14, and P21 mice and surrounding tissues were removed. Bones were flushed using a syringe (26-G) with HBSS + 2% FCS (Gibco). BM clumps were re-suspended by gentling aspirating with a 19-G needle, filtered (100μm) and kept on ice. Bones were crushed with a scissor in a way to maximize the internal bone surface area exposition and incubated with a digestion buffer (1mg/mL Collagenase VIII and 0.2 mg/mL DNase (Sigma) in HBSS with 2% FCS) for 15 min at 37ºC with rotation. Cell suspensions were collected, filtered (40μm), and kept on ice. 3 rounds of digestion were performed, and cell suspensions collected from each were pooled together with the flushed ones.

Enzymatic treatment was stopped by the addition of cold HBSS + 1%FCS followed by centrifugation. Cell suspensions were depleted of hematopoietic cells using MACS columns (Miltenyi Biotec) according to manufacturer instructions. Briefly, cells were incubated with biotinylated Ter119, CD45, CD11b and B220 antibodies for 20-30 min at 4ºC, washed twice, incubated with anti-biotin microbeads (Miltenyi Biotec) for 20 min at 4 ºC and passed through a LS column (Miltenyi Biotec). The flow-through was collected and used for cell surface staining, after filtered in a 100 μm cell strainer.

**FC and cell sorting**

5% of the cells were not passed through the MACS column and were used as before depletion control, 5% of the eluted cells were used as unstained control and the remaining were incubated for 20–30 min at 4°C in the dark with directly labeled antibodies (and streptavidin). Dead cells were excluded by incorporation of Propidium Iodide (PI). **Supplementary Table 2**, **3** and **4** shows the antibody panels used for the spectral cytometry analysis and cell sorting of FL and BM, respectively. FL stained cells were analyzed on an ID7000 Spectral Analyzer (SONY) and FL/BM were sorted with a BD FACS Aria III (BD Biosciences) according to the guidelines for the use of FC and cell sorting (**Cossarizza et al.**, **2019**). Data were analyzed with SONY ID7000 Analyzer, FlowJo software (v.10.8.2, BD Biosciences) and Jupyter Notebooks as described in '**Cytometry Analysis**' below.

**Cytometry Analysis**

Acquired unstained samples ($Ter119^{-}CD71^{-}CD45^{-}KIT^{-}$ cells) were analyzed using the AF finder function of the SONY ID7000 Analyzer. AF was defined manually in cells that show fluorescence, considering the lasers that allow better discrimination (as shown in **Figure 11**)). Once identified, the AF signals were incorporated in the unmixing matrix. Acquired full spectra are analyzed with algorithms based on the WLSM as described previously (**Futamura et al.**, **2015**). The accuracy of the unmixing is ensured by the analysis of the single-stained samples. Further manual adjustments (usually not required) can be done.

FC files were screened for abnormalities (flow rate, signal acquisitions, and dynamic range) using a quality control plugin in FlowJo, FlowAI (**Monaco et al.**, **2016**). Only "GoodEvents" were considered for analysis. UMAPs were performed to dimensionally reduction of the FC data in FlowJo (**McInnes et al.**, **2020**), on gated single, live, non-hematopoietic cells. For each stromal population defined, the corresponding channel values for the UMAP parameters were saved as .csv and plotted using Jupyter Notebooks (**Kluyver et al.**, **2016**).

**Gene expression by qRT-PCR**

Cells were sorted directly into lysis buffer, and mRNA was extracted (RNeasy Micro Kit Qiagen, Cat. 74004), reverse transcribed (PrimeScript RT Reagent Kit, Takara Bio, Cat. RR037A), and qPCR was performed with Power SYBR Green PCR Master Mix (Applied Biosystems, Cat. 4304437) (see **Supplementary Table 5**). qPCR reactions were performed on a Quantstudio3 thermocycler (Applied Biosystems). Gene expression was normalized to that of *β-actin*, and relative expression was calculated using the $2^{-\Delta Ct}$ method.

**FL sectioning, immunostaining, and optical clearing of thick sections**

FLs from time-pregnant females were collected directly into freshly prepared 2% paraformaldehyde (PFA) fixative buffer (Fischer Scientific) and kept at 4°C overnight under rotation. After washing in PBS and removing surrounding tissues, FLs were immediately sectioned or shortly stored at 4ºC until sectioning. Following FLs embedding in 4% low-melting agarose (Sigma), 150 µm frontal sections were performed using a Leica VT1200S vibratome. Sections were permeabilized and blocked with PBS containing 0.05% Tween-20 (AppliChem GmbH) [or 0.5% Triton-X 100 for nuclear staining] and 10% donkey serum (Sigma-Aldrich) for 1-2 hours (h) at room temperature (RT). This solution was also used to dilute primary and secondary antibodies. Sections were incubated with primary antibodies for 2h at RT and overnight at 4ºC, and secondary antibodies for 2h at RT, both in the dark and with rotation (see **Supplementary Table 6** and **7**). Between incubations and after secondary antibody incubation, sections were washed repeatedly with PBS containing 0.05% Tween-20 and 3% NaCl (minimum 4×, 15 min). Sections were counterstained with DAPI (D9542, Sigma-Aldrich) for 2h at RT and kept overnight in RapiClear 1.52 (SunJin Lab) for optical clearing. Sections were mounted in RapiClear and imaged on a Leica TCS SP8 using a PL APO 63x /1.40 oil immersion lens or APO 40x /1.40 oil immersion lens. Single stacks or multi-stacks tile scans were acquired at 200Hz or 400Hz, respectively, in bidirectional mode, at 12-bits and 1024×1024 resolution. Multi-stacks were acquired with z spacing of 0.3 µm.

# SUPPLEMENTARY INFORMATION

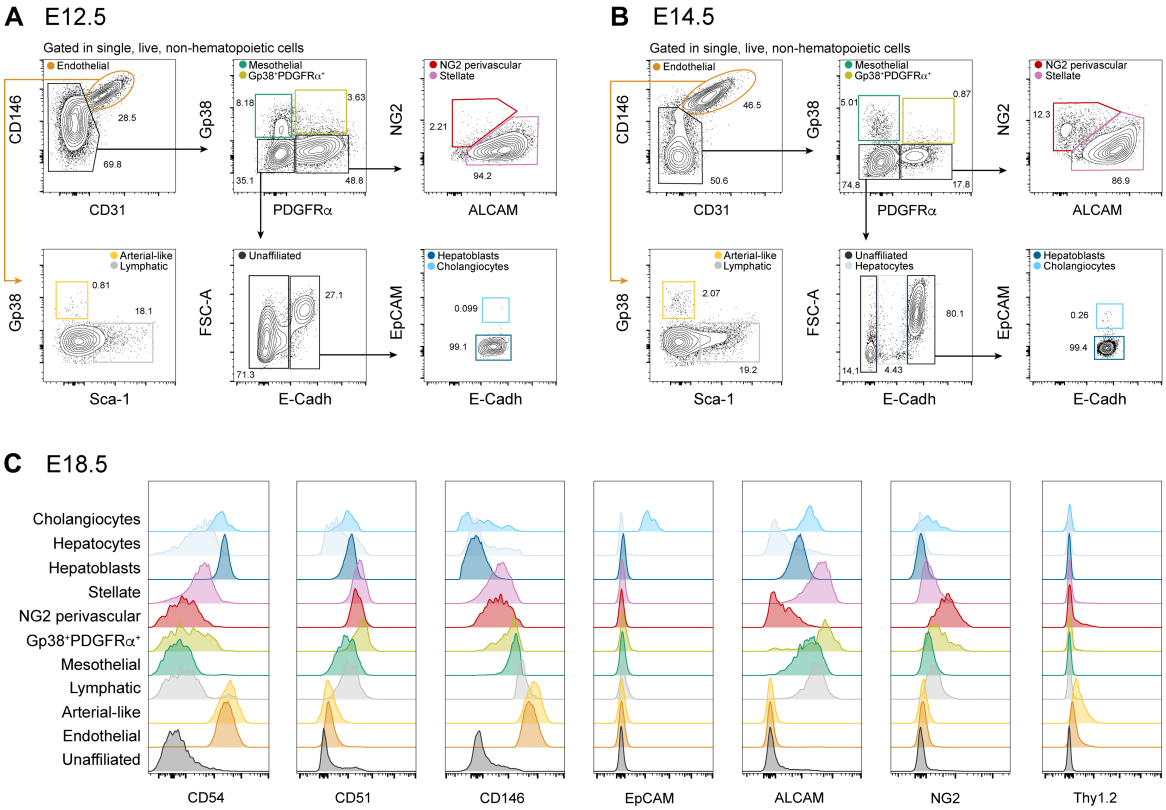


**Supplementary Figure 1. FC profile of the FL non-hematopoietic compartment during development.**

(**A, B**) Representative gating strategy used to identify and/or isolate FL non-hematopoietic cell types obtained by depletion of Ter119, CD71, KIT and CD45 cells at E12.5 (A) and E14.5 (B). (**C**) Representative histogram representation for the expression of CD54, CD51, CD146, EpCAM, ALCAM, NG2 and Thy1.2 for each gated population at E18.5.




**Supplementary Figure 2. Single-cell gene expression of FL non-hematopoietic populations.** (**A-C**) Heatmap of single cell multiplex qPCR in sorted endothelial (A), mesenchymal and MCs (B), and hepatic cells (C) of E12.5 and E18.5 FLs. Each column represents a single cell, and it is color-coded according to time point (E12.5, E18.5) and cell type. Gene expression was normalized to $\beta$-

*Actin* and *Gapdh*, and unsupervised hierarchical clustering was performed. Experiments performed and analyzed by **Soares-da-Silva, F**. For further details, see Annex V.

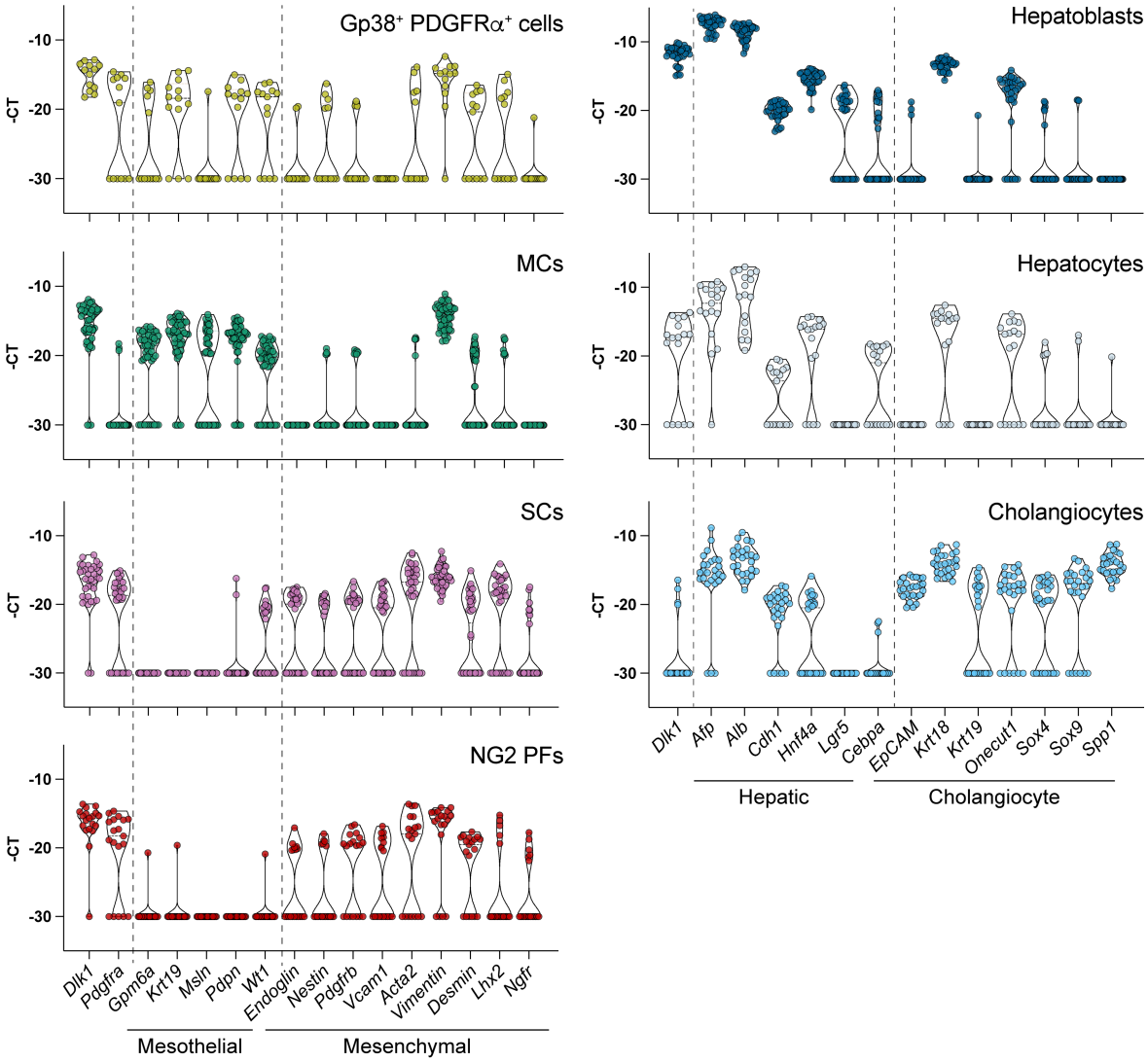


**Supplementary Figure 3. Single-cell gene expression of lineage-associated transcripts in FL non-hematopoietic populations.**
Violin plot representation of single-cell qPCR of sorted FL stromal populations at E12.5 and/or E18.5. Except for the hepatic populations, E12.5 and E18.5 data were merged. Each dot represents a cell. Gene expression was normalized to *β-Actin* and *Gapdh*. Experiments performed and analyzed by **Soares-da-Silva, F**. For further details, see Annex V.

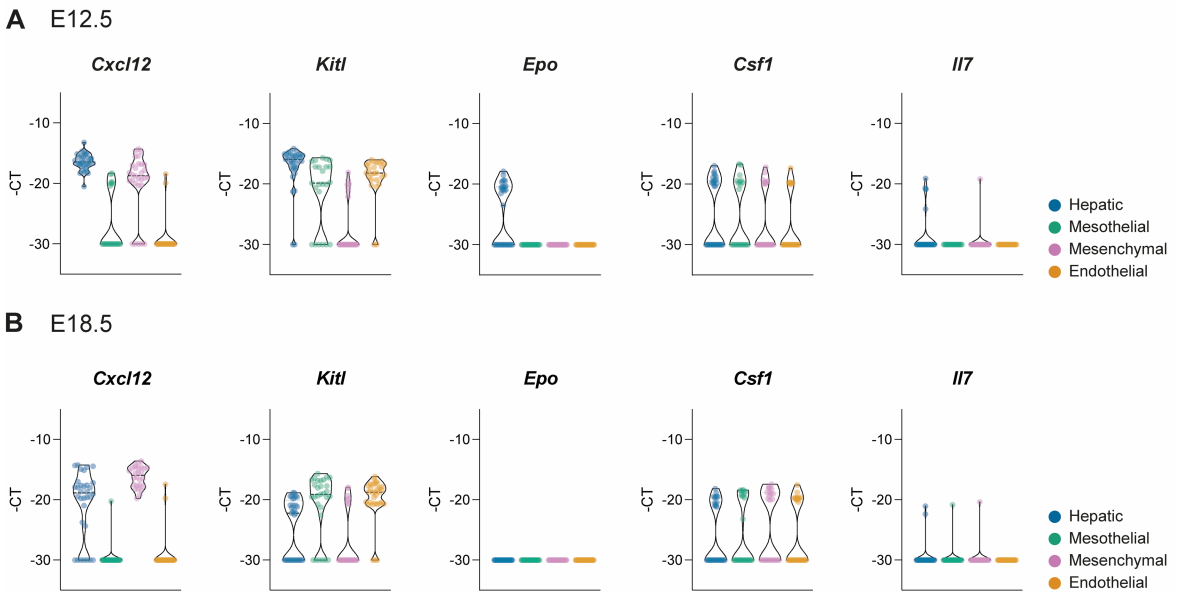


**Supplementary Figure 4. Single-cell gene expression of hematopoietic cytokines of FL major non-hematopoietic populations.**
Violin plot representation of single-cell qPCR of sorted major FL stromal populations at E12.5 and E18.5. Each dot represents a cell. Gene expression was normalized to *β-Actin* and *Gapdh*. Experiments performed and analyzed by **Soares-da-Silva, F**. For further details, see Annex V.

**Supplementary Video 1. The intricate vascular and perivascular network of the E18.5 FL.**
Video of a multi-stack or a rotative 3D view (50 μm) IF of a E18.5 FL section with Desmin (green), CD146 (red) and PDGFRα (blue). Scale bar 100 μm.

**Supplementary Video 2. ALCAM displays a widely distributed expression pattern across FL populations.**
Video of a multi-stack and a rotative 3D view (50 μm) IF of a E18.5 FL section with ALCAM (green), CD146 (red) and NG2 (magenta). Scale bar 100 μm.

**Supplementary Video 3. Pattern of expression of *Cxcl12* in *Cxcl12*-dsRed reporter mice at E12.5.**
Video of a multi-stack and a rotative 3D view (25 μm) IF of a E12.5 FL section with LHX2 (green), Cxcl12-dsRed (red) and CD146 (cyan). Scale bar 100 μm.

**Supplementary Video 4. Pattern of expression of *Kitl* in *Kitl*-tdTomato reporter mice at E12.5.**
Video of a multi-stack and a rotative 3D view (20 μm) IF of a E12.5 FL section with LHX2/HNF4α (green), Cxcl12-dsRed (red) and CD146 (cyan). Scale bar 100 μm.

**Supplementary Table 1. Percentages of FL non-hematopoietic populations throughout development.**

Data from spectral cytometry (SONY ID7000) and sorting experiments were considered (FACS Aria), following the gating strategy indicated in Figure 10 and Supplementary Figure 1. Data are represented as mean ± standard deviation percentages of single, live, $Ter119^{-}CD71^{-}KIT^{-}CD45^{-}$ cells. The number of independent experiments is indicated in between parentheses.

MCs – mesothelial cells; PFs – portal fibroblasts; SCs – stellate cells.

| *STAGE* | *Endothelial* | *Lymphatic* | *Arterial-like* | *Mesenchymal* | *NG2 PFs* | *SCs* |
|---|---|---|---|---|---|---|
| E12.5 | 33.93 ± 3.92 (3) | 0.33 ± 0.10 (3) | 6.21 ± 1.05 (3) | 28.73 ± 3.73 (3) | 0.44 ± 0.22 (3) | 27.73 ± 3.12 (3) |
| E14.5 | 50.13 ± 9,89 (13) | 0.69 ± 0.25 (13) | 9.40 ± 0.56 (7) | 7.63 ± 2.40 (13) | 1.17 ± 0.60 (11) | 5.89 ± 1.28 (11) |
| E18.5 | 62.05 ± 10. 09 (6) | 1.12 ± 0.51 (6) | 8.46 ± 0.53 (2) | 3.23 ± 0.64 (6) | 0.63 ± 0.41 (6) | 2.43 ± 0.68 (6) |

| *STAGE* | *MCs* | *$Gp38^{+}$ $CD140\alpha^{+}$* | *Hepatoblasts* | *Cholangiocytes* | *Hepatocytes* | *Unaffiliated* |
|---|---|---|---|---|---|---|
| E12.5 | 5.57 ± 0.93 (3) | 2.00 ± 0.74 (3) | 8.42 ± 3.11 (3) | - | - | 14.07 ± 2.95 (3) |
| E14.5 | 3.05 ± 1.51 (13) | 0.81 ± 0.35 (13) | 24.15 ± 10.16 (13) | 0.10 ± 0.09 (7) | 2.67 ± 0.87 (7) | 9.03 ± 5.71 (13) |
| E18.5 | 3.08 ± 1.93 (6) | 0.28 ± 0.28 (6) | 2.45 ± 0.95 (6) | 1.17 ± 0.66 (6) | 17.44 ± 8.55 (6) | 5.83 ± 4.05 (6) |

**Supplementary Table 2. List of antibodies used for the analysis of FL stromal populations by spectral FC.**

| *SPECIFICITY* | *CONJUGATION* | *CLONE* | *REFERENCE* | *SUPPLIER* |
|---|---|---|---|---|
| CD45 | Biotin | 30-F11 | 1115520 | Sony Biotechnology Inc. |
| Ter119 | Biotin | TER-119 | 1181020 | Sony Biotechnology Inc. |
| CD71 | Biotin | RI7217 | 1169015 | Sony Biotechnology Inc. |
| KIT | Biotin | 2B8 | 1129020 | Sony Biotechnology Inc. |
| E-Cadh | PE-Cy7 | DECMA-1 | 1336545 | Sony Biotechnology Inc. |
| CD31 | PerCP-Cy5.5 | MEC13.3 | 1112610 | Sony Biotechnology Inc. |
| CD166 | FITC | eBioALC48 | 11-1661-82 | eBioscience |
| PDGFRα | APC | APA5 | 135908 | BioLegend |
| Gp38 | APC-Cy7 | 8.1.1 | 1237090 | Sony Biotechnology Inc. |
| NG2/AN2 | PE | 1E6.4 | 130-100-468 | Miltenyi Biotec |
| Sca-1 | BV711 | D7 | 1140655 | Sony Biotechnology Inc. |
| CD146 | BV510 | ME-9F1 | 740200 | BD Biosciences |
| CD51 | BV421 | RMV-7 | 740062 | BD Biosciences |
| EpCAM | BV605 | G8.8 | 740389 | BD Biosciences |
| CD54 | BUV395 | 3E2 | 740222 | BD Biosciences |
| Thy1.2 | AF700 | 30-H12 | 1126595 | Sony Biotechnology Inc. |
| Streptavidin | PE-Cy5 | - | 2626025 | Sony Biotechnology Inc. |

**Supplementary Table 3. List of antibodies used for cell sorting of FL stromal populations.**

| *SPECIFICITY* | *CONJUGATION* | *CLONE* | *REFERENCE* | *SUPPLIER* |
|---|---|---|---|---|
| CD45 | Biotin | 30-F11 | 1115520 | Sony Biotechnology Inc. |
| Ter119 | Biotin | TER-119 | 1181020 | Sony Biotechnology Inc. |
| CD71 | Biotin | RI7217 | 1169015 | Sony Biotechnology Inc. |
| KIT | Biotin | 2B8 | 1129020 | Sony Biotechnology Inc. |
| E-Cadh | AF488 | DECMA-1 | 53-3249-82 | eBioscience™ |
| CD31 | PerCP-Cy5.5 | MEC13.3 | 1112610 | Sony Biotechnology Inc. |
| CD166 | APC | eBioALC48 | 17-1661-82 | eBioscience™ |
| PDGFRα | PE-Cy7 | APA5 | 1279560 | Sony Biotechnology Inc. |
| Gp38 | APC-Cy7 | 8.1.1 | 1237090 | Sony Biotechnology Inc. |
| NG2/AN2 | PE | 1E6.4 | 130-100-468 | Miltenyi Biotec |
| Sca-1 | BV711 | D7 | 1140655 | Sony Biotechnology Inc. |
| CD146 | BV510 | ME-9F1 | 740200 | BD Biosciences |
| CD51 | BV421 | RMV-7 | 740062 | BD Biosciences |

| | | | | |
|---|---|---|---|---|
| EpCAM | BV605 | G8.8 | 740389 | BD Biosciences |
| CD54 | BUV395 | 3E2 | 740222 | BD Biosciences |
| Streptavidin | BV785 | - | 2626245 | Sony Biotechnology Inc. |

**Supplementary Table 4. List of antibodies used for cell sorting of BM stromal populations.**

| *SPECIFICITY* | *CONJUGATION* | *CLONE* | *REFERENCE* | *SUPPLIER* |
|---|---|---|---|---|
| CD45 | Biotin | 30-F11 | 1115520 | Sony Biotechnology Inc. |
| Ter119 | Biotin | TER-119 | 1181020 | Sony Biotechnology Inc. |
| CD11b | Biotin | M1/70 | 1106020 | Sony Biotechnology Inc. |
| B220 | Biotin | RA3-6B2 | 1116020 | Sony Biotechnology Inc. |
| CD31 | AF488 | MEC13.3 | 1112570 | Sony Biotechnology Inc. |
| CD51 | BV421 | RMV-7 | 740062 | BD Biosciences |
| CD106 | PE-Cy7 | MVCAM.A | 105720 | BioLegend |
| Streptavidin | BV785 | - | 2626245 | Sony Biotechnology Inc. |

**Supplementary Table 5. List of primers used for qRT-PCR.**

| *PRIMER* | *GENE ID* | *FW SEQUENCE (5'-3')* | *RV SEQUENCE (5'-3')* | *PRIMERBANK ID* |
|---|---|---|---|---|
| *Actb* | 11461 | GCTTCTTTGCAGCTCCTTCGT | ATCGTCATCCATGGCGAACT | 291045236c3 |
| *Csf1* | 12977 | GTGTCAGAACACTGTAGCCAC | TCAAAGGCAATCTGGCATGAAG | 166064045c1 |
| *Cxcl12* | 20315 | TGCATCAGTGACGGTAAACCA | TTCTTCAGCCGTGCAACAATC | 7305465a1 |
| *Epo* | 13856 | ACAAAGCCATCAGTGGTCTACG | TCTGGAGGCGACATCAATTCC | 113931667c2 |
| *Il7* | 16196 | TTCCTCCACTGATCCTTGTTCT | AGCAGCTTCCTTTGTATCATCAC | 6680433a1 |
| *Kitl* | 17311 | GAATCTCCGAAGAGGCCAGAA | GCTGCAACAGGGGGTAACAT | 198596a1 |
| *Thpo* | 21832 | AACCCAGACGGAACAGAGC | GTGCTGCCATCACTCCCTC | 118130856c2 |

**Supplementary Table 6. List of primary antibodies used for IF.**

| *ANTIBODY* | *SPECIES* | *CLONE* | *REFERENCE* | *SUPPLIER* |
|---|---|---|---|---|
| αSMA | Mouse | 1A4 | A5228 | Sigma-Aldrich |
| CD146 | Sheep | Poly | AF6106 | R&D |
| CD166 | Rat | eBioALC48 | 14-1661-82 | Invitrogen |
| Desmin | Rabbit | Poly | ab8592 | abcam |
| DsRed | Rabbit | Poly | 632496 | TAKARA |
| E-Cadh | Rabbit | 24E10 | 3195S | Cell Signaling |
| EpCAM-AF647 | Rat | G8.8R | FAB8998R | R&D |
| Gp38 | Hamster | 8.1.1 | NB600-1015 | Novus Biologicals |
| HNF4α | Mouse | K9218 | MA1-199 | ThermoFischer |
| LHX2 | Rabbit | Poly | ABE1402 | Sigma-Aldrich |
| NG2 | Rabbit | Poly | AB5320 | Sigma-Aldrich |
| PDGFRα | Goat | Poly | AF1062 | R&D |
| WT1 | Rabbit | CAN-R9(IHC)-56-2 | ab89901 | abcam |

**Supplementary Table 7. List of secondary antibodies used for IF.**

| *ANTIBODY* | *CONJUGATION* | *REFERENCE* | *SUPPLIER* |
|---|---|---|---|
| Chicken anti-mouse | AF647 | A21463 | Invitrogen |
| Donkey anti-mouse | AF488 | A21202 | Invitrogen |
| Donkey anti-mouse | AF568 | A10037 | Invitrogen |
| Donkey anti-goat | AF488 | A11055 | Invitrogen |
| Donkey anti-goat | AF568 | A11057 | Invitrogen |
| Donkey anti-goat | AF647 | A21447 | Invitrogen |
| Donkey anti-rabbit | AF488 | A21206 | Invitrogen |
| Donkey anti-rabbit | AF568 | A10042 | Invitrogen |
| Donkey anti-rabbit | AF647 | A31573 | Invitrogen |
| Donkey anti-rat | AF488 | A21208 | Invitrogen |
| Donkey anti-rat | AF594 | A21209 | Invitrogen |
| Donkey anti-rat | AF647 | A48272 | Invitrogen |
| Donkey anti-sheep | AF568 | A21099 | Invitrogen |
| Donkey anti-sheep | AF647 | A21488 | Invitrogen |
| Rabbit anti-hamster | AF594 | 307-585-003 | Jackson ImmunoResearch |
| Goat anti-hamster | AF647 | 107-605-142 | Jackson ImmunoResearch |

# CHAPTER III.

## DECODING THE VISUAL NARRATIVE: THE FL IN A DATAFRAME

Part of the data in this chapter was published in the following paper:

- Peixoto, M.*; Soares-da-Silva, F.*; Bonnet, V.*; Ronteix, G.*; Faria, M.R.; Maïlhe, M.P.; Feng, X.; Pereira, J.P.; Azzoni, E.; Giorgi, A.; de Bruijn, M.; Baroud, C.#; Pinto-do-Ó, P.#; Cumano, A.# (2023) "**Spatiotemporal dynamics of cytokines expression dictate fetal liver hematopoiesis**". *BioRxiv*. doi: https://doi.org/10.1101/2023.08.24.554612 (Manuscript under review) *these authors contributed equally, #senior authorship (**Annex VI**)

## PREAMBLE

To reveal an hematopoietic niche, we aimed to understand how the different cell types (hematopoietic and stromal) position in the tissue, how they interact with each other, and the molecular milieu involved in that communication. In the preceding chapter, we conducted an identification process to determine the relevant stromal targets that warrant further investigation. While live imaging of deep organs in physiological conditions remains an elusive goal, we are limited to capturing tissue "snapshots" that give us a brief glimpse of the *in vivo* dynamics. As described before, we implemented an imaging protocol of FL thick sections to ensure tissue structure preservation and 3D resolution. Consequently, we were able to pinpoint the cell types we identified by FC *in situ* and to observe the dynamic remodeling of the tissue during development.

Although an image can be very informative *per se*, the cognitive task of drawing conclusions from such an image must go beyond mere perception. For example, we can visually search for hematopoietic progenitor cells and check if they neighbor a stromal population, but in an image with 30.000 cells, determining an actual consistent tendency for these two types of cells to be neighbors or close is not an intuitive task, and requires an analysis via measurement and quantification.

With the emergence of spatial transcriptomics and multiplexed imaging, the need to develop tools that can uncover the intricate cellular position and cell-cell interactions was reinforced (**Goltsev et al.**, **2018**; **Palla et al.**, **2022**; **Stoltzfus et al.**, **2020**). Spatial analysis of biological samples can elucidate physiological processes at both the cellular and tissue level and must accompany the technological revolution. In an era of artificial intelligence, deep learning has been revolutionizing bioimage analysis, holding great potential to handle increasingly complex multimodal image data.

In collaboration with Charles Baroud's lab, we implemented a multi-step image analysis pipeline - *Pyxidis* - to understand patterns of cell distribution of FL populations and identify potentially enriched neighbor pairs. The output of this pipeline is a dataframe with information on cell spatial position and identity in a compact format that can be visualized as a dot plot. This chapter focuses solely on the demonstration of the analysis workflow. Its application to answer our biological question is addressed in the next chapter. For a step-by-step demonstration, we will consider a single stack image of an E12.5 FL section, stained with LHX2, CD45 and KIT.

# IMAGE ANALYSIS PIPELINE

The *Pyxidis* pipeline integrates 3 major steps: nuclei segmentation, cell classification, and network analysis, compiling a series of published tools (**Figure 21**).

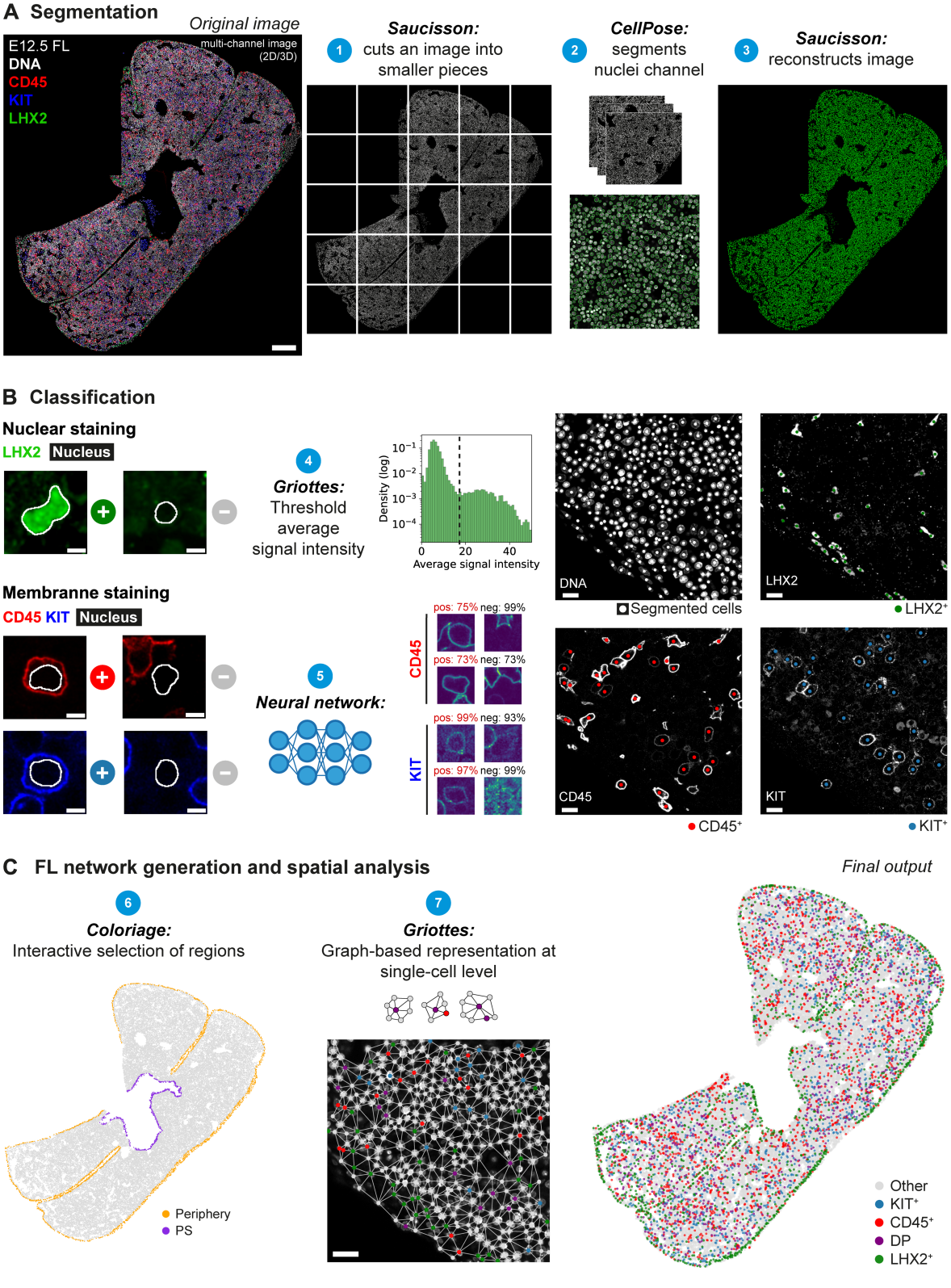


**Figure 21. Image analysis workflow.**

(**A**) Segmentation pipeline. FL multi-channel images are cut into small pieces using *Saucisson* (1). Individual tiles are segmented based on DAPI signal using *CellPose*, and then reassembled into the original shape (3). On the left, a representative single stack IF of E12.5 FL with DNA (white), LHX2 (green), KIT (blue) and CD45 (red) is shown to demonstrate the pipeline. Scale bar 200 μm. (**B**) Cell type classification pipeline. In the case of nuclear staining (e.g., LHX2, green), cells are classified according to a threshold set on the average signal intensity inside the nuclei mask using *Griottes* (4). For membrane staining (e.g., CD45/red, KIT/blue), cells are classified using a *Neural Network* (5). A representative example of a small tile post-classification is presented, displaying positive cells for DAPI, LHX2, CD45 and KIT. Scale bar 5 μm (small tiles on the left), 10 μm (on the tiles on the right). (**C**) For FL network generation and spatial analysis, *Coloriage* is used to remove or highlight specific regions of the FL sections (6). *Griottes* is used to represent the cells in a dot plot and to plot the contacts between cells (7). Scale bar 10 μm.
DP – double positive ($KIT^+CD45^+$); PS – portal sinus.

### *Nuclei segmentation*

We analyzed both single stack (2D) and multi-stack (3D) image acquisitions, with sizes ranging from 2682x2826 to 7686x8669x117 pixels (**Annex VI – Supplementary Table 2**), corresponding to 60Mb up to 50Gb in memory needs. Because operations with big files are not suitable on GPUs with 8GB RAM, a pre-processing step is performed to reduce memory consumption and allow parallel computations. Each image is divided into small tiles (3000x3000 pixels for 2D images and 600x600xZ-stacks for 3D) using the Python module *Saucisson* (**Figure 21A-1**). For each piece, we segment the nuclei, considering the DAPI signal, using *CellPose* (**Stringer et al.**, **2021**) (**Figure 21A-2**), on a GPU cluster[6]. The segmented pieces are then reconstructed to the original shape with an additional channel, with the mask for segmented nuclei (**Figure 21A-3**). At this point, we can generate a tabular file with the position (x, y, and z coordinates) of each segmented cells and some attributes (signal intensity of each channel inside the mask; area of the mask) using the package *Griottes* (**Ronteix et al.**, **2022**). To reduce artifacts created by incorrect segmentation of irregular nuclei, we filter out segmented objects whose area/volume is inferior to 50 $pixels^2$ or 3000 $pixels^3$, respectively. This segmentation limitation will be further discussed later on.

### *Cell classification*

Knowing the position of each cell, the next step is to distinguish the cell type. Therefore, we employed two different methods for cell classification depending on the type of staining: nuclear or membrane. For nuclear staining, such as LHX2, HNF4α and FLK1, a manual threshold is determined to distinguish between positive and negative cells, based on the histogram of signal intensities inside the mask of the nuclei (**Figure 21B-4**), and its accuracy is visually confirmed. Although false positives and false negatives are generally

[6] GPU cluster is a high-performance computing infrastructure.

low for this method, its precision depends on the quality of the original image and can be compromised if the background levels are not uniform across the entire section.

For membrane staining, such as CD45 and KIT, the signal intensity inside the segmented mask is very low and is not possible to robustly discriminate positive and negative cells using the threshold method. We tried to circumvent this by enlarging the nuclei mask, aiming to include the membrane staining. However, this approach often led to the inclusion of signals from neighboring cells, thereby compromising the accuracy of cell classification. Instead, the cells were classified using a deep learning-based *Neural Network*[7] (**Figure 21B-5**), that learns the fluorescence pattern around each nucleus. For that, the images were again deconstructed into small pieces, but now each one represents a single cell. Individual square images (80x80 to 120x120 pixels) were generated for each detected nucleus and centered around the geometric center of the nucleus.

The gray-scale pattern of the fluorescence inside this box was then analyzed by *SqueezeNet Networks*[4] (**Iandola et al.**, **2016**), using the transfer learning approach[8] and loaded pre-trained from *PyTorch* (**Paszke et al.**, **2019**). Training and validation datasets were manually created for each staining, using data from different images. The training was performed using a batch size of 32. An accuracy greater than 95% was achieved on validation datasets for each membrane staining (**Figure 22A, B**). Some manual corrections in the classification were performed for images with lower staining contrast. Manual verification of classification performances was done on 400 cells randomly selected for each membrane staining and each image (**Annex VI – Supplementary Table 2**). The percentage of false negatives and positives for CD45 and KIT cells is given in **Figure 22** (**A'' and B''**). The accuracy is larger than 96% for all verified sets of cells (**Table 9**).

We predefine corrections for misclassified cells that result in incompatible cell types, prioritizing the result from the nuclear marker that is typically more reliable. For instance, if a cell is classified as $LHX2^{+}CD45^{+}$, it is corrected to $LHX2^{+}CD45^{-}$. When dealing with misclassifications considering multiple nuclear markers (e.g., $LHX2^{+}HNF4\alpha^{+}$), we iteratively readjust the thresholds until the most accurate classification is achieved. For a visual confirmation of the cell classification in the entire image, we used the graphical interface *Napari*, which allows us to overlay the original image with the resulting classifications (**Supplementary Video 5**).

[7] *Neural networks* are a subset of machine learning models, inspired by the human's brain neural structure, designed to learn and make predictions from data. *SqueezeNet Networks* are a type of neural network.

[8] Transfer learning is a machine learning technique where a model developed for a task is reused as a starting point for a different but related task.

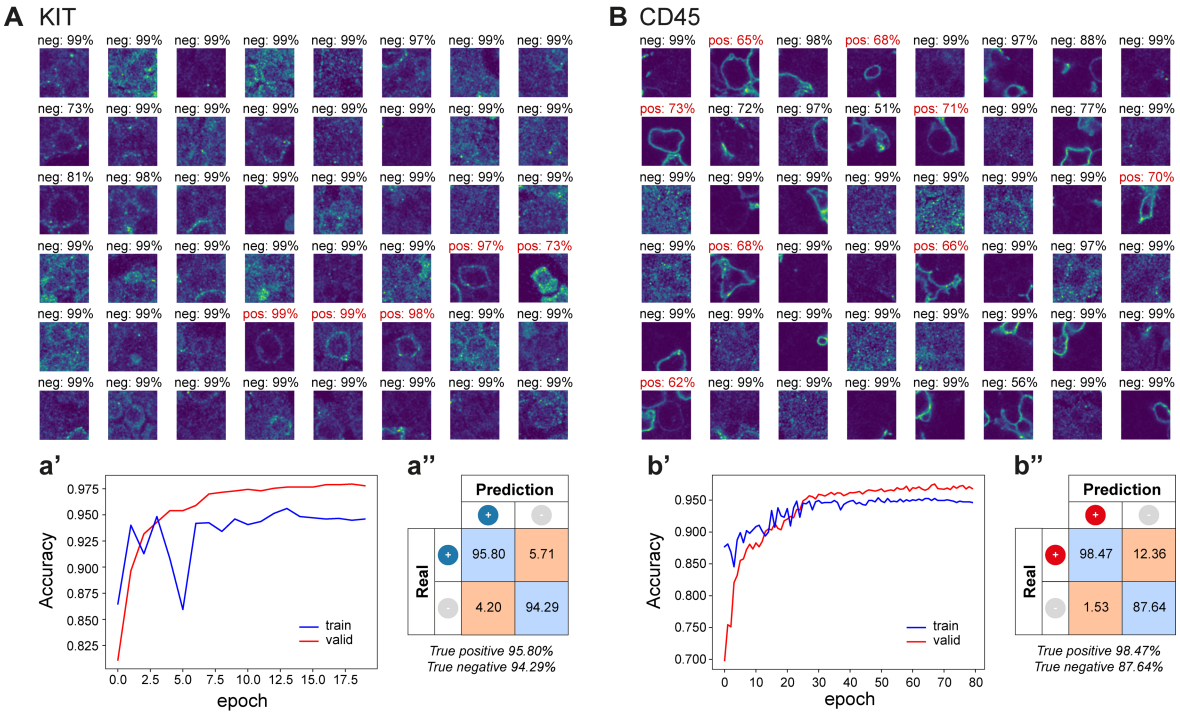


**Figure 22. Validation and quality control of image analysis.**
(**A**) Validation of KIT classification. Representative images of single cells classification and respective classification confidence. (**a'**) Accuracy of the classification during network training on training and validation datasets. (**a''**) Confusion matrix on the validation dataset. (**B**) Validation of CD45 classification. Representative images of single cells post-classification and respective classification confidence. (**b'**) Accuracy of the classification during network training on training and validation datasets. (**b''**) Confusion matrix on the validation dataset.

### *Spatial/network analysis*

#### *AF cells*

Until E14.5, nucleated erythrocytes constitute a big population in the FL. They are distributed across the parenchyma and inside the sinusoids. Those located inside the sinusoids exhibit a prominent AF signal, characterized by an intense cytoplasmic signal in one or more channels. Consequently, these cells can be incorrectly classified by the Neural Network for the membrane staining (e.g., as $KIT^+$), compromising its accuracy. To address this issue, we employed the same Neural Network approach to identify and subsequently exclude cells detected as $AF^+$ from the analysis (**Figure 23**).

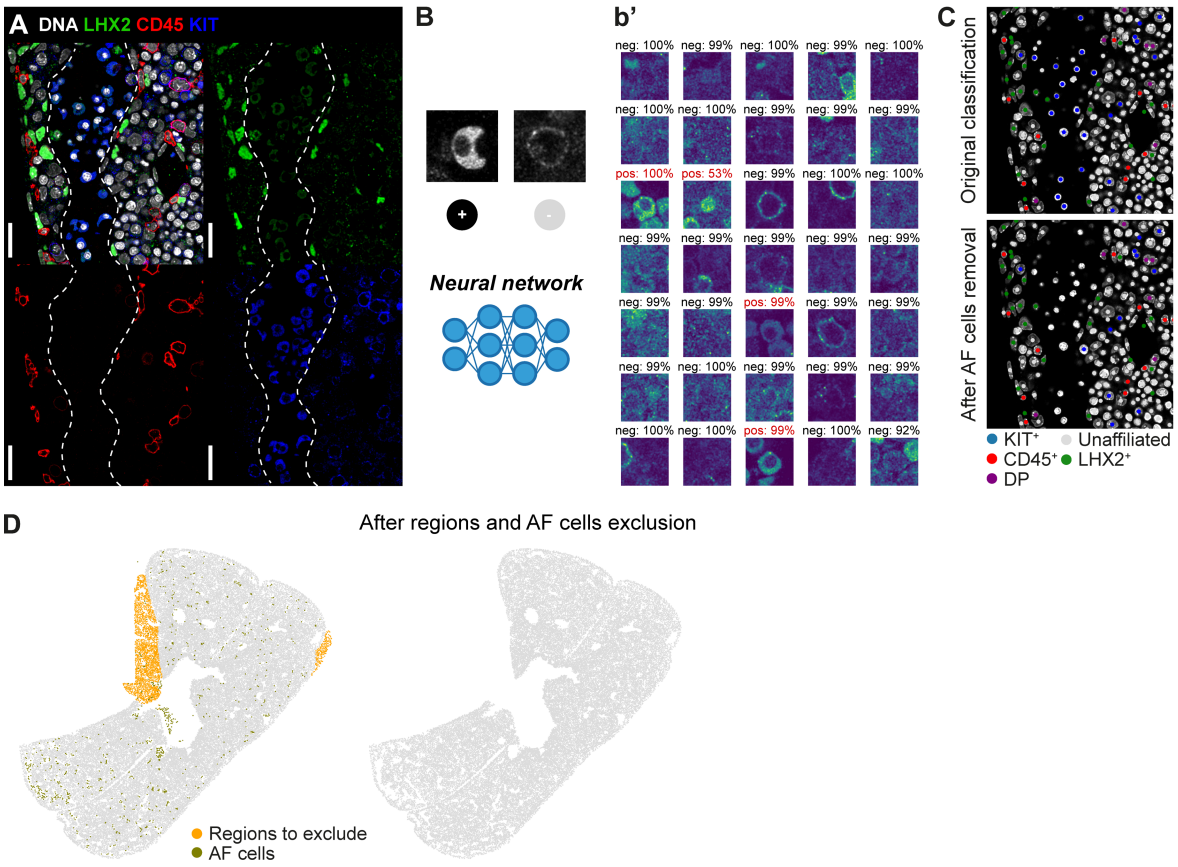


**Figure 23. Autofluorescent cells are removed from the analysis.**
(**A**) Single stack IF of E12.5 FL with DNA (white), LHX2 (green), CD45 (red), and KIT (blue), to highlight a region where AF cells (nucleated erythrocytes) can be seen inside a blood vessel (represented by the dashed line). Scale bar 25 μm. (**B**) AF cells are manually classified as positive and negative to train a *Neural Network*, so they can be later removed from the analysis. (**b'**) Representative images of single cells classification and respective classification confidence. (**C**) DNA channel of the tile depicted in (A) overlaid with classification before (top) and after (bottom) removing AF cells. (**D**) FL section (same input image as in Figure 22) before and after removing regions manually selected using *Coloriage*, and AF cells, highlighted on the left panel at orange and olive green, respectively.

### *Removal and selection of specific regions*

Parts of the tissue (e.g., disrupted lobes, other organs adjacent to the FL, or regions with lower quality) can be excluded from analysis. A specific interactive tool named *Coloriage* was created to graphically select regions in the segmented image (**Figure 21C-6)**. This tool is used to select undesired regions (**Figure 23D**) or to mark structures (e.g., the liver's periphery, vessels, individual lobes) (**Figure 21C-6)**.

### *Network construction*

After cell classification, we add to the dataframe containing the positions and properties of the nuclei additional attributes related to the cell classification. A dot plot can then be generated where each dot represents a cell, and the color code identifies the cell

phenotype (**Figure 21C**, *Final output*). A 'Delaunay' construction rule is applied to the dataframe using *Griottes* to generate a connectivity network, considering a cutoff distance to avoid incoherent links (e.g., at the image's periphery or vessels) (**Figure 21C-7**) (**Ronteix et al.**, **2022**). The returned object is a NetworkX graph (**Hagberg et al.**, **2008**), where the previously measured properties are node attributes (dots), while the neighborhood interactions and their attributes (length of the cell-cell contact) are encoded by the links.

Next, we conduct statistical analysis of the cell distributions. To differentiate between relevant and statistically significant neighboring cell pairs and patterns of cell distributions that are not merely the result of a random chance, we create randomized distributions for comparison. In this process, we shuffle the cell types on the network representation while preserving the total frequency of the types within the tissue (5-10 times) (**Figure 24A**). By labeling specific nodes in the graph as particular structures (periphery or vessels), it is possible to calculate the distances of cells to those reference points. The minimum Euclidean distance between each cell in the network and the cells attributed to the structure of interest is computed, and the minimal distance is considered for each data point (**Figure 24Bb'**). Then the relative abundance of each cell type is binned as a function of distance from the structure (**Figure 24B**). For random distributions, the distance to the periphery is re-calculated for ten repetitions of the re-shuffling operation and averaged (**Figure 24B**, dashed gray line). In the next chapter, when combining multiple images, we will present the distribution profiles as a ratio of the measured distribution to the randomized distribution (fold-change enrichment).

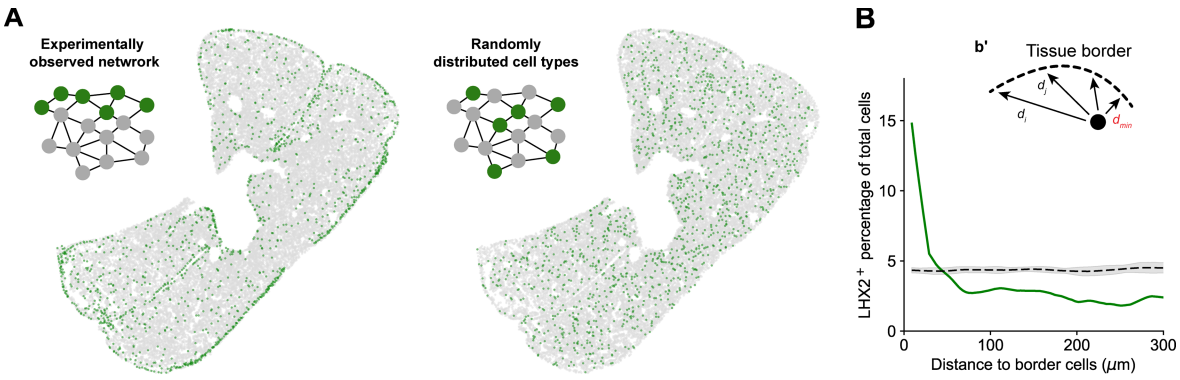


**Figure 24. Analyzing cell distribution patterns: distance to a reference point and comparison with random.**
(**A**) Experimentally observed (left) vs random (right; representative example) LHX2$^+$ cells distribution (green) (same input image as in Figure 22). (**B**) Distance to the periphery profile of LHX2$^+$ (green curve) cells and comparison with a random distribution (dashed line, average from 10 random distributions generated, with standard deviation in gray).

### *Pipeline limitations*

Regardless of the efficiency of an analysis pipeline, it will inevitably encounter constraints imposed by the inherent complexity of biological samples. Irregular nuclei, cells in division, multi-lobulated or polyploid nuclei in Mks, and phagocytosis of the expelled nuclei from erythrocytes by macrophages pose challenges for the segmentation, often leading to over-segmentation, and compromising the cell classification (**Figure 25, Supplementary Video 5**).

Filtering out very small segmented objects can help mitigate certain segmentation defects associated with irregular nuclei. However, addressing the segmentation challenges posed by Mks and macrophages presents a bigger task. While we could implement deep learning training strategies to identify Mks and macrophages to correct for the misclassification of multiple segmented nuclei, it would require in some cases to specifically allocate a channel in the staining strategy just for the identification of these cells, which might be incompatible. While we cannot categorize these cells as exceedingly rare, in the instances we investigated in this study, we assume that the errors introduced are negligible when maintaining a substantial sample size, and they do not substantially affect the results.

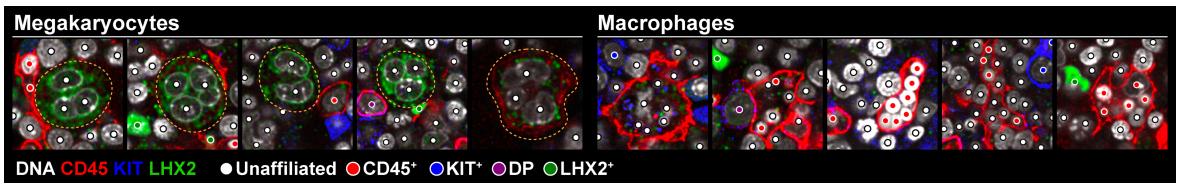


**Figure 25. Pipeline limitations.**
Representative examples where over-segmentation occurred in cases of Mks and macrophages. In the FL, Mks express no to low levels of CD45 but are often recognized by an unspecific LHX2 staining.

### *Code availability*

The analysis of the FL network images was conducted on Jupyter Notebook. All the relevant notebooks are freely accessible on the project GitHub repository (https://github.com/BaroudLab/Pyxidis). Different packages have been custom-made for the analysis of the FL images, during pre-processing and data analysis. All these functionalities (*Saucisson*, *Coloriage*) have been incorporated into the main GitHub for easier use and installation. This repository contains a step-by-step tutorial to run the entire image analysis pipeline and data analysis performed in the next chapter.

## DISCUSSION

*Pyxidis* allows the conversion of visual information from FL sections (heavy files, up to 50Gb) into a few Mb dataframe containing the same information. This dataframe compiles for each segmented cell its spatial coordinates and phenotype. A dot plot representation then recreates the original image. Compiling data from independent images enables the identification of robust and recurring spatial patterns. For the single cell neighboring analysis, the large number of screened cells provides an exceptionally robust statistical analysis.

As we strive to develop models that accurately represent biological samples, we must acknowledge that the inherent complexity of these samples imposes limitations. Additionally, successful implementation of the image analysis pipeline relies upon the quality and consistency of the input images. It is important to be aware of any technical problem regarding upstream steps to image analysis (sample preparation and image acquisition)[9], which could potentially affect accurate segmentation and classification. Identifying and addressing such problems during the analysis phase is imperative for ensuring trustworthy results.

An aspect that we miss to address here and could significantly improve the analysis of cellular interactions is the inclusion of cell topology metrics (e.g., cellular volume), in addition to relying solely on nuclei segmentation. This becomes particularly pertinent when dealing with irregularly shaped cells, like mesenchymal cells[10] and endothelial cells. Using *Cxcl12-Gfp* reporter mice, Gomariz and colleagues showed the intricate morphology of CAR cells in the BM niche, revealing their multiple cytoplasmic projections (**Gomariz et al.**, **2018**). This feature significantly expands their surface area, facilitating a multitude of connections compared to spherical cells. This effect is even more pronounced in endothelial cells, which is particularly relevant when calculating the proximity of a given cell type to vessels. Incorporating a segmentation approach for vascular networks or other cellular components akin to that employed by (**Gomariz et al.**, **2018**; **Helbling et al.**, **2023**, pre-print) could be a significant enhancement for this pipeline.

[9] As an illustrative example: in the input image in **Figure 21A**, an acquisition issue became apparent, wherein the LHX2 channel was not acquired in a single tile, clearly noticeable in **Figure 24** and **Supplementary Video 5** by the absence of $LHX2^{+}$ cells lining the mesothelium. When confronted with parts of a section with poor staining quality, we can exclude them, using the tool *Coloriage*. In this case, the effect was minimal, thus it was considered of little importance.
[10] As can be appreciated in **Figure 16D-F** considering the PDGFRα and Desmin staining.

## SUPPLEMENTARY INFORMATION

**Supplementary Video 5. Visual confirmation of the segmentation and classification using *Napari*.**
Representative demonstration of the use of the graphical interface *Napari* to visually inspect the segmentation and classification. For the demonstration, the same FL section represented in Figure 21 was used. It corresponds to a single stack, stained with DNA (white), LHX2 (green), CD45 (red) and KIT (blue).

# CHAPTER IV.

## INTERACTIONS AT THE BORDER: A NOVEL NICHE FOR HEMATOPOIETIC PROGENITORS IN THE FL

Part of the data in this chapter was published in the following paper:

- Peixoto, M.*; Soares-da-Silva, F.*; Bonnet, V.*; Ronteix, G.*; Faria, M.R.; Maïlhe, M.P.; Feng, X.; Pereira, J.P.; Azzoni, E.; Giorgi, A.; de Bruijn, M.; Baroud, C.#; Pinto-do-Ó, P.#; Cumano, A.# (2023) "**Spatiotemporal dynamics of cytokines expression dictate fetal liver hematopoiesis**". *BioRxiv*. doi: https://doi.org/10.1101/2023.08.24.554612 (Manuscript under review) *these authors contributed equally, #senior authorship (**Annex VI**)

## PREAMBLE

The location of FL HSPCs *in situ* remains elusive. Two separate studies have employed the same staining strategy ($CD150^{+}CD48^{-}CD41^{-}Lin^{-}$) to localize HSPCs within the FL (**Khan et al.**, **2016**; **Lee et al.**, **2021**). Nevertheless, these investigations have yielded conflicting outcomes. Khan et al., reported that HSPCs are predominantly close to $NG2^{+}$ PFs, whereas Lee et al. demonstrated a preferential location near SCs. By employing spatial transcriptomics analysis, two other studies claim to address the localization of HSPCs in the tissue (**Gao et al.**, **2022**; **Lu et al.**, **2021**). Nonetheless, the 10X Visium technique used by Gao et al. lacks the required spatial resolution, while the multiplexed error-robust fluorescence *in situ* hybridization (MERFISH) analysis conducted by Lu et al. offers limited coverage of the FL sections, lacking robustness.

A major goal of this work was to devise a staining strategy for the effective *in situ* identification of phenotypic HSCs, aiming that their tissue localization could provide insights into their interactions with niche cells. This includes understanding whether they form clusters, or remain dispersed, whether they exhibit proximity to particular cell types, and how their distribution compares to a random pattern. Although we developed the tools to consistently address these questions, we could not achieve a robust staining strategy with a good enrichment for HSCs. The main goal then shifted to a more simplistic approach, using only two hematopoietic markers (KIT and CD45) in combination with major stromal markers (FLK1 for endothelial cells, HNF4$\alpha$ for hepatoblasts and LHX2 for mesenchymal cells).

In **Chapter II**, we focused on resolving the FL stromal compartment, by characterizing non-hematopoietic cell types by FC, gene expression, and imaging. In this chapter, we applied the *Pyxidis* pipeline, demonstrated in **Chapter III**, aiming to understand how the HS interacts with its environment, even though lacking HSC resolution.

## THE HEMATOPOIETIC COMPARTMENT

Employing a set of defined hematopoietic markers, we analyzed the FL hematopoietic compartment at E12.5 (**Figure 26**). A considerable proportion of FL isolated cells were erythroid lineage (around 80% Ter119$^{+}$CD71$^{+}$ erythroblasts and 3% terminally differentiated erythrocytes). In the remaining hematopoietic fraction, a heterogenous population of CD45$^{-}$Ter119$^{-}$ erythroid-committed progenitors (P1, P2 and P3) previously described by Soares-da-Silva et al. and shown to be derived from the YS (**Soares-da-Silva et al., 2021**) accounted for 10%; and CD45$^{+}$ cells represented 5%. The remaining fraction consists of stromal cells, which are notably underrepresented following the isolation process. Combining the erythroid markers Ter119 and CD71, the pan-hematopoietic marker CD45, and the progenitor marker KIT, we can visualize the overwhelming majority of the hematopoietic compartment in FL sections (**Figure 26C**).

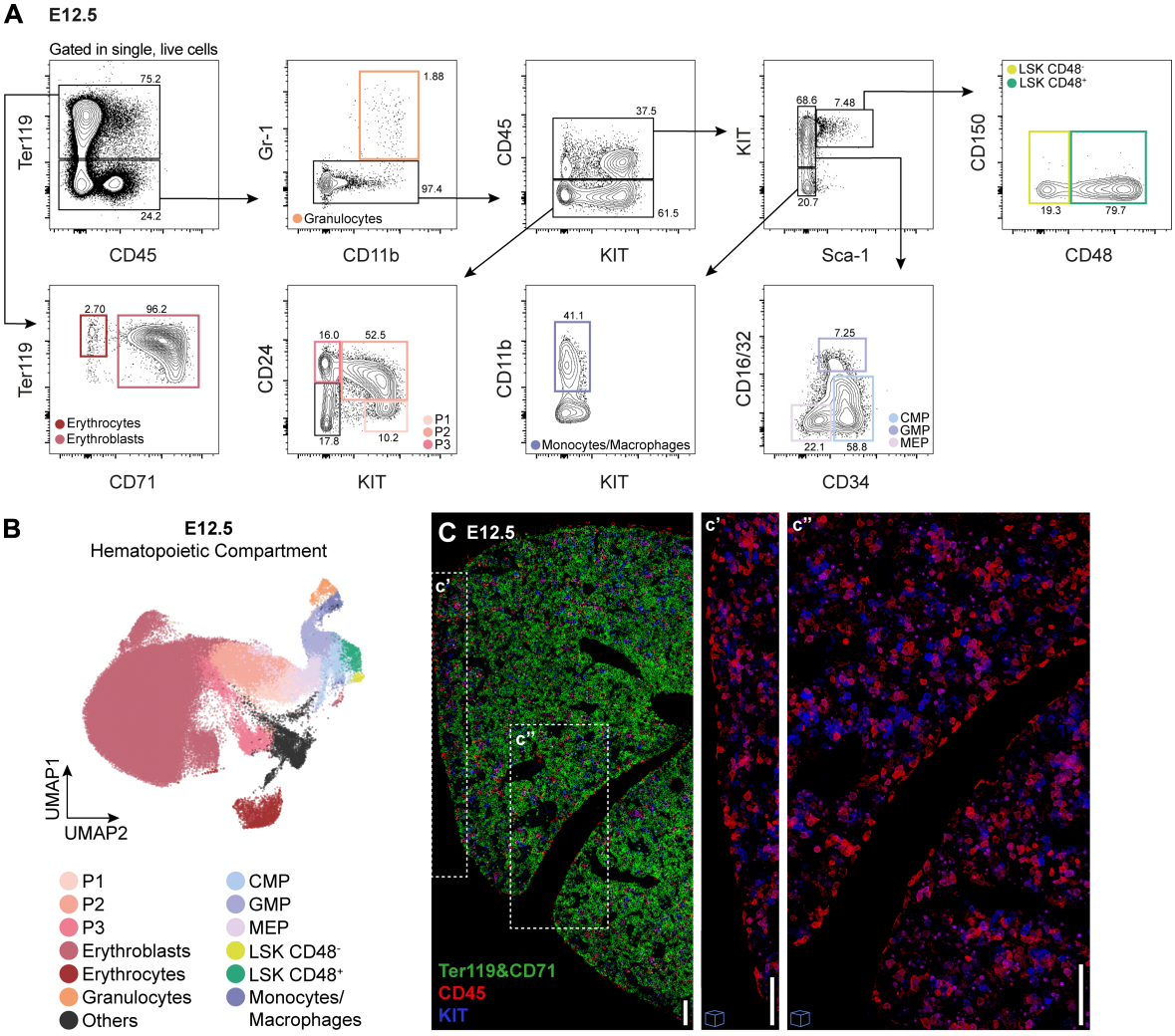


**Figure 26. Discrimination of the FL hematopoietic compartment at E12.5.**
(**A**) Representative gating strategy used for the analysis of the hematopoietic compartment of E12.5 FLs using the surface markers Ter119, CD45, CD71, CD24, Gr-1, CD11b, KIT, Sca1, CD16/32,

CD34, CD150 and CD48. (**B**) Representative UMAP representation of the hematopoietic compartment of E12.5 FLs. Color code correlates to the gating strategy shown in (A). (**C**) Single stack IF of E12.5 FL with Ter119 and CD71 (green), CD45 (red) and KIT (blue). Inserts **c'** and **c"** show an enlarged 3D view (20 μm) of the selected regions showing only CD45 and KIT. Scale bar 50 μm.

### *Wild-HSC chase – an inglorious pursuit*

The simple combination of CD150, CD48 and CD41 proved to be effective in identifying HSCs in the adult, as 1 out of 2.2 (~50%) $CD150^{+}CD48^{-}CD41^{-}$ exhibited multipotent LTR (**Kiel et al.**, **2005**). However, using the same strategy in cells isolated from E14.5 FLs, only around 18% of cells show LTR (**Kim et al.**, **2006**). Considering $CD150^{+}CD48^{-}CD41^{-}$ cells, around 50% of them are phenotypic HSCs (LSK $CD150^{+}$ $CD48^{-}$ $CD41^{-}$) at E18.5, but the percentage of enrichment decreases to around 20% at E14.5 (**Supplementary Figure 5A**). This staining strategy, previously used to locate HSCs *in situ* (**Khan et al.**, **2016**; **Lee et al.**, **2021**), is not particularly efficient. Considering that most $CD150^{+}CD48^{+}CD41^{+}$ cells are $KIT^{-}$, the combination of CD150, CD48 and KIT considerably increases the frequency of enrichment of phenotypic HSCs at E14.5 and E18.5 (**Supplementary Figure 5B**).

Combining markers for IF strategies can pose a challenge due to the limited availability of antibodies across various species that can be effectively combined. As a preliminary step, we focused on optimizing the individual antibodies (**Supplementary Table 8**). Multiple attempts were made to optimize the CD150 staining; however, none proved successful. We assessed two antibodies, one of which is commonly used in published articles for the *in situ* identification of HSPCs (**Cordeiro Gomes et al.**, **2016**; **Khan et al.**, **2016**; **Lee et al.**, **2021**; **Liu et al.**, **2022**). Various parameters, including different antibody concentrations, incubation times, incubation temperatures, and fixation procedures, were rigorously tested. These fixation procedures encompassed varying paraformaldehyde (PFA) concentrations and incubation durations. Furthermore, we explored non-fixed samples and *in vivo* perfusion of pregnant females with 2% PFA, followed by 4 hours of fixation in isolated embryos/FLs, aligning with the methodology in (**Cordeiro Gomes et al.**, **2016**).

In our quest for an alternative to CD150, we evaluated the expression profile of ESAM, a marker described to be highly enriched in HSPCs in both fetal and adult stages (**Lisa Ooi et al.**, **2009**). Nearly all HSCs, MPP1 and MPP2 expressed ESAM at both E14.5 and E18.5 (**Supplementary Figure 5C**). However, its expression in the MPP3/4 and LK cells represented less than 40 and 10%, respectively, and most mature cells did not express ESAM (except NK cells; *data not shown*). **Supplementary Table 9** displays the percentage

of enrichment for phenotypic HSCs, as well as LSK CD48$^-$ (encompassing LT- and ST-HSCs) when considering various combinations of 2/3 markers out of a total of 7 possible markers, including CD45, KIT, Sca-1, CD150, CD48, ESAM, and CD41. This analysis aimed to determine whether ESAM could serve as a reliable substitute for CD150. ESAM did not exhibit efficient enrichment for HSCs when combined with markers other than CD150. Nonetheless, certain combinations still showed promising for achieving significant enrichment for LSK CD48$^-$. Unfortunately, we encounter similar challenges in optimizing the staining for ESAM. Sca-1, on the other hand, together with KIT and CD48 was sufficient to identify LSK CD48$^-$ cells. As both antibodies for KIT and Sca-1 were raised in rats, we defined a theoretically compatible strategy to combine both, performing serial incubations of each rat antibody individually, followed by the respective secondary one. In the case of the Sca-1, which was conjugated with PE, we used a rabbit anti-PE, followed by an anti-rabbit secondary antibody.

Initially, when we simultaneously co-incubated CD48 and KIT, followed by Sca-1, we observed an overlap between Sca-1 and CD48 (excluding endothelial Sca-1$^+$ cells, **Supplementary Figure 6**). This was indicative of a potential non-specific interaction between the antibodies. This issue was resolved by incubating CD48 after Sca-1. However, in this revised strategy (**Supplementary Table 10**), we still encountered a very faint Sca-1 staining overlap with KIT. To rule out the possibility of Sca-1 interacting with the anti-rat secondary antibody, we conducted a test using an anti-rat secondary antibody specifically targeting the constant region F(ab')2. Unfortunately, this adjustment did not lead to an improvement in the background staining. As we were able to identify certain parenchymal Sca-1$^+$ cells that could potentially represent specific Sca-1 staining, we attempted to train a neural network to differentiate between background staining and genuine staining. Unfortunately, the manual classification process proved to be overly intricate and lacked consistency among different operators.

***A bird's-eye view instead***

As a working staining strategy with a good enrichment for HSCs could not be achieved, we decided to characterize the distribution of different hematopoietic populations, considering a very simplistic set of 2 markers – CD45 and KIT – that allows us to distinguish (**Figure 27**): CD45$^+$KIT$^-$ cells, referred to as CD45$^+$ cells, which comprise mainly monocytes and granulocytes; CD45$^-$KIT$^+$ cells, referred to as KIT$^+$ progenitors, that comprise the YS-derived erythroid progenitors (P1 and P2) (**Soares-da-Silva et al.**, **2021**); and CD45$^+$KIT$^+$, referred to as DP (Double Positive) progenitors, that include a broad set of hematopoietic progenitors, from less committed to more restricted ones. The majority of these are LK cells,

with proportions of CMPs, GMPs and MEPs changing along development. A smaller proportion of DP (around 10%) are LSK CD48$^-$ and LSK CD48$^+$ cells. Some of the GMPs can be of YS origin at E12.5 (not more than 8% (**Iturri et al.**, **2021**)), but the majority of these progenitors are IE. We then investigated the spatial distribution of these 3 populations within the tissue.

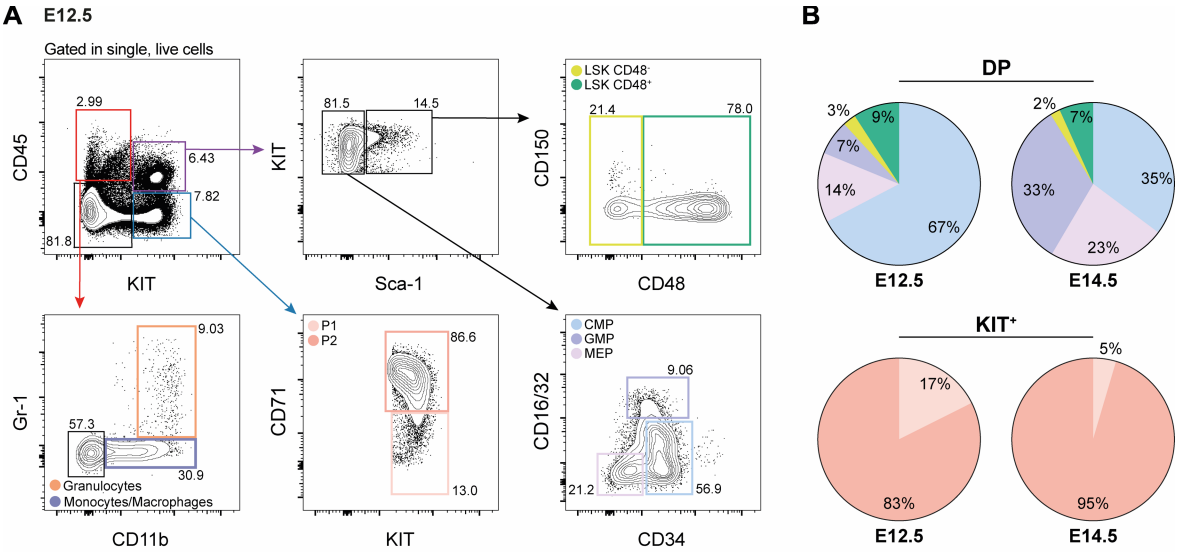


**Figure 27. Composition of the CD45$^+$, DP and KIT$^+$ FL compartments.**
(**A**) Representative gating strategy showing the cell types that are included in CD45$^+$, DP and KIT$^+$ populations. (**B**) Percentage of the progenitor cell types within DP cells (top) and KIT$^+$ cells (bottom) at E12.5 (left) or E14.5 (right).
DP – double positive (KIT$^+$CD45$^+$).

## FL NETWORK ANALYSIS

### *Tissue composition*

As described in the previous chapter, *Pyxidis* allows to recreate FL sections in a graphical representation with preserved spatial positioning and cell identity, to which multiple analyses can be performed: tissue composition, pattern of distribution of cells to specific regions, and neighborhood analysis.

To assess the FL hematopoietic and stromal components, we used a concise panel of markers: CD45 and KIT for hematopoietic cells, in combination with LHX2 (mesenchymal) or HNF4α (hepatic) or FLK1 (endothelial) for the stromal populations (**Figure 28A, B**). To accurately identify endothelial cells, we employed *Flk1*-GFP reporter mice. Due to their elongated shapes, membrane markers (e.g., CD146) are challenging to classify using the *Neural Network*, while nuclear markers are easily classified using the threshold method described before. As MCs correspond to the outer layer of the liver, they were manually selected using the tool *Coloriage* and classified as “periphery”.

We compared the frequencies of the classified cells with the frequencies obtained by FC. Except for endothelial cells, which represented the predominant stromal population isolated after dissociation of the liver, there were notable differences in the percentages of other populations between the two methods (**Figure 28C, D**). Remarkably, mesenchymal cells and hepatoblasts were 5 and 10-fold, respectively, more represented *in situ* than by FC. Curiously, the percentages of the six cell types analyzed, namely the hematopoietic types did not change considerably from E12.5 to E14.5, suggesting a nearly proportional growth of each compartment to the liver growth (**Figure 28E**).

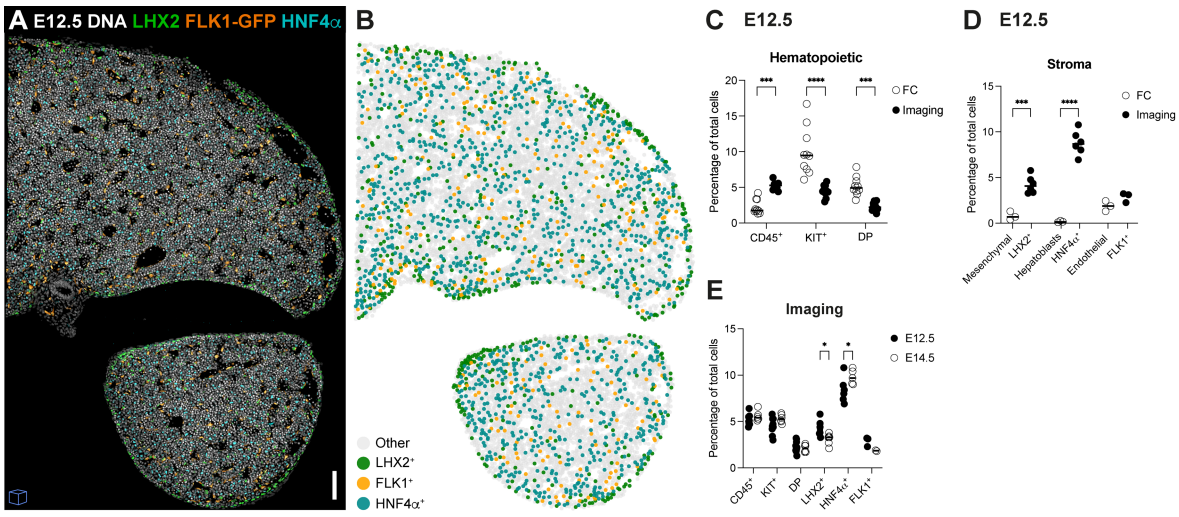


**Figure 28. Quantification of FL populations.**
(**A**) 3D view (10 μm) IF of E12.5 FL (*Flk1*-GFP mice) with DNA (white), LHX2 (green), *Flk1*-GFP (orange), and HNF4α (cyan). Scale bar 100 μm. (**B**) Dot plot representation of the FL section

represented in (A) (10 μm thick projected into a single plane). (**C**) Percentage of hematopoietic cells recovered and analyzed by FC (n=9) versus quantified by imaging of FL sections (n=9). (**D**) Percentage of stromal cells recovered and analyzed by FC (n=3) versus quantified by imaging of FL sections (LHX2 and HNF4α (n=6), FLK1 (n=3)). (**E**) Percentage of hematopoietic and stromal cells quantified by imaging of FL sections at E12.5 and E14.5 (E12.5: CD45, KIT, DP (n=10); LHX2, HNF4α (n=6); FLK1 (n=3); E14.5: CD45, KIT, DP (n=6); HNF4α (n=5); LHX2 (n=6); FLK1 (n=2)). (C-E) Statistical analysis was calculated using two-way ANOVA, followed by Šídák's multiple comparisons test.
*, P < 0.05. ***, P < 0.001; ****, P < 0.0001; DP – double positive ($KIT^+CD45^+$).

### *E12.5*

A dot plot representation (**Figure 28A, Figure 29A)** provides a global view of the spatial distribution of the different cell types. To quantify the distribution of each cell type, we calculated the relative percentage of each cell type at a given distance to the liver's periphery (**Figure 29B**) or the portal sinus (PS, central vessel structure) (**Figure 29C**) and normalized by the percentage of each cell type in an average random distribution (% observed/random). The random distribution of cells was computed by shuffling the cell types while preserving the positions and the total number of each cell type (see **Image Analysis** methodology description). The distribution profile of $CD45^+$ cells did not differ much from the random scenario, indicating that they do not have a preferential distribution within the FL. Conversely, $KIT^+$ and DP progenitor cells were found more concentrated within a 50 μm proximity to the liver's periphery, with fewer occurrences in the vicinity of the PS. As visually evident, $LHX2^+$ mesenchymal cells accumulated in the sub-mesothelium region and displayed a random distribution elsewhere. $HNF4\alpha^+$ hepatoblasts and $FLK1^+$ also displayed a higher frequency near the periphery. However, the dataset with FLK1 is unpowered statistically precluding robust conclusions.

Analysis of cell-cell contacts showed that $KIT^+$ and DP progenitors exhibited preferential contact with hepatoblasts compared to a random distribution, while they were found to be significantly less in contact with SCs and did not exhibit preferential proximity to $FLK1^+$ endothelial cells (**Figure 29D**). $CD45^+$ cells did not exhibit a preferential neighbor tendency. These results suggest that the peripheric region is a privileged site for hematopoietic progenitors at E12.5, which preferentially associate with hepatoblasts.

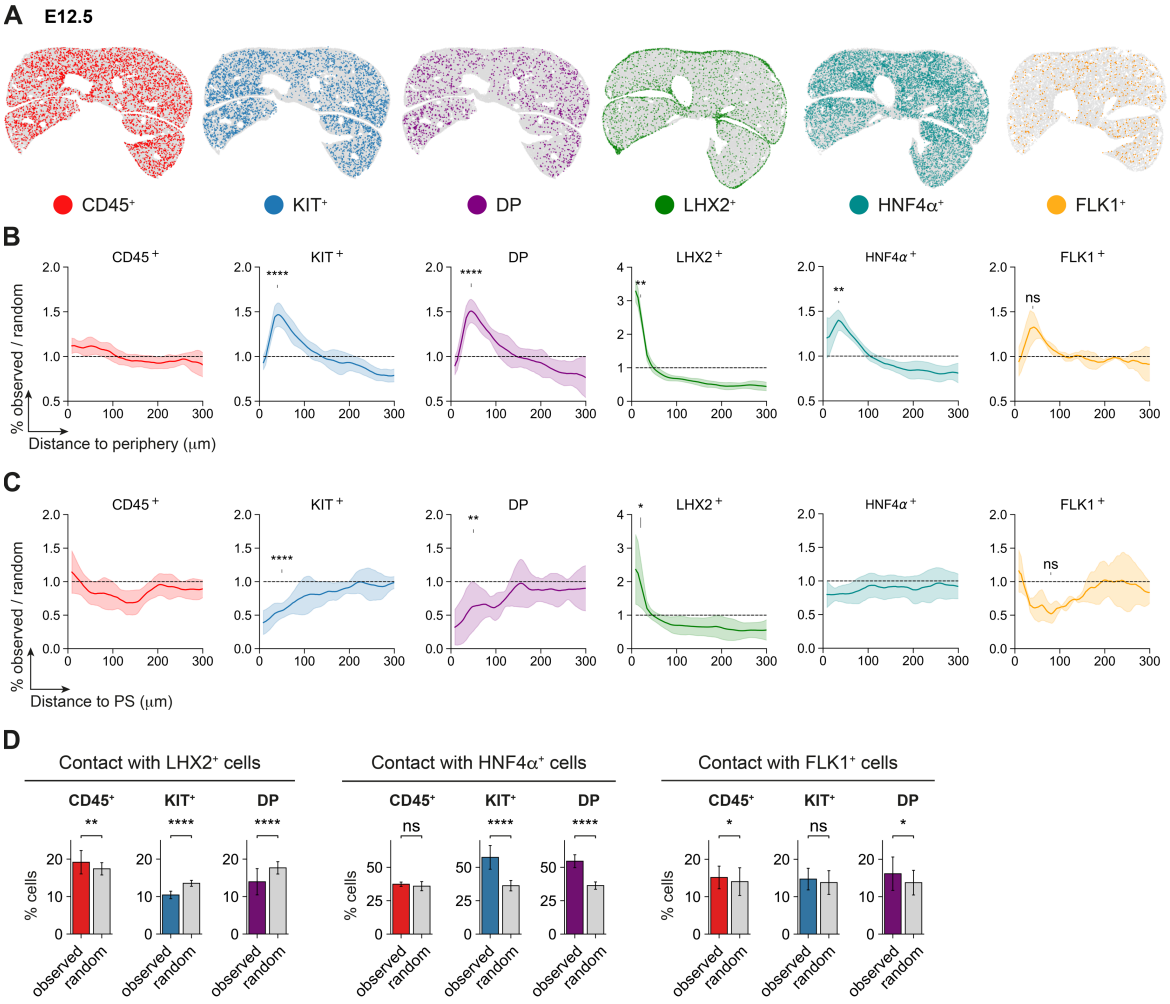


**Figure 29. KIT⁺ and DP progenitors accumulate at the periphery at E12.5 and are preferentially in contact with hepatoblasts, but not stellate or endothelial cells.**

(**A**) Dot plot representation of CD45⁺ (red), KIT⁺ (blue), DP (purple), LHX2⁺ (green), HNF4α⁺ (cyan) and FLK1⁺ (orange) cells distribution of E12.5 FL representative sections (15 μm section projected into a single plane, except for the FLK1, that corresponds to a single stack). (**D**) Distance to the periphery profile of CD45⁺ (red, n=10), KIT⁺ (blue, n=10), DP (purple, n=10), LHX2⁺ (green, n=6), HNF4α⁺ (cyan, n=6) and FLK1⁺ (orange, n=3) cells of E12.5 FLs. Curves indicate average ± standard deviation. Statistical analysis was calculated at the peak of each curve using the Mann-Whitney test, between observed and random curves. (**E**) Neighborhood composition of CD45⁺, KIT⁺ and DP⁺ cells of E12.5 FLs. Graphs display the percentage of cells that are in contact with LHX2⁺ (left, n=3), HNF4α⁺ (middle, n=3) and FLK1⁺ (right, n=2) stromal cells (observed) compared to random. Bar plots indicate average ± standard deviation. Statistical analysis was calculated using t-test Welch.
*, P < 0.05; **, P < 0.01; ****, P < 0.0001; DP – double positive (KIT⁺CD45⁺); ns – not significant; PS – portal sinus.

***E14.5***

Given that the FL is a major site of hematopoiesis during development, we investigated the distribution of hematopoietic cells at subsequent developmental stages. We found that $KIT^+$ progenitors maintained their accumulation close to the periphery (**Figure 30A, B**) at E14,5 while $CD45^+$ cells and DP progenitors changed their spatial localization. $CD45^+$ cells displayed a lower frequency within 50 μm from the periphery, and a slight increase in the frequency at the vicinity of the mesothelium, while DP progenitors were evenly dispersed in the parenchyma (**Figure 30B**). Furthermore, our analysis of cell-cell contacts demonstrated that, similar to earlier time points, $KIT^+$ and DP hematopoietic progenitors showed a preferential interaction with hepatoblasts, but not with SCs (**Figure 30C**).

As previously discussed (**Chapter II**), *Cxcl12* is mainly expressed by hepatoblasts and mesenchymal cells. At E12.5, the two cell types express similar levels, but *Cxcl12* is strongly upregulated by mesenchymal cells, reaching an 8-fold increase by E18.5, while it is maintained constant by hepatoblasts (**Figure 30D**). At E14.5, the pattern of expression in the *Cxcl12*-dsRed is similar to E12.5, with clear discrimination between perivascular *Cxcl12*-$dsRed^{bright}$ and $HNF4\alpha^+$*Cxcl12*-$dsRed^{dim}$ (**Figure 30E**). To understand how the two different hematopoietic progenitors would respond to CXCL12 signaling, we examined the expression levels of the respective receptor, CXCR4. $KIT^+$ progenitors had no expression of *Cxcr4*, but DP expressed it at low levels at E12.5 and upregulated it by a factor of 3 at E14.5 (**Figure 30F**). To confirm differences in migration responsiveness to CXCL12 of the two types of progenitors, we performed a dual-chamber migration assay. As expected, only DP progenitors migrated in response to CXCL12, and the proportion of migrating cells was higher at E14.5 (**Figure 30G**).

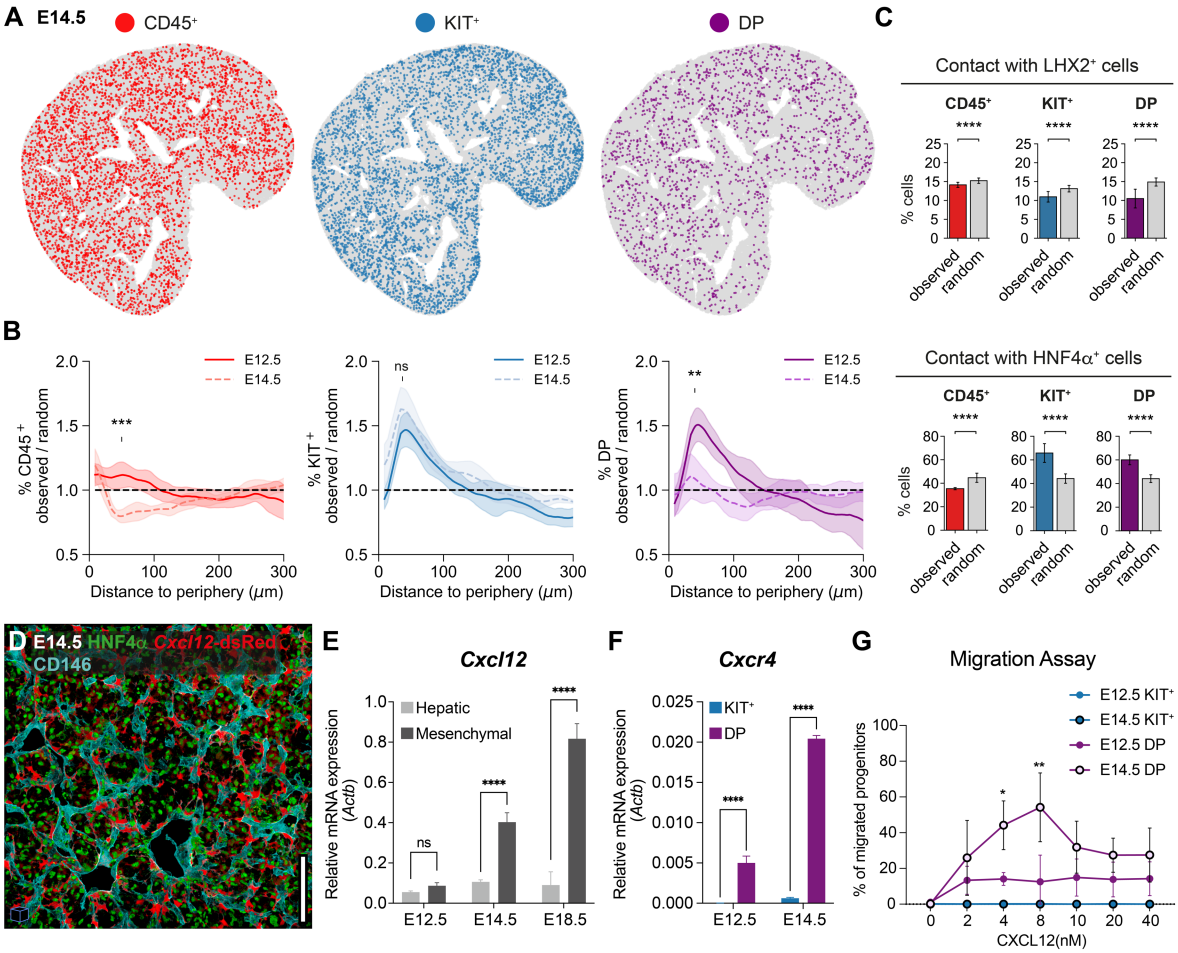


**Figure 30. At later stages, opposite to KIT⁺, DP progenitors display a homogeneous distribution throughout the parenchyma in response to CXCL12 levels.**

(**A**) Dot plot representation of CD45⁺ (red), KIT⁺ (blue) and DP (purple) cell distribution of E14.5 FL representative sections (single stack). (**B**) Distance to the periphery profile of CD45⁺ (red, n=6), KIT⁺ (blue, n=6) and DP (purple, n=6) cells of E14.5 FLs. E12.5 data from Figure 29 is overlaid for comparison. Curves indicate average ± standard deviation. Statistical analysis was calculated at the peak of each population using the Mann-Whitney test, between E12.5 and E14.5 curves. (**C**) Neighborhood composition of CD45⁺, KIT⁺ and DP⁺ cells of E14.5 FL. Graphs display the percentage of cells that are in contact with LHX2⁺ (left, n=3) and HNF4α⁺ (middle, n=3) stromal cells (observed) compared to random. Bar plots indicate average ± standard deviation. Statistical analysis was calculated using t-test Welch. (**D**) Single stack IF of E14.5 FL (*Cxcl12*-dsRed mice) with LHX2 (green), *Cxcl12*-dsRed (red) and HNF4α (blue). Scale bar 100 μm. (**E**) qRT-PCR analysis of the expression levels of the hematopoietic chemokine *Cxcl12* in hepatic (hepatoblasts, light gray), and mesenchymal (dark gray) cells in E12.5, E14.5 and E18.5 FL cells (n=3). (**F**) qRT-PCR analysis of the expression levels of the CXCL12 receptor (*Cxcr4*) in KIT⁺ (blue), and DP (purple) cells in E12.5 and E14.5 FLs (n=3). (**G**) Transwell migration assay of DP and KIT⁺ progenitors isolated from E12.5 and E14.5 FLs in response to the chemokine CXCL12a. Data are presented as the percentage of input progenitors that migrate to the bottom chamber (n=3). (E-G) Statistical analysis was calculated using two-way ANOVA, followed by Šídák's multiple comparisons test.

*, P < 0.05; **, P < 0.01; ****, P < 0.0001; DP – double positive (KIT⁺CD45⁺); ns – not significant.

### *E18.5*

At late gestation, hematopoietic cells egress from the FL and migrate to the BM, a place that will serve as a primary site for hematopoiesis for the rest of the life. To observe how the HS is organized in the maturing liver, we analyzed the distribution of $CD45^+$ cells, and specifically the two major differentiated lineages ($B220^+$ B-lineage cells or $CD11b^+$/GR-$1^+$ myeloid cells) in E18.5 FL sections (**Figure 31**). We observed frequent accumulation of $CD45^+$ cells in the major vessels and the vicinity of sub-MCs (**Figure 32A, B**). It is noteworthy that they do not cluster around all vessels or extend across the entire liver's periphery (*data not shown*). This accumulation was corroborated with the quantification of both populations in terms of distance to the vessels, and to the periphery (**Figure 32C-J; Supplementary Figure 7**). To determine whether $CD11b^+$ and $B220^+$ cells accumulate differently in the major vessels and the periphery, we compared their frequencies in these regions to the remaining tissue (**Figure 32K, L**). Our findings revealed that $CD11b^+$ cells were equally represented in major vessels and the sub-capsular region, while $B220^+$ cells were primarily located at the latter. Interestingly, we found no major differences in myeloid or lymphoid cell accumulation in $NG2^-$ or $NG2^+$ portal vessels (*data not shown*). These results point to the mesothelium/sub-mesothelium region as a supportive environment for mature lineages at later stages.

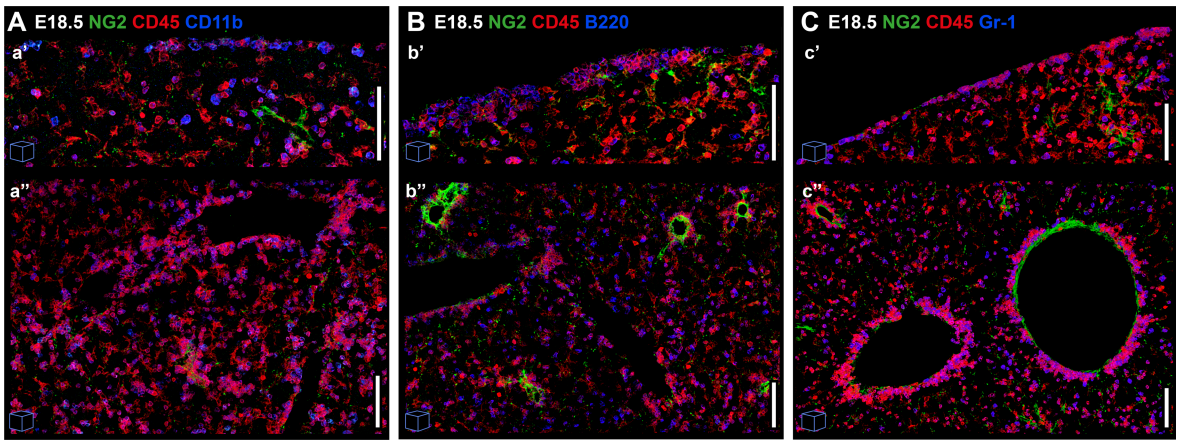


**Figure 31. Myeloid and lymphoid cells accumulate in the vessels and mesothelium at late gestation.**
(**A**) 3D view (20 μm) of IF of E18.5 peripheral (**a'**) or parenchymal (**a''**) regions with NG2 (green), CD45 (red) and CD11b (blue). (**B**) 3D view (20 μm) of IF of E18.5 peripheral (b') or parenchymal (b'') regions with NG2 (green), CD45 (red) and B220 (blue). (**C**) 3D view (20 μm) of IF of E18.5 peripheral (c') or parenchymal (c'') regions with NG2 (green), CD45 (red) and GR1 (blue). Scale bars 100 μm.

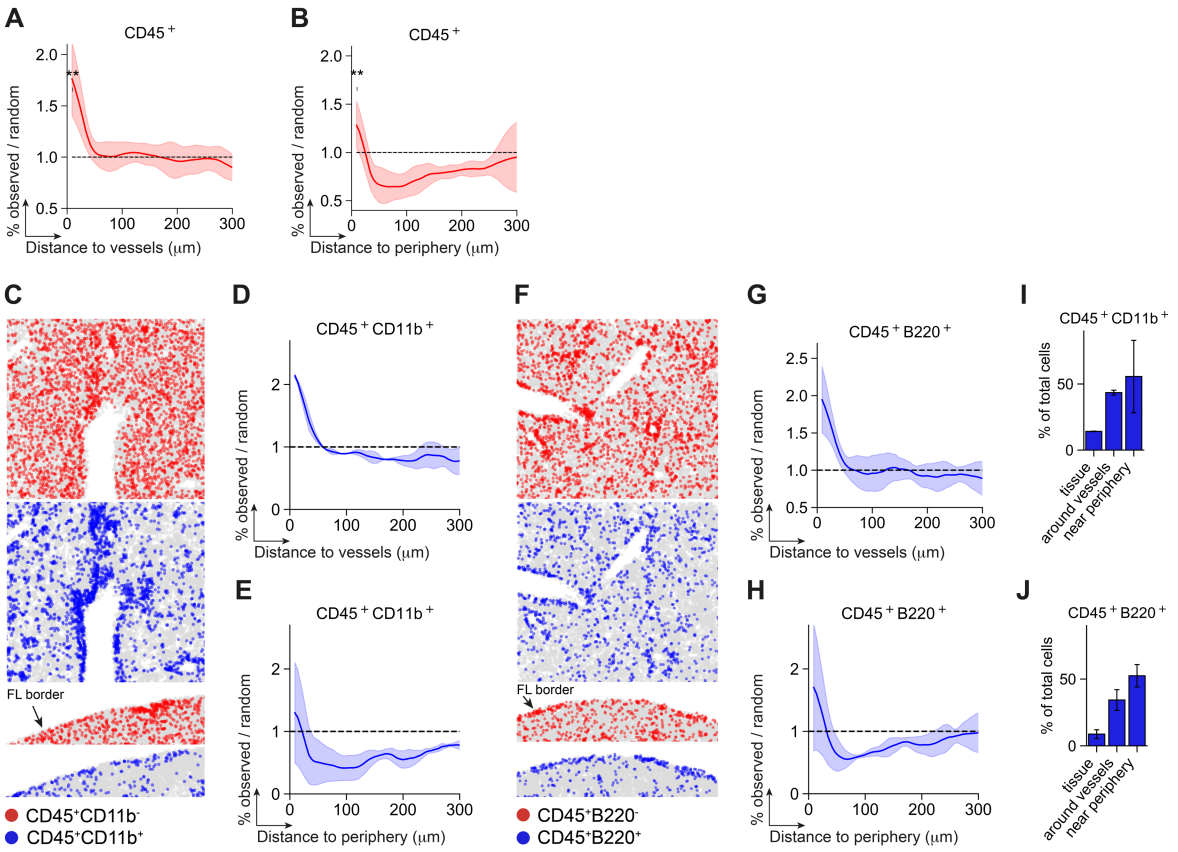


**Figure 32. Quantification of mature hematopoietic lineages around vessels and near the mesothelium at late gestation.**

(**A-B**) Distance to vessels (A) or the periphery (B) profile of CD45$^+$ cells of E18.5 FLs. Curves indicate average ± standard deviation (n=8). (**C**) Example of a dot plot representation of CD45$^+$CD11b$^-$ (red) and CD45$^+$CD11b$^+$ (blue) cells around vessels (top) and in the FL periphery (bottom) at E18.5. (**D-E**) Distance to vessels (D) or the periphery (E) profile of CD45$^+$CD11b$^+$ cells of E18.5 FLs. Curves indicate average ± standard deviation (n=2). (**F**) Example of a dot plot representation of CD45$^+$B220$^-$ (red) and CD45$^+$B220$^+$ (blue) cells around vessels (top) and in the FL periphery (bottom) at E18.5. (**G-H**) Distance to the vessels (G) or the periphery (H) profile of CD45$^+$B220$^+$ cells of E18.5 FLs. Curves indicate average ± standard deviation (n=4 in G, n=3 in H). (**I-J**) CD45$^+$CD11b$^+$ (I) or CD45$^+$B220$^+$ (J) frequency of total cells considering the entire sections analyzed (“tissue”), the regions around the vessels (‘around vessels’) or near the periphery (“near periphery”). Regions “around the vessels” or “near periphery” (3-4 cell layers) were manually selected using *Coloriage*.

## DISCUSSION

The challenge of identifying FL HSCs in their native microenvironment is not only associated with the need for combining multiple markers, or lack of specific reporter mice but also by our limited comprehension of their fetal phenotype. FL HSCs undergo maturation *in situ*, changing their surface markers' expression profile as development progresses. Even though FL HSCs do not immediately acquire CD150 upon arrival into the FL (**Kieusseian et al.**, **2012**), at E14.5, CD150 is already a fundamental marker for the identification of HSCs, as multipotent LTR is mostly restricted in the $CD150^+$ compartment (**Kim et al.**, **2006**). While other research groups have successfully assessed CD150 expression via IF in both the FL and BM (**Cordeiro Gomes et al.**, **2016**; **Khan et al.**, **2016**; **Lee et al.**, **2021**; **Liu et al.**, **2022**), we encountered difficulties in optimizing a staining strategy for this antibody. Consequently, our ability to resolve the progenitors' compartment was strongly impaired.

As we endeavored to develop a staining strategy enriching for HSCs, we simultaneously explored and fine-tuned the image analysis pipeline (described in **Chapter III**) using a simplified set of markers: KIT and CD45. Surprisingly, we noticed a small, but highly consistent tendency for $KIT^+$ and DP progenitors to be more frequently distributed around 50 μm away from the periphery at E12.5. At this stage, some regions of the liver feature a dense layer of sub-MCs that exhibit a high expression of *Cxcl12*, possibly contributing to elevated levels of this chemokine in the vicinity of the liver's periphery (**Chapter II**). Two sources of KITL were also enriched in this region: some MCs adjacent to the sub-mesothelial layer, and hepatoblasts, that were also mildly enriched 50 μm away from the periphery. As MCs secrete hepatic growth factors (PTN, HGH, EGF, MDK) (**Inagaki et al.**, **2015**; **Onitsuka et al.**, **2010**), we can hypothesize that the periphery of the liver is a privileged site for hepatoblasts proliferation or cell growth in general. As both hematopoietic progenitors were shown to be preferentially in contact with hepatoblasts, the existence of a multi-cellular circuit being established near the periphery could explain our observations. The exact chain of causality behind the localization of these cells around the periphery at this stage would need further investigation: they might be the result of the environment being rich in chemokines and cytokines, they might be accumulating as the preferential neighbors of the hepatoblasts they rely upon, or both.

By E14.5, the sub-mesothelial layer undergoes an overall reduction in thickness throughout the tissue. This reduction is likely due to the recruitment of mesenchymal cells into the parenchyma, to follow the expansion of the vascular network. Simultaneously, mesenchymal cells increase their levels of *Cxcl12*. During this stage, YS-derived progenitors, primarily comprising erythroid cells, are still located in close proximity to the

sub-mesothelial region. Notably, these cells do not express *Cxcr4*, suggesting that CXCL12 is not involved in shaping their distribution pattern. On the other hand, DP progenitors, that are responsive to CXCL12, are now randomly distributed. Our neighbor analysis shows that DP cells do not depend on direct contact with SCs, suggesting that DP cells could respond to a CXCL12 gradient instead. At E14.5, we start to see a tendency of $CD45^+$ cells to be in direct contact with MCs/sub-MCs. An environment rich in hematopoietic growth factors in the vicinity of the periphery, namely a high concentration of CXCL12 produced by the dense layer of sub-MCs might attract DP cells towards the periphery, and induce their differentiation into mature $CD45^+$ cells, explaining the distribution patterns observed at E14.5. In a similar way, as development progresses, the regions near the mesothelium and the vessels, as they are highly enriched with CXCL12-producing cells, might be zones that retain the hematopoietic cells and induce differentiation, leading to the accumulation of mature cells in these regions at later stages. Functional evidence is warranted to support these hypotheses.

Recently, by combining $\alpha$-*catulin* and *Hlf* reporter mice in a dual reporter, Helbling et al. were able to discriminate HSCs from downstream hematopoietic progenitor cells (HPCs) and characterize their distribution in FL thick sections (**Helbling et al.**, **2023**, pre-print). Interestingly, they did not find any particular pattern of spatial distribution or compartmentalization of HSCs/HPCs, nor a tendency to be closer to large vessels, sinusoids, or the liver's periphery at both stages analyzed (E13.5 and E17.5). However, at E13.5, the distribution of HSCs/HPCs was not entirely stochastic, as they exhibited clustering trends (not direct contact), which might reflect cell division. While this study is complementary to ours, it would be of interest to perform a neighbor analysis for HSCs/HPCs to see if they require direct contact with hepatoblasts and SCs.

## MATERIALS AND METHODS

### Mice

C57BL/6J mice were purchased from Envigo. *Flk1*-GFP mice (**M. Ema, Takahashi, et al.**, **2006**) were a gift from David Hardy. Timed pregnant females with vaginal plugs after overnight mating were considered to be E0.5. The day of birth was considered to be P0. Pregnant females and pups older than P21 were sacrificed by $CO_2$ inhalation, and cervical dislocation as a confirmation method. For embryos older than E15.5 and young pups, decapitation was performed. All animal manipulations were performed according to the ethics charter approved by the French Agriculture Ministry and to the European Parliament Directive 2010/63/EU.

### Isolation and FC analysis of FL hematopoietic cells

For the isolation of hematopoietic cells, E12.5, E14.5 and E18.5 FLs were dissected under a binocular magnifying lens. FLs were recovered in Hanks' balanced-salt solution (HBSS) supplemented with 1% fetal calf serum (FCS) (Gibco) and passed through a 26-gauge needle of a 1-ml syringe to obtain single-cell suspensions. Cell suspensions were filtered with a 100 µm cell strainer (BD) and stained with the antibodies listed in **Supplementary Table 11** or **12** for 20-30 min at 4ºC and analyzed on a custom BD LSR Fortessa (BD Biosciences), or the ID7000 spectral analyzer (SONY), respectively.

### FL sectioning, immunostaining, and optical clearing of thick sections

FLs from time-pregnant females were collected directly into freshly prepared 2% paraformaldehyde (PFA) fixative buffer (Fischer Scientific) and kept at 4°C overnight under rotation. After washing in PBS and removing surrounding tissues, FLs were immediately sectioned or shortly stored at 4ºC until sectioning. Following FLs embedding in 4% low-melting agarose (Sigma), 150 µm frontal sections were performed using a Leica VT1200S vibratome. Sections were permeabilized and blocked with PBS containing 0.05% Tween-20 (AppliChem GmbH) [or 0.5% Triton-X 100 for nuclear staining] and 10% donkey serum (Sigma-Aldrich) for 1-2 hours (h) at room temperature (RT). This solution was also used to dilute primary and secondary antibodies. Sections were incubated with primary antibodies for 2h at RT and overnight at 4ºC, and secondary antibodies for 2h at RT, both in the dark and with rotation (see **Supplementary Table 13** and **14**). Between incubations and after secondary antibody incubation, sections were washed repeatedly with PBS containing 0.05% Tween-20 and 3% NaCl (minimum 4×, 15 min). Sections were counterstained with DAPI (D9542, Sigma-Aldrich) for 2h at RT and kept overnight in RapiClear 1.52 (SunJin Lab) for optical clearing. Sections were mounted in RapiClear and imaged on a Leica TCS

SP8 using a PL APO 63x /1.40 oil immersion lens or APO 40x /1.40 oil immersion lens. Single stacks or multi-stacks tile scans were acquired at 200Hz or 400Hz, respectively, in bidirectional mode, at 12-bits and 1024×1024 resolution. Multi-stacks were acquired with z spacing of 0.3 µm.

## Image Analysis

### *Image processing and segmentation*

Before nuclei segmentation, images were sliced into small tiles (3000x3000 pixels for 2D images and 600x600xZ-stacks for 3D) using *Saucisson*. Each tile was then segmented based on DAPI signal using *Cellpose* (**Stringer et al.**, **2021**). Cellpose was run on parallel GPUs, and segmented tiles merged (using *Saucisson*) to reconstruct the original image. *CellPose* generates a cell mask, around the cell nuclei, that is used to extract the cell's properties (coordinates, signal intensity of each channel, area) using the package *Griottes* (**Ronteix et al.**, **2022**).

### *Cell classification*

For nuclear staining, the average signal intensity is computed using *Griottes* and a threshold is manually determined to distinguish between positive and negative cells. To classify cells based on membrane/cytoplasmic staining, images of 80x80 pixels were cropped centered around each nucleus detected containing a membrane signal in grayscale. Cell classification was conducted using a neural network specifically selected and trained for each marker. Different models were used since the image properties were highly dependent on the staining. Training and validation datasets were manually created for each staining (CD45, KIT, AF), using data from different images. A transfer learning approach has been used to train neural networks: *SqueezeNet* networks (**Iandola et al.**, **2016**) (loaded pre-trained from *PyTorch* (**Paszke et al.**, **2019**) were trained with our datasets, using 32 batch size). An accuracy > 95% has been achieved on validation datasets for each membrane staining (**Table 9**). Some manual corrections in the classification have been done for images with lower staining contrast.

**Table 9. Network training.**
Size of the training and validation datasets manually curated to implement the deep learning models used to classify different membrane markers and AF in this study, and the corresponding accuracy of the models generated.

| | *Training dataset* | | *Validation dataset* | | |
|---|---|---|---|---|---|
| | *NEGATIVE* | *POSITIVE* | *NEGATIVE* | *POSITIVE* | *Accuracy* |
| CD45 | 2410 | 1365 | 587 | 365 | 0.954 |
| KIT | 5896 | 1958 | 1406 | 280 | 0.956 |

| | | | | | |
|---|---|---|---|---|---|
| B220 | 6794 | 1480 | 2205 | 511 | 0.976 |
| CD11b | 1139 | 1104 | 231 | 432 | 0.979 |
| AF | 2033 | 861 | 293 | 167 | 0.952 |

***Removal and selection of specific regions***

AF cells were classified using the neural network approach previously described and excluded from analysis. Pieces of the tissue with lower staining quality, disrupted lobes and pieces of other organs were manually selected using the interactive tool *Coloriage*. *Coloriage* was also used to manually select specific FL structures, namely the liver's periphery and major vessels. The Minimum Euclidian distance between each cell and a cell attributed to the structure of interest was calculated. The concentration of each cell type at a given distance was normalized to the predicted one in a random distribution scenario (% observed/random). A random distribution was calculated by shuffling the cell types, while preserving the structure of the tissue and frequency of each cell type, and re-calculating the distance to the respective structure (5 iterations, averaged).

***Network construction***

The connectivity networks of the FLs were generated using *Griottes* from a data table containing the positions and properties of the cells (i.e., cell size, cell type and fluorescent intensities) using 'Delaunay' construction rule, as described in (**Ronteix et al., 2022**). A random distribution was calculated by shuffling the cell types, except the stromal cell types (fixed location), and re-calculating the contacts distributions (10 iterations).

***Code availability***

The analysis of the FL network images was conducted on Jupyter Notebook. All the relevant notebooks are freely accessible on the project GitHub repository (https://github.com/BaroudLab/FL-Image-Analysis). Different packages have been custom-made for the analysis of the FL images, during pre-processing and data analysis. All these functionalities (*Saucisson, Coloriage*) have been incorporated into the main GitHub for easier use and installation. This repository contains notebooks to reproduce all relevant panels of the article in **Annex VI** and a step-by-step tutorial to run the entire image analysis pipeline and data analysis previously described.

# SUPPLEMENTARY INFORMATION

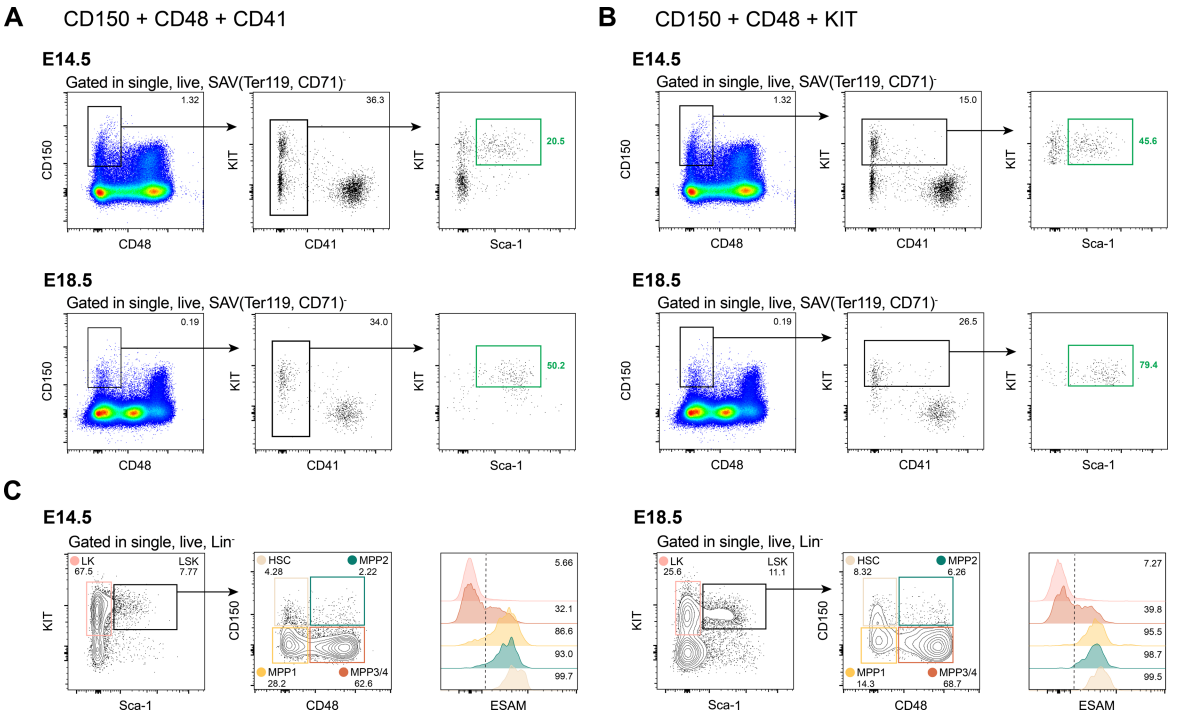


**Supplementary Figure 5. Searching for an efficient staining strategy to enrich phenotypic HSCs.**

(**A-B**) Gating strategy to quantify the percentage of enrichment in LT-HSCs by combining CD150, CD48 and CD41 (A) or CD150, CD48 and KIT (B) at E14.5 and E18.5. FL isolated cells were depleted of $Ter119^{+}CD71^{+}$ cells. (**C**) FC analysis of FC isolated cells depleted of $Ter119^{+}CD71^{+}$ cells and gated in single, live, $Lin(Gr\text{-}1, CD19, B220, NK1.1, CD41)^{-}$, to assess the expression of ESAM across different populations of hematopoietic progenitors (LK, LT-HSC, MPP1, MPP2 and MPP3/4) at E14.5 and E18.5.

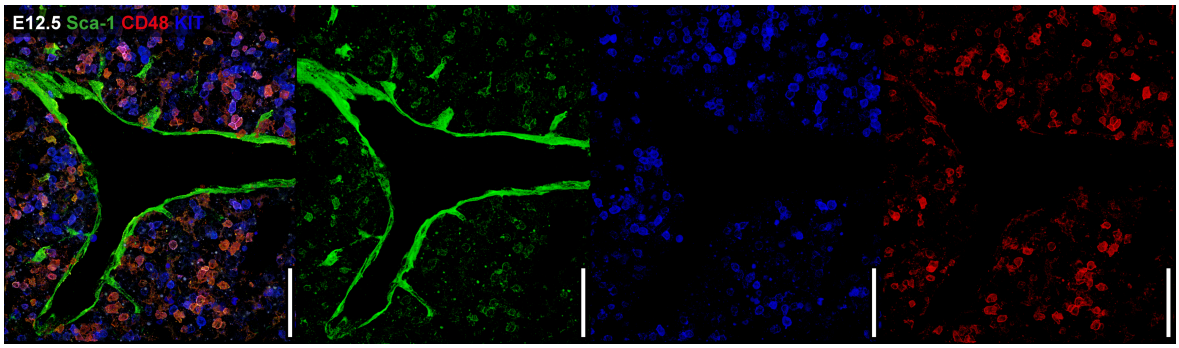


**Supplementary Figure 6. Technical difficulties encountered in the staining strategy combining KIT, CD48 and Sca-1.**
Representative 3D view (15 μm) IF of E12.5 FL with Sca-1 (green), CD48 (red) and KIT (blue). In this staining, KIT (rat) and CD48 (goat) were incubated together, followed by an incubation of their respective secondary anti-rat and anti-goat antibodies. Sca-1 was only incubated after, in an sequence of incubations: Sca-1-PE > rabbit anti-PE > anti-rabbit. Scale bar 100μm.

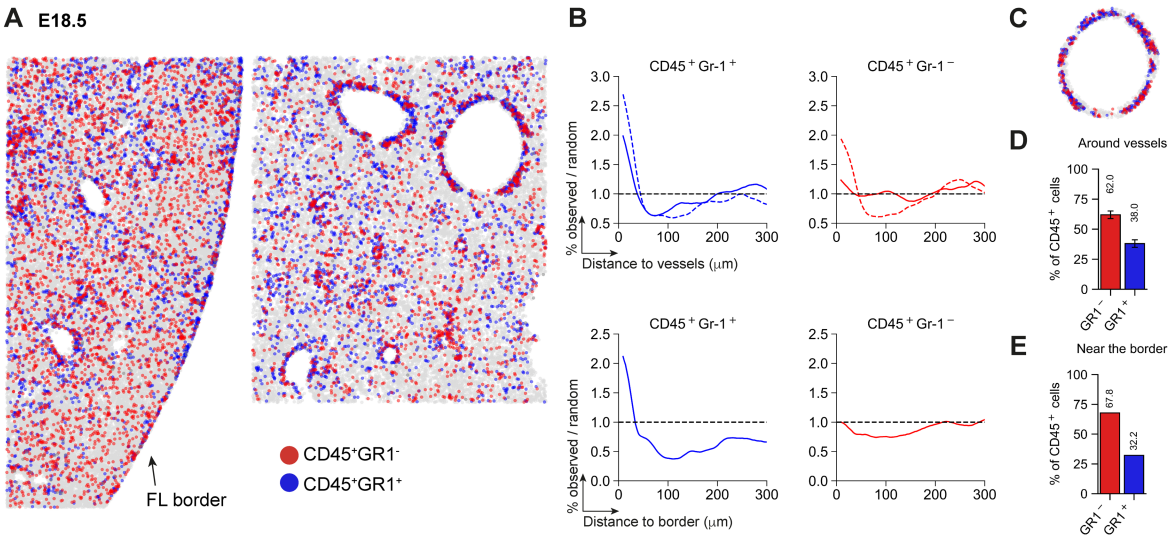


**Supplementary Figure 7. Quantification of mature hematopoietic lineages around vessels and near the mesothelium at late gestation.**

(**A**) Dot plot representation of two E18.5 FL sections, showing CD45$^+$Gr-1$^-$ cells (red) and CD45$^+$GR-1$^+$ cells (blue). (**B**) Distance to the vessels (upper panel, n=2, the two sections represented in A) or to the periphery (lower panel, n=1, section in A catching a portion of mesothelium) of CD45$^+$Gr-1$^-$ cells (red) and CD45$^+$GR-1$^+$ cells (blue). (**C**) Representative example of the selection around the vessels using the tool *Coloriage*. (**D-F**) Frequency of CD45$^+$Gr-1$^-$ cells (red) and CD45$^+$GR-1$^+$ cells (blue) in the regions selected as “vessels” or “periphery”, as exemplified in (C).

**Supplementary Table 8. List of antibodies tested to optimize an HSC-enriched staining.**
* The signal/noise ratio is very low using a streptavidin/anti-biotin, but good using an anti-goat secondary antibody.

| *ANTIBODY* | *CONJ.* | *SPECIES* | *CLONE* | *REFERENCE* | *SUPPLIER* | *WORK?* |
|---|---|---|---|---|---|---|
| CD150 | - | Rat | 9D1 | MCA2274GA | Bio-Rad | No |
| CD150 | PE | Rat | TC15-12F12.2 | 115903 | BioLegend | No |
| CD41 | biotin | Rat | MWReg30 | 133930 | BioLegend | Yes |
| CD45 | - | Goat | Poly | AF114 | R&D | Yes |
| CD45 | biotin | Rat | 30-F11 | 203104 | BioLegend | Yes |
| CD48 | - | Goat | Poly | AF3327 | R&D | Yes |
| CD48 | biotin | Goat | Poly | BAF3327 | R&D | Yes* |
| CD48 | biotin | Hamster | HM48-1 | 103409 | BioLegend | No |
| ESAM | - | Goat | Poly | PA5-48019 | Invitrogen | No |
| ESAM | APC | Rat | 1G8/ESAM | 136207 | BioLegend | No |
| KIT | APC | Rat | 2B8 | 105812 | BioLegend | Yes |
| KIT | - | Rat | 2B8 | 553352 | BD | Yes |
| KIT | FITC | Rat | 2B8 | 11-1171-82 | eBioscience | Yes |
| KIT | - | Goat | Poly | AF1356 | R6D | No |
| KIT | biotin | Rat | 2B8 | ab25022 | abcam | No |
| KIT | - | Goat | Poly | sc-1494 | Santa Cruz Biotech | No |
| KIT | - | Rabbit | Poly | sc-168 | Santa Cruz Biotech | No |
| Sca-1 | PE | Rat | D7 | 553108 | BD | Yes |
| Sca-1 | PE | Rat | D7 | 12-5981-81 | eBioscience | No |
| Sca-1 | FITC | Rat | D7 | 11-5981-82 | eBioscience | No |
| Sca-1 | - | Rat | D7 | 108101 | BioLegend | No |
| Sca-1 | biotin | Goat | Poly | BAF1226 | R&D | No |

**Supplementary Table 9. Percentages of enrichment for LT-HSCs and LSK CD48$^-$ considering different combinations of markers at E14.5 and E18.5.**

The percentage of enrichment corresponds to the percentage of cells with the Lin(Gr-1, CD19, B220, NK1.1)$^-$KIT$^+$Sca-1$^+$CD150$^{+/-}$CD48$^-$CD41$^{-/low}$ phenotype after gating accordingly to the 2/3 markers of each combination below, as exemplified. FL isolated cells were depleted of Ter119$^+$CD71$^+$ cells and analyzed in the spectral cytometer SONY ID7000.

| | | 0 | 1 | 2 | 3 | 4 | 5 | 6 | 7 | 8 | 9 | 10 | 11 | 12 | 13 | 14 | 15 | 16 | 17 | 18 |
|---|---|---|---|---|---|---|---|---|---|---|---|---|---|---|---|---|---|---|---|---|
| + | CD45 | + | + | + | + | + | + | + | + | + | + | + | + | + | + | + | + | | | |
| + | KIT | + | + | + | + | + | + | | | | | | | | | | | + | + | + |
| + | SCA-1 | | + | | | | | + | + | + | + | | | | | | | + | + | + |
| + | CD150 | | | + | | | | + | | | | + | + | + | | | | + | | |
| - | CD48 | | | | + | | | | + | | | + | | | + | + | | | + | |
| + | ESAM | | | | | + | | | | + | | | + | | + | | + | | | + |
| - | CD41 | | | | | | + | | | | + | | | + | | + | + | | | |
| E14.5 | LT-HSC | 0.31 | 6.32 | 2.06 | 6.60 | 3.30 | 0.30 | **35.5** | 4.73 | 3.93 | 0.96 | **34.0** | 19.9 | 4.64 | 5.15 | 0.74 | 2.97 | **43.9** | 7.38 | 4.52 |
| | LSK CD48$^-$ | 4.27 | 40.2 | | **82.6** | 38.3 | 4.19 | | 62.7 | 44.5 | 12.9 | | | | 62.6 | 10.2 | 32.6 | | **99.7** | 52.1 |
| E18.5 | LT-HSC | 1.25 | 8.11 | 2.75 | 15.8 | 6.05 | 1.24 | 18.2 | 1.04 | 1.74 | 0.62 | 22.9 | 15.3 | 20.9 | 1.51 | 0.10 | 1.23 | **32.2** | 17.7 | 6.25 |
| | LSK CD48$^-$ | 7.34 | 23.3 | | **81.3** | 28.6 | 6.31 | | 5.24 | 8.09 | 3.18 | | | | 7.33 | 0.52 | 5.70 | | **96.9** | 31.6 |

| | | 19 | 20 | 21 | 22 | 23 | 24 | 25 | 26 | 27 | 28 | 29 | 30 | 31 | 32 | 33 | 34 | 35 | 36 |
|---|---|---|---|---|---|---|---|---|---|---|---|---|---|---|---|---|---|---|---|
| + | CD45 | | | | | | | | | | | | | | | | | | |
| + | KIT | + | + | + | + | + | + | + | | | | | | | | | | | |
| + | SCA-1 | + | | | | | | | + | + | + | + | + | + | | | | | |
| + | CD150 | | + | + | + | | | | + | + | + | | | | + | + | + | | + |
| - | CD48 | | + | | | + | + | | + | | | + | + | | + | + | | + | + |
| + | ESAM | | | + | | + | | + | | + | | + | | + | + | | + | + | |
| - | CD41 | + | | | + | | + | + | | | + | | + | + | | + | + | + | |
| E14.5 | LT-HSC | 1.21 | **45.6** | 24.4 | 2.96 | 8.07 | 3.46 | 3.54 | **33.6** | **31.0** | **39.6** | 3.97 | 3.01 | 2.93 | 25.0 | **20.5** | 22.5 | 2.22 | 7.28 |
| | LSK CD48$^-$ | 16.9 | | | | **93.1** | 46.6 | 39.3 | | | | 45.8 | 37.3 | 33.7 | | | | 26.2 | |
| E18.5 | LT-HSC | 1.81 | **79.4** | 30.8 | 9.95 | 18.2 | 14.5 | 5.70 | 24.8 | 16.4 | 28.4 | 0.99 | 0.60 | 0.86 | 16.6 | **52.0** | 29.9 | 0.65 | 15.4 |
| | LSK CD48$^-$ | 10.2 | | | | **91.6** | **78.5** | 28.1 | | | | 4.93 | 3.17 | 4.37 | | | | 3.31 | |

**Supplementary Table 10. Staining strategy combining KIT, Sca-1 and CD48.**

| 1° | 2° | 3° | 4° | 5° | 6° | 7° |
|---|---|---|---|---|---|---|
| KIT APC (rat) | Donkey anti-rat 647 | - | - | - | - | - |
| - | - | Sca-1 PE (rat) | Rabbit anti-PE | Donkey anti-rabbit 568 | - | - |
| - | - | - | - | - | CD48 (goat) | Donkey anti-goat 488 |

**Supplementary Table 11. List of antibodies used for the analysis of FL hematopoietic populations in Figure 26 and 27.**

| *SPECIFICITY* | *CONJUGATION* | *CLONE* | *REFERENCE* | *SUPPLIER* |
|---|---|---|---|---|
| CD11b | APC-Cy7 | M1/70 | 1106130 | Sony Biotechnology Inc. |
| CD16/32 | FITC | 93 | 1106530 | Sony Biotechnology Inc. |
| CD24 | BUV496 | M1/69 | 612953 | BD Biosciences |
| CD34 | PE | RAM34 | 551387 | BD Biosciences |
| CD45 | BV786 | 30-F11 | 564225 | BD Biosciences |
| CD48 | APC | HM48-1 | 1117060 | Sony Biotechnology Inc. |
| CD71 | BV421 | RI7217 | 1169065 | Sony Biotechnology Inc. |
| CD150 | BV711 | TC15-12F12.2 | 1179705 | Sony Biotechnology Inc. |
| Gr-1 | BUV395 | RB6-8C5 | 563849 | BD Biosciences |
| KIT | BV605 | 2B8 | 563146 | BD Biosciences |
| Sca-1 | BV510 | D7 | 565507 | BD Biosciences |
| Ter119 | PE-Cy7 | TER119 | 1181110 | Sony Biotechnology Inc. |

**Supplementary Table 12. List of antibodies used for the analysis of FL hematopoietic populations in Supplementary Figure 5.**

| *SPECIFICITY* | *CONJUGATION* | *CLONE* | *REFERENCE* | *SUPPLIER* |
|---|---|---|---|---|
| KIT | BUV805 | 2B8 | 624287 | BD Biosciences |
| CD31 | BUV737 | MEC 13.3 | 565097 | BD Biosciences |
| CD19 | BUV661 | 1D3 | 565079 | BD Biosciences |
| Gr-1 | BUV395 | RB6-8C5 | 563849 | BD Biosciences |
| Streptavidin | BV785 | - | 2626245 | Sony Biotechnology Inc. |
| CD150 | BV711 | TC15-12F12.2 | 1179705 | Sony Biotechnology Inc. |
| CD45.2 | BV650 | 104 | 740490 | BD Biosciences |
| Sca-1 | BV605 | E13-161.7 | 744324 | BD Biosciences |
| CD24 | BV510 | M1/69 | 1109255 | Sony Biotechnology Inc. |
| CD34 | BV421 | RAM34 | 562608 | BD Biosciences |
| CD16/32 | PerCP-Cy5 | 93 | 1106620 | Sony Biotechnology Inc. |
| CD48 | FITC | HM48-1 | 11-0481-82 | eBioscience |
| B220 | PE-CF594 | RA3-6B2 | 562313 | BD Biosciences |
| CD41 | PE | MWReg30 | 561850 | eBioscience |
| NK1.1 | APC-Cy7 | PK136 | 1143620 | Sony Biotechnology Inc. |
| CD11b | AF700 | M1/70 | 557960 | BD Biosciences |
| ESAM | APC | 1G8/ESAM | 136207 | BioLegend |

**Supplementary Table 13. List of primary antibodies used for IF.**

| *ANTIBODY* | *SPECIES* | *CLONE* | *REFERENCE* | *SUPPLIER* |
|---|---|---|---|---|
| B220-FITC | Rat | RA3-6B2 | 103205 | BioLegend |
| CD11b-FITC | Rat | M1/70 | 101205 | BioLegend |
| GR-1-FITC | Rat | RB6-8C5 | 11-5931-82 | eBioscience |
| CD45 | Goat | Poly | AF114 | R&D |
| DsRed | Rabbit | Poly | 632496 | TAKARA |
| GFP | Rabbit | Poly | A11122 | Invitrogen |
| HNF4α | Mouse | K9218 | MA1-199 | ThermoFischer |
| HNF4α | Rabbit | EPR16885-99 | Ab201460 | abcam |
| KIT-APC | Rat | 2B8 | 116203 | BioLegend |
| LHX2 | Rabbit | Poly | ABE1402 | Sigma-Aldrich |

**Supplementary Table 14. List of secondary antibodies used for IF.**

| *ANTIBODY* | *CONJUGATION* | *REFERENCE* | *SUPPLIER* |
|---|---|---|---|
| Chicken anti-mouse | AF647 | A21463 | Invitrogen |
| Donkey anti-mouse | AF488 | A21202 | Invitrogen |
| Donkey anti-mouse | AF568 | A10037 | Invitrogen |
| Donkey anti-goat | AF488 | A11055 | Invitrogen |
| Donkey anti-goat | AF568 | A11057 | Invitrogen |
| Donkey anti-goat | AF647 | A21447 | Invitrogen |
| Donkey anti-rabbit | AF488 | A21206 | Invitrogen |
| Donkey anti-rabbit | AF568 | A10042 | Invitrogen |
| Donkey anti-rabbit | AF647 | A31573 | Invitrogen |
| Donkey anti-rat | AF488 | A21208 | Invitrogen |
| Donkey anti-rat | AF647 | A48272 | Invitrogen |
| Donkey anti-rat | AF647 | 712-606-150 | Jackson ImmunoResearch |
| Rabbit anti-PE | - | PA5-35006 | Invitrogen |

# EPILOG

While the FL has historically been acknowledged as a pivotal hematopoietic niche believed to harbor substantial HSC expansion potential (**Ema & Nakauchi**, **2000**), it remained largely underexplored until recent times. During the course of this work, multiple studies have been published regarding the FL hematopoietic niche (**Gao et al.**, **2022**; **Kayvanjoo et al.**, **2023**; **Lee et al.**, **2021**, **2022**; **Lu et al.**, **2021**; **Shao et al.**, **2023**). Our study and a parallel independent study from Nombela-Arrieta's lab, combining 3D quantitative microscopy, FC, *Kitl*- and *Cxcl12*-reporter mice models, and transcriptomic analysis, have recently been submitted back-to-back to peer revision (**Helbling et al.**, **2023**, pre-print; **Peixoto et al.**, **2023**, pre-print, Annex VI). The two studies bring an extensive and complementary characterization of the FL niche, identifying its cellular components, the cytokine producer cells and mapping the global distribution of key stromal cells and HSPCs throughout development. Remarkably, Helbling and colleagues were able to discriminate HSCs and downstream HPCs *in situ,* an unmet goal of this thesis work, through the implementation of a double reporter mouse (*Ctnnal1*$^{GFP/wt}$*Hlf*$^{dtTom/wt}$).

**Digging for the niche**

Herein, we took advantage of spectral cytometry to improve the discrimination of isolated FL cells depleted of hematopoietic cells using a relatively small antibody panel (14 colors). We identified two specific AF profiles, one attributed to SCs (AF-1) and the other to hepatic cells (AF-2), mainly hepatoblasts. These insights contributed to the refinement of our sorting strategy of FL stromal cells, ultimately leading to the identification of 10 major populations, which can be broadly categorized into 4 major compartments.

Endothelial cells (CD31$^{+}$CD146$^{+}$) are widely distributed throughout the FL, through an intricate network of sinusoids connected to portal and central veins. Although we did not find a tendency of CD45$^{+}$, KIT$^{+}$, or DP to contact with endothelial cells at E12.5 and E14.5, we acknowledge that our analysis should be refined, either by increasing the sample size and computing the distance to the vessel structures, instead of the center of the endothelial cell. Interestingly, Helbling et al. also did not observe a preferential association of HSCs with vessels (**Helbling et al.**, **2023**, pre-print), in opposition to previous reports (**Khan et al.**, **2016**; **Lee et al.**, **2021**). As gestation progressed, we found mature CD45$^{+}$ cells to accumulate in the vicinity of larger vessels (portal and central veins). Much like their counterparts in the BM, these endothelial cells express *Kitl* transcripts but are not the

primary cell type responsible for producing this factor, contrary to previously reported (**Lee et al.**, **2021**). In the BM, even though LepR$^+$ cells exhibit significantly higher levels of *Kitl* expression compared to endothelial cells, depletion of *Kitl* from either source leads to an HSC strong reduction, suggesting a dependency on endothelial-*Kitl*. The same is not true in the FL, as *Kitl*-endothelial deletion seems to be compensated by other sources (**Azzoni et al.**, **2018**; **Lee et al.**, **2021**).

Hepatoblasts (E-Cadh$^{high}$EpCAM$^-$, AF-2$^+$) are abundantly distributed throughout the FL and serve as a diverse source of hematopoietic factors, namely, KITL, CXCL12, EPO, IL-7, TPO and CSF1. KIT$^+$ and DP progenitors seem to be highly dependent on cell contact with hepatoblasts. However, at late gestation, with hepatic maturation, hepatoblasts become a rare population and downregulate hematopoietic factors, potentially contributing to the exit of the HS from the FL.

MCs (Gp38$^+$) and sub-MCs at the liver periphery were shown for the first time to play a role in hematopoietic development, by being major sources of KITL and CXCL12, respectively. Of note, our FC analysis does not allow to discriminate sub-MCs within the mesenchymal compartment, as they share the same phenotype as SCs. It is thus still not clear whether they are a distinct population from SCs or not. Curiously, we found a higher concentration of KIT$^+$ and DP cells in the vicinity (50 $\mu$m away) of the liver's periphery. The biological significance of this finding and the role of the liver periphery in this context remain to be fully understood. At late gestation, much like blood vessels, the liver periphery appears to be a preferred site for hematopoietic differentiation. Notably, we observed significant heterogeneity within the liver periphery, particularly in terms of NG2 expression in MCs, *Kitl*-expression in MCs, *Cxcl12*-expression in sub-MCs, the thickness of the sub-mesothelial layer throughout the entire region at early stages, and CD45$^+$ accumulation. Although we did not conduct an exhaustive systematic investigation into this heterogeneity, it requires further exploration.

Mesenchymal cells (PDGFR$\alpha^+$) were found to be the main source of CXCL12 and to upregulate this factor with time. The accumulation of CD45$^+$ at late gestation around vessels is likely related to the concentration of CXCL12 produced in the vessels' vicinity. Within this compartment, we were able to distinguish two primary sub-populations, reported as important niche cells (**Khan et al.**, **2016**; **Lee et al.**, **2021**): NG2 PFs (PDGFR$\alpha^+$NG2$^+$; AF-1$^-$) and SCs (PDGFR$\alpha^+$ALCAM$^+$NG2$^{-/low}$; AF-1$^{-/+}$). However, it is important to note that what we broadly refer to as SCs also encompasses sub-MCs and SLCs. Our gene expression analysis did not possess the depth required to fully resolve the heterogeneities among these populations.

In our study, we missed to address the hematopoietic compartment itself as a niche component. In the adult BM, monocytes, macrophages, dendritic cells, and Mks have been shown to regulate the HSC compartment (**Comazzetto et al.**, **2021**). Similarly, in the FL, recent studies have implicated macrophages as relevant niche players (**Gao et al.**, **2022**, **p. 202**; **Kayvanjoo et al.**, **2023**; **Mariani et al.**, **2019**). It is of paramount importance to extend the analysis to encompass other hematopoietic lineages. Namely, it would be interesting to locate HSCs/HPCs using the *Ctnnal1*$^{GFP/wt}$*Hlf*$^{dtTom/wt}$ model and analyze their neighbor composition in terms of mature lineages.

**Spatial analysis**

While there is room for improvement in our image analysis pipeline, especially in terms of incorporating a step for segmenting volumetric objects such as blood vessels, we proved its value in identifying patterns of cell distributions and its robustness for the analysis of cellular networks. This tool is publicly available, and we hope it will serve as a valuable resource for fellow scientists, potentially unlocking interesting patterns in biological tissues.

**Expansion**

The idea that the FL is a site of extensive proliferation of HSCs comes mainly from a single paper quantifying LTR HSCs throughout liver development (**Ema & Nakauchi**, **2000**). As reiterated throughout this manuscript, a higher input number of pre-HSCs colonizing the FL, and maturation rather than proliferation, could explain the over 30-fold increase in RUs from E12.5 to E16.5. In the scenario from Ganuza et al., a minimal expansion of the stem cell pool, nearly 2-fold would occur during liver development (**Ganuza et al.**, **2017**, **2022**), and 3/4 additional rounds of division would have to occur in the global population thereafter to reach the numbers of the pool in the adult. Given the overall growth of the entire organism, undergoing approximately 5 to 6 rounds of division does not seem particularly remarkable and may be indicative of a general, rather than a locally specific, mechanism. Supporting this hypothesis, we found *Igf2* to be considerably highly expressed by nearly all FL stromal cells. IGF2 is a potent embryonic growth factor, highly expressed in embryonic tissues and the blood, and strongly downregulated in the adult (**Chao & D'Amore**, **2008**). IGF2 was identified as a key factor promoting HSC expansion in co-culture systems with putative hepatoblasts, as expansion could be impaired using neutralizing anti-IGF2 antibodies (**Zhang & Lodish**, **2004**). Hence, it is plausible that while the fetal liver unquestionably plays a key role in hematopoietic development, its significance for HSCs may be comparatively less prominent and requires additional investigation.

**Final thought**

While erythrocyte development appears to be highly dependent on the FL microenvironment, particularly through direct interaction of erythroid progenitors with hepatoblasts, major producers of *Kitl* and *Epo,* the influence of the FL on HSCs remains considerably less understood. *What would be the implications for HSC development if pre-HSCs did not colonize the FL? Is it conceivable that pre-HSCs could preserve their stemness and undergo maturation within the bloodstream until they eventually colonize the BM?* Addressing these questions could offer an alternative strategy to understand the role of the FL in HSC development.

# REFERENCES


Acar, M., Kocherlakota, K. S., Murphy, M. M., Peyer, J. G., Oguro, H., Inra, C. N., Jaiyeola, C., Zhao, Z., Luby-Phelps, K., & Morrison, S. J. (2015). Deep imaging of bone marrow shows non-dividing stem cells are mainly perisinusoidal. *Nature*, *526*(7571), 126–130. https://doi.org/10.1038/nature15250

Adolfsson, J., Månsson, R., Buza-Vidas, N., Hultquist, A., Liuba, K., Jensen, C. T., Bryder, D., Yang, L., Borge, O.-J., Thoren, L. A. M., Anderson, K., Sitnicka, E., Sasaki, Y., Sigvardsson, M., & Jacobsen, S. E. W. (2005). Identification of Flt3+ Lympho-Myeloid Stem Cells Lacking Erythro-Megakaryocytic Potential. *Cell*, *121*(2), 295–306. https://doi.org/10.1016/j.cell.2005.02.013

Ajami, B., Bennett, J. L., Krieger, C., Tetzlaff, W., & Rossi, F. M. V. (2007). Local self-renewal can sustain CNS microglia maintenance and function throughout adult life. *Nature Neuroscience*, *10*(12), 1538–1543. https://doi.org/10.1038/nn2014

Akashi, K., Traver, D., Miyamoto, T., & Weissman, I. L. (2000). A clonogenic common myeloid progenitor that gives rise to all myeloid lineages. *Nature*, *404*(6774), 193–197. https://doi.org/10.1038/35004599

Alvarez-Silva, M., Belo-Diabangouaya, P., Salaün, J., & Dieterlen-Lièvre, F. (2003). Mouse placenta is a major hematopoietic organ. *Development*, *130*(22), 5437–5444. https://doi.org/10.1242/dev.00755

Ara, T., Tokoyoda, K., Sugiyama, T., Egawa, T., Kawabata, K., & Nagasawa, T. (2003). Long-Term Hematopoietic Stem Cells Require Stromal Cell-Derived Factor-1 for Colonizing Bone Marrow during Ontogeny. *Immunity*, *19*(2), 257–267. https://doi.org/10.1016/S1074-7613(03)00201-2

Ariel, P. (2017). A beginner's guide to tissue clearing. *The International Journal of Biochemistry & Cell Biology*, *84*, 35–39. https://doi.org/10.1016/j.biocel.2016.12.009

Asada, N., Kunisaki, Y., Pierce, H., Wang, Z., Fernandez, N. F., Birbrair, A., Ma'ayan, A., & Frenette, P. S. (2017). Differential cytokine contributions of perivascular haematopoietic stem cell niches. *Nature Cell Biology*, *19*(3), 214–223. https://doi.org/10.1038/ncb3475

Asahina, K. (2012). Hepatic stellate cell progenitor cells: Origin of HSCs. *Journal of Gastroenterology and Hepatology*, *27*, 80–84. https://doi.org/10.1111/j.1440-1746.2011.07001.x

Asahina, K., Sato, H., Yamasaki, C., Kataoka, M., Shiokawa, M., Katayama, S., Tateno, C., & Yoshizato, K. (2002). Pleiotrophin/Heparin-Binding Growth-Associated Molecule as a Mitogen of Rat Hepatocytes and Its Role in Regeneration and Development of Liver. *The American Journal of Pathology*, *160*(6), 2191–2205. https://doi.org/10.1016/S0002-9440(10)61167-4

Asahina, K., Tsai, S. Y., Li, P., Ishii, M., Maxson, R. E., Sucov, H. M., & Tsukamoto, H. (2009). Mesenchymal origin of hepatic stellate cells, submesothelial cells, and perivascular mesenchymal cells during mouse liver development. *Hepatology*, *49*(3), 998–1011. https://doi.org/10.1002/hep.22721

Asahina, K., Zhou, B., Pu, W. T., & Tsukamoto, H. (2011). Septum transversum-derived mesothelium gives rise to hepatic stellate cells and perivascular mesenchymal cells in developing mouse liver. *Hepatology*, *53*(3), 983–995. https://doi.org/10.1002/hep.24119

Azzoni, E., Frontera, V., Anselmi, G., Rode, C., James, C., Deltcheva, E. M., Demian, A. S., Brown, J., Barone, C., Patelli, A., Harman, J. R., Nicholls, M., Conway, S. J., Morrissey, E., Jacobsen, S. E. W., Sparrow, D. B., Harris, A. L., Enver, T., & de Bruijn, M. F. T. R. (2021). The onset of circulation triggers a metabolic switch required for endothelial to hematopoietic transition. *Cell Reports*, *37*(11), 110103. https://doi.org/10.1016/j.celrep.2021.110103

Azzoni, E., Frontera, V., McGrath, K. E., Harman, J., Carrelha, J., Nerlov, C., Palis, J., Jacobsen, S. E. W., & Bruijn, M. F. (2018). Kit ligand has a critical role in mouse yolk sac and aorta–gonad–mesonephros hematopoiesis. *EMBO Reports*, *19*(10). https://doi.org/10.15252/embr.201745477

Balazs, A. B., Fabian, A. J., Esmon, C. T., & Mulligan, R. C. (2006). Endothelial protein C receptor (CD201) explicitly identifies hematopoietic stem cells in murine bone marrow. *Blood*, *107*(6), 2317–2321. https://doi.org/10.1182/blood-2005-06-2249

Barker, J. E. (1994). Sl/Sld hematopoietic progenitors are deficient in situ. *Experimental Hematology*, *22*(2), 174–177.

Baron, M. H., Isern, J., & Fraser, S. T. (2012). The embryonic origins of erythropoiesis in mammals. *Blood*, *119*(21), 4828–4837. https://doi.org/10.1182/blood-2012-01-153486

Baryawno, N., Przybylski, D., Kowalczyk, M. S., Kfoury, Y., Severe, N., Gustafsson, K., Kokkaliaris, K. D., Mercier, F., Tabaka, M., Hofree, M., Dionne, D., Papazian, A., Lee, D., Ashenberg, O., Subramanian, A., Vaishnav, E. D., Rozenblatt-Rosen, O., Regev, A., & Scadden, D. T. (2019). A Cellular Taxonomy of the Bone Marrow Stroma in Homeostasis and Leukemia. *Cell*, *177*(7), 1915-1932.e16. https://doi.org/10.1016/j.cell.2019.04.040

Baumann, C. I., Bailey, A. S., Li, W., Ferkowicz, M. J., Yoder, M. C., & Fleming, W. H. (2004). PECAM-1 is expressed on hematopoietic stem cells throughout ontogeny and identifies a population of erythroid progenitors. *Blood*, *104*(4), 1010–1016. https://doi.org/10.1182/blood-2004-03-0989

Beaudin, A. E., Boyer, S. W., & Forsberg, E. C. (2014). Flk2/Flt3 promotes both myeloid and lymphoid development by expanding non–self-renewing multipotent hematopoietic progenitor cells. *Experimental Hematology*, *42*(3), 218-229.e4. https://doi.org/10.1016/j.exphem.2013.11.013

Beaudin, A. E., Boyer, S. W., Perez-Cunningham, J., Hernandez, G. E., Derderian, S. C., Jujjavarapu, C., Aaserude, E., MacKenzie, T., & Forsberg, E. C. (2016). A Transient Developmental Hematopoietic Stem Cell Gives Rise to Innate-like B and T Cells. *Cell Stem Cell*, *19*(6), 768–783. https://doi.org/10.1016/j.stem.2016.08.013

Becker, A. J., McCulloch, E. A., & Till, J. E. (1963). Cytological Demonstration of the Clonal Nature of Spleen Colonies Derived from Transplanted Mouse Marrow Cells. *Nature*, *197*(4866), 452–454. https://doi.org/10.1038/197452a0

Benz, C., Copley, M. R., Kent, D. G., Wohrer, S., Cortes, A., Aghaeepour, N., Ma, E., Mader, H., Rowe, K., Day, C., Treloar, D., Brinkman, R. R., & Eaves, C. J. (2012). Hematopoietic Stem Cell Subtypes Expand Differentially during Development and Display Distinct Lymphopoietic Programs. *Cell Stem Cell*, *10*(3), 273–283. https://doi.org/10.1016/j.stem.2012.02.007

Berg, T., Rountree, C. B., Lee, L., Estrada, J., Sala, F. G., Choe, A., Veltmaat, J. M., De Langhe, S., Lee, R., Tsukamoto, H., Crooks, G. M., Bellusci, S., & Wang, K. S. (2007). Fibroblast growth factor 10 is critical for liver growth during embryogenesis

and controls hepatoblast survival via beta-catenin activation. *Hepatology (Baltimore, Md.)*, *46*(4), 1187–1197. https://doi.org/10.1002/hep.21814

Berthault, C., Ramond, C., Burlen-Defranoux, O., Soubigou, G., Chea, S., Golub, R., Pereira, P., Vieira, P., & Cumano, A. (2017). Asynchronous lineage priming determines commitment to T cell and B cell lineages in fetal liver. *Nature Immunology*, *18*(10), 1139–1149. https://doi.org/10.1038/ni.3820

Bertrand, J. Y., Chi, N. C., Santoso, B., Teng, S., Stainier, D. Y. R., & Traver, D. (2010). Haematopoietic stem cells derive directly from aortic endothelium during development. *Nature*, *464*(7285), 108–111. https://doi.org/10.1038/nature08738

Bertrand, J. Y., Desanti, G. E., Lo-Man, R., Leclerc, C., Cumano, A., & Golub, R. (2006). Fetal spleen stroma drives macrophage commitment. *Development*, *133*(18), 3619–3628. https://doi.org/10.1242/dev.02510

Bertrand, J. Y., Giroux, S., Golub, R., Klaine, M., Jalil, A., Boucontet, L., Godin, I., & Cumano, A. (2005). Characterization of purified intraembryonic hematopoietic stem cells as a tool to define their site of origin. *Proceedings of the National Academy of Sciences*, *102*(1), 134–139. https://doi.org/10.1073/pnas.0402270102

Bhunchet, E., & Wake, K. (1992). Role of mesenchymal cell populations in porcine serum-induced rat liver fibrosis. *Hepatology*, *16*(6), 1452–1473. https://doi.org/10.1002/hep.1840160623

Bogue, C. W., Ganea, G. R., Sturm, E., Ianucci, R., & Jacobs, H. C. (2000). Hex expression suggests a role in the development and function of organs derived from foregut endoderm. *Developmental Dynamics*, *219*(1), 84–89. https://doi.org/10.1002/1097-0177(2000)9999:9999<::AID-DVDY1028>3.0.CO;2-5

Boisset, J.-C., van Cappellen, W., Andrieu-Soler, C., Galjart, N., Dzierzak, E., & Robin, C. (2010). In vivo imaging of haematopoietic cells emerging from the mouse aortic endothelium. *Nature*, *464*(7285), 116–120. https://doi.org/10.1038/nature08764

Bort, R., Signore, M., Tremblay, K., Barbera, J. P. M., & Zaret, K. S. (2006). Hex homeobox gene controls the transition of the endoderm to a pseudostratified, cell emergent epithelium for liver bud development. *Developmental Biology*, *290*(1), 44–56. https://doi.org/10.1016/j.ydbio.2005.11.006

Bowie, M. B., McKnight, K. D., Kent, D. G., McCaffrey, L., Hoodless, P. A., & Eaves, C. J. (2006). Hematopoietic stem cells proliferate until after birth and show a reversible phase-specific engraftment defect. *Journal of Clinical Investigation*, *116*(10), 2808–2816. https://doi.org/10.1172/JCI28310

Boyer, S. W., Schroeder, A. V., Smith-Berdan, S., & Forsberg, E. C. (2011). All Hematopoietic Cells Develop from Hematopoietic Stem Cells through Flk2/Flt3-Positive Progenitor Cells. *Cell Stem Cell*, *9*(1), 64–73. https://doi.org/10.1016/j.stem.2011.04.021

Breiteneder-Geleff, S., Soleiman, A., Kowalski, H., Horvat, R., Amann, G., Kriehuber, E., Diem, K., Weninger, W., Tschachler, E., Alitalo, K., & Kerjaschki, D. (1999). Angiosarcomas Express Mixed Endothelial Phenotypes of Blood and Lymphatic Capillaries. *The American Journal of Pathology*, *154*(2), 385–394. https://doi.org/10.1016/S0002-9440(10)65285-6

Brouard, N., Jost, C., Matthias, N., Albrecht, C., Egard, S., Gandhi, P., Strassel, C., Inoue, T., Sugiyama, D., Simmons, P. J., Gachet, C., & Lanza, F. (2017). A unique microenvironment in the developing liver supports the expansion of megakaryocyte progenitors. *Blood Advances*, *1*(21), 1854–1866. https://doi.org/10.1182/bloodadvances.2016003541

Bruns, I., Lucas, D., Pinho, S., Ahmed, J., Lambert, M. P., Kunisaki, Y., Scheiermann, C., Schiff, L., Poncz, M., Bergman, A., & Frenette, P. S. (2014). Megakaryocytes regulate hematopoietic stem cell quiescence through CXCL4 secretion. *Nature Medicine*, *20*(11), Article 11. https://doi.org/10.1038/nm.3707

Buono, M., Facchini, R., Matsuoka, S., Thongjuea, S., Waithe, D., Luis, T. C., Giustacchini, A., Besmer, P., Mead, A. J., Jacobsen, S. E. W., & Nerlov, C. (2016). A dynamic niche provides Kit ligand in a stage-specific manner to the earliest thymocyte progenitors. *Nature Cell Biology*, *18*(2), 157–167. https://doi.org/10.1038/ncb3299

Burke, Z., & Oliver, G. (2002). Prox1 is an early specific marker for the developing liver and pancreas in the mammalian foregut endoderm. *Mechanisms of Development*, *118*(1–2), 147–155. https://doi.org/10.1016/S0925-4773(02)00240-X

Busch, K., Klapproth, K., Barile, M., Flossdorf, M., Holland-Letz, T., Schlenner, S. M., Reth, M., Höfer, T., & Rodewald, H.-R. (2015). Fundamental properties of unperturbed haematopoiesis from stem cells in vivo. *Nature*, *518*(7540), 542–546. https://doi.org/10.1038/nature14242

Cabezas-Wallscheid, N., Buettner, F., Sommerkamp, P., Klimmeck, D., Ladel, L., Thalheimer, F. B., Pastor-Flores, D., Roma, L. P., Renders, S., Zeisberger, P., Przybylla, A., Schönberger, K., Scognamiglio, R., Altamura, S., Florian, C. M., Fawaz, M., Vonficht, D., Tesio, M., Collier, P., … Trumpp, A. (2017). Vitamin A-Retinoic Acid Signaling Regulates Hematopoietic Stem Cell Dormancy. *Cell*, *169*(5), 807-823.e19. https://doi.org/10.1016/j.cell.2017.04.018

Cabezas-Wallscheid, N., Klimmeck, D., Hansson, J., Lipka, D. B., Reyes, A., Wang, Q., Weichenhan, D., Lier, A., von Paleske, L., Renders, S., Wünsche, P., Zeisberger, P., Brocks, D., Gu, L., Herrmann, C., Haas, S., Essers, M. A. G., Brors, B., Eils, R., … Trumpp, A. (2014). Identification of Regulatory Networks in HSCs and Their Immediate Progeny via Integrated Proteome, Transcriptome, and DNA Methylome Analysis. *Cell Stem Cell*, *15*(4), 507–522. https://doi.org/10.1016/j.stem.2014.07.005

Cano, E., Carmona, R., & Muñoz-Chápuli, R. (2013). Wt1-expressing progenitors contribute to multiple tissues in the developing lung. *American Journal of Physiology-Lung Cellular and Molecular Physiology*, *305*(4), L322–L332. https://doi.org/10.1152/ajplung.00424.2012

Cao, H., Cao, B., Heazlewood, C. K., Domingues, M., Sun, X., Debele, E., McGregor, N. E., Sims, N. A., Heazlewood, S. Y., & Nilsson, S. K. (2019). Osteopontin is An Important Regulative Component of the Fetal Bone Marrow Hematopoietic Stem Cell Niche. *Cells*, *8*(9), 985. https://doi.org/10.3390/cells8090985

Cassiman, D., Barlow, A., Vander Borght, S., Libbrecht, L., & Pachnis, V. (2006). Hepatic stellate cells do not derive from the neural crest. *Journal of Hepatology*, *44*(6), 1098–1104. https://doi.org/10.1016/j.jhep.2005.09.023

Chan, C. K. F., Chen, C.-C., Luppen, C. A., Kim, J.-B., DeBoer, A. T., Wei, K., Helms, J. A., Kuo, C. J., Kraft, D. L., & Weissman, I. L. (2009). Endochondral ossification is required for haematopoietic stem-cell niche formation. *Nature*, *457*(7228), Article 7228. https://doi.org/10.1038/nature07547

Chen, J. Y., Miyanishi, M., Wang, S. K., Yamazaki, S., Sinha, R., Kao, K. S., Seita, J., Sahoo, D., Nakauchi, H., & Weissman, I. L. (2016). Hoxb5 marks long-term haematopoietic stem cells and reveals a homogenous perivascular niche. *Nature*, *530*(7589), 223–227. https://doi.org/10.1038/nature16943

Cheng, H., Zheng, Z., & Cheng, T. (2020). New paradigms on hematopoietic stem cell differentiation. *Protein & Cell*, *11*(1), 34–44. https://doi.org/10.1007/s13238-019-0633-0

Cheshier, S. H., Morrison, S. J., Liao, X., & Weissman, I. L. (1999). In vivo proliferation and cell cycle kinetics of long-term self-renewing hematopoietic stem cells. *Pro. Natl. Acad. Sci.*, *Medical Sciences*, 6.

Chhabra, A., Lechner, A. J., Ueno, M., Acharya, A., Van Handel, B., Wang, Y., Iruela-Arispe, M. L., Tallquist, M. D., & Mikkola, H. K. A. (2012). Trophoblasts Regulate the Placental Hematopoietic Niche through PDGF-B Signaling. *Developmental Cell*, *22*(3), 651–659. https://doi.org/10.1016/j.devcel.2011.12.022

Chou, S., Flygare, J., & Lodish, H. F. (2013). Fetal hepatic progenitors support long-term expansion of hematopoietic stem cells. *Experimental Hematology*, *41*(5), 479-490.e4. https://doi.org/10.1016/j.exphem.2013.02.003

Chou, S., & Lodish, H. F. (2010). Fetal liver hepatic progenitors are supportive stromal cells for hematopoietic stem cells. *Proceedings of the National Academy of Sciences*, *107*(17), 7799–7804. https://doi.org/10.1073/pnas.1003586107

Christensen, J. L., Wright, D. E., Wagers, A. J., & Weissman, I. L. (2004). Circulation and Chemotaxis of Fetal Hematopoietic Stem Cells. *PLoS Biology*, *2*(3), e75. https://doi.org/10.1371/journal.pbio.0020075

Christodoulou, C., Spencer, J. A., Yeh, S.-C. A., Turcotte, R., Kokkaliaris, K. D., Panero, R., Ramos, A., Guo, G., Seyedhassantehrani, N., Esipova, T. V., Vinogradov, S. A., Rudzinskas, S., Zhang, Y., Perkins, A. S., Orkin, S. H., Calogero, R. A., Schroeder, T., Lin, C. P., & Camargo, F. D. (2020). Live-animal imaging of native haematopoietic stem and progenitor cells. *Nature*, *578*(7794), 278–283. https://doi.org/10.1038/s41586-020-1971-z

Ciriza, J., Thompson, H., Petrosian, R., Manilay, J. O., & García-Ojeda, M. E. (2013). The migration of hematopoietic progenitors from the fetal liver to the fetal bone marrow: Lessons learned and possible clinical applications. *Experimental Hematology*, *41*(5), 411–423. https://doi.org/10.1016/j.exphem.2013.01.009

Comazzetto, S., Murphy, M. M., Berto, S., Jeffery, E., Zhao, Z., & Morrison, S. J. (2019). Restricted Hematopoietic Progenitors and Erythropoiesis Require SCF from Leptin Receptor+ Niche Cells in the Bone Marrow. *Cell Stem Cell*, *24*(3), 477-486.e6. https://doi.org/10.1016/j.stem.2018.11.022

Comazzetto, S., Shen, B., & Morrison, S. J. (2021). Niches that regulate stem cells and hematopoiesis in adult bone marrow. *Developmental Cell*, *56*(13), 1848–1860. https://doi.org/10.1016/j.devcel.2021.05.018

Cordeiro Gomes, A., Hara, T., Lim, V. Y., Herndler-Brandstetter, D., Nevius, E., Sugiyama, T., Tani-ichi, S., Schlenner, S., Richie, E., Rodewald, H.-R., Flavell, R. A., Nagasawa, T., Ikuta, K., & Pereira, J. P. (2016). Hematopoietic Stem Cell Niches Produce Lineage-Instructive Signals to Control Multipotent Progenitor Differentiation. *Immunity*, *45*(6), 1219–1231. https://doi.org/10.1016/j.immuni.2016.11.004

Cosgrove, J., Hustin, L. S. P., de Boer, R. J., & Perié, L. (2021). Hematopoiesis in numbers. *Trends in Immunology*, *42*(12), 1100–1112. https://doi.org/10.1016/j.it.2021.10.006

Coşkun, S., Chao, H., Vasavada, H., Heydari, K., Gonzales, N., Zhou, X., de Crombrugghe, B., & Hirschi, K. K. (2014). Development of the Fetal Bone Marrow Niche and Regulation of HSC Quiescence and Homing Ability by Emerging Osteolineage Cells. *Cell Reports*, *9*(2), 581–590. https://doi.org/10.1016/j.celrep.2014.09.013

Cossarizza, A., Chang, H., Radbruch, A., Acs, A., Adam, D., Adam-Klages, S., Agace, W. W., Aghaeepour, N., Akdis, M., Allez, M., Almeida, L. N., Alvisi, G., Anderson, G., Andrä, I., Annunziato, F., Anselmo, A., Bacher, P., Baldari, C. T., Bari, S., … Zychlinsky, A. (2019). Guidelines for the use of flow cytometry and cell sorting in immunological studies (second edition). *European Journal of Immunology*, *49*(10), 1457–1973. https://doi.org/10.1002/eji.201970107

Coutu, D. L., Kokkaliaris, K. D., Kunz, L., & Schroeder, T. (2018). Multicolor quantitative confocal imaging cytometry. *Nature Methods*, *15*(1), Article 1. https://doi.org/10.1038/nmeth.4503

Crane, G. M., Jeffery, E., & Morrison, S. J. (2017). Adult haematopoietic stem cell niches. *Nature Reviews Immunology*, *17*(9), 573–590. https://doi.org/10.1038/nri.2017.53

Crawford, L. W., Foley, J. F., & Elmore, S. A. (2010). Histology Atlas of the Developing Mouse Hepatobiliary System with Emphasis on Embryonic Days 9.5-18.5. *Toxicologic Pathology*, *38*(6), 872–906. https://doi.org/10.1177/0192623310374329

Croce, A. C., De Simone, U., Freitas, I., Boncompagni, E., Neri, D., Cillo, U., & Bottiroli, G. (2010). Human liver autofluorescence: An intrinsic tissue parameter discriminating normal and diseased conditions. *Lasers in Surgery and Medicine*, *42*(5), 371–378. https://doi.org/10.1002/lsm.20923

Croce, A. C., Ferrigno, A., Bottiroli, G., & Vairetti, M. (2018). Autofluorescence-based optical biopsy: An effective diagnostic tool in hepatology. *Liver International*, *38*(7), 1160–1174. https://doi.org/10.1111/liv.13753

Croce, A. C., Ferrigno, A., Vairetti, M., Bertone, R., Freitas, I., & Bottiroli, G. (2004). Autofluorescence properties of isolated rat hepatocytes under different metabolic conditions. *Photochemical & Photobiological Sciences*, *3*(10), 920–926. https://doi.org/10.1039/b407358d

Cumano, A., Dieterlen-Lievre, F., & Godin, I. (1996). Lymphoid Potential, Probed before Circulation in Mouse, Is Restricted to Caudal Intraembryonic Splanchnopleura. *Cell*, *86*(6), 907–916. https://doi.org/10.1016/S0092-8674(00)80166-X

Cumano, A., Ferraz, J. C., Klaine, M., Di Santo, J. P., & Godin, I. (2001). Intraembryonic, but Not Yolk Sac Hematopoietic Precursors, Isolated before Circulation, Provide Long-Term Multilineage Reconstitution. *Immunity*, *15*(3), 477–485. https://doi.org/10.1016/S1074-7613(01)00190-X

Darwiche, H., & Petersen, B. E. (2010). Biology of the Adult Hepatic Progenitor Cell: "Ghosts in the Machine." *Progress in Molecular Biology and Translational Science*, *97*, 229–249. https://doi.org/10.1016/B978-0-12-385233-5.00008-8

de Bruijn, M. F. T. R. (2000). Definitive hematopoietic stem cells first develop within the major arterial regions of the mouse embryo. *The EMBO Journal*, *19*(11), 2465–2474. https://doi.org/10.1093/emboj/19.11.2465

de Bruijn, M. F. T. R., Ma, X., Robin, C., Ottersbach, K., Sanchez, M.-J., & Dzierzak, E. (2002). Hematopoietic Stem Cells Localize to the Endothelial Cell Layer in the Midgestation Mouse Aorta. *Immunity*, *16*(5), 673–683. https://doi.org/10.1016/S1074-7613(02)00313-8

de Sauvage, F. J., Hass, P. E., Spencer, S. D., Malloy, B. E., Gurney, A. L., Spencer, S. A., Darbonne, W. C., Henzel, W. J., Wong, S. C., Kuang, W.-J., Oles, K. J., Hultgren, B., Solberg, L. A., Goeddel, D. V., & Eaton, D. L. (1994). Stimulation of megakaryocytopoiesis and thrombopoiesis by the c-Mpl ligand. *Nature*, *369*(6481), Article 6481. https://doi.org/10.1038/369533a0

Decker, M., Leslie, J., Liu, Q., & Ding, L. (2018). Hepatic thrombopoietin is required for bone marrow hematopoietic stem cell maintenance. *Science*, *360*(6384), 106–110. https://doi.org/10.1126/science.aap8861

Delgado, I., Carrasco, M., Cano, E., Carmona, R., García-Carbonero, R., Marín-Gómez, L. M., Soria, B., Martín, F., Cano, D. A., Muñoz-Chápuli, R., & Rojas, A. (2014). GATA4 loss in the septum transversum mesenchyme promotes liver fibrosis in mice. *Hepatology*, *59*(6), 2358–2370. https://doi.org/10.1002/hep.27005

Dieterlen-Lievre, F. (1975). On the origin of haemopoietic stem cells in the avian embryo: An experimental approach. *Journal of Embryology and Experimental Morphology*, *33*(3), 607–619.

Ding, L., & Morrison, S. J. (2013). Haematopoietic stem cells and early lymphoid progenitors occupy distinct bone marrow niches. *Nature*, *495*(7440), 231–235. https://doi.org/10.1038/nature11885

Ding, L., Saunders, T. L., Enikolopov, G., & Morrison, S. J. (2012). Endothelial and perivascular cells maintain haematopoietic stem cells. *Nature*, *481*(7382), 457–462. https://doi.org/10.1038/nature10783

Dixit, R., Ai, X., & Fine, A. (2013). Derivation of lung mesenchymal lineages from the fetal mesothelium requires hedgehog signaling for mesothelial cell entry. *Development*, *140*(21), 4398–4406. https://doi.org/10.1242/dev.098079

Dykstra, B., Kent, D., Bowie, M., McCaffrey, L., Hamilton, M., Lyons, K., Lee, S.-J., Brinkman, R., & Eaves, C. (2007). Long-Term Propagation of Distinct Hematopoietic Differentiation Programs In Vivo. *Cell Stem Cell*, *1*(2), 218–229. https://doi.org/10.1016/j.stem.2007.05.015

Dzierzak, E., Sanchez, M.-J., Muller, A., Miles, C., Holmes, A., Tidcombe, H., & Medvinsky, A. (1997). Hematopoietic stem cells: Embryonic beginnings. *Journal of Cellular Physiology*, *173*(2), 216–218. https://doi.org/10.1002/(SICI)1097-4652(199711)173:2<216::AID-JCP24>3.0.CO;2-C

Eaves, C. J. (2015). Hematopoietic stem cells: Concepts, definitions, and the new reality. *Blood*, *125*(17), 2605–2613. https://doi.org/10.1182/blood-2014-12-570200

Eberl, G., Marmon, S., Sunshine, M.-J., Rennert, P. D., Choi, Y., & Littman, D. R. (2004). An essential function for the nuclear receptor RORγt in the generation of fetal lymphoid tissue inducer cells. *Nature Immunology*, *5*(1), 64–73. https://doi.org/10.1038/ni1022

Elsaid, R., Meunier, S., Burlen-Defranoux, O., Soares-da-Silva, F., Perchet, T., Iturri, L., Freyer, L., Vieira, P., Pereira, P., Golub, R., Bandeira, A., Perdiguero, E. G., & Cumano, A. (2021). A wave of bipotent T/ILC-restricted progenitors shapes the embryonic thymus microenvironment in a time-dependent manner. *Blood*, *137*(8), 1024–1036. https://doi.org/10.1182/blood.2020006779

Elsaid, R., Soares-da-Silva, F., Peixoto, M., Amiri, D., Mackowski, N., Pereira, P., Bandeira, A., & Cumano, A. (2020). Hematopoiesis: A Layered Organization Across Chordate Species. *Frontiers in Cell and Developmental Biology*, *8*, 606642. https://doi.org/10.3389/fcell.2020.606642

Ema, H., & Nakauchi, H. (2000). Expansion of hematopoietic stem cells in the developing liver of a mouse embryo. *Blood*, *95*(7), 2284–2288. https://doi.org/10.1182/blood.V95.7.2284

Ema, M., Takahashi, S., & Rossant, J. (2006). Deletion of the selection cassette, but not cis-acting elements, in targeted Flk1-lacZ allele reveals Flk1 expression in

multipotent mesodermal progenitors. *Blood*, *107*(1), 111–117. https://doi.org/10.1182/blood-2005-05-1970

Ema, M., Yokomizo, T., Wakamatsu, A., Terunuma, T., Yamamoto, M., & Takahashi, S. (2006). Primitive erythropoiesis from mesodermal precursors expressing VE-cadherin, PECAM-1, Tie2, endoglin, and CD34 in the mouse embryo. *Blood*, *108*(13), 4018–4024. https://doi.org/10.1182/blood-2006-03-012872

Enzan, H., Himeno, H., Hiroi, M., Kiyoku, H., Saibara, T., & Onishi, S. (1997). Development of hepatic sinusoidal structure with special reference to the Ito cells. *Microscopy Research and Technique*, *39*(4), 336–349. https://doi.org/10.1002/(SICI)1097-0029(19971115)39:4<336::AID-JEMT4>3.0.CO;2-F

Feng, J., Pucella, J. N., Jang, G., Alcántara-Hernández, M., Upadhaya, S., Adams, N. M., Khodadadi-Jamayran, A., Lau, C. M., Stoeckius, M., Hao, S., Smibert, P., Tsirigos, A., Idoyaga, J., & Reizis, B. (2022). Clonal lineage tracing reveals shared origin of conventional and plasmacytoid dendritic cells. *Immunity*, *55*(3), 405-422.e11. https://doi.org/10.1016/j.immuni.2022.01.016

Ferkowicz, M. J., Starr, M., Xie, X., Li, W., Johnson, S. A., Shelley, W. C., Morrison, P. R., & Yoder, M. C. (2003). CD41 expression defines the onset of primitive and definitive hematopoiesis in the murine embryo. *Development*, *130*(18), 4393–4403. https://doi.org/10.1242/dev.00632

Fitch, S. R., Kimber, G. M., Wilson, N. K., Parker, A., Mirshekar-Syahkal, B., Göttgens, B., Medvinsky, A., Dzierzak, E., & Ottersbach, K. (2012). Signaling from the Sympathetic Nervous System Regulates Hematopoietic Stem Cell Emergence during Embryogenesis. *Cell Stem Cell*, *11*(4), 554–566. https://doi.org/10.1016/j.stem.2012.07.002

Frame, J. M., Fegan, K. H., Conway, S. J., McGrath, K. E., & Palis, J. (2016). Definitive Hematopoiesis in the Yolk Sac Emerges from Wnt-Responsive Hemogenic Endothelium Independently of Circulation and Arterial Identity. *Stem Cells*, *34*(2), 431–444. https://doi.org/10.1002/stem.2213

Fraser, S. T., Isern, J., & Baron, M. H. (2007). Maturation and enucleation of primitive erythroblasts during mouse embryogenesis is accompanied by changes in cell-surface antigen expression. *Blood*, *109*(1), 343–352. https://doi.org/10.1182/blood-2006-03-006569

Freyer, L., Iturri, L., Biton, A., & Perdiguero, E. G. (2020). *Overlapping Definitive Progenitor Waves Divide and Conquer to Build a Layered Hematopoietic System* [Preprint]. Immunology. https://doi.org/10.1101/2020.12.24.424302

Friedman, S. L. (2008). Hepatic Stellate Cells: Protean, Multifunctional, and Enigmatic Cells of the Liver. *Physiological Reviews*, *88*(1), 125–172. https://doi.org/10.1152/physrev.00013.2007

Futamura, K., Sekino, M., Hata, A., Ikebuchi, R., Nakanishi, Y., Egawa, G., Kabashima, K., Watanabe, T., Furuki, M., & Tomura, M. (2015). Novel full-spectral flow cytometry with multiple spectrally-adjacent fluorescent proteins and fluorochromes and visualization of in vivo cellular movement. *Cytometry Part A*, *87*(9), 830–842. https://doi.org/10.1002/cyto.a.22725

Ganuza, M., Hadland, B., Chabot, A., Li, C., Kang, G., Bernstein, I., & McKinney-Freeman, S. (2017). Murine hemogenic endothelial precursors display heterogeneous hematopoietic potential ex vivo. *Experimental Hematology*, *51*, 25-35.e6. https://doi.org/10.1016/j.exphem.2017.04.006

Ganuza, M., Hall, T., Finkelstein, D., Chabot, A., Kang, G., & McKinney-Freeman, S. (2017). Lifelong haematopoiesis is established by hundreds of precursors throughout mammalian ontogeny. *Nature Cell Biology*, *19*(10), 1153–1163. https://doi.org/10.1038/ncb3607

Ganuza, M., Hall, T., Myers, J., Nevitt, C., Sánchez-Lanzas, R., Chabot, A., Ding, J., Kooienga, E., Caprio, C., Finkelstein, D., Kang, G., Obeng, E., & McKinney-Freeman, S. (2022). Murine foetal liver supports limited detectable expansion of life-long haematopoietic progenitors. *Nature Cell Biology*. https://doi.org/10.1038/s41556-022-00999-5

Gao, S., Shi, Q., Zhang, Y., Liang, G., Kang, Z., Huang, B., Ma, D., Wang, L., Jiao, J., Fang, X., Xu, C.-R., Liu, L., Xu, X., Göttgens, B., Li, C., & Liu, F. (2022). Identification of HSC/MPP expansion units in fetal liver by single-cell spatiotemporal transcriptomics. *Cell Research*, *32*(1), 38–53. https://doi.org/10.1038/s41422-021-00540-7

Gao, X., Xu, C., Asada, N., & Frenette, P. S. (2018). The hematopoietic stem cell niche: From embryo to adult. *Development*, *145*(2), dev139691. https://doi.org/10.1242/dev.139691

Garcia-Porrero, J. A., Godin, I. E., & Dieterlen-Lièvre, F. (1995). Potential intraembryonic hemogenic sites at pre-liver stages in the mouse. *Anatomy and Embryology*, *192*(5), 425–435. https://doi.org/10.1007/BF00240375

Gazit, R., Mandal, P. K., Ebina, W., Ben-Zvi, A., Nombela-Arrieta, C., Silberstein, L. E., & Rossi, D. J. (2014). Fgd5 identifies hematopoietic stem cells in the murine bone marrow. *Journal of Experimental Medicine*, *211*(7), 1315–1331. https://doi.org/10.1084/jem.20130428

Gekas, C., Dieterlen-Lièvre, F., Orkin, S. H., & Mikkola, H. K. A. (2005). The Placenta Is a Niche for Hematopoietic Stem Cells. *Developmental Cell*, *8*(3), 365–375. https://doi.org/10.1016/j.devcel.2004.12.016

Gentek, R., Ghigo, C., Hoeffel, G., Bulle, M. J., Msallam, R., Gautier, G., Launay, P., Chen, J., Ginhoux, F., & Bajénoff, M. (2018). Hemogenic Endothelial Fate Mapping Reveals Dual Developmental Origin of Mast Cells. *Immunity*, *48*(6), 1160-1171.e5. https://doi.org/10.1016/j.immuni.2018.04.025

Géraud, C., Koch, P.-S., Zierow, J., Klapproth, K., Busch, K., Olsavszky, V., Leibing, T., Demory, A., Ulbrich, F., Diett, M., Singh, S., Sticht, C., Breitkopf-Heinlein, K., Richter, K., Karppinen, S.-M., Pihlajaniemi, T., Arnold, B., Rodewald, H.-R., Augustin, H. G., … Goerdt, S. (2017). GATA4-dependent organ-specific endothelial differentiation controls liver development and embryonic hematopoiesis. *Journal of Clinical Investigation*, *127*(3), 1099–1114. https://doi.org/10.1172/JCI90086

Gerlach, J. C., Thompson, R. L., Gridelli, B., & Schmelzer, E. (2019). Effects of Delta-Like Noncanonical Notch Ligand 1 Expression of Human Fetal Liver Hepatoblasts on Hematopoietic Progenitors. *Stem Cells International*, *2019*, e7916275. https://doi.org/10.1155/2019/7916275

Geyer, S. H., Maurer-Gesek, B., Reissig, L. F., Rose, J., Prin, F., Wilson, R., Galli, A., Tudor, C., White, J. K., Mohun, T. J., & Weninger, W. J. (2022). The venous system of E14.5 mouse embryos—Reference data and examples for diagnosing malformations in embryos with gene deletions. *Journal of Anatomy*, *240*(1), 11–22. https://doi.org/10.1111/joa.13536

Godin, I., Garcia-Porrero, J. A., Dieterlen-Lièvre, F., & Cumano, A. (1999). Stem Cell Emergence and Hemopoietic Activity Are Incompatible in Mouse Intraembryonic

Sites. *Journal of Experimental Medicine*, *190*(1), 43–52. https://doi.org/10.1084/jem.190.1.43

Goh, I., Botting, R. A., Rose, A., Webb, S., Engelbert, J., Gitton, Y., Stephenson, E., Quiroga Londoño, M., Mather, M., Mende, N., Imaz-Rosshandler, I., Yang, L., Horsfall, D., Basurto-Lozada, D., Chipampe, N.-J., Rook, V., Lee, J. T. H., Ton, M.-L., Keitley, D., … Haniffa, M. (2023). Yolk sac cell atlas reveals multiorgan functions during human early development. *Science*, *381*(6659), eadd7564. https://doi.org/10.1126/science.add7564

Goltsev, Y., Samusik, N., Kennedy-Darling, J., Bhate, S., Hale, M., Vazquez, G., Black, S., & Nolan, G. P. (2018). Deep Profiling of Mouse Splenic Architecture with CODEX Multiplexed Imaging. *Cell*, *174*(4), 968-981.e15. https://doi.org/10.1016/j.cell.2018.07.010

Gomariz, A., Helbling, P. M., Isringhausen, S., Suessbier, U., Becker, A., Boss, A., Nagasawa, T., Paul, G., Goksel, O., Székely, G., Stoma, S., Nørrelykke, S. F., Manz, M. G., & Nombela-Arrieta, C. (2018). Quantitative spatial analysis of haematopoiesis-regulating stromal cells in the bone marrow microenvironment by 3D microscopy. *Nature Communications*, *9*(1), 2532. https://doi.org/10.1038/s41467-018-04770-z

Goyama, S., Yamamoto, G., Shimabe, M., Sato, T., Ichikawa, M., Ogawa, S., Chiba, S., & Kurokawa, M. (2008). Evi-1 Is a Critical Regulator for Hematopoietic Stem Cells and Transformed Leukemic Cells. *Cell Stem Cell*, *3*(2), 207–220. https://doi.org/10.1016/j.stem.2008.06.002

Greenbaum, A., Hsu, Y.-M. S., Day, R. B., Schuettpelz, L. G., Christopher, M. J., Borgerding, J. N., Nagasawa, T., & Link, D. C. (2013). CXCL12 in early mesenchymal progenitors is required for haematopoietic stem-cell maintenance. *Nature*, *495*(7440), Article 7440. https://doi.org/10.1038/nature11926

Griffin, C. T., & Gao, S. (2017). Building discontinuous liver sinusoidal vessels. *The Journal of Clinical Investigation*, *127*(3), 790–792. https://doi.org/10.1172/JCI92823

Gualdi, R., Bossard, P., Zheng, M., Hamada, Y., Coleman, J. R., & Zaret, K. S. (1996). Hepatic specification of the gut endoderm in vitro: Cell signaling and transcriptional control. *Genes & Development*, *10*(13), 1670–1682. https://doi.org/10.1101/gad.10.13.1670

Guo, Y., Zhang, X., Huang, J., Zeng, Y., Liu, W., Geng, C., Li, K. W., Yang, D., Wu, S., Wei, H., Han, Z., Qian, X., Jiang, Y., & He, F. (2009). Relationships between Hematopoiesis and Hepatogenesis in the Midtrimester Fetal Liver Characterized by Dynamic Transcriptomic and Proteomic Profiles. *PLoS ONE*, *4*(10), e7641. https://doi.org/10.1371/journal.pone.0007641

Haas, J. D., Ravens, S., Düber, S., Sandrock, I., Oberdörfer, L., Kashani, E., Chennupati, V., Föhse, L., Naumann, R., Weiss, S., Krueger, A., Förster, R., & Prinz, I. (2012). Development of Interleukin-17-Producing γδ T Cells Is Restricted to a Functional Embryonic Wave. *Immunity*, *37*(1), 48–59. https://doi.org/10.1016/j.immuni.2012.06.003

Hagberg, A. A., Schult, D. A., & Swart, P. J. (2008). *Exploring Network Structure, Dynamics, and Function using NetworkX*.

Hall, T. D., Kim, H., Dabbah, M., Myers, J. A., Crawford, J. C., Morales-Hernandez, A., Caprio, C. E., Sriram, P., Kooienga, E., Derecka, M., Obeng, E. A., Thomas, P. G., & McKinney-Freeman, S. (2022). Murine fetal bone marrow does not support

functional hematopoietic stem and progenitor cells until birth. *Nature Communications*, *13*(1), 5403. https://doi.org/10.1038/s41467-022-33092-4

Harrison, D. E., & Zhong, R. K. (1992). The same exhaustible multilineage precursor produces both myeloid and lymphoid cells as early as 3-4 weeks after marrow transplantation. *Proceedings of the National Academy of Sciences*, *89*(21), 10134–10138. https://doi.org/10.1073/pnas.89.21.10134

Hayashi, Y., Sezaki, M., & Takizawa, H. (2019). Development of the hematopoietic system: Role of inflammatory factors. *WIREs Developmental Biology*, *8*(4), e341. https://doi.org/10.1002/wdev.341

Helbling, P. M., Piñeiro-Yáñez, E., Gerosa, R., Boettcher, S., Al-Shahrour, F., Manz, M. G., & Nombela-Arrieta, C. (2019). Global Transcriptomic Profiling of the Bone Marrow Stromal Microenvironment during Postnatal Development, Aging, and Inflammation. *Cell Reports*, *29*(10), 3313-3330.e4. https://doi.org/10.1016/j.celrep.2019.11.004

Helbling, P. M., Vijaykumar, A., Gomariz, A., Zerkatje, T., Zielińska, K. A., Loosli, K., Isringhausen, S., Nagasawa, T., Roeder, I., Manz, M. G., Yokomizo, T., & Nombela-Arrieta, C. (2023). *Tissue-scale dynamic mapping of Hematopoietic Stem Cells and supportive niche cells in the fetal liver* [Preprint]. Developmental Biology. https://doi.org/10.1101/2023.09.12.554625

Hentsch, B., Lyons, I., Li, R., Hartley, L., Lints, T. J., Adams, J. M., & Harvey, R. P. (1996). Hlx homeo box gene is essential for an inductive tissue interaction that drives expansion of embryonic liver and gut. *Genes & Development*, *10*(1), 70–79. https://doi.org/10.1101/gad.10.1.70

Herzenberg, L. A., & Herzenberg, L. A. (1989). Toward a layered immune system. *Cell*, *59*(6), 953–954. https://doi.org/10.1016/0092-8674(89)90748-4

Hikspoors, J. P. J. M., Peeters, M. M. J. P., Kruepunga, N., Mekonen, H. K., Mommen, G. M. C., Köhler, S. E., & Lamers, W. H. (2017). Human liver segments: Role of cryptic liver lobes and vascular physiology in the development of liver veins and left-right asymmetry. *Scientific Reports*, *7*(1), Article 1. https://doi.org/10.1038/s41598-017-16840-1

Hills, D., Gribi, R., Ure, J., Buza-Vidas, N., Luc, S., Jacobsen, S. E. W., & Medvinsky, A. (2011). Hoxb4-YFP reporter mouse model: A novel tool for tracking HSC development and studying the role of Hoxb4 in hematopoiesis. *Blood*, *117*(13), 3521–3528. https://doi.org/10.1182/blood-2009-12-253989

Hirsch, E., Iglesias, A., Potocnik, A. J., Hartmann, U., & Fässler, R. (1996). Impaired migration but not differentiation of haematopoietic stem cells in the absence of β1 integrins. *Nature*, *380*(6570), Article 6570. https://doi.org/10.1038/380171a0

Hoeffel, G., Chen, J., Lavin, Y., Low, D., Almeida, F. F., See, P., Beaudin, A. E., Lum, J., Low, I., Forsberg, E. C., Poidinger, M., Zolezzi, F., Larbi, A., Ng, L. G., Chan, J. K. Y., Greter, M., Becher, B., Samokhvalov, I. M., Merad, M., & Ginhoux, F. (2015). C-Myb+ Erythro-Myeloid Progenitor-Derived Fetal Monocytes Give Rise to Adult Tissue-Resident Macrophages. *Immunity*, *42*(4), 665–678. https://doi.org/10.1016/j.immuni.2015.03.011

Hoeffel, G., Wang, Y., Greter, M., See, P., Teo, P., Malleret, B., Leboeuf, M., Low, D., Oller, G., Almeida, F., Choy, S. H. Y., Grisotto, M., Renia, L., Conway, S. J., Stanley, E. R., Chan, J. K. Y., Ng, L. G., Samokhvalov, I. M., Merad, M., & Ginhoux, F. (2012). Adult Langerhans cells derive predominantly from embryonic fetal liver monocytes with a minor contribution of yolk sac–derived macrophages. *Journal of Experimental Medicine*, *209*(6), 1167–1181. https://doi.org/10.1084/jem.20120340

Houssaint, E. (1981). Differentiation of the mouse hepatic primordium. II. Extrinsic origin of the haemopoietic cell line. *Cell Differentiation*, *10*(5), 243–252. https://doi.org/10.1016/0045-6039(81)90007-5

Iandola, F. N., Han, S., Moskewicz, M. W., Ashraf, K., Dally, W. J., & Keutzer, K. (2016). *SqueezeNet: AlexNet-level accuracy with 50x fewer parameters and <0.5MB model size* (arXiv:1602.07360). arXiv. http://arxiv.org/abs/1602.07360

Ijpenberg, A., Pérez-Pomares, J. M., Guadix, J. A., Carmona, R., Portillo-Sánchez, V., Macías, D., Hohenstein, P., Miles, C. M., Hastie, N. D., & Muñoz-Chápuli, R. (2007). Wt1 and retinoic acid signaling are essential for stellate cell development and liver morphogenesis. *Developmental Biology*, *312*(1), 157–170. https://doi.org/10.1016/j.ydbio.2007.09.014

Ikuta, K., Kina, T., MacNeil, I., Uchida, N., Peault, B., Chien, Y., & Weissman, I. L. (1990). A developmental switch in thymic lymphocyte maturation potential occurs at the level of hematopoietic stem cells. *Cell*, *62*(5), 863–874. https://doi.org/10.1016/0092-8674(90)90262-D

Inagaki, N. F., Inagaki, F. F., Kokudo, N., & Miyajima, A. (2015). Use of mouse liver mesothelial cells to prevent postoperative adhesion and promote liver regeneration after hepatectomy. *Journal of Hepatology*, *62*(5), 1141–1147. https://doi.org/10.1016/j.jhep.2014.12.010

Inoue, K., Qin, Y., Xia, Y., Han, J., Yuan, R., Sun, J., Xu, R., Jiang, J. X., Greenblatt, M. B., & Zhao, B. (2023). Bone marrow Adipoq-lineage progenitors are a major cellular source of M-CSF that dominates bone marrow macrophage development, osteoclastogenesis, and bone mass. *eLife*, *12*, e82118. https://doi.org/10.7554/eLife.82118

Isern, J., Fraser, S. T., He, Z., & Baron, M. H. (2008). The fetal liver is a niche for maturation of primitive erythroid cells. *Proceedings of the National Academy of Sciences*, *105*(18), 6662–6667. https://doi.org/10.1073/pnas.0802032105

Isern, J., He, Z., Fraser, S. T., Nowotschin, S., Ferrer-Vaquer, A., Moore, R., Hadjantonakis, A.-K., Schulz, V., Tuck, D., Gallagher, P. G., & Baron, M. H. (2011). Single-lineage transcriptome analysis reveals key regulatory pathways in primitive erythroid progenitors in the mouse embryo. *Blood*, *117*(18), 4924–4934. https://doi.org/10.1182/blood-2010-10-313676

Iturri, L., Freyer, L., Biton, A., Dardenne, P., Lallemand, Y., & Gomez Perdiguero, E. (2021). Megakaryocyte production is sustained by direct differentiation from erythromyeloid progenitors in the yolk sac until midgestation. *Immunity*, *54*(7), 1433-1446.e5. https://doi.org/10.1016/j.immuni.2021.04.026

Ivanovs, A., Rybtsov, S., Ng, E. S., Stanley, E. G., Elefanty, A. G., & Medvinsky, A. (2017). Human haematopoietic stem cell development: From the embryo to the dish. *Development*, *144*(13), 2323–2337. https://doi.org/10.1242/dev.134866

Iwasaki, H., Arai, F., Kubota, Y., Dahl, M., & Suda, T. (2010). Endothelial protein C receptor–expressing hematopoietic stem cells reside in the perisinusoidal niche in fetal liver. *Blood*, *116*(4), 544–553. https://doi.org/10.1182/blood-2009-08-240903

Jaffredo, T., Gautier, R., Brajeul, V., & Dieterlen-Lièvre, F. (2000). Tracing the Progeny of the Aortic Hemangioblast in the Avian Embryo. *Developmental Biology*, *224*(2), 204–214. https://doi.org/10.1006/dbio.2000.9799

Jenkins, S. J., Ruckerl, D., Cook, P. C., Jones, L. H., Finkelman, F. D., van Rooijen, N., MacDonald, A. S., & Allen, J. E. (2011). Local Macrophage Proliferation, Rather than

Recruitment from the Blood, Is a Signature of TH2 Inflammation | Science. *Science*, *332*(6035). https://doi.org/10.1126/science.1204351

Johnson, G. R., & Moore, M. a. S. (1975). Role of stem cell migration in initiation of mouse foetal liver haemopoiesis. *Nature*, *258*(5537), Article 5537. https://doi.org/10.1038/258726a0

Jordan, C. T., Astle, C. M., Zawadzki, J., Mackarehtschian, K., Lemischka, I. R., & Harrison, D. E. (1995). Long-term repopulating abilities of enriched fetal liver stem cells measured by competitive repopulation. *Experimental Hematology*, *23*(9), 1011–1015.

Jordan, C. T., McKearn, J. P., & Lemischka, I. R. (1990). Cellular and developmental properties of fetal hematopoietic stem cells. *Cell*, *61*(6), 953–963. https://doi.org/10.1016/0092-8674(90)90061-I

Jordan, H. E. (1917). Aortic Cell Clusters in Vertebrate Embryos. *Proceedings of the National Academy of Sciences*, *3*(3), 149–156. https://doi.org/10.1073/pnas.3.3.149

Jung, J., Zheng, M., Goldfarb, M., & Zaret, K. S. (1999). Initiation of Mammalian Liver Development from Endoderm by Fibroblast Growth Factors. *Science, New Series*, *284*(5422), 1998–2003.

Kamiya, A., Kinoshita, T., Ito, Y., Matsui, T., Morikawa, Y., Senba, E., Nakashima, K., Taga, T., Yoshida, K., Kishimoto, T., & Miyajima, A. (1999). Fetal liver development requires a paracrine action of oncostatin M through the gp130 signal transducer. *The EMBO Journal*, *18*(8), 2127–2136. https://doi.org/10.1093/emboj/18.8.2127

Kasaai, B., Caolo, V., Peacock, H. M., Lehoux, S., Gomez-Perdiguero, E., Luttun, A., & Jones, E. A. V. (2017). Erythro-myeloid progenitors can differentiate from endothelial cells and modulate embryonic vascular remodeling. *Scientific Reports*, *7*(1), 43817. https://doi.org/10.1038/srep43817

Kataoka, K., Sato, T., Yoshimi, A., Goyama, S., Tsuruta, T., Kobayashi, H., Shimabe, M., Arai, S., Nakagawa, M., Imai, Y., Kumano, K., Kumagai, K., Kubota, N., Kadowaki, T., & Kurokawa, M. (2011). Evi1 is essential for hematopoietic stem cell self-renewal, and its expression marks hematopoietic cells with long-term multilineage repopulating activity. *Journal of Experimental Medicine*, *208*(12), 2403–2416. https://doi.org/10.1084/jem.20110447

Kaufmann, M. H., & Bard, J. B. L. (1999). *The Anatomical Basis of Mouse Development*. San Diego: Academic Press.

Kaushansky, K., Broudy, V. C., Lin, N., Jorgensen, M. J., McCarty, J., Fox, N., Zucker-Franklin, D., & Lofton-Day, C. (1995). Thrombopoietin, the Mp1 ligand, is essential for full megakaryocyte development. *Proceedings of the National Academy of Sciences of the United States of America*, *92*(8), 3234–3238. https://doi.org/10.1073/pnas.92.8.3234

Kaushansky, K., Lok, S., Holly, R. D., Broudy, V. C., Lin, N., Bailey, M. C., Forstrom, J. W., Buddle, M. M., Oort, P. J., Hagen, F. S., Roth, G. J., Papayannopoulou, T., & Foster, D. C. (1994). Promotion of megakaryocyte progenitor expansion and differentiation by the c-Mpl ligand thrombopoietin. *Nature*, *369*(6481), Article 6481. https://doi.org/10.1038/369568a0

Kayvanjoo, A. H., Splichalova, I., Bejarano, D. A., Huang, H., Mauel, K., Makdissi, N., Heider, D., Balzer, N. R., Osei-Sarpong, C., Baßler, K., Schultze, J. L., Uderhardt, S., Kiermaier, E., Beyer, M., Schlitzer, A., & Mass, E. (2023). *Fetal liver macrophages contribute to the hematopoietic stem cell niche by controlling*

*granulopoiesis* [Preprint]. Developmental Biology; bioRxiv preprint. https://doi.org/10.1101/2023.02.21.529403

Kent, D. G., Copley, M. R., Benz, C., Wöhrer, S., Dykstra, B. J., Ma, E., Cheyne, J., Zhao, Y., Bowie, M. B., Zhao, Y., Gasparetto, M., Delaney, A., Smith, C., Marra, M., & Eaves, C. J. (2009). Prospective isolation and molecular characterization of hematopoietic stem cells with durable self-renewal potential. *Blood*, *113*(25), 6342–6350. https://doi.org/10.1182/blood-2008-12-192054

Khan, J. A., Mendelson, A., Kunisaki, Y., Birbrair, A., Kou, Y., Arnal-Estapé, A., Pinho, S., Ciero, P., Nakahara, F., Ma'ayan, A., Bergman, A., Merad, M., & Frenette, P. S. (2016). Fetal liver hematopoietic stem cell niches associate with portal vessels. *Science*, *351*(6269), 176–180. https://doi.org/10.1126/science.aad0084

Kiel, M. J., Yilmaz, Ö. H., Iwashita, T., Yilmaz, O. H., Terhorst, C., & Morrison, S. J. (2005). SLAM Family Receptors Distinguish Hematopoietic Stem and Progenitor Cells and Reveal Endothelial Niches for Stem Cells. *Cell*, *121*(7), 1109–1121. https://doi.org/10.1016/j.cell.2005.05.026

Kieusseian, A., De La Grange, P. B., Burlen-Defranoux, O., Godin, I., & Cumano, A. (2012). Immature hematopoietic stem cells undergo maturation in the fetal liver. *Development*, *139*(19), 3521–3530. https://doi.org/10.1242/dev.079210

Kim, I., He, S., Yilmaz, Ö. H., Kiel, M. J., & Morrison, S. J. (2006). Enhanced purification of fetal liver hematopoietic stem cells using SLAM family receptors. *Blood*, *108*(2), 737–744. https://doi.org/10.1182/blood-2005-10-4135

Kimura, S., Roberts, A. W., Metcalf, D., & Alexander, W. S. (1998). Hematopoietic stem cell deficiencies in mice lacking c-Mpl, the receptor for thrombopoietin. *Proceedings of the National Academy of Sciences of the United States of America*, *95*(3), 1195–1200. https://doi.org/10.1073/pnas.95.3.1195

Kingsley, P. D., Malik, J., Fantauzzo, K. A., & Palis, J. (2004). Yolk sac–derived primitive erythroblasts enucleate during mammalian embryogenesis. *Blood*, *104*(1), 19–25. https://doi.org/10.1182/blood-2003-12-4162

Kinoshita, T., Sekiguchi, T., Xu, M., Ito, Y., Kamiya, A., Tsuji, K., Nakahata, T., & Miyajima, A. (1999). Hepatic differentiation induced by oncostatin M attenuates fetal liver hematopoiesis. *Proceedings of the National Academy of Sciences*, *96*(13), 7265–7270. https://doi.org/10.1073/pnas.96.13.7265

Kissa, K., & Herbomel, P. (2010). Blood stem cells emerge from aortic endothelium by a novel type of cell transition. *Nature*, *464*(7285), 112–115. https://doi.org/10.1038/nature08761

Kluyver, T., Ragan-Kelley, B., Pérez, F., Bussonnier, M., Frederic, J., Hamrick, J., Grout, J., Corlay, S., Ivanov, P., Abdalla, S., & Willing, C. (2016). *Jupyter Notebooks—A publishing format for reproducible computational workflows*.

Kokkaliaris, K. D. (2020). Dissecting the spatial bone marrow microenvironment of hematopoietic stem cells. *Current Opinion in Oncology*, *32*(2), 154–161. https://doi.org/10.1097/CCO.0000000000000605

Kokkaliaris, K. D., Kunz, L., Cabezas-Wallscheid, N., Christodoulou, C., Renders, S., Camargo, F., Trumpp, A., Scadden, D. T., & Schroeder, T. (2020). Adult blood stem cell localization reflects the abundance of reported bone marrow niche cell types and their combinations. *Blood*.

Komorowska, K., Doyle, A., Wahlestedt, M., Subramaniam, A., Debnath, S., Chen, J., Soneji, S., Van Handel, B., Mikkola, H. K. A., Miharada, K., Bryder, D., Larsson, J., & Magnusson, M. (2017). Hepatic Leukemia Factor Maintains Quiescence of

Hematopoietic Stem Cells and Protects the Stem Cell Pool during Regeneration. *Cell Reports*, *21*(12), 3514–3523. https://doi.org/10.1016/j.celrep.2017.11.084

Kondo, M., Weissman, I. L., & Akashi, K. (1997). Identification of Clonogenic Common Lymphoid Progenitors in Mouse Bone Marrow. *Cell*, *91*(5), 661–672. https://doi.org/10.1016/S0092-8674(00)80453-5

Kubota, H., Yao, H., & Reid, L. M. (2007). Identification and Characterization of Vitamin A-Storing Cells in Fetal Liver: Implications for Functional Importance of Hepatic Stellate Cells in Liver Development and Hematopoiesis. *Stem Cells*, *25*(9), 2339–2349. https://doi.org/10.1634/stemcells.2006-0316

Kunisaki, Y., Bruns, I., Scheiermann, C., Ahmed, J., Pinho, S., Zhang, D., Mizoguchi, T., Wei, Q., Lucas, D., Ito, K., Mar, J. C., Bergman, A., & Frenette, P. S. (2013). Arteriolar niches maintain haematopoietic stem cell quiescence. *Nature*, *502*(7473), 637–643. https://doi.org/10.1038/nature12612

Lam, E. Y. N., Hall, C. J., Crosier, P. S., Crosier, K. E., & Flores, M. V. (2010). Live imaging of Runx1 expression in the dorsal aorta tracks the emergence of blood progenitors from endothelial cells. *Blood*, *116*(6), 909–914. https://doi.org/10.1182/blood-2010-01-264382

Lassila, O., Eskola, J., Toivanen, P., Martin, C., & Dieterlen-Lievre, F. (1978). The origin of lymphoid stem cells studied in chick yolk sac–embryo chimaeras. *Nature*, *272*(5651), 353–354. https://doi.org/10.1038/272353a0

Laurenti, E., & Göttgens, B. (2018). From haematopoietic stem cells to complex differentiation landscapes. *Nature*, *553*(7689), 418–426. https://doi.org/10.1038/nature25022

Lee, Y., DiMaulo-Milk, E., Leslie, J., & Ding, L. (2022). Hematopoietic stem cells temporally transition to thrombopoietin dependence in the fetal liver. *Science Advances*, *8*(11), eabm7688. https://doi.org/10.1126/sciadv.abm7688

Lee, Y., Leslie, J., Yang, Y., & Ding, L. (2021). Hepatic stellate and endothelial cells maintain hematopoietic stem cells in the developing liver. *Journal of Experimental Medicine*, *218*(3), e20200882. https://doi.org/10.1084/jem.20200882

Li, Y., Lua, I., & Asahina, K. (2013). MACS Isolation and Culture of Mouse Liver Mesothelial Cells. *BIO-PROTOCOL*, *3*(13). https://doi.org/10.21769/BioProtoc.815

Lin, C. S., Lim, S. K., D'Agati, V., & Costantini, F. (1996). Differential effects of an erythropoietin receptor gene disruption on primitive and definitive erythropoiesis. *Genes & Development*, *10*(2), 154–164. https://doi.org/10.1101/gad.10.2.154

Lisa Ooi, A. G., Karsunky, H., Majeti, R., Butz, S., Vestweber, D., Ishida, T., Quertermous, T., Weissman, I. L., & Forsberg, E. C. (2009). The adhesion molecule ESAM1 is a novel hematopoietic stem cell marker. *Stem Cells (Dayton, Ohio)*, *27*(3), 653–661. https://doi.org/10.1634/stemcells.2008-0824

Liu, Y., Chen, Q., Jeong, H.-W., Koh, B. I., Watson, E. C., Xu, C., Stehling, M., Zhou, B., & Adams, R. H. (2022). A specialized bone marrow microenvironment for fetal haematopoiesis. *Nature Communications*, *13*(1), 1327. https://doi.org/10.1038/s41467-022-28775-x

Lopez-Tello, J., Yong, H. E. J., Sandovici, I., Dowsett, G. K. C., Christoforou, E. R., Salazar-Petres, E., Boyland, R., Napso, T., Yeo, G. S. H., Lam, B. Y. H., Constancia, M., & Sferruzzi-Perri, A. N. (2023). Fetal manipulation of maternal metabolism is a critical function of the imprinted Igf2 gene. *Cell Metabolism*, *35*(7), 1195-1208.e6. https://doi.org/10.1016/j.cmet.2023.06.007

Lu, Y., Liu, M., Yang, J., Weissman, S. M., Pan, X., Katz, S. G., & Wang, S. (2021). Spatial transcriptome profiling by MERFISH reveals fetal liver hematopoietic stem cell niche architecture. *Cell Discovery*, *7*(1), 47. https://doi.org/10.1038/s41421-021-00266-1

Lua, I., & Asahina, K. (2016). The Role of Mesothelial Cells in Liver Development, Injury, and Regeneration. *Gut and Liver*, *10*(2), 166. https://doi.org/10.5009/gnl15226

Lua, I., Li, Y., Zagory, J. A., Wang, K. S., French, S. W., Sévigny, J., & Asahina, K. (2016). Characterization of hepatic stellate cells, portal fibroblasts, and mesothelial cells in normal and fibrotic livers. *Journal of Hepatology*, *64*(5), 1137–1146. https://doi.org/10.1016/j.jhep.2016.01.010

Lyman, S. D., James, L., Bos, T. V., de Vries, P., Brasel, K., Gliniak, B., Hollingsworth, L. T., Picha, K. S., McKenna, H. J., Splett, R. R., Fletcher, F. A., Maraskovsky, E., Farrah, T., Foxworthe, D., Williams, D. E., & Beckmann, M. P. (1993). Molecular cloning of a ligand for the flt3flk-2 tyrosine kinase receptor: A proliferative factor for primitive hematopoietic cells. *Cell*, *75*(6), 1157–1167. https://doi.org/10.1016/0092-8674(93)90325-K

Maher, J. J. (1993). Cell-specific expression of hepatocyte growth factor in liver. Upregulation in sinusoidal endothelial cells after carbon tetrachloride. *The Journal of Clinical Investigation*, *91*(5), 2244–2252. https://doi.org/10.1172/JCI116451

Mariani, S. A., Li, Z., Rice, S., Krieg, C., Fragkogianni, S., Robinson, M., Vink, C. S., Pollard, J. W., & Dzierzak, E. (2019). Pro-inflammatory Aorta-Associated Macrophages Are Involved in Embryonic Development of Hematopoietic Stem Cells. *Immunity*, *50*(6), 1439-1452.e5. https://doi.org/10.1016/j.immuni.2019.05.003

Mascarenhas, M. I., Parker, A., Dzierzak, E., & Ottersbach, K. (2009). Identification of novel regulators of hematopoietic stem cell development through refinement of stem cell localization and expression profiling. *Blood*, *114*(21), 4645–4653. https://doi.org/10.1182/blood-2009-06-230037

Matsubara, A., Iwama, A., Yamazaki, S., Furuta, C., Hirasawa, R., Morita, Y., Osawa, M., Motohashi, T., Eto, K., Ema, H., Kitamura, T., Vestweber, D., & Nakauchi, H. (2005). Endomucin, a CD34-like sialomucin, marks hematopoietic stem cells throughout development. *Journal of Experimental Medicine*, *202*(11), 1483–1492. https://doi.org/10.1084/jem.20051325

Matsumoto, K., Miki, R., Nakayama, M., Tatsumi, N., & Yokouchi, Y. (2008). Wnt9a secreted from the walls of hepatic sinusoids is essential for morphogenesis, proliferation, and glycogen accumulation of chick hepatic epithelium. *Developmental Biology*, *319*(2), 234–247. https://doi.org/10.1016/j.ydbio.2008.04.021

Matsumoto, K., Yoshitomi, H., Rossant, J., & Zaret, K. S. (2001). Liver Organogenesis Promoted by Endothelial Cells Prior to Vascular Function. *Science*, *294*(5542), 559–563. https://doi.org/10.1126/science.1063889

McGrath, K. E., Frame, J. M., Fegan, K. H., Bowen, J. R., Conway, S. J., Catherman, S. C., Kingsley, P. D., Koniski, A. D., & Palis, J. (2015). Distinct Sources of Hematopoietic Progenitors Emerge before HSCs and Provide Functional Blood Cells in the Mammalian Embryo. *Cell Reports*, *11*(12), 1892–1904. https://doi.org/10.1016/j.celrep.2015.05.036

McGrath, K. E., Koniski, A. D., Malik, J., & Palis, J. (2003). Circulation is established in a stepwise pattern in the mammalian embryo. *Blood*, *101*(5), 1669–1675. https://doi.org/10.1182/blood-2002-08-2531

McInnes, L., Healy, J., & Melville, J. (2020). *UMAP: Uniform Manifold Approximation and Projection for Dimension Reduction* (arXiv:1802.03426). arXiv. http://arxiv.org/abs/1802.03426

Medvinsky, A., & Dzierzak, E. (1996). Definitive Hematopoiesis Is Autonomously Initiated by the AGM Region. *Cell*, *86*(6), 897–906. https://doi.org/10.1016/S0092-8674(00)80165-8

Medvinsky, A. L., Samoylina, N. L., Müller, A. M., & Dzierzak, E. A. (1993). An early pre-liver intraembryonic source of CFU-S in the developing mouse. *Nature*, *364*(6432), 64–67. https://doi.org/10.1038/364064a0

Melig, G., Nobuhisa, I., Saito, K., Tsukahara, R., Itabashi, A., Kanai, Y., Kanai-Azuma, M., Osawa, M., Oshima, M., Iwama, A., & Taga, T. (2023). A Sox17 downstream gene Rasip1 is involved in the hematopoietic activity of intra-aortic hematopoietic clusters in the midgestation mouse embryo. *Inflammation and Regeneration*, *43*. https://doi.org/10.1186/s41232-023-00292-4

Méndez-Ferrer, S., Michurina, T. V., Ferraro, F., Mazloom, A. R., MacArthur, B. D., Lira, S. A., Scadden, D. T., Ma'ayan, A., Enikolopov, G. N., & Frenette, P. S. (2010). Mesenchymal and haematopoietic stem cells form a unique bone marrow niche. *Nature*, *466*(7308), Article 7308. https://doi.org/10.1038/nature09262

Merad, M., Manz, M. G., Karsunky, H., Wagers, A., Peters, W., Charo, I., Weissman, I. L., Cyster, J. G., & Engleman, E. G. (2002). Langerhans cells renew in the skin throughout life under steady-state conditions. *Nature Immunology*, *3*(12), 1135–1141. https://doi.org/10.1038/ni852

Miao, R., Chun, H., Feng, X., Gomes, A. C., Choi, J., & Pereira, J. P. (2022). Competition between hematopoietic stem and progenitor cells controls hematopoietic stem cell compartment size. *Nature Communications*, *13*(1), 4611. https://doi.org/10.1038/s41467-022-32228-w

Miller, C. L., Rebel, V. I., Helgason, C. D., Lansdorp, P. M., & Eaves, C. J. (1997). Impaired Steel Factor Responsiveness Differentially Affects the Detection and Long-Term Maintenance of Fetal Liver Hematopoietic Stem Cells In Vivo. *Blood*, *89*(4), 1214–1223. https://doi.org/10.1182/blood.V89.4.1214

Miyajima, A., Kinoshita, T., Tanaka, M., Kamiya, A., Mukouyama, Y., & Hara, T. (2000). Role of Oncostatin M in hematopoiesis and liver development. *Cytokine & Growth Factor Reviews*, *11*(3), 177–183. https://doi.org/10.1016/S1359-6101(00)00003-4

Mizoguchi, T., Pinho, S., Ahmed, J., Kunisaki, Y., Hanoun, M., Mendelson, A., Ono, N., Kronenberg, H. M., & Frenette, P. S. (2014). Osterix Marks Distinct Waves of Primitive and Definitive Stromal Progenitors during Bone Marrow Development. *Developmental Cell*, *29*(3), 340–349. https://doi.org/10.1016/j.devcel.2014.03.013

Mohandas, N., & Prenant, M. (1978). Three-dimensional model of bone marrow. *Blood*, *51*(4), 633–643.

Monaco, G., Chen, H., Poidinger, M., Chen, J., de Magalhães, J. P., & Larbi, A. (2016). flowAI: Automatic and interactive anomaly discerning tools for flow cytometry data. *Bioinformatics*, *32*(16), 2473–2480. https://doi.org/10.1093/bioinformatics/btw191

Moore, K. A., Pytowski, B., Witte, L., Hicklin, D., & Lemischka, I. R. (1997). Hematopoietic activity of a stromal cell transmembrane protein containing epidermal growth factor-like repeat motifs. *Proceedings of the National Academy of Sciences*, *94*(8), 4011–4016. https://doi.org/10.1073/pnas.94.8.4011

Moore, M. A. S., & Metcalf, D. (1970). Ontogeny of the Haemopoietic System: Yolk Sac Origin of In Vivo and In Vitro Colony Forming Cells in the Developing Mouse

Embryo. *British Journal of Haematology*, *18*(3), 279–296. https://doi.org/10.1111/j.1365-2141.1970.tb01443.x

Morrison, S. J., Hemmati, H. D., Wandycz, A. M., & Weissman, I. L. (1995). The purification and characterization of fetal liver hematopoietic stem cells. *Proceedings of the National Academy of Sciences*, *92*(22), 10302–10306. https://doi.org/10.1073/pnas.92.22.10302

Morrison, S. J., & Scadden, D. T. (2014). The bone marrow niche for haematopoietic stem cells. *Nature*, *505*(7483), 327–334. https://doi.org/10.1038/nature12984

Mossadegh-Keller, N., Sarrazin, S., Kandalla, P. K., Espinosa, L., Stanley, E. R., Nutt, S. L., Moore, J., & Sieweke, M. H. (2013). M-CSF instructs myeloid lineage fate in single haematopoietic stem cells. *Nature*, *497*(7448), Article 7448. https://doi.org/10.1038/nature12026

Müller, A. M., Medvinsky, A., Strouboulis, J., Grosveld, F., & Dzierzakt, E. (1994). Development of hematopoietic stem cell activity in the mouse embryo. *Immunity*, *1*(4), 291–301. https://doi.org/10.1016/1074-7613(94)90081-7

Murray, P. D. F., & Wilson, J. T. (1997). The development in vitro of the blood of the early chick embryo. *Proceedings of the Royal Society of London. Series B, Containing Papers of a Biological Character*, *111*(773), 497–521. https://doi.org/10.1098/rspb.1932.0070

Nagasawa, T., Hirota, S., Tachibana, K., Takakura, N., Nishikawa, S., Kitamura, Y., Yoshida, N., Kikutani, H., & Kishimoto, T. (1996). Defects of B-cell lymphopoiesis and bone-marrow myelopoiesis in mice lacking the CXC chemokine PBSF/SDF-1. *Nature*, *382*(6592), Article 6592. https://doi.org/10.1038/382635a0

Nakashima, K., Zhou, X., Kunkel, G., Zhang, Z., Deng, J. M., Behringer, R. R., & de Crombrugghe, B. (2002). The Novel Zinc Finger-Containing Transcription Factor Osterix Is Required for Osteoblast Differentiation and Bone Formation. *Cell*, *108*(1), 17–29. https://doi.org/10.1016/S0092-8674(01)00622-5

Neo, W. H., Booth, C. A. G., Azzoni, E., Chi, L., Delgado-Olguín, P., de Bruijn, M. F. T. R., Jacobsen, S. E. W., & Mead, A. J. (2018). Cell-extrinsic hematopoietic impact of Ezh2 inactivation in fetal liver endothelial cells. *Blood*, *131*(20), 2223–2234. https://doi.org/10.1182/blood-2017-10-811455

Nitou, M., Sugiyama, Y., Ishikawa, K., & Shiojiri, N. (2002). Purification of Fetal Mouse Hepatoblasts by Magnetic Beads Coated with Monoclonal Anti-E-Cadherin Antibodies and Their In Vitro Culture. *Experimental Cell Research*, *279*(2), 330–343. https://doi.org/10.1006/excr.2002.5615

Nombela-Arrieta, C., Pivarnik, G., Winkel, B., Canty, K. J., Harley, B., Mahoney, J. E., Park, S.-Y., Lu, J., Protopopov, A., & Silberstein, L. E. (2013). Quantitative imaging of haematopoietic stem and progenitor cell localization and hypoxic status in the bone marrow microenvironment. *Nature Cell Biology*, *15*(5), Article 5. https://doi.org/10.1038/ncb2730

North, T. E., de Bruijn, M. F. T. R., Stacy, T., Talebian, L., Lind, E., Robin, C., Binder, M., Dzierzak, E., & Speck, N. A. (2002). Runx1 Expression Marks Long-Term Repopulating Hematopoietic Stem Cells in the Midgestation Mouse Embryo. *Immunity*, *16*(5), 661–672. https://doi.org/10.1016/S1074-7613(02)00296-0

North, T., Gu, T.-L., Stacy, T., Wang, Q., Howard, L., Binder, M., Marín-Padilla, M., & Speck, N. A. (1999). Cbfa2 is required for the formation of intra-aortic hematopoietic clusters. *Development*, *126*(11), 2563–2575. https://doi.org/10.1242/dev.126.11.2563

Nygren, J. M., Bryder, D., & Jacobsen, S. E. W. (2006). Prolonged Cell Cycle Transit Is a Defining and Developmentally Conserved Hemopoietic Stem Cell Property. *The Journal of Immunology*, *177*(1), 201–208. https://doi.org/10.4049/jimmunol.177.1.201

Ober, E. A., & Lemaigre, F. P. (2018). Development of the liver: Insights into organ and tissue morphogenesis. *Journal of Hepatology*, *68*(5), 1049–1062. https://doi.org/10.1016/j.jhep.2018.01.005

Ogawa, T., Li, Y., Lua, I., Hartner, A., & Asahina, K. (2018). Isolation of a unique hepatic stellate cell population expressing integrin α8 from embryonic mouse livers. *Developmental Dynamics*, *247*(6), 867–881. https://doi.org/10.1002/dvdy.24634

Oguro, H., Ding, L., & Morrison, S. J. (2013). SLAM Family Markers Resolve Functionally Distinct Subpopulations of Hematopoietic Stem Cells and Multipotent Progenitors. *Cell Stem Cell*, 15.

Okada, S., Nakauchi, H., Nagayoshi, K., Nishikawa, S., Miura, Y., & Suda, T. (1992). In vivo and in vitro stem cell function of c-kit- and Sca-1-positive murine hematopoietic cells. *Blood*, *80*(12), 3044–3050. https://doi.org/10.1182/blood.V80.12.3044.3044

Onitsuka, I., Tanaka, M., & Miyajima, A. (2010). Characterization and Functional Analyses of Hepatic Mesothelial Cells in Mouse Liver Development. *Gastroenterology*, *138*(4), 1525-1535.e6. https://doi.org/10.1053/j.gastro.2009.12.059

Oostendorp, R. A. J., Harvey, K. N., Kusadasi, N., de Bruijn, M. F. T. R., Saris, C., Ploemacher, R. E., Medvinsky, A. L., & Dzierzak, E. A. (2002). Stromal cell lines from mouse aorta-gonads-mesonephros subregions are potent supporters of hematopoietic stem cell activity. *Blood*, *99*(4), 1183–1189. https://doi.org/10.1182/blood.V99.4.1183

Ottersbach, K., & Dzierzak, E. (2005). The Murine Placenta Contains Hematopoietic Stem Cells within the Vascular Labyrinth Region. *Developmental Cell*, *8*(3), 377–387. https://doi.org/10.1016/j.devcel.2005.02.001

Palis, J. (2014). Primitive and definitive erythropoiesis in mammals. *Frontiers in Physiology*, *5*. https://doi.org/10.3389/fphys.2014.00003

Palis, J. (2016). Hematopoietic stem cell-independent hematopoiesis: Emergence of erythroid, megakaryocyte, and myeloid potential in the mammalian embryo. *FEBS Letters*, *590*(22), 3965–3974. https://doi.org/10.1002/1873-3468.12459

Palis, J., Chan, R. J., Koniski, A., Patel, R., Starr, M., & Yoder, M. C. (2001). Spatial and temporal emergence of high proliferative potential hematopoietic precursors during murine embryogenesis. *Proceedings of the National Academy of Sciences*, *98*(8), 4528–4533. https://doi.org/10.1073/pnas.071002398

Palis, J., Robertson, S., Kennedy, M., Wall, C., & Keller, G. (1999). Development of erythroid and myeloid progenitors in the yolk sac and embryo proper of the mouse. *Development*, *126*(22), 5073–5084. https://doi.org/10.1242/dev.126.22.5073

Palla, G., Spitzer, H., Klein, M., Fischer, D., Schaar, A. C., Kuemmerle, L. B., Rybakov, S., Ibarra, I. L., Holmberg, O., Virshup, I., Lotfollahi, M., Richter, S., & Theis, F. J. (2022). Squidpy: A scalable framework for spatial omics analysis. *Nature Methods*, *19*(2), Article 2. https://doi.org/10.1038/s41592-021-01358-2

Paszke, A., Gross, S., Massa, F., Lerer, A., Bradbury, J., Chanan, G., Killeen, T., Lin, Z., Gimelshein, N., Antiga, L., Desmaison, A., Kopf, A., Yang, E., DeVito, Z., Raison, M., Tejani, A., Chilamkurthy, S., Steiner, B., Fang, L., … Chintala, S. (2019). *PyTorch: An Imperative Style, High-Performance Deep Learning Library*.

Patel, S. H., Christodoulou, C., Weinreb, C., Yu, Q., da Rocha, E. L., Pepe-Mooney, B. J., Bowling, S., Li, L., Osorio, F. G., Daley, G. Q., & Camargo, F. D. (2022). Lifelong multilineage contribution by embryonic-born blood progenitors. *Nature*, *606*(7915), 747–753. https://doi.org/10.1038/s41586-022-04804-z

Peeters, M., Ottersbach, K., Bollerot, K., Orelio, C., de Bruijn, M., Wijgerde, M., & Dzierzak, E. (2009). Ventral embryonic tissues and Hedgehog proteins induce early AGM hematopoietic stem cell development. *Development*, *136*(15), 2613–2621. https://doi.org/10.1242/dev.034728

Pei, W., Feyerabend, T. B., Rössler, J., Wang, X., Postrach, D., Busch, K., Rode, I., Klapproth, K., Dietlein, N., Quedenau, C., Chen, W., Sauer, S., Wolf, S., Höfer, T., & Rodewald, H.-R. (2017). Polylox barcoding reveals haematopoietic stem cell fates realized in vivo. *Nature*, *548*.

Peixoto, M. M., Soares-da-Silva, F., Bonnet, V., Ronteix, G., Santos, R. F., Mailhe, M.-P., Feng, X., Pereira, J. P., Azzoni, E., Anselmi, G., Bruijn, M. de, Baroud, C. N., Pinto-do-Ó, P., & Cumano, A. (2023). *Spatiotemporal dynamics of cytokines expression dictate fetal liver hematopoiesis* (p. 2023.08.24.554612). bioRxiv. https://doi.org/10.1101/2023.08.24.554612

Perdiguero, E. G., Klapproth, K., Schulz, C., Busch, K., Azzoni, E., Crozet, L., Garner, H., Trouillet, C., De Bruijn, M., Geissmann, F., & Rodewald, H.-R. (2015). Tissue-resident macrophages originate from yolk-sac-derived erythro-myeloid progenitors. *Nature*, 17.

Peschon, J. J., Morrissey, P. J., Grabstein, K. H., Ramsdell, F. J., Maraskovsky, E., Gliniak, B. C., Park, L. S., Ziegler, S. F., Williams, D. E., Ware, C. B., Meyer, J. D., & Davison, B. L. (1994). Early lymphocyte expansion is severely impaired in interleukin 7 receptor-deficient mice. *Journal of Experimental Medicine*, *180*(5), 1955–1960. https://doi.org/10.1084/jem.180.5.1955

Pietras, E. M., Reynaud, D., Kang, Y.-A., Carlin, D., Calero-Nieto, F. J., Leavitt, A. D., Stuart, J. M., Göttgens, B., & Passegué, E. (2015). Functionally Distinct Subsets of Lineage-Biased Multipotent Progenitors Control Blood Production in Normal and Regenerative Conditions. *Cell Stem Cell*, *17*(1), 35–46. https://doi.org/10.1016/j.stem.2015.05.003

Pietras, E. M., Warr, M. R., & Passegué, E. (2011). Cell cycle regulation in hematopoietic stem cells. *Journal of Cell Biology*, *195*(5), 709–720. https://doi.org/10.1083/jcb.201102131

Pinho, S., & Frenette, P. S. (2019). Haematopoietic stem cell activity and interactions with the niche. *Nature Reviews Molecular Cell Biology*, *20*(5), Article 5. https://doi.org/10.1038/s41580-019-0103-9

Prior, N., Hindley, C. J., Rost, F., Meléndez, E., Lau, W. W. Y., Göttgens, B., Rulands, S., Simons, B. D., & Huch, M. (2019). Lgr5+ stem/progenitor cells reside at the apex of a heterogeneous embryonic hepatoblast pool. *Development*, dev.174557. https://doi.org/10.1242/dev.174557

Pucella, J. N., Upadhaya, S., & Reizis, B. (2020). The Source and Dynamics of Adult Hematopoiesis: Insights from Lineage Tracing. *Annual Review of Cell and Developmental Biology*, *36*(1), 529–550. https://doi.org/10.1146/annurev-cellbio-020520-114601

Purton, L. E., & Scadden, D. T. (2007). Limiting Factors in Murine Hematopoietic Stem Cell Assays. *Cell Stem Cell*, *1*(3), 263–270. https://doi.org/10.1016/j.stem.2007.08.016

Qian, H., Buza-Vidas, N., Hyland, C. D., Jensen, C. T., Antonchuk, J., Månsson, R., Thoren, L. A., Ekblom, M., Alexander, W. S., & Jacobsen, S. E. W. (2007). Critical Role of Thrombopoietin in Maintaining Adult Quiescent Hematopoietic Stem Cells. *Cell Stem Cell*, *1*(6), 671–684. https://doi.org/10.1016/j.stem.2007.10.008

Qian, H., Georges-Labouesse, E., Nyström, A., Domogatskaya, A., Tryggvason, K., Jacobsen, S. E. W., & Ekblom, M. (2007). Distinct roles of integrins α6 and α4 in homing of fetal liver hematopoietic stem and progenitor cells. *Blood*, *110*(7), 2399–2407. https://doi.org/10.1182/blood-2006-10-051276

Que, J., Wilm, B., Hasegawa, H., Wang, F., Bader, D., & Hogan, B. L. M. (2008). Mesothelium contributes to vascular smooth muscle and mesenchyme during lung development. *Proceedings of the National Academy of Sciences*, *105*(43), 16626–16630. https://doi.org/10.1073/pnas.0808649105

Rebel, V. I., Miller, C. L., Thornbury, G. R., Dragowska, W. H., Eaves, C. J., & Lansdorp, P. M. (1996). A comparison of long-term repopulating hematopoietic stem cells in fetal liver and adult bone marrow from the mouse. *Experimental Hematology*, *24*(5), 638–648.

Rhodes, K. E., Gekas, C., Wang, Y., Lux, C. T., Francis, C. S., Chan, D. N., Conway, S., Orkin, S. H., Yoder, M. C., & Mikkola, H. K. A. (2008). The Emergence of Hematopoietic Stem Cells Is Initiated in the Placental Vasculature in the Absence of Circulation. *Cell Stem Cell*, *2*(3), 252–263. https://doi.org/10.1016/j.stem.2008.01.001

Rinkevich, Y., Mori, T., Sahoo, D., Xu, P.-X., Bermingham, J. R., & Weissman, I. L. (2012). Identification and prospective isolation of a mesothelial precursor lineage giving rise to smooth muscle cells and fibroblasts for mammalian internal organs, and their vasculature. *Nature Cell Biology*, *14*(12), Article 12. https://doi.org/10.1038/ncb2610

Robin, C., Ottersbach, K., Durand, C., Peeters, M., Vanes, L., Tybulewicz, V., & Dzierzak, E. (2006). An Unexpected Role for IL-3 in the Embryonic Development of Hematopoietic Stem Cells. *Developmental Cell*, *11*(2), 171–180. https://doi.org/10.1016/j.devcel.2006.07.002

Rodriguez y Baena, A., Manso, B. A., & Forsberg, E. C. (2021). CFU-S assay: A historical single-cell assay that offers modern insight into clonal hematopoiesis. *Experimental Hematology*, *104*, 1–8. https://doi.org/10.1016/j.exphem.2021.10.003

Rodriguez-Fraticelli, A. E., & Camargo, F. (2021). Systems analysis of hematopoiesis using single-cell lineage tracing. *Current Opinion in Hematology*, *28*(1), 10.

Rodriguez-Fraticelli, A. E., Wolock, S. L., Weinreb, C. S., Panero, R., Patel, S. H., Jankovic, M., Sun, J., Calogero, R. A., Klein, A. M., & Camargo, F. D. (2018). Clonal analysis of lineage fate in native haematopoiesis. *Nature*, *553*(7687), 212–216. https://doi.org/10.1038/nature25168

Rojas, A., De Val, S., Heidt, A. B., Xu, S.-M., Bristow, J., & Black, B. L. (2005). Gata4 expression in lateral mesoderm is downstream of BMP4 and is activated directly by Forkhead and GATA transcription factors through a distal enhancer element. *Development (Cambridge, England)*, *132*(15), 3405–3417. https://doi.org/10.1242/dev.01913

Ronteix, G., Aristov, A., Bonnet, V., Sart, S., Sobel, J., Esposito, E., & Baroud, C. N. (2022). Griottes: A generalist tool for network generation from segmented tissue images. *BMC Biology*, *20*(1), 178. https://doi.org/10.1186/s12915-022-01376-2

Rossi, J. M., Dunn, N. R., Hogan, B. L. M., & Zaret, K. S. (2001). Distinct mesodermal signals, including BMPs from the septum transversum mesenchyme, are required

in combination for hepatogenesis from the endoderm. *Genes & Development*, *15*(15), 1998–2009. https://doi.org/10.1101/gad.904601

Rybtsov, S., Ivanovs, A., Zhao, S., & Medvinsky, A. (2016). Concealed expansion of immature precursors underpins acute burst of adult HSC activity in foetal liver. *Development*, *143*(8), 1284–1289. https://doi.org/10.1242/dev.131193

Saçma, M., Pospiech, J., Bogeska, R., de Back, W., Mallm, J.-P., Sakk, V., Soller, K., Marka, G., Vollmer, A., Karns, R., Cabezas-Wallscheid, N., Trumpp, A., Méndez-Ferrer, S., Milsom, M. D., Mulaw, M. A., Geiger, H., & Florian, M. C. (2019). Haematopoietic stem cells in perisinusoidal niches are protected from ageing. *Nature Cell Biology*, *21*(11), 1309–1320. https://doi.org/10.1038/s41556-019-0418-y

Saharinen, P., Tammela, T., Karkkainen, M. J., & Alitalo, K. (2004). Lymphatic vasculature: Development, molecular regulation and role in tumor metastasis and inflammation. *Trends in Immunology*, *25*(7), 387–395. https://doi.org/10.1016/j.it.2004.05.003

Sánchez, M.-J., Holmes, A., Miles, C., & Dzierzak, E. (1996). Characterization of the First Definitive Hematopoietic Stem Cells in the AGM and Liver of the Mouse Embryo. *Immunity*, *5*(6), 513–525. https://doi.org/10.1016/S1074-7613(00)80267-8

Sandovici, I., Georgopoulou, A., Pérez-García, V., Hufnagel, A., López-Tello, J., Lam, B. Y. H., Schiefer, S. N., Gaudreau, C., Santos, F., Hoelle, K., Yeo, G. S. H., Burling, K., Reiterer, M., Fowden, A. L., Burton, G. J., Branco, C. M., Sferruzzi-Perri, A. N., & Constância, M. (2022). The imprinted Igf2-Igf2r axis is critical for matching placental microvasculature expansion to fetal growth. *Developmental Cell*, *57*(1), 63-79.e8. https://doi.org/10.1016/j.devcel.2021.12.005

Sanjuan-Pla, A., Macaulay, I. C., Jensen, C. T., Woll, P. S., Luis, T. C., Mead, A., Moore, S., Carella, C., Matsuoka, S., Jones, T. B., Chowdhury, O., Stenson, L., Lutteropp, M., Green, J. C. A., Facchini, R., Boukarabila, H., Grover, A., Gambardella, A., Thongjuea, S., … Jacobsen, S. E. W. (2013). Platelet-biased stem cells reside at the apex of the haematopoietic stem-cell hierarchy. *Nature*, *502*(7470), 232–236. https://doi.org/10.1038/nature12495

Sasaki, T., Mizuochi, C., Horio, Y., Nakao, K., Akashi, K., & Sugiyama, D. (2010). Regulation of hematopoietic cell clusters in the placental niche through SCF/Kit signaling in embryonic mouse. *Development*, *138*(9), 1875–1875. https://doi.org/10.1242/dev.067231

Sato, Y. (2013). Dorsal aorta formation: Separate origins, lateral-to-medial migration, and remodeling. *Development, Growth & Differentiation*, *55*(1), 113–129. https://doi.org/10.1111/dgd.12010

Sawai, C. M., Babovic, S., Upadhaya, S., Knapp, D. J. H. F., Lavin, Y., Lau, C. M., Goloborodko, A., Feng, J., Fujisaki, J., Ding, L., Mirny, L. A., Merad, M., Eaves, C. J., & Reizis, B. (2016). Hematopoietic Stem Cells Are the Major Source of Multilineage Hematopoiesis in Adult Animals. *Immunity*, *45*(3), 597–609. https://doi.org/10.1016/j.immuni.2016.08.007

Schmutz, S., Valente, M., Cumano, A., & Novault, S. (2016). Spectral Cytometry Has Unique Properties Allowing Multicolor Analysis of Cell Suspensions Isolated from Solid Tissues. *PLOS ONE*, *11*(8), e0159961. https://doi.org/10.1371/journal.pone.0159961

Schofield, R. (1978). The relationship between the spleen colony-forming cell and the haemopoietic stem cell. *Blood Cells*, *4*(1–2), 7–25.

Sélénou, C., Brioude, F., Giabicani, E., Sobrier, M.-L., & Netchine, I. (2022). IGF2: Development, Genetic and Epigenetic Abnormalities. *Cells*, *11*(12), Article 12. https://doi.org/10.3390/cells11121886

Sender, R., & Milo, R. (2021). The distribution of cellular turnover in the human body. *Nature Medicine*, *27*(1), 45–48. https://doi.org/10.1038/s41591-020-01182-9

Shao, L., Paik, N. Y., Sanborn, M. A., Bandara, T., Vijaykumar, A., Sottoriva, K., Rehman, J., Nombela-Arrieta, C., & Pajcini, K. V. (2023). Hematopoietic Jagged1 is a fetal liver niche factor required for functional maturation and engraftment of fetal hematopoietic stem cells. *Proceedings of the National Academy of Sciences*, *120*(20), e2210058120. https://doi.org/10.1073/pnas.2210058120

Sigurdsson, V., Takei, H., Soboleva, S., Radulovic, V., Galeev, R., Siva, K., Leeb-Lundberg, L. M. F., Iida, T., Nittono, H., & Miharada, K. (2016). Bile Acids Protect Expanding Hematopoietic Stem Cells from Unfolded Protein Stress in Fetal Liver. *Cell Stem Cell*, *18*(4), 522–532. https://doi.org/10.1016/j.stem.2016.01.002

Siminovitch, L., McCulloch, E. A., & Till, J. E. (1963). The distribution of colony-forming cells among spleen colonies. *Journal of Cellular and Comparative Physiology*, *62*(3), 327–336. https://doi.org/10.1002/jcp.1030620313

Soares-da-Silva, F. (2020). *Environmental Signals Driving the Onset of Hematopoiesis in the Fetal Liver* [PhD]. University of Porto.

Soares-da-Silva, F., Elsaid, R., Peixoto, M. M., Nogueira, G., Pereira, P., Bandeira, A., & Cumano, A. (2023). Assembling the layers of the hematopoietic system: A window of opportunity for thymopoiesis in the embryo. *Immunological Reviews*, imr.13187. https://doi.org/10.1111/imr.13187

Soares-da-Silva, F., Freyer, L., Elsaid, R., Burlen-Defranoux, O., Iturri, L., Sismeiro, O., Pinto-do-Ó, P., Gomez-Perdiguero, E., & Cumano, A. (2021). Yolk sac, but not hematopoietic stem cell–derived progenitors, sustain erythropoiesis throughout murine embryonic life. *Journal of Experimental Medicine*, *218*(4), e20201729. https://doi.org/10.1084/jem.20201729

Soares-da-Silva, F., Peixoto, M., Cumano, A., & Pinto-do-Ó, P. (2020). Crosstalk Between the Hepatic and Hematopoietic Systems During Embryonic Development. *Frontiers in Cell and Developmental Biology*, *8*, 612. https://doi.org/10.3389/fcell.2020.00612

Souma, T., Suzuki, N., & Yamamoto, M. (2015). Renal erythropoietin-producing cells in health and disease. *Frontiers in Physiology*, *6*. https://www.frontiersin.org/articles/10.3389/fphys.2015.00167

Spangrude, G. J., Heimfeld, S., & Weissman, I. L. (1988). Purification and Characterization of Mouse Hematopoietic Stem Cells. *Science*, *241*(4861), 58–62. https://doi.org/10.1126/science.2898810

Stoltzfus, C. R., Filipek, J., Gern, B. H., Olin, B. E., Leal, J. M., Wu, Y., Lyons-Cohen, M. R., Huang, J. Y., Paz-Stoltzfus, C. L., Plumlee, C. R., Pöschinger, T., Urdahl, K. B., Perro, M., & Gerner, M. Y. (2020). CytoMAP: A Spatial Analysis Toolbox Reveals Features of Myeloid Cell Organization in Lymphoid Tissues. *Cell Reports*, *31*(3), 107523. https://doi.org/10.1016/j.celrep.2020.107523

Stremmel, C., Schuchert, R., Wagner, F., Thaler, R., Weinberger, T., Pick, R., Mass, E., Ishikawa-Ankerhold, H. C., Margraf, A., Hutter, S., Vagnozzi, R., Klapproth, S., Frampton, J., Yona, S., Scheiermann, C., Molkentin, J. D., Jeschke, U., Moser, M., Sperandio, M., … Schulz, C. (2018). Yolk sac macrophage progenitors traffic to the embryo during defined stages of development. *Nature Communications*, *9*(1), 75. https://doi.org/10.1038/s41467-017-02492-2

Stringer, C., Wang, T., Michaelos, M., & Pachitariu, M. (2021). Cellpose: A generalist algorithm for cellular segmentation. *Nature Methods*, *18*(1), 100–106. https://doi.org/10.1038/s41592-020-01018-x

Su, X., Shi, Y., Zou, X., Lu, Z.-N., Xie, G., Yang, J. Y. H., Wu, C.-C., Cui, X.-F., He, K.-Y., Luo, Q., Qu, Y.-L., Wang, N., Wang, L., & Han, Z.-G. (2017). Single-cell RNA-Seq analysis reveals dynamic trajectories during mouse liver development. *BMC Genomics*, *18*(1), 946. https://doi.org/10.1186/s12864-017-4342-x

Sugiyama, D., Kulkeaw, K., Mizuochi, C., Horio, Y., & Okayama, S. (2011). Hepatoblasts comprise a niche for fetal liver erythropoiesis through cytokine production. *Biochemical and Biophysical Research Communications*, *410*(2), 301–306. https://doi.org/10.1016/j.bbrc.2011.05.137

Sugiyama, T., Kohara, H., Noda, M., & Nagasawa, T. (2006). Maintenance of the Hematopoietic Stem Cell Pool by CXCL12-CXCR4 Chemokine Signaling in Bone Marrow Stromal Cell Niches. *Immunity*, *25*(6), 977–988. https://doi.org/10.1016/j.immuni.2006.10.016

Sugiyama, Y., Takabe, Y., Nakakura, T., Tanaka, S., Koike, T., & Shiojiri, N. (2010). Sinusoid development and morphogenesis may be stimulated by VEGF-Flk-1 signaling during fetal mouse liver development. *Developmental Dynamics*, *239*(2), 386–397. https://doi.org/10.1002/dvdy.22162

Sun, J., Ramos, A., Chapman, B., Johnnidis, J. B., Le, L., Ho, Y.-J., Klein, A. M., Hofmann, O., & Camargo, F. (2014). Clonal dynamics of native haematopoiesis. *Nature*, 17. https://doi.org/10.1038/nature13824

Sungaran, R., Markovic, B., & Chong, B. H. (1997). Localization and Regulation of Thrombopoietin mRNA Expression in Human Kidney, Liver, Bone Marrow, and Spleen Using In Situ Hybridization. *Blood*, *89*(1), 101–107. https://doi.org/10.1182/blood.V89.1.101

Suzuki, K., Tanaka, M., Watanabe, N., Saito, S., Nonaka, H., & Miyajima, A. (2008). P75 Neurotrophin Receptor Is a Marker for Precursors of Stellate Cells and Portal Fibroblasts in Mouse Fetal Liver. *Gastroenterology*, *135*(1), 270-281.e3. https://doi.org/10.1053/j.gastro.2008.03.075

Suzuki, N., Hirano, I., Pan, X., Minegishi, N., & Yamamoto, M. (2013). Erythropoietin production in neuroepithelial and neural crest cells during primitive erythropoiesis. *Nature Communications*, *4*(1), Article 1. https://doi.org/10.1038/ncomms3902

Suzuki, N., Obara, N., Pan, X., Watanabe, M., Jishage, K.-I., Minegishi, N., & Yamamoto, M. (2011). Specific Contribution of the Erythropoietin Gene 3′ Enhancer to Hepatic Erythropoiesis after Late Embryonic Stages. *Molecular and Cellular Biology*, *31*(18), 3896–3905. https://doi.org/10.1128/MCB.05463-11

Swartley, O. M., Foley, J. F., Livingston, D. P., Cullen, J. M., & Elmore, S. A. (2016). Histology Atlas of the Developing Mouse Hepatobiliary Hemolymphatic Vascular System with Emphasis on Embryonic Days 11.5–18.5 and Early Postnatal Development. *Toxicologic Pathology*, *44*(5), 705–725. https://doi.org/10.1177/0192623316630836

Szilvassy, S. J., Humphries, R. K., Lansdorp, P. M., Eaves, A. C., & Eaves, C. J. (1990). Quantitative assay for totipotent reconstituting hematopoietic stem cells by a competitive repopulation strategy. *Proceedings of the National Academy of Sciences*, *87*(22), 8736–8740. https://doi.org/10.1073/pnas.87.22.8736

Szilvassy, S. J., Ragland, P. L., Miller, C. L., & Eaves, C. J. (2003). The marrow homing efficiency of murine hematopoietic stem cells remains constant during ontogeny.

*Experimental Hematology*, *31*(4), 331–338. https://doi.org/10.1016/S0301-472X(03)00005-5

Takabe, Y., Yagi, S., Koike, T., & Shiojiri, N. (2012). Immunomagnetic exclusion of E-cadherin-positive hepatoblasts in fetal mouse liver cell cultures impairs morphogenesis and gene expression of sinusoidal endothelial cells: Sinusoidal morphogenesis during liver development. *Journal of Anatomy*, *221*(3), 229–239. https://doi.org/10.1111/j.1469-7580.2012.01532.x

Takahashi, K., Yamamura, F., & Naito, M. (1989). Differentiation, Maturation, and Proliferation of Macrophages in the Mouse Yolk Sac: A Light-Microscopic, Enzyme-Cytochemical, Immunohistochemical, and Ultrastructural Study. *Journal of Leukocyte Biology*, *45*(2), 87–96. https://doi.org/10.1002/jlb.45.2.87

Takashima, Y., Terada, M., Kawabata, M., & Suzuki, A. (2015). Dynamic three-dimensional morphogenesis of intrahepatic bile ducts in mouse liver development. *Hepatology (Baltimore, Md.)*, *61*(3), 1003–1011. https://doi.org/10.1002/hep.27436

Tamplin, O. J., Durand, E. M., Carr, L. A., Childs, S. J., Hagedorn, E. J., Li, P., Yzaguirre, A. D., Speck, N. A., & Zon, L. I. (2015). Hematopoietic Stem Cell Arrival Triggers Dynamic Remodeling of the Perivascular Niche. *Cell*, *160*(1–2), 241–252. https://doi.org/10.1016/j.cell.2014.12.032

Tan, K. S., Kulkeaw, K., Nakanishi, Y., & Sugiyama, D. (2017). Expression of cytokine and extracellular matrix mRNAs in fetal hepatic stellate cells. *Genes to Cells*, *22*(9), 836–844. https://doi.org/10.1111/gtc.12517

Tanaka, M., Okabe, M., Suzuki, K., Kamiya, Y., Tsukahara, Y., Saito, S., & Miyajima, A. (2009). Mouse hepatoblasts at distinct developmental stages are characterized by expression of EpCAM and DLK1: Drastic change of EpCAM expression during liver development. *Mechanisms of Development*, *126*(8–9), 665–676. https://doi.org/10.1016/j.mod.2009.06.939

Tanimizu, N., Kaneko, K., Itoh, T., Ichinohe, N., Ishii, M., Mizuguchi, T., Hirata, K., Miyajima, A., & Mitaka, T. (2016). Intrahepatic bile ducts are developed through formation of homogeneous continuous luminal network and its dynamic rearrangement in mice. *Hepatology*, *64*(1), 175–188. https://doi.org/10.1002/hep.28521

Tanimizu, N., Nishikawa, M., Saito, H., Tsujimura, T., & Miyajima, A. (2003). Isolation of hepatoblasts based on the expression of Dlk/Pref-1. *Journal of Cell Science*, *116*(9), 1775–1786. https://doi.org/10.1242/jcs.00388

Taoudi, S., & Medvinsky, A. (2007). Functional identification of the hematopoietic stem cell niche in the ventral domain of the embryonic dorsal aorta. *Proceedings of the National Academy of Sciences*, *104*(22), 9399–9403. https://doi.org/10.1073/pnas.0700984104

Taoudi, S., Morrison, A. M., Inoue, H., Gribi, R., Ure, J., & Medvinsky, A. (2005). Progressive divergence of definitive haematopoietic stem cells from the endothelial compartment does not depend on contact with the foetal liver. *Development*, *132*(18), 4179–4191. https://doi.org/10.1242/dev.01974

Tavian, M., Coulombel, L., Luton, D., Clemente, H., Dieterlen-Lievre, F., & Peault, B. (1996). Aorta-associated CD34+ hematopoietic cells in the early human embryo. *Blood*, *87*(1), 67–72. https://doi.org/10.1182/blood.V87.1.67.67

Till, J. E., & McCulloch, E. A. (1961). A Direct Measurement of the Radiation Sensitivity of Normal Mouse Bone Marrow Cells. *Radiation Research*, *178*(2), AV3–AV7. https://doi.org/10.1667/RRAV01.1

Tober, J., Koniski, A., McGrath, K. E., Vemishetti, R., Emerson, R., De Mesy-Bentley, K. K. L., Waugh, R., & Palis, J. (2007). The megakaryocyte lineage originates from hemangioblast precursors and is an integral component both of primitive and of definitive hematopoiesis. *Blood*, *109*(4), 1433–1441. https://doi.org/10.1182/blood-2006-06-031898

Tornack, J., Kawano, Y., Garbi, N., Hämmerling, G. J., Melchers, F., & Tsuneto, M. (2017). Flt3 ligand-eGFP-reporter expression characterizes functionally distinct subpopulations of CD150+ long-term repopulating murine hematopoietic stem cells. *European Journal of Immunology*, *47*(9), 1477–1487. https://doi.org/10.1002/eji.201646730

Trevisan, M., Yan, X., & Iscove, N. (1996). Cycle initiation and colony formation in culture by murine marrow cells with long-term reconstituting potential in vivo. *Blood*, *88*(11), 4149–4158. https://doi.org/10.1182/blood.V88.11.4149.4149

Tsuneto, M., Tokoyoda, K., Kajikhina, E., Hauser, A. E., Hara, T., Tani-ichi, S., Ikuta, K., & Melchers, F. (2013). B-Cell Progenitors and Precursors Change Their Microenvironment in Fetal Liver During Early Development. *Stem Cells*, *31*(12), 2800–2812. https://doi.org/10.1002/stem.1421

Ueda, H. R., Ertürk, A., Chung, K., Gradinaru, V., Chédotal, A., Tomancak, P., & Keller, P. J. (2020). Tissue clearing and its applications in neuroscience. *Nature Reviews Neuroscience*, *21*(2), 61–79. https://doi.org/10.1038/s41583-019-0250-1

Ueda, T., Yokota, T., Okuzaki, D., Uno, Y., Mashimo, T., Kubota, Y., Sudo, T., Ishibashi, T., Shingai, Y., Doi, Y., Ozawa, T., Nakai, R., Tanimura, A., Ichii, M., Ezoe, S., Shibayama, H., Oritani, K., & Kanakura, Y. (2019). Endothelial Cell-Selective Adhesion Molecule Contributes to the Development of Definitive Hematopoiesis in the Fetal Liver. *Stem Cell Reports*, *13*(6), 992–1005. https://doi.org/10.1016/j.stemcr.2019.11.002

Ueno, H., & Weissman, I. L. (2006). Clonal Analysis of Mouse Development Reveals a Polyclonal Origin for Yolk Sac Blood Islands. *Developmental Cell*, *11*(4), 519–533. https://doi.org/10.1016/j.devcel.2006.08.001

Ulloa, B. A., Habbsa, S. S., Potts, K. S., Lewis, A., McKinstry, M., Payne, S. G., Flores, J. C., Nizhnik, A., Feliz Norberto, M., Mosimann, C., & Bowman, T. V. (2021). Definitive hematopoietic stem cells minimally contribute to embryonic hematopoiesis. *Cell Reports*, *36*(11), 109703. https://doi.org/10.1016/j.celrep.2021.109703

Valente, M., Resende, T. P., Nascimento, D. S., Burlen-Defranoux, O., Soares-da-Silva, F., Dupont, B., Cumano, A., & Pinto-do-Ó, P. (2019). Mouse HSA+ immature cardiomyocytes persist in the adult heart and expand after ischemic injury. *PLOS Biology*, *17*(6), e3000335. https://doi.org/10.1371/journal.pbio.3000335

van Os, R., Kamminga, L. M., & de Haan, G. (2004). Stem Cell Assays: Something Old, Something New, Something Borrowed. *STEM CELLS*, *22*(7), 1181–1190. https://doi.org/10.1634/stemcells.2004-0095

Vestentoft, P. S., Jelnes, P., Hopkinson, B. M., Vainer, B., Møllgård, K., Quistorff, B., & Bisgaard, H. C. (2011). Three-dimensional reconstructions of intrahepatic bile duct tubulogenesis in human liver. *BMC Developmental Biology*, *11*(1), 56. https://doi.org/10.1186/1471-213X-11-56

Wahlestedt, M., Ladopoulos, V., Hidalgo, I., Sanchez Castillo, M., Hannah, R., Säwén, P., Wan, H., Dudenhöffer-Pfeifer, M., Magnusson, M., Norddahl, G. L., Göttgens, B., & Bryder, D. (2017). Critical Modulation of Hematopoietic Lineage Fate by Hepatic

Leukemia Factor. *Cell Reports*, *21*(8), 2251–2263. https://doi.org/10.1016/j.celrep.2017.10.112

Wake, K. (1971). “Sternzellen” in the liver: Perisinusoidal cells with special reference to storage of vitamin A. *American Journal of Anatomy*, *132*(4), 429–461. https://doi.org/10.1002/aja.1001320404

Wake, K., & Sato, T. (2015). “The Sinusoid” in the Liver: Lessons Learned from the Original Definition by Charles Sedgwick Minot (1900). *The Anatomical Record*, *298*(12), 2071–2080. https://doi.org/10.1002/ar.23263

Wang, H. U., Chen, Z.-F., & Anderson, D. J. (1998). Molecular Distinction and Angiogenic Interaction between Embryonic Arteries and Veins Revealed by ephrin-B2 and Its Receptor Eph-B4. *Cell*, *93*(5), 741–753. https://doi.org/10.1016/S0092-8674(00)81436-1

Wanner, N., Barnhart, J., Apostolakis, N., Zlojutro, V., & Asosingh, K. (2022). Using the Autofluorescence Finder on the Sony ID7000TM Spectral Cell Analyzer to Identify and Unmix Multiple Highly Autofluorescent Murine Lung Populations. *Frontiers in Bioengineering and Biotechnology*, *10*, 827987. https://doi.org/10.3389/fbioe.2022.827987

Watanabe, T., Nakagawa, K., Ohata, S., Kitagawa, D., Nishitai, G., Seo, J., Tanemura, S., Shimizu, N., Kishimoto, H., Wada, T., Aoki, J., Arai, H., Iwatsubo, T., Mochita, M., Watanabe, T., Satake, M., Ito, Y., Matsuyama, T., Mak, T. W., … Katada, T. (2002). SEK1/MKK4-Mediated SAPK/JNK Signaling Participates in Embryonic Hepatoblast Proliferation via a Pathway Different from NF-κB-Induced Anti-Apoptosis. *Developmental Biology*, *250*(2), 332–347. https://doi.org/10.1006/dbio.2002.0781

Watt, A. (2003). HNF4: A central regulator of hepatocyte differentiation and function. *Hepatology*, *37*(6), 1249–1253. https://doi.org/10.1053/jhep.2003.50273

Watts, D., Gaete, D., Rodriguez, D., Hoogewijs, D., Rauner, M., Sormendi, S., & Wielockx, B. (2020). Hypoxia Pathway Proteins are Master Regulators of Erythropoiesis. *International Journal of Molecular Sciences*, *21*(21), 8131. https://doi.org/10.3390/ijms21218131

Weissman, I. L., & Shizuru, J. A. (2008). The origins of the identification and isolation of hematopoietic stem cells, and their capability to induce donor-specific transplantation tolerance and treat autoimmune diseases. *Blood*, *112*(9), 3543–3553. https://doi.org/10.1182/blood-2008-08-078220

Wilm, B., Ipenberg, A., Hastie, N. D., Burch, J. B. E., & Bader, D. M. (2005). The serosal mesothelium is a major source of smooth muscle cells of the gut vasculature. *Development*, *132*(23), 5317–5328. https://doi.org/10.1242/dev.02141

Wittig, O., Paez-Cortez, J., & Cardier, J. E. (2010). Liver sinusoidal endothelial cells promote B lymphopoiesis from primitive hematopoietic cells. *Stem Cells and Development*, *19*(3), 341–350. https://doi.org/10.1089/scd.2009.0300

Wolber, F. M., Leonard, E., Michael, S., Orschell-Traycoff, C. M., Yoder, M. C., & Srour, E. F. (2002). Roles of spleen and liver in development of the murine hematopoietic system. *Experimental Hematology*, *30*(9), 1010–1019. https://doi.org/10.1016/S0301-472X(02)00881-0

Wong, J. B., Hewitt, S. L., Heltemes-Harris, L. M., Mandal, M., Johnson, K., Rajewsky, K., Koralov, S. B., Clark, M. R., Farrar, M. A., & Skok, J. A. (2019). B-1a cells acquire their unique characteristics by bypassing the pre-BCR selection stage. *Nature Communications*, *10*(1), 4768. https://doi.org/10.1038/s41467-019-12824-z

Wu, A. M., Till, J. E., Siminovitch, L., & McCulloch, E. A. (1967). A cytological study of the capacity for differentiation of normal hemopoietic colony-forming cells. *Journal of Cellular Physiology*, *69*(2), 177–184. https://doi.org/10.1002/jcp.1040690208

Wu, A. M., Till, J. E., Siminovitch, L., & McCulloch, E. A. (1968). Cytological evidence for a relationship between normal haematopoietic colony-forming cells and cells of the lymphoid system. *Journal of Experimental Medicine*, *127*(3), 455–464. https://doi.org/10.1084/jem.127.3.455

Wu, H., Klingmüller, U., Besmer, P., & Lodish, H. F. (1995). Interaction of the erythropoietin and stem-cell-factor receptors. *Nature*, *377*(6546), Article 6546. https://doi.org/10.1038/377242a0

Xu, C., Gao, X., Wei, Q., Nakahara, F., Zimmerman, S. E., Mar, J., & Frenette, P. S. (2018). Stem cell factor is selectively secreted by arterial endothelial cells in bone marrow. *Nature Communications*, *9*(1), Article 1. https://doi.org/10.1038/s41467-018-04726-3

Xu, M., Matsuoka, S., Yang, F.-C., Ebihara, Y., Manabe, A., Tanaka, R., Eguchi, M., Asano, S., Nakahata, T., & Tsuji, K. (2001). Evidence for the presence of murine primitive megakarycytopoiesis in the early yolk sac. *Blood*, *97*(7), 2016–2022. https://doi.org/10.1182/blood.V97.7.2016

Yamamoto, R., Morita, Y., Ooehara, J., Hamanaka, S., Onodera, M., Rudolph, K. L., Ema, H., & Nakauchi, H. (2013). Clonal Analysis Unveils Self-Renewing Lineage-Restricted Progenitors Generated Directly from Hematopoietic Stem Cells. *Cell*, *154*(5), 1112–1126. https://doi.org/10.1016/j.cell.2013.08.007

Yamazaki, S., Ema, H., Karlsson, G., Yamaguchi, T., Miyoshi, H., Shioda, S., Taketo, M. M., Karlsson, S., Iwama, A., & Nakauchi, H. (2011). Nonmyelinating Schwann Cells Maintain Hematopoietic Stem Cell Hibernation in the Bone Marrow Niche. *Cell*, *147*(5), 1146–1158. https://doi.org/10.1016/j.cell.2011.09.053

Yang, L., Bryder, D., Adolfsson, J., Nygren, J., Månsson, R., Sigvardsson, M., & Jacobsen, S. E. W. (2005). Identification of Lin–Sca1+kit+CD34+Flt3– short-term hematopoietic stem cells capable of rapidly reconstituting and rescuing myeloablated transplant recipients. *Blood*, *105*(7), 2717–2723. https://doi.org/10.1182/blood-2004-06-2159

Yang, L., Wang, W.-H., Qiu, W.-L., Guo, Z., Bi, E., & Xu, C.-R. (2017). A single-cell transcriptomic analysis reveals precise pathways and regulatory mechanisms underlying hepatoblast differentiation. *Hepatology*, *66*(5), 1387. https://doi.org/10.1002/hep.29353

Yoder, M. C., Papaioannou, V. E., Breitfeld, P. P., & Williams, D. A. (1994). Murine Yolk Sac Endoderm—And Mesoderm -Derived Cell Lines Support In Vitro Growth and Differentiation of Hematopoietic Cells. *Blood*, *83*(9), 2436–2443. https://doi.org/10.1182/blood.V83.9.2436.2436

Yokomizo, T., Ideue, T., Morino-Koga, S., Tham, C. Y., Sato, T., Takeda, N., Kubota, Y., Kurokawa, M., Komatsu, N., Ogawa, M., Araki, K., Osato, M., & Suda, T. (2022). Independent origins of fetal liver haematopoietic stem and progenitor cells. *Nature*, *609*(7928), 779–784. https://doi.org/10.1038/s41586-022-05203-0

Yokomizo, T., Ng, C. E. L., Osato, M., & Dzierzak, E. (2011). Three-dimensional imaging of whole midgestation murine embryos shows an intravascular localization for all hematopoietic clusters. *Blood*, *117*(23), 6132–6134. https://doi.org/10.1182/blood-2011-02-334037

Yokomizo, T., Watanabe, N., Umemoto, T., Matsuo, J., Harai, R., Kihara, Y., Nakamura, E., Tada, N., Sato, T., Takaku, T., Shimono, A., Takizawa, H., Nakagata, N., Mori, S., Kurokawa, M., Tenen, D. G., Osato, M., Suda, T., & Komatsu, N. (2019). Hlf marks the developmental pathway for hematopoietic stem cells but not for erythro-myeloid progenitors. *Journal of Experimental Medicine*, *216*(7), 1599–1614. https://doi.org/10.1084/jem.20181399

Yokomizo, T., Yamada-Inagawa, T., Yzaguirre, A. D., Chen, M. J., Speck, N. A., & Dzierzak, E. (2012). Whole-mount three-dimensional imaging of internally localized immunostained cells within mouse embryos. *Nature Protocols*, *7*(3), 421–431. https://doi.org/10.1038/nprot.2011.441

Yvernogeau, L., & Robin, C. (2017). Restricted intra-embryonic origin of *bona fide* hematopoietic stem cells in the chicken. *Development*, dev.151613. https://doi.org/10.1242/dev.151613

Zhang, C. C., & Lodish, H. F. (2004). Insulin-like growth factor 2 expressed in a novel fetal liver cell population is a growth factor for hematopoietic stem cells. *Blood*, *103*(7), 2513–2521. https://doi.org/10.1182/blood-2003-08-2955

Zhao, M., Perry, J. M., Marshall, H., Venkatraman, A., Qian, P., He, X. C., Ahamed, J., & Li, L. (2014). Megakaryocytes maintain homeostatic quiescence and promote post-injury regeneration of hematopoietic stem cells. *Nature Medicine*, *20*(11), 1321–1326. https://doi.org/10.1038/nm.3706

Zhao, Y., Zhou, J., Liu, D., Dong, F., Cheng, H., Wang, W., Pang, Y., Wang, Y., Mu, X., Ni, Y., Li, Z., Xu, H., Hao, S., Wang, X., Ma, S., Wang, Q., Xiao, G., Yuan, W., Liu, B., & Cheng, T. (2015). ATF4 plays a pivotal role in the development of functional hematopoietic stem cells in mouse fetal liver. *Blood*, *126*(21), 2383–2391. https://doi.org/10.1182/blood-2015-03-633354

Zorn. (2008). Liver Development. *StemBook*. https://doi.org/10.3824/stembook.1.25.1

Zorn, A. M., & Wells, J. M. (2009). Vertebrate Endoderm Development and Organ Formation. *Annual Review of Cell and Developmental Biology*, *25*(1), 221–251. https://doi.org/10.1146/annurev.cellbio.042308.113344

# ANNEX I

MOUSE DEVELOPMENT OVERVIEW

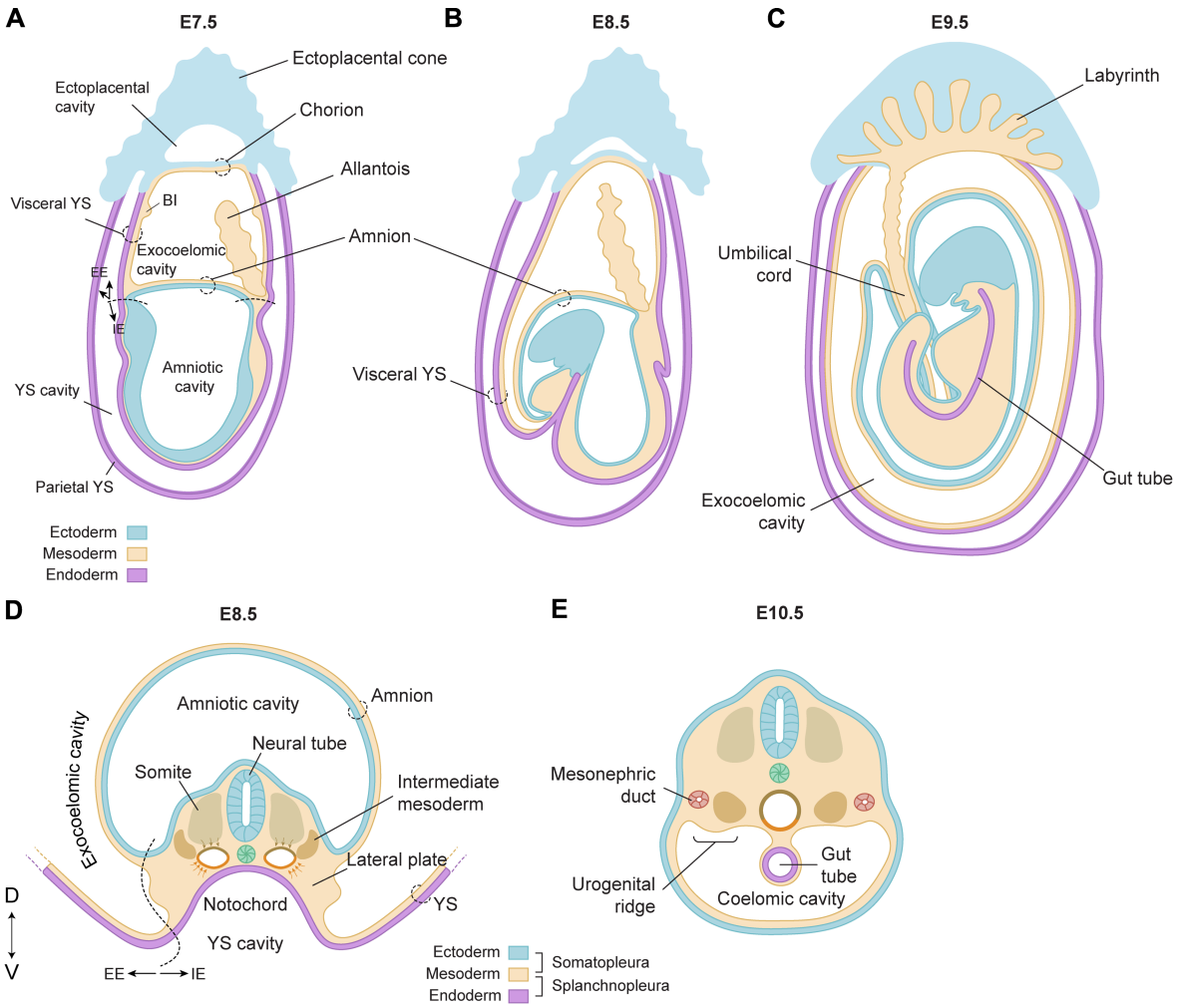


D – dorsal; V – ventral; EE – extra-embryonic; IE – intra-embryonic.

The schemes (**A-C**) represent frontal sections of mouse embryos at different stages of development and schemes (**D-E**) show transversal sections of the embryo at the level of the hindgut.

At E7.5, the mouse embryo is U-shaped, located underneath the extraembryonic structures (**A**). The YS has a bilayer structure, exclusively of extra-embryonic origin: a visceral endoderm layer on the outside, derived from the primitive endoderm (hypoblast); and mesoderm-derived layer on the inside, derived from a fraction of epiblast cells that crosses the primitive streak and migrates to extraembryonic sites. Blood islands are already visible on proximal YS. Between E8 and E9.5, the embryo turns, adopting the “fetal position”, and as result wraps itself in the amnion and YS (**B, C**). In other vertebrates, namely humans, the YS is attached to the embryo, instead of enveloping it (**Kaufmann & Bard**, **1999**).

The placenta is a transient support organ that serves as an interface between the fetal and maternal circulations, mediating the exchange of nutrients, gases, and waste products, and producing essential growth factors and hormones for embryo development. The placenta is

organized in three layers: 1. the vascular labyrinth connected to the embryo by the UVs, originated from the allantois; 2. the middle spongiotrophoblast layer; 3. the outer maternal decidua (not represented in the scheme) (**Mikkola et al.**, **2005**).

The AGM is a mesoderm-derived structure, located in the posterior part of the embryo, extending from the forelimbs to the hindlimbs, from E9.5-E12.5, with three anatomic discernible components: aorta, gonads, and mesonephros. The DA is the major blood vessel of the embryo. The genital ridge is the precursor structure of the reproductive organs (gonads), and the mesonephros serve as a transient excretory system during development (**de Bruijn**, **2000**). The DA arise as two separate bilateral vessels in the trunk (**D**) and undergoes lateral-to-medial translocation, eventually fusing into a single large vessel in the midline (**E**). Avian studies demonstrate that the DA endothelium has two distinct sources – somitic mesoderm contributes to the roof, and lateral mesoderm participates in forming the floor (**E**). This dual origin is believed to be responsible for the dorsoventral asymmetry in HSC development (**Pardanaud et al.**, **1996**).

# ANNEX II

frontiers in Cell and Developmental Biology

REVIEW
published: 22 July 2020
doi: 10.3389/fcell.2020.00612



# Crosstalk Between the Hepatic and Hematopoietic Systems During Embryonic Development

*Francisca Soares-da-Silva[1,2,3,4,5,6]†, Márcia Peixoto[1,2,3,4,5,6]†, Ana Cumano[4,5,6] and Perpetua Pinto-do-Ó[1,2,3]**

[1] Instituto de Investigação e Inovação em Saúde, Universidade do Porto, Porto, Portugal, [2] Instituto Nacional de Engenharia Biomédica, Universidade do Porto, Porto, Portugal, [3] Instituto de Ciências Biomédicas Abel Salazar, Universidade do Porto, Porto, Portugal, [4] Lymphocytes and Immunity Unit, Immunology Department, Pasteur Institute, Paris, France, [5] INSERM U1223, Paris, France, [6] Université Paris Diderot, Sorbonne Paris Cité, Paris, France

OPEN ACCESS

**Edited by:**
Joana Paiva Miranda,
University of Lisbon, Portugal

**Reviewed by:**
Kenichi Miharada,
Lund University, Sweden
Sandra Pinho,
University of Illinois at Chicago, United States

***Correspondence:**
Perpetua Pinto-do-Ó
perpetua@ineb.up.pt

† These authors have contributed equally to this work

**Specialty section:**
This article was submitted to Stem Cell Research, a section of the journal Frontiers in Cell and Developmental Biology

**Received:** 21 April 2020
**Accepted:** 19 June 2020
**Published:** 22 July 2020

**Citation:**
Soares-da-Silva F, Peixoto M, Cumano A and Pinto-do-Ó P (2020) Crosstalk Between the Hepatic and Hematopoietic Systems During Embryonic Development. Front. Cell Dev. Biol. 8:612. doi: 10.3389/fcell.2020.00612

Hematopoietic stem cells (HSCs) generated during embryonic development are able to maintain hematopoiesis for the lifetime, producing all mature blood lineages. HSC transplantation is a widely used cell therapy intervention in the treatment of hematologic, autoimmune and genetic disorders. Its use, however, is hampered by the inability to expand HSCs *ex vivo*, urging for a better understanding of the mechanisms regulating their physiological expansion. In the adult, HSCs reside in the bone marrow, in specific microenvironments that support stem cell maintenance and differentiation. Conversely, while developing, HSCs are transiently present in the fetal liver, the major hematopoietic site in the embryo, where they expand. Deeper insights on the dynamics of fetal liver composition along development, and on how these different cell types impact hematopoiesis, are needed. Both, the hematopoietic and hepatic fetal systems have been extensively studied, albeit independently. This review aims to explore their concurrent establishment and evaluate to what degree they may cross modulate their respective development. As insights on the molecular networks that govern physiological HSC expansion accumulate, it is foreseeable that strategies to enhance HSC proliferation will be improved.

**Keywords: hematopoietic stem cells, fetal liver, fetal liver microenvironment, fetal hematopoiesis, hematopoietic stem cell expansion, hematopoietic stem cell niche, self-renewal, cytokine signaling**

## INTRODUCTION

In the adult organism, hematopoietic stem cells (HSCs) constitute a rare and largely quiescent cell population residing in the bone marrow (BM) (Cheshier et al., 1999). The current dogma states that HSCs self-renew to maintain their pool throughout life and reenter cell cycle in response to stress (Wilson et al., 2008). The balance between self-renewal and differentiation in adult BM has been extensively studied, with the identification of different cellular niches and molecular cues as important elements in HSC maintenance and differentiation – reviewed in Crane et al. (2017) and Pinho and Frenette (2019).

During ontogeny, HSCs undergo a high proliferative stage, expanding in the fetal liver (FL), one of the anatomical locations of embryonic hematopoiesis (Ema and Nakauchi, 2000). Therefore, it has long been assumed that the hepatic microenvironment may drive the proliferation of HSCs while sustaining their primary "stemness" hallmark (functional capacity to reconstitute the hematopoietic compartment of irradiated recipients). So far, however, limited information is available on an HSC supportive environment in the FL and the mechanisms conveying these functional properties remain elusive, hindering effective translation into clinical applications.

A thorough dissection of the architecture and cellular organization of the liver is critical to elucidate the nature of the hematopoietic FL niche and disclose the elements (soluble and/or cell-bound signals, cell-cell contact, cell-matrix interactions, physical properties, etc.) contributing for the regulation of HSCs. This review aims to discuss the role of the FL stroma (encompassing all non-hematopoietic FL cells) and explore the interplay of the two fetal systems – hepatic and hematopoietic – in mouse (or otherwise stated) and how they mutually influence their development.

## THE EMERGENCE OF THE HEMATOPOIETIC SYSTEM DURING EMBRYOGENESIS

The adult hematopoietic system relies on a robust process whereby HSCs divide and differentiate generating all mature blood lineages. In physiological conditions, this process takes place in the BM in both humans and mice. Even though adult hematopoiesis occurs in the BM, this is merely the end-site of an otherwise thrilling journey through different anatomic locations (**Figure 1**).

The first hematopoietic cells emerge in the yolk sac (YS) in extra-embryonic structures named blood islands at around embryonic day (E) 7.5 in mice and 2–3 weeks post-conception (wpc) in humans (Bloom and Bartelmez, 1940; Palis et al., 1999). Primitive erythroid progenitors (EryP) generate primitive erythrocytes, large nucleated cells that express embryonic globins (Kingsley et al., 2006), which are found in circulation after the onset of cardiac contractions at E8.25 (∼3 wpc in humans) (Ji et al., 2003; Tavian et al., 1999) and oxygenate the developing embryo. Myeloid progenitors such as macrophage colony-forming cells or megakaryocyte colony-forming cells are also represented during early stages, concomitantly with EryP (Palis et al., 1999), suggesting that primitive hematopoiesis is limited to these three lineages.

Around 24 h later, at E8.5 (4–5 wpc in humans), a second wave of hematopoiesis initiates, with erythro-myeloid progenitors (EMPs) (Migliaccio et al., 1986; Bertrand et al., 2005b) emerging in the vascular plexus of the YS, in a process denominated endothelial to hematopoietic transition (EHT) (Frame et al., 2016; Kasaai et al., 2017). EMPs proliferate and differentiate in the YS into erythroid and myeloid cells but can also be identified in circulation and in the developing liver at later stages (E10.5) via surface expression of c-Kit, CD16/32 and low levels of CD45 (McGrath et al., 2015). These progenitors generate the first definitive erythrocytes, megakaryocytes, macrophages and other myeloid lineages such as neutrophils, granulocytes and mast cells, but lack HSC activity (Palis et al., 1999; McGrath et al., 2015). Although EMPs are a transient population at early stages of embryonic development, they generate different tissue-resident macrophages that, depending on the organ, can persist throughout adulthood (Gomez-Perdiguero et al., 2015), mast cells that are maintained until birth (Gentek et al., 2018), and are the major producers of erythrocytes throughout embryonic life (Soares-da-Silva et al., 2020, Preprint).

A third wave of hematopoiesis occurs between E9.5-E11 in mice (∼4 wpc in humans), with HSCs emergence in the aorta-gonads-mesonephros (AGM) region (Cumano et al., 1996; Medvinsky et al., 1996; Tavian et al., 1996) through EHT (Bertrand et al., 2010; Kissa and Herbomel, 2010). After generation, immature HSCs (imHSCs) undergo a maturation process as they migrate to the FL (Taoudi et al., 2008; Kieusseian et al., 2012) where they proliferate [expanding in numbers by >30-fold (Ema and Nakauchi, 2000)] and differentiate into all blood lineages: erythroid, myeloid and lymphoid. HSCs can be defined by their ability to provide long-term multilineage hematopoietic reconstitution (LTR) when transplanted to lethally irradiated mice (Morrison et al., 1995) and further repopulate secondary recipients. These cells can be found within the $Lin^{-}CD45^{+}Sca1^{+}c\text{-}Kit^{+}$ (LSK) compartment and be further divided according to their reconstitution ability in long-term (LSK $CD150^{+}CD48^{-}$ LT-HSC) or short-term (LSK $CD150^{-}CD48^{-}$ ST-HSC) reconstituting cells (Kim et al., 2006). Downstream progenitors of HSCs such as multipotent progenitors (MPPs), lympho-myeloid-primed progenitors (LMPPs), common lymphoid progenitors (CLPs) and common myeloid progenitors (CMPs) can also be found in FL and are responsible for the seeding of other hematopoietic organs such as the thymus (Ramond et al., 2014). Although adult and embryonic HSCs have similar lineage potentials, some lymphoid lineages are only produced during embryonic development, namely dendritic epidermal T cells (Ikuta et al., 1990), lymphoid tissue–inducer cells (Eberl et al., 2004), and a subset of IL-17-producer γδ T cells (Haas et al., 2012). Embryonic hematopoiesis also takes place in the placenta, starting at E10.5-E11 (∼6 wpc in humans) and declining at around E15.5 (Gekas et al., 2005; Ottersbach and Dzierzak, 2005; Robin et al., 2009). HSCs and other progenitors are also found in the fetal spleen after E15.5 (Christensen et al., 2004), even though without evidence for significant expansion and mostly differentiating into the macrophage lineage (Bertrand et al., 2006). At around E16.5 (∼10 wpc in humans) HSCs migrate to the BM, where they are maintained through adulthood (Charbord et al., 1996; Christensen et al., 2004). In the adult, BM HSCs are largely quiescent (Cheshier et al., 1999) and only divide to maintain the stem cell pool, while the replenishment of blood lineages appears to be guaranteed by downstream MPPs (Sun et al., 2014; Busch et al., 2015; Pei et al., 2017; Rodriguez-Fraticelli et al., 2018).

Thus, embryonic hematopoiesis is characterized by an overlap in time and space of three waves with distinct anatomical origins

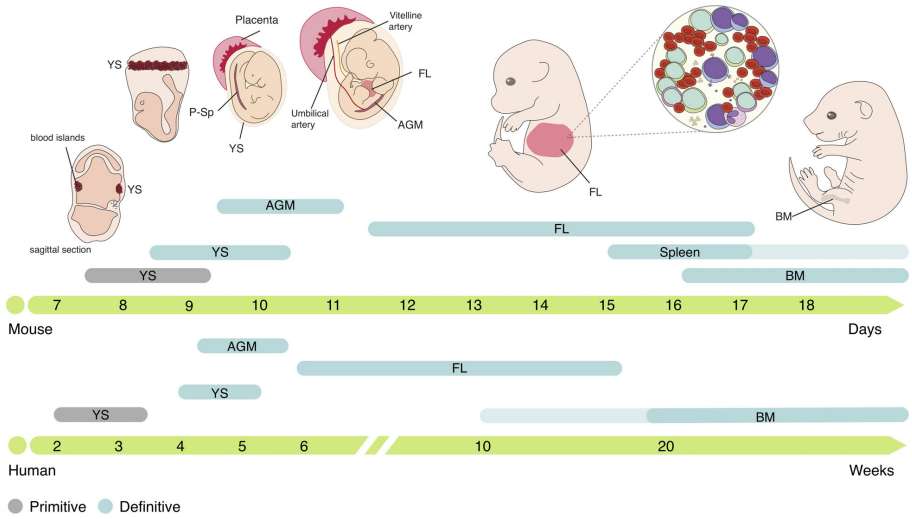


**FIGURE 1 |** Ontogeny of the hematopoietic system in mouse and human. Embryonic hematopoiesis is established in three distinct waves. The first hematopoietic cells emerge in YS blood islands, generating primitive erythrocytes, macrophages and megakaryocytes, constituting the primitive hematopoietic wave. The second hematopoietic wave initiates in the vascular plexus of the YS, generating EMPs that produce definitive erythrocytes, megakaryocytes, macrophages, neutrophils, granulocytes and mast cells, but lacks HSC activity. EMPs are the origin of tissue-resident macrophages that can persist throughout life. HSCs emerge in the AGM region and migrate to the FL, the major embryonic hematopoietic organ. In FL, HSCs expand and differentiate into all mature blood cell lineages. Small numbers of hematopoietic progenitors also colonize the fetal spleen and are still found few weeks after birth. Migration to the BM, where HSCs reside through adulthood, occurs as a continuous process and, in humans, can take several weeks. YS, yolk sac; P-Sp para-aortic splanchnopleura; FL, fetal liver; AGM, aorta-gonads-mesonephros; BM, bone marrow.

and lineage potential. All waves converge to the FL, the major hematopoietic organ during embryogenesis.

## THE COLONIZATION OF THE FL BY THE HEMATOPOIETIC SYSTEM

### Which Cells Are Present When Hematopoietic Progenitors Arrive?

As the embryo gastrulates and folds, endoderm envelops the YS ultimately forming a hollow structure, the primitive gut tube, subsequently patterned into foregut, midgut and hindgut regions. The foregut, located in the anterior endoderm, adjacent to the developing heart, generates the liver, alongside with the lungs, thyroid, and pancreas (Tremblay and Zaret, 2005). Embryonic liver development starts at around E8.5-E9 (∼4 wpc in humans) with the formation of the hepatic diverticulum, an extension of the ventral foregut epithelium that invades the septum transverse mesenchyme (STM) and forms a liver bud, by E9.5 (Severn, 1971; Wilson et al., 2006). The liver bud originates from a single-sheet of columnar endodermal epithelium with a gut morphology (**Figure 2A**), which then transitions to pseudostratified epithelial hepatoblasts (**Figure 2B**; Bort et al., 2006). At this stage, these cells are separated from the STM by a basement membrane rich in laminin and composed of other extracellular matrix (ECM) molecules, such as nidogen, type IV collagen, fibronectin, and heparan sulfate proteoglycan (Shiojiri and Sugiyama, 2004). A process of extensive hepatoblast proliferation follows, during which the cells outgrow the liver bud, disrupting the basement membrane, into the STM (**Figure 2C**; Douarin, 1975). The other constituents of the organ, sinusoidal endothelial cells (SECs), mesothelial, sub-mesothelial and hepatic stellate cells have a mesoderm origin (reviewed by Yang et al., 2019), as described below. Angioblasts or endothelial progenitor cells are found delimiting the basement membrane (**Figure 2A**), resembling a loose "necklace" of cells, and were shown to promote liver organogenesis. In Flk-1$^{-/-}$ mutant embryos, which lack endothelial cells, hepatic specification occurs, but proliferation and migration into the STM are impaired (Matsumoto et al., 2001). At E10.5–E11.0 (∼5–6 wpc in humans), hematopoietic cells colonize the FL that rapidly becomes the major fetal hematopoietic organ (Johnson and Moore, 1975; Migliaccio et al., 1986; Palis et al., 2001).

#### Hepatoblasts

Hepatoblasts are bipotent immature FL cells that differentiate into hepatocytes – the hepatic parenchyma main constituent – or cholangiocytes – the biliary epithelial cells. At the onset

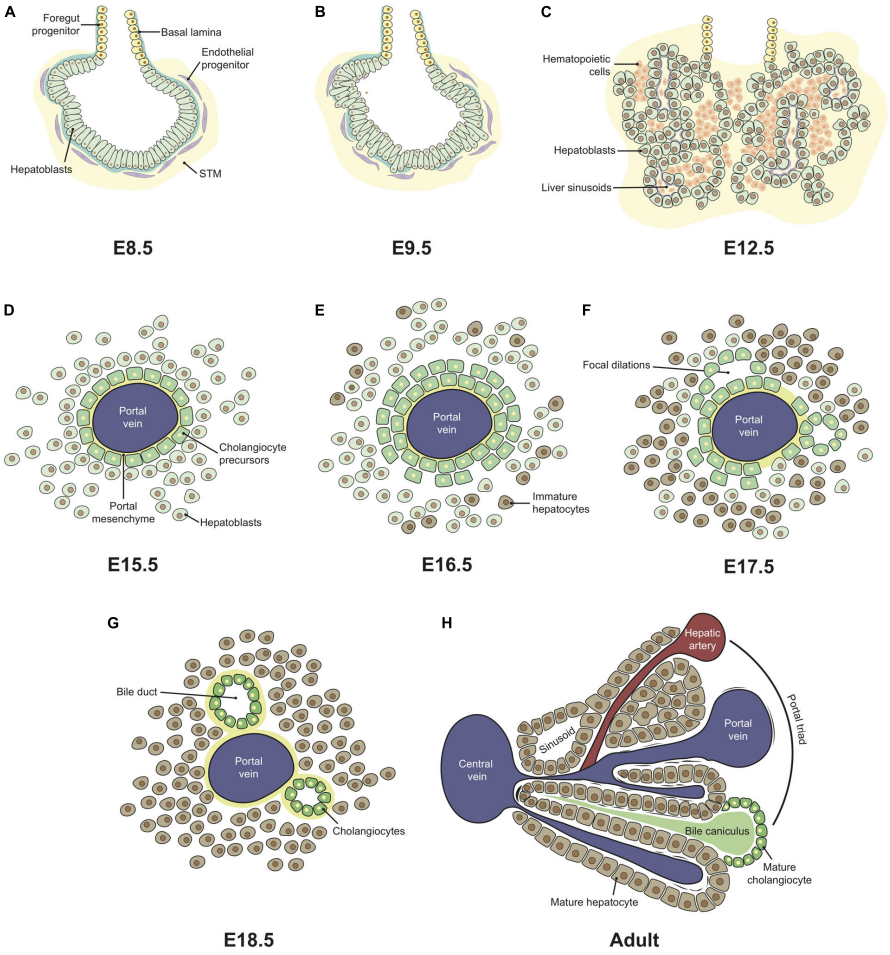


**FIGURE 2 |** Ontogeny of the fetal liver. Liver development is initiated with the formation of the hepatic diverticulum at E8.5 **(A)**. The single layer of columnar endodermal epithelial cells **(A)** thickens and transitions to a pseudostratified epithelium, followed by the delamination and migration of hepatoblasts into the STM, forming the liver bud by E9.5 **(B)**. Extensive hepatoblast proliferation follows, originating hepatic chords intermingled with the hepatic mesenchyme and surrounding the sinusoids, formed from pre-existing vitelline vessels. From E10.5, hematopoietic cells colonize the FL that rapidly becomes the major fetal hematopoietic organ up until E15.5 **(C)**. From E12.5-E15.5, the FL continues to enlarge, expanding both hematopoietic and hepatic compartments. Structural changes are only evident after hepatoblast-to-cholangiocyte specification occurs around the portal vessels, forming a monolayered ductal plate **(D)** that evolves into a bi-layer at E16.5 **(E)**. Focal dilations **(F)** evolve into bile duct structures in late gestation **(G)**. Portal triads characterize adult liver architecture where a hepatic artery, a portal vein and a bile duct form a complex structure, and a central vein, to which plates of hepatocytes lined by sinusoids converge **(H)**. This architecture is only recognizable few weeks after birth. STM, septum transversum mesenchyme.

of liver development, bipotent hepatoblasts express the liver-specific transcription factors (TFs) hematopoietically-expressed homeobox protein (HHEX) (Bogue et al., 2000), prospero homeobox protein 1 (PROX1) (Dudas et al., 2004), and co-express the hepatocytes' markers alpha-fetoprotein (AFP), albumin (ALB) (Cascio and Zaret, 1991), cytokeratin 18 (CK18) (Tanimizu et al., 2003), hepatocyte nuclear factor 4α (HNF4α) (Li et al., 2000) and cholangiocytes' markers such as cytokeratin 19 (CK19) (Tanimizu et al., 2004). Other typical hepatoblast markers are listed in **Table 1**.

**TABLE 1 |** Fetal liver non-hematopoietic compartment: cell types and associated markers.

| Cell type | Gene expression | Markers used for isolation |
|---|---|---|
| Hepatoblasts | *Hhex, Prox1, Alb, Afp, Ck8, Ck18, Ck19, Met, Hnf6, Oc2, Hnf4a, Ttr, Foxm1, Foxa2, Tbx3, Dlk1, Lgr5, Epcam, Cdh1, Trgb1, Itga6, Liv2, Prom1, Anpep* | $DLK1^+$ (Tanimizu et al., 2003; Tan et al., 2017)<br>E-$Cadherin^+$ (Nitou et al., 2002; Nierhoff et al., 2005)<br>$EpCAM^+DLK1^+$ (Tanaka et al., 2009)<br>$Liv2^+CD31^-CD45^-Lgr5\text{-}eGFP^+$ (Prior et al., 2018)<br>$Ter119^-CD45^-c\text{-}Kit^-CD49f^+CD29^+$ (Suzuki et al., 2000)<br>$VCAM1^+ALCAM^+DLK1^+$ (Tsuneto et al., 2013)<br>$Ter119^-CD45^-CD51^+VCAM1^+PDGFR\alpha^-$ (Brouard et al., 2017) |
| Hepatocytes | *Alb, Afp, Ttr, G6p, Apoa1, Apoh Por, Cps1* | – |
| Cholangiocytes | *Sox9, Hnf6, Oc2, Spp1, Ck19, Epcam, Krt7* | $EpCAM^+$ (Yang et al., 2017) |
| Endothelial cells | *Flk1, Flt1, Ve-cadh, Pecam1, Mcam, Tek, Tie, Lyve1, Kdr* | $CD45^-Ter119^-CD31^+$ (Khan et al., 2016)<br>$DLK1^-CD45^-Ter119^-CD31^+LYVE\text{-}1^+$ and<br>$DLK1^-CD45^-Ter119^-CD31^+LYVE\text{-}1^-$ (Tan et al., 2017) |
| Mesothelial cells | *Cytokeratin, Cd200, Gpm6a, Alcam, Gp38, Wt1, Podxl, Msln* | $Flk1^-PODXL^{high}$ (Onitsuka et al., 2010) |
| Sub-mesothelial cells | *Alcam, Desmin, Nestin, p75tnr, Pdgfra, Wt1* | – |
| Hepatic stellate cells | *Vimentin, Acta2, Desmin, p75NTR, Foxf1, Lhx2, Hlx* | $DLK1^-Ter119^-CD45^-CD31^-LYVE\text{-}1^-p75NTR^+$ (Tan et al., 2017) |
| Pericytes | *NG2, Nestin, Vimentin, Acta2, Pdgfra, Pdgfrb, Dlk1, Itgav, Endoglin, Vcam, Mcam, Nr2f2* | $Ter119^-CD45^-CD31^-Nestin^+NG2^+$ (Khan et al., 2016)<br>$CD45^-CD56^-CD34^-CD146^{+1}$ (Gerlach et al., 2012) |

[1]*Study performed in humans.*

Different markers have been used to isolate hepatoblasts, namely delta like non-canonical Notch ligand [DLK1 or preadipocyte factor 1 (Pref-1)] (Tanimizu et al., 2003), epithelial cadherin (E-cadherin) or CD324 (Nitou et al., 2002), epithelial cell adhesion molecule (EpCAM) or CD326 (Tanaka et al., 2009), and leucine-rich repeat-containing G-protein coupled receptor 5 (LGR5) (Prior et al., 2018). DLK1 is strongly expressed by hepatoblasts in the E10.5 liver bud and continues to be highly expressed until around E16.5, being significantly downregulated thereafter and absent in mature hepatocytes and cholangiocytes (Tanimizu et al., 2003; Tanaka et al., 2009). E-Cadherin, present at the onset of liver outgrowth, is downregulated by the time hepatoblasts migrate to the STM, disrupting the epithelial sheet, although it can be used as a hepatoblast-specific marker after E12.5 (Nitou et al., 2000; Margagliotti et al., 2007). Transient EpCAM expression labels newly formed hepatoblasts but is significantly reduced after E12, while expression after E16 specifically labels bile duct cells (Tanaka et al., 2009). Recently, combining multicolor clonal genetic lineage tracing, organoid cultures and analysis of single-cell RNA sequencing, LGR5 was shown to mark a subpopulation of *bonafide* bipotential hepatoblasts at E9.5–E10 as the origin of the hepatoblast pool (Prior et al., 2018).

## Endothelial Cells

The main blood vessels in the adult liver are the portal and central veins and the hepatic artery. Up until birth, the hepatic artery is absent and embryonic circulation is sustained by a transient afferent vascular system, the extraembryonic umbilical and vitelline veins (Collardeau-Frachon and Scoazec, 2008). The portal vein arises early in the liver development, between E10.5–E12.5 in mouse (4–6 wpc in human) (Collardeau-Frachon and Scoazec, 2008; Swartley et al., 2016). The hepatic sinusoids are the first vessels to appear, by E10–E10.5, originating from the pre-existing vitelline vessels. The latter sprouts throughout the STM, by angiogenesis, receiving signals from the surrounding mesenchyme (**Figure 2C**; Swartley et al., 2016). Hepatoblasts were also identified as a positive stimulator of sinusoid morphogenesis and maturation (Takabe et al., 2012). Stabilin 2 (STAB-2) and lymphatic vessel endothelial hyaluronan receptor 1 (LYVE-1) (commonly used as a marker of lymphatics) – hyaluronan receptors – start to be expressed in SECs at E9.5 and E10.5, respectively, and continue to be expressed thereafter (Nonaka et al., 2007; Takabe et al., 2012). Of note, lymphatic vessels were only reported after birth (Swartley et al., 2016). At E9.5, endothelial cells located around the liver diverticulum (**Figure 2A**) express both CD31/PECAM-1 and Flk-1 (Sugiyama et al., 2010b). CD31 and Flk1 expression in SECs is strong in the early stages of liver development, but is downregulated with time. In adult livers, endothelial cells of portal and hepatic veins strongly express CD31, while it is absent or weakly detected in SECs (Sugiyama et al., 2010b; Takabe et al., 2012). Primitive SECs also strongly express Flk-1, contrarily to endothelial cells of portal and hepatic veins (Sugiyama et al., 2010b). During embryonic liver development, portal vessels express the arterial markers Ephrin-B2 and Neuropilin-1, but not the venous marker EphB4. This expression profile is inverted at the end of gestation, with the transition into a venular phenotype (Wang et al., 1998; Khan et al., 2016). Liver endothelial cells constitute a heterogeneous cellular compartment and different markers should be used for their identification according to vascular location and developmental stage.

### Mesothelial and Sub-Mesothelial Cells

Mesothelial cells (MCs) compose a single epithelial layer (mesothelium) lining the liver parenchyma on the surface of lobes. From E12.5, MCs are characterized by the expression of cytokeratin, CD200, glycoprotein M6A (GPM6A), podoplanin (PDPN/Gp38), podocalyxin-like protein 1 (PODXL), and mesothelin (MSLN) (Lua and Asahina, 2016). PODXL is highly expressed in immature MCs, being downregulated during development, while MSLN is upregulated. MCs proliferate during liver development and remain quiescent after birth. Wilm's tumor-1 (WT1) is mainly expressed by MCs (Onitsuka et al., 2010). $WT1^{-/-}$ embryos show incomplete lobulation compared to control littermates at E13.5, reduced numbers of $Flk1^{-}PODXL^{high}$ MCs, $DLK1^{+}$ hepatoblasts, and total FL cells, suggesting that hepatic development was impaired due to defective MCs (Ijpenberg et al., 2007; Onitsuka et al., 2010). This is supported by the observation that fetal MCs express growth factors (PTN, MDK, and HGF) involved in hepatic development (Onitsuka et al., 2010).

Underneath the MC sheet lays a population of cells expressing Desmin, Nerve growth factor receptor (NGFR/p75NTR) and platelet-derived growth factor receptor α (PDGFRα/CD140a), associated with type IV collagen of the basal lamina, commonly referred as "sub-mesothelial cells" (sub-MC) or capsular fibroblasts. The expression of activated leukocyte cell adhesion molecule (ALCAM/CD166) and WT1 was also observed in MC and sub-MC around E11–E14 and, before that, in the STM by E9–E10 (Asahina et al., 2011; Lua and Asahina, 2016).

### Hepatic Stellate Cells and/or Pericytes

Although the terms hepatic stellate cells and pericytes have been used by many authors as synonyms, it is not consensual they represent the same population. In adult liver, there is a population of perisinusoidal cells residing in the space of Disse between hepatocytes and SECs, that stores vitamin D lipids (Wake, 1971), and is a major player in liver fibrogenesis (Guyot et al., 2006). MesP1-expressing mesoderm has been considered its earliest ancestry, as it gives rise to the STM – the origin of the liver mesothelium and mesenchymal cells. Migration inward of MC and sub-MC from the liver surface is assumed to give rise to hepatic stellate cells and perivascular mesenchymal cells (Asahina, 2012). Hepatic stellate cells express Desmin, p75NTR, but not the MC markers ALCAM, WT1, and Gp38 (Asahina et al., 2010).

Gerlach et al. (2012) isolated $CD146^{+}CD45^{-}CD56^{-}CD34^{-}$ cells from fetal and adult human livers and identified them as pericytes, a distinct population from hepatic stellate cells. They showed that these cells express NG2 and vimentin, but not GFAP *in situ*, and are found around periportal but not pericentral blood vessels neither within the space of Disse. These cells exhibit high osteogenic and myogenic, but low adipogenic or chondrogenic differentiation potential, in *in vitro* differentiation assays. In mice, a population characterized by the expression of Nestin and NG2 was identified as periportal pericytes, which expresses mesenchymal markers and shows trilineage mesenchymal capacity *in vitro* (Khan et al., 2016).

## Law of Attraction: What Brings Hematopoietic Progenitors to the Developing Liver?

Hematopoietic stem cells emerge from the dorsal aorta directly into circulation and can, therefore, be found in different locations (Cumano et al., 1996; Medvinsky et al., 1996). These cells can travel through the umbilical arteries to the placenta and return to the embryo through the umbilical veins. The umbilical veins drain directly into the liver by fusing with the intrahepatic vascular plexus of the vitelline veins, forming the hepatic sinus. Cells traveling in the right umbilical vein can bypass the liver directly to the vena cava through the *ductus venosus*, a structure only present during fetal development, and can be directed into other embryonic regions through the heart. The liver is also irrigated by the vitelline veins, which transport blood from the YS, and eventually mature to become the portal vein. Another route for newly formed HSCs is to travel from the dorsal aorta through the subcardinal vein to the liver or inferior cardinal vein to the heart. From the heart, circulating cells can reach the developing lungs or upper half of the body (Kiserud, 2005). However, it is in the developing FL that HSCs establish and remain until they migrate to the BM. Transplantation studies show that HSCs can also be found in the placenta (Gekas et al., 2005; Ottersbach and Dzierzak, 2005). The placenta of a mouse model lacking a functional circulatory system was shown to still harbor hematopoietic activity, suggesting that the placenta could generate *de novo* hematopoietic cells with multilineage potential (Rhodes et al., 2008), however, direct evidence for HSC emergence from the placenta is yet to attain.

Hematopoietic stem or progenitor cells (HSPCs) but also EMPs, colonize the FL after liver bud formation at E10.5 (Johnson and Moore, 1975; Palis et al., 2001). Distinct mechanisms of FL colonization have been proposed, mostly relying on cell adhesion-mediated processes and/or chemoattraction (cytokines, chemokine signaling, and growth factors) (**Figure 3**; Hayashi et al., 2019).

Several cell adhesion molecules have been identified in embryonic HSPCs, including integrins, selectins, cadherins, and others. Hematopoietic progenitors express vascular-endothelial cadherin (VE-Cadherin/CD144) as they emerge from the YS (in the case of EMPs) or AGM (in the case of HSCs) that is downregulated thereafter and undetectable in BM HSCs (Fraser et al., 2002; Taoudi et al., 2005). FL $CD34^{+}$ progenitors express higher levels of the integrins β1 (CD29), α2 (CD49b), and α5 (CD49e), similar levels of integrins α4 (CD49d) and α6 (CD49f), E- and P-selectins (CD62E and CD62P, respectively) and CD11b and CD11c molecules, but lower levels of integrin β2 (CD18), CD11a and CD44 than their adult BM equivalent (Roy and Verfaillie, 1999). Seminal studies showed that HSPCs lacking β1 integrin were unable to colonize the FL but were still present in the circulation and capable of generating all blood lineages, suggesting a role for integrin-mediated cell adhesion in FL colonization (Hirsch et al., 1996). Integrin receptors result from the dimerization of α and β subunits and analysis of the expression of the α chain partner of β1 integrin in LSK progenitors revealed integrins α4 and α6 as the most

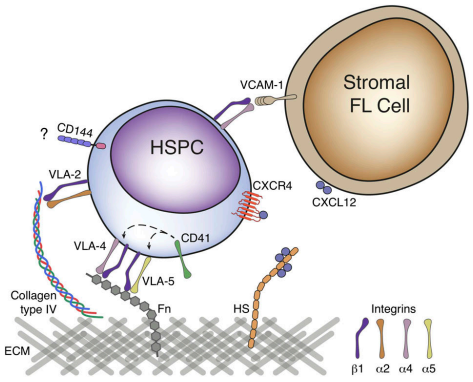


**FIGURE 3 |** Molecular mechanisms of fetal liver colonization. HSPC express a variety of cell adhesion molecules in their surface that can favor attachment to a specific location. β1 integrin is essential for colonization of FL by HSPC and can bind to the ECM components fibronectin and type IV collagen through dimerization with α4 and α5 or α2 integrins, respectively. VLA-4 and VLA-5 binding to fibronectin has been proposed to be modulated by CD41. VLA-4 (α4β1 integrin) can also mediate cell-cell interactions by binding with VCAM-1, expressed on the surface of FL stromal cells. Expression of the cadherin CD144 in HSCs as they emerge is assumed to play a role in the organ colonization, although no binding partner has been described in FL. CXCL12, a potent chemoattractant is expressed by FL stromal cells and binds to CXCR4, expressed on the surface of HSPC. CXCL12 gradients can be generated as this chemokine binds to proteoglycans in the ECM, namely to heparan sulfate (HS). HSPC, hematopoietic stem and progenitor cell; FL, fetal liver; ECM, extracellular matrix; VLA, very late antigen; Fn, fibronectin; HS, heparan sulfate.

predominant (Sugiyama et al., 2013). FL CD34$^+$ progenitors bind the ECM component fibronectin through the integrin receptors α4β1 and α5β1 (also known as VLA-4 and VLA-5) and this binding has been proposed to be modulated by the integrin α2b (GPIIb or CD41), also expressed in these cells (**Figure 3**; Roy and Verfaillie, 1999; Emambokus and Frampton, 2003). Other ECM components have been tested for adhesion of FL CD34$^+$ progenitors such as type I and type IV collagen and laminin, however, only type IV collagen promotes adherence at levels equivalent to that of fibronectin, through α2β1 integrin (VLA-2) (Roy and Verfaillie, 1999). In the FL, hepatoblasts (defined as DLK1$^+$ cells) are the major producers of ECM components, namely vitronectin and fibronectin (Sugiyama et al., 2013). Embryos lacking hepatoblasts can still form the liver bud but die between E10.5–E12.5 (Nishina et al., 1999). These FL show decreased expression of vitronectin and fibronectin that may play an important role in FL colonization by HSCs and YS EMPs, although this role has not been specifically assessed (Sugiyama et al., 2013). Integrins can also mediate cell-cell interactions. Cellular bound counterparts of VLA-4 include the vascular cell adhesion molecule-1 (VCAM-1/CD106), expressed by FL hepatoblasts (Sugiyama et al., 2010a).

Cytokine and chemokine signaling can also stand at the basis of FL colonization. The stromal cell-derived factor-1 (SDF-1), commonly known as CXC chemokine ligand 12 (CXCL12), acts through binding to its receptor CXCR4 present in HSPCs and has been extensively studied in the adult BM – reviewed in Yu and Scadden (2016); and Wei and Frenette (2018). CXCL12 expression is stabilized at the cell surface or in the surrounding ECM through proteoglycans binding, allowing the creation of chemokine gradients essential for cell migration (Schumann et al., 2010). In the FL, CXCL12 is expressed by DLK1$^+$ hepatoblasts (Chou and Lodish, 2010) and Nestin$^+$NG2$^+$ pericytes (Khan et al., 2016). The role of CXCL12 in FL colonization was analyzed using CXCL12$^{-/-}$ embryos. At early stages (E12.5–E14.5), the number of HSCs was similar in the FL of mutant animals and controls. By E16.5 FL HSCs were reduced by more than twofold and an abnormally high number was found in circulation. These observations indicate that CXCL12 is an important factor for retaining HSCs in FL, but not for its initial colonization (Ara et al., 2003).

Owing to the particular architecture of fetal circulation, FL is in an anatomically privileged location. Even if HSCs are traveling directly within the embryo through the subcardinal vein, or the umbilical veins after passing in the placenta, the FL is the first intraembryonic organ they encounter. Whether a passive retainment of circulating cells (e.g., through β1-integrin) occurs, or specific signals directly promote chemoattraction of HSPCs to FL is still unclear.

## How Do the Hepatic and Hematopoietic Cell Types Organize During Development?

The structure of the FL changes dramatically during embryonic development. Crawford et al. (2010) extensively characterized the mouse developing hepatobiliary system from E9.5 to E18.5 creating a histology atlas. At initial stages (E10.5–E12.5), the liver is mainly constituted by a vascular plexus and migrating hepatoblasts that later form hepatic chords. At E11.5, the hepatic sinusoids are wide, which may favor the access and establishment of the newly generated hematopoietic progenitors. From E12.5 onward, the organization of the cells in the FL changes as the frequency of hematopoietic cells increases. At E13.5, the most frequent FL population are nucleated erythrocytes that, at early stages, are located throughout the liver parenchyma, in between the hepatic chords, but after E14.5 more mature enucleated erythroid cells are found within the vessels (Ayres-Silva et al., 2011). At this stage, megakaryocytes and erythroblastic islands, which consist of a central macrophage surrounded by erythroid cells, are also distinguishable in the liver parenchyma. These macrophages are responsible for the phagocytosis of the expelled nuclei during erythroid maturation (Bessis et al., 1978). Megakaryocytes are essential to thrombosis and hemostasis and may be determinant in an organ that is mostly constituted by erythroid cells. Moreover, the developing liver seems to provide a unique microenvironment for the expansion of megakaryocyte progenitors (Brouard et al., 2017).

From E13.5 to late gestation, no dramatic changes occur in the histology of the FL. Other hematopoietic cells such as B cell progenitors identified by Pax5 expression, can be found interspersed in the tissue by E12.5 and also forming perivascular aggregates by E18.5. Granulocytes are scattered throughout the tissue from E16.5 onward, concentrating/converging around central veins and in the periphery by E17.5, correlating with the presence of mesenchymal cells and suggesting a crosstalk between these distinct cell types (Ayres-Silva et al., 2011). By this time-point, as hematopoietic cells exit the organ and migrate to the BM, hepatoblasts and hepatocytes regain contact (Crawford et al., 2010).

Disclosure of HSCs distribution within the FL has been hindered by the multi-marker assessment required, i.e., $Lin^-$c-$Kit^+Sca1^+CD150^+CD48^-$, to phenotypically identify these cells. Hematopoietic progenitors (defined by c-Kit expression) are found in close association with $DLK1^+$ hepatoblasts at E14.5 (Sugiyama et al., 2013). Nevertheless, c-$Kit^+$ cells could mostly represent erythroid progenitors as they are the most frequent population at this stage (Soares-da-Silva et al., 2020, Preprint). Other approaches include the use of transgenic Ly6a-GFP (labeling $Sca1^+$ cells) mice, that together with Runx1 localized HSPCs at E11.5 in close contact with endothelial cells (Tamplin et al., 2015). HSCs, profiled as $CD150^+CD48^-Lin^-$, have been found in close association with $Nestin^+NG2^+$ pericytes surrounding the portal vessels (Khan et al., 2016). Although this characterization more closely identifies a potential HSC, FL studies using mouse models that directly label HSCs are still missing. Generation of a mouse with a single-color reporter driven by endogenous *Hoxb5* (*Hoxb5*–tri-mCherry), which expression in the BM is limited to LT-HSCs and *in situ* imaging evidenced the close proximity of LT-HSCs with VE-$Cadherin^+$ cells (Chen et al., 2016). Recently, another HSC-specific reporter line has been described, yet also only analyzed in the adult bone (Christodoulou et al., 2020).

## THE INTERPLAY BETWEEN THE DEVELOPING HEPATIC-HEMATOPOIETIC TISSUES

### How Does the FL Environment Modulate Hematopoiesis? A Role in Maturation, Expansion and Differentiation of HSCs?

Emerging imHSCs lack long-term reconstitution activity in conventional or $Rag2^{-/-}$ immunocompromised mice but can reconstitute NK-deficient $Rag2\gamma c^{-/-}$ animals (Cumano et al., 2001; Bertrand et al., 2005a). After co-culture with the OP9 BM stromal cell line in the presence of thrombopoietin (TPO) or with E10.5 FL rudiments, $CD31^+$c-$Kit^+CD45^-$ imHSCs acquire an adult HSC phenotype (LSK $CD150^+CD48^-$) and develop LTR activity in $Rag2^{-/-}$ or conventional mice as they upregulate MHC class I molecules (Kieusseian et al., 2012). These experiments suggest that the FL provides the signals necessary for the maturation of newly formed HSCs. FL stroma also supports the differentiation of committed hematopoietic progenitors towards distinct lineages. Interleukine 7 (IL-7) promotes the survival and proliferation of lymphoid progenitors and controls the determination of the B cell lineage (Sudo et al., 1989; Peschon et al., 1994). In FL, IL-7 is produced by $VCAM1^+ALCAM^+DLK1^+$ hepatoblasts (Tsuneto et al., 2013) and controls the number of lymphoid progenitors that develop into the B-cell lineage by stabilizing the B-cell transcriptional signature (Berthault et al., 2017). For instance, erythropoietin (EPO) is produced by $DLK1^+$ hepatoblasts and is required for proliferation and terminal differentiation of erythroid progenitors (Sugiyama et al., 2011). Also, TPO expressing $Ter119^-CD45^-CD51^+VCAM1^+PDGFR\alpha^-$ FL hepatoblasts support the production of megakaryocytes from adult BM HSCs in a contact-dependent manner (Brouard et al., 2017). TPO is the main regulator of megakaryocyte differentiation and platelet production (Kaushansky, 1995; Eaton and de Sauvage, 1997) but has also been shown to promote survival and proliferation of BM HSPCs *in vitro* (Borge et al., 1996; Ku et al., 1996), the proliferation of fetal hematopoietic progenitors *in vivo* (Alexander et al., 1996) or expansion of BM HSCs following transplantation (Fox et al., 2002). Lack of TPO signaling causes decreased HSC function and numbers (Kimura et al., 1998; Solar et al., 1998), a consequence from the exit of a quiescent state (Nakamura et al., 2007; Qian et al., 2007), possibly leading to a premature exhaustion of the stem cell pool. The survival and proliferation effects of TPO are enhanced when used in combination with other early cytokines, namely FMS-like tyrosine kinase 3 ligand (FLT3L) and c-Kit ligand [KITL, also known as stem cell factor (SCF) or steel factor (SF)] both in murine and human adult BM cells (Ramsfjell et al., 1996; Borge et al., 1997). The highest levels of TPO in the adult are found in the liver (Lok et al., 1994). Systemic TPO produced by hepatocytes, but not by hematopoietic, osteoblast or BM mesenchymal stromal cells is required for BM HSC maintenance (Decker et al., 2018). It can be detected in FL as early as E10.5, having a strong impact on HSC expansion and survival in this organ (Petit-Cocault et al., 2007). Indeed, several cytokines/chemokines/growth factors are important for HSC proliferation, maintenance and survival, namely KITL, FLT3L, insulin growth factor (IGF), angiopoietin-3, angiopoietin-like 2, Wnt family growth factors, Ephrin2a, CSF1, EPO, CXCL12, and IL-6 – reviewed in Sauvageau et al. (2004). In FL, some of these cytokines are expressed by hepatoblasts or other stromal cells, such as stellate cells or pericytes (see **Table 2** and **Figure 4**; Charbord and Moore, 2005; Chou and Lodish, 2010; Khan et al., 2016; Tan et al., 2017).

The hypothesis that stem cells are regulated by their environment has been proposed by Schofield (1978) and postulates that stem cell properties are maintained by the surrounding cells designated "niche." Stromal regulation of hematopoiesis has been proposed by many and early studies of co-culture of hematopoietic progenitors with either FL fibroblast or epithelial-stromal cell lines showed erythroid and myeloid support (Tsai et al., 1986; Hata et al., 1993). More than 200 FL stromal cell lines have been developed and tested for maintenance or expansion of HSCs, however, only a few were able to maintain their repopulating activity

**TABLE 2 |** Cytokine signaling in fetal liver.

| FL Supportive Stroma | | Hematopoietic progenitors | |
|---|---|---|---|
| **Pathway involved** | **Expressing cell** | **Receptor** | **Effect** |
| KITL | DLK1$^+$ hepatoblasts (Chou and Lodish, 2010; Sugiyama et al., 2011)<br>Nestin$^+$ cells (Khan et al., 2016)<br>Stellate cells (Tan et al., 2017) | c-Kit (CD117) (Yarden et al., 1987) | BM HSC survival and self-renewal (Barker, 1994; Miller et al., 1997) |
| ANGPTL2 | Nestin$^+$ cells (Khan et al., 2016) | PirB (Zheng et al., 2012) | BM HSC proliferation (Zhang et al., 2006) |
| ANGPTL3 | DLK1$^+$ hepatoblasts (Chou and Lodish, 2010) | PirB (Zheng et al., 2012) | BM HSC maintenance (Zheng et al., 2011)<br>BM HSC proliferation (Zhang et al., 2006) |
| FLT3L | Stellate cells (Tan et al., 2017) | Flt3 (CD135) (Matthews et al., 1991) | FL HSPC proliferation (Lyman et al., 1993) |
| TPO | DLK1$^+$ hepatoblasts (Chou and Lodish, 2010; Sugiyama et al., 2011; Brouard et al., 2017)<br>Stellate cells (Tan et al., 2017) | MPL (TPO-R, CD110) (Vigon et al., 1992) | FL HSC survival and proliferation (Petit-Cocault et al., 2007)<br>BM HSC quiescence (Nakamura et al., 2007; Qian et al., 2007) |
| CSF1 | Stellate cells (Tan et al., 2017) | Csf-1 Receptor (Guilbert and Stanley, 1980) | Commitment to macrophage lineage (Rieger et al., 2009) |
| EPO | DLK1$^+$ hepatoblasts (Sugiyama et al., 2011)<br>Stellate cells (Tan et al., 2017) | EPO receptor (Sawyer et al., 1987) | Proliferation and differentiation of FL erythroid progenitors (Lin et al., 1996) |
| CXCL12 | Dlk1$^+$ hepatoblasts (Chou and Lodish, 2010)<br>Nestin$^+$ cells (Khan et al., 2016)<br>Stellate cells (Kubota et al., 2007) | CXCR4 (Bleul et al., 1996) | FL and FBM B-cell lymphopoiesis and FBM myelopoiesis (Nagasawa et al., 1996)<br>BM HSC engraftment post-transplantation (Lai et al., 2014; McDermott et al., 2015)<br>FL HSC retainment (Ara et al., 2003)<br>BM HSC retainment (Sugiyama et al., 2006) |
| IL-7 | VCAM1$^+$ALCAM$^+$DLK1$^+$ hepatoblasts (Tsuneto et al., 2013) | IL-7Rα (Park et al., 1990) | Lymphocyte expansion (Peschon et al., 1994) |
| IGF2 | Dlk1$^+$ hepatoblasts (Chou and Lodish, 2010)<br>Nestin$^+$ cells (Khan et al., 2016)<br>Stellate cells (Tan et al., 2017) | IGF1-R (Rubin et al., 1983)<br>IGF2-R (Morgan et al., 1987)<br>Insulin receptor (House and Weidemann, 1970) | F L and BM HSC proliferation (Zhang and Lodish, 2004) |

over a 3-week co-culture period (Wineman et al., 1996). The functional heterogeneity observed was not due to distinct cytokine production as all cell lines expressed similar cytokine profiles, including *Flt3l*, *Kitl*, *Tpo*, *Igf1, Il6*, *Il11*, leukemia inhibitory factor *(Lif)*, granulocyte-colony stimulating factor (G-CSF/*Csf3*), granulocyte/macrophage-colony stimulating factor (GM-CSF/*Csf2*), and transforming growth factor, beta 1 (*Tgfb1*). Importantly, the successful stromal cell lines have in common the expression of *Dlk1*, and overexpression of this factor is sufficient to enable hematopoietic support (Moore et al., 1997). Although these cell lines only maintain HSC potential and do not promote HSC expansion, some FL cells have been described to do so. Recent studies have addressed the role of specific FL populations *in vivo* or *in vitro*. It is the case of DLK1$^+$ hepatoblasts that are able to expand LT-HSC around 20-fold after a 3-week co-culture period (Chou et al., 2013). This expansion seems to be contact-dependent as DLK1$^+$ conditioned medium only allows expansion of ST-HSC and cells cultured in transwell inserts did not show the same expansion levels. Although promising, it is worth mentioning that these cultures were supplemented with KITL, TPO, and FLT3L and, therefore, it remains unclear which mechanisms underlie HSCs expansion in DLK1$^+$ cell co-cultures. Moreover, DLK1 knockdown in human hepatoblasts results in decreased hematopoietic support *in vitro* (Gerlach et al., 2019). The role of hepatoblasts *in vivo* has been difficult to assess as transgenic mice with hepatoblast deficiencies die between E10.5 and E12.5 and studies of liver development do not usually investigate the hematopoietic compartment (Nishina et al., 1999). DLK1 has been used to identify hepatoblasts but it is also expressed by the majority of Nestin$^+$ cells surrounding the portal vessels, a cell type that has been implicated as part of the FL niche (Tanimizu et al., 2003; Chou and Lodish, 2010; Chou et al., 2013; Khan et al., 2016). HSCs numbers are modestly reduced when Nestin$^+$NG2$^+$ pericytes are selectively eliminated and the remaining HSCs are less proliferative (Khan et al., 2016). So far, this is the only study that addresses the role of a specific cell type in HSC expansion and maintenance *in vivo*. Nestin$^+$ cells are the major producers of *Cxcl12* at E14.5 when compared to Nestin$^-$ cells, therefore, the reduction in FL HSCs could result from a defect in HSC expansion together with a displacement

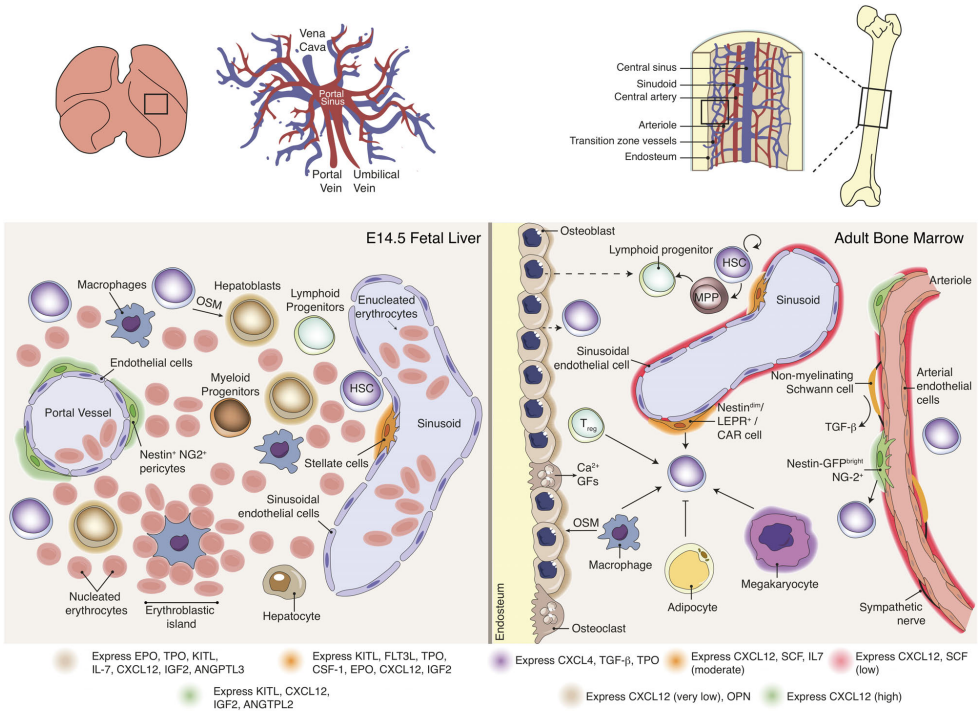


**FIGURE 4 |** Hematopoietic stem cell niche in fetal liver *versus* bone marrow. Distinct BM stromal cell populations have been described as modulators of HSC functions via expression of soluble and membrane-bound factors. Data available for FL stromal populations is scarce and consequently evidence for a direct role of stromal populations in HSC expansion or differentiation is not reported. The FL microenvironment includes cytokine-producing hepatoblasts, pericytes and stellate cells, together with high number of hematopoietic progenitors and distinct developmental stage erythroid cells. BM Nestin-GFP$^{high}$, NG2$^{+}$ perisinusoidal cells and Nestin-GFP$^{dim}$, LepR$^{+}$, CAR sinusoidal cells are key regulators of HSC maintenance, contributing differentially for cytokine production. Macrophages, $T_{reg}$ and megakaryocytes were also reported to contribute to HSC maintenance and mobilization. Sympathetic nerves regulate HSC mobilization through a tightly control of CXCL12 expression by stromal cells. Non-myelinating Schwann cells activate latent TGF-β into its active form, which may contribute for HSC maintenance. The role of osteoblasts in HSPC is still unclear. Adipocytes may negatively affect HSC maintenance.

of cells into circulation. Moreover, Nestin$^{+}$ cells seem to be a transient population, important for HSC localization around the portal vessels during FL hematopoiesis but are no longer present postnatally, a stage at which HSCs migrate and reside in the BM. These cells have also been described in adult BM and ablation of Nestin$^{+}$NG2$^{+}$ pericytes alters HSCs localization away from arterioles (Kunisaki et al., 2013). In the rat, fetal hepatic stellate cells were shown to express VCAM-1 and to secrete *Cxcl12* and hepatocyte growth factor *(Hgf)*, revealing a potential role for the hematopoietic and hepatic development (Kubota et al., 2007). Accordingly, mouse FL hepatic stellate cells (defined as p75NTR$^{+}$) express a range of hematopoietic cytokines, *Csf1*, *Igf2*, *Tpo*, *Kitl*, *Epo*, *Igf1*, *Il11*, *Flt3l* and Oncostatin M (*Osm*, involved in hepatic maturation) and were therefore proposed as potential niche components (Tan et al., 2017).

To date, researchers have undertaken a cell type-directed approach, however, it is conceivable that different FL populations play distinct roles in the maintenance and expansion of HSCs and act through cellular networks. Only an unsupervised analysis of the FL constituents as a whole will shed light on the part each cell type takes in the support of hematopoiesis.

The vascular labyrinthine of the placenta (where embryonic circulation meets maternal circulation) has also been proposed as a niche for HSC expansion (Gekas et al., 2005; Ottersbach and Dzierzak, 2005; Robin et al., 2009). Human placenta-derived stromal cell lines with pericyte characteristics were shown to support *in vitro* maintenance of cord blood (CB) hematopoietic progenitors and hematopoietic cells were found in close contact with pericytes/perivascular cells in the placenta by immunostaining (Robin et al., 2009). Taken together with what

has already been described for the FL (Khan et al., 2016), pericyte-like cells are likely to play a role on supporting hematopoiesis.

## Can the Adult Liver Be a Hematopoietic Site?

Extramedullary hematopoiesis (EMH) is a process in which HSPCs leave their microenvironment in the BM and establish in distinct anatomical locations wherein they continue to produce mature blood cells. Although it is a physiologic process during embryonic development (YS, AGM, FL, and fetal spleen), in the adult it only occurs in pathological settings of BM failure, myelostimulation, tissue inflammation, or abnormal cytokine production (Johns and Christopher, 2012). EMH can occur sporadically in lymph nodes, spinal cord, kidneys, gastrointestinal tract, and lung (Chiu et al., 2015). It is interesting, however, that the predominant sites of EMH are shared between the embryo and the adult: the spleen and the liver. In fact, splenic or liver hematopoiesis can still be observed postnatally in many mammals but disappears before adulthood. Hematopoietic foci in the adult liver can be found within sinusoids and in close association with macrophages (Barberá-Guillem et al., 1989). BM HSPCs co-cultured with liver sinusoid endothelial cells (LSECs) were maintained for more than 6 weeks in cytokine supplemented media, demonstrating a putative niche role of endothelial cells in the adult liver (Cardier and Barberá-Guillem, 1997). An adherent layer of liver cells has been suggested to support megakaryopoiesis by the production of TPO and B lymphopoiesis by the production of *Il7* and *Flt3l* (Cardier and Dempsey, 1998; Wittig et al., 2010). Although endothelial cells have been reported to express TPO, this cytokine is mostly produced by the liver parenchyma (hepatocytes) (Nomura et al., 1997). In the adult, EPO is produced by the kidney, although hepatocytes can also support hepatic erythropoiesis in physiological or pathological conditions (Ploemacher and van Soest, 1977; Semenza et al., 1991; Eckardt et al., 1994; Weidemann and Johnson, 2009). In conclusion, under physiologic conditions, the liver harbors low numbers of HSPCs and supports extramedullary hematopoiesis (Taniguchi et al., 1996; Watanabe et al., 1996). Thus, it is conceivable that adult liver may keep some of its embryonic niche properties.

## Is the Development of the FL and Hematopoietic Cells Symbiotic?

In mid-gestation, embryonic liver functions as a "bag" accommodating the expanding hematopoietic system before BM development. During the temporal window in which the organ is essentially a hematopoietic tissue – from E12.5 to E16.5 (∼6–18 wpc in humans) – and the ratio of non-hematopoietic cells/total liver cells is very low, the organ's architecture is far less complex than that of its adult counterpart. In the adult, hepatocytes are the main parenchymal cell type, organized in cords interspaced by an intricate vascular and biliary system (**Figure 2H**). Alongside with the massive migration of hematopoietic cells to the BM at E16.5 (Christensen et al., 2004), the liver tissue starts to mature – hepatocytes and cholangiocytes differentiate from hepatoblasts and cellular adhesion increases, creating tight hepatic parenchyma with dense hepatocyte cords (Crawford et al., 2010). Transcriptomic and proteomic analysis throughout FL development identified E15.5 as the time of onset of metabolic, detoxification and immune programs (Guo et al., 2009).

Hepatoblasts differentiate into hepatocytes starting at ∼E13.5 in mice and around 14 wpc in humans (Haruna et al., 1996; Yang et al., 2017). Single-cell transcriptomic studies along development (E10.5–E17.5) of hepatoblasts/hepatocytes/cholangiocytes (sorted based on the expression of DLK-1 and EpCAM) suggest that hepatoblast-to-hepatocyte lineage specification is the default process. Cholangiocyte specification occurs as early as E11.5 and is completed by E14.5 (Yang et al., 2017). Hepatoblasts fate decision is modulated by a gradient of Activin/TGF-β signaling, controlled by Onecut (OC) TFs (OC-1/HNF-6 and OC-2) (Clotman, 2005). Cholangiocyte-primed hepatoblasts appear in low numbers at E13.5 around the portal vein and portal sinus, forming a single-layered ductal plate at E15.5, that evolves to a double-layer by E16.5 (**Figures 2D,E**), characterized by CK19 and CK8 cytokeratins and β2 integrin (CD18) (Van Eyken et al., 1988; Tanimizu et al., 2009). At this stage, CK19 expression becomes specific to ductal plate cells (Van Eyken et al., 1988). Focal dilations between the two ductal plate cell layers give rise to the bile ducts (**Figures 2F,G**), whereas the remaining tissue progressively regresses (Clotman et al., 2002). This ductal plate remodeling involves tubulogenesis (Antoniou et al., 2009) and apoptosis (Terada and Nakanuma, 1995). Around birth, the portal mesenchyme encircles the cells of the ductal plate (Swartley et al., 2016). Hepatoblasts located away from the portal vein will gradually differentiate into hepatocytes and by E17 start to exhibit a characteristic polarized epithelial morphology disposed in hepatic cords alongside the bile canaliculi (Zorn, 2008). Because cholangiocyte differentiation occurs along the hilum-to-periphery axis, different maturation states can be observed at a given developmental time (Yang et al., 2017). Three-dimensional reconstructions of serial cross-sections/whole-mount immunostained FL and carbon ink injection have been used to disclose the morphogenesis of intrahepatic bile ducts (Vestentoft et al., 2011; Takashima et al., 2015; Tanimizu et al., 2016).

Kinoshita et al. (1999) showed that hematopoietic cells expand when cultured in a monolayer of primary fetal hepatic cells (in presence of hematopoietic cytokines) and that the addition of OSM suppresses *in vitro* hematopoiesis, by inducing the maturation of the hepatic cells. Since hematopoietic cells produce OSM, its expansion increases the local OSM concentration, consequently promoting hepatic development (Kamiya et al., 1999). It was hypothesized that a metabolically active liver no longer supports hematopoiesis (Miyajima et al., 2000). However, it is still not clear whether the displacement of the hematopoietic cells out of the FL facilitates liver maturation or if the changes in the microenvironment no longer support hematopoiesis.

Impaired hematopoiesis in *c-Myb* mutant (Mucenski et al., 1991) or $Ubc^{-/-}$ mice (Ryu et al., 2012) and abnormal erythropoiesis in *Rb*-deficient mice (Lee et al., 1992) also results in impaired liver growth. However, the

early embryonic lethality (at around E15) has hindered the analysis of the impact of the hematopoietic compartment in liver development.

The vasculature remodeling at the end of gestation was also correlated with the rapid loss of HSCs in the postnatal liver (Khan et al., 2016). After birth, the portal vein no longer receives blood from the vitelline vein, collecting the blood from the gut, draining it to the central vein and the hepatic artery arises. With the ligation of the umbilical inlet, the portal vessels acquire a vein phenotype and lose the periportal pericytes (Khan et al., 2016).

## HEMATOPOIETIC EXIT FROM FL AND ESTABLISHMENT IN THE BM

### What Makes the Hematopoietic System Move? How Is the BM Niche Established?

The BM is the ultimate destination of the hematopoietic system journey in the embryo, being the production hub for blood cells throughout life. LSK cell homing and colonization of mouse BM was reported at E15.5–E16.5, coinciding with the fetal bone marrow (FBM) vascularization (Gekas et al., 2005; Coşkun et al., 2014; Cao et al., 2019), although LT-HSC activity cannot be detected before E17.5 (Christensen et al., 2004). In mice, HSCs migrating out of the FL also seed the spleen, starting at E15.5, with HSC activity still being detected a few weeks after birth (Wolber et al., 2002; Christensen et al., 2004; Bertrand et al., 2006). In humans, although early colonization of fetal long bones was reported at ∼10 wpc (Charbord et al., 1996), the hematopoietic shift from the FL to the FBM occurs later, around 20 wpc (**Figure 1**).

Coşkun et al. (2014) showed that hematopoietic progenitor cells reside in the vascularized regions of fetal long bones, stage at which they are still proliferative. Previous work showed that in the BM, HSCs are cycling during the first 3 weeks after birth and become quiescent thereafter (Bowie et al., 2006). The shift to a quiescence state seems to be dependent on the cellular composition of the microenvironment (Coşkun et al., 2014). LSK cells isolated from *Osx*$^{-/-}$ FBM [that lack osteolineage cells (Nakashima et al., 2002) and some stromal populations (Mizoguchi et al., 2014)] form multi-lineage colonies *in vitro*, but fail to repopulate transplanted recipients (Mizoguchi et al., 2014). LSK cells exhibited dysregulated cell cycle progression and defective homing ability, suggesting that osteolineage and/or mesenchymal cells are necessary to establish and sustain BM LT-HSCs (Coşkun et al., 2014). Additionally, E15.5 CD105$^{+}$Thy1$^{-}$ mesenchymal progenitors transplanted under the kidney capsule give rise to donor-derived chondrocytes and can create an ectopic niche with the recruitment of host-derived marrow and HSCs, evidencing the importance of endochondral ossification for HSC niche formation (Chan et al., 2009).

Osteopontin (OPN), also known as secreted phosphoprotein 1 (SPP1) has been suggested to be an important niche factor in BM. Its concentration in stromal cells is inversely correlated with HSC proliferation in the adult BM (Stier et al., 2005). The OPN dominant form thrombin-cleaved osteopontin (trOPN) is highly expressed in FBM (at the trabecular bone surface), but neglectable-to-none in the early-mid gestation FL (Cao et al., 2019). trOPN receptor α4β1 integrin is upregulated in fetal compared to adult HSCs. The differential concentration of the divalent metal cations, $Ca^{2+}$, $Mg^{2+}$, and $Mn^{2+}$ between FL and FBM, being highly prevalent in the latter, was assumed to activate α4β1 in HSCs, possibly hindering their expansion in the BM (Cao et al., 2019).

CXCL12 expression in the vicinity of vascular endothelial cells in FBM supports the hematopoietic colonization of the organ (Nagasawa et al., 1996; Ara et al., 2003). HSCs isolated from CXCL12$^{-/-}$ embryos failed to colonize the BM in long-term repopulation assays whereas their migration ability could be rescued by enforced expression of CXCL12 under the control of vascular-specific Tie-2 regulatory sequences (Ara et al., 2003). Moreover, the CXCL12-mediated migration of HSPCs *in vitro* seems to be enhanced by the presence of KITL, indicating an additive effect, only found in fetal HSCs (Christensen et al., 2004). This suggests an important role of KITL for HSC seeding and homing during embryonic development.

*CXCL12-GFP* knock-in mice allowed the identification of CXCL12-abundant reticular (CAR) cells, a population with high expression of CXCL12, distributed near SECs and at a lower extent near the endosteum (Sugiyama et al., 2006). These cells show *in vitro* potential to differentiate into adipocytic and osteoblastic lineages (Omatsu et al., 2010). Specific markers have been identified for mesenchymal cells in BM. Leptin receptor (Lepr) is highly enriched in *Scf-GFP*-expressing perivascular stromal cells (Ding et al., 2012) and Lepr$^{+}$ cells were shown to largely overlap with CAR cells (Zhou et al., 2014). A rare population of Nestin$^{+}$ cells that contains all of the fibroblastic CFU (CFU-F) activity within the mouse BM, capable of generating mesenspheres (mesenchymal spheres) *in vitro*, multipotent and with self-renewal potential was identified as a mesenchymal stem cell (MSC) population (Méndez-Ferrer et al., 2010). Later, two different Nestin-GFP populations were discriminated based on the fluorescence intensity by microscopy. Rare quiescent *Nestin-GFP$^{bright}$* cells, positive for the pericyte marker NG2 and α-smooth muscle actin, are enriched for CFU-F activity and express *Cxcl12* and *Kitl*. These cells are located alongside arterioles, close to dormant HSCs (Kunisaki et al., 2013), and associated with sympathetic nerves, that regulate their CXCL12 expression through the $\beta_3$-adrenergic receptor (Méndez-Ferrer et al., 2010). *Nestin-GFP$^{dim}$* cells have a reticular shape, are mitotically active and line sinusoids, largely overlapping with Lepr$^{+}$ cells (∼80%) (Kunisaki et al., 2013). Selective ablation of mouse Nestin$^{+}$ cells (Méndez-Ferrer et al., 2010) or CAR cells (Omatsu et al., 2010) significantly impacts the maintenance of HSCs. The structural differences of the blood vessels and perivascular populations seem to be associated with heterogeneity in HSC function. Besides, the selective deletion of *Cxcl12* from arteriolar NG2$^{+}$ cells, but not sinusoidal Lepr$^{+}$ cells, significantly reduced the HSCs compartment in the BM and a similar effect was observed by deletion of *Kitl* in LepR$^{+}$; but not NG2$^{+}$ cells, evidencing the differential contribution of

perivascular populations in the cytokine production (Asada et al., 2017). BM microenvironment is illustrated in **Figure 4**.

Nestin$^+$ cells can be prospectively isolated using PDGFRα and CD51 markers in the mouse and human fetal and adult BM (Pinho et al., 2013) and show MSC's properties and enrichment of *Cxcl12*, *Vcam1*, *Angpt1*, *Opn*, and *Scf* genes. Of note, in humans, these cells represent a small subset of CD146$^+$ cells (Pinho et al., 2013), the latter harboring all the CFU-F activity in BM (Sacchetti et al., 2007). Co-culture of human PDGFRα$^+$CD51$^+$ mesenspheres with human FBM CD34$^+$ cells in a serum-free, but cytokine supplemented (TPO, SCF, FLT3L) culture media can expand MPPs that engraft immunodeficient mice (Pinho et al., 2013).

In the FL, Nestin-GFP$^+$NG2$^+$ cells, associated with portal vessels, form a niche promoting HSC expansion during the FL development that is no longer found after birth. Concomitantly, the phenotype of the portal vessel transits from Neuropilin-1$^+$Ephrin-B2$^+$ arterial to EphB4$^+$ venular vessels (Khan et al., 2016). This role of Nestin$^+$NG2$^+$ cells in FL is opposite to that in BM, where Nestin$^+$NG2$^+$arteriolar pericytes were proposed to maintain HSC quiescent (Kunisaki et al., 2013).

## UNRESOLVED QUESTIONS – *EX VIVO* EXPANSION OF HSCs

Hematopoietic stem cells are the only cells of the hematopoietic compartment with the potential to replenish all mature blood cells and to divide without triggering differentiation programs, a process known as self-renewal. The mechanisms conveying these properties have been under investigation over the last 60 years, however, to date, they remain poorly understood. The concept that specific BM niche/microenvironment components regulate the fate of HSCs has been proposed by many authors. Cordeiro Gomes et al. (2016) analyzed not only HSCs but also different hematopoietic progenitors and found both HSCs and MPPs locate near or in contact with the same mesenchymal progenitor CAR-cells, expressing CXCL12 and SCF, fundamental to maintain the HSC pool and IL-7 that acts as a short-range signal for lymphoid differentiation. These observations suggest that both maintenance and multilineage differentiation are locally regulated by the same niche (Cordeiro Gomes et al., 2016). In the FL, HSCs expand considerably and differentiate, producing different mature lineages. If a given stromal population is also involved in the regulation of both processes, by the expression of various cytokines, or different cell populations contribute with distinct cytokines is still unresolved.

Hematopoietic stem cell transplantation is a widely used cell therapy intervention in the treatment of hematologic, autoimmune and genetic disorders. However, this therapy is still associated with high mortality rates, mainly due to infection, graft-versus-host disease (GvHD) and organ dysfunction, urging the need for improvement (Tanaka et al., 2016). The most common source of HSCs for transplantation is the BM or mobilized circulating HSPCs. However, matching of major histocompatibility complex antigens is needed to avoid GvHD (Schuster et al., 2012; Walasek et al., 2012). CB can be successfully used as a source of partially mismatched HSCs, as it is readily available through CB banks and elicits low levels of GvHD. Low numbers of HSCs in CB and consequent absent or delayed reconstitution leads to post-transplantation infections, limiting the use of CB in adult patients (Ruggeri et al., 2014).

*In vitro* generation of HSCs would overcome some of the current clinical difficulties that transplantation faces, however, despite countless efforts to derive HSCs from pluripotent stem cell sources, generation of HSC *in vitro* has not yet been achieved – reviewed in Freire and Butler (2020). Another possibility to obtain higher numbers of HSCs would be to expand them *ex vivo* prior to transplantation. Distinct cytokine/growth factor cocktails have shown promising for expansion of HSCs, yet, limited success was reported in clinical studies due to a lack of LT-HSC expansion and rather proliferation of downstream progenitors together with undesirable stem cell differentiation – reviewed in Kumar and Geiger (2017) and Tajer et al. (2019). Cytokines currently used for *ex vivo* HSC expansion include KITL, TPO, IL-3, and FLT3L. *Kitl* and *Tpo* knockout mice show normal fetal development but reduced HSC numbers in the adult, suggesting that these cytokines are important for stem cell survival and proliferation in adulthood but might not be the drivers of HSC expansion during the embryonic period (Fujita et al., 1989; de Sauvage et al., 1996). There is growing evidence that the physical and mechanical properties of the microenvironment could impact on HSC decisions – reviewed in Kumar and Geiger (2017). A combination of cytokines with stroma derived ECM components – fibronectin and collagen – has shown encouraging results (Wohrer et al., 2014; Wilkinson et al., 2019). Moreover, culture of BM HSPCs in tropoelastin, the most elastic biomaterial known, induces a sixfold increase of LSK cells without supplementation with cytokines, suggesting that tropoelastin mediates a similar effect in survival and proliferation of LSK cells and its use could replace exogenous cytokines (Holst et al., 2010). Most cytokines studied have a role in HSC function in the BM, a site where HSC expansion does not occur in physiological conditions. The same cytokines have been found in FL stroma, but whether these are responsible for fetal HSC expansion is not known. Most likely, the FL expansion of newly generated HSCs results from intrinsic cellular properties together with a suitable microenvironment, physical cues included. Efforts have been made to replicate the embryonic microenvironment where HSCs expand, particularly by co-culture with FL hepatic or mesenchymal cells (Wineman et al., 1996; Chou and Lodish, 2010; Chou et al., 2013; Khan et al., 2016). Most strategies used so far focused on specific cell populations, either hepatoblasts or mesenchymal cells, but overlooked the possibility that distinct populations might need to interact. Only the co-culture of HSCs in a system where all the cytokine-expressing populations of the FL are present would reproduce the FL microenvironment. Such a system where hepatoblasts, endothelial and mesenchymal cells are cultured together in a 3D aggregate has already been devised, but no co-culture with hematopoietic cells has been attempted (Takebe et al., 2015). Liver cell culture models have been extensively developed for pharmacological and toxicological research or as a source for transplantation, to obtain an *in vitro* system that resembles a mature liver – reviewed in

Godoy et al. (2013), and for that reason are not suitable for recreating the FL niche environment.

Whereas the FL interactions between different cell types have been correlated with their contribution to the massive transient expansion of the hematopoietic system, other niche factors need to be addressed. Sigurdsson et al. (2016) reported the role of FL bile acids (BAs) as chemical chaperones, critical to sustain high protein production by expanding LT-HSCs without triggering endoplasmic reticulum (ER) stress. Inhibiting the biosynthesis of BAs *in vivo* resulted in reduced numbers of $Lin^{-}$, LSKs, and LSK $CD48^{-}CD150^{+}$ in the FL, with no apparent effect in the number of HSCs in the mother's BM (Sigurdsson et al., 2016). Comparison of FL and BM HSCs transcriptomes demonstrated that FL HSCs metabolism relies on oxygen-dependent pathways, which may be a requirement for extensive energy production during expansion. Contrary to BM HSCs, FL HSCs use oxidative phosphorylation (aside from glycolysis), have higher number of mitochondria and up regulate genes associated with antioxidant and DNA repair pathways, that are speculated to confer protection from reactive oxygen species-mediated (geno)toxicity (Manesia et al., 2015).

Exploring the complexity of HSC niches (cellular composition, cytokine and growth factors milieu, physical properties, oxygen availability, etc.) will improve into our understanding of HSC self-renewal capacity (recently reviewed by Wilkinson et al., 2020), that is currently insufficient to devise efficient strategies for HSC expansion *ex vivo*.

## CONCLUDING REMARKS

Distinct studies have identified and characterized FL stromal populations that may contribute with specific cues, enabling the HSC expansion in this organ. Despite the efforts, the role of the FL microenvironment has not been directly shown. The possibility that HSCs proliferate exclusively due to intrinsic properties is however remote. Therefore, a model in which distinct populations cooperate is conceivable. An analysis that contemplates such complex multicellular networks has not been attempted. This review aimed to compile information on the cellular populations that could signal to HSCs during development, highlighting the advances and the unresolved questions in the field.

## AUTHOR CONTRIBUTIONS

FS-d-S and MP: conceptualization and writing. AC: discussion and revision. PP-d-Ó: conceptualization and revision. All authors contributed to the article and approved the submitted version.

## FUNDING

FS-d-S funded by FCT grants PD/BD/114128/2015 and POCI-0100145-FEDER-01638. MP funded by FCT grant SFRH/BD/143605/2019. AC financed by the Institut Pasteur, INSERM, ANR (grant Twothyme and EpiDev) and REVIVE Future Investment Program and Pasteur-Weizmann Foundation. PP-d-Ó financed by Portuguese funds through FCT/MCTES in the framework of the projects PTDC/MED-OUT/32656/2017, POCI-01-0145-FEDER-032656, and by – FCT – UIDB/04293/2020.

## ACKNOWLEDGMENTS

We thank the members of PP-d-Ó and AC laboratories for critical discussions.

## REFERENCES

Alexander, W. S., Roberts, A. W., Nicola, N. A., Li, R., and Metcalf, D. (1996). Deficiencies in progenitor cells of multiple hematopoietic lineages and defective megakaryocytopoiesis in mice lacking the thrombopoietic receptor c-Mpl. *Blood* 87, 2162–2170.

Antoniou, A., Raynaud, P., Cordi, S., Zong, Y., Tronche, F., Stanger, B. Z., et al. (2009). Intrahepatic bile ducts develop according to a new mode of tubulogenesis regulated by the transcription factor SOX9. *Gastroenterology* 136, 2325–2333. doi: 10.1053/j.gastro.2009.02.051

Ara, T., Tokoyoda, K., Sugiyama, T., Egawa, T., Kawabata, K., and Nagasawa, T. (2003). Long-term hematopoietic stem cells require stromal cell-derived factor-1 for colonizing bone marrow during ontogeny. *Immunity* 19, 257–267. doi: 10.1016/S1074-7613(03)00201-2

Asada, N., Kunisaki, Y., Pierce, H., Wang, Z., Fernandez, N. F., Birbrair, A., et al. (2017). Differential cytokine contributions of perivascular haematopoietic stem cell niches. *Nat. Cell Biol.* 19, 214–223. doi: 10.1038/ncb3475

Asahina, K. (2012). Hepatic stellate cell progenitor cells. *J. Gastroenterol. Hepatol.* 27(Suppl. 2), 80–84. doi: 10.1111/j.1440-1746.2011.07001.x

Asahina, K., Tsai, S. Y., Li, P., Ishii, M. Jr., and Henry, M. (2010). Mesenchymal origin of hepatic stellate cells, submesothelial cells, and perivascular mesenchymal cells during mouse liver development. *Hepatology* 49, 998–1011. doi: 10.1002/hep.22721.Mesenchymal

Asahina, K., Zhou, B., Pu, W. T., and Tsukamoto, H. (2011). Septum transversum-derived mesothelium gives rise to hepatic stellate cells and perivascular mesenchymal cells in developing mouse liver. *Hepatology* 53, 983–995. doi: 10.1002/hep.24119

Ayres-Silva, J. D. P., Manso, P. P. D. A., Madeira, M. R. D. C., Pelajo-Machado, M., and Lenzi, H. L. (2011). Sequential morphological characteristics of murine fetal liver hematopoietic microenvironment in Swiss Webster mice. *Cell Tissue Res.* 344, 455–469. doi: 10.1007/s00441-011-1170-1

Barberá-Guillem, E., Ayala, R., and Vidal-Vanaclocha, F. (1989). Differential location of hemopoietic colonies within liver acini of postnatal and phenylhydrazine-treated adult mice. *Hepatology* 9, 29–36. doi: 10.1002/hep.1840090106

Barker, J. E. (1994). Sl/Sld hematopoietic progenitors are deficient in situ. *Exp. Hematol.* 22, 174–177.

Berthault, C., Ramond, C., Burlen-Defranoux, O., Soubigou, G., Chea, S., Golub, R., et al. (2017). Asynchronous lineage priming determines commitment to T cell and B cell lineages in fetal liver. *Nat. Immunol.* 18, 1139–1149. doi: 10.1038/ni.3820

Bertrand, J., Chi, N. C., Santoso, B., Teng, S., Stainier, D. Y. R., and Traver, D. (2010). Haematopoietic stem cells derive directly from aortic endothelium during development. *Nature* 464, 108–111. doi: 10.1038/nature08738

Bertrand, J., Desanti, G. E., Lo-Man, R., Leclerc, C., Cumano, A., and Golub, R. (2006). Fetal spleen stroma drives macrophage commitment. *Development* 133, 3619–3628. doi: 10.1242/dev.02510

Bertrand, J., Giroux, S., Golub, R., Klaine, M., Jalil, A., Boucontet, L., et al. (2005a). Characterization of purified intraembryonic hematopoietic stem cells as a tool to define their site of origin. *Proc. Natl. Acad. Sci. U.S.A.* 102, 134–139. doi: 10.1073/pnas.0402270102

Bertrand, J., Jalil, A., Klaine, M., Jung, S., Cumano, A., and Godin, I. (2005b). Three pathways to mature macrophages in the early mouse yolk sac. *Blood* 106, 3004–3011. doi: 10.1182/blood-2005-02-0461

Bessis, M., Mize, C., and Prenant, M. (1978). Erythropoiesis: comparison of in vivo and in vitro amplification. *Blood Cells* 4, 155–174.

Bleul, C. C., Farzan, M., Choe, H., Parolin, C., Clark-Lewis, I., Sodroski, J., et al. (1996). The lymphocyte chemoattractant SDF-1 is a ligand for LESTR/fusin and blocks HIV-1 entry. *Nature* 382, 829–833. doi: 10.1038/382829a0

Bloom, W., and Bartelmez, G. W. (1940). Hematopoiesis in young human embryos. *Am. J. Anat.* 67, 21–53. doi: 10.1002/aja.1000670103

Bogue, C. W., Ganea, G. R., Sturm, E., Ianucci, R., and Jacobs, H. C. (2000). Hex expression suggests a role in the development and function of organs derived from foregut endoderm. *Dev. Dyn.* 219, 84–89.

Borge, O., Ramsfjell, V., Cui, L., and Jacobsen, S. E. (1997). Ability of early acting cytokines to directly promote survival and suppress apoptosis of human primitive CD34+CD38- bone marrow cells with multilineage potential at the single-cell level: key role of thrombopoietin. *Blood* 90, 2282–2292.

Borge, O., Ramsfjell, V., Veiby, O., Murphy, M., Lok, S., and Jacobsen, S. (1996). Thrombopoietin, but not erythropoietin promotes viability and inhibits apoptosis of multipotent murine hematopoietic progenitor cells in vitro. *Blood* 88, 2859–2870. doi: 10.1182/blood.V88.8.2859.bloodjournal8882859

Bort, R., Signore, M., Tremblay, K., Barbera, J. P. M., and Zaret, K. S. (2006). Hex homeobox gene controls the transition of the endoderm to a pseudostratified, cell emergent epithelium for liver bud development. *Dev. Biol.* 290, 44–56. doi: 10.1016/j.ydbio.2005.11.006

Bowie, M. B., McKnight, K. D., Kent, D. G., McCaffrey, L., Hoodless, P. A., and Eaves, C. J. (2006). Hematopoietic stem cells proliferate until after birth and show a reversible phase-specific engraftment defect. *J. Clin. Invest.* 116, 2808–2816. doi: 10.1172/JCI28310

Brouard, N., Jost, C., Matthias, N., Albrecht, C., Egard, S., Gandhi, P., et al. (2017). A unique microenvironment in the developing liver supports the expansion of megakaryocyte progenitors. *Blood Adv.* 1, 1854–1866. doi: 10.1182/bloodadvances.2016003541

Busch, K., Klapproth, K., Barile, M., Flossdorf, M., Holland-Letz, T., Schlenner, S. M., et al. (2015). Fundamental properties of unperturbed haematopoiesis from stem cells in vivo. *Nature* 518, 542–546. doi: 10.1038/nature14242

Cao, H., Cao, B., Heazlewood, C. K., Domingues, M., Sun, X., Debele, E., et al. (2019). Osteopontin is an important regulative component of the fetal bone marrow hematopoietic stem cell niche. *Cells* 8:985. doi: 10.3390/cells8090985

Cardier, J., and Barberá-Guillem, E. (1997). Extramedullary hematopoiesis in the adult mouse liver is associated with specific hepatic sinusoidal endothelial cells. *Hepatology* 26, 165–175. doi: 10.1002/hep.510260122

Cardier, J., and Dempsey, J. (1998). Thrombopoietin and its receptor, c-mpl, are constitutively expressed by mouse liver endothelial cells: evidence of thrombopoietin as a growth factor for liver endothelial cells. *Blood* 91, 923–929. doi: 10.1182/blood.V91.3.923

Cascio, S., and Zaret, K. S. (1991). Hepatocyte differentiation initiates during endodermal-mesenchymal interactions prior to liver formation. *Development* 113, 217–225.

Chan, C. K. F., Chen, C.-C., Luppen, C. A., Kim, J.-B., DeBoer, A. T., Wei, K., et al. (2009). Endochondral ossification is required for haematopoietic stem-cell niche formation. *Nature* 457, 490–494. doi: 10.1038/nature07547

Charbord, P., and Moore, K. A. (2005). Gene expression in stem cell-supporting stromal cell lines. *Ann. N. Y. Acad. Sci.* 1044, 159–167. doi: 10.1196/annals.1349.020

Charbord, P., Tavian, M., Humeau, L., and Peault, B. (1996). Early ontogeny of the human marrow from long bones: an immunohistochemical study of hematopoiesis and its microenvironment. *Blood* 87, 4109–4119. doi: 10.1182/blood.V87.10.4109.bloodjournal87104109

Chen, J. Y., Miyanishi, M., Wang, S. K., Yamazaki, S., Sinha, R., Kao, K. S., et al. (2016). Hoxb5 marks long-term haematopoietic stem cells and reveals a homogenous perivascular niche. *Nature* 530, 223–227. doi: 10.1038/nature16943

Cheshier, S. H., Morrison, S. J., Liao, X., and Weissman, I. L. (1999). In vivo proliferation and cell cycle kinetics of long-term self-renewing hematopoietic stem cells. *Proc. Natl. Acad. Sci. U.S.A.* 96, 3120–3125. doi: 10.1073/pnas.96.6.3120

Chiu, S.-C., Liu, H.-H., Chen, C.-L., Chen, P.-R., Liu, M.-C., Lin, S.-Z., et al. (2015). Extramedullary hematopoiesis (EMH) in laboratory animals: offering an insight into stem cell research. *Cell Transplant.* 24, 349–366. doi: 10.3727/096368915X686850

Chou, S., Flygare, J., and Lodish, H. F. (2013). Fetal hepatic progenitors support long-term expansion of hematopoietic stem cells. *Exp. Hematol.* 41, 479–490. doi: 10.1016/j.exphem.2013.02.003

Chou, S., and Lodish, H. F. (2010). Fetal liver hepatic progenitors are supportive stromal cells for hematopoietic stem cells. *Proc. Natl. Acad. Sci. U.S.A.* 107, 7799–7804. doi: 10.1073/pnas.1003586107

Christensen, J. L., Wright, D. E., Wagers, A. J., and Weissman, I. L. (2004). Circulation and chemotaxis of fetal hematopoietic stem cells. *PLoS Biol.* 2:e020075. doi: 10.1371/journal.pbio.0020075

Christodoulou, C., Spencer, J. A., Yeh, S.-C. A., Turcotte, R., Kokkaliaris, K. D., Panero, R., et al. (2020). Live-animal imaging of native haematopoietic stem and progenitor cells. *Nature* 578, 278–283. doi: 10.1038/s41586-020-1971-z

Clotman, F. (2005). Control of liver cell fate decision by a gradient of TGF signaling modulated by Onecut transcription factors. *Genes Dev.* 19, 1849–1854. doi: 10.1101/gad.340305

Clotman, F., Lannoy, V. J., Reber, M., Cereghini, S., Cassiman, D., Jacquemin, P., et al. (2002). The onecut transcription factor HNF6 is required for normal development of the biliary tract. *Development* 129, 1819–1828.

Collardeau-Frachon, S., and Scoazec, J. Y. (2008). Vascular development and differentiation during human liver organogenesis. *Anat. Rec.* 291, 614–627. doi: 10.1002/ar.20679

Cordeiro Gomes, A., Hara, T., Lim, V. Y., Herndler-Brandstetter, D., Nevius, E., Sugiyama, T., et al. (2016). Hematopoietic stem cell niches produce lineage-instructive signals to control multipotent progenitor differentiation. *Immunity* 45, 1219–1231. doi: 10.1016/j.immuni.2016.11.004

Coşkun, S., Chao, H., Vasavada, H., Heydari, K., Gonzales, N., Zhou, X., et al. (2014). Development of the fetal bone marrow niche and regulation of HSC quiescence and homing ability by emerging osteolineage cells. *Cell Rep.* 9, 581–590. doi: 10.1016/j.celrep.2014.09.013

Crane, G. M., Jeffery, E., and Morrison, S. J. (2017). Adult haematopoietic stem cell niches. *Nat. Rev. Immunol.* 17, 573–590. doi: 10.1038/nri.2017.53

Crawford, L. W., Foley, J. F., and Elmore, S. A. (2010). Histology atlas of the developing mouse hepatobiliary system with emphasis on embryonic days 9.5-18.5. *Toxicol. Pathol.* 38, 872–906. doi: 10.1177/0192623310374329

Cumano, A., Dieterlen-Lievre, F., and Godin, I. (1996). Lymphoid potential, probed before circulation in mouse, is restricted to caudal intraembryonic splanchnopleura. *Cell* 86, 907–916. doi: 10.1016/S0092-8674(00)80166-X

Cumano, A., Ferraz, J. C., Klaine, M., Di Santo, J. P., and Godin, I. (2001). Intraembryonic, but Not Yolk Sac hematopoietic precursors, isolated before circulation, provide long-term multilineage reconstitution. *Immunity* 15, 477–485. doi: 10.1016/S1074-7613(01)00190-X

de Sauvage, F. J., Carver-Moore, K., Luoh, S. M., Ryan, A., Dowd, M., Eaton, D. L., et al. (1996). Physiological regulation of early and late stages of megakaryocytopoiesis by thrombopoietin. *J. Exp. Med.* 183, 651–656. doi: 10.1084/jem.183.2.651

Decker, M., Leslie, J., Liu, Q., and Ding, L. (2018). Hepatic thrombopoietin is required for bone marrow hematopoietic stem cell maintenance. *Science* 360, 106–110. doi: 10.1126/science.aap8861

Ding, L., Saunders, T. L., Enikolopov, G., and Morrison, S. J. (2012). Endothelial and perivascular cells maintain haematopoietic stem cells. *Nature* 481, 457–462. doi: 10.1038/nature10783

Douarin, N. M. (1975). An experimental analysis of liver development. *Med. Biol.* 53, 427–455.

Dudas, J., Papoutsi, M., Hecht, M., Elmaouhoub, A., Saile, B., Christ, B., et al. (2004). The homeobox transcription factor Prox1 is highly conserved in embryonic hepatoblasts and in adult and transformed hepatocytes, but is absent

from bile duct epithelium. *Anat. Embryol.* 208, 359–366. doi: 10.1007/s00429-004-0403-4

Eaton, D. L., and de Sauvage, F. J. (1997). Thrombopoietin: the primary regulator of megakaryocytopoiesis and thrombopoiesis. *Exp. Hematol.* 25, 1–7.

Eberl, G., Marmon, S., Sunshine, M. J., Rennert, P. D., Choi, Y., and Littmann, D. R. (2004). An essential function for the nuclear receptor RORγt in the generation of fetal lymphoid tissue inducer cells. *Nat. Immunol.* 5, 64–73. doi: 10.1038/ni1022

Eckardt, K. U., Pugh, C. W., Meier, M., Tan, C. C., Ratcliffe, P. J., and Kurtz, A. (1994). Production of erythropoietin by liver cells in vivo and in vitro. *Ann. N. Y. Acad. Sci.* 718, 50–60. doi: 10.1111/j.1749-6632.1994.tb55703.x

Ema, H., and Nakauchi, H. (2000). Expansion of hematopoietic stem cells in the developing liver of a mouse embryo. *Blood* 95, 2284–2289.

Emambokus, N. R., and Frampton, J. (2003). The glycoprotein IIb molecule is expressed on early murine hematopoietic progenitors and regulates their numbers in sites of hematopoiesis. *Immunity* 19, 33–45. doi: 10.1016/S1074-7613(03)00173-0

Fox, N., Priestley, G., Papayannopoulou, T., and Kaushansky, K. (2002). Thrombopoietin expands hematopoietic stem cells after transplantation. *J. Clin. Invest.* 110, 389–394. doi: 10.1172/JCI15430

Frame, J. M., Fegan, K. H., Conway, S. J., McGrath, K. E., and Palis, J. (2016). Definitive hematopoiesis in the yolk sac emerges from wnt-responsive hemogenic endothelium independently of circulation and arterial identity. *Stem Cells* 34, 431–444. doi: 10.1002/stem.2213

Fraser, S. T., Ogawa, M., Yu, R. T., Nishikawa, S., Yoder, M. C., and Nishikawa, S. I. (2002). Definitive hematopoietic commitment within the embryonic vascular endothelial-cadherin+ population. *Exp. Hematol.* 30, 1070–1078. doi: 10.1016/S0301-472X(02)00887-1

Freire, A. G., and Butler, J. M. (2020). Blood making: learning what to put into the dish. *F1000Research* 9:38. doi: 10.12688/f1000research.21245.1

Fujita, J., Onoue, H., Ebi, Y., Nakayama, H., and Kanakura, Y. (1989). In vitro duplication and in vivo cure of mast-cell deficiency of Sl/Sld mutant mice by cloned 3T3 fibroblasts. *Proc. Natl. Acad. Sci. U.S.A.* 86, 2888–2891. doi: 10.1073/pnas.86.8.2888

Gekas, C., Dieterlen-Lièvre, F., Orkin, S. H., and Mikkola, H. K. A. (2005). The placenta is a niche for hematopoietic stem cells. *Dev. Cell* 8, 365–375. doi: 10.1016/j.devcel.2004.12.016

Gentek, R., Ghigo, C., Hoeffel, G., Bulle, M. J., Msallam, R., Gautier, G., et al. (2018). Hemogenic endothelial fate mapping reveals dual developmental origin of mast cells. *Immunity* 48, 1160–1171. doi: 10.1016/j.immuni.2018.04.025

Gerlach, J. C., Over, P., Turner, M. E., Thompson, R. L., Foka, H. G., Chen, W. C. W., et al. (2012). *Perivascular mesenchymal* progenitors in human fetal and adult liver. *Stem Cells Dev.* 21, 3258–3269. doi: 10.1089/scd.2012.0296

Gerlach, J. C., Thompson, R. L., Gridelli, B., and Schmelzer, E. (2019). Effects of delta-like noncanonical Notch ligand 1 expression of human fetal liver hepatoblasts on hematopoietic progenitors. *Stem Cells Intern.* 2019:7916275. doi: 10.1155/2019/7916275

Godoy, P., Hewitt, N. J., Albrecht, U., Andersen, M. E., Ansari, N., Bhattacharya, S., et al. (2013). Recent advances in 2D and 3D in vitro systems using primary hepatocytes, alternative hepatocyte sources and non-parenchymal liver cells and their use in investigating mechanisms of hepatotoxicity, cell signaling and ADME. *Arch. Toxicol.* 87:1315. doi: 10.1007/s00204-013-1078-5

Gomez-Perdiguero, E., Klapproth, K., Schulz, C., Busch, K., Azzoni, E., Crozet, L., et al. (2015). Tissue-resident macrophages originate from yolk-sac-derived erythro-myeloid progenitors. *Nature* 518, 547–551. doi: 10.1038/nature13989

Guilbert, L. J., and Stanley, E. R. (1980). Specific interaction of murine colony-stimulating factor with mononuclear phagocytic cells. *J. Cell Biol.* 85, 153–159. doi: 10.1083/jcb.85.1.153

Guo, Y., Zhang, X., Huang, J., Zeng, Y., Liu, W., Geng, C., et al. (2009). Relationships between hematopoiesis and hepatogenesis in the midtrimester fetal liver characterized by dynamic transcriptomic and proteomic profiles. *PLoS One* 4:e7641. doi: 10.1371/journal.pone.0007641

Guyot, C., Lepreux, S., Combe, C., Doudnikoff, E., Bioulac-Sage, P., Balabaud, C., et al. (2006). Hepatic fibrosis and cirrhosis: the (myo)fibroblastic cell subpopulations involved. *Intern. J. Biochem. Cell Biol.* 38, 135–151. doi: 10.1016/j.biocel.2005.08.021

Haas, J. D., Ravens, S., Düber, S., Sandrock, I., Oberdörfer, L., Kashani, E., et al. (2012). Development of interleukin-17-producing γδ T cells is restricted to a functional embryonic wave. *Immunity* 37, 48–59. doi: 10.1016/j.immuni.2012.06.003

Haruna, Y., Saito, K., Spaulding, S., Nalesnik, M. A., and Gerber, M. A. (1996). Identification of bipotential progenitor cells in human liver development. *Hepatology* 23, 476–481. doi: 10.1002/hep.510230312

Hata, M., Nanno, M., Doi, H., Satomi, S., Sakata, T., Suzuki, R., et al. (1993). Establishment of a hepatocytic epithelial cell line from the murine fetal liver capable of promoting hemopoietic cell proliferation. *J. Cell. Physiol.* 154, 381–392. doi: 10.1002/jcp.1041540222

Hayashi, Y., Sezaki, M., and Takizawa, H. (2019). Development of the hematopoietic system: Role of inflammatory factors. *Wil. Interdiscipl. Rev. Dev. Biol.* 8, 1–17. doi: 10.1002/wdev.341

Hirsch, E., Iglesias, A., Potocnik, A. J., Hartmann, U., and Fässler, R. (1996). Impaired migration but not differentiation of haematopoietic stem cells in the absence of β1 integrins. *Nature* 380, 171–175. doi: 10.1038/380171a0

Holst, J., Watson, S., Lord, M. S., Eamegdool, S. S., Bax, D. V., Nivison-Smith, L. B., et al. (2010). Substrate elasticity provides mechanical signals for the expansion of hemopoietic stem and progenitor cells. *Nat. Biotechnol.* 28, 1123–1128. doi: 10.1038/nbt.1687

House, P. D. R., and Weidemann, M. J. (1970). Characterization of an [125I]-Insulin binding plasma membrane fraction from rat liver. *Biochem. Biophys. Res. Commun.* 41, 541–548. doi: 10.1016/0006-291X(70)90046-X

Ijpenberg, A., Pérez-Pomares, J. M., Guadix, J. A., Carmona, R., Portillo-Sánchez, V., Macías, D., et al. (2007). Wt1 and retinoic acid signaling are essential for stellate cell development and liver morphogenesis. *Dev. Biol.* 312, 157–170. doi: 10.1016/j.ydbio.2007.09.014

Ikuta, K., Kina, T., MacNeil, I., Uchida, N., Peault, B., Chien, Y., et al. (1990). A developmental switch in thymic lymphocyte maturation potential occurs at the level of hematopoietic stem cells. *Cell* 62, 863–874. doi: 10.1016/0092-8674(90)90262-D

Ji, R. P., Phoon, C. K. L., Aristizábal, O., McGrath, K. E., Palis, J., and Turnbull, D. H. (2003). Onset of cardiac function during early mouse embryogenesis coincides with entry of primitive erythroblasts into the embryo proper. *Circ. Res.* 92, 133–135. doi: 10.1161/01.RES.0000056532.18710.C0

Johns, J. L., and Christopher, M. M. (2012). Extramedullary hematopoiesis: a new look at the underlying stem cell niche, theories of development, and occurrence in animals. *Vet. Pathol.* 49, 508–523. doi: 10.1177/0300985811432344

Johnson, G. R., and Moore, M. A. S. (1975). Role of stem cell migration in initiation of mouse foetal liver haemopoiesis. *Nature* 258, 726–728. doi: 10.1038/258726a0

Kamiya, A., Kinoshita, T., Ito, Y., Matsui, T., Morikawa, Y., Senba, E., et al. (1999). Fetal liver development requires a paracrine action of oncostatin M through the gp130 signal transducer. *EMBO J.* 18, 2127–2136. doi: 10.1093/emboj/18.8.2127

Kasaai, B., Caolo, V., Peacock, H. M., Lehoux, S., Gomez-Perdiguero, E., Luttun, A., et al. (2017). Erythro-myeloid progenitors can differentiate from endothelial cells and modulate embryonic vascular remodeling. *Sci. Rep.* 7, 25–28. doi: 10.1038/srep43817

Kaushansky, K. (1995). Thrombopoietin: the primary regulator of platelet production. *Blood* 86, 419–431. doi: 10.1182/blood.V86.2.419.bloodjournal862419

Khan, J., Mendelson, A., Kunisaki, Y., Birbrair, A., Kou, Y., Arnal-Estapé, A., et al. (2016). Fetal liver hematopoietic stem cell niches associate with portal vessels. *Science* 351, 176–180. doi: 10.1126/science.aad0084

Kieusseian, A., de la Grange, P. B., Burlen-Defranoux, O., Godin, I., and Cumano, A. (2012). Immature hematopoietic stem cells undergo maturation in the fetal liver. *Development* 139, 3521–3530. doi: 10.1242/dev.079210

Kim, I., He, S., Yilmaz, O. H., Kiel, M. J., Morrison, S. J., and Yilmaz, H. (2006). Enhanced purification of fetal liver hematopoietic stem cells using SLAM family receptors. *Blood* 108, 737–744. doi: 10.1182/blood-2005-10-4135

Kimura, S., Roberts, A. W., Metcalf, D., and Alexander, W. S. (1998). Hematopoietic stem cell deficiencies in mice lacking c-Mpl, the receptor for thrombopoietin. *Proc. Natl. Acad. Sci. U.S.A.* 95, 1195–1200. doi: 10.1073/pnas.95.3.1195

Kingsley, P. D., Malik, J., Emerson, R. L., Bushnell, T. P., McGrath, K. E., Bloedorn, L. A., et al. (2006). "Maturational" globin switching in primary primitive erythroid cells. *Blood* 107, 1665–1672. doi: 10.1182/blood-2005-08-3097

Kinoshita, T., Sekiguchi, T., Xu, M.-J., Ito, Y., Kamiya, A., Tsuji, K.-I., et al. (1999). Hepatic differentiation induced by oncostatin M attenuates fetal liver hematopoiesis. *Proc. Natl. Acad. Sci. U.S.A.* 96, 7265–7270. doi: 10.2177/jsci.21.supplement_215

Kiserud, T. (2005). Physiology of the fetal circulation. *Semin. Fet. Neonat. Med.* 10, 493–503. doi: 10.1016/j.siny.2005.08.007

Kissa, K., and Herbomel, P. (2010). Blood stem cells emerge from aortic endothelium by a novel type of cell transition. *Nature* 464, 112–115. doi: 10.1038/nature08761

Ku, H., Yonemura, Y., Kaushansky, K., and Ogawa, M. (1996). Thrombopoietin, the ligand for the Mpl receptor, synergizes with steel factor and other early acting cytokines in supporting proliferation of primitive hematopoietic progenitors of mice. *Blood* 87, 4544–4551.

Kubota, H., Yao, H., and Reid, L. M. (2007). Identification and characterization of vitamin a-storing cells in fetal liver: implications for functional importance of hepatic stellate cells in liver development and hematopoiesis. *Stem Cells* 25, 2339–2349. doi: 10.1634/stemcells.2006-0316

Kumar, S., and Geiger, H. (2017). HSC niche biology and hsc expansion Ex *Vivo*. *Trends Mol. Med.* 23, 799–819. doi: 10.1016/j.molmed.2017.07.003

Kunisaki, Y., Bruns, I., Scheiermann, C., Ahmed, J., Pinho, S., Zhang, D., et al. (2013). Arteriolar niches maintain haematopoietic stem cell quiescence. *Nature* 502, 637–643. doi: 10.1038/nature12612

Lai, C.-Y., Yamazaki, S., Okabe, M., Suzuki, S., Maeyama, Y., Iimura, Y., et al. (2014). Stage-specific roles for Cxcr4 signaling in murine hematopoietic stem/progenitor cells in the process of bone marrow repopulation. *Stem Cells* 32, 1929–1942. doi: 10.1002/stem.1670

Lee, E. Y.-H. P., Chang, C.-Y., Hu, N., Wang, Y.-C. J., Lai, C.-C., Herrup, K., et al. (1992). Mice deficient for Rb are nonviable and show defects in neurogenesis and haematopoiesis. *Nature* 359, 288–294. doi: 10.1038/359288a0

Li, J., Ning, G., and Duncan, S. A. (2000). Mammalian hepatocyte differentiation requires the transcription factor HNF-4alpha. *Genes Dev.* 14, 464–474. doi: 10.1128/MMBR.66.1.39-63.2002

Lin, C. S., Lim, S. K., D'Agati, V., and Costantini, F. (1996). Differential effects of an erythropoietin receptor gene disruption on primitive and definitive erythropoiesis. *Genes Dev.* 10, 154–164. doi: 10.1101/gad.10.2.154

Lok, S., Kaushansky, K., Holly, R. D., Kuijper, J. L., Lofton-Day, C. E., Oort, P. J., et al. (1994). Cloning and expression of murine thrombopoietin cDNA and stimulation of platelet production in vivo. *Nature* 369, 565–568. doi: 10.1038/369565a0

Lua, I., and Asahina, K. (2016). The role of mesothelial cells in liver development. *Injury Regener. Gut Liver* 10:166. doi: 10.5009/gnl15226

Lyman, S. D., James, L., Bos, T., Vanden de Vries, P., Brasel, K., Gliniak, B., et al. (1993). Molecular cloning of a ligand for the flt3flk-2 tyrosine kinase receptor: a proliferative factor for primitive hematopoietic cells. *Cell* 75, 1157–1167. doi: 10.1016/0092-8674(93)90325-K

Manesia, J. K., Xu, Z., Broekaert, D., Boon, R., van Vliet, A., Eelen, G., et al. (2015). Highly proliferative primitive fetal liver hematopoietic stem cells are fueled by oxidative metabolic pathways. *Stem Cell Res.* 15, 715–721. doi: 10.1016/j.scr.2015.11.001

Margagliotti, S., Clotman, F., Pierreux, C. E., Beaudry, J. B., Jacquemin, P., Rousseau, G. G., et al. (2007). The onecut transcription factors HNF-6/OC-1 and OC-2 regulate early liver expansion by controlling hepatoblast migration. *Dev. Biol.* 311, 579–589. doi: 10.1016/j.ydbio.2007.09.013

Matsumoto, K., Yoshitomi, H., Rossant, J., and Zaret, K. S. (2001). Liver organogenesis promoted by endothelial cells prior to vascular function. *Science* 294, 559–563. doi: 10.1126/science.1063889

Matthews, W., Jordan, C. T., Wiegand, G. W., Pardoll, D., and Lemischka, I. R. (1991). A receptor tyrosine kinase specific to hematopoietic stem and progenitor cell-enriched populations. *Cell* 65, 1143–1152. doi: 10.1016/0092-8674(91)90010-V

McDermott, D. H., Gao, J.-L., Liu, Q., Siwicki, M., Martens, C., Jacobs, P., et al. (2015). Chromothriptic cure of WHIM syndrome. *Cell* 160, 686–699. doi: 10.1016/j.cell.2015.01.014

McGrath, K. E., Frame, J. M., Fegan, K. H., Bowen, J. R., Conway, S. J., Catherman, S. C., et al. (2015). Distinct sources of hematopoietic progenitors emerge before HSCS and provide functional blood cells in the mammalian Embryo. *Cell Rep.* 11, 1892–1904. doi: 10.1016/j.celrep.2015.05.036

Medvinsky, A., Dzierzak, E., Ridgeway, T., and Hill, M. (1996). Definitive hematopoiesis is autonomously initiated by the AGM region. *Cell* 86, 897–906. doi: 10.1016/S0092-8674(00)80165-8

Méndez-Ferrer, S., Michurina, T. V., Ferraro, F., Mazloom, A. R., MacArthur, B. D., Lira, S. A., et al. (2010). Mesenchymal and haematopoietic stem cells form a unique bone marrow niche. *Nature* 466, 829–834. doi: 10.1038/nature09262

Migliaccio, G., Migliaccio, A. R., Petti, S., Mavilio, F., Russo, G., Lazzaro, D., et al. (1986). Human embryonic hemopoiesis. Kinetics of progenitors and precursors underlying the yolk sac-liver transition. *J. Clin. Invest.* 78, 51–60. doi: 10.1172/JCI112572

Miller, C. L., Rebel, V. I, Helgason, C. D., Lansdorp, D., and Eaves, C. J. (1997). Impaired steel factor responsiveness differentially affects the detection and long-term maintenance of fetal liver hematopoietic stem cells in vivo. *Blood* 89, 1214–1223. doi: 10.1182/blood.v89.4.1214

Miyajima, A., Kinoshita, T., Tanaka, M., Kamiya, A., Mukouyama, Y., and Hara, T. (2000). Role of oncostatin M in hematopoiesis and liver development. *Cytokine Growth. Factor. Rev.* 11, 177–183. doi: 10.1016/S1359-6101(00)00003-4

Mizoguchi, T., Pinho, S., Ahmed, J., Kunisaki, Y., Hanoun, M., Mendelson, A., et al. (2014). Osterix marks distinct waves of primitive and definitive stromal progenitors during bone marrow development. *Dev. Cell* 29, 340–349. doi: 10.1016/j.devcel.2014.03.013

Moore, K. A., Pytowski, B., Witte, L., Hicklin, D., and Lemischka, I. R. (1997). Hematopoietic activity of a stromal cell transmembrane protein containing epidermal growth factor-like repeat motifs. *Proc. Natl. Acad. Sci. U.S.A.* 94, 4011–4016. doi: 10.1073/pnas.94.8.4011

Morgan, D. O., Edman, J. C., Standring, D. N., Fried, V. A., Smith, M. C., Roth, R. A., et al. (1987). Insulin-like growth factor II receptor as a multifunctional binding protein. *Nature* 329, 301–307. doi: 10.1038/329301a0

Morrison, S. J., Hemmati, H. D., Wandycz, A. M., and Weissman, I. L. (1995). The purification and characterization of fetal liver hematopoietic stem cells. *Proc. Natl. Acad. Sci. U.S.A.* 92, 10302–10306. doi: 10.1073/pnas.92.22.10302

Mucenski, M. L., Mclain, K., Kier, A., Swerdlow, S. H., Schreiner, C. M., Miller, T. A., et al. (1991). A functional c-myb Gene is required for normal murine fetal hepatic hematopoiesis. *Cell* 65, 677–689.

Nagasawa, T., Hirota, S., Tachibana, K., Takakura, N., Nishikawa, S. I., Kitamura, Y., et al. (1996). Defects of B-cell lymphopoiesis and bone-marrow myelopoiesis in mice lacking the CXC chemokine PBSF/SDF-1. *Nature* 382, 635–638. doi: 10.1038/382635a0

Nakamura, Y., Hagiwara, T., Hosokawa, K., Iwasaki, H., Matsuoka, S., Takahashi, T., et al. (2007). Thrombopoietin/MPL signaling regulates hematopoietic stem cell quiescence and interaction with the osteoblastic niche. *Cell Stem Cell* 1, 685–697. doi: 10.1016/j.stem.2007.10.020

Nakashima, K., Zhou, X., Kunkel, G., Zhang, Z., Deng, J. M., Behringer, R. R., et al. (2002). The novel zinc finger-containing transcription factor osterix is required for osteoblast differentiation and bone formation. *Cell* 108, 17–29. doi: 10.1016/S0092-8674(01)00622-5

Nierhoff, D., Ogawa, A., Oertel, M., Chen, Y.-Q., and Shafritz, D. A. (2005). Purification and characterization of mouse fetal liver epithelial cells with high in vivo repopulation capacity. *Hepatology* 42, 130–139. doi: 10.1002/hep.20735

Nishina, H., Vaz, C., Billia, P., Nghiem, M., Sasaki, T., De la Pompa, J. L., et al. (1999). Defective liver formation and liver cell apoptosis in mice lacking the stress signaling kinase SEK1/MKK4. *Development* 126, 505–516.

Nitou, M., Ishikawa, K., and Shiojiri, N. (2000). Immunohistochemical analysis of development of desmin-positive hepatic stellate cells in mouse liver. *J. Anat.* 197, 635–646. doi: 10.1046/j.1469-7580.2000.19740635.x

Nitou, M., Sugiyama, Y., Ishikawa, K., and Shiojiri, N. (2002). Purification of fetal mouse hepatoblasts by magnetic beads coated with monoclonal anti-E-cadherin antibodies and their in vitro culture. *Exper. Cell Res.* 279, 330–343. doi: 10.1006/excr.2002.5615

Nomura, S., Ogami, K., Kawamura, K., Tsukamoto, I., Kudo, Y., Kanakura, Y., et al. (1997). Cellular localization of thrombopoietin mRNA in the liver by in situ hybridization. *Exp. Hematol.* 25, 565–572.

Nonaka, H., Tanaka, M., Suzuki, K., and Miyajima, A. (2007). Development of murine hepatic sinusoidal endothelial cells characterized by the expression of hyaluronan receptors. *Dev. Dyn.* 236, 2258–2267. doi: 10.1002/dvdy.21227

Omatsu, Y., Sugiyama, T., Kohara, H., Kondoh, G., Fujii, N., Kohno, K., et al. (2010). The essential functions of adipo-osteogenic progenitors as the hematopoietic stem and progenitor cell niche. *Immunity* 33, 387–399. doi: 10.1016/j.immuni.2010.08.017

Onitsuka, I., Tanaka, M., and Miyajima, A. (2010). Characterization and functional analyses of hepatic mesothelial cells in mouse liver development. *Gastroenterology* 138, 1525–1535. doi: 10.1053/j.gastro.2009.12.059

Ottersbach, K., and Dzierzak, E. (2005). The murine placenta contains hematopoietic stem cells within the vascular labyrinth region. *Dev. Cell* 8, 377–387. doi: 10.1016/j.devcel.2005.02.001

Palis, J., Chan, R. J., Koniski, A., Patel, R., Starr, M., and Yoder, M. C. (2001). Spatial and temporal emergence of high proliferative potential hematopoietic precursors during murine embryogenesis. *Proc. Natl. Acad. Sci. U.S.A.* 98, 4528–4533. doi: 10.1073/pnas.071002398

Palis, J., Robertson, S., Kennedy, M., Wall, C., and Keller, G. (1999). Development of erythroid and myeloid progenitors in the yolk sac and embryo proper of the mouse. *Development* 126, 5073–5084.

Park, L. S., Friend, D. J., Schmierer, A. E., Dower, S. K., and Namen, A. E. (1990). Murine interleukin 7 (IL-7) receptor: characterization on an IL-7-dependent Cell Line. *J. Exper. Med.* 171, 1073–1089. doi: 10.1084/jem.171.4.1073

Pei, W., Feyerabend, T. B., Rössler, J., Wang, X., Postrach, D., Busch, K., et al. (2017). Polylox barcoding reveals haematopoietic stem cell fates realized *in vivo*. *Nature* 548, 456–460. doi: 10.1038/nature23653

Peschon, J. J., Morrissey, P. J., Grabstein, K. H., Ramsdell, F. J., Maraskovsky, E., Gliniak, B. C., et al. (1994). Early lymphocyte expansion is severely impaired in interleukin 7 receptor-deficient mice. *J. Exp. Med.* 180, 1955–1960. doi: 10.1084/jem.180.5.1955

Petit-Cocault, L., Volle-Challier, C., Fleury, M., Peault, B., and Souyri, M. (2007). Dual role of Mpl receptor during the establishment of definitive hematopoiesis. *Development* 134, 3031–3040. doi: 10.1242/dev.001818

Pinho, S., and Frenette, P. S. (2019). Haematopoietic stem cell activity and interactions with the niche. *Nat. Rev. Mol. Cell Biol.* 20, 303–320. doi: 10.1038/s41580-019-0103-9

Pinho, S., Lacombe, J., Hanoun, M., Mizoguchi, T., Bruns, I., Kunisaki, Y., et al. (2013). PDGFRα and CD51 mark human Nestin+ sphere-forming mesenchymal stem cells capable of hematopoietic progenitor cell expansion. *J. Exper. Med.* 210, 1351–1367. doi: 10.1084/jem.20122252

Ploemacher, R. E., and van Soest, P. L. (1977). Morphological investigation on phenylhydrazine-induced erythropoiesis in the adult mouse liver. *Cell Tissue Res.* 178, 435–461. doi: 10.1007/bf00219567

Prior, N., Hindley, C. J., Rost, F., Esteban, E. M., Lau, W. W. Y., Göttgens, B., et al. (2018). Lgr5+ stem/progenitor cells reside at the apex of the embryonic hepatoblast pool. *bioRxiv* [Preprint]. doi: 10.1101/485870

Qian, H., Buza-Vidas, N., Hyland, C. D., Jensen, C. T., Antonchuk, J., Månsson, R., et al. (2007). Critical role of thrombopoietin in maintaining adult quiescent hematopoietic stem cells. *Cell Stem Cell* 1, 671–684. doi: 10.1016/j.stem.2007.10.008

Ramond, C., Berthault, C., Burlen-Defranoux, O., De Sousa, A. P., Guy-Grand, D., Vieira, P., et al. (2014). Two waves of distinct hematopoietic progenitor cells colonize the fetal thymus. *Nat. Immunol.* 15, 27–35. doi: 10.1038/ni.2782

Ramsfjell, V., Borge, O. J., Veiby, O. P., Cardier, J., Murphy, M. J., Lyman, S. D., et al. (1996). Thrombopoietin, but not erythropoietin, directly stimulates multilineage growth of primitive murine bone marrow progenitor cells in synergy with early acting cytokines: distinct interactions with the ligands for c-kit and FLT3. *Blood* 88, 4481–4492.

Rhodes, K. E., Gekas, C., Wang, Y., Lux, C. T., Francis, C. S., Chan, D. N., et al. (2008). The emergence of hematopoietic stem cells is initiated in the placental vasculature in the absence of circulation. *Cell Stem Cell* 2, 252–263. doi: 10.1016/j.stem.2008.01.001

Rieger, M. A., Hoppe, P. S., Smejkal, B. M., Eitelhuber, A. C., and Schroeder, T. (2009). Hematopoietic cytokines can instruct lineage choice. *Science* 325, 217–218. doi: 10.1126/science.1171461

Robin, C., Bollerot, K., Mendes, S., Haak, E., Crisan, M., Cerisoli, F., et al. (2009). Human placenta is a potent hematopoietic niche containing hematopoietic stem and progenitor cells throughout development. *Cell Stem Cell* 5, 385–395. doi: 10.1016/j.stem.2009.08.020

Rodriguez-Fraticelli, A. E., Wolock, S. L., Weinreb, C. S., Panero, R., Patel, S. H., Jankovic, M., et al. (2018). Clonal analysis of lineage fate in native haematopoiesis. *Nature* 553, 212–216. doi: 10.1038/nature25168

Roy, V., and Verfaillie, C. M. (1999). Expression and function of cell adhesion molecules on fetal liver, cord blood and bone marrow hematopoietic progenitors: implications for anatomical localization and developmental stage specific regulation of hematopoiesis. *Exp. Hematol.* 27, 302–312. doi: 10.1016/S0301-472X(98)00031-9

Rubin, J. B., Shia, M. A., and Pilch, P. F. (1983). Stimulation of tyrosine-specific phosphorylation in vitro by insulin-Like growth factor I. *Nature* 305, 438–440. doi: 10.1038/305438a0

Ruggeri, A., Labopin, M., Sormani, M. P., Sanz, G., Sanz, J., Volt, F., et al. (2014). Engraftment kinetics and graft failure after single umbilical cord blood transplantation using a myeloablative conditioning regimen. *Haematologica* 99, 1509–1515. doi: 10.3324/haematol.2014.109280

Ryu, K. Y., Park, H., Rossi, D. J., Weissman, I. L., and Kopito, R. R. (2012). Perturbation of the hematopoietic system during embryonic liver development due to disruption of polyubiquitin gene Ubc in mice. *PLoS One* 7:32956. doi: 10.1371/journal.pone.0032956

Sacchetti, B., Funari, A., Michienzi, S., Di Cesare, S., Piersanti, S., Saggio, I., et al. (2007). Self-renewing osteoprogenitors in bone marrow sinusoids can organize a hematopoietic microenvironment. *Cell* 131, 324–336. doi: 10.1016/j.cell.2007.08.025

Sauvageau, G., Iscove, N. N., and Humphries, R. K. (2004). In vitro and in vivo expansion of hematopoietic stem cells. *Oncogene* 23, 7223–7232. doi: 10.1038/sj.onc.1207942

Sawyer, S. T., Krantz, S. B., and Luna, J. (1987). Identification of the receptor for erythropoietin by cross-linking to Friend virus-infected erythroid cells. *Proc. Natl. Acad. Sci. U.S.A.* 84, 3690–3694. doi: 10.1073/pnas.84.11.3690

Schofield, R. (1978). The relationship between the spleen colony-forming cell and the haemopoietic stem cell. *Blood Cells* 4, 7–25.

Schumann, K., Lämmermann, T., Bruckner, M., Legler, D. F., Polleux, J., Spatz, J. P., et al. (2010). Immobilized chemokine fields and soluble chemokine gradients cooperatively shape migration patterns of dendritic cells. *Immunity* 32, 703–713. doi: 10.1016/j.immuni.2010.04.017

Schuster, J. A., Stupnikov, M. R., Ma, G., Liao, W., Lai, R., Ma, Y., et al. (2012). Expansion of hematopoietic stem cells for transplantation: current perspectives. *Exper. Hematol. Oncol.* 1:12. doi: 10.1186/2162-3619-1-12

Semenza, G. L., Koury, S. T., Nejfelt, M. K., Gearhart, J. D., and Antonarakis, S. E. (1991). Cell-type-specific and hypoxia-inducible expression of the human erythropoietin gene in transgenic mice. *Proc. Natl. Acad. Sci. U.S.A.* 88, 8725–8729. doi: 10.1073/pnas.88.19.8725

Severn, C. B. (1971). A morphological study of the development of the human liver. I. Development of the hepatic diverticulum. *Am. J. Anat.* 131, 133–158. doi: 10.1002/aja.1001310202

Shiojiri, N., and Sugiyama, Y. (2004). Immunolocalization of extracellular matrix components and integrins during mouse liver development. *Hepatology* 40, 346–355. doi: 10.1002/hep.20303

Sigurdsson, V., Takei, H., Soboleva, S., Radulovic, V., Galeev, R., and Siva, K. (2016). Bile acids protect expanding hematopoietic stem cells from unfolded protein stress in fetal liver short article bile acids protect expanding hematopoietic stem cells from unfolded protein stress in fetal liver. *Stem Cell* 18, 522–532. doi: 10.1016/j.stem.2016.01.002

Soares-da-Silva, F., Burlen-Defranoux, O., Elsaid, R., Iturri, L., Freyer, L., Sismeiro, O., et al. (2020). Yolk sac erythromyeloid progenitors sustain erythropoiesis throughout embryonic life. *bioRxiv* [Preprint]. doi: 10.1101/2020.02.27.968230

Solar, G. P., Kerr, W. G., Zeigler, F. C., Hess, D., Donahue, C., Sauvage, F. J., et al. (1998). Role of c-mpl in early hematopoiesis. *Blood* 92, 4–10.

Stier, S., Ko, Y., Forkert, R., Lutz, C., Neuhaus, T., Grunewald, E., et al. (2005). Osteopontin is a hematopoietic stem cell niche component that negatively regulates stem cell pool size. *J. Exper. Med.* 201, 1781–1791. doi: 10.1084/jem.20041992

Sudo, T., Ito, M., Ogawa, Y., Iizuka, M., Kodama, H., Kunisada, T., et al. (1989). Interleukin 7 production and function in stromal cell-dependent B cell development. *J. Exp. Med.* 170, 333–338. doi: 10.1084/jem.170.1.333

Sugiyama, D., Kulkeaw, K., and Mizuochi, C. (2013). TGF-beta-1 up-regulates extra-cellular matrix production in mouse hepatoblasts. *Mech. Dev.* 130, 195–206. doi: 10.1016/j.mod.2012.09.003

Sugiyama, D., Kulkeaw, K., Mizuochi, C., Horio, Y., and Okayama, S. (2011). Hepatoblasts comprise a niche for fetal liver erythropoiesis through cytokine production. *Biochem. Biophys. Res. Commun.* 410, 301–306. doi: 10.1016/j.bbrc.2011.05.137

Sugiyama, T., Kohara, H., Noda, M., and Nagasawa, T. (2006). Maintenance of the hematopoietic stem cell pool by CXCL12-CXCR4 chemokine signaling in bone marrow stromal cell niches. *Immunity* 25, 977–988. doi: 10.1016/j.immuni.2006.10.016

Sugiyama, Y., Koike, T., and Shiojiri, N. (2010a). Developmental changes of cell adhesion molecule expression in the fetal mouse liver. *Anat. Rec.* 293, 1698–1710. doi: 10.1002/ar.21204

Sugiyama, Y., Takabe, Y., Nakakura, T., Tanaka, S., Koike, T., and Shiojiri, N. (2010b). Sinusoid development and morphogenesis may be stimulated by VEGF-Flk-1 signaling during fetal mouse liver development. *Dev. Dyn.* 239, 386–397. doi: 10.1002/dvdy.22162

Sun, J., Ramos, A., Chapman, B., Johnnidis, J. B., Le, L., Ho, Y.-J., et al. (2014). Clonal dynamics of native haematopoiesis. *Nature* 514, 322–327. doi: 10.1038/nature13824

Suzuki, A., Zheng, Y. W., Kondo, R., Kusakabe, M., Takada, Y., Fukao, K., et al. (2000). Flow-cytometric separation and enrichment of hepatic progenitor cells in the developing mouse liver. *Hepatology* 32, 1230–1239. doi: 10.1053/jhep.2000.20349

Swartley, O. M., Foley, J. F., Livingston, D. P., Cullen, J. M., and Elmore, S. A. (2016). Histology atlas of the developing mouse hepatobiliary hemolymphatic vascular system with emphasis on embryonic days 11.5-18.5 and early postnatal development. *Toxicol. Pathol.* 44, 705–725. doi: 10.1177/0192623316630836

Tajer, P., Pike-Overzet, K., Arias, S., Havenga, M., and Staal, F. (2019). Ex vivo expansion of hematopoietic stem cells for therapeutic purposes: lessons from development and the niche. *Cells* 8:169. doi: 10.3390/cells8020169

Takabe, Y., Yagi, S., Koike, T., and Shiojiri, N. (2012). Immunomagnetic exclusion of E-cadherin-positive hepatoblasts in fetal mouse liver cell cultures impairs morphogenesis and gene expression of sinusoidal endothelial cells. *J. Anat.* 221, 229–239. doi: 10.1111/j.1469-7580.2012.01532.x

Takashima, Y., Terada, M., Kawabata, M., and Suzuki, A. (2015). Dynamic three-dimensional morphogenesis of intrahepatic bile ducts in mouse liver development. *Hepatology* 61, 1003–1011. doi: 10.1002/hep.27436

Takebe, T., Enomura, M., Yoshizawa, E., Kimura, M., Koike, H., Ueno, Y., et al. (2015). Vascularized and complex organ buds from diverse tissues via mesenchymal cell-driven condensation. *Cell Stem Cell* 16, 556–565. doi: 10.1016/j.stem.2015.03.004

Tamplin, O. J., Durand, E. M., Carr, L. A., Childs, S. J., Hagedorn, E. J., Li, P., et al. (2015). Hematopoietic stem cell arrival triggers dynamic remodeling of the perivascular niche. *Cell* 160, 241–252. doi: 10.1016/j.cell.2014.12.032

Tan, K. S., Kulkeaw, K., Nakanishi, Y., and Sugiyama, D. (2017). Expression of cytokine and extracellular matrix mRNAs in fetal hepatic stellate cells. *Genes Cells* 22, 836–844. doi: 10.1111/gtc.12517

Tanaka, M., Okabe, M., Suzuki, K., Kamiya, Y., Tsukahara, Y., Saito, S., et al. (2009). Mouse hepatoblasts at distinct developmental stages are characterized by expression of EpCAM and DLK1: drastic change of EpCAM expression during liver development. *Mech. Dev.* 126, 665–676. doi: 10.1016/j.mod.2009.06.939

Tanaka, Y., Kurosawa, S., Tajima, K., Tanaka, T., Ito, R., Inoue, Y., et al. (2016). Analysis of non-relapse mortality and causes of death over 15 years following allogeneic hematopoietic stem cell transplantation. *Bone Marrow Transplant.* 51, 553–559. doi: 10.1038/bmt.2015.330

Taniguchi, H., Toyoshima, T., Fukao, K., and Nakauchi, H. (1996). Presence of hematopoietic stem cells in the adult liver. *Nat. Med.* 2, 198–203. doi: 10.1038/nm0296-198

Tanimizu, N., Kaneko, K., Itoh, T., Ichinohe, N., Ishii, M., Mizuguchi, T., et al. (2016). Intrahepatic bile ducts are developed through formation of homogeneous continuous luminal network and its dynamic rearrangement in mice. *Hepatology* 64, 175–188. doi: 10.1002/hep.28521

Tanimizu, N., Miyajima, A., and Mostov, K. E. (2009). Liver progenitor cells fold up a cell monolayer into a double-layered structure during tubular morphogenesis. *Mol. Biol. Cell* 20, 2486–2494. doi: 10.1091/mbc.e08-02-0177

Tanimizu, N., Nishikawa, M., Saito, H., Tsujimura, T., and Miyajima, A. (2003). Isolation of hepatoblasts based on the expression of Dlk/Pref-1. *J. Cell Sci.* 116, 1775–1786. doi: 10.1242/jcs.00388

Tanimizu, N., Saito, H., Mostov, K., and Miyajima, A. (2004). Long-term culture of hepatic progenitors derived from mouse Dlk+ hepatoblasts. *J. Cell Sci.* 117, 6425–6434. doi: 10.1242/jcs.01572

Taoudi, S., Gonneau, C., Moore, K., Sheridan, J. M., Blackburn, C. C., Taylor, E., et al. (2008). Extensive hematopoietic stem cell generation in the AGM region via maturation of VE-Cadherin+CD45+ pre-definitive HSCs. *Cell Stem Cell* 3, 99–108. doi: 10.1016/j.stem.2008.06.004

Taoudi, S., Morrison, A. M., Inoue, H., Gribi, R., Ure, J., and Medvinsky, A. (2005). Progressive divergence of definitive haematopoietic stem cells from the endothelial compartment does not depend on contact with the foetal liver. *Development* 132, 4179–4191. doi: 10.1242/dev.01974

Tavian, M., Coulombel, L., Luton, D., Clemente, H. S., Dieterlen-Lièvre, F., and Péault, B. (1996). Aorta-associated CD34+ hematopoietic cells in the early human embryo. *Blood* 87, 67–72.

Tavian, M., Hallais, M. F., and Péault, B. (1999). Emergence of intraembryonic hematopoietic precursors in the pre-liver human embryo. *Development* 126, 793–803.

Terada, T., and Nakanuma, Y. (1995). Detection of apoptosis and expression of apoptosis-related proteins during human intrahepatic bile duct development. *Am. J. Pathol.* 146, 67–74.

Tremblay, K. D., and Zaret, K. S. (2005). Distinct populations of endoderm cells converge to generate the embryonic liver bud and ventral foregut tissues. *Dev. Biol.* 280, 87–99. doi: 10.1016/j.ydbio.2005.01.003

Tsai, S., Emerson, S. G., Sieff, C. A., and Nathan, D. G. (1986). Isolation of a human stromal cell strain secreting hemopoietic growth factors. *J. Cell. Physiol.* 127, 137–145. doi: 10.1002/jcp.1041270117

Tsuneto, M., Tokoyoda, K., Kajikhina, E., Hauser, A. E., Hara, T., Tani-ichi, S., et al. (2013). B-cell progenitors and precursors change their microenvironment in fetal liver during early development. *Stem Cells* 31, 2800–2812. doi: 10.1002/stem.1421

Van Eyken, P., Sciot, R., Callea, F., Steen, K., Van Der Moerman, P., and Desmet, V. J. (1988). The development of the intrahepatic bile ducts in man: a keratin-immunohistochemical study. *Hepatology* 8, 1586–1595. doi: 10.1002/hep.1840080619

Vestentoft, P. S., Jelnes, P., Hopkinson, B. M., Vainer, B., Møllgård, K., Quistorff, B., et al. (2011). Three-dimensional reconstructions of intrahepatic bile duct tubulogenesis in human liver. *BMC Dev. Biol.* 11:56. doi: 10.1186/1471-213X-11-56

Vigon, I., Mornon, J. P., Cocault, L., Mitjavila, M. T., Tambourin, P., Gisselbrecht, S., et al. (1992). Molecular cloning and characterization of MPL, the human homolog of the v- mpl oncogene: identification of a member of the hematopoietic growth factor receptor superfamily. *Proc. Natl. Acad. Sci. U.S.A.* 89, 5640–5644. doi: 10.1073/pnas.89.12.5640

Wake, K. (1971). "Sternzellen" in the liver: perisinusoidal cells with special reference to storage of vitamin A. *Am. J. Anat.* 132, 429–461. doi: 10.1002/aja.1001320404

Walasek, M. A., van Os, R., and de Haan, G. (2012). Hematopoietic stem cell expansion: challenges and opportunities. *Ann. N. Y. Acad. Sci.* 1266, 138–150. doi: 10.1111/j.1749-6632.2012.06549.x

Wang, H. U., Chen, Z. F., and Anderson, D. J. (1998). Molecular distinction and angiogenic interaction between embryonic arteries and veins revealed by ephrin-B2 and its receptor Eph-B4. *Cell* 93, 741–753. doi: 10.1016/S0092-8674(00)81436-1

Watanabe, H., Miyaji, C., Seki, S., and Abo, T. (1996). c-kit+ stem cells and thymocyte precursors in the livers of adult mice. *J. Exp. Med.* 184, 687–693. doi: 10.1084/jem.184.2.687

Wei, Q., and Frenette, P. S. (2018). Niches for hematopoietic stem cells and their progeny. *Immunity* 48, 632–648. doi: 10.1016/j.immuni.2018.03.024

Weidemann, A., and Johnson, R. S. (2009). Nonrenal regulation of EPO synthesis. *Kidney Int.* 75, 682–688. doi: 10.1038/ki.2008.687

Wilkinson, A. C., Igarashi, K. J., and Nakauchi, H. (2020). Haematopoietic stem cell self-renewal in vivo and ex vivo. *Nat. Rev. Genet.* 27, 273–278. doi: 10.1038/s41576-020-0241-0

Wilkinson, A. C., Ishida, R., Kikuchi, M., Sudo, K., Morita, M., Crisostomo, R. V., et al. (2019). Long-term ex vivo haematopoietic-stem-cell expansion allows nonconditioned transplantation. *Nature* 571, 117–121. doi: 10.1038/s41586-019-1244-x

Wilson, A., Laurenti, E., Oser, G., van der Wath, R. C., Blanco-Bose, W., Jaworski, M., et al. (2008). Hematopoietic stem cells reversibly switch from dormancy to self-renewal during homeostasis and repair. *Cell* 135, 1118–1129. doi: 10.1016/j.cell.2008.10.048

Wilson, W., Groat, C. S., and Leduc, E. H. (2006). Histogenesis of the liver. *Ann. N. Y. Acad. Sci.* 111, 8–24. doi: 10.1111/j.1749-6632.1963.tb36945.x

Wineman, J., Moore, K., Lemischka, I., and Müller-Sieburg, C. (1996). Functional heterogeneity of the hematopoietic microenvironment: rare stromal elements maintain long-term repopulating stem cells. *Blood* 87, 4082–4090.

Wittig, O., Paez-Cortez, J., and Cardier, J. E. (2010). Liver sinusoidal endothelial cells promote b lymphopoiesis from primitive hematopoietic cells. *Stem Cells Dev.* 19, 341–350. doi: 10.1089/scd.2009.0300

Wohrer, S., Knapp, D. J. H. F., Copley, M. R., Benz, C., Kent, D. G., Rowe, K., et al. (2014). Distinct stromal cell factor combinations can separately control hematopoietic stem cell survival, proliferation, and self-renewal. *Cell Rep.* 7, 1956–1967. doi: 10.1016/j.celrep.2014.05.014

Wolber, F. M., Leonard, E., Michael, S., Orschell-Traycoff, C. M., Yoder, M. C., and Srour, E. F. (2002). Roles of spleen and liver in development of the murine hematopoietic system. *Exp. Hematol.* 30, 1010–1019. doi: 10.1016/S0301-472X(02)00881-0

Yang, L., Li, L. C., Lamaoqiezhong, L., Wang, X., Wang, W. H., Wang, Y. C., et al. (2019). The contributions of mesoderm-derived cells in liver development. *Semin. Cell Dev. Biol.* 92, 63–76. doi: 10.1016/j.semcdb.2018.09.003

Yang, L., Wang, W. H., Qiu, W. L., Guo, Z., Bi, E., and Xu, C. R. (2017). A single-cell transcriptomic analysis reveals precise pathways and regulatory mechanisms underlying hepatoblast differentiation. *Hepatology* 66, 1387–1401. doi: 10.1002/hep.29353

Yarden, Y., Kuang, W. J., Yang-Feng, T., Coussens, L., Munemitsu, S., Dull, T. J., et al. (1987). Human proto-oncogene c-kit: a new cell surface receptor tyrosine kinase for an unidentified ligand. *EMBO J.* 6, 3341–3351. doi: 10.1002/j.1460-2075.1987.tb02655.x

Yu, V. W. C., and Scadden, D. T. (2016). Hematopoietic stem cell and its bone marrow niche. *Curr. Top. Dev. Biol.* 118, 21–44. doi: 10.1016/bs.ctdb.2016.01.009

Zhang, C. C., Kaba, M., Ge, G., Xie, K., Tong, W., Hug, C., et al. (2006). Angiopoietin-like proteins stimulate ex vivo expansion of hematopoietic stem cells. *Nat. Med.* 12, 240–245. doi: 10.1038/nm1342

Zhang, C. C., and Lodish, H. F. (2004). Insulin-like growth factor 2 expressed in a novel fetal liver cell population is a growth factor for hematopoietic stem cells. *Blood* 103, 2513–2521. doi: 10.1182/blood-2003-08-2955

Zheng, J., Huynh, H., Umikawa, M., Silvany, R., and Zhang, C. C. (2011). Angiopoietin-like protein 3 supports the activity of hematopoietic stem cells in the bone marrow niche. *Blood* 117, 470–479. doi: 10.1182/blood-2010-06-291716

Zheng, J., Umikawa, M., Cui, C., Li, J., Chen, X., Zhang, C. C. C., et al. (2012). Inhibitory receptors bind ANGPTLs and support blood stem cells and leukaemia development. *Nature* 485, 656–660. doi: 10.1038/nature11095

Zhou, B. O., Yue, R., Murphy, M. M., Peyer, J. G., and Morrison, S. J. (2014). Leptin-receptor-expressing mesenchymal stromal cells represent the main source of bone formed by adult bone marrow. *Cell Stem Cell* 15, 154–168. doi: 10.1016/j.stem.2014.06.008

Zorn, A. M. (2008). Liver development. *Stembook* 2, 1–26. doi: 10.3824/stembook.1.25.1

**Conflict of Interest:** The authors declare that the research was conducted in the absence of any commercial or financial relationships that could be construed as a potential conflict of interest.

*Copyright © 2020 Soares-da-Silva, Peixoto, Cumano and Pinto-do-Ó. This is an open-access article distributed under the terms of the Creative Commons Attribution License (CC BY). The use, distribution or reproduction in other forums is permitted, provided the original author(s) and the copyright owner(s) are credited and that the original publication in this journal is cited, in accordance with accepted academic practice. No use, distribution or reproduction is permitted which does not comply with these terms.*

# ANNEX III

frontiers in Cell and Developmental Biology

REVIEW
published: 16 December 2020
doi: 10.3389/fcell.2020.606642



## Hematopoiesis: A Layered Organization Across Chordate Species

*Ramy Elsaid[1,2,3†], Francisca Soares-da-Silva[1,2,3,4,5,6†], Marcia Peixoto[1,2,3,4,5], Dali Amiri[1,2,3], Nathan Mackowski[1,2,3], Pablo Pereira[1,2,3], Antonio Bandeira[1,2,3*] and Ana Cumano[1,2,3*]*

[1] Unit of Lymphocytes and Immunity, Immunology Department, Institut Pasteur, Paris, France, [2] INSERM U1223, Paris, France, [3] Université de Paris, Céllule Pasteur, Paris, France, [4] I3S—Instituto de Investigação e Inovação em Saúde and INEB—Instituto Nacional de Engenharia Biomédica, Universidade do Porto, Porto, Portugal, [5] Instituto de Ciências Biomédicas Abel Salazar, Universidade do Porto, Porto, Portugal, [6] Graduate Program in Areas of Basic and Applied Biology, Instituto de Ciências Biomeidicas Abel Salazar, Universidade do Porto, Porto, Portugal

OPEN ACCESS

***Edited by:***
*Emanuele Azzoni,*
*University of Milano Bicocca, Italy*

***Reviewed by:***
*Romualdo Ciau-Uitz,*
*University of Oxford, United Kingdom*
*Owen Tamplin,*
*University of Wisconsin-Madison, United States*
*Miguel Ganuza Fernandez,*
*Queen Mary University of London, United Kingdom*

****Correspondence:***
*Antonio Bandeira*
*antonio.bandeira-ferreira@pasteur.fr;*
*bandeira@pasteur.fr*
*Ana Cumano*
*ana.cumano@pasteur.fr*

*† These authors have contributed equally to this work*

***Specialty section:***
*This article was submitted to Stem Cell Research, a section of the journal Frontiers in Cell and Developmental Biology*

***Received:*** *15 September 2020*
***Accepted:*** *19 November 2020*
***Published:*** *16 December 2020*

***Citation:***
*Elsaid R, Soares-da-Silva F, Peixoto M, Amiri D, Mackowski N, Pereira P, Bandeira A and Cumano A (2020) Hematopoiesis: A Layered Organization Across Chordate Species. Front. Cell Dev. Biol. 8:606642. doi: 10.3389/fcell.2020.606642*

The identification of distinct waves of progenitors during development, each corresponding to a specific time, space, and function, provided the basis for the concept of a "layered" organization in development. The concept of a layered hematopoiesis was established by classical embryology studies in birds and amphibians. Recent progress in generating reliable lineage tracing models together with transcriptional and proteomic analyses in single cells revealed that, also in mammals, the hematopoietic system evolves in successive waves of progenitors with distinct properties and fate. During embryogenesis, sequential waves of hematopoietic progenitors emerge at different anatomic sites, generating specific cell types with distinct functions and tissue homing capacities. The first progenitors originate in the yolk sac before the emergence of hematopoietic stem cells, some giving rise to progenies that persist throughout life. Hematopoietic stem cell-derived cells that protect organisms against environmental pathogens follow the same sequential strategy, with subsets of lymphoid cells being only produced during embryonic development. Growing evidence indicates that fetal immune cells contribute to the proper development of the organs they seed and later ensure life-long tissue homeostasis and immune protection. They include macrophages, mast cells, some γδ T cells, B-1 B cells, and innate lymphoid cells, which have "non-redundant" functions, and early perturbations in their development or function affect immunity in the adult. These observations challenged the view that all hematopoietic cells found in the adult result from constant and monotonous production from bone marrow-resident hematopoietic stem cells. In this review, we evaluate evidence for a layered hematopoietic system across species. We discuss mechanisms and selective pressures leading to the temporal generation of different cell types. We elaborate on the consequences of disturbing fetal immune cells on tissue homeostasis and immune development later in life.

**Keywords: hematopoieisis, lymphopoieis, embryo, evo devo biology, layered**

## LAYERED HEMATOPOIESIS: A HISTORICAL PERSPECTIVE

Hematopoiesis, the process by which blood cells are produced, has been considered to be initiated by hematopoietic stem cells (HSC) that develop through multiple differentiation intermediates and give rise to all blood lineages. Recent studies have challenged this view by showing that specialized embryonic-derived subsets persist throughout life.

During embryogenesis, successive waves of mesoderm-derived hematopoietic progenitors contribute to the formation of erythroid, myeloid, and lymphoid lineages. In the 1920s, studies on embryonic hematopoiesis revealed that the first blood cells appear in the yolk sac (YS): red blood cells were found in clusters surrounded by an endothelial layer, named blood islands. The order of events that resulted in the formation of these structures led embryologists to hypothesize that both hematopoietic and endothelial cells had a common origin, a bipotent cell designated hemangioblast (see **Table 1**; Choi et al., 1998). In the 1970s, Moore and Owen (1967) showed that the embryonic day (E) 7 chicken YS generated mostly erythroid and also myeloid and lymphoid progeny after transplantation into irradiated embryos, pointing to a YS origin of HSCs. In mammals, the first single-cell assays showed the existence of multilineage progenitors in the YS, shortly after the beginning of circulation (Moore and Metcalf, 1970). Subsequent studies using chick–quail or chick–chick chimeras challenged the view that YS was the source of HSCs and showed that long-lasting hematopoietic potential was only found in intra-embryonic progenitors (Dieterlen-Lievre, 1975; Lassila et al., 1978). In mouse, culture of YS vs. the intra-embryonic aorta-gonad-mesonephros (AGM) region before the establishment of circulation demonstrated that the origin of HSCs is exclusively intra-embryonic (Cumano et al., 1996). It is now accepted that three waves of hematopoietic progenitors are generated in the mammalian embryo. The first wave is generated during gastrulation in the YS blood islands (Godin and Cumano, 2002). Soon after, a second wave of progenitors emerges in the YS vascular plexus (Frame et al., 2016). These two hematopoietic waves, which generate primitive and definitive erythrocytes, respectively, provide the oxygen needed for embryo survival as well as megakaryocytes and myeloid cells that are important for tissue remodeling and hemostasis. The third wave occurs in the great vessels of the embryo and generates HSCs that will migrate to the fetal liver (FL) where they expand (Ema and Nakauchi, 2000). This pool of HSCs will sustain hematopoiesis throughout adult life, generating not only erythroid and myeloid cells but also lymphoid cells.

The notion that YS populations are only produced and necessary during embryonic development has recently been challenged. Inducible lineage-tracing mouse models formally demonstrated that YS progenitors generate unique tissue-resident macrophage populations that persist throughout adulthood (Ginhoux et al., 2010; Gomez Perdiguero et al., 2015). These studies challenged the dogma that HSCs were the source of all hematopoietic lineages in the adult and provided evidence for the concept of a "layered" hematopoietic system.

Embryonic hematopoiesis is thus characterized by the partial overlap of distinct waves of progenitors that transit through different organs in embryonic and adult life. Each wave is well-orchestrated in time and space, each serving specific internal and external environmental needs. We will speculate on the selective advantages of a layered system across evolution that relates to hematopoiesis in general and to lymphopoiesis.

**Abbreviations:** a, anterior; AGM, aorta, gonads, mesonephros; BM, bone marrow; BMP4, bone morphogenic protein 4; c, cortical; CFC, colony-forming cells; CHT, caudal hematopoietic tissue; CLP, common lymphoid progenitor; CS, Carnegie stage; DA, dorsal aorta; DETC, dendritic epidermal T cells; DLP, dorsal lateral plate; dpf, days post-fertilization; E, embryonic day; EHT, endothelial-to-hematopoietic transition; EMP, erythromyeloid progenitors; Ery-P, primitive erythroid; Epo, erythropoietin; ES, embryonic stem; FL, fetal liver; HE, hemogenic endothelium; hpf, hours post-fertilization; HSC, hematopoietic stem cells; HIAC, hematopoietic intra-aortic clusters; ICM, intermediate cell mass; IL, interleukin; LMP, lympho-myeloid-restricted progenitors; LTi, lymphoid tissue inducer; m, medullary; p, posterior; PAF, para-aortic foci; PBI, posterior blood islands; PLM, posterior-lateral mesoderm; RA, retinoic acid; RBI, rostral blood islands; Shh, sonic hedgehog; TdT, terminal deoxynucleotidyl transferase; TEC, thymic epithelial cell; TSP, thymic seeding progenitors; VBI, ventral blood islands; YS, yolk sac.

## EMBRYONIC HEMATOPOIESIS IN DIFFERENT SPECIES: A COMMON STRATEGY TO MAKE BLOOD

### Foreword

Hemocytoblasts or primordial HSCs, derived from mesoderm, generate multiple hematopoietic cell types and are found across species starting in coelomic invertebrates. Key transcription factors that modulate the divergence of different hematopoietic cell types are conserved. For example, orthologs of *Gata*, *Fog*, and *Runx* have been identified in *Drosophila*. These transcription factors regulate the production of plasmatocytes, which exert phagocytic activity, granulocytes, with metabolic activity and immune function, and oxygen-transporting red blood cells (Evans et al., 2003; Hartenstein, 2006). In contrast, Metazoa without coelom are devoid of well-defined mesoderm and have a gelatinous matrix between ectoderm and endoderm enclosing large numbers of amoebocytes. These cells move using pseudopodia and fulfill functions that differ among species, ranging from defending the organism against pathogens, digesting food, or disposing of waste.

A major accomplishment in the transition of invertebrate to vertebrate metazoans was the development of a closed circulatory system and that of a centralized pumping organ, the heart, which ensures a rapid distribution of oxygen and nutrients to tissues, and the deployment of immune surveillance in the organism. Most invertebrates rely on myoepithelial cells with contractile capabilities to ensure that cells transit from the hemal spaces (fluid-filled sinus without a lining) and channels to the tissues, collectively designated as an open circulatory system (Muñoz-Chápuli et al., 2005; Hartenstein, 2006). However, there are several exceptions to this rule. For example, annelids have a closed

**TABLE 1 |** Glossary.

**Hemangioblast**. A bipotent hematopoietic and endothelial progenitor. The most common example is yolk sac blood islands in mice where primitive erythrocytes and the endothelial cells lining these structures are thought to have a common progenitor. In the mouse embryo, multiple progenitors contribute to blood island formation, and therefore, their common origin remains to be formally demonstrated.
**Endothelial-to-hematopoietic transition (EHT)**. The process whereby cells with morphology, phenotype, and spatial position of endothelial cells convert into a hematopoietic cell. This process has been identified to be at the origin of erythromyeloid bipotent cells in the vasculature of the yolk sac and of multipotent hematopoietic stem cell progenitors in the dorsal aorta. This conversion has been clearly visualized in the zebrafish embryo and is independent of cell division. In the fish embryo, newly converted single hematopoietic cells appear to rapidly egress into the space between the vein and the artery. By contrast, in mammalian and chicken embryos, newly converted cells extensively expand *in situ* forming hematopoietic intra-aortic clusters budding into the lumen, before being released into blood circulation.
**Hemogenic endothelium**. Designates the endothelial cells in the yolk sac and dorsal aorta that have the capacity to convert into a hematopoietic cell through a process named EHT.
**Hematopoietic intra-aortic clusters (HIAC)**. Clusters of hematopoietic cells adjacent to the endothelium protruding in the lumen of the dorsal aorta after being generated through EHT. They are found in birds and mammalian embryos, but not in zebrafish.
**Primitive wave**. The first hematopoietic cells with a given identity. Designates the first hematopoietic cells that generate primitive erythrocytes. Primitive erythrocytes derive from erythroid progenitors in the YS blood islands and are large nucleated cells that express embryonic hemoglobins Hbb-bh1 and Hbb-y. This concept also includes macrophages and megakaryocytes.
**Definitive wave**. Refers to the hematopoietic cells that generate definitive erythrocytes. These are enucleated cells that express embryonic and adult forms of hemoglobin (Hbb-bh1 and Hbb-b1) but lack Hbb-y hemoglobin expression. They can originate from either erythromyeloid progenitors that derive from the YS or from hematopoietic stem cells of intra-embryonic origin, during embryonic or post-natal life, respectively.
**Somatic recombination**. Genomic recombination that occurs in somatic cells. It is the process whereby the genes coding for the antigen receptors in T and B lymphocytes are assembled from the random assortment of variable (V), diversity (D), and joining (J) elements on immunoglobulin heavy chain, TCRβ and TCRδ chains, or from V and J elements in Ig light chains, TCRα and TCRγ chains.
**T cell negative selection**. Elimination of T lymphocytes expressing a self-reactive antigen receptor occurring in the thymus. Negative selection is mediated through the interaction of immature thymocytes with thymic epithelial cells located in the thymic medulla (mTEC) and dendritic cells (DC) that express a large collection of tissue-specific peptides.
**Antigen receptor repertoire**. Collection of the diverse antigen receptors expressed by B or T lymphocytes and generated by somatic recombination (see above). The diversity of the antigen receptor repertoire is further increased by trimming of the ends of the segments and addition of nucleotides without templated (N sequence addition) prior to the joining.
**Tolerance**. The absence of reactivity toward a given antigenic determinant. Often referred to self-tolerance, it designates the absence of lymphocytes that recognize antigen determinants from the organism where they reside. Defective tolerance induction results in autoimmune disorders.

circulatory system with pumping muscular blood vessels. Molluscs, instead, have an open circulatory system and one (or several) centralized hearts composed of cavities (atria and ventricles).

The emergence of a closed circulatory system with a centralized heart is linked to the appearance of vascular endothelial cells, the origin of which has long been a matter of debate. It was hypothesized that endothelial cells originate from the amoebocytes that, in acoelomatic invertebrates, adhere to the basement membrane that lines the hemal cavities (Muñoz-Chápuli et al., 2005). This hypothesis links the development of endothelial and hematopoietic cells throughout vertebrate evolution. We analyzed here different model systems of chordates in which independent generations of hematopoietic cells and different primary hematopoietic organs have been documented (**Table 2**).

## Cephalochordates (Amphioxus)

The amphioxus are invertebrates that together with Tunicates stand in close phylogenetic proximity to vertebrates (Delsuc et al., 2006; **Figure 1**). They appear, therefore, to be the model of choice to understand the evolution of a circulatory system. Developmental studies in amphioxus demonstrated that their cardiac region is decentralized and that blood is pumped by contractile vessels throughout life. By contrast, analysis of orthologs of *Pax2/5/8*, together with those of key vessel and hematopoietic development markers *Flk1* and *Scl*, identified specific expression in an AGM-like region, thus pointing to a similar origin of hematopoietic cells in amphioxus and vertebrates (Pascual-Anaya et al., 2013). This hypothesis was reinforced by experiments showing that the treatment of amphioxus larva with retinoic acid (RA) inhibited the expression of hematopoietic genes, reminiscent of what was observed in zebrafish larva and mouse embryonic stem (ES) cells where treatment with RA inhibited primitive hematopoiesis (Pascual-Anaya et al., 2013). Altogether, these data indicate that despite lacking a centralized heart, amphioxus developed a process that resembles hemogenic endothelium (HE) and endothelial-to-hematopoietic transition (EHT) (see **Table 1**). These studies were performed up to the stage of 2 day-old larva and, therefore, do not allow to assert whether invertebrates also generate hematopoietic progenitors at independent sites.

## Tunicates

Tunicates are currently considered as the closest relatives to vertebrates (Delsuc et al., 2006; **Figure 1**). Unlike cephalochordates, they have a centralized pumping organ (the heart) and an established network of blood vessels (Rosental et al., 2020). They have, therefore, in the sessile adult animal, circulating blood cells composed of myeloid cells. They also have a progenitor compartment located in the endostyle, tentatively considered as a functional equivalent to the bone marrow (BM) (Rosental et al., 2018). Cells endowed with cytotoxic activity that reject allografts could represent the equivalent population to NK cells. There is presently no experimental evidence on the origin of these cells.

**TABLE 2 |** Models to study hematopoiesis.

| Species | Advantages | Disadvantages | Methodologies used for the study of hematopoiesis |
|---|---|---|---|
| Mouse | Broad availability of transgenic and gene-deficient strains | Species-specific differences in basic biology (e.g., replicative rate, DNA damage response, etc.)<br>Inbred mouse strains do not account with genetic diversity; the choice of a specific genetic background can influence the observed phenotype | *In vitro* clonal assays (CAFCs, LTC-IC, CFU assays)<br>Flow cytometry phenotyping<br>Functional repopulation assays (competitive and non-competitive transplantation assays)<br>Lineage tracing models<br>Clonal analysis of lineage fate in native hematopoiesis (Sun et al., 2014)<br>Single-cell transcriptomics and proteomic analysis |
| Human | Extensively characterized hematopoietic system<br>Higher translational value for clinical applications | Limited sources of human hematopoietic cells and tissues<br>Limited accessibility to steady-state human hematopoiesis: limited studies of human hematopoietic cells on their natural microenvironment; no clonal tracking possible out of transplantation setting<br>*In vivo* xenotransplantation murine models only capture part of the cell-intrinsic properties of human hematopoiesis<br>Cell-extrinsic aspects of human hematopoiesis are difficult to access and study<br>*In vivo* assays are time-consuming | Characterization of hematopoietic populations by surface markers expression—flow cytometry (Notta et al., 2011, 2016)<br>Evaluation of differentiation potential—*in vitro* colony-forming assays (Notta et al., 2016)<br>*In vivo* functional repopulation assays in immunodeficient mice—xenograft models (Kamel-Reid et al., 1989; Beer and Eaves, 2015)<br>Repopulation dynamics of HSCs in humans—post-transplantation clonal tracking (Scala and Aiuti, 2019)<br>Single-cell transcriptomics and proteomic analysis |
| Zebrafish | Rapid and external development<br>Embryo optical transparency<br>Easy high-resolution optical imaging in live animals<br>Large-scale genetic and chemical screens<br>Several transgenic lines available (reviewed in Stachura and Traver, 2016) | Lack of antibodies for phenotypic characterization<br>Lack of knock-in technologies<br>Need to establish breeding standards; Inbreed and outbreed depression | Genome targeting (ZFNs, TALENs, CRISPR, and morpholino-mediated gene knockdown) to produce mutants of interest (reviewed in Sertori et al., 2016)<br>Major blood lineages isolation by size and granularity using FACS (Traver et al., 2003)<br>Hematopoietic cell transplantation (Traver et al., 2003, 2004; Hess et al., 2013)<br>Stromal culture assays (Stachura et al., 2011; Wolf et al., 2017)<br>Clonal methylcellulose assays (Stachura et al., 2011)<br>Parabiotic embryos for cell migration and homing studies (Demy et al., 2013)<br>High-resolution time-lapse live imaging (e.g., Bertrand et al., 2010; Kissa and Herbomel, 2010)<br>Xenotransplantation (Hess and Boehm, 2016; Parada-Kusz et al., 2018)<br>*In vivo* lineage tracing (e.g., Murayama et al., 2006; Jin et al., 2007; He et al., 2020) |
| Axolotl | Neoteny (no metamorphosis)<br>Regeneration without scar tissue formation | Lack of antibodies for phenotypic characterization<br>Gene manipulation difficult to perform<br>Long periods of generation | Transplantation (Lopez et al., 2014) |
| Xenopus | Large embryo size<br>Lineage tracing strategies<br>Available chimeric procedures to determine cell origin | Lack of antibodies for phenotypic characterization<br>Gene manipulation difficult to perform | Chimeras (Du Pasquier et al., 1989)<br>Lineage tracing of blastomeres (Ciau-Uitz et al., 2000) |
| Chicken | Large egg size<br>Amenable to surgical manipulation<br>Quail–chicken chimeric system | Lack of antibodies for phenotypic characterization<br>Lack of growth factors for *in vitro* cultures<br>Gene manipulation technologies difficult to perform | Quail–chicken and chicken–chicken chimeras (Le Douarin, 1969)<br>Corio-allantoid transplantation (Yvernogeau and Robin, 2017)<br>Lineage tracing (Jaffredo et al., 2000) |

*DIC, differential interference contrast; FACS, fluorescence-activated cell sorting; TALENs, transcription activator-like effector nucleases; ZFNs, zinc finger nucleases.*

**TABLE 3 |** Hematopoietic waves.

| Species | Adult hematopoietic sites | Embryonic hematopoietic waves | Location | Potential |
|---|---|---|---|---|
| Mouse | Bone marrow<br>Spleen | Primitive | YS | Primitive erythrocytes, macrophage colony-forming cells, and megakaryocyte colony-forming cells (Palis et al., 1999) |
| | | Definitive | YS | Erythromyeloid progenitors (Palis et al., 1999; Bertrand et al., 2005) |
| | | | AGM | HSC (Cumano et al., 1996; Medvinsky and Dzierzak, 1996) |
| Human | Bone marrow | Primitive | YS | Primitive erythrocytes and myeloid cells (Tavian et al., 1999) |
| | | Definitive | YS | Erythromyeloid progenitors (Migliaccio et al., 1986) |
| | | | AGM | HSCs (Tavian et al., 1996) |
| Zebrafish | Kidney marrow (pronephros)<br>Thymus | Primitive | VLM, RBI | Primitive macrophages and granulocytes (Herbomel et al., 1999) |
| | | | PLM, ICM | Primitive erythrocytes (Dietrich et al., 1995; Thompson et al., 1998) |
| | | Definitive (transient) | PBI | Erythromyeloid progenitors (mammalian EMP-like) (Bertrand et al., 2007) |
| | | | | Lympho-myeloid and myeloid progenitors* (He et al., 2020) |
| | | | | CD4 Tαβ lymphocytes (HSC-independent) (Tian et al., 2017) |
| | | Definitive | VDA | |
| Axolotl | Spleen<br>Thymus | ? | ? | HSC (Bertrand et al., 2010; Kissa and Herbomel, 2010)<br>HSC? (Lopez et al., 2014) |
| Xenopus | Liver periphery (HSC)<br>Spleen<br>Bone marrow (GMP and lymphocytes)<br>Thymus | Primitive<br>Definitive<br>Definitive (HSC) | aVBI pVBI DLP | Primitive erythrocytes (Ciau-Uitz et al., 2010)<br>Definitive erythrocytes (Ciau-Uitz et al., 2010)<br>HSC (Ciau-Uitz et al., 2010) |
| Chicken | Bone marrow<br>Thymus<br>Bursa of Fabricius | Primitive | YS | Macrophages and erythrocytes |
| | | Definitive | Dorsal aorta | HSC (Yvernogeau and Robin, 2017) |

*BM, bone marrow; ICM, intermediate cell mass; HSCs, hematopoietic stem cells; PBI, posterior blood island; PLM, posterior-lateral mesoderm; VDA, ventral dorsal aorta; VLM, ventrolateral mesoderm; YS, yolk sac; VBI, ventral blood islands; DLP, dorsal lateral plate; GMP, granulocyte-macrophage progenitor. *Erythroid potential was not assessed for these progenitors.*

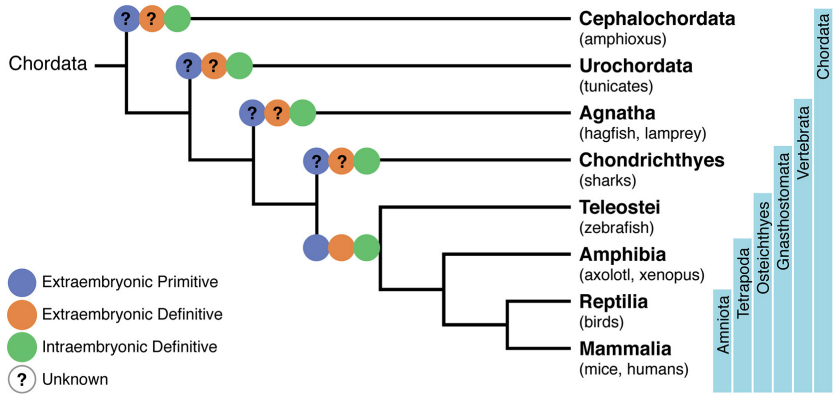


**FIGURE 1 |** Phylogenetic tree of chordates showing the evolutionary relationships of the hematopoietic system. A phylogeny representing Cephalochordata to Amniota, illustrating the development of a layered hematopoietic system with (i) yolk sac (YS) or extra-embryonic primitive hematopoietic cell generation in blue, (ii) YS definitive hematopoietic cell generation in orange, and (iii) intra-embryonic definitive hematopoiesis in green. Osteichthyes (which include zebrafish, axolotl, Xenopus, birds, mice, and humans) were the first where the distinct origins of hematopoietic cells have been demonstrated. Lack of information on specific processes are represented with a question mark.

## Agnathes or Jawless Chordates (Lampreys and Hagfish)

Lampreys possess circulating erythrocytes, myeloid and lymphoid cells, and were the most ancient vertebrates to show a robust adaptive immunity with the capacity to reject allografts, to produce specific antibodies, and to develop immunological memory. The molecular basis of this sophisticated immune system is a unique set of "building blocks" that encode lymphocyte antigen receptors (Pancer et al., 2004). They differ from those in higher vertebrates but are assembled in a similar manner, undergoing a process of somatic recombination (see **Table 1**) and exerting similar functions, illustrating an unprecedented example of parallel evolution. An independent site for T cell development, equivalent in function to the mammalian thymus, has been identified in the gills (Bajoghli et al., 2011). Lampreys have three different loci of the "building blocks" that encode antigen receptors of three distinct lymphoid cells reminiscent of the mammalian B, αβ-T, and γδ-T cells, indicating strong selective pressures for non-redundant functions of these different cell types (Boehm et al., 2018).

Lampreys develop through a complex life cycle with a larval stage, called ammocoetes, a metamorphosis that lasts for several months and an adult stage. In ammocoetes, the first hematopoietic cells are found in the typhlosole, which is a longitudinal fold of the intestinal inner wall, and also in the adipose tissue of the nephric fold. During metamorphosis, blood cell formation is displaced from these sites to the supra-neural body, a unique organ equivalent to the mammalian BM. The typhlosole is composed of mesenchymal cells located close to the dorsal aorta, and that form blood islands where the first hematopoietic cells are found. These hematopoietic cells appear by morphology to belong to the myeloid, erythroid, and lymphoid lineages and many of them are actively proliferating (Amemiya et al., 2007). Although it has proven difficult to identify, in lampreys, equivalent anatomical sites to the higher vertebrate YS or dorsal aorta (DA), it is possible that the first hematopoietic cells are generated in the typhlosole blood islands.

## Chondrichthyes or Cartilaginous Fish (Sharks)

Sharks are the most primitive organisms to have a functional adaptive immune system that is, unlike Agnathes, similar to that found in mammals. It is also in cartilaginous fish where the spleen is found for the first time in phylogeny and where hematopoietic progenitors were first detected and identified (Manca et al., 2018). It appears, therefore, that the spleen is the major hematopoietic organ already active in the embryo. The limited information concerning the hematopoietic development in these organisms suggests that HSC originated in the YS and transit later to the Leydig organ (located close to the esophagus) and to the spleen (Manca et al., 2019). In summary, there are different sites where hematopoiesis occurs over time, but the emergence of hematopoietic cells at multiple sites have not been documented.

## Teleosts or Bony Fish (Zebrafish)

Zebrafish (*Danio rerio*) is the most well-studied teleost species and has been an important model to study hematopoietic development, given that it is uniquely suitable for large-scale mutagenesis experiments, genome editing, chemical screenings, and high-resolution live imaging (**Table 2**).

Similar to other vertebrates, zebrafish hematopoiesis develops through successive waves emerging at different locations (**Table 3** and **Figure 2**). Contrary to mammals, birds, and other teleosts, zebrafish primitive hematopoiesis initiates intra-embryonically,

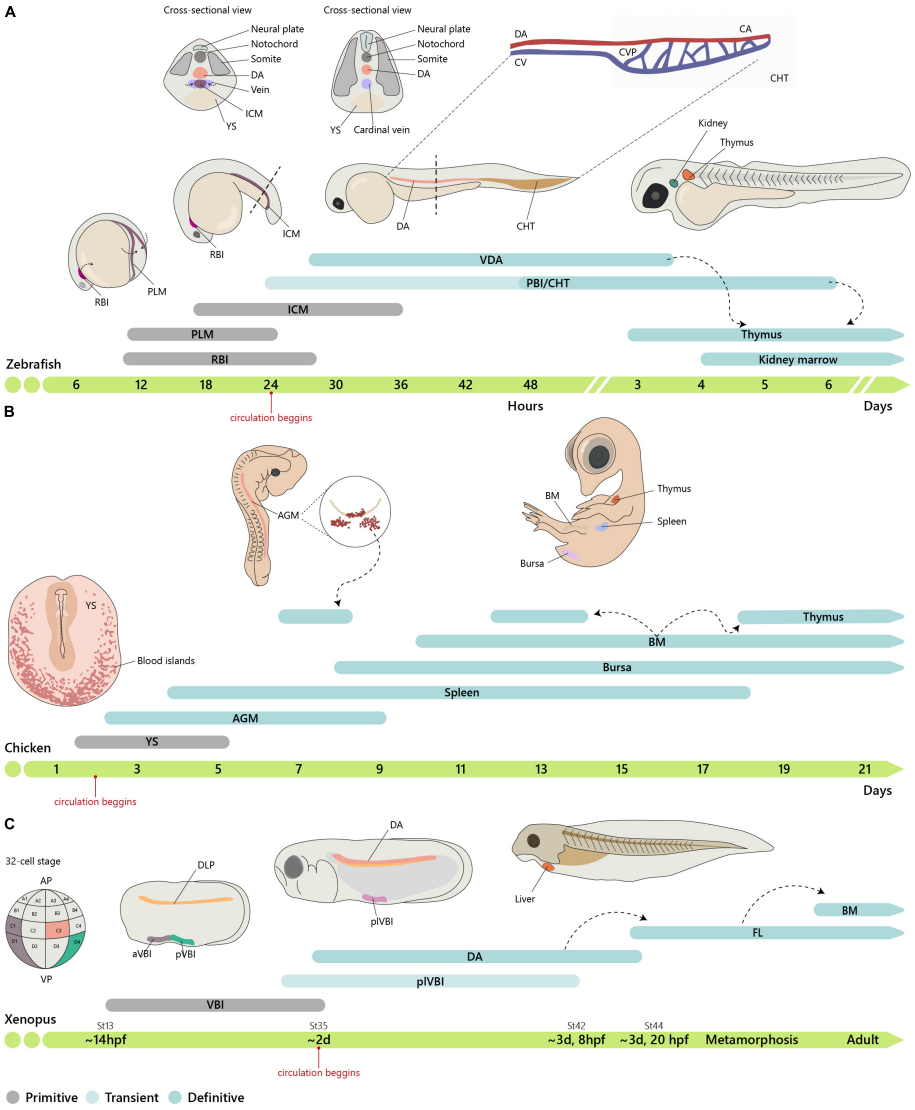


**FIGURE 2 |** Embryonic origin of the hematopoietic system. **(A)** Timeline of hematopoietic development in zebrafish. In zebrafish, primitive hematopoiesis occurs in the RBI and ICM region generating primitive macrophages and erythrocytes, respectively. The CHT, consisting of the CA (the continuation of the DA as it enters the tail), CV, and an endothelial network in between, the CVP, hosts a niche for HSC expansion and differentiation, reaching a peak at around E6. **(B)** In chicken, primitive hematopoiesis *at* E1.5 occurs in the YS blood islands. IAHCs are first detected at E2.25, reach a peak at E3, and gradually decrease, being residual at E5.5. PAF cells are detected at E2.5, rapidly surpassing the number of HIAC and last until around E9. **(C)** In Xenopus, the first hematopoietic site is the VBI (YS equivalent). Subsequent generation occurs after progenitor cells from the DLP migrate to the midline where they coalesce to give rise to the dorsal aorta (AGM). Cells from the two waves colonize the liver, which is the definitive site of hematopoiesis in both larval and adult stages. Xenopus were staged according to Nieuwkoop and Faber. See http://www.xenbase.org/anatomy/alldev.do for equivalences to dpf. AGM, aorta-gonad-mesonephros; aVBI, anterior VBI; BM, bone marrow; CA, caudal artery; CHT, caudal hematopoietic tissue; CVP, caudal vein plexus; DA, dorsal aorta; ICM, intermediate cell mass; FL, fetal liver; *PAF, para-aortic foci;* PBI, posterior blood island; PLM, posterior-lateral mesoderm; pVBI, posterior VBI; plVBI, posterior-lateral VBI; RBI, rostral blood islands; YS, yolk sac; VBI, ventral blood island.

in a structure known as intermediate cell mass (ICM). This structure results from the migration of two posterior bilateral stripes of lateral mesoderm (posterior-lateral mesoderm, PLM) to the trunk midline. It is in this structure where primitive erythroid progenitors and endothelial cells were found (Detrich et al., 1995; Thompson et al., 1998). Hematopoietic commitment, defined by the expression of the erythroid-specific transcription factor *Gata1*, occurs as early as the 2-somite stage [around 11 h post-fertilization (hpf)] in the PLM. Another site of primitive hematopoiesis was identified in the rostral blood island (RBI) region of the anterior mesoderm. This site produces macrophage-like cells that migrate into the yolk syncytial layer and disseminate through different tissues (Herbomel et al., 1999).

The DA resembles the mammalian AGM and was first suggested to harbor hematopoietic stem cell activity based on the identification of transcripts for the zebrafish orthologs of *cmyb*, *lmo2* (Thompson et al., 1998), and *runx1* (Kalev-Zylinska et al., 2002). Co-expression of these markers with vascular markers (*fli1*, *flk1*, and *flk4*) suggested they are hemangioblasts (Thompson et al., 1998). Challenging this idea, the emergence of definitive HSCs in the DA was directly visualized as an EHT mechanism where cells in endothelial position and morphology adopted a spherical shape and migrated ventrally toward the caudal vein (Bertrand et al., 2010). This process did not require cell division and EHT was taken as direct evidence for HSC originating from HE (Kissa and Herbomel, 2010).

The endothelial lineage branch to create HE before cells migrate across the ventral somites to reach the ventral aspect of the dorsal aorta (Kobayashi et al., 2014). This process involves the expression of adhesion molecules (Jam) that ensure the required strength of Notch signaling delivered by the somite cells (Kobayashi et al., 2014). Attempts to dissect the molecular events that shape EHT identified Runx1 as an essential player inducing the survival of newly generated hematopoietic cells (Kissa and Herbomel, 2010). Bmp4 is expressed in the ventral aspect of the dorsal aorta and promotes the hematopoietic stem cell program, whereas the expression of Shh in the roof maintains the arterial program (Wilkinson et al., 2009). More recently, it was shown that myeloid cells (Espín-Palazón et al., 2014) and metabolic alterations that promote inflammasome-induced IL1β-signaling in macrophages enhance HSC production, and inflammasome inhibition results in decreased hematopoietic generation (Frame et al., 2020). Taken together, these observations indicate that the EHT is a complex process involving several key molecular players and different cell types. The sequence of events and the precise molecular requirements essential for EHT remain largely incomplete, and attempts to recreate the conditions to promote EHT *in vitro* are still being developed (Gomes et al., 2018).

Contrary to mammals and birds, intra-aortic clusters were not observed in zebrafish and newly formed HSCs did not directly enter circulation (**Figure 3**). HSCs migrate and reside transiently in the posterior region in the tail, called caudal hematopoietic tissue (CHT) (Murayama et al., 2006). At earlier stages, before 36 hpf, this region, which also generates hematopoietic progenitor cells, independently of HSCs (discussed below), is more commonly referred as posterior blood island (PBI) and corresponds to the ventral portion of the tail immediately caudal to the yolk tube extension (Bertrand et al., 2007). Like the mammalian FL, the CHT environment promotes the expansion and differentiation of newly formed HSCs. This niche is modulated by the incoming hematopoietic cells that remodel the vascular niche (Tamplin et al., 2015). Migration of the hematopoietic cells toward the CHT depends on CxCL8/CXCR1 chemokine signaling that also promotes residency (Blaser et al., 2017); Klf6a promotes their maintenance and expansion in the CHT through CCL25b-Ccr7 chemokine signaling (Xu et al., 2015).

Fate-mapping studies revealed erythromyeloid progenitors (EMP), analogous to the mammalian EMP, arise at 24–30 hpf in the vascular plexus of the PBI (Bertrand et al., 2007). These cells have both erythroid and myeloid differentiation potentials but lack lymphoid potential. In mice, it is currently accepted that the microglia (brain-resident macrophages) are exclusively derived from the YS (Ginhoux et al., 2010; Gomez Perdiguero et al., 2015). By contrast, in zebrafish, embryonic/larval and adult microglia were shown to have different sources: the RBI, the YS equivalent for the former and the ventral wall of the DA for the latter (Xu et al., 2015). These differences may be species-specific and/or reflect different timing in the establishment of the blood–brain barrier.

Fate-mapping analysis using high temporal–spatial resolution cell labeling techniques identified two waves of T lymphopoiesis. One, which is HSC-independent, originates in the DA and PBI regions and generates predominantly CD4 αβ T cells found only in the larval stage. A later HSC-dependent wave develops from progenitors restricted to the DA and gives rise to various types of T cells from the larval stage up to adulthood (Tian et al., 2017). Lymphopoiesis is initiated in the thymus after 3 days post-fertilization (dpf), with the onset of *rag1* expression, although the first progenitor immigrants arrive in the thymus by 54 hpf (Kissa et al., 2008). Live imaging of these progenitors revealed that besides extravasation from the nearest vessels, most of them migrate to the thymus through the mesenchyme with remote sites of extravasation (Kissa et al., 2008). By 4 dpf, hematopoietic cells seed the kidney marrow (pronephros), the BM counterpart in the zebrafish, where they establish the adult hematopoietic system (Murayama et al., 2006).

## Amphibians (Axolotl and *Xenopus*)

Two major amphibian models have contributed to our understanding of biological processes. One is the urodele *Axolotl mexicanum*, a model of tissue regeneration without scar tissue formation. The other is the anuran *Xenopus laevis* (allotetraploid) and *tropicalis* (diploid) that are the most-studied amphibian model systems for vertebrate embryonic development, cell and molecular biology, immunology, and, more recently, evolutionary diversification following genome duplication.

## Axolotl

The *Axolotl mexicanum* has been used to study tissue regeneration without fibrosis. Although little is known of

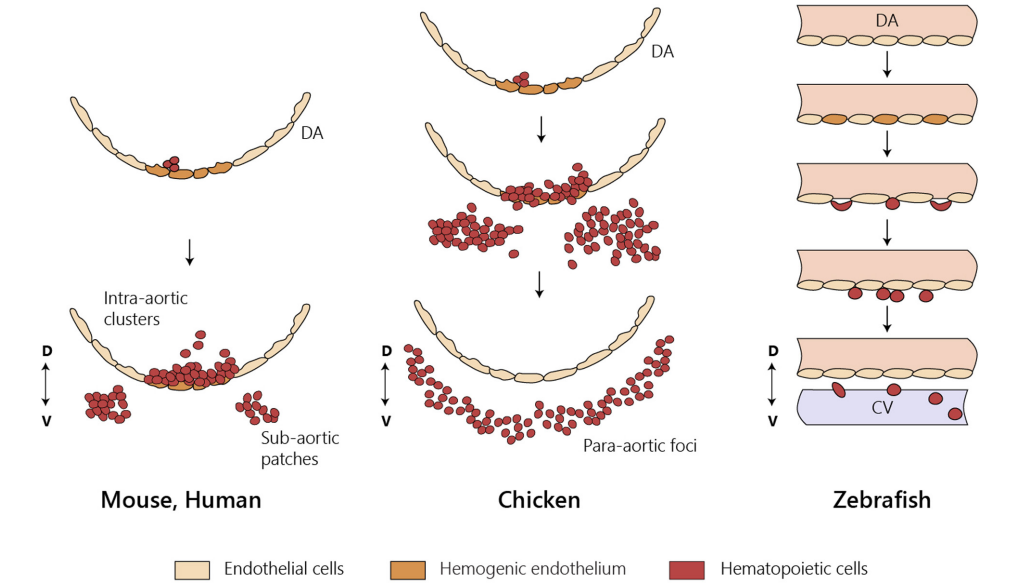


**FIGURE 3 |** HSC emergence at the dorsal aorta in mice, chicken, and zebrafish. Intra-embryonic hematopoietic clusters (IAHCs) containing newly formed HSCs in birds and in mammals. IAHC originate from PAF in chicken and sub-aortic patches in mice. Contrary to mammals and birds, IAHCs are not observed in zebrafish and newly formed HSCs do not enter directly into circulation. CV, caudal vein; D, dorsal; DA, dorsal aorta; V, ventral; PAF, para-aortic foci.

its hematopoietic system, this is nevertheless an interesting model to study hematopoiesis because, unlike *Xenopus*, adult animals retain many embryonic features (neoteny) and do not undergo a clear stage of metamorphosis. The main hematopoietic organs were recently identified (Lopez et al., 2014). Using cell transplantation assays with minimal graft-vs.-host reaction, it was shown that the liver is the first site of hematopoiesis. High expression of the lymphocyte-specific enzyme terminal deoxynucleotidyl transferase (TdT) was found transiently in the liver and later being restricted to the spleen (Golub et al., 2004) where it remains throughout life. So, like in other model systems lacking hematopoietic BM, the spleen is the adult hematopoietic organ. These recent advances, however, did not indicate the origin of the hematopoietic cells that colonize these organs.

## Frogs

The *Xenopus* model has been extensively used to study hematopoiesis because larval chimeras are easy to make and early embryos have large cells that can be marked and traced in fate-mapping studies (Ciau-Uitz and Patient, 2016). Natural polyploids have also been used as models to study the regulation of gene duplication and gene silencing and to identify donor and recipient cells in transplantation experiments (Du Pasquier et al., 1989). Transplantation and chimera experiments indicated that hematopoietic cells originate first in the ventral blood islands (VBI) and later in the tissues originated from the dorsal lateral plate (DLP) (Chen and Turpen, 1995). Lineage tracing experiments established that these two territories are independent. Thus, blastomeres from 32-cell stage embryos that contribute to the DLP and to adult HSCs do not contribute to VBI, and conversely, blastomeres that contribute to VBI do not participate in the generation of adult HSCs (Ciau-Uitz et al., 2000). The VBI, the equivalent site to the mammalian YS, comprises an initial anterior region (aVBI) where primitive erythrocytes are first found along with myeloid cells and, at later stages, a posterior VBI (pVBI) that contains definitive erythrocytes, myeloid cells, and, similar to what was found in the zebrafish, also lymphocytes (Smith et al., 1989; Turpen et al., 1997). A third wave of hematopoietic generation occurs in the AGM, formed by the midline migration of the DLP, with the emergence of HSC and hematopoietic intra-aortic clusters (HIAC) formation.

It has been proposed that in aVBI, hemangioblast-like cells are at the origin of the first hematopoietic cells (Ciau-Uitz et al., 2010). By contrast, hemangioblast-like cells were not found in the pVBI, and hematopoietic cells are produced through an EHT process similar to that operating in fish, birds, and mammals in the DA and large arteries. Thus, hematopoiesis in frogs appears to occur in three independent waves similar to bony fish, birds, and mammals. Recently, a fourth myeloid cell generation has

been described to occur in the mesenchyme posterior to the DLP (Imai et al., 2017).

The peripheral region of the liver was shown to be the primary hematopoietic organ throughout life containing HSC and erythroid progenitors, whereas the BM contains myeloid progenitors that respond to myeloid growth factors (Yaparla et al., 2019). Lymphocytes are produced in the thymus and the spleen in juvenile frogs, whereas the BM and the thymus have lymphopoietic activity in the adult (Greenhalgh et al., 1993).

## Birds

The large size and the easy manipulation of the avian fertilized egg allowed the construction of xenogeneic and congenic chimeras. The quail–chicken chimera system devised by Nicole Le Douarin combined with a rigorous identification of tissues originated from each species provided a reliable lineage-tracing tool (Le Douarin, 1969). Seminal experiments using this chimeric system established the intra-embryonic origin of HSC at a time when the YS was the consensual source of definitive hematopoiesis (Dieterlen-Lievre, 1975). Similar experiments using congenic chicken strains reinforced this notion (Lassila et al., 1978). The DA was soon designated as the site of origin of the hematopoietic progenitors of intra-embryonic origin because it harbored intra-aortic hematopoietic clusters (IAHC) comprising hematopoietic cells (Le Douarin and Dieterlen-Lièvre, 2013). IAHCs are the origin of another hematopoietic cell structure called para-aortic foci (PAF) formed later below the endothelial cell layer (**Figure 3**). A similar structure was described in the mouse and designated sub-aortic patches (Manaia et al., 2000). Cells within the IAHC or PAF contain HSC able of long-term reconstitution of the hematopoietic system (Dunon et al., 1998). Although it is presently difficult to phenotypically distinguish cells from the two structures, it is thought that PAF are an intermediate site where HSC mature before colonizing the thymus, the bursa of Fabricius, and the BM (Yvernogeau and Robin, 2017). The quail–chicken chimera system was also used to demonstrate the YS origin of most macrophages found in the central nervous system (microglia) (Cuadros et al., 1993).

Another important contribution from the Dieterlen-Lièvre group was the observation that two independent sources of endothelial cells contributed to the formation of the DA (Pardanaud et al., 1996). Thus, the roof and the sides of the DA are formed by endothelial cells originated in the somites whereas the floor of the DA, where hematopoietic cell generation occurs, is of splanchnopleural origin (ventral mesoderm). After hematopoietic cell generation, the endothelial cells in the floor of the DA are replaced by somite-derived cells similar to the remaining vessel wall (Pouget et al., 2006). This replacement process might not be evolutionarily conserved across vertebrates and is currently under investigation in other species. Additional experiments showed that expression of *Runx1* and activation of the Notch signaling pathway in HE required contact with the underlying mesenchymal cells. Both signals are essential for EHT, reinforcing the notion that EHT is an exceptional phenomenon that occurs under unique developmental conditions (Richard et al., 2013). Cell-labeling experiments targeting endothelial cells in embryos prior to IAHC emergence provided further evidence for an endothelial origin of the emerging hematopoietic cells (Jaffredo et al., 2000).

In summary, the chicken hematopoietic development also appears to occur in layers, although the precise contribution of YS to hematopoiesis has not been determined and no EMPs have been identified, either because they do not exist or because their identification was hampered by the absence of antibodies specific for the different hematopoietic lineages.

## Mice

The first hematopoietic cells arise in the mouse YS around E6.5–E7 in blood islands (Moore and Metcalf, 1970). Colony-forming assays identified bipotent erythroid/megakaryocyte (Xu et al., 2001; Tober et al., 2007) and macrophage progenitors (Palis et al., 1999) within these structures. Primitive erythroid progenitors (Ery-P) are exclusively present in the YS from E7.5 to E8.5 (Palis et al., 1999) and generate primitive erythrocytes. These primitive erythrocytes are larger than their BM counterparts and lack adult globin expression (Wong et al., 1986). Similar to other non-mammalian species, mouse Ery-P maintain their nucleus for several days (Kingsley et al., 2004). In contrast to those found in adult BM, primitive macrophages do not differentiate through a monocyte stage but directly from monopotent macrophage precursors (Mac-CFC/YS-Mp) (Bertrand et al., 2005).

The second hematopoietic wave starts at E8.5, with EMPs emerging from HE in the recently formed YS vascular bed, through a process of EHT (Goldie et al., 2008; Bertrand et al., 2010; McGrath et al., 2015; Frame et al., 2016; Kasaai et al., 2017). These progenitors proliferate extensively during the following 48 h and are found in circulation by E9 and in the hepatic primordium by E10.5 (Palis et al., 1999). This second wave generates definitive erythroid progenitors, the first mast cells, and bipotent macrophage granulocyte progenitors. Embryonic definitive erythrocytes can be found in circulation around E11.5–E12.5 and are distinguished from primitive erythrocytes by their small size (similar to adult erythrocytes) and the absence of nucleus. They originate from a novel population of progenitors of YS-EMP origin, recently identified, that ensures erythrocyte production and oxygenation up until birth (Soares-da-Silva et al. bioRxiv 2020.02.27.968230; doi: https://doi.org/10.1101/2020.02.27.968230).

Of note, the second hematopoietic wave generates tissue-resident macrophages (Gomez Perdiguero et al., 2015; Hoeffel et al., 2015). They have self-renewal ability and persist throughout life (Merad et al., 2002; Ajami et al., 2007; Jenkins et al., 2011).

The third and last wave of hematopoietic cell generation starts around E9.5, when multipotent progenitors emerge through EHT in the embryo DA and other large blood vessels (de Bruijn et al., 2000; Zovein et al., 2008; Boisset et al., 2010; Yzaguirre and Speck, 2016). Opposite to the first two hematopoietic waves, this third wave generates the progenitors of HSC and is the only capable to give rise to lymphocytes (Cumano et al., 1996; Medvinsky and Dzierzak, 1996). Similar to zebrafish, Notch signaling in the

mouse AGM is determinant for hematopoietic cell generation (Kumano et al., 2003), and YS-derived macrophages, which are the most represented mature cells in this location, have been shown to enhance HSC emergence (Mariani et al., 2019). The total number of hematopoietic cells generated in the AGM has been estimated to be in the order of several hundreds of cells (Godin et al., 1999; Ganuza et al., 2017). According to some authors, HSC can also be generated in extraembryonic structures such as the placenta (Gekas et al., 2005; Ottersbach and Dzierzak, 2005). HSC then migrate to the FL where they mature, proliferate [expanding by more than 30-fold (Ema and Nakauchi, 2000)], and differentiate. Although adult and embryonic HSCs produce all major blood cell types, some specific lymphoid lineages are only produced during embryonic development, namely, the dendritic epidermal T cells (DETC) ($V\gamma5^+$) (Ikuta et al., 1990), lymphoid tissue inducer (LTi) cells (Eberl et al., 2004), and a subset of IL-17-producer γδ T cells ($V\gamma6^+$) (Haas et al., 2012).

## Humans

The development of the human hematopoietic system also follows a layered strategy. The first hematopoietic cells are found in the YS [starting at around E16–18, Carnegie stage (CS) 7–8]. At this stage, $CD45^+$ cells are found in the cardiac cavities and mark the onset of circulation (Tavian et al., 1999). Whereas in mice the generation of hematopoietic cells and their detection in the FL and placenta are largely overlapping, in humans, the spatial–temporal progression of hematopoiesis is better discriminated (Ivanovs et al., 2017). In the YS, few megakaryocytes and macrophages are found in addition to erythrocytes. Although a population of EMP has not been formally identified, data suggests a second wave of hematopoietic cell emergence in the YS at around CS 13–15. IAHC emerge in the DA between CS 13 and 17 and $CD34^+CD45^+$ progenitors colonize the FL by CS 13, suggesting that HSC initiate liver colonization as they are generated (Tavian et al., 1996; Ivanovs et al., 2011). $CD34^+CD45^{lo}$ HSC are found in the placenta only after the 9th week of gestation (4 weeks after the first $CD34^+$ cells reach this site). For this reason, the placenta is not considered a site of HSC generation in humans. The BM formation in humans marks the end of the embryonic period (CS 23 or E56) and colonization by HSC is initiated shortly after, although the exact time of HSC activity in the BM remains undetermined. Like in the mouse, human HSC initially express endothelial and hematopoietic markers that together with the detection of IAHC suggest a generation through an EHT. Curiously, and unlike in mice, the umbilical artery does not appear to be a site of hematopoietic cell generation in humans (Ivanovs et al., 2011).

## An Evolutionarily Conserved Design

From the comparison of hematopoietic development across species, it appears that the sequential generation of different hematopoietic progenitors was an evolutionarily successful strategy. Establishment of circulation was the key step toward the establishment of a vertebrate hematopoietic system.

Paradoxically, the first hematopoietic cells to be produced are differentiated rather than multipotent progenitors and fulfill the most basic functions like oxygen delivery, hemostasis, and tissue remodeling. Overall, despite some variations, distinct YS and DA hematopoietic generations are well conserved. Although controversial (Ueno and Weissman, 2006), the notion that bipotent hemangioblast-like cells contribute to hematopoietic cell generation is associated with that of primitive erythrocytes, megakaryocytes, and macrophages that occur in the YS blood islands.

With tissue complexity, subsequent hematopoietic waves have to fulfill increasingly specialized functions, and for that, multipotent progenitors are better adapted to generate a diverse array of cells with specific and diversified functions.

Remarkably, gene expression analysis in cephalochordates led to the identification of HE (Pascual-Anaya et al., 2013), which places EHT process as ancient and highly conserved through phylogeny. EHT appears to be the mechanism operating in the generation of multipotent progenitors in late YS and in the AGM and the only one to contribute to HSC production.

There is a consistent contribution of YS to the microglia and other tissue-resident macrophages and to primitive erythrocytes (Godin and Cumano, 2002). It is also generally accepted that YS hematopoietic cells do not contribute to the lymphoid compartment, although some minor and transient lymphocyte subsets have been suggested to emerge in the YS (discussed below). Other sites of hematopoietic cell generation, the most discussed being the placenta (Gekas et al., 2005; Ottersbach and Dzierzak, 2005; Rhodes et al., 2008), have been proposed but are not consensual, and the allantois that was hypothesized to be an alternative hematopoietic site in the chicken was recently shown to have no contribution to HSC generation (Yvernogeau and Robin, 2017). Recent evidence points to a role of YS-derived macrophages in the generation of HSC (Mariani et al., 2019). It is tempting to speculate that a selective pressure for an early generation of this unique type of macrophages lies not only in their capacity to ensure general tissue homeostasis, as the embryo develops, but also in their contribution to HSC emergence. It remains to be determined whether the unique properties of YS-derived macrophages are cell autonomous or whether they are modulated by cues received from the environment where they reside.

As different hematopoietic cells emerge, they transit through different primary hematopoietic organs: the FL and later the BM or their equivalents in the different species. Due to the pronounced differences in cell composition of the primary hematopoietic organs, it is to be expected that the cues that hematopoietic progenitors receive are substantially different in distinct organs and that this may influence their development. A recent example of this selective pressure is the lower requirements for erythropoietin (Epo) of embryonic erythrocytes compared to those in BM. They develop in the FL where Epo concentrations are lower than those produced in the kidney of adults. The recent discovery that these embryonic erythrocytes are of YS origin and outcompete those of HSC origin in the FL exemplifies how the environment can select for progenitors of different origins in space and time (Soares-da-Silva et al. bioRxiv 2020.02.27.968230; doi: https://doi.org/10.1101/2020.02.27.968230). The generally low concentration

of other cytokines (i.e., IL-7) in FL also impacts lymphocyte development (see below).

## LYMPHOCYTE DEVELOPMENT: A STRATEGY DESIGNED FOR LIFE-LONG TISSUE HOMEOSTASIS AND IMMUNE PROTECTION

Lymphopoiesis, the process of lymphocyte generation, is the best-documented system where successive waves of progenitors differentiate and migrate to specific tissues thus generating the basis of a layered developmental organization. In this section, we will describe the development of embryonic lymphoid lineage populations and why they are selectively produced within an embryonic environment resulting in a diverse adult lymphoid compartment.

### B Cell Development

The "layered immune system" concept was initially proposed by Herzenberg (1989), with the identification of functionally distinct "lineages" of B cells that are generated during ontogeny. B-1a cells, which reside mainly in the peritoneal and pleural cavities and produce natural antibodies in a T cell-independent manner, are usually obtained from embryonic precursors and contribute to innate-like immunity (reviewed in Herzenberg, 2000; Montecino-Rodriguez and Dorshkind, 2012; Elsaid et al., 2019). There are different explanations for the unique capacity of fetal progenitors to generate specific lymphoid cells (**Figure 4**).

The identification of a specific B1 progenitor only found in the embryo led to the hypothesis that these cells could derive from progenitors distinct from those that generate classical B-2 B cells. Recent studies show that innate-like B and T cells preferentially originate from developmentally restricted progenitors (Beaudin et al., 2016). These cells are exclusively found in fetal and neonatal stages, suggesting that they represent a distinct lineage from HSC.

However, experiments of cellular barcoding coupled with transplantation showed that FL HSCs can generate both B-1a and B-2 cells and that the capacity to generate B-1a cells is lost during development and upon transplantation (Kristiansen et al., 2016). Moreover, it was recently shown that antigen receptor specificity is sufficient to induce cell proliferation and acquisition of the B-1 phenotype and function (Graf et al., 2019). Lin28b, a regulator of fetal hematopoiesis, is important in the generation of B1a lineage, and loss of its expression controls the switch from neonatal to adult B cell production (Vanhee et al., 2019). Low levels of IL-7, a cytokine crucial for adult B cell development, in FL favors the generation of B1, highlighting the impact of the microenvironment on the preferential production of particular cell types (Wong et al., 2019).

### Thymopoiesis

In the thymus, T lymphocyte differentiation occurs from hematopoietic progenitors migrating from either the FL or the BM at later developmental stages in a process called "thymopoiesis." In general, thymopoiesis resembles B lymphopoiesis in many ways, as it is also a stepwise process of rearrangement of antigen receptor genes and selection to ensure self-tolerance (Abramson and Anderson, 2017; Hosokawa and Rothenberg, 2020). The thymus produces T lymphocytes that are important for protection against environmental pathogens. Thymus architecture is key to T cell tolerance and a normal immune system. The first thymic seeding progenitors (TSP) that colonize the embryonic thymus display a unique capacity to generate innate and innate-like lymphocytes. These cells are required to shape the thymic architecture, thus ensuring life-long efficient T cell tolerance and avoiding autoimmunity (Elsaid et al., 2020).

The layered organization of thymopoiesis has been reported in all species studied from zebrafish to humans. During development, multiple waves of hematopoietic progenitors derived from distinct anatomical sites colonize the thymus. These waves give rise to T cells that fulfill distinct functions at distinct developmental stages. We will discuss below embryonic thymopoiesis across species and how cells from different waves contribute to diverse T cell compartments.

### Zebrafish

Fate-mapping analysis using high temporal–spatial resolution cell labeling techniques identified two waves of T cell progenitors: an early HSC-independent, from the DA and PBI regions, generating predominantly αβ T cells that do not persist beyond the larva stage and a late HSC-dependent T lymphopoiesis, restricted to the DA, giving rise to various types of T cells from the larval stage up to adulthood (Tian et al., 2017). This first wave shares two properties with the corresponding population in mice: they are important in thymic architecture and they differentiate fast (Hess and Boehm, 2012). In-depth characterization of the phenotype and function of T cells generated from this HSC-independent precursor is presently not available.

### Frogs

*Xenopus laevis* have two major hematopoietic organs, the liver, which is predominant in the larvae, and the spleen, the major hematopoietic organ in adult animals. B cells are produced in the liver in larval stages and the spleen takes over that function after metamorphosis (Du Pasquier et al., 1989). The diversity of the B cell repertoire is apparent in larvae and it is achieved through the combinatorial rearrangement of a large number VH, DH, and JH segments. Somatic hypermutation also operates in *Xenopus* larvae possibly as a response to the complex biota of their environment. Interestingly, terminal deoxynucleotidyl transferase (TdT) expression and N sequence additions are only detected after metamorphosis (Lee and Hsu, 1994), indicating further diversification of the antigen receptor repertoire (see **Table 1**) in adult animals.

Two waves of TSP, predominantly of DLP origin, have been identified during the larval stages. The first wave generates a transient population of T lymphocytes, whereas the progeny of the second wave persists in the adult (Turpen and Smith, 1989). It has been reported that T and B cells can also originate in the VBI (Smith et al., 1989). A third wave of progenitors enters the

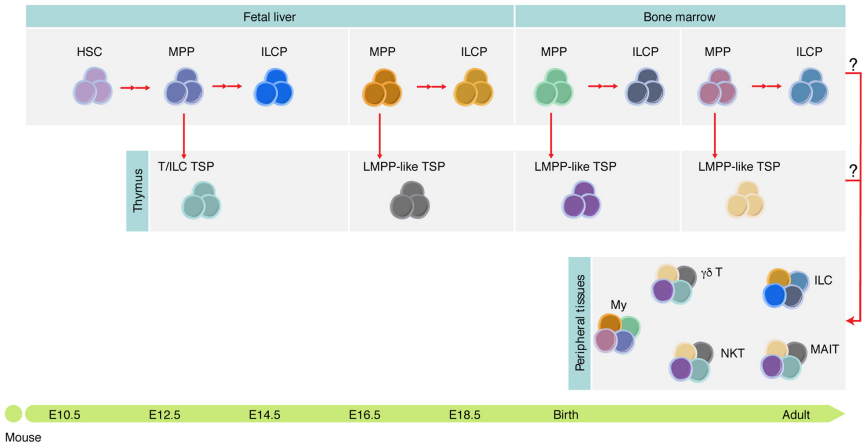


**FIGURE 4 |** Tissue-resident immune cells are mosaic of cells derived at different developmental stages. Different hematopoietic progenitors are generated during development, some of which contribute to the adult tissue-resident immune cell compartment diversity. It is still unknown which functions these cells play during development and whether they persist in adulthood. ILCP, ILC progenitor; My, myeloid cells; NKT, NK T cells; MAIT, mucosal-associated invariant T cells.

thymus at the beginning of metamorphosis and provides T cells throughout adult life.

In conclusion, T lymphopoiesis in frogs is organized in waves, and B and T lymphocytes with a limited repertoire diversity are produced early in embryonic life. The exposure of frog and fish larvae to a biota-rich environment compared to chicken and mammals might account for some differences in timing and the type of lymphocyte responses in the different species.

## Birds

An interesting and unique property of the chicken lymphoid development is that B cells develop in a unique environment called bursa of Fabricius where they acquire a diverse antigen receptor repertoire (Reynaud et al., 1987). Sequential transplantation of thymic lobes demonstrated for the first time that the embryonic thymus is discontinuously seeded by hematopoietic cells. In total, three waves of hematopoietic cells reach the thymus: the first at E6.5 and the third at E18, 1 day before hatching (Coltey et al., 1987). It was subsequently shown that the first wave of TSP is derived from cells located in the para-aortic clusters shortly after their generation in the DA. These observations raised the possibility that, in chickens, the first wave of TSP is composed of multipotent hematopoietic cells. The refractory periods where no hematopoietic progenitors reach the thymus are consequent to the absence of circulating progenitors because the injection in circulation of cells derived from para-aortic foci during refractory periods resulted in efficient thymic colonization (Dunon et al., 1998, 1999).

## Mice

Two waves of distinct TSP colonize the fetal thymus where they contribute to thymic organogenesis. First wave TSP are first detected around E12.5 and persist until E15.5. These progenitors differentiate rapidly, exhibit low proliferative capacity, express transcripts related to the ILC lineage, and are the only ones with the capacity to generate Vγ5$^+$ T cells and LTi cells. A second wave of more immature hematopoietic progenitors colonize the thymus after E15 and ensure thymopoiesis thereafter (**Figure 5**; Ramond et al., 2014; Elsaid et al., 2020).

The thymic rudiment is detected around E11.5 in the mouse embryo (Takahama et al., 2017). The thymic epithelial cells (TEC) divide into cortical TEC (cTEC) and medullary TEC (mTEC). Aire$^+$ mTECs ensure the expression of tissue-specific peptides that mediate T cell negative selection (see **Table 1**). Vγ5$^+$ T cells and LTi cells, a subset of group 3 innate lymphoid cells (ILC3), are required to establish a mature compartment (*Aire*-expressing) of mTEC (Roberts et al., 2012). In line with this work, Elsaid et al. (2020) showed that the first wave of TSP generates invariant γδ T cells and LTi within a thymic microenvironment and that temporal depletion of this wave resulted in loss of (Aire)-expressing mTEC at birth (**Figure 4**). The crosstalk between the progeny of the first TSP and immature mTEC ensures that mature Aire$^+$ mTEC are in time and place to induce tolerance (see **Table 1**) in the nascent αβ T cell repertoire during the neonatal period.

The first wave of TSP originates from a particular subset of FL common lymphoid progenitor (CLP), no longer detected after E15, that preferentially arises in the poor IL-7 environment of the FL (Berthault et al., 2017).

Before HSC activity, lympho-myeloid-restricted progenitors (LMP) co-expressing lymphoid- and myeloid-associated genes were reported in YS (Böiers et al., 2013) and proposed to be the origin of the first wave of TSPs (Luis et al., 2016). These studies challenged the notion that the first TSP derived from HSC

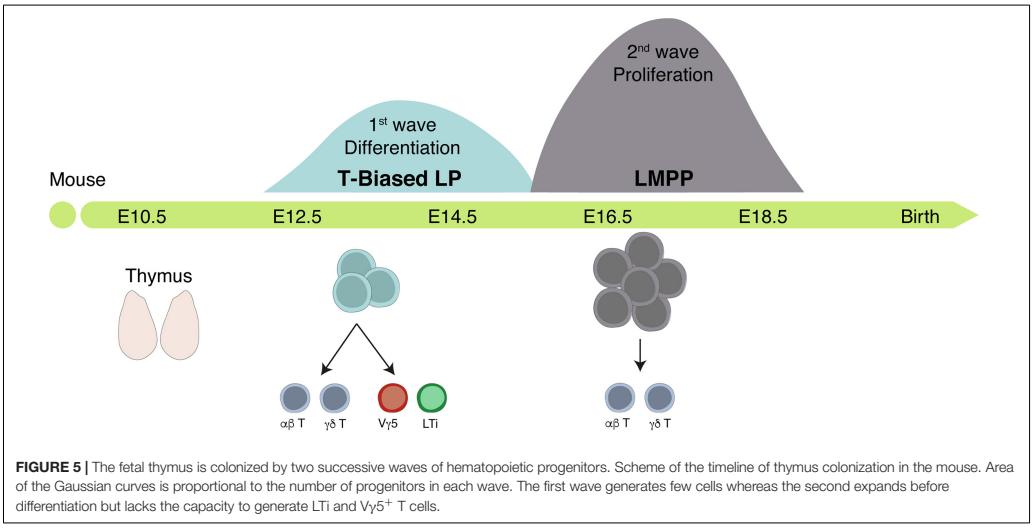


**FIGURE 5 |** The fetal thymus is colonized by two successive waves of hematopoietic progenitors. Scheme of the timeline of thymus colonization in the mouse. Area of the Gaussian curves is proportional to the number of progenitors in each wave. The first wave generates few cells whereas the second expands before differentiation but lacks the capacity to generate LTi and $V\gamma5^+$ T cells.

relied on the analysis of reporter and lineage tracing mouse lines. Corroborating these observations, single-cell transcriptional and epigenetic analysis of IAHC detected a population of lympho-myeloid-primed progenitors, suggesting an early differentiation process or an HSC-independent generation (Zhu et al., 2020). Alternatively, or complementarily, despite a transient expression of lymphoid transcripts, the reported YS-derived LMP were devoid of lymphoid potential and therefore do not qualify as lymphoid progenitors (Elsaid et al., 2020).

## Humans

Growing evidence suggests that, as in mice, the human fetal thymus is colonized by distinct waves of hematopoietic progenitors. Unlike their adult counterpart (Tieppo et al., 2020), fetal thymic progenitors expressing low levels of TdT generate invariant γδ T cells and promote tolerance (Mold et al., 2010; Ng et al., 2019). It was further shown that, like that of innate B-1 cells in mice, the generation of fetal invariant γδ T cell subsets was Lin28b-dependent. Further studies are required to identify the phenotype and functions of these fetal-derived T cells in fetal immunity and organ development.

## Why a Layered Lymphoid Compartment?

Similar to what was described for hematopoietic cells, not all lymphocyte subsets are produced simultaneously nor throughout life. In the mouse, whereas lymphocytes with a highly variable receptor repertoire are produced constantly after birth, some particular subsets that comprise B1 B cells and $V\gamma5^+$ and $V\gamma6^+$ T cells are exclusively or preferentially produced during embryonic life and persist in adults. These subsets share some general properties: (1) they express invariant or restricted antigen receptor repertoires and are, therefore, not devoted to highly specific immune responses. Rather, they fulfill broader functions and are, therefore, commonly designated as "innate-like" cells; (2) they are produced in small numbers; and (3) rather than circulating, they reside in tissues. These lymphocyte subsets that might confer a first line of protection before adaptive immune cells are fully functional also contribute to tissue architecture and homeostasis. Due to their stage-restricted development, it is tempting to hypothesize that these particular lymphoid subsets originate from specialized cells that develop independent from HSC. The demonstration that B1 and B2 cells share a similar cellular origin (Kristiansen et al., 2016), that Vγ5-expressing T cells do not differentiate from conventional YS progenitors, and that embryonic hematopoietic progenitors often express lymphoid specific transcripts, regardless of their differentiation potential, offer alternative possibilities that need to be further investigated (Elsaid et al., 2020).

B1 cells make natural circulating immunoglobulin that provides a first line of defense against pathogens. Although B2 cells can also produce IgM, their development is delayed and transient protection is better achieved through immunoglobulins of B1 cell origin. In the absence of $V\gamma5^+$ T cells in the skin, wound healing is delayed (Jameson et al., 2002). Similarly, in the absence of $V\gamma6^+$ T cells, there is increased susceptibility to airway viral infections as epithelium integrity is easily compromised (Guo et al., 2018). Because IL-17, the main effector cytokine in epithelium regeneration, can also be produced by conventional T cells, γδ T cells might only be crucial in neonates and juveniles before conventional T cell immunity is mature. Both $V\gamma5^+$ T cells and LTi that contribute to the maturation of mTEC in the thymus have a common origin in specialized TSP only present in the embryo. Other cell types such as $CD4^+$ T cells can produce RANKL and induce mTEC maturation. LTi are no longer found in the adult thymus, suggesting that, together with γδ T cells, they fulfill a very specific role in late gestation and around birth.

The fact that they originate from a particular progenitor cell arising specifically in the low-IL-7 FL environment (Berthault et al., 2017) and that in some mouse strains neonatal tolerance induction is required for prevention of autoimmune disease later in life (Guerau-de-Arellano et al., 2009) suggests a role of these developmental-restricted cells in the establishment of peripheral tolerance.

A selective pressure including environmental constraints appears to favor the early development of less diverse and sophisticated immune cells that are important in the establishment of basic immune functions and that confer protection before the highly complex diverse immune system is operational. An early development before large numbers of lymphoid cells circulate also ensures an efficient colonization of peripheral tissues where niches are possibly limited. Cell-autonomous mechanisms that condition the differentiation of developmentally restricted progenitors are still largely unknown. The HSC-independent origin proposed by some authors will have to be probed against a possible loss of the expression of embryo-specific genes such as loss of Lin28b and of the B1 differentiation capacity as HSC transit from FL to BM, through either an internal clock-type mechanism or environmentally induced.

## CONCLUDING REMARKS

It is interesting to realize that cells usually considered as pro-inflammatory such as macrophages have been also involved in organogenesis and in maintenance of tissue integrity, throughout evolution. It follows that what is considered to be the adult inflammasome might have tissue-remodeling functions during development and that therefore both functions co-evolved. This notion can be extended to specific subsets of innate-like T cells and ILCs.

The first waves of immune cells appear to be also devoted to tissue remodeling although they can also engage in defense, namely, in species whose embryos are released in microbiota-rich environment. However, they appear to be prone to mount low inflammatory responses compatible with the integrity of tissues, as elsewhere described in *X. laevis* tadpoles.

## AUTHOR CONTRIBUTIONS

MP and FS also contributed to the figures. AB, AC, FS, and RE conceptualized and assembled the manuscript. All authors reviewed the literature, discussed, contributed to writing, and approved the submitted version.

## FUNDING

This work was financed by the PPU Pasteur Ph.D. program. This work was financed by the Institut Pasteur, INSERM, Pasteur-Weizmann Foundation and ANR (grant Twothyme and Epi-Dev) through grants to AC; by REVIVE (Investissement d'Avenir; ANR-10-LABX-73) through grants to AC and RE; by FCT through the grants PD/BD/114128/2015 and POCI-0100145-FEDER-01638 to FS; and the grant SFRH/BD/143605/2019 to MP.

## ACKNOWLEDGMENTS

We are grateful to L. du Pasquier for the advice and critical reading of the manuscript. We are also grateful to Eliza Gomez-Perdiguero (Institut Pasteur) and the members of her laboratory for stimulating discussions.

## REFERENCES

Abramson, J., and Anderson, G. (2017). Thymic epithelial cells. *Annu. Rev. Immunol.* 35, 85–118. doi: 10.1146/annurev-immunol-051116-052320

Ajami, B., Bennett, J. L., Krieger, C., Tetzlaff, W., and Rossi, F. M. (2007). Local self-renewal can sustain CNS microglia maintenance and function throughout adult life. *Nat. Neurosci.* 10, 1538–1543. doi: 10.1038/nn2014

Amemiya, C. T., Saha, N. R., and Zapata, A. (2007). Evolution and development of immunological structures in the lamprey. *Curr. Opin. Immunol.* 19, 535–541. doi: 10.1016/j.coi.2007.08.003

Bajoghli, B., Guo, P., Aghaallaei, N., Hirano, M., Strohmeier, C., McCurley, N., et al. (2011). A thymus candidate in lampreys. *Nature* 470, 90–94. doi: 10.1038/nature09655

Beaudin, A. E., Boyer, S. W., Perez-Cunningham, J., Hernandez, G. E., Derderian, S. C., Jujjavarapu, C., et al. (2016). A transient developmental hematopoietic stem cell gives rise to innate-like B and T Cells. *Cell Stem Cell* 19, 768–783. doi: 10.1016/j.stem.2016.08.013

Beer, P. A., and Eaves, C. J. (2015). Modeling normal and disordered human hematopoiesis. *Trends Cancer* 1, 199–210. doi: 10.1016/j.trecan.2015.09.002

Berthault, C., Ramond, C., Burlen-Defranoux, O., Soubigou, G., Chea, S., Golub, R., et al. (2017). Asynchronous lineage priming determines commitment to T cell and B cell lineages in fetal liver. *Nat. Immunol.* 18, 1139–1149. doi: 10.1038/ni.3820

Bertrand, J. Y., Chi, N. C., Santoso, B., Teng, S., Stainier, D. Y., and Traver, D. (2010). Haematopoietic stem cells derive directly from aortic endothelium during development. *Nature* 464, 108–111. doi: 10.1038/nature08738

Bertrand, J. Y., Jalil, A., Klaine, M., Jung, S., Cumano, A., and Godin, I. (2005). Three pathways to mature macrophages in the early mouse yolk sac. *Blood* 106, 3004–3011. doi: 10.1182/blood-2005-02-0461

Bertrand, J. Y., Kim, A. D., Violette, E. P., Stachura, D. L., Cisson, J. L., and Traver, D. (2007). Definitive hematopoiesis initiates through a committed erythromyeloid progenitor in the zebrafish embryo. *Development* 134, 4147–4156. doi: 10.1242/dev.012385

Blaser, B. W., Moore, J. L., Hagedorn, E. J., Li, B., Riquelme, R., Lichtig, A., et al. (2017). CXCR1 remodels the vascular niche to promote hematopoietic stem and progenitor cell engraftment. *J. Exp. Med.* 214, 1011–1027. doi: 10.1084/jem.20161616

Boehm, T., Hirano, M., Holland, S. J., Das, S., Schorpp, M., and Cooper, M. D. (2018). Evolution of alternative adaptive immune systems in vertebrates. *Annu. Rev. Immunol.* 36, 19–421.

Böiers, C., Carrelha, J., Lutteropp, M., Luc, S., Green, J. C., Azzoni, E., et al. (2013). Lymphomyeloid contribution of an immune-restricted progenitor emerging prior to definitive hematopoietic stem cells. *Cell Stem Cell* 13, 535–548. doi: 10.1016/j.stem.2013.08.012

Boisset, J. C., van Cappellen, W., Andrieu-Soler, C., Galjart, N., Dzierzak, E., and Robin, C. (2010). In vivo imaging of haematopoietic cells emerging from the mouse aortic endothelium. *Nature* 464, 116–120. doi: 10.1038/nature08764

Chen, X. D., and Turpen, J. B. (1995). Intraembryonic origin of hepatic hematopoiesis in *Xenopus laevis*. *J. Immunol.* 154, 2557–2567.

Choi, K., Kennedy, M., Kazarov, A., Papadimitriou, J. C., and Keller, G. (1998). A common precursor for hematopoietic and endothelial cells. *Development* 125, 725–732.

Ciau-Uitz, A., Liu, F., and Patient, R. (2010). Genetic control of hematopoietic development in *Xenopus* and zebrafish. *Int. J. Dev. Biol.* 54, 1139–1149. doi: 10.1387/ijdb.093055ac

Ciau-Uitz, A., and Patient, R. (2016). The embryonic origins and genetic programming of emerging haematopoietic stem cells. *FEBS Lett.* 590, 4002–4015. doi: 10.1002/1873-3468.12363

Ciau-Uitz, A., Walmsley, M., and Patient, R. (2000). Distinct origins of adult and embryonic blood in *Xenopus*. *Cell* 102, 787–796. doi: 10.1016/s0092-8674(00)00067-2

Coltey, M., Jotereau, F. V., and Le Douarin, N. M. (1987). Evidence for a cyclic renewal of lymphocyte precursor cells in the embryonic chick thymus. *Cell Differ.* 22, 71–82.

Cuadros, M. A., Martin, C., Coltey, P., Almendros, A., and Navascués, J. (1993). First appearance, distribution, and origin of macrophages in the early development of the avian central nervous system. *J. Comp. Neurol.* 330, 113–129. doi: 10.1002/cne.903300110

Cumano, A., Dieterlen-Lievre, F., and Godin, I. (1996). Lymphoid potential, probed before circulation in mouse, is restricted to caudal intraembryonic splanchnopleura. *Cell* 86, 907–916.

de Bruijn, M. F., Speck, N. A., Peeters, M. C., and Dzierzak, E. (2000). Definitive hematopoietic stem cells first develop within the major arterial regions of the mouse embryo. *Embo J.* 19, 2465–2474. doi: 10.1093/emboj/19.11.2465

Delsuc, F., Brinkmann, H., Chourrout, D., and Philippe, H. (2006). Tunicates and not cephalochordates are the closest living relatives of vertebrates. *Nature* 439, 965–968. doi: 10.1038/nature04336

Demy, D. L., Ranta, Z., Giorgi, J. M., Gonzalez, M., Herbomel, P., and Kissa, K. (2013). Generating parabiotic zebrafish embryos for cell migration and homing studies. *Nat. Methods* 10, 256–258. doi: 10.1038/nmeth.2362

Detrich, H. W., Kieran, M. W., Chan, F. Y., Barone, L. M., Yee, K., Rundstadler, J. A., et al. (1995). Intraembryonic hematopoietic cell migration during vertebrate development. *Proc. Natl. Acad. Sci. U.S.A.* 92, 10713–10717. doi: 10.1073/pnas.92.23.10713

Dieterlen-Lievre, F. (1975). On the origin of haemopoietic stem cells in the avian embryo: an experimental approach. *J. Embryol. Exp. Morphol.* 33, 607–619.

Du Pasquier, L., Schwager, J., and Flajnik, M. F. (1989). The immune system of *Xenopus*. *Annu. Rev. Immunol.* 7, 251–275. doi: 10.1146/annurev.iy.07.040189.001343

Dunon, D., Allioli, N., Vainio, O., Ody, C., and Imhof, B. A. (1998). Renewal of thymocyte progenitors and emigration of thymocytes during avian development. *Dev. Comp. Immunol.* 22, 279–287. doi: 10.1016/s0145-305x(98)00010-x

Dunon, D., Allioli, N., Vainio, O., Ody, C., and Imhof, B. A. (1999). Quantification of T-cell progenitors during ontogeny: thymus colonization depends on blood delivery of progenitors. *Blood* 93, 2234–2243.

Eberl, G., Marmon, S., Sunshine, M. J., Rennert, P. D., Choi, Y., and Littman, D. R. (2004). An essential function for the nuclear receptor RORgamma(t) in the generation of fetal lymphoid tissue inducer cells. *Nat. Immunol.* 5, 64–73. doi: 10.1038/ni1022

Elsaid, R., Meunier, S., Burlen-Defranoux, O., Soares-da-Silva, F., Perchet, T., Iturri, L., et al. (2020). A wave of bipotent T/ILC-restricted progenitors shapes the embryonic thymus microenvironment in a time-dependent manner. *Blood* [Epub ahead of print]. doi: 10.1182/blood.2020006779

Elsaid, R., Yang, J., and Cumano, A. (2019). The influence of space and time on the establishment of B cell identity. *Biomed. J.* 42, 209–217. doi: 10.1016/j.bj.2019.07.008

Ema, H., and Nakauchi, H. (2000). Expansion of hematopoietic stem cells in the developing liver of a mouse embryo. *Blood* 95, 2284–2288.

Espín-Palazón, R., Stachura, D. L., Campbell, C. A., García-Moreno, D., Del Cid, N., Kim, A. D., et al. (2014). Proinflammatory signaling regulates hematopoietic stem cell emergence. *Cell* 159, 1070–1085. doi: 10.1016/j.cell.2014.10.031

Evans, C. J., Hartenstein, V., and Banerjee, U. (2003). Thicker than blood: conserved mechanisms in *Drosophila* and vertebrate hematopoiesis. *Dev. Cell* 5, 673–690. doi: 10.1016/s1534-5807(03)00335-6

Frame, J. M., Fegan, K. H., Conway, S. J., McGrath, K. E., and Palis, J. (2016). definitive hematopoiesis in the yolk sac emerges from Wnt-responsive hemogenic endothelium independently of circulation and arterial identity. *Stem Cells* 34, 431–444. doi: 10.1002/stem.2213

Frame, J. M., Kubaczka, C., Long, T. L., Esain, V., Soto, R. A., Hachimi, M., et al. (2020). Metabolic regulation of inflammasome activity controls embryonic hematopoietic stem and progenitor cell production. *Dev. Cell* 55, 133.e6–149.e6. doi: 10.1016/j.devcel.2020.07.015

Ganuza, M., Hall, T., Finkelstein, D., Chabot, A., Kang, G., and McKinney-Freeman, S. (2017). Lifelong haematopoiesis is established by hundreds of precursors throughout mammalian ontogeny. *Nat. Cell Biol.* 19, 1153–1163. doi: 10.1038/ncb3607

Gekas, C., Dieterlen-Lièvre, F., Orkin, S. H., and Mikkola, H. K. (2005). The placenta is a niche for hematopoietic stem cells. *Dev. Cell* 8, 365–375. doi: 10.1016/j.devcel.2004.12.016

Ginhoux, F., Greter, M., Leboeuf, M., Nandi, S., See, P., Gokhan, S., et al. (2010). Fate mapping analysis reveals that adult microglia derive from primitive macrophages. *Science* 330, 841–845. doi: 10.1126/science.1194637

Godin, I., and Cumano, A. (2002). The hare and the tortoise: an embryonic haematopoietic race. *Nat. Rev. Immunol.* 2, 593–604. doi: 10.1038/nri857

Godin, I., Garcia-Porrero, J. A., Dieterlen-Lièvre, F., and Cumano, A. (1999). Stem cell emergence and hemopoietic activity are incompatible in mouse intraembryonic sites. *J. Exp. Med.* 190, 43–52.

Goldie, L. C., Lucitti, J. L., Dickinson, M. E., and Hirschi, K. K. (2008). Cell signaling directing the formation and function of hemogenic endothelium during murine embryogenesis. *Blood* 112, 3194–3204. doi: 10.1182/blood-2008-02-139055

Golub, R., André, S., Hassanin, A., Affaticati, P., Larijani, M., and Fellah, J. S. (2004). Early expression of two TdT isoforms in the hematopoietic system of the Mexican axolotl. Implications for the evolutionary origin of the N-nucleotide addition. *Immunogenetics* 56, 204–213. doi: 10.1007/s00251-004-0681-2

Gomes, A. M., Kurochkin, I., Chang, B., Daniel, M., Law, K., Satija, N., et al. (2018). Cooperative transcription factor induction mediates hemogenic reprogramming. *Cell Rep.* 25, 2821.e7–2835.e7. doi: 10.1016/j.celrep.2018.11.032

Gomez Perdiguero, E., Klapproth, K., Schulz, C., Busch, K., Azzoni, E., Crozet, L., et al. (2015). Tissue-resident macrophages originate from yolk-sac-derived erythro-myeloid progenitors. *Nature* 518, 547–551. doi: 10.1038/nature13989

Graf, R., Seagal, J., Otipoby, K. L., Lam, K. P., Ayoub, S., Zhang, B., et al. (2019). BCR-dependent lineage plasticity in mature B cells. *Science* 363, 748–753. doi: 10.1126/science.aau8475

Greenhalgh, P., Olesen, C. E., and Steiner, L. A. (1993). Characterization and expression of recombination activating genes (RAG-1 and RAG-2) in *Xenopus laevis*. *J. Immunol.* 151, 3100–3110.

Guerau-de-Arellano, M., Martinic, M., Benoist, C., and Mathis, D. (2009). Neonatal tolerance revisited: a perinatal window for Aire control of autoimmunity. *J. Exp. Med.* 206, 1245–1252. doi: 10.1084/jem.20090300

Guo, X. J., Dash, P., Crawford, J. C., Allen, E. K., Zamora, A. E., Boyd, D. F., et al. (2018). Lung γδ T Cells mediate protective responses during neonatal influenza infection that are associated with Type 2 Immunity. *Immunity* 49, 531.e6–544.e6. doi: 10.1016/j.immuni.2018.07.011

Haas, J. D., Ravens, S., Düber, S., Sandrock, I., Oberdörfer, L., Kashani, E., et al. (2012). Development of interleukin-17-producing γδ T cells is restricted to a functional embryonic wave. *Immunity* 37, 48–59. doi: 10.1016/j.immuni.2012.06.003

Hartenstein, V. (2006). Blood cells and blood cell development in the animal kingdom. *Annu. Rev. Cell Dev. Biol.* 22, 677–712. doi: 10.1146/annurev.cellbio.22.010605.093317

He, S., Tian, Y., Feng, S., Wu, Y., Shen, X., Chen, K., et al. (2020). In vivo single-cell lineage tracing in zebrafish using high-resolution infrared laser-mediated gene induction microscopy. *eLife* 9:e52024. doi: 10.7554/eLife.52024

Herbomel, P., Thisse, B., and Thisse, C. (1999). Ontogeny and behaviour of early macrophages in the zebrafish embryo. *Development* 126, 3735–3745.

Herzenberg, L. A. (1989). Toward a layered immune system. *Cell* 59, 953–954. doi: 10.1016/0092-8674(89)90748-4

Herzenberg, L. A. (2000). B-1 cells: the lineage question revisited. *Immunol. Rev.* 175, 9–22.

Hess, I., and Boehm, T. (2012). Intravital imaging of thymopoiesis reveals dynamic lympho-epithelial interactions. *Immunity* 36, 298–309. doi: 10.1016/j.immuni.2011.12.016

Hess, I., and Boehm, T. (2016). Stable multilineage xenogeneic replacement of definitive hematopoiesis in adult zebrafish. *Sci. Rep.* 6:19634. doi: 10.1038/srep19634

Hess, I., Iwanami, N., Schorpp, M., and Boehm, T. (2013). Zebrafish model for allogeneic hematopoietic cell transplantation not requiring preconditioning. *Proc. Natl. Acad. Sci. U.S.A.* 110, 4327–4332. doi: 10.1073/pnas.1219847110

Hoeffel, G., Chen, J., Lavin, Y., Low, D., Almeida, F. F., See, P., et al. (2015). C-Myb(+) erythro-myeloid progenitor-derived fetal monocytes give rise to adult tissue-resident macrophages. *Immunity* 42, 665–678. doi: 10.1016/j.immuni.2015.03.011

Hosokawa, H., and Rothenberg, E. V. (2020). How transcription factors drive choice of the T cell fate. *Nat. Rev. Immunol.* [Epub ahead of print]. doi: 10.1038/s41577-020-00426-6

Ikuta, K., Kina, T., MacNeil, I., Uchida, N., Peault, B., Chien, Y. H., et al. (1990). A developmental switch in thymic lymphocyte maturation potential occurs at the level of hematopoietic stem cells. *Cell* 62, 863–874.

Imai, Y., Ishida, K., Nemoto, M., Nakata, K., Kato, T., and Maéno, M. (2017). Multiple origins of embryonic and tadpole myeloid cells in *Xenopus laevis*. *Cell Tissue Res.* 369, 341–352. doi: 10.1007/s00441-017-2601-4

Ivanovs, A., Rybtsov, S., Ng, E. S., Stanley, E. G., Elefanty, A. G., and Medvinsky, A. (2017). Human haematopoietic stem cell development: from the embryo to the dish. *Development* 144, 2323–2337. doi: 10.1242/dev.134866

Ivanovs, A., Rybtsov, S., Welch, L., Anderson, R. A., Turner, M. L., and Medvinsky, A. (2011). Highly potent human hematopoietic stem cells first emerge in the intraembryonic aorta-gonad-mesonephros region. *J. Exp. Med.* 208, 2417–2427. doi: 10.1084/jem.20111688

Jaffredo, T., Gautier, R., Brajeul, V., and Dieterlen-Lièvre, F. (2000). Tracing the progeny of the aortic hemangioblast in the avian embryo. *Dev. Biol.* 224, 204–214. doi: 10.1006/dbio.2000.9799

Jameson, J., Ugarte, K., Chen, N., Yachi, P., Fuchs, E., Boismenu, R., et al. (2002). A role for skin gammadelta T cells in wound repair. *Science* 296, 747–749. doi: 10.1126/science.1069639

Jenkins, S. J., Ruckerl, D., Cook, P. C., Jones, L. H., Finkelman, F. D., van Rooijen, N., et al. (2011). Local macrophage proliferation, rather than recruitment from the blood, is a signature of TH2 inflammation. *Science* 332, 1284–1288. doi: 10.1126/science.1204351

Jin, H., Xu, J., and Wen, Z. (2007). Migratory path of definitive hematopoietic stem/progenitor cells during zebrafish development. *Blood* 109, 5208–5214. doi: 10.1182/blood-2007-01-069005

Kalev-Zylinska, M. L., Horsfield, J. A., Flores, M. V., Postlethwait, J. H., Vitas, M. R., Baas, A. M., et al. (2002). Runx1 is required for zebrafish blood and vessel development and expression of a human RUNX1-CBF2T1 transgene advances a model for studies of leukemogenesis. *Development* 129, 2015–2030.

Kamel-Reid, S., Letarte, M., Sirard, C., Doedens, M., Grunberger, T., Fulop, G., et al. (1989). A model of human acute lymphoblastic leukemia in immune-deficient SCID mice. *Science* 246, 1597–1600. doi: 10.1126/science.2595371

Kasaai, B., Caolo, V., Peacock, H. M., Lehoux, S., Gomez-Perdiguero, E., Luttun, A., et al. (2017). Erythro-myeloid progenitors can differentiate from endothelial cells and modulate embryonic vascular remodeling. *Sci. Rep.* 7:43817. doi: 10.1038/srep43817

Kingsley, P. D., Malik, J., Fantauzzo, K. A., and Palis, J. (2004). Yolk sac-derived primitive erythroblasts enucleate during mammalian embryogenesis. *Blood* 104, 19–25. doi: 10.1182/blood-2003-12-4162

Kissa, K., and Herbomel, P. (2010). Blood stem cells emerge from aortic endothelium by a novel type of cell transition. *Nature* 464, 112–115. doi: 10.1038/nature08761

Kissa, K., Murayama, E., Zapata, A., Cortés, A., Perret, E., Machu, C., et al. (2008). Live imaging of emerging hematopoietic stem cells and early thymus colonization. *Blood* 111, 1147–115610. doi: 1182/blood-2007-07-099499

Kobayashi, I., Kobayashi-Sun, J., Kim, A. D., Pouget, C., Fujita, N., Suda, T., et al. (2014). Jam1a-Jam2a interactions regulate haematopoietic stem cell fate through Notch signalling. *Nature* 512, 319–323. doi: 10.1038/nature13623

Kristiansen, T. A., Jaensson Gyllenbäck, E., Zriwil, A., Björklund, T., Daniel, J. A., Sitnicka, E., et al. (2016). Cellular barcoding Links B-1a B cell potential to a fetal hematopoietic stem cell state at the single-cell level. *Immunity* 45, 346–357. doi: 10.1016/j.immuni.2016.07.014

Kumano, K., Chiba, S., Kunisato, A., Sata, M., Saito, T., Nakagami-Yamaguchi, E., et al. (2003). Notch1 but not Notch2 is essential for generating hematopoietic stem cells from endothelial cells. *Immunity* 18, 699–711. doi: 10.1016/s1074-7613(03)00117-1

Lassila, O., Eskola, J., Toivanen, P., Martin, C., and Dieterlen-Lievre, F. (1978). The origin of lymphoid stem cells studied in chick yold sac-embryo chimaeras. *Nature* 272, 353–354. doi: 10.1038/272353a0

Le Douarin, N. (1969). [Details of the interphase nucleus in Japanese quail (Coturnix coturnix japonica)]. *Bull. Biol. Fr Belg.* 103, 435–452.

Le Douarin, N. M., and Dieterlen-Lièvre, F. (2013). How studies on the avian embryo have opened new avenues in the understanding of development: a view about the neural and hematopoietic systems. *Dev. Growth Differ.* 55, 1–14. doi: 10.1111/dgd.12015

Lee, A., and Hsu, E. (1994). Isolation and characterization of the *Xenopus* terminal deoxynucleotidyl transferase. *J. Immunol.* 152, 4500–4507.

Lopez, D., Lin, L., Monaghan, J. R., Cogle, C. R., Bova, F. J., Maden, M., et al. (2014). Mapping hematopoiesis in a fully regenerative vertebrate: the axolotl. *Blood* 124, 1232–1241. doi: 10.1182/blood-2013-09-526970

Luis, T. C., Luc, S., Mizukami, T., Boukarabila, H., Thongjuea, S., Woll, P. S., et al. (2016). Initial seeding of the embryonic thymus by immune-restricted lympho-myeloid progenitors. *Nat. Immunol.* 17, 1424–1435. doi: 10.1038/ni.3576

Manaia, A., Lemarchandel, V., Klaine, M., Max-Audit, I., Romeo, P., Dieterlen-Lièvre, F., et al. (2000). Lmo2 and GATA-3 associated expression in intraembryonic hemogenic sites. *Development* 127, 643–653.

Manca, R., Glomski, C., and Pica, A. (2019). Hematopoietic stem cells debut in embryonic lymphomyeloid tissues of elasmobranchs. *Eur. J. Histochem.* 63:3060. doi: 10.4081/ejh.2019.3060

Manca, R., Glomski, C. A., and Pica, A. (2018). Evolutionary intraembryonic origin of vertebrate hematopoietic stem cells in the elasmobranch spleen. *Eur. J. Histochem.* 62:2987. doi: 10.4081/ejh.2018.2987

Mariani, S. A., Li, Z., Rice, S., Krieg, C., Fragkogianni, S., Robinson, M., et al. (2019). Pro-inflammatory aorta-associated macrophages are involved in embryonic development of hematopoietic stem cells. *Immunity* 50, 1439.e5–1452.e5. doi: 10.1016/j.immuni.2019.05.003

McGrath, K. E., Frame, J. M., Fegan, K. H., Bowen, J. R., Conway, S. J., Catherman, S. C., et al. (2015). Distinct sources of hematopoietic progenitors emerge before HSCs and provide functional blood cells in the mammalian embryo. *Cell Rep.* 11, 1892–1904. doi: 10.1016/j.celrep.2015.05.036

Medvinsky, A., and Dzierzak, E. (1996). Definitive hematopoiesis is autonomously initiated by the AGM region. *Cell* 86, 897–906.

Merad, M., Manz, M. G., Karsunky, H., Wagers, A., Peters, W., Charo, I., et al. (2002). Langerhans cells renew in the skin throughout life under steady-state conditions. *Nat. Immunol.* 3, 1135–1141. doi: 10.1038/ni852

Migliaccio, G., Migliaccio, A. R., Petti, S., Mavilio, F., Russo, G., Lazzaro, D., et al. (1986). Human embryonic hemopoiesis. Kinetics of progenitors and precursors underlying the yolk sac—-liver transition. *J. Clin. Invest.* 78, 51–60. doi: 10.1172/JCI112572

Mold, J. E., Venkatasubrahmanyam, S., Burt, T. D., Michaëlsson, J., Rivera, J. M., Galkina, S. A., et al. (2010). Fetal and adult hematopoietic stem cells give rise to distinct T cell lineages in humans. *Science* 330, 1695–1699. doi: 10.1126/science.1196509

Montecino-Rodriguez, E., and Dorshkind, K. (2012). B-1 B cell development in the fetus and adult. *Immunity* 36, 13–21. doi: 10.1016/j.immuni.2011.11.017

Moore, M. A., and Metcalf, D. (1970). Ontogeny of the haemopoietic system: yolk sac origin of in vivo and in vitro colony forming cells in the developing mouse embryo. *Br. J. Haematol.* 18, 279–296. doi: 10.1111/j.1365-2141.1970.tb01443.x

Moore, M. A., and Owen, J. J. (1967). Chromosome marker studies in the irradiated chick embryo. *Nature* 215, 1081–1082. doi: 10.1038/2151081a0

Muñoz-Chápuli, R., Carmona, R., Guadix, J. A., Macías, D., and Pérez-Pomares, J. M. (2005). The origin of the endothelial cells: an evo-devo approach for the invertebrate/vertebrate transition of the circulatory system. *Evol. Dev.* 7, 351–3581.

Murayama, E., Kissa, K., Zapata, A., Mordelet, E., Briolat, V., Lin, H. F., et al. (2006). Tracing hematopoietic precursor migration to successive hematopoietic

organs during zebrafish development. *Immunity* 25, 963–975. doi: 10.1016/j.immuni.2006.10.015

Ng, M. S. F., Roth, T. L., Mendoza, V. F., Marson, A., and Burt, T. D. (2019). Helios enhances the preferential differentiation of human fetal CD4+ naïve T cells into regulatory T cells. *Sci. Immunol.* 4:eaav5947. doi: 10.1126/sciimmunol.aav5947

Notta, F., Doulatov, S., Laurenti, E., Poeppl, A., Jurisica, I., and Dick, J. E. (2011). Isolation of single human hematopoietic stem cells capable of long-term multilineage engraftment. *Science* 333, 218–221. doi: 10.1126/science.1201219

Notta, F., Zandi, S., Takayama, N., Dobson, S., Gan, O. I., Wilson, G., et al. (2016). Distinct routes of lineage development reshape the human blood hierarchy across ontogeny. *Science* 351:aab2116. doi: 10.1126/science.aab2116

Ottersbach, K., and Dzierzak, E. (2005). The murine placenta contains hematopoietic stem cells within the vascular labyrinth region. *Dev. Cell* 8, 377–387. doi: 10.1016/j.devcel.2005.02.001

Palis, J., Robertson, S., Kennedy, M., Wall, C., and Keller, G. (1999). Development of erythroid and myeloid progenitors in the yolk sac and embryo proper of the mouse. *Development* 126, 5073–5084.

Pancer, Z., Amemiya, C. T., Ehrhardt, G. R., Ceitlin, J., Gartland, G. L., and Cooper, M. D. (2004). Somatic diversification of variable lymphocyte receptors in the agnathan sea lamprey. *Nature* 430, 174–180. doi: 10.1038/nature02740

Parada-Kusz, M., Penaranda, C., Hagedorn, E. J., Clatworthy, A., Nair, A. V., Henninger, J. E., et al. (2018). Generation of mouse-zebrafish hematopoietic tissue chimeric embryos for hematopoiesis and host-pathogen interaction studies. *Dis. Model. Mech.* 11:dmm034876. doi: 10.1242/dmm.034876

Pardanaud, L., Luton, D., Prigent, M., Bourcheix, L. M., Catala, M., and Dieterlen-Lievre, F. (1996). Two distinct endothelial lineages in ontogeny, one of them related to hemopoiesis. *Development* 122, 1363–1371.

Pascual-Anaya, J., Albuixech-Crespo, B., Somorjai, I. M., Carmona, R., Oisi, Y., Alvarez, S., et al. (2013). The evolutionary origins of chordate hematopoiesis and vertebrate endothelia. *Dev. Biol.* 375, 182–192. doi: 10.1016/j.ydbio.2012.11.015

Pouget, C., Gautier, R., Teillet, M. A., and Jaffredo, T. (2006). Somite-derived cells replace ventral aortic hemangioblasts and provide aortic smooth muscle cells of the trunk. *Development* 133, 1013–1022. doi: 10.1242/dev.02269

Ramond, C., Berthault, C., Burlen-Defranoux, O., de Sousa, A. P., Guy-Grand, D., Vieira, P., et al. (2014). Two waves of distinct hematopoietic progenitor cells colonize the fetal thymus. *Nat. Immunol.* 15, 27–35. doi: 10.1038/ni.2782

Reynaud, C. A., Anquez, V., Grimal, H., and Weill, J. C. (1987). A hyperconversion mechanism generates the chicken light chain preimmune repertoire. *Cell* 48, 379–388. doi: 10.1016/0092-8674(87)90189-9

Rhodes, K. E., Gekas, C., Wang, Y., Lux, C. T., Francis, C. S., Chan, D. N., et al. (2008). The emergence of hematopoietic stem cells is initiated in the placental vasculature in the absence of circulation. *Cell Stem Cell* 2, 252–263. doi: 10.1016/j.stem.2008.01.001

Richard, C., Drevon, C., Canto, P. Y., Villain, G., Bollérot, K., Lempereur, A., et al. (2013). Endothelio-mesenchymal interaction controls runx1 expression and modulates the notch pathway to initiate aortic hematopoiesis. *Dev. Cell* 24, 600–611. doi: 10.1016/j.devcel.2013.02.011

Roberts, N. A., White, A. J., Jenkinson, W. E., Turchinovich, G., Nakamura, K., Withers, D. R., et al. (2012). Rank signaling links the development of invariant γδ T cell progenitors and Aire(+) medullary epithelium. *Immunity* 36, 427–437. doi: 10.1016/j.immuni.2012.01.016

Rosental, B., Kowarsky, M., Seita, J., Corey, D. M., Ishizuka, K. J., Palmeri, K. J., et al. (2018). Complex mammalian-like haematopoietic system found in a colonial chordate. *Nature* 564, 425–429. doi: 10.1038/s41586-018-0783-x

Rosental, B., Raveh, T., Voskoboynik, A., and Weissman, I. L. (2020). Evolutionary perspective on the hematopoietic system through a colonial chordate: allogeneic immunity and hematopoiesis. *Curr. Opin. Immunol* 62, 91–98. doi: 10.1016/j.coi.2019.12.006

Scala, S., and Aiuti, A. (2019). In vivo dynamics of human hematopoietic stem cells: novel concepts and future directions. *Blood Adv.* 3, 1916–1924. doi: 10.1182/bloodadvances.2019000039

Sertori, R., Trengove, M., Basheer, F., Ward, A. C., and Liongue, C. (2016). Genome editing in zebrafish: a practical overview. *Brief. Funct. Genomics* 15, 322–330. doi: 10.1093/bfgp/elv051

Smith, P. B., Flajnik, M. F., and Turpen, J. B. (1989). Experimental analysis of ventral blood island hematopoiesis in *Xenopus* embryonic chimeras. *Dev. Biol.* 131, 302–312. doi: 10.1016/s0012-1606(89)80003-x

Stachura, D. L., Svoboda, O., Lau, R. P., Balla, K. M., Zon, L. I., Bartunek, P., et al. (2011). Clonal analysis of hematopoietic progenitor cells in the zebrafish. *Blood* 118, 1274–1282. doi: 10.1182/blood-2011-01-331199

Stachura, D. L., and Traver, D. (2016). Cellular dissection of zebrafish hematopoiesis. *Methods Cell Biol.* 133, 11–53. doi: 10.1016/bs.mcb.2016.03.022

Sun, J., Ramos, A., Chapman, B., Johnnidis, J. B., Le, L., Ho, Y. J., et al. (2014). Clonal dynamics of native haematopoiesis. *Nature* 514, 322–327. doi: 10.1038/nature13824

Takahama, Y., Ohigashi, I., Baik, S., and Anderson, G. (2017). Generation of diversity in thymic epithelial cells. *Nat. Rev. Immunol.* 17, 295–305. doi: 10.1038/nri.2017.12

Tamplin, O. J., Durand, E. M., Carr, L. A., Childs, S. J., Hagedorn, E. J., Li, P., et al. (2015). Hematopoietic stem cell arrival triggers dynamic remodeling of the perivascular niche. *Cell* 160, 241–252. doi: 10.1016/j.cell.2014.12.032

Tavian, M., Coulombel, L., Luton, D., Clemente, H. S., Dieterlen-Lièvre, F., and Péault, B. (1996). Aorta-associated CD34+ hematopoietic cells in the early human embryo. *Blood* 87, 67–72.

Tavian, M., Hallais, M. F., and Péault, B. (1999). Emergence of intraembryonic hematopoietic precursors in the pre-liver human embryo. *Development* 126, 793–803.

Thompson, M. A., Ransom, D. G., Pratt, S. J., MacLennan, H., Kieran, M. W., Detrich, H. W., et al. (1998). The cloche and spadetail genes differentially affect hematopoiesis and vasculogenesis. *Dev. Biol.* 197, 248–269. doi: 10.1006/dbio.1998.8887

Tian, Y., Xu, J., Feng, S., He, S., Zhao, S., Zhu, L., et al. (2017). The first wave of T lymphopoiesis in zebrafish arises from aorta endothelium independent of hematopoietic stem cells. *J. Exp. Med.* 214, 3347–3360. doi: 10.1084/jem.20170488

Tieppo, P., Papadopoulou, M., Gatti, D., McGovern, N., Chan, J. K. Y., Gosselin, F., et al. (2020). The human fetal thymus generates invariant effector γδ T cells. *J. Exp. Med.* [Epub ahead of print]. doi: 10.1084/jem.20190580

Tober, J., Koniski, A., McGrath, K. E., Vemishetti, R., Emerson, R., de Mesy-Bentley, K. K., et al. (2007). The megakaryocyte lineage originates from hemangioblast precursors and is an integral component both of primitive and of definitive hematopoiesis. *Blood* 109, 1433–1441. doi: 10.1182/blood-2006-06-031898

Traver, D., Paw, B. H., Poss, K. D., Penberthy, W. T., Lin, S., and Zon, L. I. (2003). Transplantation and in vivo imaging of multilineage engraftment in zebrafish bloodless mutants. *Nat. Immunol.* 4, 1238–1246. doi: 10.1038/ni1007

Traver, D., Winzeler, A., Stern, H. M., Mayhall, E. A., Langenau, D. M., Kutok, J. L., et al. (2004). Effects of lethal irradiation in zebrafish and rescue by hematopoietic cell transplantation. *Blood* 104, 1298–1305. doi: 10.1182/blood-2004-01-0100

Turpen, J. B., Kelley, C. M., Mead, P. E., and Zon, L. I. (1997). Bipotential primitive-definitive hematopoietic progenitors in the vertebrate embryo. *Immunity* 7, 325–334. doi: 10.1016/s1074-7613(00)80354-4

Turpen, J. B., and Smith, P. B. (1989). Precursor immigration and thymocyte succession during larval development and metamorphosis in *Xenopus*. *J. Immunol.* 142, 41–47.

Ueno, H., and Weissman, I. L. (2006). Clonal analysis of mouse development reveals a polyclonal origin for yolk sac blood islands. *Dev. Cell* 11, 519–533. doi: 10.1016/j.devcel.2006.08.001

Vanhee, S., Åkerstrand, H., Kristiansen, T. A., Datta, S., Montano, G., Vergani, S., et al. (2019). Lin28b controls a neonatal to adult switch in B cell positive selection. *Sci. Immunol.* 4:eaax4453. doi: 10.1126/sciimmunol.aax4453

Wilkinson, R. N., Pouget, C., Gering, M., Russell, A. J., Davies, S. G., Kimelman, D., et al. (2009). Hedgehog and Bmp polarize hematopoietic stem cell emergence in the zebrafish dorsal aorta. *Dev. Cell* 16, 909–916. doi: 10.1016/j.devcel.2009.04.014

Wolf, A., Aggio, J., Campbell, C., Wright, F., Marquez, G., Traver, D., et al. (2017). Zebrafish caudal haematopoietic embryonic stromal tissue (CHEST) cells support haematopoiesis. *Sci. Rep.* 7:44644. doi: 10.1038/srep44644

Wong, J. B., Hewitt, S. L., Heltemes-Harris, L. M., Mandal, M., Johnson, K., Rajewsky, K., et al. (2019). B-1a cells acquire their unique characteristics by bypassing the pre-BCR selection stage. *Nat. Commun.* 10:4768. doi: 10.1038/s41467-019-12824-z

Wong, P. M., Chung, S. W., Reicheld, S. M., and Chui, D. H. (1986). Hemoglobin switching during murine embryonic development: evidence for

two populations of embryonic erythropoietic progenitor cells. *Blood* 67, 716–721.

Xu, J., Zhu, L., He, S., Wu, Y., Jin, W., Yu, T., et al. (2015). Temporal-spatial resolution fate mapping reveals distinct origins for embryonic and adult microglia in Zebrafish. *Dev. Cell* 34, 632–641. doi: 10.1016/j.devcel.2015.08.018

Xu, M. J., Matsuoka, S., Yang, F. C., Ebihara, Y., Manabe, A., Tanaka, R., et al. (2001). Evidence for the presence of murine primitive megakaryocytopoiesis in the early yolk sac. *Blood* 97, 2016–2022. doi: 10.1182/blood.v97.7.2016

Yaparla, A., Reeves, P., and Grayfer, L. (2019). Myelopoiesis of the Amphibian *Xenopus laevis* is segregated to the bone marrow, away from their hematopoietic peripheral liver. *Front. Immunol.* 10:3015. doi: 10.3389/fimmu.2019.03015

Yvernogeau, L., and Robin, C. (2017). Restricted intra-embryonic origin of bona fide hematopoietic stem cells in the chicken. *Development* 144, 2352–2363. doi: 10.1242/dev.151613

Yzaguirre, A. D., and Speck, N. A. (2016). Extravascular endothelial and hematopoietic islands form through multiple pathways in midgestation mouse embryos. *Dev. Biol.* 415, 111–121. doi: 10.1016/j.ydbio.2016.04.004

Zhu, Q., Gao, P., Tober, J., Bennett, L., Chen, C., Uzun, Y., et al. (2020). Developmental trajectory of prehematopoietic stem cell formation from endothelium. *Blood* 136, 845–856. doi: 10.1182/blood.2020004801

Zovein, A. C., Hofmann, J. J., Lynch, M., French, W. J., Turlo, K. A., Yang, Y., et al. (2008). Fate tracing reveals the endothelial origin of hematopoietic stem cells. *Cell Stem Cell* 3, 625–636. doi: 10.1016/j.stem.2008.09.018

**Conflict of Interest:** The authors declare that the research was conducted in the absence of any commercial or financial relationships that could be construed as a potential conflict of interest.

*Copyright © 2020 Elsaid, Soares-da-Silva, Peixoto, Amiri, Mackowski, Pereira, Bandeira and Cumano. This is an open-access article distributed under the terms of the Creative Commons Attribution License (CC BY). The use, distribution or reproduction in other forums is permitted, provided the original author(s) and the copyright owner(s) are credited and that the original publication in this journal is cited, in accordance with accepted academic practice. No use, distribution or reproduction is permitted which does not comply with these terms.*

# ANNEX IV

Check for updates

Received: 17 January 2022 | Revised: 7 April 2022 | Accepted: 28 April 2022

DOI: 10.1002/cyto.a.24567

ORIGINAL ARTICLE

ISAC CYTOMETRY Journal of Quantitative Cell Science PART A

## Identification of fetal liver stroma in spectral cytometry using the parameter autofluorescence

Márcia Mesquita Peixoto[1,2,3,4,5,6] | Francisca Soares-da-Silva[1,2,3] | Sandrine Schmutz[7] | Marie-Pierre Mailhe[1,2,3] | Sophie Novault[7] | Ana Cumano[1,2,3] | Cedric Ait-Mansour[8]

[1]Immunology Department, Unit Lymphocytes and Immunity, Institut Pasteur, Paris, France

[2]INSERM U1223, Paris, France

[3]Université de Paris, Sorbonne Paris Cité, Paris, France

[4]Instituto de Investigação e Inovação em Saúde, Universidade do Porto, Porto, Portugal

[5]Instituto Nacional de Engenharia Biomédica, Universidade do Porto, Porto, Portugal

[6]Instituto de Ciências Biomédicas Abel Salazar, Universidade do Porto, Porto, Portugal

[7]Flow cytometry core facility, CRT2, Institut Pasteur, Paris, France

[8]Sony Europe B.V, Weybridge, United Kingdom

**Correspondence**
Ana Cumano, Immunology Department, Institut Pasteur 25 Rue du Dr. Roux 75724 Paris, CEDEX 15, France.
Email: ana.cumano@pasteur.fr

**Funding information**
This work was supported by grants from Institut Pasteur, INSERM, ANR and FCT/MCTES.

**Abstract**

The fetal liver (FL) is the main hematopoietic organ during embryonic development. The FL is also the unique anatomical site where hematopoietic stem cells expand before colonizing the bone marrow, where they ensure life-long blood cell production and become mostly resting. The identification of the different cell types that comprise the hematopoietic stroma in the FL is essential to understand the signals required for the expansion and differentiation of the hematopoietic stem cells. We used a panel of monoclonal antibodies to identify FL stromal cells in a 5-laser equipped spectral flow cytometry (FCM) analyzer. The "Autofluorescence Finder" of SONY ID7000 software identified two distinct autofluorescence emission spectra. Using autofluorescence as a fluorescence parameter we could assign the two autofluorescent signals to three distinct cell types and identified surface markers that characterize these populations. We found that one autofluorescent population corresponds to hepatoblast-like cells and cholangiocytes whereas the other expresses mesenchymal transcripts and was identified as stellate cells. Importantly, after birth, autofluorescence becomes the unique identifying property of hepatoblast-like cells because mature cholangiocytes are no longer autofluorescent. These results show that autofluorescence used as a parameter in spectral FCM is a useful tool to identify new cell subsets that are difficult to analyze in conventional FCM.

**KEYWORDS**
autofluorescence, fetal liver, hepatoblast-like cells/hepatocytes, spectral flow cytometry

### 1 | INTRODUCTION

Flow cytometry (FCM) has rapidly evolved over the past few decades [1]. The development of more advanced technologies including mass cytometry [2], imaging FCM [3], genomic FCM [4] and spectral FCM [5], has expanded our ability to study immune responses, by characterizing more cellular parameters simultaneously in single cells with higher resolution than ever before. FCM characterizes physical and fluorescent properties of cells in suspension by using fluorochrome-conjugated antibodies to measure proteins expressed by distinct immune cell subpopulations [6].

Spectral FCM was first proposed by J. Paul Robinson at Purdue University in 2004 [7]. The first commercial instrument (Sony SP6800) was launched by Sony Biotechnology in 2012, using prisms along with PMT detectors to collect and amplify light beyond the capability of

Marcia Mesquita Peixoto, Francisca Soares-da-Silva contributed equally. Sophie Novault, Ana Cumano, and Cedric Ait-Mansour are Co-senior authors.

This is an open access article under the terms of the Creative Commons Attribution-NonCommercial License, which permits use, distribution and reproduction in any medium, provided the original work is properly cited and is not used for commercial purposes.
© 2022 The Authors. *Cytometry Part A* published by Wiley Periodicals LLC on behalf of International Society for Advancement of Cytometry.

conventional flow cytometers [8]. The Sony SP6800 is equipped with three lasers 405/488/638 nm and two pinholes such that two excitation lasers can be used in a given experiment. Using the 405/488 nm excitation lasers we assembled a 19-fluorescent probe panel to analyze immune cells in the mouse adult spleen [9, 10]. Moreover, analysis of antibody-stained preparations of embryonic, neonatal, and adult heart, which is a highly auto-fluorescent tissue, allowed the robust identification of new surface markers of different cardiac populations [11]. In addition, intra-epithelial lymphocytes were efficiently analyzed in mouse intestinal epithelium cell preparations because the autofluorescence management allowed eliminating from the analysis the autofluorescent epithelial cells [9]. Recently, the Sony ID7000 became available with different laser configurations that can be remodeled. The ID7000 Software analysis is based on the previously described Weighted Least Squares Method algorithm [8] that allows the easy detection of auto-fluorescence (AF) that can be incorporated in the panel as independent fluorescent parameters.

The fetal liver (FL) is a highly auto-fluorescent tissue where hepatic and hematopoietic cells differentiate alongside and where hepatic and mesenchymal cells play, yet ill-defined, roles in hematopoietic differentiation [12] and in the establishment of the hematopoietic stem cell compartment [13]. In addition, although surface markers for different populations have been identified, a global analysis of the FL stroma using epithelial and mesenchymal markers has not been undertaken.

Here we sought to analyze the nonhematopoietic stromal compartment in mouse FL using a 14-fluorochrome antibody panel and distinct AF parameters that were unique in the identification of cell populations. We found two major AF signals at embryonic day (E)18.5 of mouse gestation. One AF signal has different emission spectra in the 355 nm laser and in the 405 nm laser. It defines stellate cells that accumulate autofluorescent vitamin A in cytoplasmic granules [14]. The second AF signal is visible in the 355 nm laser, in the 405 nm and also with a lower intensity and different emission spectra in the 488 and 561 nm lasers and marks hepatoblasts/hepatocytes and cholangiocytes. Importantly, AF is an invaluable tool to distinguish cells with the characteristics of E14.5 hepatoblasts, after birth, hereafter designated as hepatoblast-like cells. In addition, defining the true fluorescence associated with each autofluorescent population helped design a sorting strategy to be used in conventional FCM. These results indicate that AF treated as a fluorescence parameter in spectral FCM is essential to the characterization of cell subsets in solid tissues.

## 2 | MATERIALS AND METHODS

The experiment was designed to identify populations of stromal cells in the mouse FL at different stages of gestation.

### 2.1 | Cell suspension

E14.5, E18.5 FLs, P3 and P9 livers were dissected under a binocular magnifying lens. Cells were recovered in Hanks' balanced-salt solution (HBSS) supplemented with 1% fetal calf serum (FCS) (Gibco) or RPMI medium (Gibco) supplemented with 10% FCS (P3 and P9) and treated with 0.05 mg/ml Liberase TH (Roche) and 0.2 mg/ml DNAse (Sigma) for 6–8 min at 37°C. Cells were resuspended by gentle pipetting. Before staining, cell suspensions were filtered with a 100 μm cell strainer (BD). All experiments using E14.5 and E18.5 embryos were done by pooling FL cells from the same litter in each experiment, in three or more biological replicates. In an independent experiment, FL cells were analyzed after mechanical dissociation (in two biological replicates; *data not shown*).

### 2.2 | Flow sample and specimen description

All antibodies were titrated to give the highest signal-to-noise ratio. The antibody panel has been optimized in a conventional flow cytometer (LSR Fortessa with five lasers (BD Biosciences) and then used in the ID7000 (Sony) to study the autofluorescence. Liver cells were depleted of $Ter119^+$ $CD45^+$ $CD71^+$ $CD117^+$ cells by magnetic cell separation using LS MACS Columns (Miltenyi Biotec). Cell suspensions were stained in two steps. First, cell suspensions of FL were incubated with the biotinylated antibodies for 15–20 min at 4°C. Cells were washed to eliminate excess of antibody, incubated for 15 min with anti-biotin beads (Miltenyi Biotec) and applied to a LS MACS

**TABLE 1** List of the antibodies used in this study and their specificity

| Marker | Conjugation | |
|---|---|---|
| SAV | PE-Cy5 | CD45, TER119, CD71, CD117 (all hematopoietic cells) biotin |
| Dead | PI | – |
| CD324 | PE-Cy7 | (Epithelial-Cadherin) hepatoblasts, hepatocytes and cholangiocytes |
| CD31 | PerCP-Cy5.5 | (Platelet and endothelial cell adhesion molecule) endothelial cells |
| CD166 | FITC | (Activated Leukocyte Cell Adhesion Molecule) hepatoblasts and stellate cells |
| CD140a | APC | (Platelet derived growth factor receptor a) stellate cells and pericytes |
| Gp38 | APC-Cy7 | (Podoplanin) mesenchymal cells, lymphatic endothelial cells |
| NG2 | PE | (Chondroitin sulphate proteoglycan 4) pericytes |
| Sca-1 | BV711 | (Stem Cell antigen 1) endothelial cells |
| CD146 | BV510 | (Melanoma cell adhesion molecule) endothelial cells and mesenchymal cells |
| CD51 | BV421 | (Integrin alpha V) mesenchymal cells |
| CD326 | BV605 | (Epithelial cell adhesion molecule) cholangiocytes (bile duct cells) |
| CD54 | BUV395 | (Intercellular Adhesion Molecule 1) hepatoblasts and endothelial cells |
| Thy1.2 | AF700 | (Cluster of differentiation 90) mesenchymal cells |

Column (Miltenyi Biotec). The 5% of the cells were not passed through the MACS column and were used as depletion control. The 5% of the eluted cells were used as unstained control and the remaining were incubated for 20–30 min at 4°C in the dark with directly labeled antibodies (and streptavidin (SAV) listed in Table 1/Supplemental Table 1. PI was added to depleted stained and to the depletion control samples.

## 2.3 | Instrument details

Stained cells were analyzed in the Sony ID7000 spectral cytometer. The LE-ID7000E used in this study has five lasers 355/405/488/561/637 nm (Supplemental Figure 1), PMT gains/voltages can be independently adjusted for each laser, and there are seven pinholes allowing for additional lasers to be installed. The schematic optical configuration is shown in Supplemental Figure 1, framed by a black box. The detection capacity of the ID7000 spans from 360 nm to 820 nm in the 5-laser configuration. The signals are captured with 32-, 26-, and 19-channel PMT arrays and individual PMT, as shown.

Before the analysis, the Sony ID7000 was calibrated using the align-check and the performance 8-peak beads, following the guidelines of the instrument provider. A minimum of 100,000 events were acquired for cell-stained samples and a minimum of 20,000 events for unstained samples. In every experiment single-stained samples in

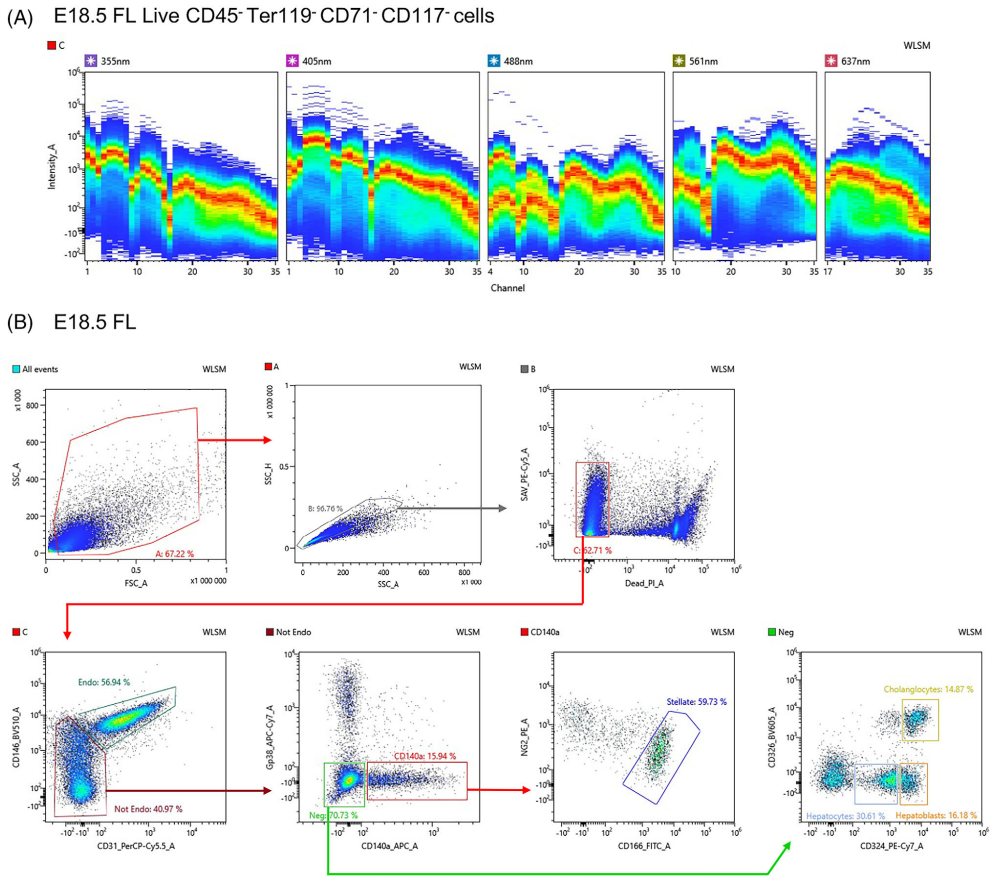


**FIGURE 1** Gating strategy to identify stellate cells, hepatoblasts-like cells, hepatocytes and cholangiocytes. E18.5 mouse fetal liver cell suspensions were stained with biotin labeled antibodies recognizing CD45, TER119, CD71, CD117. Negative cells were magnetically sorted and labeled with the antibodies in Table 1. (A) The spectra of emission of fetal liver cells after depletion (marked with streptavidin in a dump channel) and gated out of PI labeled cells. (B) After unmixing, cells were manually gated to define endothelial, hepatic and stellate cells. The analysis started with a FSC_A/SSC_A gate, doublet exclusion and PI positive/SAV positive cell exclusion. The gate for SAV exclusion was set by the depletion control sample (not depleted). CD324 was defined as a marker of epithelial cells, cholangiocytes CD324$^{high}$CD326$^{+}$; hepatocytes CD324$^{low}$CD326$^{-}$; hepatoblasts-like cells CD324$^{high}$CD326$^{-}$. Stellate cells are defined by as PDGFRa$^{+}$ CD166$^{+}$. [Color figure can be viewed at wileyonlinelibrary.com]

Ultracomp eBeads (Thermo Fisher), for each individual fluorochrome, were provided and a minimum of 2000 events were collected. Total FL cells stained with propidium iodide (PI) were used as the control for dead cell exclusion. Unstained cells after depletion were always included. Stained cells with the full panel, before depletion of hematopoietic cells, were analyzed as a control for lineage staining.

## 3 | DATA ANALYSIS DETAILS

### 3.1 | Autofluorescence analysis

The unstained samples, after depletion of hematopoietic cells, were analyzed using the autofluorescence finder function as shown in Figure 2. This is a nonautomatic visualization tool where scanning across the emission wavelengths on each laser detects the best display of autofluorescence. The scanning is done by moving the cursor (bar under top plots in Figure 2) and the signal in the different combined detectors can be adjusted to find the best separation between the different autofluorescence signals. The autofluorescence signals are then manually gated and checked for their emission spectra (see Figure 2, lower panels). Distinct autofluorescence signals will separate in one of the laser combinations and will have distinct emission spectra. Once identified the autofluorescence signals are incorporated in the unmixing matrix.

Acquired full spectrum are analyzed with algorithms based on the WLSM as described previously [8]. The accuracy of the unmixing is ensured by the analysis of the single stained samples. Further manual adjustments (usually not required) can be done. Acquisitions were done with similar settings of the laser PMT.

Cells were sorted with a BD FACSAria III (BD Biosciences) according to the guidelines for the use of FCM and cell sorting [6]. The FACSAria III was calibrated with CST beads following the manufacturer's protocols. Data were analyzed with the ID7000 (Sony, Inc) or FlowJo (v.10.7.3, BD Biosciences) software.

### 3.2 | Gene expression by RT-PCR

Cells were sorted directly into lysis buffer and mRNA was extracted with a RNeasy Micro Kit (Qiagen). After extraction mRNA was reverse-transcribed into cDNA with PrimeScript RT Reagent Kit (Takara Bio), followed by quantitative PCR with Power SYBR Green PCR Master Mix (Applied Biosystems). Primers used were as follows: Actb FW: GCTTCTTTGCAGCTCCTTCGT; Actb RV: ATCGTCATCCATGGCGAACT; Afp FW: CTTCCCTCATCCTCCTGCTAC; Afp RV: ACAAACTGGGTAAAGGTGATGG; Alb FW: TGCTTTTTCCAGGGGTGTGTT; Alb RV: TTACTTCCTGCACTAATTTGGCA; Des FW: GTGGATGCAGCCACTCTAGC; Des RV: GTGGATGCAGCCACTCTAGC; Onecut1 FW: GCCCTGGAGCAAACTCAAGT; Onecut1 RV: TTGGACGGACGCTTATTTTCC; Pdgfrb FW: TTCCAGGAGTGATACCAGCTT; Pdgfrb RV: AGGGGGCGTGATGACTAGG; Sox9 FW: CTCCTCCACGAAGGGTCTCT; Sox 9 RV: AGGAAGCTGGCAGACCAGTA. qPCR reactions were performed on a Quantstudio3 thermocycler (Applied Biosystems), gene expression was normalized to that of β-actin and relative expression was calculated using the $2^{-\Delta Ct}$ method.

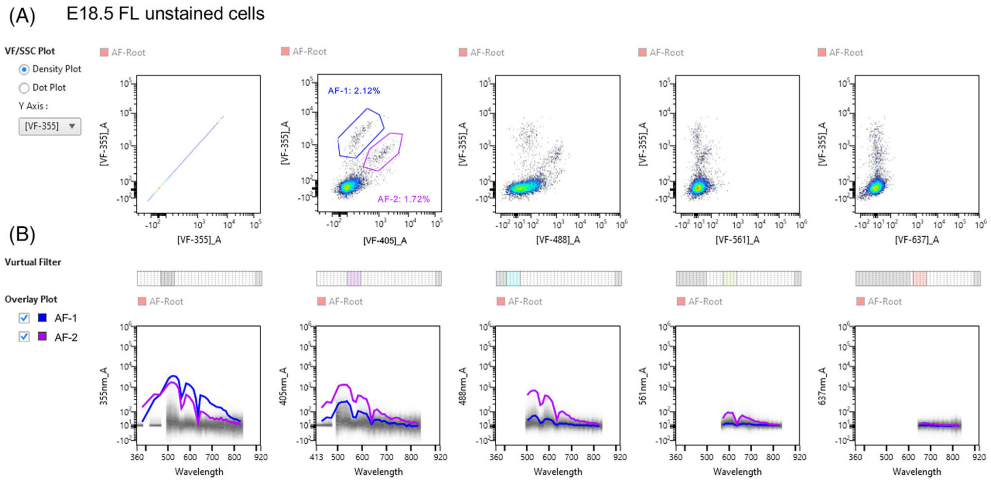


**FIGURE 2** Autofluorescence finder. The analytical tool autofluorescence applied to unstained cells before unmixing. (A) Autofluorescence is defined manually in cells that show fluorescence in the different lasers, as defined in Materials and Methods. (B) The spectra of emission of the two defined autofluorescent (AF) signals in the different lasers. [Color figure can be viewed at wileyonlinelibrary.com]

### 3.3 | Statistical analysis

All results are shown as mean ± standard deviation (SD). Statistical significance was determined using one-way ANOVA followed by Tukey's multiple comparison test where a $p$ value <0.05 was considered significant and a $p$ value >0.05 was considered not significant.

## 4 | RESULTS

### 4.1 | A strategy to characterize nonhematopoietic cell populations in FL

To characterize nonhematopoietic (hereafter referred to as stromal) populations in the FL we assembled a panel of 14 fluorescent dyes (Table 1) that included propidium iodide (PI-dead cell exclusion) and 13 fluorescence conjugated antibodies that mark cells belonging to the hepatic, endothelial and mesenchymal lineages (liver fibroblasts, also called stellate cells - see Table 1). The analysis was done in FL cell suspensions depleted of hematopoietic cells in a dump channel that includes the erythroid marker TER119, the pan-hematopoietic marker CD45, and CD71 and CD117 that together mark embryonic erythroid progenitors [15]. Cells were depleted of hematopoietic cells, that represent more than 80% of total FL cells, by magnetic sorting. We analyzed liver cells isolated from embryonic days (E) 14.5 and E18.5 (1 day prior to birth), and from days 3 and 9 postbirth (P3 and P9). Figure 1A shows the spectra of emission of E18.5 cells after the elimination of hematopoietic and dead cells. Figure 1B shows the gating strategy used to identify known cell subsets with CD31 and CD146 defining endothelial cells, and, in nonendothelial cells, CD140a (PDGFRa), Gp38 (podoplanin), and CD166 (ALCAM) define stellate cells as CD140a$^{+}$ Gp38$^{-}$CD116$^{+}$ [13]. In the Gp38$^{-}$CD140a$^{-}$ subset, CD326 and CD324 (E-Cadherin) define cholangiocytes (CD324$^{+}$CD326$^{+}$) [16] and hepatic cells (CD324$^{high/low}$ CD326$^{-}$) [17] . This analysis shows that at E18.5 all major FL populations are detected, and hepatocytes are difficult to discriminate from the decreasing numbers of hepatoblasts that are undergoing differentiation.

### 4.2 | Two different autofluorescence patterns identified by the autofluorescence finder

AF is a property of many tissues defined as signal emission by cells excited at particular wavelengths, in the absence of specific fluorescence. AF can mask or distort true fluorescence and is usually subtracted to facilitate the fluorescence detection. The ID7000 spectral cytometer is equipped with an analytical software that provides a tool to identify independent AF signals called AF finder (Figure 2, see Materials and Methods). In unstained cells this tool allowed the detection of two AF signals (Figure 2A). AF-1 shows an emission spectra with 3 emission peaks detected in the 355 and 405 lasers(around 510nm, 590nm and 655nm) and 2 smaller emission peaks in the 488 laser (around510nm and 590nm). AF-2 shows a similar emission spectra as AF-1 with the addition of anemission peak at 655nm in the 488 laser and 2 emission peaks in the 561 laser (around600nm and 655nm). The differences in the spectra of emission found in most laser channels suggested that these two AF signals correspond to two independent cell types. Efficient single cell suspension that minimizes cell death requires an enzymatic digestion of the FL. To test whether the two autofluorescence signals were impacted by the enzymatic digestion we analyzed E14.5 FL after mechanic dissociation. The autofluorescent signals were detected after mechanic dissociation (*data not shown*) indicating that they are an intrinsic property of the two subsets. The frequencies and numbers of cells exhibiting AF-1 and AF-2 were, however, strongly reduced consistent with our previous observation that mechanical dissociation is not suited for FL viable cell recovery.

After unmixing, we used AF-1 and AF-2 as independent parameters to define two different populations and proceeded to identify their identity (Figure 3A–D). Figure 3 shows two independent gating strategies, one that analyzes cells within AF-1 (Figure 3B) compared to the conventional strategy previously shown in Figure 1 (Figure 3A). AF-1 cells correspond to a majority of CD31$^{-}$ (85%), CD140a$^{+}$ (85%) cells and CD116$^{+}$ (95%) cells (Figure 3B) that define, with a high degree of enrichment, stellate cells.

CD324$^{+}$ hepatocytes and CD324$^{+}$CD326$^{+}$ cholangiocytes (bile duct cells) are known to derive during embryonic development from bipotent progenitors called hepatoblasts [18]. AF-2 gated cells (Figure 3C) comprise a majority (83%) of CD31$^{-}$ nonendothelial cells, 94% of CD140a$^{-}$ gp38$^{-}$ and > 90% of CD324$^{high}$. We designated this population hepatoblasts-like cells because they closely resemble cells with similar phenotype and autofluorescent properties in E14.4 FL, before cholangiocyte differentiation (Supplemental Figure 2), known to be bipotent progenitors [16]. Within AF-2 in E18.5 FL we also found CD324$^{+}$ CD326$^{+}$ cholangiocytes [19]. Interestingly, the analysis done in AF-2 did not detect the subset that expresses low levels of CD324 that we classify as hepatocytes [17] (Figure 3C). AF-2 is, therefore, an important parameter to distinguish hepatoblasts-like cells from hepatocytes, at this stage of development. When auto-fluorescent cells were gated out, stellate cells are virtually absent from the plots (Figure 3D) whereas a subset of hepatoblasts-like cells and cholangiocytes are still detected (30% and 50%, respectively) indicating that AF-2 distinguishes two different cell subsets (AF-2$^{+}$ and AF-2$^{-}$ cells) in each of these populations. The cells designated as nonAF correspond to cells with low AF-1 and AF-2 and comprise all other cell populations in the FL that exhibit background levels of AF.

### 4.3 | Properties and identity of FL stromal cells

To further characterize the AF of FL cells and determine whether this is a cell-intrinsic property or if it is lost upon manipulation we sorted hepatic cells, hepatoblast-like cells and stellate cells from E18.5 FL

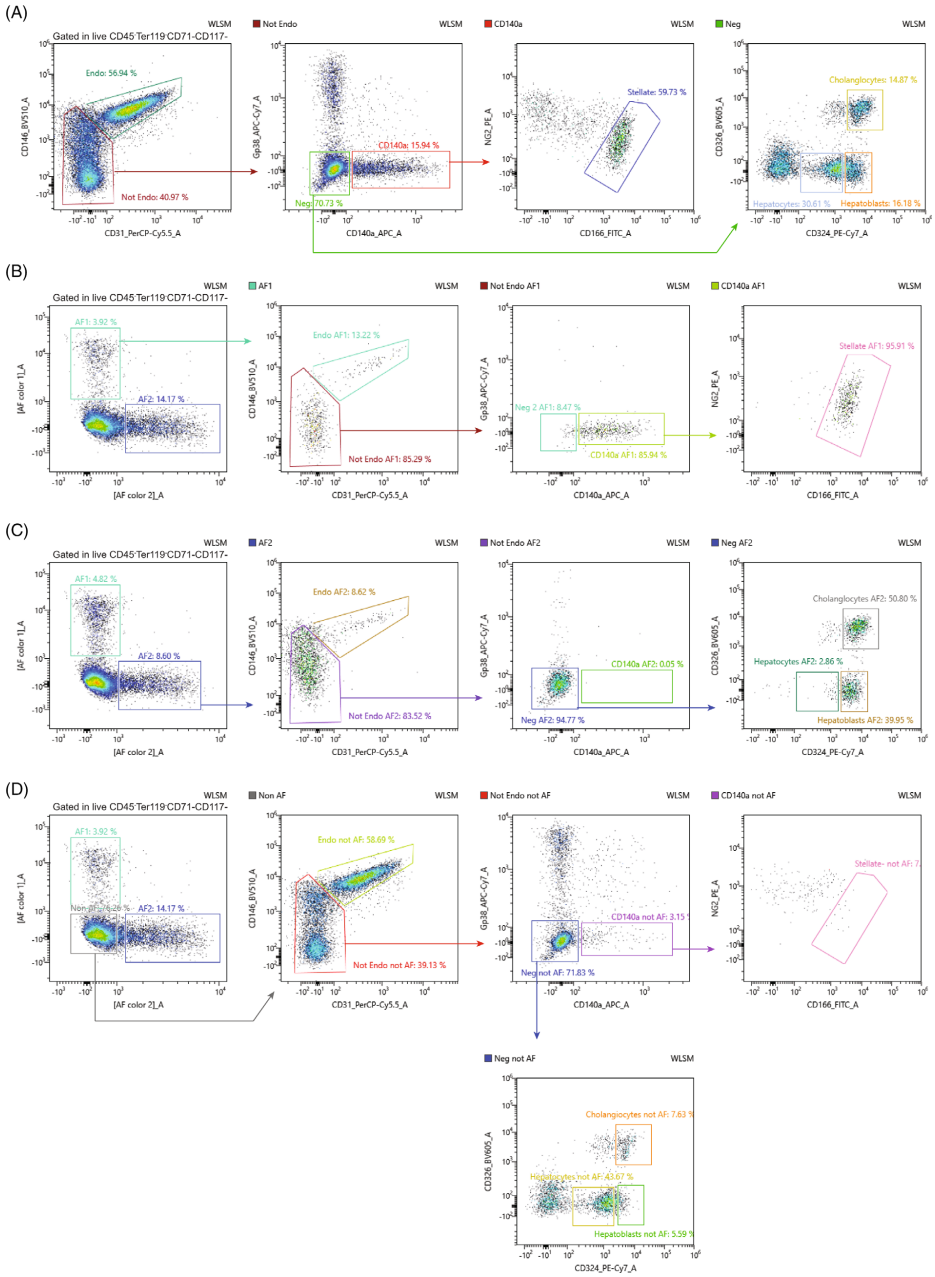


**FIGURE 3** Two distinct autofluorescent signals: AF-1 defines stellate cells and AF-2 defines a subset of hepatic cells and cholangiocytes. After unmixing the two AF signals can be used as two additional fluorescent parameters. (A) E18.5 FL live CD45$^-$TER119$^-$CD71$^-$CD117$^-$ cells were analyzed as in Figure 1B. (B) Analysis of E18.5 FL live CD45$^-$TER119$^-$CD71$^-$CD117$^-$AF1$^+$ cells using the same strategy as in Figure 1B. (C) Analysis of E18.5 FL live CD45$^-$TER119$^-$CD71$^-$CD117$^-$AF2$^+$ cells using the same strategy as in Figure 1B. (D) Analysis of E18.5 FL live CD45$^-$TER119$^-$CD71$^-$CD117$^-$AF1$^-$AF2$^-$ cells using the same strategy as in Figure 1B. [Color figure can be viewed at wileyonlinelibrary.com]

using a simplified panel in a conventional flow cytometer (Figure 4A, presort). All populations before and after cell sorting were analyzed in spectral FCM (Figure 4B, sorted populations). Stellate cells (lower plots) show persistent levels of AF whereas hepatocytes (upper plots) remained negative for this parameter. As previously observed, hepatoblast-like cells sorted as CD324$^{high}$ cells yield a mixed population of AF-2$^{+}$ and AF-2$^{-}$ cell (middle plots). These results indicated that AF in FL populations is a cell-specific property.

In order to unambiguously ascertain the lineage affiliation of these three cell subsets we subjected the cells sorted to quantitative RT-PCR. We show that cells classified as cholangiocytes by FCM express the cholangiocytic markers *Sox9* and *Onecut 1* (*Hnf6*) [16], the hepatoblasts-like cells express *Onecut 1* [18], *Alb* and *Afp* whereas stellate cells express *Desmin* and *Pdgfrb* (Figure 4C) [20]. This transcriptional profile is specific for the three subsets thus confirming the lineage affiliation inferred by the surface marker expression.

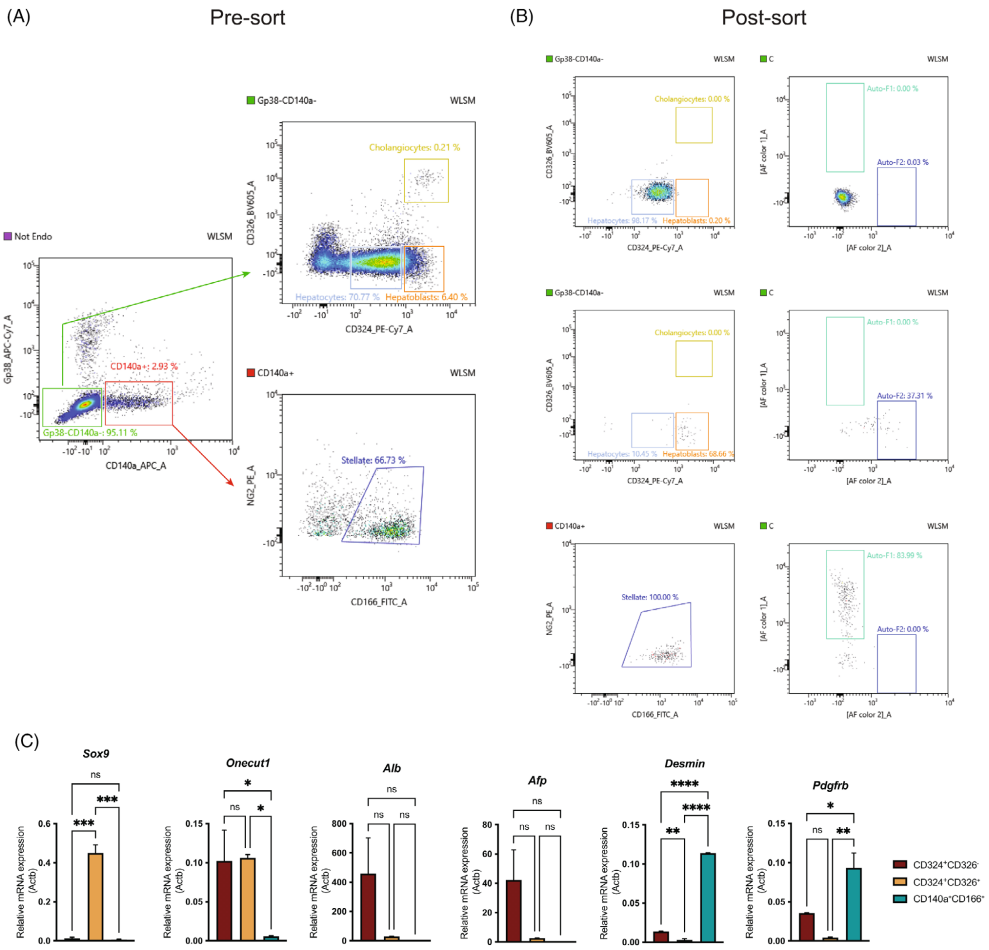


**FIGURE 4** Autofluorescence is a cell intrinsic property. (A) Fetal liver cells negative for the dump channel and for PI expressing cells were sorted after being stained with a simplified antibody panel including Gp38, CD140a, NG2, CD166, CD324 and CD326. Hepatocytes, hepatoblast-like cells and stellate cells were sorted according to the strategy shown (presort). Sorted cells were reanalyzed in the ID7000 spectral analyzer (sorted populations). Left plots show purity control, right plots show AF of sorted cells. (B) Sorted cholangiocytes, hepatoblast-like cells and stellate cells as in A were subjected quantitative RT-PCR in triplicate samples of two independent experiments for *Sox9*, *Onecut1*, *Alb*, *Afp*, *Desmin* and *Pdgfrb*, and normalized to the expression of β-actin used as house-keeping gene. Data are represented as mean +/− SD. *$p < 0.05$, **$p < 0.01$, ***$p < 0.001$, ****$p < 0.0001$. [Color figure can be viewed at wileyonlinelibrary.com]

### 4.4 | Autofluorescence defines hepatoblast-like cells after birth

Hepatoblast-like cells decrease in numbers as development progresses, so we used AF-2 to detect these cells, after birth. However, hepatocytes that are the dominant liver population after birth are fragile epithelial cells, highly sensitive to manipulation ex vivo and to the disruption of the tight junctions, required for single-cell suspensions. Consequently, we detected decreasing numbers of hepatocytes with age. At P3 and P9 the levels of AF were very similar in spectrum and intensity to those seen at E18.5. At P3 and P9 AF-2 represents a majority of hepatoblast-like cells with high expression of CD324, and by high AF-2 (Figure 5A). Interestingly, at these stages, most cholangiocytes lost expression of AF-2. This result is reinforced at P9 (Figure 5B) where gating in AF-2 yields 93% of hepatoblast-like cells. These results further indicate that AF-2 is essential for the identification of hepatoblast-like cells, after birth.

## 5 | DISCUSSION

In this report we used a spectral flow cytometer equipped with five lasers to analyze a highly autofluorescent tissue, the FL, in single-cell suspensions. The software analysis of the Sony ID7000 is equipped with an analytical tool for easy detection of different autofluorescent signals. The unmixing algorithm subtracts the AF to find true fluorescent signals but importantly, by using the AF signals as independent parameters, it increased the panel of 14-fluorescent dyes into a 16-fluorescence panel.

The "Autofluorescence finder" tool identified independent AF signals that differed in shape and intensity in the different laser

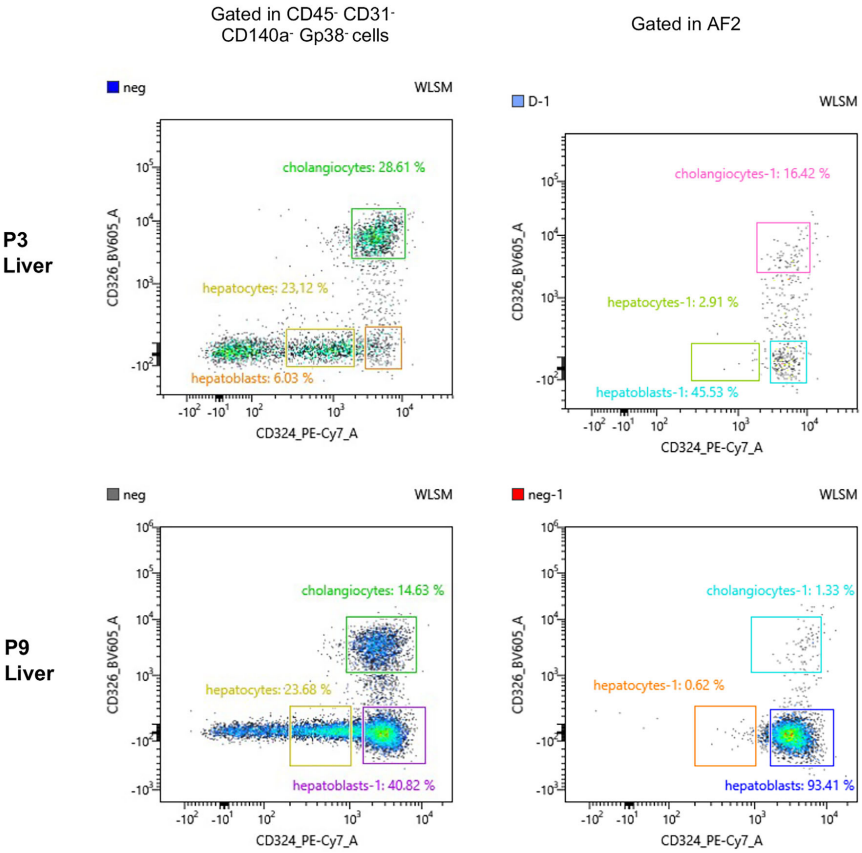


**FIGURE 5** AF2 defines hepatoblast-like cells after birth. Analysis of live CD45⁻TER119⁻CD71⁻CD117⁻ P3 and P9 liver cells in a plot of CD324/CD326 after the conventional gating strategy defined in Figure 1 (left plots) or on the cells gated for AF2 expression (right plots). [Color figure can be viewed at wileyonlinelibrary.com]

detectors. Gating on AF-1 we identified a dominant population with the phenotype that defines stellate cells, the fibroblasts specific to the liver. This population has previously been reported to be endowed with AF in a limited analysis using conventional FCM because stellate cells store vitamin A in cytoplasm granules [14]. The second AF signal, AF-2, was found in epithelial cells (expressing CD324) that, at E18.5, could be subdivided into two subsets. The first expressed CD326 which is specific, at this stage, of newly differentiated cholangiocytes [19], and the second expressed the highest levels of CD324 while lacking CD326 and was consequently classified as hepatoblasts-like cells because they resemble E14.5 hepatoblasts [16, 17].

Irrespective of the cell preparation method, enzymatic digestion or mechanical dissociation, the two autofluorescent signals were detected, although mechanical dissociation resulted in lower representation of stellate cells and hepatoblast-like cells. We conclude that the two independent AF signals in stromal FL populations were intrinsic properties of the cells which confers reliability to the analysis. The transcriptional profile of the AF populations unambiguously confirmed the lineage affiliation proposed by the surface marker analysis.

The AF-2 parameter allowed the distinction of hepatocytes from hepatoblast-like cells ($CD324^+$ $CD326^-$ cells), by clearly demarcating the limits between the two cell types. Because hepatoblast-like cells rapidly decrease after birth, as most proliferative activity in the adult liver is driven by hepatocytes, we analyzed liver cells after birth. We found that the two different AF signals persisted at these later time points with AF-2 marking a majority of hepatoblast-like cells. Interestingly, most cholangiocytes lost AF-2 at P3 and virtually all were $AF2^-$ at P9. AF-2 is therefore the only property specific for hepatoblast-like cells, after birth. Although hepatocytes are the most numerous cells in the adult liver, they comprised less than 20% of the cell suspension analyzed here. This observation is consistent with the well-documented fragility of hepatocytes. The protocols currently recommended to isolate viable hepatocytes include enzymatic digestion similar to the procedure used in this study [21]. Alternatively, a perfusion with an enzymatic solution is followed by a purification in a Percoll gradient [22]. In any of these methods, $5–20 \times 10^6$ hepatocytes [21] (1%–6%) can be obtained out of the $3 \times 10^8$ hepatocytes in a mouse liver [23] indicating that no efficient procedure is currently available to isolate hepatocytes.

Our study presents several innovations: (1) The ID7000 software analysis provides an easy tool to detect independent AF signals; (2) The unmixing algorithm subtracts the AF signals to allow accurate true fluorescence detection, a feature already present in the SP6800; (3) Importantly, the analytical tool treats the AF signals as fluorescence and increases, therefore, the panel of analyzed parameters. We provide evidence that these advances will be invaluable to the characterization of single-cell suspensions obtained from autofluorescent tissues, difficult to analyze in conventional FCM.

## ACKNOWLEDGMENTS

We thank all members of the FCM core facility, the members of the Institut Pasteur laboratory, Antonio Bandeira, Paulo Vieira, Rachel Golub and Pablo Pereira. This work was financed by the Institut Pasteur, INSERM, ANR (grant Twothyme, grant DELSTAR and grant EPI-DEV), REVIVE Future Investment Program and Pasteur-Weizmann Foundation through grants to A.C. This work was financed by Portuguese funds through FCT/MCTES in the framework of the project PTDC/MED-OUT/32656/2017 (POCI-01-0145-FEDER-032656). F.S.S is funded by the REVIVE Future investments postdoctoral grant (Investissement d'Avenir; ANR-10-LABX-73). MP is funded by FCT grant SFRH/BD/143605/2019.

## AUTHOR CONTRIBUTIONS

**Marcia Peixoto:** Conceptualization (equal); data curation (equal); formal analysis (equal); investigation (equal); methodology (equal); writing – original draft (equal); writing – review and editing (equal). **Francisca Soares da Silva:** Conceptualization (equal); data curation (equal); formal analysis (equal); investigation (equal); methodology (equal); writing – original draft (equal); writing – review and editing (equal). **Sandrine Schmutz:** Data curation (equal); formal analysis (equal); methodology (equal). **Marie-Pierre Mailhe:** Data curation (equal); formal analysis (equal). **Sophie Novault:** Conceptualization (equal); data curation (equal); formal analysis (equal); investigation (equal); methodology (equal); project administration (equal); supervision (equal); writing – original draft (equal). **Ana Cumano:** Conceptualization (equal); data curation (equal); funding acquisition (equal); project administration (equal); supervision (equal). **Cedric Ait-Mansour:** Conceptualization (equal); data curation (equal); formal analysis (equal); investigation (equal); methodology (equal); project administration (equal); supervision (equal); validation (equal).

## CONFLICT OF INTEREST

Cedric Ait-Mansour is working for the company Sony Europe B.v as a global senior manager market development-new products. All other authors declare no competing interests.

## DATA AVAILABILITY STATEMENT

A version of this manuscript is available in BioRxiv bioRxiv 2021.09.29.462345; doi: https://doi.org/10.1101/2021.09.29.462345. FCM data has been deposited in Flow Repository under the name "FL autofluorescence."

## ORCID

*Francisca Soares-da-Silva* https://orcid.org/0000-0003-1312-7601
*Sophie Novault* https://orcid.org/0000-0001-5708-3597
*Ana Cumano* https://orcid.org/0000-0002-4578-959X

## REFERENCES

1. Robinson JP. Spectral flow cytometry-quo vadimus. Cytometry A. 2019;95:823.
2. Spitzer MH, Nolan GP. Mass cytometry: single cells. Many Features Cell. 2016;165:780–91.
3. Basiji DA. Principles of Amnis imaging flow cytometry. Methods Mol Biol. 2016;1389:13.
4. Stoeckius M, Hafemeister C, Stephenson W, Houck-Loomis B, Chattopadhyay PK, Swerdlow H, et al. Simultaneous epitope and transcriptome measurement in single cells. Nat Methods. 2017;14:865–8.
5. Nolan JP, Condello D. Spectral flow cytometry. Curr Protoc Cytom. 2013;63:1–13.

6. Cossarizza A, Chang HD, Radbruch A, Acs A, Adam D, Adam-Klages S, et al. Guidelines for the use of flow cytometry and cell sorting in immunological studies (second edition). Eur J Immunol. 2019;49:1457–973.
7. Grégori G, Patsekin V, Rajwa B, Jones J, Ragheb K, Holdman C, et al. Hyperspectral cytometry at the single-cell level using a 32-channel photodetector. Cytometry A. 2012;81:35–44.
8. Futamura K, Sekino M, Hata A, Ikebuchi R, Nakanishi Y, Egawa G, et al. Novel full-spectral flow cytometry with multiple spectrally-adjacent fluorescent proteins and fluorochromes and visualization of in vivo cellular movement. Cytometry A. 2015;87:830–42.
9. Schmutz S, Valente M, Cumano A, Novault S. Spectral cytometry has unique properties allowing multicolor analysis of cell suspensions isolated from solid tissues. PLoS One. 2016;11:e0159961.
10. Schmutz S, Valente M, Cumano A, Novault S. Analysis of cell suspensions isolated from solid tissues by spectral flow cytometry. J Vis Exp. 2017;123:55578.
11. Valente M, Resende TP, Nascimento DS, Burlen-Defranoux O, Soares-da-Silva F, Dupont B, et al. Mouse HSA+ immature cardiomyocytes persist in the adult heart and expand after ischemic injury. PLoS Biol. 2019;17:e3000335.
12. Pinho S, Frenette PS. Haematopoietic stem cell activity and interactions with the niche. Nat Rev Mol Cell Biol. 2019;20:303–20.
13. Soares-da-Silva F, Peixoto M, Cumano A, Pinto-do-Ó P. Crosstalk between the hepatic and hematopoietic systems during embryonic development. Front Cell Dev Biol. 2020;8:612.
14. Kubota H, Yao HL, Reid LM. Identification and characterization of vitamin A-storing cells in fetal liver: implications for functional importance of hepatic stellate cells in liver development and hematopoiesis. Stem Cells. 2007;25:2339–49.
15. Soares-da-Silva F, Freyer L, Elsaid R, Burlen-Defranoux O, Iturri L, Sismeiro O, et al. Yolk sac, but not hematopoietic stem cell-derived progenitors, sustain erythropoiesis throughout murine embryonic life. J Exp Med. 2021;218(4):e20201729.
16. Yang L, Wang WH, Qiu WL, Guo Z, Bi E, Xu CR. A single-cell transcriptomic analysis reveals precise pathways and regulatory mechanisms underlying hepatoblast differentiation. Hepatology. 2017;66:1387–401.
17. Nierhoff D, Levoci L, Schulte S, Goeser T, Rogler LE, Shafritz DA. New cell surface markers for murine fetal hepatic stem cells identified through high density complementary DNA microarrays. Hepatology. 2007;46:535–47.
18. Si-Tayeb K, Lemaigre FP, Duncan SA. Organogenesis and development of the liver. Dev Cell. 2010;18:175–89.
19. Tanaka M, Okabe M, Suzuki K, Kamiya Y, Tsukahara Y, Saito S, et al. Mouse hepatoblasts at distinct developmental stages are characterized by expression of EpCAM and DLK1: drastic change of EpCAM expression during liver development. Mech Dev. 2009;126:665–76.
20. Tan KS, Kulkeaw K, Nakanishi Y, Sugiyama D. Expression of cytokine and extracellular matrix mRNAs in fetal hepatic stellate cells. Genes Cells. 2017;22:836–44.
21. Jung Y, Zhao M, Svensson KJ. Isolation, culture, and functional analysis of hepatocytes from mice with fatty liver disease. STAR Protoc. 2020;1:100222.
22. Fry JR, Jones CA, Wiebkin P, Bellemann P, Bridges JW. The enzymic isolation of adult rat hepatocytes in a functional and viable state. Anal Biochem. 1976;71:341–50.
23. Falconer DS, Gauld IK, Roberts RC. Cell numbers and cell sizes in organs of mice selected for large and small body size. Genet Res. 1978;31:287–301.


## SUPPORTING INFORMATION

Additional supporting information may be found in the online version of the article at the publisher's website.

**How to cite this article:** Peixoto MM, Soares-da-Silva F, Schmutz S, Mailhe M-P, Novault S, Cumano A, et al. Identification of fetal liver stroma in spectral cytometry using the parameter autofluorescence. Cytometry. 2022. https://doi.org/10.1002/cyto.a.24567

# ANNEX V

Check for updates

DOI: 10.1111/imr.13187

INVITED REVIEW

Immunological Reviews WILEY

# Assembling the layers of the hematopoietic system: A window of opportunity for thymopoiesis in the embryo

Francisca Soares-da-Silva[1,2,3] | Ramy Elsaid[1,2,3] | Marcia Mesquita Peixoto[1,2,4,5] | Gonçalo Nogueira[1,2,3] | Pablo Pereira[1,2,3] | Antonio Bandeira[1,2,3] | Ana Cumano[1,2,3]

[1]Unit of Lymphocytes and Immunity, Immunology Department, Institut Pasteur, Paris, France

[2]INSERM U1223, Paris, France

[3]Université Paris Cité, Cellule Pasteur, Paris, France

[4]I3S – Instituto de Investigação e Inovação em Saúde & INEB – Instituto Nacional de Engenharia Biomédica, Universidade do Porto, Porto, Portugal

[5]Abel Salazar Biomedical Sciences Institute, University of Porto, Porto, Portugal

**Correspondence**
Ana Cumano, Lymphocytes and Immunity Unit – Immunology Department, 25 Rue du Dr Roux, 75015 Paris France.
Email: ana.cumano@pasteur.fr

**Present address**
Ramy Elsaid, Unit Genetics and Developmental Biology, Institut Curie, UMR3215/U934, Paris, France

**Funding information**
Agence Nationale de la Recherche; Faculdade de Ciências e Tecnologia, Universidade Nova de Lisboa, Grant/Award Number: SFRH/BD/143605/2019; Institut National de la Santé et de la Recherche Médicale, Grant/Award Number: U1223; Institut Pasteur; Ligue Contre le Cancer, Grant/Award Number: Departmental Committee "Ile-de-France"

**Summary**

During embryonic development, several independent generations of hematopoietic cells were identified. They occur in the yolk sac and the intra-embryonic major arteries, in a narrow window of development. They arise sequentially, starting with primitive erythrocytes in the yolk sac blood islands, progressing to less differentiated erythromyeloid progenitors still in the yolk sac, and culminating with multipotent progenitors, some of which will generate the adult hematopoietic stem cell compartment. All these cells contribute to the formation of a layered hematopoietic system that reflects adaptative strategies to the fetal environment and the embryo's needs. It is mostly composed, at these stages, of erythrocytes and tissue-resident macrophages both of yolk sac origin, the latter persisting throughout life. We propose that subsets of lymphocytes of embryonic origin derive from a different intra-embryonic generation of multipotent cells occurring before the emergence of hematopoietic stem cell progenitors. These multipotent cells have a limited lifespan and generate cells that provide basic protection against pathogens before the adaptive immune system is functional, contribute to tissue development and homeostasis, and shape the establishment of a functional thymus. Understanding the properties of these cells will impact the understanding of childhood leukemia and of adult autoimmune pathology and thymic involution.

KEYWORDS
fetal hematopoiesis, hematopoietic stem cells, lymphoid tissue inducer cells, thymic seeding progenitors, thymus

Francisca Soares-da-Silva, Ramy Elsaid, Marcia Mesquita Peixoto and Gonçalo Nogueira contributed equally to this work.

Pablo Pereira, Antonio Bandeira and Ana Cumano contributed equally as senior authors

This article is part of a series of reviews covering Ontogenic Waves of Immune Cell Development appearing in Volume 315 of *Immunological Reviews*

This is an open access article under the terms of the Creative Commons Attribution License, which permits use, distribution and reproduction in any medium, provided the original work is properly cited.
© 2023 INSERM. *Immunological Reviews* published by John Wiley & Sons Ltd.

## 1 | FOREWORD

More than 30 years ago, Herzenberg and Herzenberg proposed that the mammalian hematopoietic system is composed of cells originated from different waves of hematopoietic stem cells (HSC) with specific differentiation potential, emerging sequentially during embryonic development.[1] This notion integrated findings suggesting the embryonic origin of some adult lymphocyte subsets that were not easily generated from adult bone marrow (BM) progenitors and was published in a paper entitled "Toward a Layered Immune System". Although the tools to analyze hematopoiesis and the knowledge on progenitor subsets evolved, the notion that the hematopoietic compartment is composed of cells that originate from developmentally restricted progenitors and that persist for life is of actuality.

## 2 | A HISTORIC PERSPECTIVE

### 2.1 | Extra-embryonic generation: the yolk sac

Colony-forming cells in the spleen (CFU-S) is an in vivo assay that measures the presence of highly proliferative hematopoietic progenitors considered, for a long time, to comprise HSC.[2]

The first multilineage colony-forming cells were identified in the yolk sac (YS) at embryonic day (E)8 as CFU-S analyzed 8 days after transplantation ($CFU\text{-}S_8$).[3] In vitro colony formation in semi-solid medium was also first detected at this stage, peaked in numbers at E10 and decreased thereafter.[3] These results were consistent with a YS origin of HSC. However, pioneer experiments in the avian model challenged this idea. Chicken chimeras derived from chick embryos that developed in a major histocompatibility complex (MHC) allogeneic egg showed that adult hematopoietic cells derive from the embryo proper and not from the YS.[4]

Primitive erythrocytes were initially identified as the first embryonic hematopoietic cells of YS origin.[5] Circulating primitive erythrocytes are nucleated and express specific hemoglobin chains that have increased capacity to transport oxygen compared to adult hemoglobin.[6] They can be found around E7 of mouse gestation in YS blood islands, peak by the time circulation is established (E8-8.5), and decrease after E12.5, although a few were detected after birth.[5] They circulate but are also found in the fetal liver (FL), the first main site of embryonic hematopoietic differentiation. Limited numbers of primitive macrophages and megakaryocytes have also been reported in the YS blood islands.[5]

Around E8-8.5, a second layer of hematopoietic progenitors emerges in the vasculature of the YS. It is composed of erythro-myeloid progenitors (EMP) that generate definitive erythrocytes and multiple myeloid lineages.[7,8] However, they fail to generate lymphocytes in vitro or in vivo. The YS has long been considered a provider of cells that transiently ensure embryo survival. It came therefore as a surprise that YS EMP-derived macrophages persist for life as tissue-resident macrophages.[9] The best example are microglia, the macrophages residing in the central nervous system (CNS) that, under physiologic conditions, stay throughout adult life with the same original cell composition and are not replaced by BM-derived cells (discussed below). Subsequently, YS mast cells were also found to have a long lifespan.[10] This observation indicates that mature blood cells emerging in the embryo in an HSC-independent manner persist and are functional for long periods of time, thus challenging the paradigm that all adult hematopoietic cells are derived from HSC.

### 2.2 | Intra-embryonic generation: major arteries

Experiments in several models including the chicken,[4,11] the mouse,[12–14] and the zebrafish[15,16] indicated an intra-embryonic origin of lymphoid progenitors that paralleled that of HSC. This generation was restricted to the major arteries (aorta, omphalo-mesenteric, and vitelline arteries)[17] and occurred in close vicinity to endothelial cells lining the vessel. The emergence of hematopoietic progenitors was directly observed in the zebrafish larvae.[15,16] These observations indicated that hematopoietic progenitors emerge from endothelial cells through a process, designated endothelial-to-hematopoietic transition (EHT), that involves progressive morphological alterations, loss of endothelial cell markers, and acquisition of hematopoietic specific transcripts. It was subsequently proposed that EMP in the YS emerge by a similar mechanism.[18] For the purpose of this review, we will use the term "embryo-derived" for all hematopoietic progenitors that are generated within the embryo proper.

The above experiments indicated that a third layer of hematopoietic progenitors emerges in the intra-embryonic dorsal aorta also called aorta-gonads-mesonephros (AGM) and in the omphalo-mesenteric and vitelline arteries that connect circulation between the embryo proper and the extra-embryonic tissues (YS and placenta).[17] These progenitors can generate erythroid, megakaryocyte, myeloid, and lymphoid cells at the clonal level. They migrate to the FL where they establish the adult HSC compartment. The emergence of the third layer is limited to the period between E9 and E11.5 and partially overlaps in time, in the mouse, with the previous EMP generation.[19]

The first emerging multipotent progenitors were assessed for their capacity to reconstitute the hematopoietic compartment of myeloablated recipient mice for long periods of time. This ability designated long-term reconstitution (LTR) activity is taken as the golden standard to evaluate HSC. These experiments revealed a poor LTR capacity of E9-E10 progenitors.[20] Although CFU-S were detected in the intra-embryonic compartment earlier than in YS,[13,21] very low numbers of cells with LTR activity were found before E12. It was subsequently shown that emerging multipotent progenitors needed to undergo maturation in an organ culture of AGM or FL in order to acquire LTR activity and that these newly generated multipotent progenitors were designated pre-HSC[22] or immature-HSC.[23] One reason for their inefficient reconstitution capacity is their low expression of MHC-class I on the surface that activates host NK cell activity,[14] but other factors are probably also involved in their fast elimination from hosts by innate immune mechanisms. These experiments dissociated $CFU\text{-}S_{11}$ and LTR activity, indicating that the

16000656, 0, Downloaded from https://onlinelibrary.wiley.com/doi/10.1111/imr.13187 by Institut Pasteur, Wiley Online Library on [10/04/2023]. See the Terms and Conditions (https://onlinelibrary.wiley.com/terms-and-conditions) on Wiley Online Library for rules of use; OA articles are governed by the applicable Creative Commons License

CFU-S assay does not detect HSC.[24] They also indicated that testing the in vivo activity of the emerging multipotent progenitors should not be done in the same assays used to detect adult HSC.

## 2.3 | The fetal liver, the major embryonic hematopoietic organ

The FL is the main hematopoietic organ in the mouse embryo. It develops from the hepatic endodermal bud (that gives rise to the liver parenchyma), that proliferates in cords that invade the mesodermal septum transversum (giving liver fibroblasts or stellate cells, mesothelial and endothelial cells), and it provides the environmental signals that support hematopoietic differentiation and the establishment of the HSC compartment.[25,26] It was early recognized that hematopoietic cells in FL are originated elsewhere.[25,27] CFU-$S_8$ were detected in FL at E10.5[3] and CFU-$S_{11}$[21] at E11.5. Using a competitive in vivo assay, it was shown that LTR activity was first detected in FL at E12.5.[28] Later studies, using organ cultures and, again, in vivo reconstitution assays, confirmed that the FL is initially colonized at E10.5 (30 somite [S] stage), that is, shortly after being produced in the AGM, by immature HSC, which will fully develop to HSC in situ.[23] Ema and Nakauchi further showed that, in FL, the number of cells displaying LTR activity increased more than 30-fold between E12.5 and E16.5, and decreased thereafter. These observations were interpreted as reflecting a single wave of HSC expansion in FL and a progressive exit to colonize the BM or the spleen. Interestingly, E12.5 is also the time when the first B cell progenitors were detected in FL.[29,30]

Although these conclusions remain unchallenged, the extent to which HSC expand in the FL is a matter of debate (see below).

Little is known about the properties of the FL stromal cells that sustain hematopoiesis. Endothelial cells,[31,32] hepatic stellate cells,[32] hepatoblasts[33] and portal vessels associated pericytes[34] have been reported to be involved in HSC expansion and hematopoiesis in FL.[26] These apparently conflicting reports may indicate that several cell types contribute to fetal hematopoiesis and that both compartments, hepatic and hematopoietic, evolve as development progresses. It is, therefore, required to take into consideration how the properties of the different stromal cells evolve along gestation, to understand the factors governing FL hematopoiesis.

## 2.4 | A layered immune system

In the late 80s it was reported that a small subset of B cells (designated B1 cells to differentiate them from B2 conventional B cells), reside in the peritoneal and pleural cavities, expressed the T cell marker CD5 and were endowed with some surprising properties.[35] B1 cells could expand extensively when transferred into neonatal mice,[36] expressed B cell receptors biased toward the recognition of bacterial products,[37,38] appeared to secrete most natural antibodies[39] and originated from B1 specific B cell progenitors that reside in FL,[40] (BM cells being less efficient than FL in reconstituting the B1 compartment upon transfer[35]). These properties led to the proposal that B1 cells originated from an embryonic-specific progenitor and not from HSC.[41] However, additional experiments indicated that: 1. B1 and conventional B2 cells can share the same progenitors[42]; 2. an antigen receptor from B1 cells can confer B1 properties to conventional B2 cells[43]; 3. some properties of B1 cells can be explained by an inefficient pre-B cell receptor selection in FL, that fails to delete some autoreactive receptors[44]; 4. induction of *Rag* in the BM of *Rag*$^{-/-}$ mice results in the production of B1 cells.[45] In the absence of a consensual view, we will consider here that FL progenitors contribute more efficiently to the B1 compartment than their BM counterparts.

Around the time B1 cells were described it became also evident that subsets of mouse γδ T cells expressing invariant T cell receptors (TCR)[46] also had specific properties not shared with other T cells. They reside in tissues (skin for Vγ5Vδ1- expressing cells, also called dendritic epidermal T cells [DETC], and lung for Vγ6Vδ1-expressing cells), precede by several days conventional αβ T cells in the embryonic thymus[47] and appeared to be of strict embryonic origin.[48–50] Vγ5 and Vγ7 (residing in the intestinal epithelium) expressing T cells were later shown to be positively selected by butyrophilin-like molecules (called Skint1 for Vγ5 and *Btnl1* for Vγ7) expressed by epithelial cells in the thymus and in the intestine, respectively.[51,52] Vγ5 T cells in turn induce the up-regulation of *Skint1* in mTEC (Figure 2).[53] It should be pointed out that γδ T cells have multiple nomenclatures which can be a source of confusion. Thus, Vγ5 and Vγ6 T cells in Heilig and Tonegawa[54] now a widely used nomenclature, have been called Vγ3 and Vγ4 in Garman, Doherty, and Raulet,[55] also used by Havran and Allison. We will use here the Heilig and Tonegawa nomenclature and full correspondence between the different nomenclatures can be found in Raulet.[56]

The basis for the developmental restriction of invariant γδ T cell subsets has not been elucidated. Several possibilities to explain this developmental restriction include 1. an HSC-independent embryonic origin, possibly from YS, 2. epigenetic modifications of HSC as they transit from FL into BM that restricts rearrangement of specific segments within the TCRγ and TCRδ loci, and 3. environmental changes modulating the selection of these subsets.

Although injection of progenitors in embryonic environments is still challenging and difficult to achieve with low cell numbers, fetal thymic organ cultures (FTOC) are highly efficient. BM progenitors seeded in fetal thymic lobes generate αβ and γδ T cells but no Vγ5- or Vγ6-expressing cells indicating different cell intrinsic properties in fetal and adult thymic seeding progenitors (TSP).[49] The embryonic restriction of invariant T cells appears to be more complete than that of B1 B cells because there are no reports of a possible adult BM HSC origin for Vγ5 or Vγ6 T cells. This observation raises the possibility of different underlying mechanisms in the restricted generation of B1 or invariant γδ T cells.

Similar to B1 cells and γδ T cells, a population of lymphoid cells, called lymphoid tissue inducer cells (LTi), that induces lymph node and Peyer's patches formation, appear also to be restricted to the embryonic period. Their development depends on the expression of the orphan receptor Rorc encoded by RoRγt[57] and, although cells

16000625, 0, Downloaded from https://onlinelibrary.wiley.com/doi/10.1111/imr.13187 by Institut Pasteur, Wiley Online Library on [10/04/2023]. See the Terms and Conditions (https://onlinelibrary.wiley.com/terms-and-conditions) on Wiley Online Library for rules of use; OA articles are governed by the applicable Creative Commons License

with similar properties have been found in the progeny of BM HSC, only in the FL is RoRγt expressed in lymphoid progenitors before tissue residency.[58]

Thus, the immune system, like embryonic erythroid and myeloid cells, is composed of cells that were generated in a developmentally restricted manner. The origin and function of these different hematopoietic progenitors will be discussed below.

## 3 | WAVES OF HEMATOPOIESIS

### 3.1 | Yolk Sac Hematopoiesis –longer than expected

As previously mentioned, the hematopoietic system is established by multiple waves of progenitors. This includes all multipotent progenitors that may or may not undergo maturation into HSC and their progenies (Figure 1).

The YS waves generate mostly erythrocytes responsible for carrying oxygen across the developing embryo, macrophages that play important roles in tissue development and remodeling and megakaryocytes that produce platelets responsible for clotting processes. The idea that these YS populations are only produced and required during embryonic development has been recently challenged.[8,59] Two major recent contributions, using inducible lineage-tracing mouse models, directly showed that distinct tissue-resident macrophage populations, generated during embryonic development from YS progenitors, persist throughout adulthood. By pulsing Runx1$^{MerCreMer}$Rosa26$^{EYFP}$ embryos with 4-hydroxytamoxifen (OH-TAM) at E7.5, that labels YS progenitors and their progeny, Hoeffel and colleagues showed that around 30% of microglia cells (resident macrophages of the brain) were labeled in adult mice.[59] Using two distinct lineage-tracing models Csf1r$^{MeriCreMer}$Rosa26$^{YFP}$ pulsed with OH-TAM at E8.5 and Tie2$^{MeriCreMer}$Rosa26$^{YFP}$ pulsed with OH-TAM at E7.5 or E8.5, Gomez-Perdiguero and colleagues showed that most tissue-resident macrophages (microglia cells from brain, Kupffer

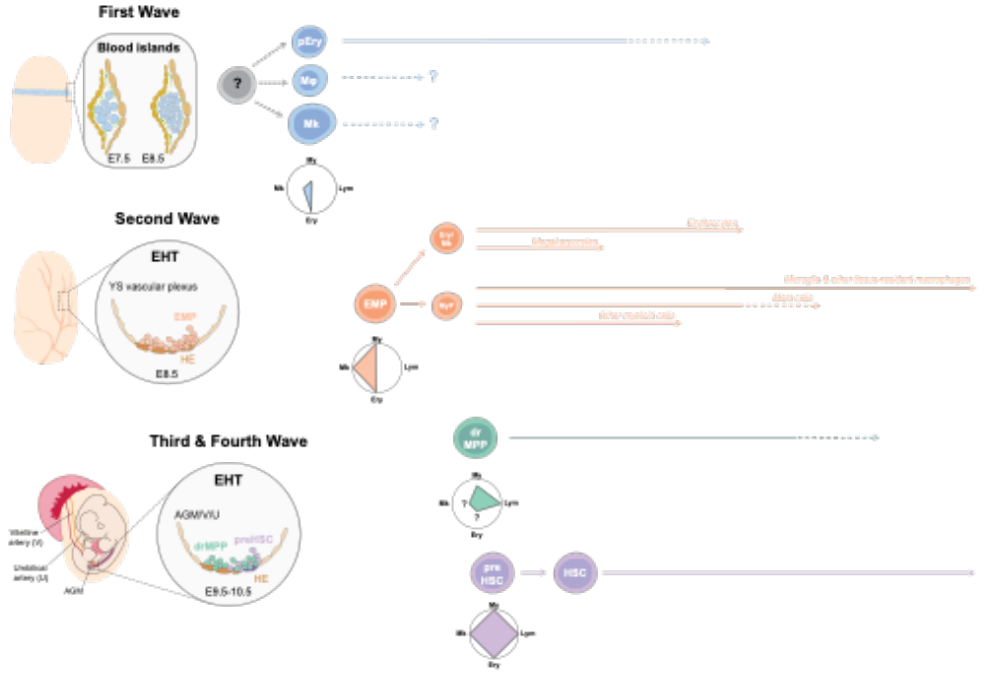


FIGURE 1 Model of hematopoietic progenitor emergence in the embryo: sequential but overlapping waves.

10990026, 0, Downloaded from https://onlinelibrary.wiley.com/doi/10.1111/imr.13187 by Institut Pasteur, Wiley Online Library on [19/04/2023]. See the Terms and Conditions (https://onlinelibrary.wiley.com/terms-and-conditions) on Wiley Online Library for rules of use; OA articles are governed by the applicable Creative Commons License

cells from liver, Langerhans cells from skin and alveolar macrophages from lung) originate from a Tie2 expressing EMP progenitor.[9] While about half of those cells were slowly replaced by HSC-derived progeny, microglia cells were only marginally replaced during a year period.[9,60] In fact, the contribution of BM-derived precursors and/or circulating monocytes to the microglia pool has only been observed in situations where the integrity of the blood-brain barrier (BBB) has been disrupted, e.g., using radiation, or in the context of disease.[61–63]

In the developing CNS of rodents, primates and humans, microglia cells were progressively found at key sites of neurogenesis such as the ventricular and subventricular zone,[64–66] where they regulate the size of the neural precursor pool by phagocytosis.[67,68] Dysfunctions in these cells can lead to neuropsychiatric diseases, since they have also been implicated in synaptic pruning and remodeling and have important functions in learning and memory (reviewed in 69,70). YS-derived microglia cells colonize the brain starting at E9, a time when there are still no embryo-derived macrophages, and participate in the BBB formation. This occurs at a specific window of opportunity since no more myeloid precursors colonize the CNS after this period.

YS-derived hematopoiesis has proven to also have a higher relevance than initially thought regarding other blood populations. Indeed, lineage-tracing analysis of YS versus HSC-derived hematopoiesis showed that there is a minimal contribution of HSC to various cellular subsets in the embryo. It is the case for mast cells, which are predominantly YS-derived in the embryo and at perinatal stages in most connective tissues.[10,70] Furthermore, recent evidence showed that, until birth, red blood cell production is maintained by YS EMP with minimal contribution from HSC.[71] Remarkably, YS-derived erythrocyte progenitors require 10-fold lower concentrations of erythropoietin (Epo) than their HSC-derived counterparts and have, therefore, a selective advantage in an Epo-poor environment such as the embryo. This can explain why patients with mutations altering the receptor-binding kinetics of Epo only display anemia postnatally.[72]

These studies have challenged the dogma by which HSC assume blood production from the moment they are generated and are the source of all hematopoietic lineages in the adult, thus providing evidence for the existence of a developmentally regulated "layered" hematopoietic system. The obvious selective pressure for such phenomenon lies in the differences in environments that exist in FL and BM for hematopoiesis. The FL exhibits lower cytokine concentrations and, therefore, progenitors that respond to lower concentrations of chemokines and cytokines, like YS progenitors will have a selective advantage over HSC and their progeny.[44,71,73] One can speculate that, by taking over the production of myeloid and erythroid cells throughout embryonic development, the YS-derived progenitors, or other transient progenitors, are liberating the embryo-derived progenitors, from where HSC are derived, from fulfilling the needs of the embryo, allowing them to set up the stem cell pool and to generate the lymphoid counterparts that are exclusively embryo-derived.

### 3.2 | Embryo-derived progenitors – multipotency versus stemness

The first embryo-derived hematopoietic progenitors appear in clusters in the dorsal aorta and other major arteries through a process of EHT performed by specialized endothelial cells named hemogenic endothelium (HE).[15,16,74] These progenitors are multipotent, giving rise to all blood lineages, and the only ones with lymphoid potential.[12,13] The EHT process starts with the up-regulation of the transcription factor Runx1, essential for HSC generation, that activates the hematopoietic transcriptional program.[75–77] This leads to a series of morphological changes that manifest as endothelial cells budding and forming intra-aortic hematopoietic cell clusters (IAHC). IAHC can be identified as c-Kit$^+$ and constitute a heterogeneous group of cells with expression of endothelial markers such as CD31 and Flk-1 at the basal level of the cluster, while CD45 can be detected in some cells of the cluster outer region. c-Kit$^+$ cells in the AGM peak at E10.5 (around 800 c-Kit$^+$ cells per aorta) and the majority localized ventrally.[78] At this stage, all c-Kit$^+$ cells are multipotent at the clonal level, but only about 20–30 are pre-HSC.[79] Studies aiming at identifying the distribution of HSC within the IAHC showed their preferential localization in the ventral side of the aorta, hinting a ventral polarity in the development of these cells.[80,81] Major efforts have been made to identify the molecular and signaling pathways that induce the specification of the HE and coordinate HSC emergence (reviewed in 82).

Whether all multipotent progenitors generated in the major arteries will give rise to HSC has recently been questioned.[83] The fact that most of the c-Kit$^+$ cells present in IAHC do not show HSC activity may have two different explanations: All c-Kit$^+$ cells may be HSC precursors at different stages of development and with different LTR activity. Alternatively, they may represent a heterogeneous population of cells generated by two developmental pathways, one that will give rise to HSC and the other fated to differentiate. Whether this heterogeneity is defined at the HE stage or in response to extrinsic cues is not yet clarified. Recently, Dignum and colleagues[84] reported that Cxcr4 expression in the HE associates with HSC activity, whereas Cxcr4$^-$ HE cells generate HSC-independent progenitors that can give rise to all lineages in vitro but lack engraftment post-transplantation. In fact, Cxcr4$^-$ HE represents a heterogeneous progenitor compartment with cells displaying distinct lineage-restricted potential (multipotent, lymphomyeloid, erythromyeloid, and myeloid-only) in culture assays. Another study points to heterogeneity in the HE in terms of HSC potential as *Mecom*, a critical regulator of HSC, is preferentially expressed in progenitors that will mature into phenotypic HSC.[83] Accumulating evidence points, therefore, to the existence of multipotent progenitors independent of HSC that will be further described below.

16000625, 0, Downloaded from https://onlinelibrary.wiley.com/doi/10.1111/imr.13187 by Institut Pasteur, Wiley Online Library on [10/04/2023]. See the Terms and Conditions (https://onlinelibrary.wiley.com/terms-and-conditions) on Wiley Online Library for rules of use; OA articles are governed by the applicable Creative Commons License

### 3.3 | The establishment of the HSC compartment

At this stage, we will discuss the attempts to evaluate the degree of expansion of the different hematopoietic compartments, as well as how the existence of multiple layers can be integrated in these views. The organization of the hematopoietic system is classically viewed as a hierarchical tree, with HSC continuously sustaining all mature blood lineages throughout life. However, this concept has only been based on a "retrospective" assessment of the two hallmarks of HSC (self-renewal and multipotency), upon isolation and transplantation into myeloablated recipients, which might not reflect hematopoiesis in intact animals. In the last years, different lineage-tracing mouse models, genetic barcoding technologies and RNA sequencing have been increasingly implemented to analyze the hematopoietic system in unperturbed settings (reviewed in 85,86). These studies were quite informative on the physiological hematopoietic flux throughout its hierarchical structure and revealed a minimal contribution of adult HSC to downstream compartments.[87–89] These findings were in line with the fact that the adult stem cell compartment is mainly quiescent at steady-state.[90,91] Whereas downstream multipotent progenitors proved robust in vivo self-renewability and sustained adult hematopoiesis,[89] their repopulating ability, when transplanted, was limited, being exhausted after a few weeks,[92] and are, therefore, not clinical targets for LTR. The mechanisms regulating the cell fate decision between self-renewal or differentiation are still largely unknown and their understanding is expected to open doors to the development of efficient HSC manipulation and expansion protocols ex vivo.

In contrast to the adult system, it has been widely accepted that HSC are highly proliferative during embryonic development, expanding significantly in the FL,[28] thus rendering this organ an ideal site to study the mechanisms driving HSC proliferation. However, this dogma was recently challenged.[93,94] To dissect how the adult HSC pool is established, from its generation in the AGM region until its settlement in the BM, reports that aimed to quantify HSC throughout development are here revisited (Table 1).

Only 1–2 HSC (cells with LTR potential) were detected in the AGM at E10.5-E11.5.[13,20] Given the extremely low repopulation activity of the emerging hematopoietic cells in this region, the term pre-HSC was introduced to identify immature precursors that acquired LTR potential after ex vivo cultures.[79] Using this system, Rybtsov and colleagues identified around 20 pre-HSC in E10.5 AGM, peaking at E11.5 (40–60 cells). They further showed that the number of pre-HSC in E11.5 AGM matched the number of mature HSC in E12.5 FL (~60 cells), suggesting that maturation, rather than proliferation, takes place during the migration of cells from the AGM to the FL. This latter value compares well with the ~50 repopulating units (RU) described by[28] in E12.5 FL.

The notion that the FL is a site of significant HSC expansion comes mainly from the work of Ema and Nakauchi who quantified LTR potential from FL cells at different developmental stages. They showed a 33-fold expansion from E12.5 (~50 cells) to E16.5 (~1500), corresponding to about 5 rounds of symmetric division. Despite variable estimates in the number of RUs in E14 FL, ranging from 440 to 2000 (Table 1), most studies converge to the conclusion that the FL contributes to the generation of 1000–2000 HSC. These numbers represent about 10% of the estimated number of HSC in the adult (Table 1). Accordingly, 3 additional rounds of symmetric division should take place after HSC leave the FL (see below).

Recent reports,[93,94] not only questioned the concept that the FL is a privileged niche for active HSC expansion without differentiation, but also concluded that the estimated cohort of HSC generated in the AGM only doubles in size during fetal stages of mouse development. Using a multi-color ROSA26 – Confetti reporter system and based on mouse-to-mouse variance in the composition of adult blood, the authors traced back the hemopoietic hierarchical tree to ~600 E7-E10.5 AGM precursors, a number 10-fold higher than the above-cited number of pre-HSC in E11.5 AGM. In *Conf-Ubiq*$^{ERT2\text{-}Cre}$ mice treated with tamoxifen (TAM) at different stages, they further refined their estimations by showing that the HSC compartment in the BM of 6-month-old mice derived from about 850 E8-E10 endothelial progenitors and 1.700 E12–14 hematopoietic progenitors, this number remaining constant up at least 9 days postnatally. Altogether, these results indicated that the size of the embryonic pool of HSC is primarily determined by the very high number of pre-HSC generated in the AGM, with not more than 1 round of division occurring at a later stage during embryonic development, eventually in the FL.[94]

Numerous studies showed that essentially all FL cells are in active division. Between E12.5 and E14.5, all FL Sca-1$^+$c-Kit$^+$ cells are in cycle, as demonstrated by BrdU uptake analysis.[95] Notably, Ganuza et al. also estimated 4 rounds of division of CD45$^+$c-Kit$^+$Lin$^-$ progenitors from E12.5 to E14.5[94] in line with Ema et al. This notwithstanding, an active cycling HSC population is not necessarily in contradiction with a low net expansion, as asymmetric division or differentiation might occur, not duplicating the stem cell pool at each division. This is what Ganuza et al. suggest: FL HSC are actively dividing but most daughter cells are biased for differentiation, implying that the FL is not a privileged niche for active HSC expansion without differentiation.

Although HSC migrate to the BM as early as E15.5, only minimal HSC activity is detected in this tissue during fetal stages.[96–98] This might indicate that, either the migration from the FL to the BM occurs progressively (or massively only after birth), or that the establishment in the new niche might temporarily compromise their LTR potential. Although quantification of transplantable HSC throughout the first days after birth has not been performed, the entire HSC population was reported to be in cycle during the first two weeks after birth, switching progressively to a quiescence state that is fully acquired by the end of the fourth week.[96] An increasing contribution of precursor cells to the adult BM pool could be estimated using the *Conf-Ubiq*$^{ERT2\text{-}Cre}$ model, from ~2.000 around birth to ~5.700 at 3 weeks.[94] Overall, these results are also in line with the classical notion that, after birth, the HSC compartment must expand about 10-fold (~3 rounds of symmetric division) to reach the 10.000–20.000 HSC in adult BM (Table 1).

16000656, 0, Downloaded from https://onlinelibrary.wiley.com/doi/10.1111/imr.13187 by Institut Pasteur, Wiley Online Library on [10/04/2023]. See the Terms and Conditions (https://onlinelibrary.wiley.com/terms-and-conditions) on Wiley Online Library for rules of use; OA articles are governed by the applicable Creative Commons License

**TABLE 1** Reports quantifying HSC at different developmental stages.

| | AGM | | | | | | FL | | | | | BM | | | | |
|---|---|---|---|---|---|---|---|---|---|---|---|---|---|---|---|---|
| Method | E8 | E9 | E10 | E11 | E12 | E11 | E12 | E14 | E16 | E18 | E18 | 2 wk | 3 wk | 4 wk | Adult | Reference |
| LTRA; LDA | – | – | – | – | – | – | – | – | – | – | – | – | – | – | 1 CRU/ 10.000 (20.000)[a] | 99 |
| LTRA; LDA | – | – | – | – | – | – | – | – | – | – | – | – | – | – | 1 CRU/ 11.200 (18.000)[a] | 100 |
| LTRA | – | – | – | – | – | – | – | 1/15.700 (1300)[b] | – | – | – | – | – | – | – | 101 |
| LTRA | – | – | – | – | – | – | – | 1/17.300 (1200)[b] | – | – | – | – | – | – | – | 102 |
| LTRA; LDA | – | – | – | – | – | – | – | 1.100 CRU | – | – | – | – | – | – | – | 103 |
| LTRA ; LDA | – | – | – | – | – | n. d | 1/39.840 (50) 40 CRU | 1/40.980 (488) | 1/36.900 (1.626) 1.538 CRU | 1/43.487 (1.035) | – | – | – | – | – | 28 |
| LTRA | – | – | – | – | – | – | – | 1/23.000 (900)[b] | – | – | – | – | – | – | 1/20.000 (10.000)[a] | 104 |
| LTRA | – | – | – | n. d | < 5 | n. d | 30 | 500 | 1.000 | – | <10 | – | – | – | – | 105 |
| LTRA; LDA | – | – | – | – | – | – | – | 2.000 CRU 1/35.000 ($Ter119^-$) | – | 1/73.000 | 1/95.000 or 1/6.600 ($Lin^-$) | – | 1/6.500 ($Lin^-$) | 1/6.300 ($Lin^-$) | 1/5.500 ($Lin^-$) | 96 |
| LTRA | – | – | – | – | – | – | – | 443 ESLAM[c] | – | 1044 ESLAM | 7 ESLAM | – | 1016 ESLAM | 983 ESLAM | 1700 ESLAM | 106 |
| LTRA; LDA | – | – | – | – | – | <1 | 35 30 CRU | 600 SLAM[c] | 600 (E15.5) | – | – | – | – | – | – | 107 |
| LTRA (cultured explants) | – | – | – | 55 | 10 | n. d | 60 | – | – | – | – | – | – | – | – | 79 |
| *MtMV of Confetti—reporter labeling* | 600 Pre. (E7.5) | 850 Pre. | – | – | – | 1700 Pre. | – | – | – | 3.000 Pre. | 5.700 Pre. | – | 1/18.320 (11.000)[a] | 93,94 | | |

*Note*: Unless otherwise stated, cell numbers or frequencies are indicated as RUs relative to the respective organ's total cell number and some values were rounded for simplification.

Abbreviations: CRU, competitive repopulating unit; LDA, limiting dilution assay; LTRA, long-term repopulation assay (transplantation assays) – repopulation potential was considered for at least 16 weeks after transplantation; n.d, not detected; Pre., precursors.

[a]Total cell number estimated considering $2\times10^8$ total BM cells.

[b]Total cell number estimated using the total cell number per FL from (Ema & Nakauchi, 2000).

[c]ESLAM ($CD45^+$ $EPCR^+$ $CD48^-$ $CD150^+$) or SLAM (LSK $CD48^-$ $CD150^+$) cells with LTR potential.







16000054, 0, Downloaded from https://onlinelibrary.wiley.com/doi/10.1111/imr.13187 by Institut Pasteur, Wiley Online Library on [10/04/2023]. See the Terms and Conditions (https://onlinelibrary.wiley.com/terms-and-conditions) on Wiley Online Library for rules of use; OA articles are governed by the applicable Creative Commons License

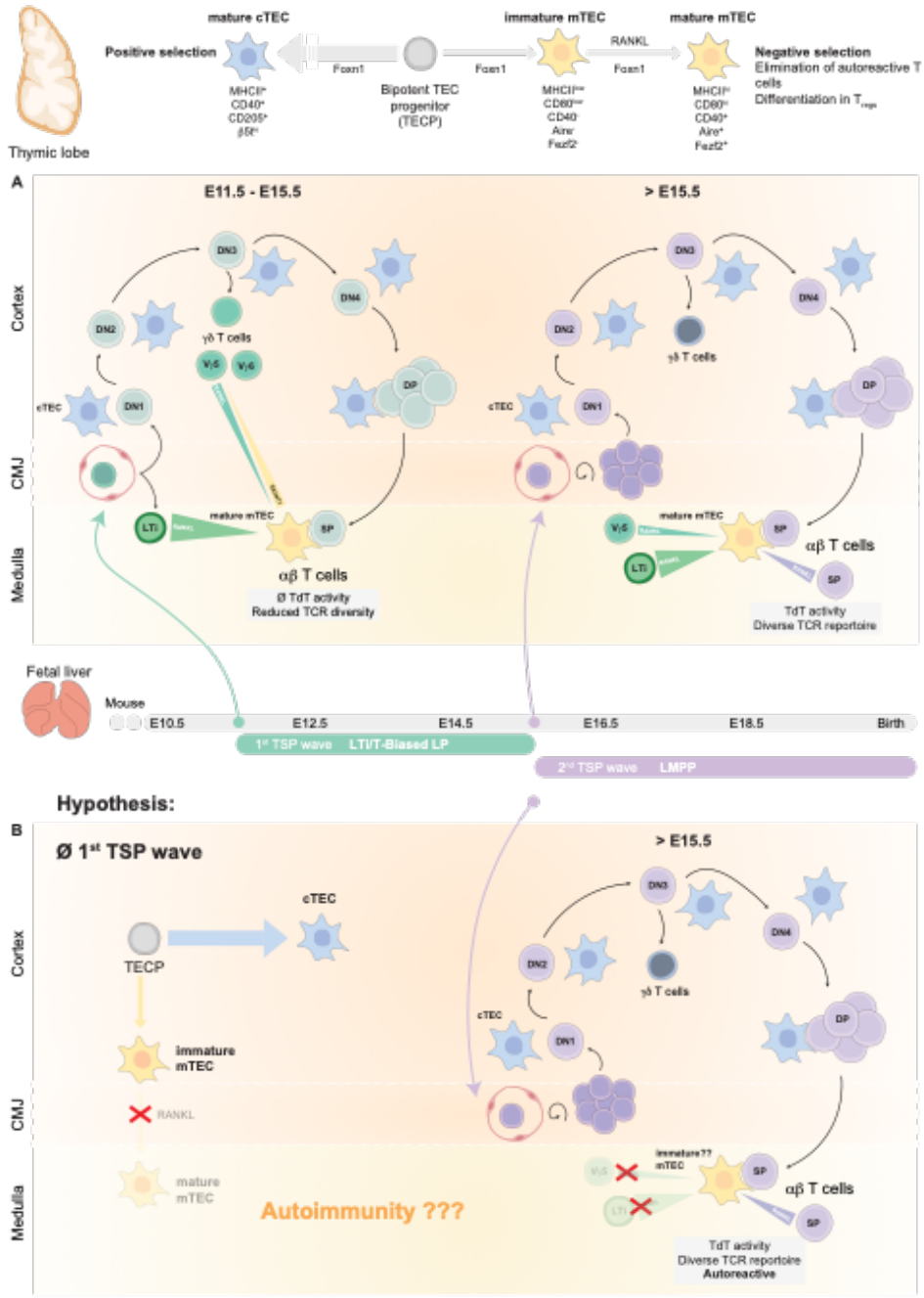


FIGURE 2 Importance of an orchestrated TSP colonization for thymocyte selection and thymic architecture.

10990684, 0, Downloaded from https://onlinelibrary.wiley.com/doi/10.1111/imr.13187 by Institut Pasteur, Wiley Online Library on [19/04/2023]. See the Terms and Conditions (https://onlinelibrary.wiley.com/terms-and-conditions) on Wiley Online Library for rules of use; OA articles are governed by the applicable Creative Commons License

### 3.3.1 | Is HSC embryonic expansion in FL a dogma on the edge?

Although there is some variability in the estimations of fetal HSC numbers (Table 1), the most conflicting value that impacts the extent of embryonic HSC expansion is the starting number of AGM progenitors: ~60 immature HSC precursors[79] vs. ~600 precursors fated to become HSC.[93] Numbers based on transplantation systems are likely prone to underestimations. Also, it should be noted that the work of Ema and Nakauchi[28] is not informative as to whether the increase in RU they observed was due to expansion of HSC or to maturation of multipotent progenitors into cells with LTR activity. While the strategy of Ganuza et al[94] is of considerable interest, they assume that the linear correlation they found between sample-to-sample variance and numbers of precursors established with fibroblastic cell lines in vitro also applies to hematopoietic progenitors in vivo. Their system is prone to overestimations because newly generated progenitors are actively cycling and the progeny of single cells can be marked more than once during the period of TAM activity. Furthermore, their view does not easily accommodate increasing evidence suggesting that, similar to adult HSC, the bulk of embryonic HSC are not actively contributing to blood production, which is essentially ensured by other multipotent progenitors (originated from HSC-independent AGM or YS waves).[71,83,108]

A precise quantification of the stem/progenitor cell compartments throughout ontogeny, contemplating the layered organization, is still missing. Understanding the kinetics of the different waves and progenitors in the FL and fetal and neonatal BM will be fundamental to comprehending the establishment of the adult hematopoietic system and the impact of different niches in hematopoietic development.

Many questions remain unresolved: What is the fraction of multipotent cells generated in the intra-embryonic vessels that evolve to become HSC? Does the FL microenvironment have a role in HSC proliferation? Does the neonatal BM also sustain HSC expansion? Is HSC expansion niche-dependent or a cell-intrinsic property? What contributes to the HSC shift into quiescence? Knowing that HSC expansion only occurs during the initial stages of development, when the whole organism is growing, the possibility that a general mechanism, rather than a local one is the key to the conundrum, cannot be disregarded.

## 4 | LAYERED THYMOPOIESIS AND THE THYMIC ARCHITECTURE

### 4.1 | The thymus

Within the thymus, thymic epithelial cells (TEC) provide the unique microenvironment required for developing functionally diverse T cells expressing TCR reactive to foreign antigens while tolerant to self. TEC coordinate virtually all stages of T cell development, providing key cytokines, chemokines, and ligands for the commitment, survival, proliferation, and selection of T cell precursors (thymocytes).[109] Deficits in thymic function arise with aging, cytoablative protocols or during pregnancy and infection, contributing to poor T-cell responses to newly encountered pathogens and predisposing to autoimmunity and cancer. This deficit is due to an involution of the organ that is characterized by a progressive loss of architectural integrity, size, as well as cellularity that, in turn, results in reduced T lymphopoiesis. While the involution observed with aging appears to be irreversible, transient involution, such as the one occurring in pregnancy, after irradiation, cytostatic drugs, or infection, is reversible indicating that the adult epithelial compartment has regenerative capacity (reviewed in 110).

The TEC compartment is classically subdivided into functionally distinct cortical (c) and medullary (m) TEC and develops from the endoderm of the third pharyngeal pouch.[111] The use of specific surface markers[112,113] and clonal analysis[114,115] established that cTEC and mTEC derive from common bipotent TEC progenitors (TECP). Bipotent TECP have also been identified in the adult thymus up to 9 months of age.[116] These cells resemble cTEC by phenotype.[117,118] Interestingly, the bipotent compartment has recently been characterized as biased toward cTEC differentiation during neonatal life, shifting to biased toward mTEC differentiation thereafter.[119]

Whereas cTEC regulate T cell lineage commitment and positive selection, mTEC contribute to the elimination of autoreactive T cells and to the differentiation of regulatory T cells. The key role of mTEC in tolerance induction depends on their capacity to express tissue-restricted antigens (TRA), a process that is determined in part by *Aire*[120] and *Fezf2*.[121] TRA expression by mTEC anticipates the presentation of peripheral self-antigens to mature T cells,[122] such that potentially autoreactive thymocytes are eliminated or deviated to the T regulatory cell lineage. Thus, genetic defects that impair TEC function will result in a broad range of life-threatening pathologies that range from immunodeficiency to autoimmunity.

The developmental pathway of cTEC remains elusive, whereas our understanding of the molecular events that regulate mTEC differentiation is far more detailed. The development of mTEC depends on instructive signals provided by distinct hematopoietic cells, including lymphoid tissue inducer (LTi) cells, γδT cells, and $CD4^+$ T cells.[53] These lymphoepithelial interactions, commonly termed "thymic crosstalk", engage specific members of the tumor necrosis factor receptor superfamily (TNFRSF), including receptor activator of NF-kB (RANK) and lymphotoxin a receptor (LTaR) in mTEC and their progenitors, and CD40 and lymphotoxin a in thymocytes, which, in turn, activate nuclear factor kappa B (NF-kB) signaling pathways required for mTEC maturation.

### 4.2 | Thymic epithelial regeneration

The thymus is a highly dynamic organ that increases in size for the first 3–4 weeks of post-natal life, in the mouse. After that, the thymus starts a long involution process with decreased numbers of

16000658, 0, Downloaded from https://onlinelibrary.wiley.com/doi/10.1111/imr.13187 by Institut Pasteur, Wiley Online Library on [10/04/2023]. See the Terms and Conditions (https://onlinelibrary.wiley.com/terms-and-conditions) on Wiley Online Library for rules of use; OA articles are governed by the applicable Creative Commons License

thymocytes and of epithelial cells such that, in aging mice and humans, few naïve T cells are produced. *Foxn1* is a transcription factor required for the formation of a functional epithelium. Loss of function mutations in *Foxn1* (like the one found in the nude mouse) results in the absence of thymus and hair follicles, although TECP are still present.[123] Most TEC express *Foxn1* during embryonic development and this expression is reduced in post-natal mice.[124] Reduced Foxn1 expression results in decreased levels of the target genes *Dll4*, *Kitl*, and *Cxcl12*, that are important for the earlier stages of thymocyte development. Delayed involution and regeneration of aging thymus function and architecture are observed when TEC are forced to upregulate *Foxn1* expression. Aging mice with increased *Foxn1* expression have an augmented TEC compartment that comprises MHCII$^{low}$ TECP, and mTEC with an increase in *Aire* and TRA expression.[125]

Other environmental factors impact the cellularity of the thymus and its architecture. Possibly the most relevant is the myeloablative treatment required for BM transplantation. IL-22 is an important factor produced by ILC3, that is triggered by a decrease in double-positive thymocytes that follows total body irradiation (TBI). In the absence of IL-22 or ILC3, the TEC compartment does not recover as assessed up to 28 days after TBI.[126] RANK ligand (RANKL), that is produced by LTi and CD4$^+$ T cells, appears to be upregulated after myeloablative treatment and induces thymic regeneration.[127] Increased levels of lymphotoxin α in LTi cells upon RANKL upregulation take part in epithelial regeneration, raising the possibility that their clinical administration could improve thymic regeneration in transplanted patients. Two other molecules are upregulated in the thymus after irradiation. One is BMP4[128] that is produced by endothelial cells and regulates the expression of *Foxn1* and its targets and the other is *Fgf7* or keratinocyte growth factor (KGF). KGF treatment in vivo was shown to expand a population of Ly51$^+$Foxn1$^+$ cTEC[129] and to improve thymocyte recovery after myeloablation or BM transplantation (reviewed in 110). However, treatment with KGF after BM transplantation failed to improve T cell production in humans,[130] indicating species-specific variations in the regulation of factors that determine the thymus epithelial compartment.

Several TEC subsets were shown to be in cycle in the adult thymus and more precise BrdU incorporation experiments have shown that the *Aire*$^+$ mTEC cells are continuously renewed with a half-life of 2 weeks.[131]

Altogether the observations summarized above indicated that TEC respond to direct injury or massive thymocyte depletion by activating several mechanisms that restore their numbers indicating that it is a highly dynamic compartment. It is interesting to notice that some of these mechanisms of regenerative process specifically involve ILC3/LTi cells, highlighting their fundamental role in the homeostasis of the adult TEC compartment. It is intriguing to observe that these cells are very infrequent in the adult thymus.[132]

Thymomas are malignant hyperplasias of TEC, frequently associated with a decreased expression of *Aire* and a disorganized thymic architecture. This disease is also frequently associated with multiorgan autoimmune disorders,[133] including myasthenia gravis characterized by the presence of autoantibodies against acetylcholine receptors. This association of pathologies indicates that loss of *Aire* expression in the adult thymus results in a loss of self-tolerance.

### 4.3 | Embryonic thymus colonization: two waves of TSP

Continuous colonization of the thymus by hematopoietic progenitors is required for normal T cell production. The thymus anlage is initially colonized after E11 of mouse gestation[111] and fetal thymopoiesis occurs in two phases, initiated by two distinct waves of hematopoietic TSP, corresponding to the most immature subset of ETP[134] (Figure 2A). TSP of the first wave bear surface markers of common lymphoid progenitors (CLP) but have lost B cell differentiation potential. They have limited proliferative capacity and rapidly differentiate into mature T cells.[135] First wave TSP are the only progenitors that generate LTi cells and invariant Vγ5- or Vγ6-expressing T cells, which are exclusively produced before birth. Of note, thymic LTi appear to derive from a common T/ILC progenitor, in contrast to all other LTi that are generated in the FL and exit the organ to form the lymph nodes and Payer's patches anlage.[58,136] Of interest, bipotent ILC/Vγ5 progenitors were detected among first wave TSP (10% of all T/ILC progenitors).[135]

LTi and invariant Vγ5$^+$ T cells are the first mature cells to be produced in the embryonic thymus and both were shown to play a role in the maturation of mTEC through the expression of RANKL.[53,109] Although many mature T cells express RANKL, it is tempting to speculate that embryonic restricted cells operate in a time-window that ensures early maturation of the epithelial compartment. Loss of both populations leads to a transient impairment in mTEC maturation and to an altered thymic architecture.[53] The impact that a defective progeny of the first wave TSP has in the thymic epithelial compartment throughout adult life has not been directly assessed although *Aire* deficiency in the first days of post-natal life-induced autoimmunity.[137] This observation raises the possibility that Vγ5 T cells and LTi cells generated from the first wave TSP are essential for proper adult immune function. Thus, the first wave of TSP would fulfill the essential function of inducing TEC maturation before TCRαβ T cells develop, thereby shaping the thymic architecture required for thymocyte selection (Figure 2B). It is also conceivable that the TEC compartment has a window of opportunity for adequate maturation and that the equilibrium between mature TEC and TECP determines, at this stage, the proper response to disturbances in the adult TEC compartment. If that were the case, a late or inadequate crosstalk between thymocytes and TEC would result in a life-long defective compartment with potential consequences for development of autoimmunity and premature thymic involution.

After birth, invariant Vγ5$^+$ T cells migrate to the skin where they expand and contribute to the integrity of the epithelial barrier, and to

16000656, 0, Downloaded from https://onlinelibrary.wiley.com/doi/10.1111/imr.13187 by Institut Pasteur, Wiley Online Library on [10/04/2023]. See the Terms and Conditions (https://onlinelibrary.wiley.com/terms-and-conditions) on Wiley Online Library for rules of use; OA articles are governed by the applicable Creative Commons License

the tissue repair upon injury.[48,138] Thymic LTi are also gradually lost although their fate is presently unknown.[132] To date, the role of invariant Vγ6$^+$ T cells in thymic organogenesis has not been addressed. These cells are also of exclusive embryonic origin, and their development is coupled with their capacity to produce high levels of IL-17. While some stay resident in the thymus, the vast majority leave to the periphery in the perinatal period and colonize the mucosa of the genitourinary tract as well as the airway epithelia where they play an important role in acute inflammation, and tissue repair.[139] Although the first TSP also produce αβ T cells, the absence of terminal deoxynucleotidyltransferase (TdT) and, therefore, of N sequence additions at that stage limits the diversity of their TCR.[135] They are thought to be rapidly replaced by the highly diverse T cells produced from the second wave TSP that colonize the thymus after E15.5. These progenitors are endowed with high proliferative capacity and generate large numbers of TCR-diverse, αβ- and γδ-T cells (Figure 2A). Second wave TSP share essentially all key properties with adult TSP.[134]

### 4.4 | The origin of fetal TSP

The first TSP display general hallmarks of CLP but also express high levels of *Ccr7*, *Ccr9*, *Cd7*, and *Glis3*, typical of FL CLP that have lost B-cell potential. Indeed, in vitro and in vivo studies demonstrated that they have restricted T/ILC potential.[73] Of interest, these cells were identified by the surface expression of paired immunoglobulin-like receptors (PIR).[73]

A subset of CLP expressing PIR A/B was identified in FL exclusively between E11 and E14.[73] This subset had the same transcriptional signature of first-wave TSP, suggesting a lineage relationship. Similarly, again exclusively in the referred time window, the FL also harbors a subset of lymphomyeloid-primed progenitors (LMPP) that are PIR$^+$, whose transcription signature is already biased toward restricted T/ILC potential.[73] However, the capacity of PIR$^+$ LMPP and PIR$^+$ CLP to generate LTi and invariant Vγ5$^+$ T-cells has not been addressed experimentally. The second wave of TSP is made of cells with the hallmarks of LMPP (PIR-), that is, still retaining full lymphoid and limited myeloid potentials. It is worth noting that they only appear in the thymus after E15.5 despite the fact that their LMPP (PIR$^-$) FL equivalents largely outnumber FL PIR$^+$ LMPP and PIR$^+$ CLP between E11 and E14.[73,134]

#### 4.4.1 | First wave of TSP may be HSC-independent

As mentioned above, HSC are first detected in E12 FL where they increase in numbers up to E16.[28] The fact that PIR$^+$ LMPP and PIR$^+$ CLP are already detected in FL and in circulation at E11, coincident with the onset of thymic colonization, implies that first-wave TSP must be HSC-independent.

Whether the first wave of TSP originates from YS or intra-embryonic multilineage progenitors that emerge from the dorsal aorta has been a matter of debate due to the fact that, in mice, the time window of hematopoiesis at both sites largely overlaps. It has been proposed that YS-derived cells have the potential to generate lymphoid cells.[140] These results were based on the observation that lymphoid-associated transcripts (namely Il7Ra, Rag1, and Rag2) were detected in YS cells, prior to the emergence of HSC.[140] Along the same line, it was also suggested that YS progenitors were the source of first wave TSP, as assessed by the emergence of invariant Vγ5$^+$ T cells, in experiments using a temporally-controlled lineage tracing model.[141] However, as the authors themselves acknowledged, the results were as well compatible with an intra-embryonic, HSC-independent, origin of these cells.

Recently, Elsaid et al[135] using a fate-mapping mouse line allowing the identification of the first emerging Il7Rα-expressing cells in E9.5 embryos, demonstrated that the expression of lymphoid-associated genes by YS progenitors, including EMP, was transient, and that IL7Rα-expressing YS cells had no T or B cell potential, as assessed in highly sensitive in vitro assays and in FTOC. Although Vγ5$^+$ T cells and LTi do not appear to derive from EMP, it has been difficult to determine the exact origin of these cells. These cells are labeled to the same extent as HSC in the Csf1R$^{MERCreMER}$ mouse model[135] but not in the Cdh5$^{CreERT2}$ model[141] when induced at E10.5. The former targets all hematopoietic and myeloid progenitors whereas the latter targets cells at their origin in the HE, in a shorter time window. Taken together, the results are compatible with the first TSP originating from a late YS multipotent progenitor independent from EMP, or from early intra-embryonic multipotent progenitors that have low probability to integrate the HSC compartment. Heterogeneity in the capacity of multipotent progenitors to integrate the HSC compartment has previously been reported.[142] A population of Flk2-expressing cells, detected in the FL prior to E12.5 that appear to preferentially differentiate into lymphocytes, particularly of the embryonic type.[142] Furthermore, intra-embryonic, HSC-independent progenitors with T-cell potential revealed by in vitro clonal assays and single-cell transcriptomics have also been observed.[84] All these experiments point to a fourth generation of transient progenitors biased for differentiation that generate embryonic-type lymphoid cells independently from HSC.

#### 4.4.2 | Zebrafish and humans

Using high-resolution spatiotemporal laser-induced lineage tracing technology in zebrafish Tian et al[143] showed the emergence of HSC-independent and HSC-dependent progenitors emerge at non-overlapping time windows. Specifically, they showed that the first T-cells identified in the embryonic thymus arise from HSC-independent progenitors. T cells generated from this first wave were no longer detectable at the juvenile stage. These results were recently confirmed by Ulloa et al[144] using different experimental strategies.

In humans, evidence also exists supporting the concept of a layered organization of thymopoiesis during development. It has

16000656, 0, Downloaded from https://onlinelibrary.wiley.com/doi/10.1111/imr.13187 by Institut Pasteur, Wiley Online Library on [10/04/2023]. See the Terms and Conditions (https://onlinelibrary.wiley.com/terms-and-conditions) on Wiley Online Library for rules of use; OA articles are governed by the applicable Creative Commons License

16000656, 0, Downloaded from https://onlinelibrary.wiley.com/doi/10.1111/imr.13187 by Institut Pasteur, Wiley Online Library on [10/04/2023]. See the Terms and Conditions (https://onlinelibrary.wiley.com/terms-and-conditions) on Wiley Online Library for rules of use; OA articles are governed by the applicable Creative Commons License

been proposed that fetal and adult HSC give rise to distinct T-cell lineages.[145] This study adds to a long series of publications demonstrating that the fetal and the adult T-cell immune systems are quite distinct, in line with the very old concept that the fetal environment is prone to tolerance induction. However, it does not directly inform on whether fetal and adult HSC are intrinsically distinct.

Vermijlen et al.[146] identified human semi-invariant and invariant γδ T-cell populations exclusively produced in the fetus, whose development was coupled to an effector program, namely the production of IFNγ and granzymes. These developmental properties appear analogous to those of first wave TSP-dependent invariant Vγ5-expressing T cells in the mouse thymus. Recently the same group demonstrated that the above-cited properties of fetal γδ T-cells were due to the expression of high levels of the RNA-binding protein Lin28b, and that this type of cells could only be generated in vitro from fetal HSC precursors or Lin28b-transduced post-natal HSC.[147] Whether expression levels of Lin28b might distinguish waves of TSP, or HSC-dependent from HSC-independent multipotent progenitors, remains at this stage speculative. Interestingly, forced expression of Lin28b in mice confers adult BM progenitors with the capacity to generate fetal-type cells like B1 B and NKTγδ cells, in mice.[148]

Highlights of current knowledge on fetal thymopoiesis, as here summarized, add to the many studies in recent years that converged to the concept that, in the mouse embryo, hematopoiesis is essentially driven by YS-derived and intra-embryonic HSC-independent progenitors. A contribution of HSC to late fetal thymopoiesis is likely to occur in species with long gestation periods. However, as discussed elsewhere,[149] even in these cases the evolutionary strategy of a layered organization of thymopoiesis is, in all likelihood, conserved

## 5 | A NEW HSC-INDEPENDENT INTRA-EMBRYONIC WAVE OF HEMATOPOIETIC GENERATION

Considerations relevant when studying the embryonic origin of the hematopoietic populations are 1. In the mouse, the three generations of hematopoietic progenitors occur sequentially but overlap 2. It has been challenging to find specific markers that are uniquely expressed in YS or intra-embryonic HE; 3. After circulation is established (E8.5) it is difficult to define the intra- or extra-embryonic origin of the cells because blood vessels connect YS and embryo proper 4. Lymphoid potential does not equate with HSC generation because some lymphoid progenitors could be HSC-independent[141,142]; 5. However, the absence of LTR activity in embryonic cells does not preclude the presence of pre- or immature HSC; 6. A third event of EHT occurs in the omphalo-mesenteric and vitelline arteries that connect the embryo proper with the placenta and YS. Therefore, isolation of extra-embryonic tissue including these vessels will exhibit multipotent hematopoietic activity. Ultimately, given these considerations, the YS versus AGM origin of the progenitors becomes of limited functional relevance. Instead, it is their differentiation potential and their capacity to contribute to adult hematopoiesis that are of key significance.

The fundamentally different properties of embryonic restricted lymphocytes compared with their adult counterparts raise the problem of their origin. If all lymphoid cells originate from HSC, it is not obvious why a cell that is in nature multipotent becomes unable to generate a very specific subset of cells as they transit from the FL to the BM. As discussed above, however, FL and BM are very different environments and could exert selective pressures on the progeny of HSC. FL exhibit low levels of Epo, but also possibly of most hematopoietic cytokines including interleukin (IL)-7, a potent regulator of lymphoid development. Low levels of IL-7 favor the accumulation of T/ILC versus B progenitors in the FL[73] and modulate the repertoire of B1 B cells.[44] It could be argued that irrespective of their site of origin, the first layer of lymphoid cells exhibits properties that were primarily selected as an adaptation to environmental cues, determining different cell fates. The transition from FL to the BM could also induce epigenetic modifications modulating the differentiation potential and rendering some *loci* inaccessible in HSC.

However, functional properties of embryonic lymphoid cells appear to be specific of the developmental stage and to be cell autonomous, and, therefore, it is tempting to consider the possibility that they derive from different progenitors that are developmentally restricted (Figure 2). These cells would derive from an independent wave of hematopoietic generation between the emergence of YS EMP and that of the dorsal aorta HSC. They would have multipotent differentiation properties but would have low probability to integrate the adult HSC pool. They would rather devote to differentiate into embryonic type lymphocytes that have fundamental roles in organ development.

Several lines of evidence support this notion and are outlined below.

The possibility to follow the progeny of cells by permanently inducing the expression of a fluorescent protein (lineage tracing, fate map) revolutionized developmental hematology. Because it has been difficult to identify specific markers to distinguish the hemogenic endothelium that generates EMP and multipotent progenitors, experiments that fate map the second and third layer of hematopoietic generation relied in an induction of fluorescence at different developmental stages:

1. Lineage tracing studies[141] show low frequency of fluorescent-labeled invariant γδ T cells and LTi cells were observed in conditions that label YS-EMP, indicating that they originate from different progenitors also found by Elsaid et al.[135] However, also conditions that label a majority of HSC yield low frequency of YFP labeled embryonic lymphoid cells, suggesting that they do not originate from HSC or their immediate progenitors.
2. A transient population of multipotent progenitors appears biased to the production of B1 cells and invariant γδ T cells in vivo,

and these cells emerge in the mouse embryo before HSC are detected.[142]

3. Human fetal hematopoietic progenitors were shown to generate T cells with different properties than their adult BM counterparts.[150]
4. CXCR4 expression in the dorsal aorta HE distinguishes an early and a late hematopoietic generation that differ in their capacity to integrate the HSC compartment.[84]

Another compelling argument is the analysis of the incidence of childhood leukemias:

1. The higher incidence of myeloid leukemias in aged individuals contrasts with the higher incidence of acute lymphoid leukemias (ALL) in infants.[151] It was recently suggested that the target of childhood ALL is a progenitor cell that is lymphoid biased and can only be found during embryonic development.
2. Another interesting observation is the high susceptibility of children with Down syndrome (DS) to develop leukemias, not found in adult DS patients.[152] It is, therefore, tempting to speculate that the target cell for the infant DS leukemia is no longer present in the adult BM thus accounting for the discrepancy between young and adult DS patients in developing the disease.[153]
3. The common ALL translocation, MLL-AF9, induces different diseases depending on whether it is induced in neonatal human progenitors or in adult CD34$^+$ cells. It is therefore tempting to speculate that, in humans, lymphoid-biased transient multipotent cells, equivalent to the ones we propose here, are targets of the translocations that lead to ALL.[154]

The first wave of TSP induces the maturation of the thymic architecture, essential to the selection of conventional T cell.[53,135] Genetic or environmentally induced variations in the maturation of the thymic epithelial compartment might impact immunity for life, increasing risks of autoimmune disorders or premature thymic involution. The invariant γδ T cells also have roles in the periphery by improving wound healing, in the skin,[155] and epithelial regeneration, in the lungs.[139] Likewise, it could be speculated that altering the dynamic of secondary lymphoid organ formation initiated by LTi could modulate memory immune responses and even cancer development. The natural antibody repertoire of B1 cells appears to be selected by early exposure to bacterial products and might be essential as first line of defense specially in newborns where the adaptive immune system is immature.[38] All these properties would have conferred a selective pressure to maintain this new, yet transient, generation of progenitors that do not contribute to the HSC compartment and possibly also not to adult hematopoiesis.

Further studies are required to assess how long these hematopoietic progenitors persist, whether they can reach the BM, how to distinguish them from other multipotent cells and what are the molecular basis for their different behavior.

## ACKNOWLEDGEMENTS

We thank all members from the Lymphocyte and Immunity Unit, Elisa Gomez-Perdiguero and the members from her laboratory for excellent discussions.

## FUNDING INFORMATION

Institut Pasteur, INSERM, ANR (grant Twothyme, grant EPI-DEV and grant DELSTAR), Ligue contre le cancer, and REVIVE Future Investment Program through grants to A.C. FSS is financed by a post-doctoral grant from REVIVE (ANR-10-LABX-73), GN is financed by a PhD grant from REVIVE and MMP is financed by a grant from FCT SFRH/BD/143605/2019.

## CONFLICT OF INTEREST

All authors declare no have a conflict of interest.

## DATA AVAILABILITY STATEMENT

Data available on request from the authors.

## ORCID

*Ana Cumano* https://orcid.org/0000-0002-4578-959X

## REFERENCES

1. Herzenberg LA. Toward a layered immune system. *Cell*. 1989;59(6):953-954.
2. Becker AJ, McCulloch EA, Till JE. Cytological demonstration of the clonal nature of spleen colonies derived from transplanted mouse marrow cells. *Nature*. 1963;197:452-454.
3. Moore MA, Metcalf D. Ontogeny of the haemopoietic system: yolk sac origin of in vivo and in vitro colony forming cells in the developing mouse embryo. *Br J Haematol*. 1970;18(3):279-296.
4. Lassila O, Eskola J, Toivanen P, Martin C, Dieterlen-Lievre F. The origin of lymphoid stem cells studied in chick yold sac-embryo chimaeras. *Nature*. 1978;272(5651):353-354.
5. Palis J. Primitive and definitive erythropoiesis in mammals. *Front Physiol*. 2014;5:53.
6. Stefanska M, Batta K, Patel R, Florkowska M, Kouskoff V, Lacaud G. Primitive erythrocytes are generated from hemogenic endothelial cells. *Sci Rep*. 2017;7(1):6401.
7. Bertrand JY, Jalil A, Klaine M, Jung S, Cumano A, Godin I. Three pathways to mature macrophages in the early mouse yolk sac. *Blood*. 2005;106(9):3004-3011.
8. McGrath KE, Frame JM, Fegan KH, et al. Distinct sources of hematopoietic progenitors emerge before HSCs and provide functional blood cells in the mammalian embryo. *Cell Rep*. 2015;11(12):1892-1904.
9. Gomez Perdiguero E, Klapproth K, Schulz C, et al. Tissue-resident macrophages originate from yolk-sac-derived erythro-myeloid progenitors. *Nature*. 2015;518(7540):547-551.
10. Gentek R, Ghigo C, Hoeffel G, et al. Hemogenic endothelial fate mapping reveals dual developmental origin of mast cells. *Immunity*. 2018;48(6):1160-1171.
11. Jaffredo T, Gautier R, Brajeul V, Dieterlen-Lièvre F. Tracing the progeny of the aortic hemangioblast in the avian embryo. *Dev Biol*. 2000;224(2):204-214.
12. Cumano A, Dieterlen-Lievre F, Godin I. Lymphoid potential, probed before circulation in mouse, is restricted to caudal intraembryonic splanchnopleura. *Cell*. 1996;86(6):907-916.

16000656, 0, Downloaded from https://onlinelibrary.wiley.com/doi/10.1111/imr.13187 by Institut Pasteur, Wiley Online Library on [10/04/2023]. See the Terms and Conditions (https://onlinelibrary.wiley.com/terms-and-conditions) on Wiley Online Library for rules of use; OA articles are governed by the applicable Creative Commons License

13. Medvinsky A, Dzierzak E. Definitive hematopoiesis is autonomously initiated by the AGM region. *Cell*. 1996;86(6):897-906.
14. Cumano A, Ferraz JC, Klaine M, Di Santo JP, Godin I. Intraembryonic, but not yolk sac hematopoietic precursors, isolated before circulation, provide long-term multilineage reconstitution. *Immunity*. 2001;15(3):477-485.
15. Bertrand JY, Chi NC, Santoso B, Teng S, Stainier DY, Traver D. Haematopoietic stem cells derive directly from aortic endothelium during development. *Nature*. 2010;464(7285):108-111.
16. Kissa K, Herbomel P. Blood stem cells emerge from aortic endothelium by a novel type of cell transition. *Nature*. 2010;464(7285):112-115.
17. de Bruijn MF, Speck NA, Peeters MC, Dzierzak E. Definitive hematopoietic stem cells first develop within the major arterial regions of the mouse embryo. *EMBO J*. 2000;19(11):2465-2474.
18. Frame JM, Fegan KH, Conway SJ, McGrath KE, Palis J. Definitive hematopoiesis in the yolk sac emerges from Wnt-responsive Hemogenic endothelium independently of circulation and arterial identity. *Stem Cells*. 2016;34(2):431-444.
19. Godin I, Garcia-Porrero JA, Dieterlen-Lièvre F, Cumano A. Stem cell emergence and hemopoietic activity are incompatible in mouse intraembryonic sites. *J Exp Med*. 1999;190(1):43-52.
20. Müller AM, Medvinsky A, Strouboulis J, Grosveld F, Dzierzak E. Development of hematopoietic stem cell activity in the mouse embryo. *Immunity*. 1994;1(4):291-301.
21. Medvinsky AL, Samoylina NL, Müller AM, Dzierzak EA. An early pre-liver intraembryonic source of CFU-S in the developing mouse. *Nature*. 1993;364(6432):64-67.
22. Taoudi S, Gonneau C, Moore K, et al. Extensive hematopoietic stem cell generation in the AGM region via maturation of VE-cadherin+CD45+ pre-definitive HSCs. *Cell Stem Cell*. 2008;3(1):99-108.
23. Kieusseian A, Brunet de la Grange P, Burlen-Defranoux O, Godin I, Cumano A. Immature hematopoietic stem cells undergo maturation in the fetal liver. *Development*. 2012;139(19):3521-3530.
24. Benveniste P, Frelin C, Janmohamed S, et al. Intermediate-term hematopoietic stem cells with extended but time-limited reconstitution potential. *Cell Stem Cell*. 2010;6(1):48-58.
25. Houssaint E. Differentiation of the mouse hepatic primordium. I. An analysis of tissue interactions in hepatocyte differentiation. *Cell Differ*. 1980;9(5):269-279.
26. Soares-da-Silva F, Peixoto M, Cumano A, Pinto-do-Ó P. Crosstalk between the hepatic and hematopoietic systems during embryonic development. *Front Cell Dev Biol*. 2020;8:612.
27. Johnson GR, Moore MA. Role of stem cell migration in initiation of mouse foetal liver haemopoiesis. *Nature*. 1975;258(5537):726-728.
28. Ema H, Nakauchi H. Expansion of hematopoietic stem cells in the developing liver of a mouse embryo. *Blood*. 2000;95(7):2284-2288.
29. Paige CJ, Gisler RH, McKearn JP, Iscove NN. Differentiation of murine B cell precursors in agar culture. Frequency, surface marker analysis and requirements for growth of clonable pre-B cells. *Eur J Immunol*. 1984;14(11):979-987.
30. Cumano A, Paige CJ, Iscove NN, Brady G. Bipotential precursors of B cells and macrophages in murine fetal liver. *Nature*. 1992;356(6370):612-615.
31. Ding L, Saunders TL, Enikolopov G, Morrison SJ. Endothelial and perivascular cells maintain haematopoietic stem cells. *Nature*. 2012;481(7382):457-462.
32. Lee Y, Leslie J, Yang Y, Ding L. Hepatic stellate and endothelial cells maintain hematopoietic stem cells in the developing liver. *J Exp Med*. 2021;218(3):e20200882.
33. Chou S, Lodish HF. Fetal liver hepatic progenitors are supportive stromal cells for hematopoietic stem cells. *Proc Natl Acad Sci U S A*. 2010;107(17):7799-7804.
34. Khan JA, Mendelson A, Kunisaki Y, et al. Fetal liver hematopoietic stem cell niches associate with portal vessels. *Science*. 2016;351(6269):176-180.
35. Hayakawa K, Hardy RR, Herzenberg LA, Herzenberg LA. Progenitors for Ly-1 B cells are distinct from progenitors for other B cells. *J Exp Med*. 1985;161(6):1554-1568.
36. Förster I, Rajewsky K. Expansion and functional activity of Ly-1+ B cells upon transfer of peritoneal cells into allotype-congenic, newborn mice. *Eur J Immunol*. 1987;17(4):521-528.
37. Martin F, Kearney JF. B-cell subsets and the mature preimmune repertoire. Marginal zone and B1 B cells as part of a "natural immune memory". *Immunol Rev*. 2000;175:70-79.
38. New JS, Dizon BLP, Fucile CF, Rosenberg AF, Kearney JF, King RG. Neonatal exposure to commensal-bacteria-derived antigens directs polysaccharide-specific B-1 B cell repertoire development. *Immunity*. 2020;53(1):172-186.
39. Hayakawa K, Asano M, Shinton SA, et al. Positive selection of natural autoreactive B cells. *Science*. 1999;285(5424):113-116.
40. Montecino-Rodriguez E, Leathers H, Dorshkind K. Identification of a B-1 B cell-specified progenitor. *Nat Immunol*. 2006;7(3):293-301.
41. Herzenberg LA. Layered evolution in the immune system: a view from history. *Ann N Y Acad Sci*. 2015;1362:1-5.
42. Kristiansen TA, Jaensson Gyllenbäck E, Zriwil A, et al. Cellular barcoding links B-1a B cell potential to a fetal hematopoietic stem cell state at the single-cell level. *Immunity*. 2016;45(2):346-357.
43. Graf R, Seagal J, Otipoby KL, et al. BCR-dependent lineage plasticity in mature B cells. *Science*. 2019;363(6428):748-753.
44. Wong JB, Hewitt SL, Heltemes-Harris LM, et al. B-1a cells acquire their unique characteristics by bypassing the pre-BCR selection stage. *Nat Commun*. 2019;10(1):4768.
45. Düber S, Hafner M, Krey M, et al. Induction of B-cell development in adult mice reveals the ability of bone marrow to produce B-1a cells. *Blood*. 2009;114(24):4960-4967.
46. Asarnow DM, Kuziel WA, Bonyhadi M, Tigelaar RE, Tucker PW, Allison JP. Limited diversity of gamma delta antigen receptor genes of Thy-1+ dendritic epidermal cells. *Cell*. 1988;55(5):837-847.
47. Havran WL, Allison JP. Developmentally ordered appearance of thymocytes expressing different T-cell antigen receptors. *Nature*. 1988;335(6189):443-445.
48. Havran WL, Allison JP. Origin of Thy-1+ dendritic epidermal cells of adult mice from fetal thymic precursors. *Nature*. 1990;344(6261):68-70.
49. Ikuta K, Kina T, MacNeil I, et al. A developmental switch in thymic lymphocyte maturation potential occurs at the level of hematopoietic stem cells. *Cell*. 1990;62(5):863-874.
50. Haas JD, Ravens S, Düber S, et al. Development of interleukin-17-producing γδ T cells is restricted to a functional embryonic wave. *Immunity*. 2012;37(1):48-59.
51. Boyden LM, Lewis JM, Barbee SD, et al. Skint1, the prototype of a newly identified immunoglobulin superfamily gene cluster, positively selects epidermal gammadelta T cells. *Nat Genet*. 2008;40(5):656-662.
52. Di Marco Barros R, Roberts NA, Dart RJ, et al. Epithelia use Butyrophilin-like molecules to shape organ-specific γδ T cell compartments. *Cell*. 2016;167(1):203-218.
53. Roberts NA, White AJ, Jenkinson WE, et al. Rank signaling links the development of invariant γδ T cell progenitors and Aire(+) medullary epithelium. *Immunity*. 2012;36(3):427-437.
54. Heilig JS, Tonegawa S. Diversity of murine gamma genes and expression in fetal and adult T lymphocytes. *Nature*. 1986;322(6082):836-840.
55. Garman RD, Doherty PJ, Raulet DH. Diversity, rearrangement, and expression of murine T cell gamma genes. *Cell*. 1986;45(5):733-742.
56. Raulet DH. The structure, function, and molecular genetics of the gamma/delta T cell receptor. *Annu Rev Immunol*. 1989;7:175-207.


16000656, 0, Downloaded from https://onlinelibrary.wiley.com/doi/10.1111/imr.13187 by Institut Pasteur, Wiley Online Library on [10/04/2023]. See the Terms and Conditions (https://onlinelibrary.wiley.com/terms-and-conditions) on Wiley Online Library for rules of use; OA articles are governed by the applicable Creative Commons License

57. Eberl G, Marmon S, Sunshine MJ, Rennert PD, Choi Y, Littman DR. An essential function for the nuclear receptor RORgamma(t) in the generation of fetal lymphoid tissue inducer cells. *Nat Immunol*. 2004;5(1):64-73.
58. Possot C, Schmutz S, Chea S, et al. Notch signaling is necessary for adult, but not fetal, development of RORγt(+) innate lymphoid cells. *Nat Immunol*. 2011;12(10):949-958.
59. Hoeffel G, Chen J, Lavin Y, et al. C-Myb(+) erythro-myeloid progenitor-derived fetal monocytes give rise to adult tissue-resident macrophages. *Immunity*. 2015;42(4):665-678.
60. Schulz C, Gomez Perdiguero E, Chorro L, et al. A lineage of myeloid cells independent of Myb and hematopoietic stem cells. *Science*. 2012;336(6077):86-90.
61. Mildner A, Schmidt H, Nitsche M, et al. Microglia in the adult brain arise from Ly-6ChiCCR2+ monocytes only under defined host conditions. *Nat Neurosci*. 2007;10(12):1544-1553.
62. Varvel NH, Grathwohl SA, Baumann F, et al. Microglial repopulation model reveals a robust homeostatic process for replacing CNS myeloid cells. *Proc Natl Acad Sci U S A*. 2012;109(44):18150-18155.
63. Ajami B, Bennett JL, Krieger C, McNagny KM, Rossi FM. Infiltrating monocytes trigger EAE progression, but do not contribute to the resident microglia pool. *Nat Neurosci*. 2011;14(9):1142-1149.
64. Antony JM, Paquin A, Nutt SL, Kaplan DR, Miller FD. Endogenous microglia regulate development of embryonic cortical precursor cells. *J Neurosci Res*. 2011;89(3):286-298.
65. Arnò B, Grassivaro F, Rossi C, et al. Neural progenitor cells orchestrate microglia migration and positioning into the developing cortex. *Nat Commun*. 2014;5:5611.
66. Squarzoni P, Oller G, Hoeffel G, et al. Microglia modulate wiring of the embryonic forebrain. *Cell Rep*. 2014;8(5):1271-1279.
67. Nandi S, Gokhan S, Dai XM, et al. The CSF-1 receptor ligands IL-34 and CSF-1 exhibit distinct developmental brain expression patterns and regulate neural progenitor cell maintenance and maturation. *Dev Biol*. 2012;367(2):100-113.
68. Cunningham CL, Martínez-Cerdeño V, Noctor SC. Microglia regulate the number of neural precursor cells in the developing cerebral cortex. *J Neurosci*. 2013;33(10):4216-4233.
69. Prinz M, Priller J. Microglia and brain macrophages in the molecular age: from origin to neuropsychiatric disease. *Nat Rev Neurosci*. 2014;15(5):300-312.
70. Li Q, Barres BA. Microglia and macrophages in brain homeostasis and disease. *Nat Rev Immunol*. 2018;18(4):225-242.
71. Soares-da-Silva F, Freyer L, Elsaid R, et al. Yolk sac, but not hematopoietic stem cell-derived progenitors, sustain erythropoiesis throughout murine embryonic life. *J Exp Med*. 2021;218(4):e20201729.
72. Kim AR, Ulirsch JC, Wilmes S, et al. Functional selectivity in cytokine signaling revealed through a pathogenic EPO mutation. *Cell*. 2017;168(6):1053-1064.
73. Berthault C, Ramond C, Burlen-Defranoux O, et al. Asynchronous lineage priming determines commitment to T cell and B cell lineages in fetal liver. *Nat Immunol*. 2017;18(10):1139-1149.
74. Zovein AC, Hofmann JJ, Lynch M, et al. Fate tracing reveals the endothelial origin of hematopoietic stem cells. *Cell Stem Cell*. 2008;3(6):625-636.
75. Chen MJ, Yokomizo T, Zeigler BM, Dzierzak E, Speck NA. Runx1 is required for the endothelial to haematopoietic cell transition but not thereafter. *Nature*. 2009;457(7231):887-891.
76. Okuda T, van Deursen J, Hiebert SW, Grosveld G, Downing JR. AML1, the target of multiple chromosomal translocations in human leukemia, is essential for normal fetal liver hematopoiesis. *Cell*. 1996;84(2):321-330.
77. Lie-A-Ling M, Marinopoulou E, Lilly AJ, et al. Regulation of RUNX1 dosage is crucial for efficient blood formation from hemogenic endothelium. *Development*. 2018;145(5):dev149419.
78. Yokomizo T, Dzierzak E. Three-dimensional cartography of hematopoietic clusters in the vasculature of whole mouse embryos. *Development*. 2010;137(21):3651-3661.
79. Rybtsov S, Ivanovs A, Zhao S, Medvinsky A. Concealed expansion of immature precursors underpins acute burst of adult HSC activity in foetal liver. *Development*. 2016;143(8):1284-1289.
80. Taoudi S, Medvinsky A. Functional identification of the hematopoietic stem cell niche in the ventral domain of the embryonic dorsal aorta. *Proc Natl Acad Sci U S A*. 2007;104(22):9399-9403.
81. Mascarenhas MI, Parker A, Dzierzak E, Ottersbach K. Identification of novel regulators of hematopoietic stem cell development through refinement of stem cell localization and expression profiling. *Blood*. 2009;114(21):4645-4653.
82. Gritz E, Hirschi KK. Specification and function of hemogenic endothelium during embryogenesis. *Cell Mol Life Sci*. 2016;73(8):1547-1567.
83. Yokomizo T, Ideue T, Morino-Koga S, et al. Independent origins of fetal liver haematopoietic stem and progenitor cells. *Nature*. 2022;609(7928):779-784.
84. Dignum T, Varnum-Finney B, Srivatsan SR, et al. Multipotent progenitors and hematopoietic stem cells arise independently from hemogenic endothelium in the mouse embryo. *Cell Rep*. 2021;36(11):109675.
85. Pucella JN, Upadhaya S, Reizis B. The source and dynamics of adult hematopoiesis: insights from lineage tracing. *Annu Rev Cell Dev Biol*. 2020;36:529-550.
86. Rodriguez-Fraticelli AE, Camargo F. Systems analysis of hematopoiesis using single-cell lineage tracing. *Curr Opin Hematol*. 2021;28(1):18-27.
87. Pei W, Feyerabend TB, Rössler J, et al. Polylox barcoding reveals haematopoietic stem cell fates realized in vivo. *Nature*. 2017;548(7668):456-460.
88. Rodriguez-Fraticelli AE, Wolock SL, Weinreb CS, et al. Clonal analysis of lineage fate in native haematopoiesis. *Nature*. 2018;553(7687):212-216.
89. Sun J, Ramos A, Chapman B, et al. Clonal dynamics of native haematopoiesis. *Nature*. 2014;514(7522):322-327.
90. Cheshier SH, Morrison SJ, Liao X, Weissman IL. In vivo proliferation and cell cycle kinetics of long-term self-renewing hematopoietic stem cells. *Proc Natl Acad Sci U S A*. 1999;96(6):3120-3125.
91. Pietras EM, Warr MR, Passegué E. Cell cycle regulation in hematopoietic stem cells. *J Cell Biol*. 2011;195(5):709-720.
92. Harrison DE, Zhong RK. The same exhaustible multilineage precursor produces both myeloid and lymphoid cells as early as 3-4 weeks after marrow transplantation. *Proc Natl Acad Sci U S A*. 1992;89(21):10134-10138.
93. Ganuza M, Hall T, Finkelstein D, Chabot A, Kang G, McKinney-Freeman S. Lifelong haematopoiesis is established by hundreds of precursors throughout mammalian ontogeny. *Nat Cell Biol*. 2017;19(10):1153-1163.
94. Ganuza M, Clements W, McKinney-Freeman S. Specification of hematopoietic stem cells in mammalian embryos: a rare or frequent event. *Blood*. 2022;140(4):309-320.
95. Nygren JM, Bryder D, Jacobsen SE. Prolonged cell cycle transit is a defining and developmentally conserved hemopoietic stem cell property. *J Immunol*. 2006;177(1):201-208.
96. Bowie MB, McKnight KD, Kent DG, McCaffrey L, Hoodless PA, Eaves CJ. Hematopoietic stem cells proliferate until after birth and show a reversible phase-specific engraftment defect. *J Clin Invest*. 2006;116(10):2808-2816.
97. Hall TD, Kim H, Dabbah M, et al. Murine fetal bone marrow does not support functional hematopoietic stem and progenitor cells until birth. *Nat Commun*. 2022;13(1):5403.
98. Qian H, Georges-Labouesse E, Nyström A, et al. Distinct roles of integrins alpha6 and alpha4 in homing of fetal liver hematopoietic stem and progenitor cells. *Blood*. 2007;110(7):2399-2407.

16000656, 0, Downloaded from https://onlinelibrary.wiley.com/doi/10.1111/imr.13187 by Institut Pasteur, Wiley Online Library on [10/04/2023]. See the Terms and Conditions (https://onlinelibrary.wiley.com/terms-and-conditions) on Wiley Online Library for rules of use; OA articles are governed by the applicable Creative Commons License

99. Szilvassy SJ, Humphries RK, Lansdorp PM, Eaves AC, Eaves CJ. Quantitative assay for totipotent reconstituting hematopoietic stem cells by a competitive repopulation strategy. *Proc Natl Acad Sci U S A*. 1990;87(22):8736-8740.
100. Trevisan M, Yan XQ, Iscove NN. Cycle initiation and colony formation in culture by murine marrow cells with long-term reconstituting potential in vivo. *Blood*. 1996;88(11):4149-4158.
101. Morrison SJ, Hemmati HD, Wandycz AM, Weissman IL. The purification and characterization of fetal liver hematopoietic stem cells. *Proc Natl Acad Sci U S A*. 1995;92(22):10302-10306.
102. Rebel VI, Miller CL, Thornbury GR, Dragowska WH, Eaves CJ, Lansdorp PM. A comparison of long-term repopulating hematopoietic stem cells in fetal liver and adult bone marrow from the mouse. *Exp Hematol*. 1996;24(5):638-648.
103. Miller CL, Rebel VI, Helgason CD, Lansdorp PM, Eaves CJ. Impaired steel factor responsiveness differentially affects the detection and long-term maintenance of fetal liver hematopoietic stem cells in vivo. *Blood*. 1997;89(4):1214-1223.
104. Szilvassy SJ, Ragland PL, Miller CL, Eaves CJ. The marrow homing efficiency of murine hematopoietic stem cells remains constant during ontogeny. *Exp Hematol*. 2003;31(4):331-338.
105. Gekas C, Dieterlen-Lièvre F, Orkin SH, Mikkola HK. The placenta is a niche for hematopoietic stem cells. *Dev Cell*. 2005;8(3):365-375.
106. Benz C, Copley MR, Kent DG, et al. Hematopoietic stem cell subtypes expand differentially during development and display distinct lymphopoietic programs. *Cell Stem Cell*. 2012;10(3):273-283.
107. Zhao Y, Zhou J, Liu D, et al. ATF4 plays a pivotal role in the development of functional hematopoietic stem cells in mouse fetal liver. *Blood*. 2015;126(21):2383-2391.
108. Patel SH, Christodoulou C, Weinreb C, et al. Lifelong multilineage contribution by embryonic-born blood progenitors. *Nature*. 2022;606(7915):747-753.
109. Abramson J, Anderson G. Thymic epithelial cells. *Annu Rev Immunol*. 2017;35:3585-3118.
110. Alawam AS, Anderson G, Lucas B. Generation and regeneration of Thymic epithelial cells. *Front Immunol*. 2020;11:858.
111. Rodewald HR. Thymus organogenesis. *Annu Rev Immunol*. 2008;26:26355-26388.
112. Gill J, Malin M, Hollander GA, Boyd R. Generation of a complete thymic microenvironment by MTS24(+) thymic epithelial cells. *Nat Immunol*. 2002;3(7):635-642.
113. Bennett AR, Farley A, Blair NF, Gordon J, Sharp L, Blackburn CC. Identification and characterization of thymic epithelial progenitor cells. *Immunity*. 2002;16(6):803-814.
114. Bleul CC, Corbeaux T, Reuter A, Fisch P, Mönting JS, Boehm T. Formation of a functional thymus initiated by a postnatal epithelial progenitor cell. *Nature*. 2006;441(7096):992-996.
115. Rossi SW, Jenkinson WE, Anderson G, Jenkinson EJ. Clonal analysis reveals a common progenitor for thymic cortical and medullary epithelium. *Nature*. 2006;441(7096):988-991.
116. Ulyanchenko S, O'Neill KE, Medley T, et al. Identification of a Bipotent epithelial progenitor population in the adult thymus. *Cell Rep*. 2016;14(12):2819-2832.
117. Ribeiro AR, Rodrigues PM, Meireles C, Di Santo JP, Alves NL. Thymocyte selection regulates the homeostasis of IL-7-expressing thymic cortical epithelial cells in vivo. *J Immunol*. 2013;191(3):1200-1209.
118. Ribeiro AR, Meireles C, Rodrigues PM, Alves NL. Intermediate expression of CCRL1 reveals novel subpopulations of medullary thymic epithelial cells that emerge in the postnatal thymus. *Eur J Immunol*. 2014;44(10):2918-2924.
119. Nusser A, Sagar, Swann JB, et al. Developmental dynamics of two bipotent thymic epithelial progenitor types. *Nature*. 2022;606(7912):165-171.
120. Mathis D, Benoist C. Aire. *Annu Rev Immunol*. 2009;27:27287-27312.
121. Takaba H, Morishita Y, Tomofuji Y, et al. Fezf2 orchestrates a Thymic program of self-antigen expression for immune tolerance. *Cell*. 2015;163(4):975-987.
122. Michelson DA, Hase K, Kaisho T, Benoist C, Mathis D. Thymic epithelial cells co-opt lineage-defining transcription factors to eliminate autoreactive T cells. *Cell*. 2022;185(14):2542-2558.
123. Blackburn CC, Augustine CL, Li R, et al. The nu gene acts cell-autonomously and is required for differentiation of thymic epithelial progenitors. *Proc Natl Acad Sci U S A*. 1996;93(12):5742-5746.
124. Corbeaux T, Hess I, Swann JB, Kanzler B, Haas-Assenbaum A, Boehm T. Thymopoiesis in mice depends on a Foxn1-positive thymic epithelial cell lineage. *Proc Natl Acad Sci U S A*. 2010;107(38):16613-16618.
125. Bredenkamp N, Nowell CS, Blackburn CC. Regeneration of the aged thymus by a single transcription factor. *Development*. 2014;141(8):1627-1637.
126. Dudakov JA, Hanash AM, Jenq RR, et al. Interleukin-22 drives endogenous thymic regeneration in mice. *Science*. 2012;336(6077):91-95.
127. Lopes N, Vachon H, Marie J, Irla M. Administration of RANKL boosts thymic regeneration upon bone marrow transplantation. *EMBO Mol Med*. 2017;9(6):835-851.
128. Wertheimer T, Velardi E, Tsai J, et al. Production of BMP4 by endothelial cells is crucial for endogenous thymic regeneration. *Sci Immunol*. 2018;3(19):eaal2736.
129. Rode I, Martins VC, Kühlbeck G, Maltry N, Tessmer C, Rodewald HR. Foxn1 protein expression in the developing, aging, and regenerating thymus. *J Immunol*. 2015;195(12):5678-5687.
130. Coles AJ, Azzopardi L, Kousin-Ezewu O, et al. Keratinocyte growth factor impairs human thymic recovery from lymphopenia. *JCI Insight*. 2019;5:e125377.
131. Gray D, Abramson J, Benoist C, Mathis D. Proliferative arrest and rapid turnover of thymic epithelial cells expressing Aire. *J Exp Med*. 2007;204(11):2521-2528.
132. Jones R, Cosway EJ, Willis C, et al. Dynamic changes in intrathymic ILC populations during murine neonatal development. *Eur J Immunol*. 2018;48(9):1481-1491.
133. Cheng MH, Fan U, Grewal N, et al. Acquired autoimmune polyglandular syndrome, thymoma, and an AIRE defect. *N Engl J Med*. 2010;362(8):764-766.
134. Ramond C, Berthault C, Burlen-Defranoux O, et al. Two waves of distinct hematopoietic progenitor cells colonize the fetal thymus. *Nat Immunol*. 2014;15(1):27-35.
135. Elsaid R, Meunier S, Burlen-Defranoux O, et al. A wave of bipotent T/ILC-restricted progenitors shapes the embryonic thymus microenvironment in a time-dependent manner. *Blood*. 2021;137(8):1024-1036.
136. Simic M, Manosalva I, Spinelli L, et al. Distinct waves from the Hemogenic endothelium give rise to layered lymphoid tissue inducer cell ontogeny. *Cell Rep*. 2020;32(6):108004.
137. Guerau-de-Arellano M, Martinic M, Benoist C, Mathis D. Neonatal tolerance revisited: a perinatal window for Aire control of autoimmunity. *J Exp Med*. 2009;206(6):1245-1252.
138. Keyes BE, Liu S, Asare A, et al. Impaired epidermal to dendritic T cell signaling slows wound repair in aged skin. *Cell*. 2016;167(5):1323-1338.
139. Guo XJ, Dash P, Crawford JC, et al. Lung γδ T cells mediate protective responses during neonatal influenza infection that are associated with type 2 immunity. *Immunity*. 2018;49(3):531-544.
140. Böiers C, Carrelha J, Lutteropp M, et al. Lymphomyeloid contribution of an immune-restricted progenitor emerging prior to definitive hematopoietic stem cells. *Cell Stem Cell*. 2013;13(5):535-548.
141. Gentek R, Ghigo C, Hoeffel G, et al. Epidermal γδ T cells originate from yolk sac hematopoiesis and clonally self-renew in the adult. *J Exp Med*. 2018;215(12):2994-3005.


16000656, 0, Downloaded from https://onlinelibrary.wiley.com/doi/10.1111/imr.13187 by Institut Pasteur, Wiley Online Library on [10/04/2023]. See the Terms and Conditions (https://onlinelibrary.wiley.com/terms-and-conditions) on Wiley Online Library for rules of use; OA articles are governed by the applicable Creative Commons License

142. Beaudin AE, Boyer SW, Perez-Cunningham J, et al. A transient developmental hematopoietic stem cell gives rise to innate-like B and T cells. *Cell Stem Cell*. 2016;19(6):768-783.
143. Tian Y, Xu J, Feng S, et al. The first wave of T lymphopoiesis in zebrafish arises from aorta endothelium independent of hematopoietic stem cells. *J Exp Med*. 2017;214(11):3347-3360.
144. Ulloa BA, Habbsa SS, Potts KS, et al. Definitive hematopoietic stem cells minimally contribute to embryonic hematopoiesis. *Cell Rep*. 2021;36(11):109703.
145. Dimova T, Brouwer M, Gosselin F, et al. Effector Vγ9Vδ2 T cells dominate the human fetal γδ T-cell repertoire. *Proc Natl Acad Sci U S A*. 2015;112(6):E556-E565.
146. Vermijlen D, Gatti D, Kouzeli A, Rus T, Eberl M. γδ T cell responses: how many ligands will it take till we know. *Semin Cell dev Biol*. 2018;84:75-86.
147. Tieppo P, Papadopoulou M, Gatti D, et al. The human fetal thymus generates invariant effector γδ T cells. *J Exp Med*. 2020;217(3):jem.20190580.
148. Yuan J, Nguyen CK, Liu X, Kanellopoulou C, Muljo SA. Lin28b reprograms adult bone marrow hematopoietic progenitors to mediate fetal-like lymphopoiesis. *Science*. 2012;335(6073):1195-1200.
149. Elsaid R, Soares-da-Silva F, Peixoto M, et al. Hematopoiesis: a layered organization across chordate species. *Front Cell Dev Biol*. 2020;8:606642.
150. Mold JE, Venkatasubrahmanyam S, Burt TD, et al. Fetal and adult hematopoietic stem cells give rise to distinct T cell lineages in humans. *Science*. 2010;330(6011):1695-1699.
151. Böiers C, Richardson SE, Laycock E, et al. A human IPS model implicates embryonic B-myeloid fate restriction as developmental susceptibility to B acute lymphoblastic leukemia-associated ETV6-RUNX1. *Dev Cell*. 2018;44(3):362-377.
152. Marlow EC, Ducore J, Kwan ML, et al. Leukemia risk in a cohort of 3.9 million children with and without down syndrome. *J Pediatr*. 2021;234:172-180.
153. Khan I, Malinge S, Crispino J. Myeloid leukemia in down syndrome. *Crit Rev Oncog*. 2011;16(1–2):25-36.
154. Horton SJ, Jaques J, Woolthuis C, et al. MLL-AF9-mediated immortalization of human hematopoietic cells along different lineages changes during ontogeny. *Leukemia*. 2013;27(5):1116-1126.
155. MacLeod AS, Rudolph R, Corriden R, Ye I, Garijo O, Havran WL. Skin-resident T cells sense ultraviolet radiation-induced injury and contribute to DNA repair. *J Immunol*. 2014;192(12):5695-5702.

**How to cite this article:** Soares-da-Silva F, Elsaid R, Peixoto MM, et al. Assembling the layers of the hematopoietic system: A window of opportunity for thymopoiesis in the embryo. *Immunol Rev*. 2023;00:1-17. doi:10.1111/imr.13187

16000065x, 0, Downloaded from https://onlinelibrary.wiley.com/doi/10.1111/imr.13187 by Institut Pasteur, Wiley Online Library on [10/04/2023]. See the Terms and Conditions (https://onlinelibrary.wiley.com/terms-and-conditions) on Wiley Online Library for rules of use; OA articles are governed by the applicable Creative Commons License

# ANNEX VI

bioRxiv preprint doi: https://doi.org/10.1101/2023.08.24.554612; this version posted August 25, 2023. The copyright holder for this preprint (which was not certified by peer review) is the author/funder. All rights reserved. No reuse allowed without permission.

**Spatiotemporal dynamics of cytokines expression dictate fetal liver hematopoiesis.**

Marcia Mesquita Peixoto[1-4,*], Francisca Soares-da-Silva[1,2,5,*], Valentin Bonnet[6,7*], Gustave Ronteix[6,7*], Rita Faria Santos[3,4], Marie-Pierre Mailhe[1,2,5], Xing Feng[8], João Pedro Pereira[8], Emanuele Azzoni[9], Giorgio Anselmi[10], Marella de Bruijn[10], Charles N. Baroud[6,7#], Perpétua Pinto-do-Ó[3,4#$], Ana Cumano[1,2,5#$]

Affiliation

[1]Unit of Lymphocytes and Immunity, Immunology Department, Institut Pasteur, Paris, France

[2]INSERM U1223, Paris, France

[3]I3S – Instituto de Investigação e Inovação em Saúde & INEB – Instituto Nacional de Engenharia Biomédica, Universidade do Porto, Porto, Portugal

[4]Abel Salazar Biomedical Sciences Institute, University of Porto, Porto, Portugal

[5]Université Paris Cité, Cellule Pasteur, Paris, France

[6]Institut Pasteur, Université Paris Cité, Physical microfluidics and Bioengineering, 25-28 Rue du Dr. Roux, 75015 Paris, France

[7]Laboratoire d'Hydrodynamique, CNRS, École Polytechnique, Institut Polytechnique de Paris, 91120 Palaiseau, France

[8]Department of Immunobiology and Yale Stem Cell Center, Yale University School of Medicine, New Haven, United States.

[9]School of Medicine and Surgery, University of Milano-Bicocca, Monza, Italy

[10]MRC Weatherall Institute of Molecular Medicine, University of Oxford, UK

*equal contribution

#senior authorship

$corresponding author

Contact information: Ana Cumano, Lymphocytes and Immunity Unit – Immunology Department, 25 Rue du Dr Roux, 75015 Paris France. Email: ana.cumano@pasteur.fr

bioRxiv preprint doi: https://doi.org/10.1101/2023.08.24.554612; this version posted August 25, 2023. The copyright holder for this preprint (which was not certified by peer review) is the author/funder. All rights reserved. No reuse allowed without permission.

**Abstract**

During embryogenesis, yolk-sac and intra-embryonic-derived hematopoietic progenitors, comprising the precursors of adult hematopoietic stem cells, converge into the fetal liver. With a new staining strategy, we defined all non-hematopoietic components of the fetal liver and found that hepatoblasts are the major producers of hematopoietic growth factors. We identified mesothelial cells, a novel component of the stromal compartment, producing Kit ligand, a major hematopoietic cytokine.

A high-definition imaging dataset analyzed using a deep-learning based pipeline allowed the unambiguous identification of hematopoietic and stromal populations, and enabled determining a neighboring network composition, at the single cell resolution.

Throughout active hematopoiesis, progenitors preferentially associate with hepatoblasts, but not with stellate or endothelial cells. We found that, unlike yolk sac-derived progenitors, intra-embryonic progenitors respond to a chemokine gradient created by CXCL12-producing stellate cells. These results revealed that FL hematopoiesis is a spatiotemporal dynamic process, defined by an environment characterized by low cytokine concentrations.

bioRxiv preprint doi: https://doi.org/10.1101/2023.08.24.554612; this version posted August 25, 2023. The copyright holder for this preprint (which was not certified by peer review) is the author/funder. All rights reserved. No reuse allowed without permission.

**Introduction**

The generation of hematopoietic cells occurs in different embryonic locations at successive, overlapping, time windows[1,2]. In the mouse, multipotent erythro-myeloid progenitors (EMP)[3] are produced through an endothelial-to-hematopoietic transition (EHT) process, in the vasculature of the YS[4], between E8-8.5. These progenitors differentiate into definitive erythrocytes[5], tissue resident macrophages that can persist for life[6], neutrophils and mast cells[7,8] but are devoid of lymphoid potential[3,9]. Starting at E9, a subset of endothelial cells in the intra-embryonic (IE) vasculature (dorsal aorta, omphalo-mesenteric and vitelline arteries) undergoes EHT, spanning for around 48 hours and resulting in the emergence of the first lympho-myeloid progenitors[10–15]. Newly generated multipotent progenitors rapidly enter the circulation and home to the FL, where all hematopoietic generations converge. It is in this environment that the multipotent progenitors give rise to the hematopoietic stem cell (HSC) compartment. To acquire long-term reconstitution (LTR) capacity, IE multipotent progenitors require maturation that can occur in the dorsal aorta but primarily takes place in the FL[16–18]. Therefore, only few LTR HSC have been detected in E11.5 dorsal aorta and are only consistently found in the FL at around E12.5[11,19,20]. KIT is expressed from very early stages but other adult markers of HSC, such as Sca-1 and CD150, are only clearly detectable at E12.5 and E13.5, respectively[18]. The most substantial increase in FL reconstitution capacity occurs between E12.5-E16.5[20]. The early stages after FL colonization (E12.5-E14.5) constitute a unique environment where the HSC compartment is established.

The FL is an organ composed of hepatoblasts, of endodermal origin, that later differentiate into hepatocytes and cholangiocytes, being the latter dependent on signals from mesenchymal cells around the portal vessels, for differentiation[21,22]. Mesothelial cells that form the liver capsule derive from the septum transversum and can generate fibroblasts through epithelial-to-mesenchymal transition (EMT)[21]. Stellate cells that mature into vitamin A storing cells, can be found adjacent to mesothelial cells and lining the sinusoids[23,24]. An additional population of perivascular fibroblasts identified as $NG2^+$, are found exclusively around portal vessels[25]. After E16.5 the liver transits from a hematopoietic to a metabolic organ and hepatoblasts rapidly differentiate into hepatocytes and cholangiocytes.

Several studies identified stromal compartments involved in fetal hematopoiesis. DLK1 expressing cells (defining hepatoblasts) were reported as main producers of erythropoietin (Epo) but also of stem cell factor (also called Kit-ligand (KITL)), and CXCL12[26]. Endothelial[27,28] and stellate cells have been found to produce KITL[29] and peri-portal $NG2^+$ cells producing CXCL12 postulated as essential for HSC maintenance[25]. However, deletion of NG2 expressing peri-portal cells[25] and constitutive deletion of KITL in hepatoblasts resulted in subtle reductions, or no changes, in the HSC compartment before birth[29]. In addition, most studies of the FL stroma restricted their analysis to particular subsets, concentrated in single time-points and did not consider the early stages of hematopoiesis.

Here we optimized 2D-3D imaging to the analysis of all stromal cell populations. The high-quality images were analyzed in a pipeline based in deep learning to determine the identity of individual cells and to describe their immediate neighbors. We show that hematopoietic progenitors of YS and IE

bioRxiv preprint doi: https://doi.org/10.1101/2023.08.24.554612; this version posted August 25, 2023. The copyright holder for this preprint (which was not certified by peer review) is the author/funder. All rights reserved. No reuse allowed without permission.

have a higher frequency at the vicinity of the FL sub-mesothelial region, dominated by CXCL12-producing stellate cells and KITL-producing hepatoblasts and mesothelial cells. Later in development, mesenchymal cells (mainly perivascular) increase CXCL12 expression and CXCR4-expressing IE progenitors, but not CXCR4$^{-}$ YS-progenitors, distribute away from the sub-mesothelial region. We identified mesothelial cells as producers of KITL and stellate cells/pericytes of CXCL12. Hepatoblasts, however, are major producers of KITL, CXCL12, and the only subset that produces Epo and interleukin7 (IL-7). Through E12.5 and E14.5 hematopoietic progenitors preferentially associate with hepatoblasts, but not with stellate or endothelial cells. By E18.5 hepatic cells that now consist of a majority of hepatocytes and cholangiocytes produce decreased levels of KITL, CXCL12, Epo and IL-7. This is coincident with the onset of BM hematopoiesis. Throughout FL development cytokine and chemokine production is strikingly lower compared with BM derived stromal cells, a feature that might be determinant for FL hematopoiesis.

bioRxiv preprint doi: https://doi.org/10.1101/2023.08.24.554612; this version posted August 25, 2023. The copyright holder for this preprint (which was not certified by peer review) is the author/funder. All rights reserved. No reuse allowed without permission.

**Results**

**The non-hematopoietic compartment of the FL comprises endothelial, hepatic, mesenchymal and mesothelial cells.**

We integrated spectral flow cytometry and single-cell transcriptional profiling of isolated FL cells with an imaging pipeline capable of spatial analysis at the cellular level (Fig 1A). Using a set of defined surface markers (TableS1) we characterized the hematopoietic compartment at E12.5 (Fig1B), which predominantly consisted of erythroblasts (80% of total FL cells), a population of CD45$^-$ erythroid progenitors (P1, P2, P3) that we previously showed derive from the YS (10%)[5], and CD45$^+$ IE-derived cells (5%) (Fig1B; FigS1A). These three major components of the hematopoietic compartment can be identified in the tissue with the combination of the erythroid markers Ter119 and CD71, the pan-hematopoietic marker CD45 and the progenitor marker KIT (Fig1C). A combination of CD45 and KIT staining allows the identification of three major non-erythroid populations in the FL. These include CD45$^+$KIT$^-$ cells, referred to as CD45$^+$ cells, which comprise monocytes and granulocytes; CD45$^-$KIT$^+$ cells, referred to as KIT$^+$ progenitors, that comprise the YS-derived erythroid progenitors[5]; and CD45$^+$KIT$^+$, referred to as DP (Double Positive) progenitors, that include a majority of common myeloid progenitors (CMP), granulocyte-monocyte progenitors (GMP), some of which can be of YS origin at E12.5 (not more than 8%[30]), megakaryocyte-erythroid progenitors (MEP), as well as LSK CD48$^-$ and LSK CD48$^+$ multipotent progenitors (FigS1B-D).

We performed spectral flow cytometry analysis of the refined non-hematopoietic compartment (Ter119$^-$CD45$^-$CD117$^-$CD71$^-$) with a panel of 14 surface markers (TableS1) (FigS2A-C). We identified 10 cell types that could be classified into 4 major populations: endothelial (CD31$^+$CD146$^+$), hepatic (CD31$^-$Gp38$^-$PDGFRa$^-$E-Cadh$^+$), mesenchymal (CD31$^-$Gp38$^-$PDGFRa$^+$), and mesothelial (CD31$^-$PDGFRa$^-$Gp38$^+$) cells (Fig1D, FigS2A-C).

During the early stages of development (E12.5), E-Cadh$^+$ hepatic cells consist primarily of E-Cadh$^{hi}$EpCAM$^-$ hepatoblasts (FigS2A-C) that express high levels of *Dlk1*, *Afp*, *Alb*, *Vcam1*, *Alcam* and *Hnf4a*, as well as the progenitor marker *Lgr5* and the proliferation marker *Ki-67* (Fig1E; FigS2D, Cluster IV) and are identified in the tissue by their expression of HNF4a (Fig1F). At E18.5, E-Cadh$^{int}$ cells were classified as hepatocytes because of lower expression levels of *Dlk1*, *Afp*, *Igf2*, *Vcam1*, the absence of *Lgr5* and *Vimentin* expression (FigS2A and S2D, Cluster II) and by the expression of the mature marker *Cebpa*. Starting from E16.5, E-Cadh$^{hi}$EpCAM$^+$ biliary duct cells or cholangiocytes, which express *Sox4*, *Sox9*, and *Spp1* but not *Dlk1* (FigS2A, D, Cluster I) can be identified in the tissue exclusively close to NG2$^+$ cells, around portal vessels (FigS2G, H).

Throughout all stages analyzed, CD31$^+$ endothelial cells expressed *Cdh5*, *Tek*, *Kdr*, *Endoglin* and *Efnb2*, and intermediate levels of *Nestin* and *Lepr* (Fig1E, FigS2E). We identified an endothelial subset co-expressing Sca-1, and another, co-expressing Gp38 (Podoplanin), associated with lymphatic vessels[31] (FigS2A-C). Gp38$^+$ endothelial cells clustered separately and were characterized by expression of *Dlk1*, *Wt1*, *Alcam*, *Krt18* and *Krt19* and lower levels of *Endoglin*, *Cdh5* and *Tek* (Cluster II, FigS2E). In the tissue, endothelial cells were detected by the expression of CD146, (Fig1F-H) that also labeled the mesothelial layer, identified by Gp38 co-expression (Fig1G).

bioRxiv preprint doi: https://doi.org/10.1101/2023.08.24.554612; this version posted August 25, 2023. The copyright holder for this preprint (which was not certified by peer review) is the author/funder. All rights reserved. No reuse allowed without permission.

PDGFRa$^{+}$CD166$^{+}$NG2low/$^{-}$ fibroblasts represented an enriched population of maturing stellate cells co-expressing *Lhx2* and *Desmin* that acquire a specific autofluorescent profile as they accumulate vitamin A[24] (FigS2F, Cluster I, II). In contrast, PDGFRa$^{+}$CD166$^{-}$NG2$^{+}$ perivascular fibroblasts do not accumulate vitamin A granules, were barely detectable at E12.5 and increased in frequency as development progressed. We found that NG2$^{+}$ cells and stellate cells exhibited similar transcriptional profiles based on the expression of *Endoglin*, *Nestin*, *Pdgfrb*, and *Vcam1* and clustered together (FigS2F, Cluster I, II). However, stellate cells, that co-express PDGFRa and LHX2 or Desmin, were located in the sub-mesothelial region and lining CD146$^{+}$ endothelial cells (FigS2I) whereas NG2$^{+}$ fibroblasts were exclusively found lining portal vessels, as previously described[25] (Fig1F-G; FigS2H).

Mesothelial cells expressed *Gpm6a*, *Msln*, and *Wt1*, but stellate markers (Fig1H; FigS2F, Cluster III). A small subset of cells co-expressed PDGFRa, Gp38 and NG2, but not CD166 and co-expressed transcripts of both mesothelial and mesenchymal cells, consistent with a mesothelial origin of stellate cells[32] (FigS2F, Cluster III). In the tissue, mesothelial cells formed a single epithelial sheet followed by an irregular layer of sub-mesothelial PDGFRa$^{+}$LHX2$^{+}$ cells, that can reach a thickness of 3-5 cells at E12.5. As development progresses, the sub-mesothelial region was consistently found to be a single cell layer, due to the relocation of stellate cells to a perivascular position (FigS2I). Sub-mesothelial and the peri-vascular stellate cells were only distinguishable by position in the tissue.

Interestingly, both mesenchymal and mesothelial cells expressed the *Dlk1* transcript, which has been used as a marker for the identification and isolation of hepatoblasts[26] (Fig1H).

Overall, three markers are sufficient to identify the stromal compartment. LHX2$^{+}$ stellate cells that localize in the sub-mesothelium and around blood vessels, HNF4a$^{+}$ hepatoblasts that distribute throughout the parenchyma and CD146$^{+}$ endothelial and mesothelial cells that are distinguishable by their specific locations (Fig1F).

**YS and IE-derived progenitors accumulate at the border at E12.5 and are preferentially in contact with hepatoblasts, but not stellate or endothelial cells.**

The spatial distribution of different cell types was quantified by building a multi-step image analysis pipeline, that we named Pyxidis, to identify the phenotype and position of each cell within 2D and 3D images (Fig2, FigS3). The output of this pipeline was a graph-based representation of the cells that preserved spatial positioning and cell identity in a compact format[33], thus enabling information from many different images to be pooled together for statistical analysis. Details of the analysis are described in materials and methods.

Classification of endothelial cells using a nuclear marker was more accurate than with surface CD146, therefore we analyzed FLs from the FLK1-GFP mouse reporter line (FigS4A). To validate the cell classification, we compared the frequencies of classified cells in the tissue with the frequencies obtained by flow cytometry analysis. Cells from the hematopoietic compartment were found with similar frequencies in the two methods (FigS4B). Stromal cells, in contrast, were over-represented by a factor of 3 in the imaging analysis due to constraints in the single cell isolation procedure (FigS4C). Overall, the image analysis pipeline provided a robust method for the study of different cell types in the tissue.

bioRxiv preprint doi: https://doi.org/10.1101/2023.08.24.554612; this version posted August 25, 2023. The copyright holder for this preprint (which was not certified by peer review) is the author/funder. All rights reserved. No reuse allowed without permission.

The graph-based description of the FL provided a global view of the spatial distribution of the cell types. CD45$^+$ cells were spread in the parenchyma, while YS-derived KIT$^+$ and IE-derived DP progenitors displayed a biased distribution towards the periphery, that we further quantified (Fig3A, C, E). For that, a random distribution of cells was computed (See Methods for detailed description) and compared to the frequency of a given cell type at a certain position (% observed/random). CD45$^+$ cells had a random distribution. Conversely, KIT$^+$ and DP progenitors were found close to the capsule (Fig 3E). Mesenchymal cells accumulate in the sub-mesothelial region (within 30 µm of the border) or distributed throughout the parenchyma, lining the vasculature, as mentioned above (Fig3B, D, F). Endothelial cells were evenly distributed throughout the parenchyma (Fig3F). Interestingly, HNF4a$^+$ hepatoblasts displayed a similar distribution profile as hematopoietic progenitors with significantly higher frequencies near the sub-mesothelial region (Fig3F). In contrast, when analyzing the distribution of these populations in relation to a central region, the portal sinus (PS), we found that CD45$^+$ cells were also randomly distributed, while KIT$^+$ and DP progenitors were located further away (FigS4E). LHX2$^+$ cells lined this vessel indicating that LHX2 is also expressed around non-sinusoidal vasculature (FigS4E).

Analysis of cell-cell contacts showed that KIT$^+$ and DP progenitors exhibited a preferential contact with hepatoblasts while they were found to be significantly less in contact with stellate cells (Fig3G). Unlike previous reports, we failed to find any preferential proximity of hematopoietic progenitors with FLK1$^+$ endothelial cells at E12.5[25,29] (Fig3G). Our results identify the sub-capsular region as a privileged site for hematopoietic progenitors of YS and IE origin at E12.5, that preferentially associate with hepatoblasts.

**Supportive hematopoietic cytokines are produced by distinct stromal populations and accumulate at the mesothelial and sub-mesothelial regions.**

We analyzed cytokine expression in single cells of the four major stromal populations and found that hepatoblasts were the major cytokine producers at E12.5 (Fig4A) expressing high levels of *Cxcl12* and *Kitl*, intermediate levels of *Csf1* and were the only producers of *Epo* and *Il7*. Mesothelial and endothelial cells were also major producers of *Kitl* and expressed intermediate levels of *Csf1*. *Cxcl12* was produced at high levels by virtually all mesenchymal cells (Fig4A, FigS2, Cluster I and II). Hepatoblasts that co-expressed *Epo* and *Il7* in addition to *Cxcl12* and *Kitl*, clustered together (FigS2D, Cluster IV). They were also the most immature cells because they co-expressed *Lgr5* and *Ki67*. In contrast, *Csf1* and *Cxcl12* were co-expressed by different cells within cluster IV and in E18.5 cluster II. *Csf1* expressing mesenchymal cells were mostly represented in Cluster II, that differ from Cluster I by the expression of the stellate markers *Lhx2* and *Ngfr* (FigS2F). Interestingly, *Igf2*, a crucial embryonic growth factor, was highly expressed in all analyzed stromal populations (FigS2D-F).

To characterize the tissue distribution of the two most expressed cytokines, CXCL12 and KITL, we analyzed FL from reporter *Cxcl12*-dsRed[34] and *Kitl*-dTomato mice[35]. The cells with high levels of *Cxcl12*-dsRed co-expressed LHX2 and were predominantly located in the sub-mesothelial and perivascular regions (Fig4B, D). The expression of *Cxcl12* in the sub-mesothelial region was heterogeneous, with some regions with the accumulation of cells expressing bright *Cxcl12*-dsRed

bioRxiv preprint doi: https://doi.org/10.1101/2023.08.24.554612; this version posted August 25, 2023. The copyright holder for this preprint (which was not certified by peer review) is the author/funder. All rights reserved. No reuse allowed without permission.

(indicated by red arrowheads in Fig4B). Cells with dull expression of *Cxcl12* were found in the parenchyma, and co-expressed HNF4a (Fig4C, D). Nearly all mesenchymal cells and hepatoblasts expressed *Cxcl12* (Fig4E).

A heterogeneous pattern of *Kitl*-tdTomato expression was found in CD146$^+$ mesothelial cells (Fig4A, F-f', G-g'). *Kitl* expression was also found in HNF4a+ hepatoblasts (Fig4F) but not in endothelial and mesenchymal cells (Fig4G, H). These results indicate that distinct stromal populations can express the same cytokines expression is shared distinct stromal populations regardless of cell distribution within the tissue.

**At later stages, IE-derived but not YS-derived progenitors display a homogeneous distribution throughout the parenchyma.**

Given that the FL is a major site of hematopoiesis during development, we investigated the distribution of hematopoietic cells at subsequent developmental stages. We found that KIT$^+$ progenitors maintained their accumulation close to the capsule (Fig5A, B) at E14,5 while CD45$^+$ cells and DP progenitors changed their spatial localization. CD45$^+$ cells displayed a lower frequency within 50 μm from the capsule, while DP progenitors were evenly dispersed in the parenchyma (Fig5B). Analysis of cell-cell contacts showed that as for the earlier time-points, hematopoietic progenitors (KIT+ and DP) preferentially interacted with hepatoblasts rather than with stellate cells (Fig5C).

To investigate the mechanisms underlying the changes in spatial distribution of progenitors we analyzed the CXCL12-CXCR4 axis, involved in hematopoietic cell migration[36]. We observed strong *Cxcl12*-dsRed expression in perivascular cells at E14.5 (Fig5D). While hepatoblasts maintained similar *Cxcl12* transcript expression at all stages, mesenchymal cells expressed significantly higher levels with time (Fig5E). Whereas KIT$^+$ progenitors have no expression of *Cxcr4*, DP progenitors express low levels of the chemokine receptor at E12.5, which were further increased at E14.5 (Fig5F). In a dual-chamber migration assay, KIT$^+$ progenitors did not migrate in response to CXCL12 at either E12.5 or E14.5 whereas E12.5 DP progenitors migrate in response to CXCL12, which was more pronounced at E14.5 (Fig5G). We propose that E14.5 DP progenitors migrate from sub-capsular region into the parenchyma, between E12.5 and E14.5 in response to the redistribution of CXCL12 expressing mesenchymal cells.

At later stages of mouse development, hematopoietic cells transit from the FL to the BM, where hematopoiesis is sustained throughout adulthood. This migration to the BM starts at around E15.5-E16.5, and few progenitors are found in the FL before birth[37,38]. We observed an accumulation of CD45$^+$ cells in the major vessels and in the vicinity of sub-mesothelial cells in E18.5 FLs (FigS5A-D). At E18.5 we found clusters of both CD11b$^+$ myeloid and B220$^+$ lymphoid cells around the vessels and in sub-capsular regions (FigS5E-J). CD11b$^+$ cells were equally represented in major vessels and the sub-capsular region, while B220$^+$ cells were primarily located at the latter (FigS5K, L). These results point to the sub-mesothelial region as a supportive site for hematopoiesis also at late developmental stages.

**The fetal liver is a low-cytokine environment.**

bioRxiv preprint doi: https://doi.org/10.1101/2023.08.24.554612; this version posted August 25, 2023. The copyright holder for this preprint (which was not certified by peer review) is the author/funder. All rights reserved. No reuse allowed without permission.

To understand the cytokine expression dynamics in the FL we compared transcript expression in all stromal populations from E12.5 up to E18.5 (FigS6A, B). Mesenchymal cells were the major producers of *Cxcl12* after E12.5, with increasing levels at later stages. Conversely, *Kitl*, *Epo* and *Il7* were predominantly expressed by hepatoblasts and exhibited a decrease in expression at E18.5, with few hepatoblasts expressing *Cxcl12* and *Kitl* at this timepoint. *Thpo*, primarily expressed by hepatoblasts, was increased at later stages. We observed higher levels of the cytokines *Flt3* and *Csf1* in mesothelial and perivascular cells at E18.5, possibly supporting the accumulation of lymphoid and myeloid cells in these regions.

We compared of the highest stromal producer in the FL with BM endothelial and $CD51^{+}CD106^{+}$ cells (a mesenchymal stromal population reported to be highly enriched for hematopoietic cytokines)[39], from postnatal days 7, 14, and 21 to better understand the differences in cytokine expression (Fig6A; FigS6C). Except for *Epo*, known to be produced in the post-natal kidney, all cytokines were expressed at significantly higher levels in the BM. Moreover, we observed that $CD51^{+}CD106^{+}$ cells were the primary cytokine producers, in neonatal BM (Fig6A) where *Cxcl12*, *Kitl*, and *Il7* transcripts were more than 10 times higher than in FL. These observations indicate that the FL is a low-cytokine environment.

bioRxiv preprint doi: https://doi.org/10.1101/2023.08.24.554612; this version posted August 25, 2023. The copyright holder for this preprint (which was not certified by peer review) is the author/funder. All rights reserved. No reuse allowed without permission.

**Discussion**

We analyzed FL hematopoiesis between E12.5 and E14.5 because it corresponds to the period when HSC are found in increasing numbers[20]. Although the degree of expansion of HSC in FL is still under debate[40,41], understanding how the FL stromal compartment regulates fetal hematopoiesis is essential to understand the mechanism leading to HSC formation and to the pathogenesis of childhood hematologic disorders.

The comparative analysis of all non-hematopoietic stromal subsets at E12.5 showed the hepatoblasts as major producers of *Kitl* and *Cxcl12* and the only cells that expressed *Epo* and *Il7*. Cytokine production decreases by E18.5 consistent with previous reports[29]. *Kitl*, however, is also produced by mesothelial and endothelial cells, whereas *Cxcl12* is found in stellate cells/pericytes and NG2 peri-portal cells. This promiscuous distribution of two major hematopoietic modulators explains why inhibiting cytokine production in defined cell types had limited impact in hematopoiesis and in the HSC FL compartment. The NG2 expressing cells are found, in FL, only around large portal vessels rather than around sinusoids and they have been proposed to play important roles in fetal hematopoiesis[25]. However, NG2 expressing cells are rarely found at the early stages of active hematopoiesis (E12.5) and later (E14.5) they accumulate around the nascent portal network where cholangiocytes differentiate. NG2 is also expressed in mesothelial cells that we identify as a new element of the FL stroma, constituting the FL capsule and producing *Kitl*. Disrupting NG2 expression might, therefore, have unpredictable consequences for the integrity of the mesothelial compartment and for the organ architecture and could explain the modest decrease in HSC, previously reported[25]. Proximity to NG2+ cells was previously evaluated for 105 cells from 12 E14.5 FL (an average of 9 cells per FL that contains more than 1000 HSC), a number that may not be representative of the entire HSC compartment at that stage. Constitutive deletion of KITL in both endothelial and PDGFRa expressing cells significantly impacted HSC numbers but only postnatally[29], indicating that KITL produced by these two cell subsets did not impact the HSC compartment before birth. DLK1 expression has been considered a marker for hepatoblasts, however, we found it expressed in lymphatic endothelial cells, mesothelial and stellate cells.

At E12.5, the sub-mesothelial thick layer of stellate cells producie *Cxcl12*, but not *Kitl*. Proliferating hepatoblasts also concentrate in this area where they receive signals from mesothelial cells to expand (hepatocyte growth factor, midkine and pleiotropin)[42]. Mesothelial cells and hepatoblasts are the main producers of KITL and hematopoietic progenitors of YS and IE origin converge to this region, where they are in direct contact with hepatoblasts, but not with endothelial or stellate cells. At this stage, this FL region is also highly hypoxic which might contribute to the highest levels of Epo detected in hepatoblasts[43]. At E14.5, CXCL12-producing stellate cells have invaded the parenchyma possibly recruited by the expansion of the vascular network, and $NG2^+$ peri-vascular cells accumulate around the portal vessels. The sub-mesothelial layer of stellate cells is reduced and IE hematopoietic progenitors no longer concentrate in this region. At this stage, *Cxcl12* expression by stellate cells increased and the levels of *Cxcr4* in hematopoietic progenitors also increased with augmented response to chemokine gradients. YS-derived progenitors that comprise mostly erythroid

bioRxiv preprint doi: https://doi.org/10.1101/2023.08.24.554612; this version posted August 25, 2023. The copyright holder for this preprint (which was not certified by peer review) is the author/funder. All rights reserved. No reuse allowed without permission.

cells do not express *Cxcr4* and are still found in the sub-mesothelial region, at E14.5. Later, at E18.5, hematopoietic cytokines are no longer produced by hepatoblasts, that become rare. Cholangiocytes accumulate around portal vessels close to NG2 expressing cells and where $CD45^+$ $B220^+$ or $CD11b^+$ cells now converge. $B220^+$ and $CD11b^+$ lymphoid and myeloid cells respectively also accumulate in the sub-capsular region. Stellate cells that also surround sinusoids are likely to drive the exit of mature cells and progenitors from FL, after E15.5.

The modest impact observed on fetal hematopoiesis by deleting cytokines or chemokines in specific cell types can be due to the redundant production of these factors, as discussed above. It could, however, also indicate that HSC are largely independent from these factors before BM colonization. We found that YS-derived erythroid progenitors outcompete HSC derived progenitors, for access to low concentrations of EPO present in FL, because they have a lower threshold response to this factor[5]. Moreover, the low concentration of IL-7 in the FL allows B1 B cell selection for autoreactive specificities[44]. We show here that the FL is generally a low cytokine environment compared to BM. It is therefore possible that YS or IE-derived cells endowed with low HSC potential, previously reported[45,46], are particularly efficient in consuming the limited environmental resources available. HSC or their progenitors could complete a limited number of rounds of division in the FL, in a cytokine independent manner after migrating from in the dorsal aorta. Their higher threshold for cytokine response prevents differentiation and explains their limited contribution to fetal hematopoiesis[47]. In the present study we did not analyze HSC, so it is possible that DP cells that neighbor hepatoblasts are the progeny of multipotent cells that do not integrate the stem cell compartment. Because expansion in the FL might be limited, HSC expansion would occur preferentially in the BM shortly after colonization, as suggested[41]. In this scenario the FL HSC niche properties would have to be revised: it would be a cytokine protected environment rather than being a cytokine rich environment.

bioRxiv preprint doi: https://doi.org/10.1101/2023.08.24.554612; this version posted August 25, 2023. The copyright holder for this preprint (which was not certified by peer review) is the author/funder. All rights reserved. No reuse allowed without permission.

**References**


1. Elsaid, R. et al. Hematopoiesis: A Layered Organization Across Chordate Species. *Front Cell Dev Biol* **8**, 606642 (2020).
2. Soares-da-Silva, F. et al. Assembling the layers of the hematopoietic system: A window of opportunity for thymopoiesis in the embryo. *Immunol Rev* (2023).
3. Bertrand, J. Y. et al. Three pathways to mature macrophages in the early mouse yolk sac. *Blood* **106**, 3004-3011 (2005).
4. Frame, J. M., Fegan, K. H., Conway, S. J., McGrath, K. E. & Palis, J. Definitive Hematopoiesis in the Yolk Sac Emerges from Wnt-Responsive Hemogenic Endothelium Independently of Circulation and Arterial Identity. *Stem Cells* **34**, 431-444 (2016).
5. Soares-da-Silva, F. et al. Yolk sac, but not hematopoietic stem cell-derived progenitors, sustain erythropoiesis throughout murine embryonic life. *J Exp Med* **218**, (2021).
6. Gomez Perdiguero, E. et al. Tissue-resident macrophages originate from yolk-sac-derived erythro-myeloid progenitors. *Nature* **518**, 547-551 (2015).
7. Li, Z. et al. Adult Connective Tissue-Resident Mast Cells Originate from Late Erythro-Myeloid Progenitors. *Immunity* **49**, 640-653.e5 (2018).
8. Gentek, R. et al. Hemogenic Endothelial Fate Mapping Reveals Dual Developmental Origin of Mast Cells. *Immunity* **48**, 1160-1171.e5 (2018).
9. McGrath, K. E. et al. Distinct Sources of Hematopoietic Progenitors Emerge before HSCs and Provide Functional Blood Cells in the Mammalian Embryo. *Cell Rep* **11**, 1892-1904 (2015).
10. Cumano, A., Dieterlen-Lievre, F. & Godin, I. Lymphoid potential, probed before circulation in mouse, is restricted to caudal intraembryonic splanchnopleura. *Cell* **86**, 907-916 (1996).
11. Medvinsky, A. & Dzierzak, E. Definitive hematopoiesis is autonomously initiated by the AGM region. *Cell* **86**, 897-906 (1996).
12. de Bruijn, M. F., Speck, N. A., Peeters, M. C. & Dzierzak, E. Definitive hematopoietic stem cells first develop within the major arterial regions of the mouse embryo. *EMBO J* **19**, 2465-2474 (2000).
13. Godin, I., Garcia-Porrero, J. A., Dieterlen-Lièvre, F. & Cumano, A. Stem cell emergence and hemopoietic activity are incompatible in mouse intraembryonic sites. *J Exp Med* **190**, 43-52 (1999).
14. Yokomizo, T. & Dzierzak, E. Three-dimensional cartography of hematopoietic clusters in the vasculature of whole mouse embryos. *Development* **137**, 3651-3661 (2010).
15. Yokomizo, T., Ng, C. E., Osato, M. & Dzierzak, E. Three-dimensional imaging of whole midgestation murine embryos shows an intravascular localization for all hematopoietic clusters. *Blood* **117**, 6132-6134 (2011).
16. Taoudi, S. et al. Extensive hematopoietic stem cell generation in the AGM region via maturation of VE-cadherin+CD45+ pre-definitive HSCs. *Cell Stem Cell* **3**, 99-108 (2008).

bioRxiv preprint doi: https://doi.org/10.1101/2023.08.24.554612; this version posted August 25, 2023. The copyright holder for this preprint (which was not certified by peer review) is the author/funder. All rights reserved. No reuse allowed without permission.

17. Rybtsov, S., Ivanovs, A., Zhao, S. & Medvinsky, A. Concealed expansion of immature precursors underpins acute burst of adult HSC activity in foetal liver. *Development* **143**, 1284-1289 (2016).
18. Kieusseian, A., Brunet de la Grange, P., Burlen-Defranoux, O., Godin, I. & Cumano, A. Immature hematopoietic stem cells undergo maturation in the fetal liver. *Development* **139**, 3521-3530 (2012).
19. Müller, A. M., Medvinsky, A., Strouboulis, J., Grosveld, F. & Dzierzak, E. Development of hematopoietic stem cell activity in the mouse embryo. *Immunity* **1**, 291-301 (1994).
20. Ema, H. & Nakauchi, H. Expansion of hematopoietic stem cells in the developing liver of a mouse embryo. *Blood* **95**, 2284-2288 (2000).
21. Asahina, K. Hepatic stellate cell progenitor cells. *J Gastroenterol Hepatol* **27 Suppl 2**, 80-84 (2012).
22. Yin, C., Evason, K. J., Asahina, K. & Stainier, D. Y. Hepatic stellate cells in liver development, regeneration, and cancer. *J Clin Invest* **123**, 1902-1910 (2013).
23. Kubota, H., Yao, H. L. & Reid, L. M. Identification and characterization of vitamin A-storing cells in fetal liver: implications for functional importance of hepatic stellate cells in liver development and hematopoiesis. *Stem Cells* **25**, 2339-2349 (2007).
24. Peixoto, M. M. et al. Identification of fetal liver stroma in spectral cytometry using the parameter autofluorescence. *Cytometry A* **101**, 960-969 (2022).
25. Khan, J. A. et al. Fetal liver hematopoietic stem cell niches associate with portal vessels. *Science* **351**, 176-180 (2016).
26. Chou, S. & Lodish, H. F. Fetal liver hepatic progenitors are supportive stromal cells for hematopoietic stem cells. *Proc Natl Acad Sci U S A* **107**, 7799-7804 (2010).
27. Ding, L., Saunders, T. L., Enikolopov, G. & Morrison, S. J. Endothelial and perivascular cells maintain haematopoietic stem cells. *Nature* **481**, 457-462 (2012).
28. Azzoni, E. et al. Kit ligand has a critical role in mouse yolk sac and aorta-gonad-mesonephros hematopoiesis. *EMBO Rep* **19**, (2018).
29. Lee, Y., Leslie, J., Yang, Y. & Ding, L. Hepatic stellate and endothelial cells maintain hematopoietic stem cells in the developing liver. *J Exp Med* **218**, (2021).
30. Iturri, L. et al. Megakaryocyte production is sustained by direct differentiation from erythromyeloid progenitors in the yolk sac until midgestation. *Immunity* **54**, 1433-1446.e5 (2021).
31. Ruddle, N. H. Lymphatic vessels and tertiary lymphoid organs. *J Clin Invest* **124**, 953-959 (2014).
32. Asahina, K., Zhou, B., Pu, W. T. & Tsukamoto, H. Septum transversum-derived mesothelium gives rise to hepatic stellate cells and perivascular mesenchymal cells in developing mouse liver. *Hepatology* **53**, 983-995 (2011).
33. Ronteix, G. et al. Griottes: a generalist tool for network generation from segmented tissue images. *BMC Biol* **20**, 178 (2022).

bioRxiv preprint doi: https://doi.org/10.1101/2023.08.24.554612; this version posted August 25, 2023. The copyright holder for this preprint (which was not certified by peer review) is the author/funder. All rights reserved. No reuse allowed without permission.


34. Ding, L. & Morrison, S. J. Haematopoietic stem cells and early lymphoid progenitors occupy distinct bone marrow niches. *Nature* **495**, 231-235 (2013).
35. Buono, M. et al. A dynamic niche provides Kit ligand in a stage-specific manner to the earliest thymocyte progenitors. *Nat Cell Biol* **18**, 157-167 (2016).
36. Bleul, C. C. et al. Formation of a functional thymus initiated by a postnatal epithelial progenitor cell. *Nature* **441**, 992-996 (2006).
37. Christensen, J. L., Wright, D. E., Wagers, A. J. & Weissman, I. L. Circulation and chemotaxis of fetal hematopoietic stem cells. *PLoS Biol* **2**, E75 (2004).
38. Hall, T. D. et al. Murine fetal bone marrow does not support functional hematopoietic stem and progenitor cells until birth. *Nat Commun* **13**, 5403 (2022).
39. Baryawno, N. et al. A Cellular Taxonomy of the Bone Marrow Stroma in Homeostasis and Leukemia. *Cell* **177**, 1915-1932.e16 (2019).
40. Ganuza, M. et al. Lifelong haematopoiesis is established by hundreds of precursors throughout mammalian ontogeny. *Nat Cell Biol* **19**, 1153-1163 (2017).
41. Ganuza, M., Clements, W. & McKinney-Freeman, S. Specification of hematopoietic stem cells in mammalian embryos: a rare or frequent event. *Blood* **140**, 309-320 (2022).
42. Onitsuka, I., Tanaka, M. & Miyajima, A. Characterization and functional analyses of hepatic mesothelial cells in mouse liver development. *Gastroenterology* **138**, 1525-35, 1535.e1 (2010).
43. Imanirad, P. et al. HIF1α is a regulator of hematopoietic progenitor and stem cell development in hypoxic sites of the mouse embryo. *Stem Cell Res* **12**, 24-35 (2014).
44. Wong, J. B. et al. B-1a cells acquire their unique characteristics by bypassing the pre-BCR selection stage. *Nat Commun* **10**, 4768 (2019).
45. Beaudin, A. E. et al. A Transient Developmental Hematopoietic Stem Cell Gives Rise to Innate-like B and T Cells. *Cell Stem Cell* **19**, 768-783 (2016).
46. Dignum, T. et al. Multipotent progenitors and hematopoietic stem cells arise independently from hemogenic endothelium in the mouse embryo. *Cell Rep* **36**, 109675 (2021).
47. Yokomizo, T. et al. Independent origins of fetal liver haematopoietic stem and progenitor cells. *Nature* **609**, 779-784 (2022).

bioRxiv preprint doi: https://doi.org/10.1101/2023.08.24.554612; this version posted August 25, 2023. The copyright holder for this preprint (which was not certified by peer review) is the author/funder. All rights reserved. No reuse allowed without permission.

**Acknowledgements**

We thank A. Bandeira, P. Vieira, E. Maikranz, and P. Pereira and the members of the P. Pinto-do-Ó, C. Baroud and A. Cumano laboratories for critical discussions. We thank C. Ait-Mansour (SONY Europe B.V) for help with spectral cytometry and critical discussions. We thank D. Hardy (Institut Pasteur, Paris, France) for the FLK1-GFP reporter mice. We acknowledge the Center for Translational Science (CRT) - Cytometry and Biomarkers Unit of Technology and Service (CB UTechS) at Institut Pasteur for support in conducting this study, namely S. Novault, S. Megharba, S. Schmutz, V. Libri, and T. Stephen; and the staff of the animal facility of the Institut Pasteur for mouse care. We acknowledge the Histology Platform, Image Analysis Hub, The Cluster Team and Gpulab of Institut Pasteur for technical support. We gratefully acknowledge the UtechS Photonic BioImaging (Imagopole), C2RT, Institut Pasteur, supported by the French National Research Agency (France BioImaging; ANR-10–INSB–04; Investments for the Future). We acknowledge Investissement d'Avenir grant ANR-16-CONV-0005 for funding computing resources used for simulations. We acknowledge the support of i3S facilities: Animal Facility, Translational Cytometry Unit, HEMS (Histology and Electron Microscopy), and ALM (Advanced Light Microscopy), the latter, member of the national infrastructure PPBI-Portuguese Platform of BioImaging (supported by POCI-01-0145-FEDER-022122).

**Funding**

This work was financed by the Institut Pasteur, Institut National de la Santé et de la Recherche Médicale, Agence Nationale de la Recherche (grant Twothyme, grant EPI-DEV and grant DELSTAR), REVIVE Future Investment Program and Ligue Nationale contre le Cancer through grants to A. Cumano. The P. Pinto-do-Ó laboratory was funded by Fundo Europeu de Desenvolvimento Regional funds through the COMPETE 2020–Operational Program for Competitiveness and Internationalization, Portugal 2020, and Portuguese funds through Fundação para a Ciência e Tecnologia do Ministério da Ciência, Tecnologia e Ensino Superior in the framework of the project POCI-01-0145-FEDER-032656. M.P. was funded by FCT grant SFRH/BD/143605/2019. F.S.S. was financed by a post-doctoral grant from REVIVE (ANR-10-LABX-73). G.R. was funded by ANR grant UniBAC ANR-17-CE13-0010. These studies were funded by the NIH (RO1AI113040 awarded to JP Pereira); X Feng was funded by the NIH (T32 DK007356).

**Author contributions**

Conceptualization: F.S.S., M.M.P., P.P.O., A.C.; Methodology: F.S.S., M.M.P., V.B., G.R.; Software: M.M.P., V.B., G.R.; Resources: X.F, J.P.P., E.A., G.A., M.d.B.; Formal Analysis: F.S.S., M.M.P., V.B.; Investigation: F.S.S., M.M.P., R.F.S., M.P.M.; Writing - Original Draft: F.S.S., A.C.; Writing - Review and Editing: F.S.S., M.M.P., V.B., A.C., P.P.O., C.B.; Visualization: F.S.S., M.M.P., V.B.; Supervision: A.C., P.P.O., C.N.B.; Funding Acquisition: A.C., P.P.O., C.N.B..

**Declaration of interest**

The authors declare no competing interests.

bioRxiv preprint doi: https://doi.org/10.1101/2023.08.24.554612; this version posted August 25, 2023. The copyright holder for this preprint (which was not certified by peer review) is the author/funder. All rights reserved. No reuse allowed without permission.

**Data availability**

All raw data is available in the open repository Zenodo with the following unique identifiers: microscopy images-doi: 10.5281/zenodo.7866578; gene Expression-doi: 10.5281/zenodo.7867188; flow cytometry-doi: 10.5281/zenodo.7867212.

bioRxiv preprint doi: https://doi.org/10.1101/2023.08.24.554612; this version posted August 25, 2023. The copyright holder for this preprint (which was not certified by peer review) is the author/funder. All rights reserved. No reuse allowed without permission.

**Figure legends**

**Figure 1. The non-hematopoietic compartment of the FL comprises endothelial, hepatic, mesenchymal and mesothelial cells.**

**(A)** Schematic representation of the strategy for the analysis of the FL from E12.5 to E18.5.

**(B)** UMAP analysis of flow cytometry data of E12.5 FLs stained with the surface markers Ter119, CD45, CD71, Gr1, CD11b, KIT, Sca1, CD16/32, CD34, CD150 and CD48. See gating strategy used in Fig S1A.

**(C)** Single-stack immunohistochemistry (IHC) of E12.5 FL with the hematopoietic markers Ter119&CD71 (green), CD45 (red) and KIT (blue). Inserts c' and c'' show an enlarged 3D view (20 um) of the selected regions with the markers CD45 and KIT. Scale bar 50 um.

**(D)** UMAP analysis of flow cytometry data of $Ter119^{-}CD45^{-}CD71^{-}KIT^{-}$ cells from E12.5 FLs stained with the surface markers CD146, CD31, Gp38, PDGFRa, NG2, CD166, Sca1, E-Cadh and EpCAM that identify the four major populations highlighted by dashed circles: endothelial, hepatic, mesothelial and mesenchymal. See gating strategy used in Fig S2A.

**(E)** Violin plots of single-cell gene expression analysis of lineage associated transcripts of sorted hepatic ($CD31^{-}Gp38^{-}PDGFRa^{-}EpCAM\text{-}E\text{-}Cadh^{hi}$ cells, blue), endothelial ($CD31^{+}CD146^{+}$ cells, orange), mesenchymal ($CD31^{-}Gp38^{-}PDGFRa^{+}$ cells, pink), and mesothelial ($CD31^{-}PDGFRa^{-}Gp38^{+}$ cells, green) cells.

**(F)** Single-stack IHC of E12.5 FL with DAPI (white), LHX2 (green), the hepatic marker HNF4a (red) and CD146 (cyan). Insert f' shows an enlarged 3D view (15 um) of the selected region. Scale bar 50 um.

**(G)** Single-stack IHC of the capsular region of E12.5 FL with DAPI (white), the endothelial and mesothelial marker CD146 (green) and the mesothelial marker Gp38 (red) (left), Gp38 alone (middle), and a 3D lateral view (50 um) of both CD146 and Gp38 (right). Scale bar 50 um.

**(H)** Single-stack IHC of the border region of E12.5 FL with DAPI (white), CD146 (red), the mesenchymal markers LHX2 (green) and PDGFRa (blue) (left), and a 3D view (20 um) (right). Scale bar 50 um.

All images with cubes are 3D projections.

**Figure 2. Image analysis workflow.**

**(A)** Segmentation pipeline. FL multi-channel images are cut into small pieces using *Saucisson* (1), Individual tiles are segmented based on DAPI signal using *CellPose* (2), and then reassembled into the original shape (3). On the left, a representative single-stack IHC of E12.5 FL with DAPI (white), LHX2 (green), KIT (blue) and CD45 (red) is shown to demonstrate the pipeline. Scale bar 200 μm.

**(B)** Cell type classification pipeline. In case of nuclear staining (as for LHX2, green), cells are classified according to a threshold set on the average signal intensity inside the nuclei mask using *Griottes* (4). For membrane staining (as for CD45/red, KIT/blue), cells are classified using a *Neural Network* (5). A representative example of a small tile post-classification is presented, displaying positive cells for LHX2 (green), CD45 (red) and KIT (blue). Scale bar 5 μm (small tiles on the left), 10 μm (on the tiles on the right).

bioRxiv preprint doi: https://doi.org/10.1101/2023.08.24.554612; this version posted August 25, 2023. The copyright holder for this preprint (which was not certified by peer review) is the author/funder. All rights reserved. No reuse allowed without permission.

**(C)** Single-stack IHC of E12.5 FL (*Cxcl12*-dsRed mice) with LHX2 (green), *Cxcl12*-dsRed (red) and HNF4a (blue). Scale bar 100 μm.
**(D)** Quantification of *Cxcl12*-dsRed$^{bright+}$ and *Cxcl12*-dsRed$^{dim+}$ cells in the stromal compartment. Bar plots indicate average ± standard deviation (n=6).
**(E)** Quantification of Cxcl12-dsRed cells with distinct signal intensities in LHX2$^+$ (left) and HNF4a$^+$ (right) stromal cells. Bar plots indicate average ± standard deviation (n=6).
**(F)** Single-stack IHC of E12.5 FL (*Kitl*-tdTomato mice) with HNF4a (green), *Kitl*-tdTomato (red) and CD146 (cyan). Inserts f' show an enlarged 3D view (20 μm) of the selected regions. Scale bar 100 μm.
**(G)** IHC of E12.5 FL (*Kitl*-tdTomato mice) with PDGFRa (green), *Kitl*-tdTomato (red) and CD146 (cyan), 3D view (15 μm). Inserts g' and g'' show an enlarged 3D view or single-stack of the selected regions, respectively. Scale bar 100 μm.
**(H)** Quantification of *Kitl*-tdTomato$^+$ cells in HNF4a$^+$ cells. HNF4a$^+$ classified cells from a single-image (3D image, 16.000 total cells) were selected and Kitl-dTomato$^+$ cells manually classified (n=1).

**Figure 5. At later stages, opposite to YS-derived, IE-derived progenitors display a homogeneous distribution throughout the parenchyma in response to *Cxcl12* levels.**
**(A)** Dot plot representation of CD45$^+$ (red), KIT$^+$ (blue) and DP (purple) cell distribution of E14.5 FL representative sections (single-stack).
**(B)** Distance to the border profile of CD45$^+$ (red, n=6), KIT$^+$ (blue, n=6) and DP (purple, n=6) cells of E14.5 FLs. E12.5 data from Figure 3D is overlaid for comparison. Curves indicate average ± standard deviation. Statistical analysis was calculated at the peak of each population using the Mann-Whitney test, between E12.5 and E14.5 curves. *, P < 0.05; **, P < 0.01; ****, P < 0.0001; ns, not significant.
**(C)** Neighborhood composition of CD45$^+$, KIT$^+$ and DP cells of E14.5 FL. Graphs display the percentage of cells that are in contact with LHX2$^+$ (left, n=3) and HNF4a$^+$ (middle, n=3) stromal cells (observed) compared to random. Bar plots indicate average ± standard deviation. Statistical analysis was calculated using t-test Welch. *, P < 0.05; **, P < 0.01; ****, P < 0.0001; ns, not significant.
**(D)** Single-stack IHC of E14.5 FL (*Cxcl12*-dsRed mice) with LHX2 (green), *Cxcl12*-dsRed (red) and HNF4a (blue). Scale bar 100 μm.
**(E)** Quantitative RT-PCR analysis of the expression levels of the hematopoietic chemokine *Cxcl12* in hepatic (light gray), and mesenchymal (dark gray) cells in E12.5, E14.5 and E18.5 FL cells (n=3). Statistical analysis was calculated using two-way ANOVA, followed by Šídák's multiple comparisons test. ****, P < 0.0001; ns, not significant.
**(F)** Quantitative RT-PCR analysis of the expression levels of the CXCL12 receptor (*Cxcr4*) in KIT$^+$ (blue), and DP (purple) cells in E12.5, E14.5 FLs (n=3). Statistical analysis was calculated using two-way ANOVA, followed by Šídák's multiple comparisons test. ****, P < 0.0001.
**(G)** Transwell migration assay of DP and KIT$^+$ progenitors of E12.5 and E14.5 FL in response to the chemokine CXCL12a. Data are presented as the percentage of input progenitors that migrate to the bottom chamber (n=3). Statistical analysis was calculated using two-way ANOVA, followed by Šídák's multiple comparisons test. *, P < 0.05; **, P < 0.01.

bioRxiv preprint doi: https://doi.org/10.1101/2023.08.24.554612; this version posted August 25, 2023. The copyright holder for this preprint (which was not certified by peer review) is the author/funder. All rights reserved. No reuse allowed without permission.

**(C)** For FL network generation and spatial analysis, *Coloriage* is used to remove or highlight specific regions of the FL sections (6). *Griottes* is used to represent the cells in a dot plot and to plot the contacts between cells (7). Scale bar 10 μm.
PV – *portal sinus*.

**Figure 3. YS and IE-derived progenitors accumulate at the border at E12.5 and are preferentially in contact with hepatoblasts, but not stellate or endothelial cells.**
**(A)** IHC of 2 lobes of E12.5 FL with DAPI (white), CD45 (red) and KIT (blue), 3D view (15 μm).
**(B)** IHC of 2 lobes of E12.5 FL (FLK1-GFP mice) with DAPI (white), LHX2 (green), FLK-1 GFP (orange), and HNF4a (cyan), 3D view (10 μm).
**(C)** Dot plot representation of $CD45^+$ (red), $KIT^+$ (blue), and DP (purple) cells distribution of E12.5 FL representative sections (15 μm section projected into a single plane).
**(D)** Dot plot representation of $LHX2^+$ (green), $FLK1^+$ (orange), and $HNF4a^+$ (cyan) cells distribution of E12.5 FL representative sections (15 μm section projected into a single plane, except for the FLK1, that corresponds to a single-stack).
**(E)** Distance to the capsule profile of $CD45^+$ (red, n=10), $KIT^+$ (blue, n=10), and DP (purple, n=10) cells of E12.5 FLs. Curves indicate average ± standard deviation. Statistical analysis was calculated at the peak of each curve using the Mann-Whitney test, between observed and random curves. *, $P < 0.05$; **, $P < 0.01$; ****, $P < 0.0001$; ns, not significant.
**(F)** Distance to the capsule profile of $LHX2^+$ (green, n=6), $FLK1^+$ (orange, n=3), and $HNF4a^+$ (cyan, n=6) cells of E12.5 FLs. Curves indicate average ± standard deviation. Statistical analysis was calculated at the peak of each curve using the Mann-Whitney test, between observed and random curves. *, $P < 0.05$; **, $P < 0.01$; ****, $P < 0.0001$; ns, not significant.
**(G)** Neighborhood composition of $CD45^+$, $KIT^+$ and DP cells of E12.5 FLs. Graphs display the percentage of cells that are in contact with $HNF4a^+$ (left, n=3), $LHX2^+$ (middle, n=3) and $FLK1^+$ (right, n=2) stromal cells (observed) compared to random. Bar plots indicate average ± standard deviation. Statistical analysis was calculated using t-test Welch. *, $P < 0.05$; **, $P < 0.01$; ****, $P < 0.0001$; ns, not significant.
Images with cubes are 3D projections.

**Figure 4. Supportive hematopoietic cytokines are produced by distinct stromal populations and accumulate at the mesothelial and sub-mesothelial regions.**
**(A)** Violin plots of single-cell gene expression analysis of the cytokines *Cxcl12, Kitl, Epo, Csf1* and *Il7* in Hepatic (blue), Mesothelial (green), Mesenchymal (pink) and Endothelial (orange) cells at E12.5.
**(B)** IHC of E12.5 FL (*Cxcl12*-dsRed mice) with LHX2 (green), *Cxcl12*-dsRed (red) and CD146 (cyan), 3D view (25 μm). Red arrowheads point to a border region with bright *Cxcl12*-dsRed cells, while green arrowheads indicate a region with dim *Cxcl12*-dsRed cells. Insert b' shows an enlarged single-stack view of the selected region. Yellow arrowheads indicate cells with high expression of *Cxcl12*, that co-stain LHX2. White arrowheads indicate cells with low expression of *Cxcl12*, $LHX2^-$. Scale bar 100 μm.

bioRxiv preprint doi: https://doi.org/10.1101/2023.08.24.554612; this version posted August 25, 2023. The copyright holder for this preprint (which was not certified by peer review) is the author/funder. All rights reserved. No reuse allowed without permission.

**Figure 6. The fetal liver is a low cytokine environment.**

**(A)** Quantitative RT-PCR analysis of the expression levels of the hematopoietic cytokines *Cxcl12, Kitl, Epo, Thpo, Csf1* and *Il7* in mesenchymal (pink) or hepatic (blue) cells of E12.5, E14.5 and E18.5 FL and endothelial (dark red) or $CD51^{+}CD106^{+}$ (yellow) cells of P7, P14 and P21 BM. For each cytokine, only the FL population with highest expression levels is represented: Mesen (pink) for *Cxcl12* and *Csf1* and Hepa (blue) for *Kitl, Epo, Thpo* and *Il7* (n=3).

bioRxiv preprint doi: https://doi.org/10.1101/2023.08.24.554612; this version posted August 25, 2023. The copyright holder for this preprint (which was not certified by peer review) is the author/funder. All rights reserved. No reuse allowed without permission.

## Figure 1

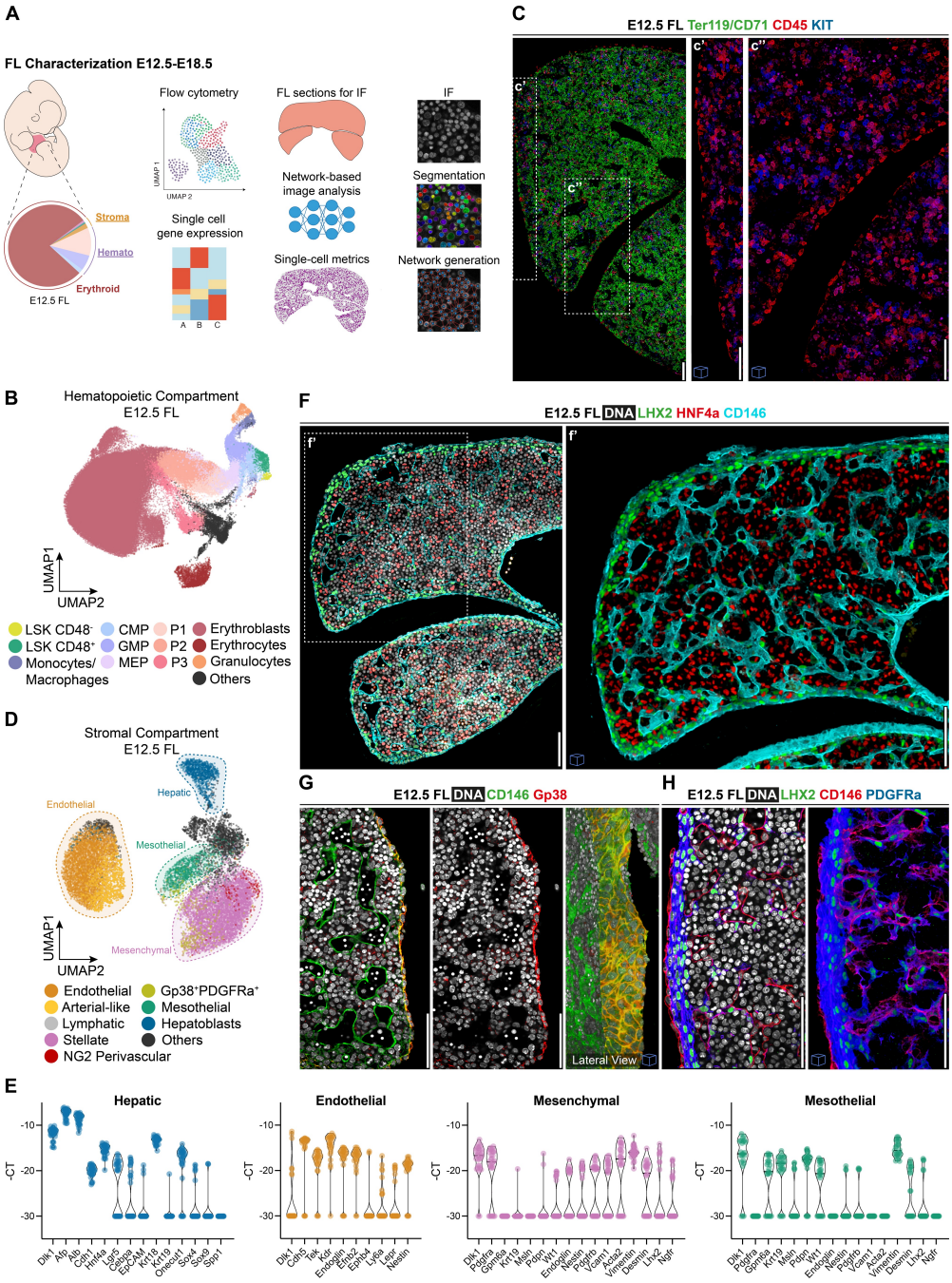

bioRxiv preprint doi: https://doi.org/10.1101/2023.08.24.554612; this version posted August 25, 2023. The copyright holder for this preprint (which was not certified by peer review) is the author/funder. All rights reserved. No reuse allowed without permission.

## Figure 2

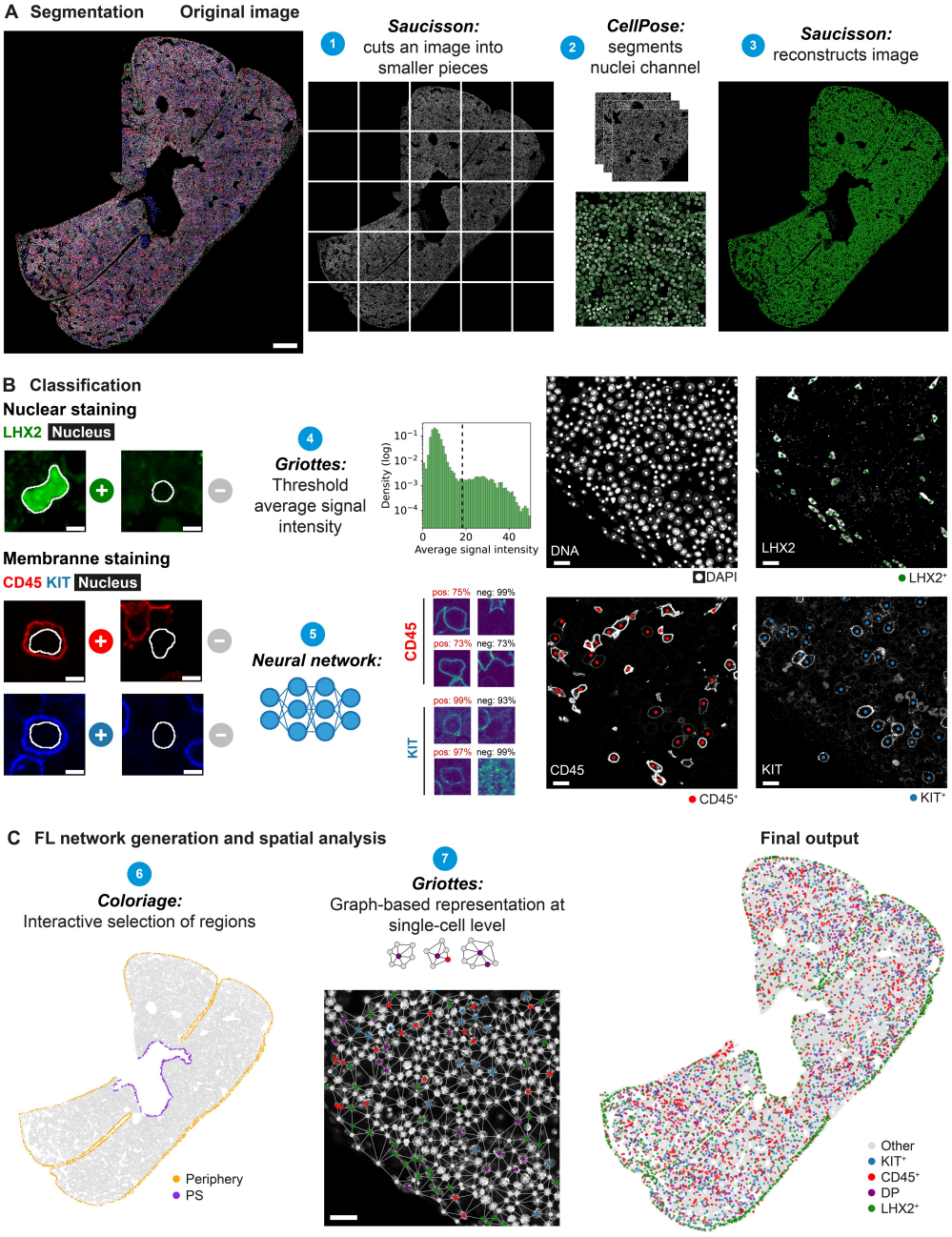

bioRxiv preprint doi: https://doi.org/10.1101/2023.08.24.554612; this version posted August 25, 2023. The copyright holder for this preprint (which was not certified by peer review) is the author/funder. All rights reserved. No reuse allowed without permission.

**Figure 3**

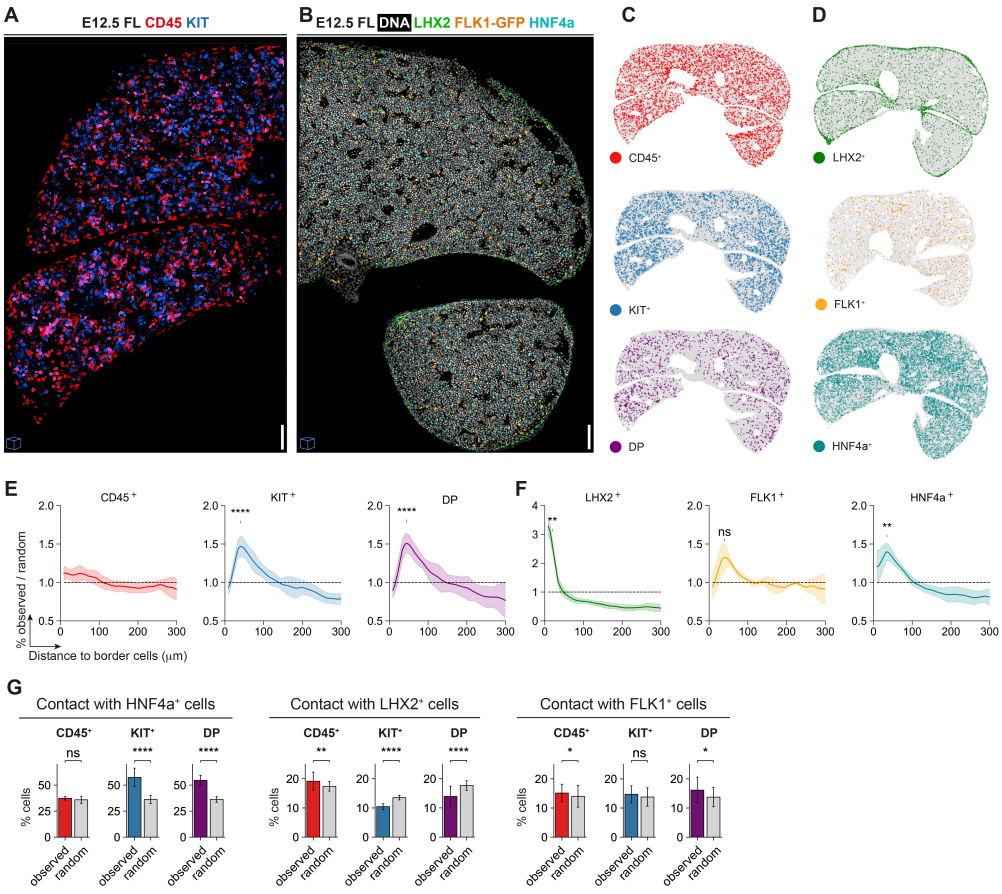

bioRxiv preprint doi: https://doi.org/10.1101/2023.08.24.554612; this version posted August 25, 2023. The copyright holder for this preprint (which was not certified by peer review) is the author/funder. All rights reserved. No reuse allowed without permission.

## Figure 5

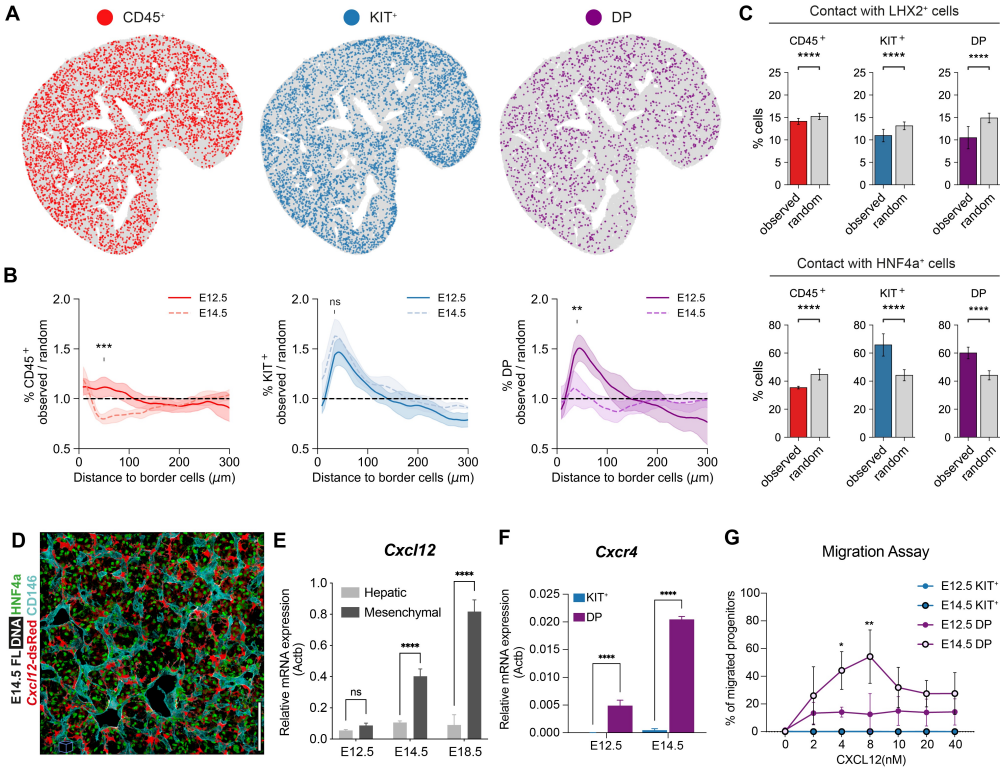

bioRxiv preprint doi: https://doi.org/10.1101/2023.08.24.554612; this version posted August 25, 2023. The copyright holder for this preprint (which was not certified by peer review) is the author/funder. All rights reserved. No reuse allowed without permission.

## Figure 6

**A**

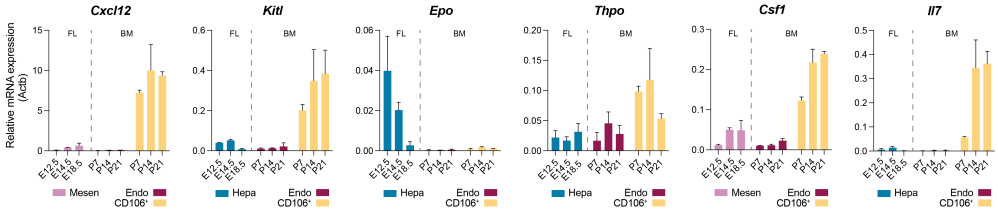

bioRxiv preprint doi: https://doi.org/10.1101/2023.08.24.554612; this version posted August 25, 2023. The copyright holder for this preprint (which was not certified by peer review) is the author/funder. All rights reserved. No reuse allowed without permission.

**Supplementary Figure legends**

**Figure S1 (related to Figure 1). Discrimination of the hematopoietic compartment.**

**(A)** Gating strategy used for the analysis of the hematopoietic compartment of E12.5 FLs using the surface markers Ter119, CD45, CD71, Gr1, CD11b, KIT, Sca1, CD16/32, CD34, CD150 and CD48. (Related to Figure 1B).

**(B)** Gating strategy and **(C)** UMAP analysis showing the cell types that are included in the image analysis with CD45 and KIT.

**(D)** Percentage of the progenitor cell types within DP cells (top) and $KIT^+$ cells (bottom) at E12 (left) or E14 (right).

**Figure S2 (related to Figure 1). Characterization of the stromal compartment.**

**(A)** Gating strategy used for the analysis of of $Ter119^-CD45^-CD71^-KIT^-$ FL cells using the surface markers CD146, CD31, Gp3, PDGFRa, NG2, CD166, Sca1, E-Cadh and EpCAM. Represented is the profile of an E18.5. The same strategy was applied to all time-points.

**(B)** UMAP analysis of flow cytometry data of $Ter119^-CD45^-CD71^-KIT^-$ cells from E14.5 (left) and E18.5 (right) FLs stained with the surface markers CD146, CD31, Gp3, PDGFRa, NG2, CD166, Sca1, E-Cadh and EpCAM.

**(C)** Distribution profile of live non-hematopoietic cells at E12.5, E14.5 and E18.5 as obtained from flow cytometry data.

**(D)** Heatmap of single-cell multiplex qPCR in sorted hepatic cells of E12.5 and E18.5 FLs. Each column represents a single cell, and it is color-coded according to time-point (E12.5, E18.5) and cell type (Hepatoblasts, Hepatocytes and Cholangiocytes). Gene expression was normalized to *β-actin* and *Gapdh*, and unsupervised hierarchical clustering was performed.

**(E)** Heatmap of single-cell multiplex qPCR in sorted endothelial cells of E12.5 and E18.5 FLs. Each column represents a single cell, and it is color-coded according to time-point (E12.5, E18.5) and cell type (Endothelial, arterial-like and lymphatic). Gene expression was normalized to *β-actin* and *Gapdh*, and unsupervised hierarchical clustering was performed.

**(F)** Heatmap of single-cell multiplex qPCR in sorted mesenchymal and mesothelial cells of E12.5 and E18.5 FLs. Each column represents a single cell, and it is color-coded according to time-point (E12.5, E18.5) and cell type (Mesothelial, $Gp38^+PDGFRa^+$, NG2 Perivascular and Stellate). Gene expression was normalized to *β-actin* and *Gapdh*, and unsupervised hierarchical clustering was performed.

**(G)** Single-stack IHC of E18.5 FL with DAPI (white) and E-Cadherin (red). Scale bar 100 μm.

**(H)** Single-stack IHC of E18.5 FL with DAPI (white), NG2 (green), aSMA (red) and EpCAM (blue). Insert h' shows an enlarged view of a portal vessel and the respective single-channels below. Scale bar 50 μm.

**(I)** 3D view (25 μm) of IHC of E16.5 with LHX2 (green), CD146 (red), and PDGFRa (blue). Scale bar 50 μm.

**Figure S3 (related to Figure 2). Validation and quality control of image analysis.**

bioRxiv preprint doi: https://doi.org/10.1101/2023.08.24.554612; this version posted August 25, 2023. The copyright holder for this preprint (which was not certified by peer review) is the author/funder. All rights reserved. No reuse allowed without permission.

**(A)** Validation of KIT classification. Representative images of single cells classification and respective classification confidence. (A') Accuracy of the classification during network training on training and validation datasets. (A'') Confusion matrix on the validation dataset.
**(B)** Validation of CD45 classification. Representative images of single cells post-classification and respective classification confidence. (B') Accuracy of the classification during network training on training and validation datasets. (B'') Confusion matrix on the validation dataset.
**(C)** Single-stack IHC of E12.5 FL with DAPI (white), LHX2 (green), CD45 (red), and KIT (blue), to highlight a region where nucleated erythrocytes (autofluorescent - AF - cells) can be seen inside a blood vessel (represented by the dashed line).
**(D)** AF cells are manually classified as positive and negative to train a neural network, so that negative cells can be later removed from the analysis. (D') Representative images of single cells classification and respective classification confidence.
**(E)** DAPI channel of the tile depicted in **(C)** overlaid with classification before (top) and after (bottom) removing AF cells.
**(F)** FL section (same as in Figure 2) before and after removing regions manually selected using *Coloriage*, and AF cells, highlighted on the left panel at orange and olive green, respectively.

**Figure S4 (related to Figure 3)**
**(A)** Dot plot representation of $LHX2^+$ (green), $HNF4a^+$ (cyan) and $FLK1^+$ (orange) cells distribution of E12.5 FL section represented in Figure 3 (10 μm thick projected into a single plane).
**(B)** Percentage of hematopoietic cells recovered and analyzed by flow cytometry (n=9) versus quantified by imaging of FL sections (n=9). Statistical analysis was calculated using two-way ANOVA, followed by Šídák's multiple comparisons test. ***, $P < 0.001$; ****, $P < 0.0001$.
**(C)** Percentage of stromal cells recovered and analyzed by flow cytometry (n=3) versus quantified by imaging of FL sections (LHX2 and HNF4a (n=6), FLK1 (n=3)). Statistical analysis was calculated using two-way ANOVA, followed by Šídák's multiple comparisons test. ***, $P < 0.001$; ****, $P < 0.0001$.
**(D)** Percentage of hematopoietic and stromal cells quantified by imaging of FL sections at E12.5 and E14.5 (E12.5: CD45, KIT, DP (n=10); LHX2, HNF4a (n=6); FLK1 (n=3); E14.5: CD45, KIT, DP (n=6); HNF4a (n=5); LHX2 (n=6); FLK1 (n=2)). Statistical analysis was calculated using two-way ANOVA, followed by Šídák's multiple comparisons test. *, $P < 0.05$.
**(E)** Distance to *portal sinus* (PS) profile of CD45+ (red, n=10), $KIT^+$ (blue, n=10), DP (purple, n=10), LHX2+ (green, n=6), HNF4a+ (cyan, n=6) and FLK1+ (orange, n=3) cells of E12.5 FL sections. Curves indicate average ± standard deviation. Statistical analysis was calculated at the peak of each population using the Mann-Whitney test, between observed and random curves. *, $P < 0.05$; **, $P < 0.01$; ****, $P < 0.0001$; ns, not significant.

**Figure S5. Myeloid and lymphoid cells accumulate in the vessels and mesothelium at late gestation.**
(**A**) Distance to vessels profile of $CD45^+$ cells of E18.5 FLs. Curves indicate average ± standard deviation (n=8).

bioRxiv preprint doi: https://doi.org/10.1101/2023.08.24.554612; this version posted August 25, 2023. The copyright holder for this preprint (which was not certified by peer review) is the author/funder. All rights reserved. No reuse allowed without permission.

(**B**) Distance to the border profile of $CD45^+$ cells of E18.5 FLs. Curves indicate average ± standard deviation (n=6).

(**C**) 3D view (20 μm) of IHC of E18.5 mesothelial region (left) or parenchyma (right) with NG2 (green), CD45 (red) and CD11b (blue). Scale bar 50 μm.

(**D**) Distance to vessels profile of $CD45^+CD11b^+$ cells of E18.5 FLs. Curves indicate average ± standard deviation (n=2).

(**E**) Example of a dot plot representation of $CD45^+CD11b^-$ (red) and $CD45^+CD11b^+$ (blue) cells around vessels (top) and in the FL border (bottom) at E18.5.

(**F**) Distance to vessels profile of $CD45^+CD11b^+$ cells of E18.5 FLs. Curves indicate average ± standard deviation (n=2).

(**G**) Distance to the border profile of $CD45^+CD11b^+$ cells of E18.5 FLs. Curves indicate average ± standard deviation (n=2).

(**H**) Example of a dot plot representation of $CD45^+B220^-$ (red) and $CD45^+B220^+$ (blue) cells around vessels (top) and in the FL border (bottom) at E18.5.

(**I**) Distance to the vessels profile of $CD45^+B220^+$ cells of E18.5 FLs. Curves indicate average ± standard deviation (n=4).

(**J**) Distance to the border profile of $CD45^+B220^+$ cells of E18.5 FLs. Curves indicate average ± standard deviation (n=3).

(**K**) $CD45^+CD11b^+$ frequency of total cells considering the entire sections analyzed ("tissue"), the regions around the vessels ('around vessels') or near the border ("near border").

(**L**) $CD45^+B220^+$ frequency of total cells considering the entire sections analyzed ("tissue"), the regions around the vessels ('around vessels') or near the border ("near border").

Regions "around the vessels" or "near border" (3-4 cell layers) were manually selected using *Coloriage*.

**Figure S6 (related to Figure 6). Cytokines expression along time.**

**(A)** Quantitative RT-PCR analysis of the expression levels of the hematopoietic cytokines *Cxcl12, Kitl, Epo, Thpo, Il7, Flt3l, Csf1, Csf2* and *Csf3* in endothelial (Endo), hepatic (Hepa), mesothelial (Meso), and mesenchymal (Mesen) cells in E12.5 (light blue), E14.5 (blue) and E18.5 (dark blue) FL cells (n=3).

**(B)** Violin plots of single-cell gene expression analysis of the cytokines *Cxcl12, Kitl, Epo, Csf1* and *Il7* in Hepatic (blue), Mesothelial (green), Mesenchymal (pink) and Endothelial (orange) cells at E18.5.

**(C)** Gating strategy used for the analysis of the stroma of P7, P14 and P21 BM using the surface markers CD51, CD31 and CD106. Representative profile of a P7 BM. The same strategy was applied to all time-points.

bioRxiv preprint doi: https://doi.org/10.1101/2023.08.24.554612; this version posted August 25, 2023. The copyright holder for this preprint (which was not certified by peer review) is the author/funder. All rights reserved. No reuse allowed without permission.

**Figure S1 (related to Figure 1)**

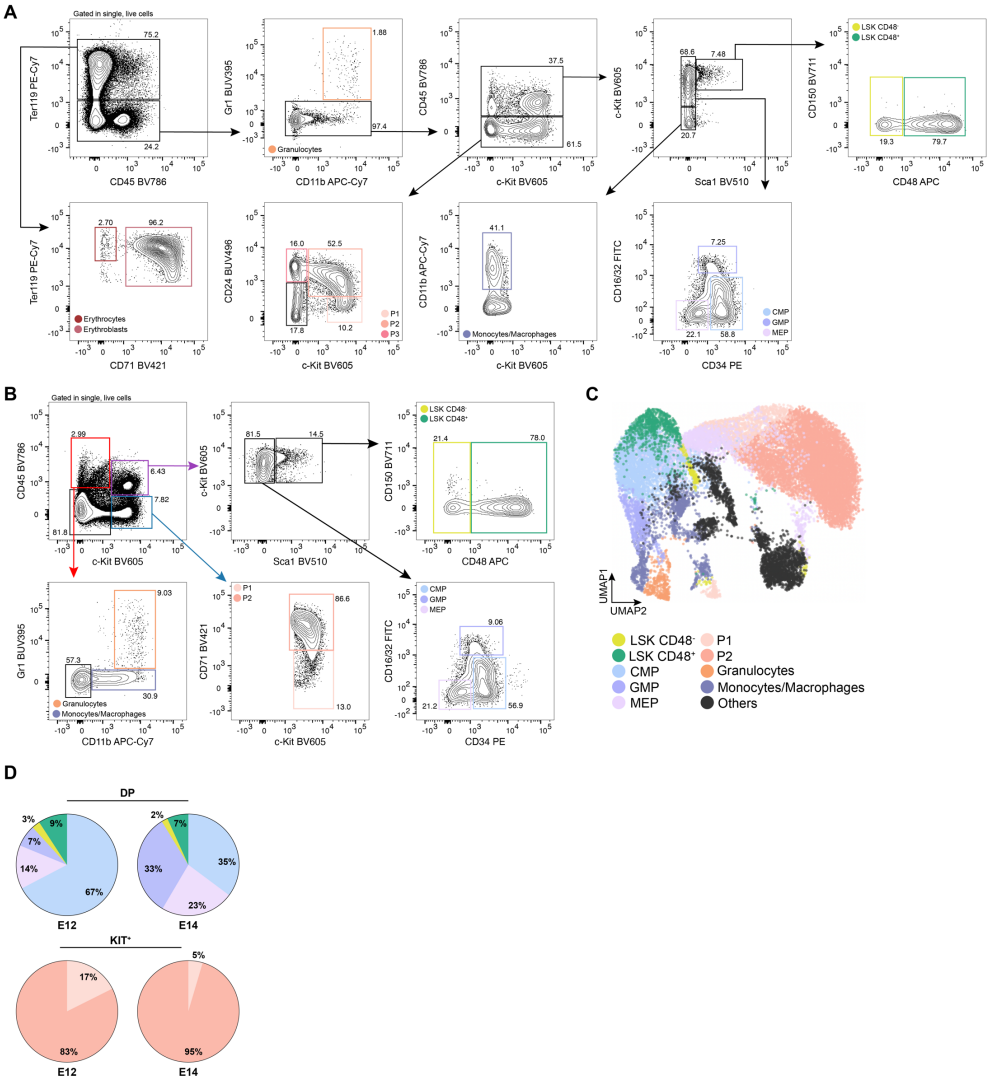

bioRxiv preprint doi: https://doi.org/10.1101/2023.08.24.554612; this version posted August 25, 2023. The copyright holder for this preprint (which was not certified by peer review) is the author/funder. All rights reserved. No reuse allowed without permission.

**Figure S2 (related to Figure 1)**

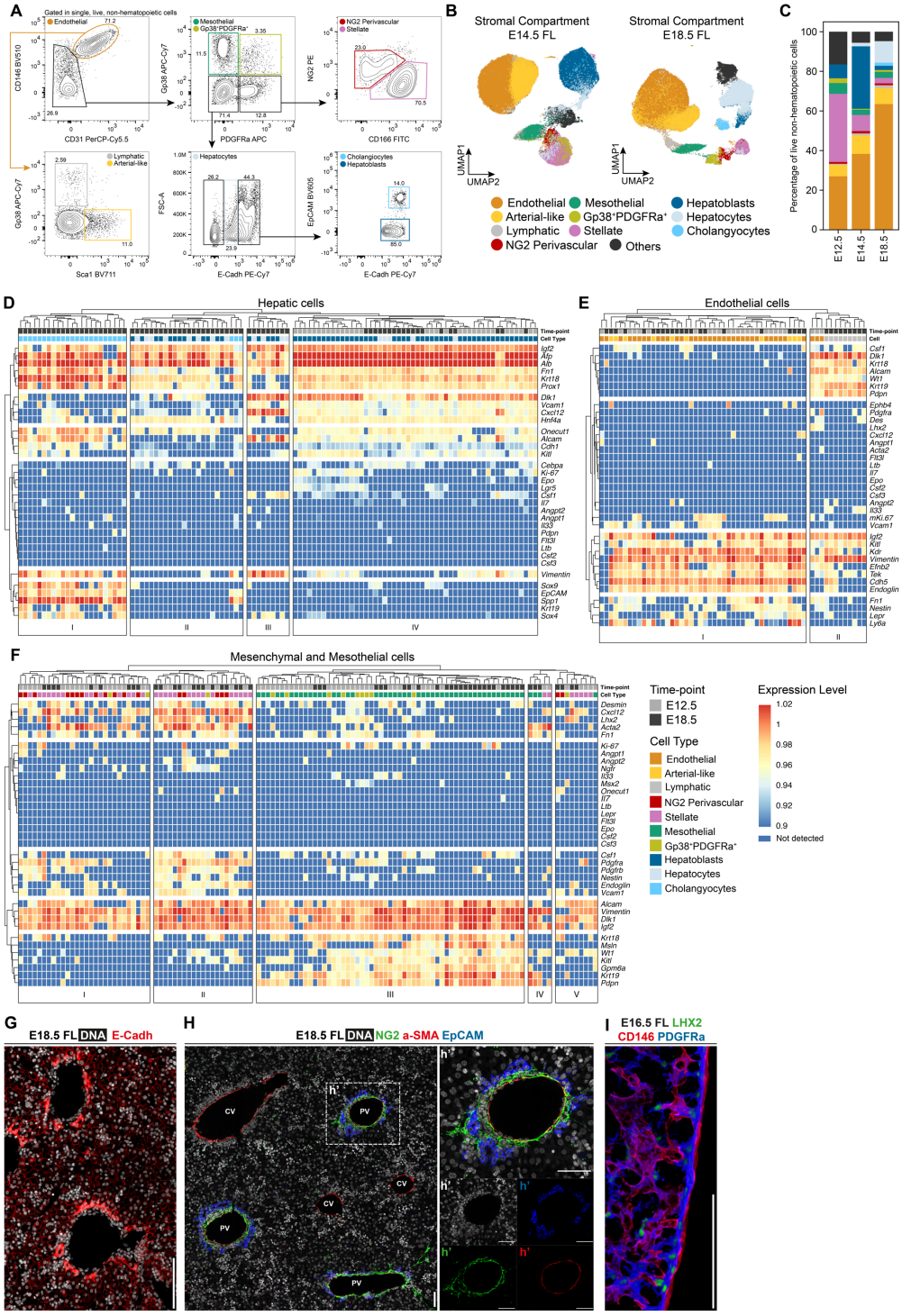

bioRxiv preprint doi: https://doi.org/10.1101/2023.08.24.554612; this version posted August 25, 2023. The copyright holder for this preprint (which was not certified by peer review) is the author/funder. All rights reserved. No reuse allowed without permission.

## Figure S3 (related to Figure 2)

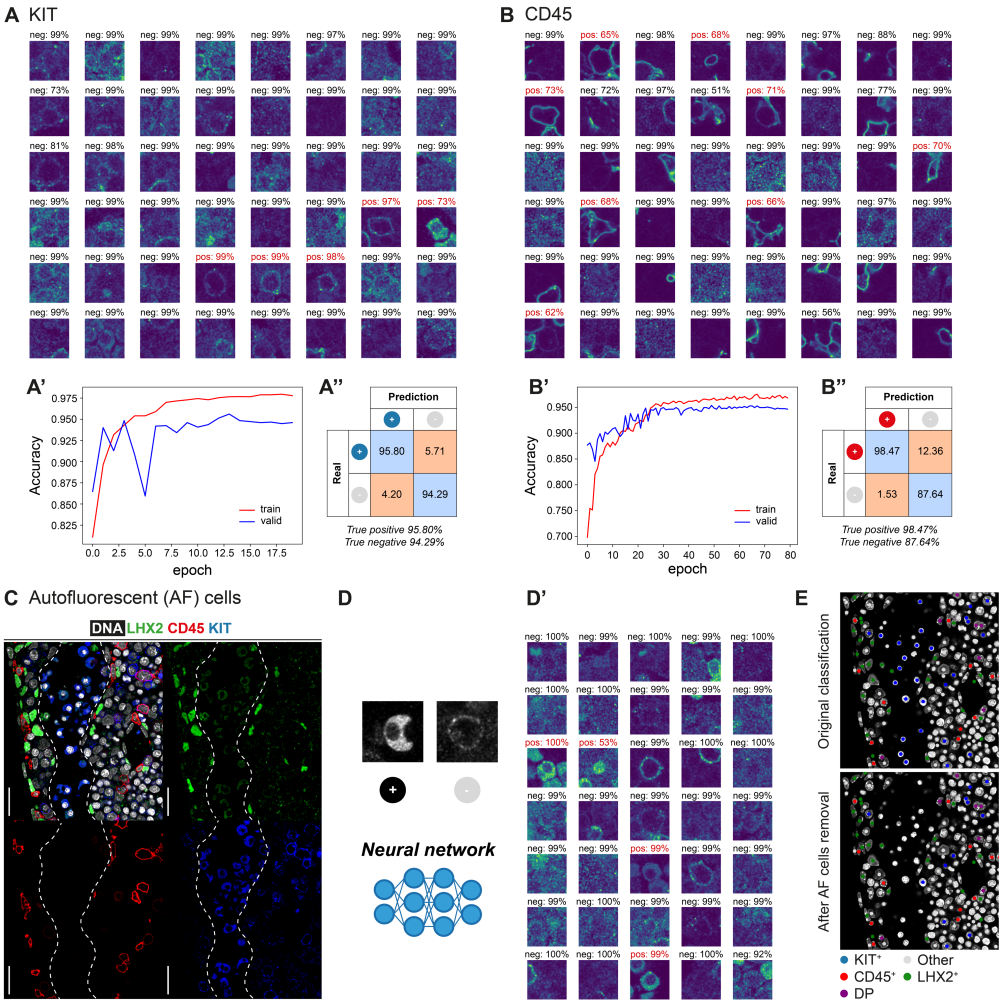

bioRxiv preprint doi: https://doi.org/10.1101/2023.08.24.554612; this version posted August 25, 2023. The copyright holder for this preprint (which was not certified by peer review) is the author/funder. All rights reserved. No reuse allowed without permission.

## Figure S4 (related to Figure 3)

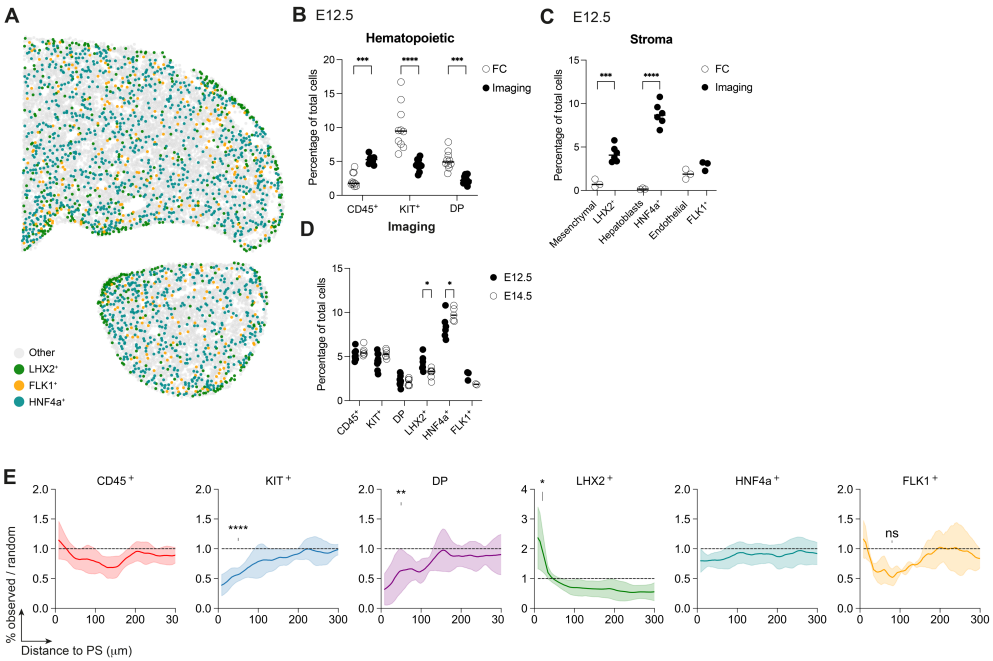

bioRxiv preprint doi: https://doi.org/10.1101/2023.08.24.554612; this version posted August 25, 2023. The copyright holder for this preprint (which was not certified by peer review) is the author/funder. All rights reserved. No reuse allowed without permission.

## Figure S5

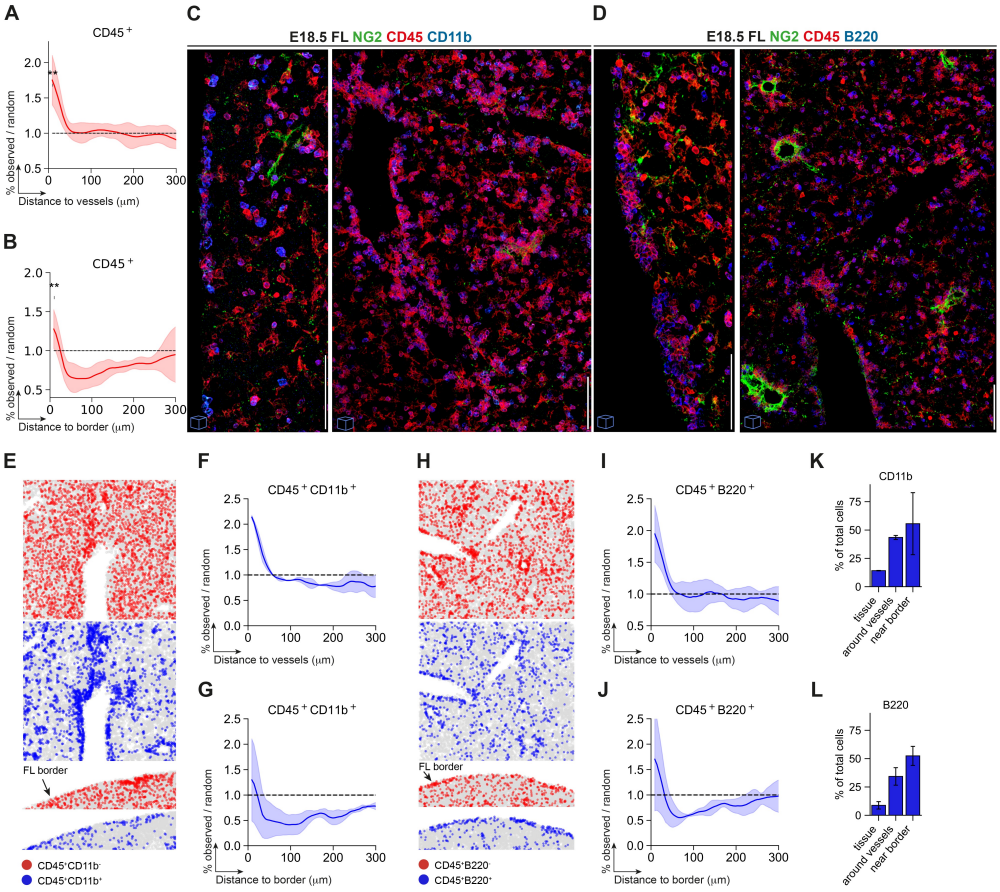

bioRxiv preprint doi: https://doi.org/10.1101/2023.08.24.554612; this version posted August 25, 2023. The copyright holder for this preprint (which was not certified by peer review) is the author/funder. All rights reserved. No reuse allowed without permission.

**Figure S6 (related to Figure 6)**

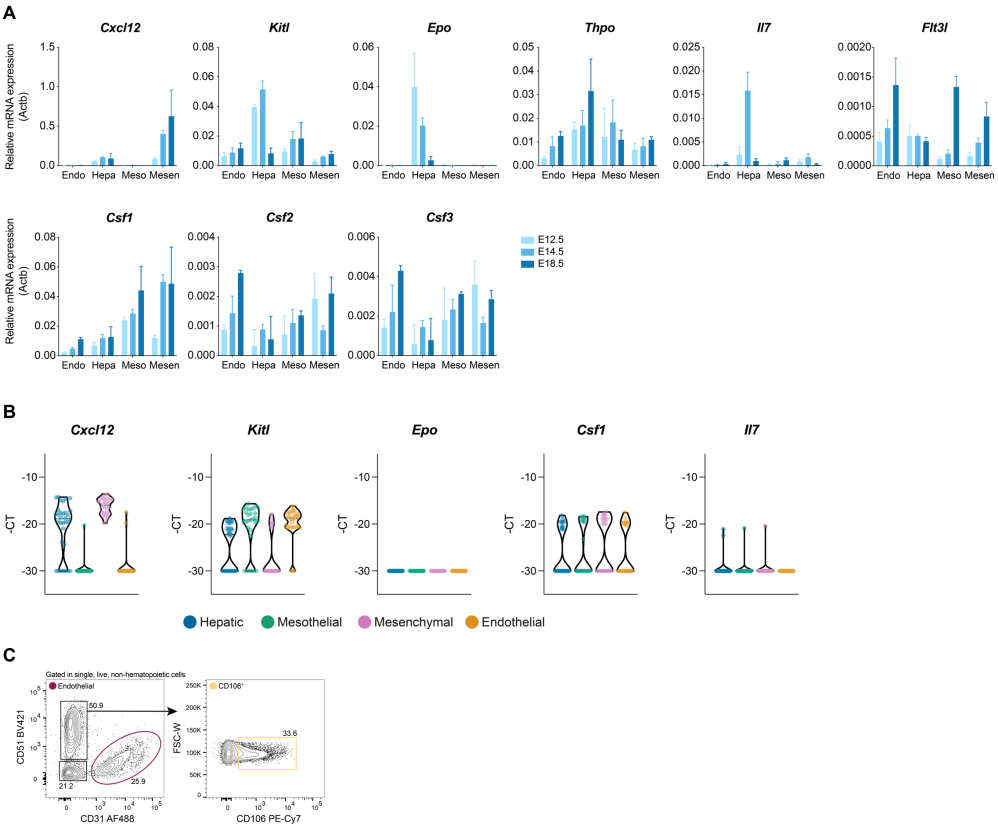

**Experimental Model and Subject Details**

**Mice**

C57BL/6J mice were purchased from Envigo. Flk1-GFP mice were a gift from David Hardy[1]. Fixed FLs from Cxcl12-dsRed[2] mice were kindly provided by João Pedro Pereira. Fixed FLs from Kitl-tdTomato[3] mice were kindly provided by Marella de Bruijn.
6 to 8-week-old mice or timed pregnant females were used. Timed pregnancies were generated after overnight mating, the following morning females with vaginal plugs were considered to be at E0.5. All animal manipulations were performed according to the ethics charter approved by the French Agriculture ministry and to the European Parliament Directive 2010/63/EU.

**Method Details**

**Cell Suspension**

For the isolation of non-hematopoietic populations, E12.5-E18.5 FLs were dissected under a binocular magnifying lens. FLs were recovered in Hanks' balanced-salt solution (HBSS) supplemented with 1% fetal calf serum (FCS) (Gibco), cut in 1 $mm^2$ pieces and incubated with 0,05 mg/ml Liberase TH (Roche) for 6-8 minutes at 37ºC. Enzymatic treatment was stopped by addition of cold HBSS+1% FCS followed by centrifugation. FLs were depleted of hematopoietic cells ($Ter119^+CD45^+Kit^+CD71^+$) using MACS columns (Miltenyi Biotec) according to manufacturer instructions. Briefly, for MACS columns depletion, cells were incubated with biotinylated Ter119, CD45, Kit and CD71 antibodies for 20-30 min at 4ºC, washed twice, incubated with anti-biotin microbeads (Miltenyi Biotec) for 20 min at 4ºC and passed through a LS column (Miltenyi Biotec). The flow-through was collected and used for cell surface staining. Before staining, cell suspensions were filtered with a 100 µm cell strainer (BD).
For the isolation of hematopoietic cells, E12.5-E14.5 FLs were dissected under a binocular magnifying lens. FLs were recovered in HBSS+1% FCS (Gibco) and passed through a 26-gauge needle of a 1-ml syringe to obtain single-cell suspensions. Before staining, cell suspensions were filtered with a 100 µm cell strainer (BD).
For the isolation of BM non-hematopoietic populations, femurs and tibias were isolated from P7, P14, and P21 mice and surrounding tissues removed. Bones were flushed using a 26-gauge needle of a 1-ml syringe with HBSS+2% FCS (Gibco). BM clumps were re-suspended by gentling aspirating with a 19-gauge needle, filtered (100 µm) and kept on ice. Bones were crushed with a scissor in a way to maximize the internal bone surface area exposition and incubated with a digestion buffer (1mg/mL Collagenase VIII and X DNase I in HBSS+2% FCS) for 15 min at 37ºC with rotation. Cell suspensions were collected, filtered (40 µm), and kept on ice. 3 rounds of digestion were performed, and cell suspensions collected from each were pooled together with the flushed ones. Enzymatic treatment was stopped by addition of cold HBSS+2% FCS followed by centrifugation. Cell suspensions were depleted of hematopoietic cells using MACS columns (Miltenyi Biotec) according to manufacturer instructions. Briefly, cells were incubated with biotinylated Ter119, CD45, CD11b and B220 antibodies for 20-30 min at 4ºC, washed twice, incubated with anti-biotin microbeads (Miltenyi Biotec) for 20 min at 4 ºC and passed through a LS column (Miltenyi Biotec). The flow-through was collected and used for cell surface staining. Before staining, cell suspensions were filtered with a 100 µm cell strainer (BD).

**Flow cytometry and cell sorting**

MACS depleted non-hematopoietic cells were stained with the antibodies listed in Table S1 for 20 min at 4ºC and analyzed on a spectral cytometer ID7000 (SONY) as described[4] or sorted with a BD FACS Aria III (BD Biosciences) according to the guidelines for the use of flow cytometry and cell sorting[5].

Hematopoietic cells were stained with the antibodies listed in Supp Table S1 for 20-30 min at 4ºC and analyzed on a custom BD LSR Fortessa (BD Biosciences). For sorting, FL were depleted of mature cells using MACS columns (Miltenyi Biotec) according to manufacturer instructions. Briefly, cells were incubated with biotinylated Ter119, Gr-1, CD19, CD3, CD4, CD8, NK1.1, CD11c antibodies (listed in Supp Table S1) for 20-30 min at 4ºC, washed, incubated with anti-biotin microbeads (Miltenyi Biotec) for 20 min at 4ºC and passed through a LS column (Miltenyi Biotec). The flow-through was collected and used for cell surface staining with the antibodies listed in Table S1, for 20-30 min at 4ºC. Stained cells were sorted with a BD FACSAria III (BD Biosciences) according to the guidelines for the use of flow cytometry and cell sorting[5]. Data were analyzed with FlowJo software (v.10.5.3, BD Biosciences).

**Flow Cytomety Analysis**

Flow cytometry files were screened for abnormalities (flow rate, signal acquisitions, and dynamic range) using a quality control plugin in FlowJo, FlowAI[6]. Only ”GoodEvents” were considered for analysis. To perform dimensionality reduction of the flow cytometry data, UMAPs were performed in FlowJo, on gated single, live, non-hematopoietic cells. For each stromal population defined, the corresponding channel values for the UMAP parameters were saved as .csv and plotted using Jupyter Notebook (University of Southampton Institutional Repository).

**Imaging**

**FL sectioning, immunostaining and optical clearing of thick sections**

FLs from timed-pregnant females were collected directly into freshly prepared 2% PFA fixative buffer (Fischer Scientific) and kept at 4°C overnight under rotation. After washing in PBS and removing surrounding tissues, FLs were immediately sectioned or shortly stored at 4ºC until sectioning. Following FLs embedding in 4% low-melting agarose (Sigma), 150 µm frontal sections were performed using a Leica VT1200S vibratome. Sections were permeabilized and blocked with PBS containing 0.05% Tween-20 (AppliChem GmbH) [or 0.5% Triton-X 100 for nuclear staining] and 10% donkey serum (Sigma-Aldrich) for 1-2 hr at RT. This solution was also used to dilute primary and secondary antibodies. Sections were incubated with primary antibodies for 2 hours at room temperature (RT) and overnight at 4ºC, and secondary antibodies for 2h at RT, both in the dark and with rotation. Between incubations and after secondary antibody incubation, sections were washed repeatedly with PBS containing 0.05% Tween-20 and 3% NaCl (minimum 4x, 15 min). Sections were counterstained with DAPI (D9542, Sigma-Aldrich) for 2 hours at RT and kept overnight in RapiClear 1.52 (SunJin Lab) for optical clearing. Sections were mounted in RapiClear and imaged on a Leica TCS SP8 using a PL APO 63x /1.40 oil immersion lens or APO 40x /1.40 oil immersion lens. Single-stacks or multi-stacks tile scans were acquired at 200Hz or 400Hz, respectively, bidirectional mode, at 12-bits and 1024×1024 resolution. Multi-stacks were acquired with z spacing of 0.3 µm. Table S2 compiles all information regarding image acquisition.

**Image Analysis**

**Image processing and segmentation**

The first step to obtain these graphs consisted of segmenting the nuclei within each image, based on their DAPI signal, using CellPose[7]. The FL images acquired in this study ranged in size from 2682x2826 to 7686x8669x117 pixels (See Table S2), which corresponded to 60Mb up to 50Gb in memory needs. As a result, some were too large for analysis on graphics processing unit (GPU)s with 8GB RAM. These images were pre-processed to reduce memory consumption by dividing them into smaller tiles using a Python module named *Saucisson* before being segmented (Fig 2A-1). Tiles of 3000x3000 pixels were used for 2D images and 600x600xZ-stacks for 3D images (See Table S2 for number of z-stacks). These tiles size allow to fit data sizes to GPUs memory and parallel computations. These separate files were then segmented in

parallel on a GPU cluster, using the Cellpose package (Fig. 2A-2). After segmentation, the masks from each of the individual tiles were stitched together again using Saucisson (Fig. 2A-3).

**Cell classification**

As a result of the image segmentation pipeline, the position of each cell is known only by the segmented domain of its nucleus. The next step is to distinguish the cell phenotype, which is obtained from the expression levels of nuclear or membrane-bound proteins to which specific fluorescent antibodies can attach.

In order to classify cells based on staining in the nucleus (such as LHX2 and HNF4a), the average signal intensity, within the mask of the nucleus, is computed using *Griottes*[8] and a threshold is applied, robustly distinguishing between positive and negative cells (Fig 2B-4). To classify cells based on membrane staining, it is necessary to analyze the fluorescence pattern around each nucleus. In this case measuring average fluorescence intensity inside or around the nucleus isn't precise enough, since neighboring positive cells can cause a local high fluorescence signal, despite little or no expression of the relevant protein by the cell itself (Fig 2B-5). Instead, the cells were classified using a deep learning based Neural Network. An individual square image was generated for each detected nucleus, with dimensions between 18 to 22µm (80x80 to 120x120 pixels) and centered around the geometric center of the nucleus (See Fig.2B and S3 for examples). The gray-scale pattern of the fluorescence inside this box was then analyzed by using *SqueezeNet* networks[9], using the transfer learning approach and loaded pre-trained from *PyTorch*[10]. Training and validation datasets were manually created (Fig 2B) for each staining, using data from different images. Training was performed using a batch size of 32. As a result, an accuracy larger than 95% was achieved on validation datasets for each membrane staining (Fig S3A-B), although some manual corrections in the classification were performed for images with lower staining contrast. A different network was trained for each marker in order to manage differences that appeared for the different membrane stainings. Manual verification of classification performances was done on 400 cells randomly selected for each membrane staining and each image. The number of false negative and positive cells is given in Table S2. The accuracy is larger than 96% for all verified set of cells.

**Removal and selection of specific regions**

In FL sections, nucleated erythrocytes are frequently found in blood vessels. Due to a very specific auto fluorescent (AF) signal, intense cytoplasmatic signal in one or more channels, they can be misclassified for membrane staining (e.g., as $CD45^+$ and/or $KIT^+$). To correct this, we used the same neural network approach, previously described, to detect these cells, and cells identified as $AF^+$ were excluded from analysis (Fig S3C-E). Some images also contain disrupted lobes and pieces of tissues coming from other organs. A specific interactive tool named *Coloriage* was created to graphically select regions in the segmented image. This tool is used to eliminate these undesired regions (Fig. 2C-6; Fig S3F).

**Network construction**

The outcome of this pipeline was to replace the pixel/voxel-scale description with a cell-scale representation of the complete image, either in 2D or in 3D. In this representation each cell was identified by its position and was characterized by its expression of the different nuclear or membrane markers (Fig. 2C). This representation was stored as a connected graph using the Griottes package[8] (Fig. 2C-7). The connectivity network of the FLs was generated using *Griottes* from a data table containing the positions and properties of the nuclei cells using the 'Delaunay' construction rule. Further information on *Griottes* can be found in[8]. This network construction allows us to estimate the connectivity between any two cells and to build the statistics of proximity between specific cell types and stromal cells (Fig 2C).

The graph-based description provides a method to extract key information from large fluorescence images, including cell phenotype and position, and condensing it into a generic format. This condensation allows the data size to be reduced from several Gb (up to 50Gb for the analyzed images) to a few Mb per image, without loss of information. Moreover, by labeling specific nodes in the graph as being at the periphery, it is possible to calculate distances of cells from this periphery from independent images and to pool the information together, which in turn enables the identification of robust and recurring spatial patterns (as demonstrated in Figs. 3 and 5).

**Calculation of the cell enrichment in different regions**

The relative enrichment or depletion of each cell type was calculated by comparing the relative abundance at any region with a random distribution of cell types. In particular, we focused on the enrichment near the periphery and the vessels in the FL. This procedure began by graphically selecting the specific structure to be studied, using *Coloriage*. The minimum Euclidean distance between each cell in the network and the cells attributed to the structure of interest was computed. Then the relative abundance of each cell type was binned as a function of distance from the structure.
In parallel the cell types were numerically shuffled on the network representation, while preserving the total frequency of the types in the tissue. The distance to the periphery was re-calculated for ten repetitions of the re-shuffling operation, thus providing a randomized position graph of the different cell types.
The ratio of the measured distribution to the randomized distribution provided a robust measure of the enrichment at different distances from the periphery and the vessels within the tissue. This allows us to distinguish relevant and statistically significant patterns that are not a consequence of random cell distribution.

**Code availability**

The analysis on the FL network images was conducted on Jupyter Notebook. All the relevant notebooks are freely accessible on the project GitHub repository (https://github.com/BaroudLab/Pyxidis). Different packages have been custom-made for the analysis of the FL images, during pre-processing and data analysis. All these functionalities (*Saucisson*, *Coloriage*) have been incorporated in the main GitHub for easier use and installation. This repository contains a step-by-step tutorial to run the entire image analysis pipeline and data analysis previously described.

**Multiplex single-cell qPCR**

Single cells were sorted directly into 96-well plates loaded with RT-STA Reaction mix (CellsDirect™ One-Step qRTPCR Kit, Invitrogen, according to the manufacturer's procedures) and 0.2x specific TaqMan® Assay mix (see Table S3 for the TaqMan® assays list) and were kept at −80°C at least overnight. For each subset analyzed, a control well with 20 cells was also sorted. Pre-amplified cDNA (20 cycles) was obtained according to the manufacturer's note and was diluted 1:5 in TE buffer for qPCR. Multiplex qPCR was performed using the microfluidics Biomark HD system for 40 cycles (Fluidigm) as previously described[11]. The same TaqMan probes were used for both RT/pre-amp and qPCR. Only single cells for which at least 2 housekeeping genes could be detected before 20 cycles were included in the analysis.

**Gene expression by RT-PCR**

Cells were sorted directly into lysis buffer and mRNA was extracted with a RNeasy Plus Micro Kit (Qiagen). After extraction, mRNA was reverse-transcribed into cDNA with PrimeScript RT Reagent Kit (Takara Bio), followed by quantitative PCR with Power SYBR Green PCR Master Mix (Applied Biosystems). Primers used can be found in Supplementary Table S4. qPCR reactions were performed on a Quantstudio3 thermocycler (Applied Biosystems), gene expression was normalized to that of b-actin and relative expression was calculated using the $2^{-\Delta Ct}$ method.

**Transwell migration assays**

FL KIT$^+$ and DP cells were prepared as for flow cytometry and cell sorting. For sorting of E14.5 cells, lineage depletion (Ter119, CD19, B220, Gr1, CD3, CD4, CD8a, NK1.1 and CD11c) was performed using magnetic LS columns (Miltenyi Biotec). Dual-chamber chemotaxis assays were performed using 24-well plates with 5-µm pore size inserts (Cat# PTMP24H48, Sigma), as previously described[12]. CXCL12a (Cat# 460-SD-050, R&D Systems) was added to the lower chamber at defined concentrations, and 100 µl of a cell suspension (1 × $10^6$ cells/ml) of KIT$^+$ or DP cells was placed in the upper chamber. Cells were allowed to migrate for 2h at 37°C. A known quantity of fluorescent beads was added to the lower chamber for normalization of migrated progenitors. Migrated cells were collected from the lower chamber and analyzed by FACS to enumerate migrated progenitors.

**Bioinformatic analysis of multiplex single-cell qPCR**

Gene expression raw data (BioMarkTM, Fluidigm) of single cells was normalized with Gapdh and Actb. Heatmaps and hierarchical clustering were generated using R packages “pheatmap” and “Rphenograph”[13].

**Quantification and Statistical Analysis**

All results are shown as mean ± standard deviation (SD). Statistical significance was determined using two-way ANOVA, followed by Šídák's multiple comparisons test where a P value of <0.05 was considered significant and a P value >0.05 was considered not significant.

References

1. Hardy, D. et al. Defective angiogenesis in CXCL12 mutant mice impairs skeletal muscle regeneration. *Skelet Muscle* **9**, 25 (2019).
2. Ding, L. & Morrison, S. J. Haematopoietic stem cells and early lymphoid progenitors occupy distinct bone marrow niches. *Nature* **495**, 231-235 (2013).
3. Buono, M. et al. A dynamic niche provides Kit ligand in a stage-specific manner to the earliest thymocyte progenitors. *Nat Cell Biol* **18**, 157-167 (2016).
4. Peixoto, M. M. et al. Identification of fetal liver stroma in spectral cytometry using the parameter autofluorescence. *Cytometry A* **101**, 960-969 (2022).
5. Cossarizza, A. et al. Guidelines for the use of flow cytometry and cell sorting in immunological studies (third edition). *Eur J Immunol* **51**, 2708-3145 (2021).
6. Monaco, G. et al. flowAI: automatic and interactive anomaly discerning tools for flow cytometry data. *Bioinformatics* **32**, 2473-2480 (2016).
7. Stringer, C., Wang, T., Michaelos, M. & Pachitariu, M. Cellpose: a generalist algorithm for cellular segmentation. *Nat Methods* **18**, 100-106 (2021).
8. Ronteix, G. et al. Griottes: a generalist tool for network generation from segmented tissue images. *BMC Biol* **20**, 178 (2022).
9. Iandola FN et al. SqueezeNet: AlexNet-level accuracy with 50x fewer parameters and <0.5MB model size. **arXiv.1602.07360**, (2016).
10. Paszke A et al. PyTorch: An Imperative Style, High-Performance Deep Learning Library. **arXiv:1912.01703**, (2019).
11. Chea, S. et al. Notch signaling in group 3 innate lymphoid cells modulates their plasticity. *Sci Signal* **9**, ra45 (2016).
12. Christensen, J. L., Wright, D. E., Wagers, A. J. & Weissman, I. L. Circulation and chemotaxis of fetal hematopoietic stem cells. *PLoS Biol* **2**, E75 (2004).
13. Levine, J. H. et al. Data-Driven Phenotypic Dissection of AML Reveals Progenitor-like Cells that Correlate with Prognosis. *Cell* **162**, 184-197 (2015).

## Supplementary Tables:

## Table S1. List of antibodies for Flow Cytometry (FC) and Immunostaining (IF).

| *PROTEIN* | *CONJUGATION* | *CLONE* | *CATALOG #* | *MANUFACTURER* | *SPECIES* | *USED FOR* | *USED FOR DETECTION OF* |
|---|---|---|---|---|---|---|---|
| a-SMA | - | 1A4 | A5228 | Sigma-Aldrich | Mouse | IHC | Smooth Muscle Cells |
| B220 | FITC | RA3-6B2 | 103205 | BioLegend | Rat | IHC | B Lineage Cells |
| CD106 | PE-Cy7 | MVCAM.A | 105720 | BioLegend | Rat | FC | Mesenchymal Cells |
| CD117 (KIT) | BV605 | 2B8 | 563146 | BD Biosciences | Rat | FC | Hematopoietic Progenitors |
| CD117 (KIT) | Biotin | 2B8 | 1129020 | SONY | Rat | FC | Lineage Depletion (Stroma) |
| CD117 (KIT) | APC | 2B8 | 105812 | BioLegend | Rat | IHC | Hematopoietic Progenitors |
| CD11b | APC-Cy7 | M1/70 | 1106130 | SONY | Rat | FC | Myeloid Lineage Cells |
| CD11b | FITC | M1/70 | 101205 | BioLegend | Rat | IHC | Myeloid Lineage Cells |
| CD11c | Biotin | N418 | 1186520 | SONY | Rat | FC | Lineage Depletion (Hemato) |
| CD140a (PDGFRa) | APC | APA5 | 1279540 | SONY | Rat | FC | Mesenchymal Cells |
| CD140a (PDGFRa) | - | Polyclonal | AF1062 | R&D Systems | Goat | IHC | Mesenchymal Cells |
| CD146 | BV510 | ME-9F1 | 740200 | BD Biosciences | Rat | FC | Endothelial, Mesothelial and Mesenchymal Cells |
| CD146 | - | Polyclonal | AF6106 | R&D Systems | Sheep | IHC | Endothelial, Mesothelial and Mesenchymal Cells |
| CD150 | BV711 | TC15-12F12.2 | 1179705 | SONY | Rat | FC | Hematopoietic Progenitors |
| CD16/32 | FITC | 93 | 1106530 | SONY | Rat | FC | Hematopoietic Progenitors |
| CD166 | FITC | eBioALC48 | 11-1661-80 | eBioscience | Rat | FC | Hepatoblasts and Mesenchymal Cells |
| CD24 | BUV496 | M1/69 | 612953 | BD Biosciences | Rat | FC | Erythroid Cells |
| CD31 | PerCP-Cy5.5 | 390 | 102420 | BioLegend | Rat | FC | Endothelial Cells |
| CD31 | AF488 | MEC13.3 | 1112570 | SONY | Rat | FC | Endothelial Cells |
| CD324 (E-Cadh) | PE-Cy7 | DECMA-1 | 1336545 | SONY | Rat | FC | Hepatic Cells |
| CD324 (E-Cadh) | - | 24E10 | 3195S | Cell Signaling Technology | Rabbit | IHC | Hepatic Cells |
| CD326 (EpCAM) | BV605 | G8.8 | 1191135 | SONY | Rat | FC | Cholangiocytes |
| CD326 (EpCAM) | AF647 | G8.8R | FAB8998R | R&D Systems | Rat | IHC | Cholangiocytes |
| CD34 | PE | RAM34 | 551387 | BD Biosciences | Rat | FC | Hematopoietic Progenitors |
| CD3e | Biotin | 145-2C11 | 1101520 | SONY | Rat | FC | Lineage Depletion (Hemato) |
| CD4 | Biotin | GK1.5 | 1102020 | SONY | Rat | FC | Lineage Depletion (Hemato) |
| CD45 | BV786 | 30-F11 | 564225 | BD Biosciences | Rat | FC | Hematopoietic Cells |
| CD45 | Biotin | 30-F11 | 1115520 | SONY | Rat | FC | Lineage Depletion (Stroma) |
| CD45 | - | Polyclonal | AF114 | R&D Systems | Goat | IHC | Hematopoietic Cells |
| CD48 | APC | HM48-1 | 1117060 | SONY | Rat | FC | Hematopoietic Progenitors |
| CD51 | BV421 | RMV-7 | 740062 | BD Biosciences | Rat | FC | Mesenchymal Cells |
| CD71 | BV421 | RI7217 | 1169065 | SONY | Rat | FC | Erythroid Cells |
| CD71 | Biotin | RI7217 | 1169015 | SONY | Rat | FC | Lineage Depletion (Stroma) |
| CD71 | Biotin | RI7217 | 113803 | BioLegend | Rat | IHC | Erythroid Cells |
| CD8a | Biotin | 53-6.7 | 1103520 | SONY | Rat | FC | Lineage Depletion (Hemato) |
| Desmin | - | Polyclonal | ab8592 | abcam | Rabbit | IHC | Stellate Cells |
| Gp38 | APC-Cy7 | 8.1.1 | 1237090 | SONY | Rat | FC | Mesothelial Cells |
| Gp38 | - | 8.1.1 | NB600-1015 | Novus Biologicals | Hamster | IHC | Mesothelial Cells |
| Gr-1 | BUV395 | RB6-8C5 | 563849 | BD Biosciences | Rat | FC | Granulocytes |
| Gr-1 | Biotin | RB6-8C5 | 553125 | BD Biosciences | Rat | FC | Lineage Depletion (Hemato) |
| HNF4a | - | K9218 | MA1-199 | Invitrogen | Mouse | IHC | Hepatic Cells |
| HNF4a | - | EPR16885-99 | ab201460 | abcam | Rabbit | IHC | Hepatic Cells |
| LHX2 | - | Polyclonal | ABE1402 | Merck Millipore | Rabbit | IHC | Stellate cells |
| NG2 | PE | 1E6.4 | 130-100-468 | Miltenyi Biotec | Rat | FC | Mesenchymal Cells |
| NG2 | - | Polyclonal | AB5320 | Merck Millipore | Rabbit | IHC | Mesenchymal Cells |
| NK1.1 | Biotin | PK136 | 1143520 | SONY | Rat | FC | Lineage Depletion (Hemato) |
| Sca1 | BV510 | D7 | 565507 | BD Biosciences | Rat | FC | Hematopoietic Progenitors and Endothelial cells |
| Sca1 | BV711 | D7 | 1140655 | SONY | Rat | FC | Hematopoietic Progenitors and Endothelial cells |
| Ter119 | PE-Cy7 | TER-119 | 1181110 | SONY | Rat | FC | Erythroid Cells |
| Ter119 | Biotin | TER-119 | 1181020 | SONY | Rat | FC | Lineage Depletion (Hemato and Stroma) |
| Ter119 | Biotin | TER-119 | 116203 | BioLegend | Rat | IHC | Erythroid Cells |
| Streptavidin | BV785 | - | 2626245 | SONY | - | FC | |
| Streptavidin | PE-Cy5 | - | 2626025 | SONY | - | FC | |
| Streptavidin | AF488 | - | 405235 | BioLegend | - | IHC | |
| Secondary Chicken anti-mouse | AF647 | - | A21463 | Invitrogen | - | IHC | |
| Secondary Donkey anti-goat | AF488 | - | A11055 | Invitrogen | - | IHC | |
| Secondary Donkey anti-goat | AF568 | - | A11057 | Invitrogen | - | IHC | |
| Secondary Donkey anti-goat | AF647 | - | A21447 | Invitrogen | - | IHC | |
| Secondary Donkey anti-mouse | AF488 | - | A21202 | Invitrogen | - | IHC | |
| Secondary Donkey anti-mouse | AF568 | - | A10037 | Invitrogen | - | IHC | |
| Secondary Donkey anti-rabbit | AF488 | - | A21206 | Invitrogen | - | IHC | |
| Secondary Donkey anti-rabbit | AF568 | - | A10042 | Invitrogen | - | IHC | |
| Secondary Donkey anti-rabbit | AF647 | - | A31573 | Invitrogen | - | IHC | |
| Secondary Donkey anti-rat | AF488 | - | A21208 | Invitrogen | - | IHC | |
| Secondary Donkey anti-rat | AF594 | - | A21209 | Invitrogen | - | IHC | |
| Secondary Donkey anti-rat | AF647 | - | A48272 | Invitrogen | - | IHC | |
| Secondary Donkey anti-sheep | AF568 | - | A21099 | Invitrogen | - | IHC | |
| Secondary Donkey anti-sheep | AF647 | - | A21488 | Invitrogen | - | IHC | |
| Secondary Rabbit anti-hamster | AF594 | - | 307-585-003 | Jackson ImmunoResearch | - | IHC | |
| Anti-GFP | - | - | A11122 | Invitrogen | Rabbit | IHC | |

## Table S2. Metadata regarding the image analysis.

| | | | FLUORESCENT CHANNELS | | | | | | | | | | | | manual verification of AVN classification on AVN patient images | | | | | | |
|---|---|---|---|---|---|---|---|---|---|---|---|---|---|---|---|---|---|---|---|---|---|
| | | | | | | | | | | | | | | | C1 | | C2 | | | C3 | |
| IMAGE | IMAGE CODE | C0 | C1 | C2 | C3 | TIME POINT | ANIMAL MODEL | DIMENSION | # STACKS | ANALYZED W/ PYXIDIS | SECTION REGION | IMAGE DIMENSIONS (Pixels) | VOXEL SIZE | FALSE POS | FALSE NEG | FALSE POS | FALSE NEG | FALSE POS | FALSE NEG |
| 210909_1 | 210909_1 | DNA | NG2 | CD45 | KIT | E12.5 | WT | 3D | 52 | | all RL | 10479x11405 | 0.2405x0.2405x0.2985 | - | - | - | - | - | - |
| 210911_3 | 210911_3 | DNA | Ter119/CD71 | CD45 | KIT | E12.5 | WT | 3D | 69 | | 2 lobes | 8577x5752 | 0.2405x0.2405x0.2985 | - | - | 8 | 4 | 7 | 1 |
| 221205_4 | 221205_4 | DNA | LHX2 | CD45 | KIT | E12.5 | WT | 2D | 1 | | all RL | 14677x14871 | 0.1804x0.1804 | - | - | 5 | 1 | 2 | 3 |
| 221205_5 | 221205_5 | DNA | LHX2 | CD45 | KIT | E12.5 | WT | 2D | 1 | | all RL | 14073x13271 | 0.1804x0.1804 | - | - | 3 | 4 | 1 | 4 |
| 221212_6 | 221212_6 | DNA | LHX2 | CD45 | KIT | E12.5 | WT | 2D | 1 | | all RL | 13913x14962 | 0.1804x0.1804 | - | - | 1 | 2 | 0 | 0 |
| 221212_1 | 221212_1 | DNA | CD45 | HNF4a | KIT | E12.5 | WT | 2D | 1 | | all RL | 14752x10998 | 0.1804x0.1804 | 1 | 3 | - | - | 0 | 1 |
| 221212_2 | 221212_2 | DNA | CD45 | HNF4a | KIT | E12.5 | WT | 2D | 1 | | all RL | 12214x16772 | 0.1804x0.1804 | 9 | 1 | - | - | 3 | 0 |
| 221212_3 | 221212_3 | DNA | CD45 | HNF4a | KIT | E12.5 | WT | 2D | 1 | | all RL | 13905x15986 | 0.1804x0.1804 | 0 | 9 | - | - | 0 | 5 |
| 230326_1 | 230326_1_1 | DNA | RLK1 | CD45 | KIT | E12.5 | RLK1-GFP | 2D | 1 | | 1 lobe | 7420x7499 | 0.2841x0.2841 | - | - | 10 | 5 | 3 | 4 |
| | 230326_1_2 | DNA | RLK1 | CD45 | KIT | E12.5 | RLK1-GFP | 2D | 1 | | 1 lobe | 2504x4232 | 0.2841x0.2841 | - | - | 25 | 4 | 5 | 8 |
| | 230326_1_3 | DNA | RLK1 | CD45 | KIT | E12.5 | RLK1-GFP | 2D | 1 | | 1 lobe | 6526x8724 | 0.2841x0.2841 | - | - | 15 | 5 | 7 | 2 |
| | 230326_1_4 | DNA | RLK1 | CD45 | KIT | E12.5 | RLK1-GFP | 2D | 1 | | all RL | 10208x10206 | 0.2841x0.2841 | - | - | 5 | 4 | 6 | 3 |
| 230326_3 | 230326_3 | DNA | RLK1 | CD45 | KIT | E12.5 | RLK1-GFP | 2D | 1 | | 3 lobes | 6603x8404 | 0.2841x0.2841 | - | - | 19 | 3 | 4 | 4 |
| 221020_7 | 221021_7_63x | DNA | LHX2 | - | HNF4a | E12.5 | WT | 2D | 1 | | all RL | 11485x12526 | 0.2405x0.2405 | - | - | - | - | - | - |
| | 221020_7_40x | DNA | LHX2 | - | HNF4a | E12.5 | WT | 3D | 117 | | all RL | 11422x8616 | 0.3788x0.3788x0.3467 | - | - | - | - | - | - |
| 221020_9 | 221020_9_63x | DNA | LHX2 | - | HNF4a | E12.5 | WT | 2D | 117 | | all RL | 7686x8669 | 0.2405x0.2405 | - | - | - | - | - | - |
| | 221020_9_40x | DNA | LHX2 | - | HNF4a | E12.5 | WT | 3D | 117 | | all RL | 7686x8669 | 0.3788x0.3788x0.3467 | - | - | - | - | - | - |
| 230226_5 | 220326_5_1 | DNA | RLK1 | LHX2 | HNF4a | E12.5 | RLK1-GFP | 3D | 1 | | 2 lobes | 4705x6543 | 0.2841x0.2841x0.35 | - | - | - | - | - | - |
| | 220326_5_2 | DNA | RLK1 | LHX2 | HNF4a | E12.5 | RLK1-GFP | 2D | 1 | | 2 lobes | 5764x4736 | 0.2841x0.2841 | - | - | - | - | - | - |
| 220518_8_1 | 220518_8_1 | DNA | HNF4a | Kit-tdTomato | CD146 | E12.5 | Kit-tdTomato | 2D | 1 | | all RL | 6574x8383 | 0.2841x0.2841 | - | - | - | - | - | - |
| 220323_3 | 220323_3 | DNA | LHX2 | Cxcl12-dsRed | CD146 | E12.5 | Cxcl12-dsRed | 3D | 88 | | part of 1 lobe | 11223x93945 | 0.1202x0.1202 | - | - | - | - | - | - |
| 220323_3_1 | 220323_3_1 | DNA | LHX2 | Cxcl12-dsRed | - | E12.5 | Cxcl12-dsRed | 3D | 52 | YES | part of 2 lobes | 5760x9252 | 0.2841x0.2841 | - | - | - | - | - | - |
| 220325_4 | 220325_4 | DNA | LHX2 | Cxcl12-dsRed | HNF4a | E12.5 | Cxcl12-dsRed | 3D | 70 | | part of 1 lobe | 2913x2915 | 0.2841x0.2841 | - | - | - | - | - | - |
| 220123_1 | 220123_1 | DNA | LHX2 | Cxcl12-dsRed | - | E14.5 | Cxcl12-dsRed | 2D | 1 | | part of 1 lobe | 1943x1943 | 0.2841x0.2841 | - | - | - | - | - | - |
| 220125_2 | 220125_2 | DNA | LHX2 | Cxcl12-dsRed | - | E14.5 | Cxcl12-dsRed | 2D | 1 | | all RL | 14924x12135 | 0.2841x0.2841 | - | - | - | - | - | - |
| 220123_3_2 | 220123_3_2 | DNA | HNF4a | Cxcl12-dsRed | CD146 | E14.5 | Cxcl12-dsRed | 3D | 86 | | all RL | 14156x10362 | 0.2841x0.2841 | - | - | - | - | - | - |
| 230124_1 | 230124_1_1 | DNA | CD45 | HNF4a | KIT | E14.5 | WT | 2D | 1 | | 2 lobes | 1951x1931 | 0.2841x0.2841 | - | - | - | - | - | - |
| | 230124_1_2 | DNA | CD45 | HNF4a | KIT | E14.5 | WT | 2D | 1 | | piece | 2882x2826 | 0.1804x0.1804 | 8 | 12 | - | - | 6 | 3 |
| | 230124_1_3 | DNA | CD45 | HNF4a | KIT | E14.5 | WT | 2D | 1 | | piece | 5597x6524 | 0.1804x0.1804 | 6 | 5 | - | - | 4 | 3 |
| | 230124_1_4 | DNA | CD45 | HNF4a | KIT | E14.5 | WT | 2D | 1 | | piece | 5632x8380 | 0.1804x0.1804 | 8 | 6 | - | - | 6 | 0 |
| | 230124_1_5 | DNA | CD45 | HNF4a | KIT | E14.5 | WT | 2D | 1 | | piece | 4474x10248 | 0.1804x0.1804 | 11 | 6 | - | - | 5 | 1 |
| 230213_5 | 230213_5 | DNA | CD45 | HNF4a | KIT | E14.5 | WT | 2D | 1 | | piece | 8342x7487 | 0.1804x0.1804 | 10 | 4 | - | - | 4 | 1 |
| 230213_6 | 230213_6 | DNA | CD45 | HNF4a | KIT | E14.5 | WT | 2D | 1 | | all RL | 17426x18518 | 0.1804x0.1804 | 7 | 8 | - | - | 5 | 9 |
| 230213_9 | 230213_9 | DNA | CD45 | LHX2 | KIT | E14.5 | WT | 2D | 1 | | all RL | 19331x19278 | 0.1804x0.1804 | 4 | 5 | - | - | 3 | 6 |
| 230215_7 | 230215_7 | DNA | CD45 | LHX2 | KIT | E14.5 | WT | 2D | 1 | | all RL | 20171x20328 | 0.1804x0.1804 | 4 | 13 | - | - | 4 | 4 |
| 230215_8 | 230215_8 | DNA | CD45 | LHX2 | KIT | E14.5 | WT | 2D | 1 | | all RL | 19281x19418 | 0.1804x0.1804 | 6 | 8 | - | - | 3 | 6 |
| 221110_4 | 221110_4 | DNA | RLK1 | LHX2 | HNF4a | E14.5 | RLK1-GFP | 3D | 117 | | all RL | 23863x22160 | 0.1804x0.1804 | 5 | 6 | - | - | 5 | 11 |
| 221117_1 | 221117_1 | DNA | RLK1 | - | HNF4a | E14.5 | RLK1-GFP | 3D | 89 | | 2 lobes | 4859x2961 | 0.3788x0.3788x0.3467 | - | - | - | - | - | - |
| 210527_11 | 210527_11 | DNA | - | CD45 | - | E18.5 | WT | 3D | 67 | | 2 lobes | 2857x2856 | 0.3788x0.3788x0.3467 | - | - | - | - | - | - |
| 210528_11 | 210528_11 | DNA | - | CD45 | - | E18.5 | WT | 3D | 84 | | piece | 4919x5847 | 0.2393x0.2393x0.2985 | - | - | 0 | 4 | - | - |
| 210626_3 | 210626_3 | DNA | B220 | CD45 | - | E18.5 | WT | 3D | 69 | | piece | 3965x7770 | 0.2393x0.2393x0.2985 | - | - | 4 | 5 | - | - |
| 210629_3 | 210629_3 | DNA | B220 | CD45 | NG2 | E18.5 | WT | 3D | 68 | | piece | 4911x8779 | 0.2393x0.2393x0.2985 | 4 | 0 | 4 | 5 | - | - |
| 210825_2 | 210825_2 | DNA | B220 | CD45 | - | E18.5 | WT | 3D | 68 | | piece | 5879x5224 | 0.2393x0.2393x0.2985 | 5 | 4 | 5 | 8 | - | - |
| 210827_2 | 210827_2 | DNA | B220 | CD45 | - | E18.5 | WT | 3D | 68 | | piece | 4782x4741 | 0.2393x0.2393x0.2985 | 0 | 4 | 3 | 9 | - | - |
| 210630_5 | 210630_5 | DNA | NG2 | CD45 | CD11b | E18.5 | WT | 3D | 68 | | piece | 6511x5599 | 0.2393x0.2393x0.2985 | 2 | 3 | 1 | 2 | - | - |
| 210630_5_1 | 210630_5_1 | DNA | - | CD45 | CD11b | E18.5 | WT | 2D | 1 | | piece | 5866x7775 | 0.2393x0.2393x0.2985 | - | - | 0 | 7 | 6 | 0 |
| 211216_3 | - | DNA | LHX2 | CD146 | HNF4a | E12.5 | WT | 3D | 69 | | piece | 3952x10620 | 0.2405x0.2405x1 | - | - | 7 | 10 | 22 | 0 |
| 210704_6 | - | DNA | Gp38 | CD146 | - | E12.5 | WT | 3D | 174 | | | | | | | | | | |
| 211217_2 | - | DNA | LHX2 | CD146 | PDGFRa | E12.5 | WT | 3D | 71 | | | | | | | | | | |
| 220518_8_2 | - | DNA | HNF4a | Kit-tdTomato | CD146 | E12.5 | Kit-tdTomato | 3D | 68 | NO | | | | | | | | | |
| 220520_9 | - | DNA | PDGFRa | Kit-tdTomato | CD146 | E12.5 | Kit-tdTomato | 3D | 50 | | | | | | | | | | |
| 200821 | - | DNA | CD31 | E-Cadh | - | E18.5 | WT | 2D | 1 | | | | | | | | | | |
| 210827_5 | - | DNA | NG2 | aSMA | EpCAM | E18.5 | WT | 3D | 18 | | | | | | | | | | |
| 211217_2 | - | DNA | LHX2 | CD146 | PDGFRa | E16.5 | WT | 3D | 85 | | | | | | | | | | |

| IMAGE | Images used for each pannel | | | | | | | | | | | | | | | | | | | | | | | | | | | | | | | | | |
|---|---|---|---|---|---|---|---|---|---|---|---|---|---|---|---|---|---|---|---|---|---|---|---|---|---|---|---|---|---|---|---|---|---|---|
| | *Fig1C* | *Fig1F* | *Fig1G* | *Fig1H* | *Fig3A* | *Fig3B* | *Fig3E* | *Fig3F* | *Fig3G* | *Fig4B* | *Fig4C* | *Fig4D* | *Fig4E* | *Fig4F* | *Fig4F_f'* | *Fig4G* | *Fig4H* | *Fig5B* | *Fig5C* | *Fig5D* | *FigS1G* | *FigS1H* | *FigS1I* | *FigS4A* | *FigS4C* | *FigS4D* | *FigS4E* | *FigS4F* | *FigS5A* | *FigS5B* | *FigS5C* | *FigS5D* | *FigS5F/G/K* | *FigS5I/J/L* |
| 210909_1 | | | | | ✓ | | ✓ | | | | | | | | | | | ✓ | | | | | | | ✓ | | ✓ | ✓ | | | | | | |
| 210911_3 | ✓ | | | | | | ✓ | | | | | | | | | | | ✓ | | | | | | | ✓ | | ✓ | ✓ | | | | | | |
| 221205_4 | | | | | | | ✓ | ✓ | ✓ | | | | | | | | | ✓ | | | | | | | ✓ | ✓ | ✓ | ✓ | | | | | | |
| 221205_5 | | | | | | | ✓ | ✓ | ✓ | | | | | | | | | ✓ | | | | | | | ✓ | ✓ | ✓ | ✓ | | | | | | |
| 221212_6 | | | | ✓ | | | ✓ | ✓ | ✓ | | | | | | | | | ✓ | | | | | | | ✓ | ✓ | ✓ | ✓ | | | | | | |
| 221212_1 | | | | | | | ✓ | ✓ | ✓ | | | | | | | | | ✓ | | | | | | | ✓ | ✓ | ✓ | ✓ | | | | | | |
| 221212_2 | | | | | | | ✓ | ✓ | ✓ | | | | | | | | | ✓ | | | | | | | ✓ | ✓ | ✓ | ✓ | | | | | | |
| 221212_3 | | | | | | | ✓ | ✓ | ✓ | | | | | | | | | ✓ | | | | | | | ✓ | ✓ | ✓ | ✓ | | | | | | |
| 230326_1 | | | | | | | ✓ | ✓ | ✓ | | | | | | | | | ✓ | | | | | | | ✓ | ✓ | ✓ | ✓ | | | | | | |
| 230326_3 | | | | | | | ✓ | ✓ | ✓ | | | | | | | | | ✓ | | | | | | | | ✓ | ✓ | | | | | | | |
| 221020_7 | | | | | | | | | | | | | | | | | | | | | | | | ✓ | | | | | | | | | | |
| | | | | | | | | ✓ | | | | | | | | | | | | | | | | ✓ | | ✓ | ✓ | ✓ | | | | | | |
| 221020_9 | | | | | | | | | | | | | | | | | | | | | | | | ✓ | | | | | | | | | | |
| | | | | | | | | ✓ | | | | | | | | | | | | | | | | ✓ | | ✓ | ✓ | ✓ | | | | | | |
| 230226_5 | | | | | | ✓ | | | | | | | | | | | | | | | | | | ✓ | | | | | | | | | | |
| | | | | | | | | ✓ | | | | | | | | | | | | | | | | ✓ | | ✓ | ✓ | ✓ | | | | | | |
| 220518_8_1 | | | | | | | | | | | | | | ✓ | | | ✓ | | | | | | | | | | | | | | | | | |
| 220323_3 | | | | | | | | | | ✓ | | ✓ | ✓ | | | | | | | | | | | | | | | | | | | | | |
| 220323_3_1 | | | | | | | | | | | | ✓ | ✓ | | | | | | | | | | | | | | | | | | | | | |
| 220325_4 | | | | | | | | | | | ✓ | ✓ | ✓ | | | | | | | | | | | | | | | | | | | | | |
| 220123_1 | | | | | | | | | | | | ✓ | ✓ | | | | | | | | | | | | | | ✓ | | | | | | | |
| 220125_2 | | | | | | | | | | | | ✓ | ✓ | | | | | | | | | | | | | | ✓ | | | | | | | |
| 220123_3_2 | | | | | | | | | | | | ✓ | ✓ | | | | | | | ✓ | | | | | | | | | | | | | | |
| 230124_1 | | | | | | | | | | | | | | | | | | ✓ | ✓ | | | | | | | | ✓ | | | | | | | |
| 230213_5 | | | | | | | | | | | | | | | | | | ✓ | ✓ | | | | | | | | ✓ | | | | | | | |
| 230213_6 | | | | | | | | | | | | | | | | | | ✓ | ✓ | | | | | | | | ✓ | | | | | | | |
| 230213_9 | | | | | | | | | | | | | | | | | | ✓ | ✓ | | | | | | | | ✓ | | | | | | | |
| 230215_7 | | | | | | | | | | | | | | | | | | ✓ | ✓ | | | | | | | | ✓ | | | | | | | |
| 230215_8 | | | | | | | | | | | | | | | | | | ✓ | ✓ | | | | | | | | ✓ | | | | | | | |
| 221110_4 | | | | | | | | | | | | | | | | | | | | | | | | | | | ✓ | | | | | | | |
| 221117_1 | | | | | | | | | | | | | | | | | | | | | | | | | | | ✓ | | | | | | | |
| 210527_11 | | | | | | | | | | | | | | | | | | | | | | | | | | | | ✓ | | | | | | |
| 210528_11 | | | | | | | | | | | | | | | | | | | | | | | | | | | | ✓ | ✓ | | | | | |
| 210626_3 | | | | | | | | | | | | | | | | | | | | | | | | | | | | ✓ | | | | | | ✓ |
| 210629_3 | | | | | | | | | | | | | | | | | | | | | | | | | | | | ✓ | ✓ | | ✓ | | | ✓ |
| 210825_2 | | | | | | | | | | | | | | | | | | | | | | | | | | | | ✓ | ✓ | | | | | ✓ |
| 210827_2 | | | | | | | | | | | | | | | | | | | | | | | | | | | | ✓ | ✓ | | | | | ✓ |
| 210630_5 | | | | | | | | | | | | | | | | | | | | | | | | | | | | ✓ | ✓ | ✓ | | ✓ | | |
| 210630_5_1 | | | | | | | | | | | | | | | | | | | | | | | | | | | | ✓ | ✓ | | | ✓ | | |
| 211216_3 | | ✓ | | | | | | | | | | | | | | | | | | | | | | | | | | | | | | | | |
| 210704_6 | | | ✓ | | | | | | | | | | | | | | | | | | | | | | | | | | | | | | | |
| 211217_2 | | | | ✓ | | | | | | | | | | | | | | | | | | | | | | | | | | | | | | |
| 220518_8_2 | | | | | | | | | | | | | | | ✓ | | | | | | | | | | | | | | | | | | | |
| 220520_9 | | | | | | | | | | | | | | | | ✓ | | | | | | | | | | | | | | | | | | |
| 200821 | | | | | | | | | | | | | | | | | | | | | ✓ | | | | | | | | | | | | | |
| 210827_5 | | | | | | | | | | | | | | | | | | | | | | ✓ | | | | | | | | | | | | |
| 211217_2 | | | | | | | | | | | | | | | | | | | | | | | ✓ | | | | | | | | | | | |

**Table S3. TaqMan Assays used for single-cell multiplexed qRT-PCR.**

| *GENE* | *GENE ID* | *TAQMAN ASSAY ID* |
|---|---|---|
| *Acta2* | 11475 | Mm01546133_m1 |
| *Afp* | 11576 | Mm00431715_m1 |
| *Alb* | 11657 | Mm00802090_m1 |
| *Alcam* | 11658 | Mm00711623_m1 |
| *Angpt1* | 11600 | Mm00456503_m1 |
| *Angpt2* | 11601 | Mm00545822_m1 |
| *Cdh1* | 12550 | Mm01247357_m1 |
| *Cdh5* | 12562 | Mm00486938_m1 |
| *Cebpa* | 12606 | Mm00514283_s1 |
| *Csf1* | 12977 | Mm00432686_m1 |
| *Csf2* | 12981 | Mm01290062_m1 |
| *Csf3* | 12985 | Mm00438334_m1 |
| *Cspg4* | 121021 | Mm00507257_m1 |
| *Cxcl12* | 20315 | Mm00445553_m1 |
| *Des* | 13346 | Mm00802455_m1 |
| *Dlk1* | 13386 | Mm00494477_m1 |
| *Efnb2* | 13642 | Mm00438670_m1 |
| *Endoglin* | 13805 | Mm00468252_m1 |
| *Epcam* | 17075 | Mm00493214_m1 |
| *Ephb4* | 13846 | Mm01201157_m1 |
| *Epo* | 13856 | Mm01202755_m1 |
| *Flt3l* | 14256 | Mm00442801_m1 |
| *Fn1* | 14268 | Mm01256744_m1 |
| *Gpm6a* | 234267 | Mm00463812_m1 |
| *Hnf4a* | 15378 | Mm01247712_m1 |
| *Igf2* | 16002 | Mm00439564_m1 |
| *Il33* | 77125 | Mm00505403_m1 |
| *Il7* | 16196 | Mm00434291_m1 |
| *Kdr* | 16542 | Mm01222421_m1 |
| *Kitl* | 17311 | Mm00442972_m1 |
| *Krt18* | 16668 | Mm01601704_g1 |
| *Krt19* | 16669 | Mm00492980_m1 |
| *Lepr* | 16847 | Mm00440181_m1 |
| *Lgr5* | 14160 | Mm00438890_m1 |
| *Lhx2* | 16870 | Mm00839783_m1 |
| *Ltb* | 16994 | Mm00434774_g1 |
| *Ly6a* | 110454 | Mm00726565_s1 |
| *mKi-67* | 17345 | Mm01278617_m1 |

| | | |
|---|---|---|
| *Msln* | 56047 | Mm00450770_m1 |
| *Msx2* | 17702 | Mm00442992_m1 |
| *Nes* | 18008 | Mm00450205_m1 |
| *Ngfr* | 18053 | Mm00446296_m1 |
| *Onecut1* | 15379 | Mm00839394_m1 |
| *Pdgfra* | 18595 | Mm00440701_m1 |
| *Pdgfrb* | 18596 | Mm00435553_m1 |
| *Pdpn* | 14726 | Mm00494716_m1 |
| *Prox1* | 19130 | Mm00435969_m1 |
| *Runx1* | 12394 | Mm01213404_m1 |
| *Sox4* | 20677 | Mm00486320_s1 |
| *Sox9* | 20682 | Mm00448840_m1 |
| *Spp1* | 20750 | Mm00436767_m1 |
| *Tek* | 21687 | Mm00443243_m1 |
| *Thpo* | 21832 | Mm00437040_m1 |
| *Vcam1* | 22329 | Mm01320970_m1 |
| *Vim* | 22352 | Mm01333430_m1 |
| *Wt1* | 22431 | Mm01337048_m1 |
| *Actb* | 11461 | Mm01205647_g1 |
| *Gapdh* | 14433 | Mm99999915_g1 |
| *Hprt* | 15452 | Mm03024075_m1 |

**Table S4. Primers used for RT-PCR.**

| *PRIMER* | *GENE ID* | *FW SEQUENCE (5'-3')* | *RV SEQUENCE (5'-3')* | *PRIMERBANK ID* |
|---|---|---|---|---|
| *Csf1* | 12977 | GTGTCAGAACACTGTAGCCAC | TCAAAGGCAATCTGGCATGAAG | 166064045c1 |
| *Csf2* | 12981 | GGCCTTGGAAGCATGTAGAGG | GGAGAACTCGTTAGAGACGACTT | 22094089a1 |
| *Csf3* | 12985 | ATGGCTCAACTTTCTGCCCAG | CTGACAGTGACCAGGGGAAC | 6753536a1 |
| *Cxcl12* | 20315 | TGCATCAGTGACGGTAAACCA | TTCTTCAGCCGTGCAACAATC | 7305465a1 |
| *Epo* | 13856 | ACAAAGCCATCAGTGGTCTACG | TCTGGAGGCGACATCAATTCC | 113931667c2 |
| *Flt3l* | 14256 | GCCTGGAGCCCAAATTCCTC | GCTGAAGTAACAGTCAGGTGTC | 18043820a1 |
| *Il7* | 16196 | TTCCTCCACTGATCCTTGTTCT | AGCAGCTTCCTTTGTATCATCAC | 6680433a1 |
| *Kitl* | 17311 | GAATCTCCGAAGAGGCCAGAA | GCTGCAACAGGGGGTAACAT | 198596a1 |
| *Thpo* | 21832 | AACCCAGACGGAACAGAGC | GTGCTGCCATCACTCCCTC | 118130856c2 |
| *Actb* | 11461 | GCTTCTTTGCAGCTCCTTCGT | ATCGTCATCCATGGCGAACT | 291045236c3 |